

Soil Mechanics

T. William Lambe • Robert V. Whitman

Massachusetts Institute of Technology

1969

JOHN WILEY & SONS, New York • Chichester • Brisbane • Toronto • Singapore

KARL TERZAGHI

Karl Terzaghi, born October 2, 1883 in Prague and died October 25, 1963 in Winchester, Massachusetts, is generally recognized as the Father of Soil Mechanics. His early professional life was spent in a search for a rational approach to earthwork engineering problems. His efforts were rewarded with the publication in 1925 of his famous book on soil mechanics: this publication is now credited as being the birth of soil mechanics.

Between 1925 and 1929, Terzaghi was at M.I.T. initiating the first U.S. program in soil mechanics and causing soil mechanics to be widely recognized as an important discipline in civil engineering. In 1938 he joined the faculty at Harvard University where he developed and gave his course in engineering geology.

Terzaghi's amazing career is well documented in the book *From Theory to Practice in Soil Mechanics* (Wiley, 1960). All of Terzaghi's publications through 1960 (256) are listed in this book. Terzaghi won many honors, including the Norman Medal of the American Society of Civil Engineers in 1930, 1943, 1946, and 1955. Terzaghi was given nine honorary doctorate degrees coming from universities in eight different countries. He served for many years as President of the International Society of Soil Mechanics and Foundation Engineering.

Not only did Terzaghi start soil mechanics but he exerted a profound influence on it until his death. Two days before he died he was diligently working on a professional paper. Terzaghi's writings contain significant contributions on many topics, especially consolidation theory, foundation design and construction, cofferdam analysis, and landslide mechanisms. Probably Terzaghi's most important contribution to the profession was his approach to engineering problems, which he taught and demonstrated.

To commemorate Terzaghi's great work, the American Society of Civil Engineers created the Terzaghi Lecture and the Terzaghi Award.



PREFACE

Soil Mechanics is designed as a text for an introductory course in soil mechanics. An intensive effort was made to identify the truly fundamental and relevant principles of soil mechanics and to present them clearly and thoroughly. Many numerical examples and problems are included to illustrate these key principles. This text has been used successfully both in an introductory undergraduate course and in an introductory graduate course. Although *Soil Mechanics* has been written principally for the student, practicing engineers should find it valuable as a reference document.

The book is divided into five parts. Part I describes the nature of soil problems encountered in civil engineering and gives an overall preview of the behavior of soil. Part II describes the nature of soil, especially the transmission of stresses between soil particles. Part III is devoted primarily to dry soil since many aspects of soil behavior can best be understood by considering the interaction of soil particles without the presence of water. Part IV builds upon the principles given in Parts II and III to treat soils in which the pore water is either stationary or flowing under steady conditions. Part V considers the most complex situation in soil mechanics, that wherein pore pressures are influenced by applied loads and hence the pore water is flowing under transient conditions. This organization of the book permits the subject matter to be presented in sequential fashion, progressively building up to the more complex principles.

Parts III, IV, and V all have the same general format. First there are several chapters that set forth the basic principles of soil behavior. Then follow several chapters in which these principles are applied to the practical analysis and design of earth retaining structures, earth slopes, and shallow foundations. For example, chapters concerning shallow foundations appear in Part III, Part IV, and Part V. Special chapters on deep foundations and soil improvement appear at the end of Part V. These problem-oriented chapters illustrate the blending of theory, laboratory testing, and empirical evidence from past experience to provide practical but sound methods for analysis and design. *Soil Mechanics* does not attempt to cover all the details of these practical problems; numerous references are provided to guide the student in additional study.

Soil Mechanics deliberately includes far more material than can or should be covered in a single introductory course, thus making it possible for the instructor to choose the topics to be used to illustrate the basic principles. We have found that numerical examples of practical problems should be introduced very early in an introductory course in soil mechanics—preferably within the first eight periods. Thus we organize the early portion of our courses as follows:

1. Part I is covered in two lectures, giving students motivation for the study of soil mechanics and an understanding of the organization of the course.
2. Chapter 3 is covered in detail, but Chapters 4 to 7 are surveyed only hastily. As questions arise later in the course, reference is made to the material in these chapters.
3. Chapter 8 describes several basic methods for calculating and displaying the stresses; students must master these techniques. Chapters 9 to 12 contain certain key concepts concerning soil behavior plus descriptive matter and tables and charts of typical values. These chapters may be covered rapidly, stressing only the key concepts. Then the student is ready for an intensive study of retaining structures (Chapter 13) and shallow foundations (Chapter 14). Three or four periods may profitably be spent on each chapter. Chapter 15 serves to introduce the increasingly important problem of soil dynamics, and serves as supplementary reading for an introductory course.
4. In Chapter 16 the definition and manipulation of effective stress is emphasized and the mechanistic interpretation of effective stress serves as supplementary reading. The depth of study of

Chapters 17 to 19 will vary with the treatment given this topic in other courses such as fluid mechanics. Chapters 20 to 22 are largely descriptive and may be studied quickly with emphasis on the main features of soil behavior. This again leaves time for a detailed study of topics from Chapters 23 to 25. The choice of topics will depend on the interests of the instructor and the material to be covered in later courses. We attempt to cover only portions of two of the three chapters.

5. Chapters 26 and 27 contain key concepts and computational procedures and detailed coverage is needed for comprehension. Similarly, detailed coverage of Chapter 28 is required to give understanding of the key connection between drained and undrained behavior. Chapters 29 and 30 are largely descriptive and can be covered quickly leaving time for detailed study of selected topics from the remaining chapters.

The material not covered in an introductory course will serve to introduce students to more advanced courses and can be used as reference material for those courses.

As the reader will see, our book presents photographs of and biographical data on six pioneers in soil mechanics. These men have made significant contributions to soil mechanics knowledge and have had a major impact on soil mechanics students. There is a second generation of leaders whose works are having and will have an impact on soil mechanics. The extensive references in our book to the works of these people attest to this fact.

We thank the many authors and publishers for permission to reproduce tables and figures. The Council of the Institution of Civil Engineers granted permission to reproduce material from *Géotechnique*.

The early stages of the preparation of this text was supported in part by a grant made to the Massachusetts Institute of Technology by the Ford Foundation for the purpose of aiding in the improvement of engineering education. This support is gratefully acknowledged. We thank Professor Charles L. Miller, Head of the Department of Civil Engineering, for his encouragement in the undertaking of this book. We also acknowledge the contributions of our many colleagues at M.I.T. and the important role of our students who subjected several drafts to such careful scrutiny and criticism. Special recognition is due Professors Charles C. Ladd and Leslie G. Bromwell who offered comments on most of the text. Professor Bromwell contributed revisions to Part II and to Chapter 34. Professor John T. Christian helped considerably with theoretical portions of the text, as did Dr. Robert T. Martin on Part II and Dr. David D'Appolonia on Chapters 15 and 33. Professor James K. Mitchell of the University of California (Berkeley) contributed valuable comments regarding Part II, as did Professor Robert L. Schiffman of the University of Illinois (Chicago) regarding Chapter 27. Finally, we thank Miss Evelyn Perez and especially Mrs. Alice K. Viano for their indefatigable and meticulous typing of our many drafts.

T. William Lambe
Robert V. Whitman

PART I *Introduction*

CHAPTER 1	Soil Problems in Civil Engineering	3
CHAPTER 2	A Preview of Soil Behavior	18

PART II *The Nature of Soil*

CHAPTER 3	Description of an Assemblage of Particles	29
CHAPTER 4	Description of an Individual Soil Particle	40
CHAPTER 5	Normal Stress between Soil Particles	52
CHAPTER 6	Shear Resistance between Soil Particles	61
CHAPTER 7	Soil Formation	71

PART III *Dry Soil*

CHAPTER 8	Stresses within a Soil Mass	97
CHAPTER 9	Tests to Measure Stress-Strain Properties	116
CHAPTER 10	General Aspects of Stress-Strain Behavior	122
CHAPTER 11	Shear Strength of Cohesionless Soil	137
CHAPTER 12	Stress-Strain Relationships	151
CHAPTER 13	Earth Retaining Structures and Slopes	162
CHAPTER 14	Shallow Foundations	195
CHAPTER 15	Dynamic Loading of Soil	227

PART IV *Soil with Water—No Flow or
Steady Flow*

CHAPTER 16	Effective Stress Concept	241
CHAPTER 17	One-Dimensional Fluid Flow	251
CHAPTER 18	Two-Dimensional Fluid Flow	266
CHAPTER 19	Soil Permeability and Filter Requirements	281
CHAPTER 20	General Aspects of Drained Stress-Strain Behavior	295
CHAPTER 21	Drained Shear Strength	304
CHAPTER 22	Stress-Strain Relations for Drained Conditions	318
CHAPTER 23	Earth Retaining Structures with Drained Conditions	328
CHAPTER 24	Earth Slopes with Drained Conditions	352
CHAPTER 25	Shallow Foundations with Drained Conditions	374

PART V *Soil with Water—Transient Flow*

CHAPTER 26	Pore Pressures Developed During Undrained Loading	391
CHAPTER 27	Consolidation Theory	406
CHAPTER 28	Drained and Undrained Stress-Strain Behavior	423
CHAPTER 29	Undrained Shear Strength	439
CHAPTER 30	Stress-Strain Relations for Undrained Conditions	455
CHAPTER 31	Earth Retaining Structures and Earth Slopes with Undrained Conditions	464
CHAPTER 32	Shallow Foundations with Undrained Conditions	484
CHAPTER 33	Deep Foundations	498
CHAPTER 34	The Improvement of Soil	514
Appendix A	Symbols	525
Appendix B	Conversion	531
Appendix C	References	535
Index		547

DONALD WOOD TAYLOR



Donald Wood Taylor was born in Worcester, Massachusetts in 1900 and died in Arlington, Massachusetts on December 24, 1955. After graduating from Worcester Polytechnic Institute in 1922, Professor Taylor worked nine years with the United States Const and Geodetic Survey and with the New England Power Association. In 1932 he joined the staff of the Civil Engineering Department at M.I.T. where he remained until his death.

Professor Taylor was active in both the Boston Society of Civil Engineers and the American Society of Civil Engineers. Just prior to his death he had been nominated for the Presidency of the Boston Society. From 1948 to 1953 he was International Secretary for the International Society of Soil Mechanics and Foundation Engineering.

Professor Taylor, a quiet and unassuming man, was highly respected among his peers for his very careful and accurate research work. He made major contributions to the fundamentals of soil mechanics, especially on the topics of consolidation, shear strength of cohesive soils, and the stability of earth slopes. His paper "Stability of Earth Slopes" was awarded the Desmond Fitzgerald Medal, the highest award of the Boston Society of Civil Engineers. His textbook, *Fundamentals of Soil Mechanics*, has been widely used for many years.

PART I

Introduction

Part I attempts to motivate the beginning student and alert him to the few really fundamental concepts in soil mechanics. Chapter 1 gives a general picture of civil engineering problems that can be successfully attacked

by using the principles of soil mechanics. Chapter 2 describes, in terms familiar to the budding engineer, the essential principles that are covered in detail in the main portion of the book.

CHAPTER 1

Soil Problems in Civil Engineering

In his practice the civil engineer has many diverse and important encounters with soil. He uses soil as a foundation to support structures and embankments; he uses soil as a construction material; he must design structures to retain soils from excavations and underground openings; and he encounters soil in a number of special problems. This chapter deals with the nature and scope of these engineering problems, and with some of the terms the engineer uses to describe and solve these problems. Several actual jobs are described in order to illustrate the types of questions that a soil engineer must answer.

1.1 FOUNDATIONS

Nearly every civil engineering structure—building, bridge, highway, tunnel, wall, tower, canal, or dam—must be founded in or on the surface of the earth. To perform satisfactorily each structure must have a proper foundation.

When firm soil is near the ground surface, a feasible means of transferring the concentrated loads from the walls or columns of a building to the soil is through *spread footings*, as illustrated in Fig. 1.1. An arrangement of spread footings is called a *spread foundation*. In the past, timber or metal grillages, cobble pads, etc., were used to form spread footings, but today footings almost invariably are of reinforced concrete.

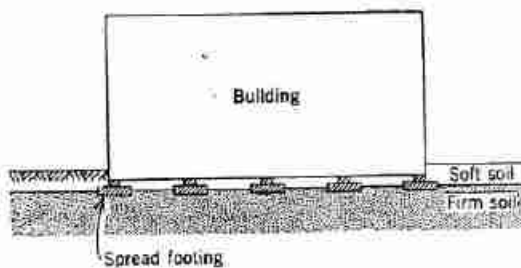


Fig. 1.1 Building with spread foundation.

When firm soil is not near the ground surface, a common means of transferring the weight of a structure to the ground is through vertical members such as *piles* (Fig. 1.2), *caissons*, or *piers*. These terms do not have sharp definitions that distinguish one from another. Generally, caissons and piers are larger in diameter than piles and are installed by an excavation technique, whereas piles are installed by driving. The weight of the building is carried through the soft soil to firm material below with essentially no part of the building load being applied to the soft soil.

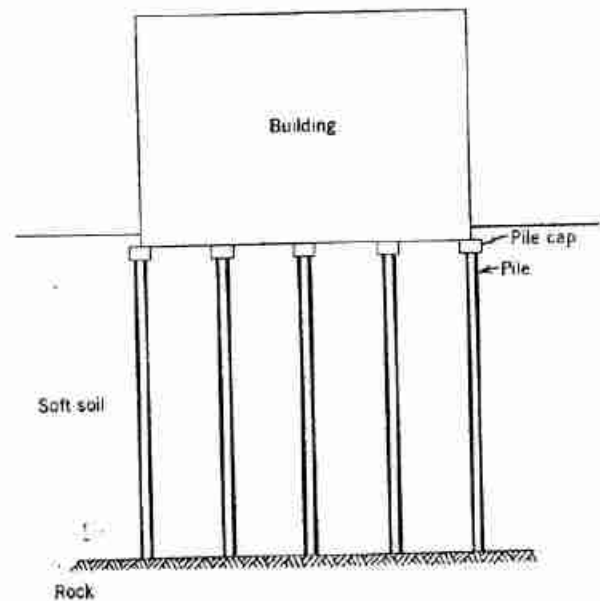


Fig. 1.2 Building with pile foundation.

There is much more to successful foundation engineering than merely selecting sizes of footings or choosing the right number and sizes of piles. In many cases, the cost of supporting a building can be significantly reduced by

applying certain treatments to the soil. Further, some structures, such as steel storage tanks, can be supported directly on a specially prepared pad of soil without the benefit of intervening structural members. Thus the word *foundation* refers to the soil under the structure as well as any intervening load carrying member, i.e., *foundation* refers to the material whose behavior the civil engineer has analyzed in order to provide satisfactory and economical support for the structure. Indeed, the word *foundation* is used to describe the material that supports any type of engineering structure such as building, dam, highway embankment, or airfield runway. In modern usage, the term *shallow foundation* is used to describe an arrangement where structural loads are carried by the soil directly under the structure, and *deep foundation* is used for the case where piles, caissons, or piers are used to carry the loads to firm soil at some depth.

In the design of any foundation system, the central problem is to prevent settlements large enough to damage the structure or impair its functions. Just how much settlement is permissible depends on the size, type, and use of structure, type of foundation, source in the subsoil of the settlement, and location of the structure. In most cases, the critical settlement is not the *total settlement* but rather the *differential settlement*, which is the relative movement of two parts of the structure.

In most metropolitan areas of the United States and Western Europe, owners of buildings usually are unwilling to accept settlements greater than a few inches, since unattractive cracks are likely to occur if the settlements are larger. For example, experience has shown that settlements in excess of approximately 5 in. will

cause the brick and masonry walls of buildings on the M.I.T. campus to crack.

However, where soil conditions are very bad, owners sometimes willingly tolerate large settlements with resulting cracking in order to avoid very significant additional costs of deep foundations over shallow ones. For example, along the waterfront in Santos, Brazil, 15-story apartment buildings are founded directly upon soft soil. Settlements as large as 1 ft are common. Cracks in these buildings are apparent, but most of them have remained in continuous use.

Perhaps the classic case of bad foundation conditions exists in Mexico City. Here, for example, one building, the Palace of Fine Arts, shown in Fig. 1.3, is in continuous use even though it has sunk 12 ft into the surrounding soil. Where a visitor used to walk up steps to the first floor, he must now walk down steps to this floor because of the large settlement.

With structures other than buildings, large settlements often are tolerated. Settlements as large as several feet are quite common in the case of flexible structures such as storage tanks and earth embankments. On the other hand, foundation movements as small as 0.01 in. may be intolerable in the case of foundations for precision tracking radars and nuclear accelerators.

Example of Shallow Foundation

Figure 1.4 shows the M.I.T. Student Center, which has a shallow foundation consisting of a slab under the entire building. Such a slab is called a *mat*. The subsoils at the site consist of the following strata starting from ground surface and working downward: a 15-ft layer of soft fill



Fig. 1.3 Palacio de las Bellas Artes, Mexico City. The 2-m differential settlement between the street and the building on the right necessitated the steps which were added as the settlement occurred. The general subsidence of this part of the city is 7 m (photograph compliments of Raul Marsal).

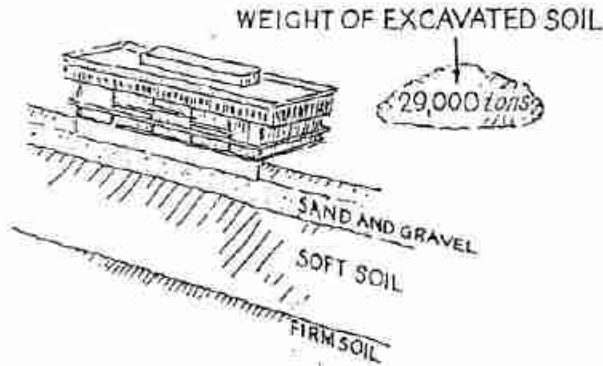


Fig. 1.4 Building on shallow mat foundation.

Weight of building	= 32,000 tons
Weight of furniture, people, etc. (time average)	= 5,000 tons
	<hr/>
	37,000 tons
Weight of excavated soil	= 29,000 tons
Net load to clay	= 8,000 tons

and organic silt; a 20-ft layer of sand and gravel; 75-ft of soft clay; and, finally, firm soil and rock. The weight of the empty building (called the *dead load*) is 32,000 tons. The weight of furniture, people, books, etc. (called *live load*) is 5000 tons. Had this building with its total load of 37,000 tons been placed on the ground surface, a settlement of approximately 1 ft would have occurred due to the compression of the soft underlying soil. A settlement of such large magnitude would damage the structure. The solution of this foundation problem was to place the building in an excavation. The weight of excavated soil was 29,000 tons, so that the net building load applied to the underlying soil was only 8000 tons. For this arrangement the estimated settlement of the building is 2–3 in., a value which can be tolerated.

This technique of reducing the net load by removing soil is called *flotation*. When the building is partly compensated by relief of load through excavation the technique is called *partial flotation*; when entirely compensated, it is called *full flotation*. Full flotation of a structure in soil is based on the same principle as the flotation of a boat. The boat displaces a weight of water equal to the weight of the boat so that the stress at a given depth in the water below the boat is the same, independent of the presence of the boat. Since the building in Fig. 1.4, has an average unit weight equal to about one-half that of water, and the unit weight of the excavated soil is about twice that of water, the building should be placed with about one-fourth of its total height under the ground surface in order to get full flotation.

On this particular project, the soil engineer was called upon to study the relative economy of this special shallow foundation versus a deep foundation of piles or caissons.

After having concluded that the shallow foundation was desirable, he had to answer questions such as the following.

1. Just how deep into the soil should the building be placed?
2. Would the excavation have to be enclosed by a wall during construction to prevent cave-ins of soil?
3. Would it be necessary to lower the water table in order to excavate and construct the foundation and, if so, what means should be used to accomplish this lowering of the ground water (*dewatering*)?
4. Was there a danger of damage to adjacent buildings? (In later chapters it will be demonstrated that lowering the water table under a building can cause serious settlements. The question of just how and for what duration the water table is lowered can thus be very important.)
5. How much would the completed building settle and would it settle uniformly?
6. For what stresses and what stress distribution should the mat of the building be designed?

Example of Pile Foundation

Figure 1.5 shows the M.I.T. Materials Center, which has a deep pile foundation. The subsoils at the site of the Materials Building are similar to those at the Student Center with the important exception that there is little or no sand and gravel at the Materials Center site. The total load of the Materials Building is 28,000 tons made up of a dead load of 16,000 tons and a live load of 12,000 tons. The dead load of the Materials Center is less than that of the Student Center primarily because the Materials Building is made of lighter materials than the Student

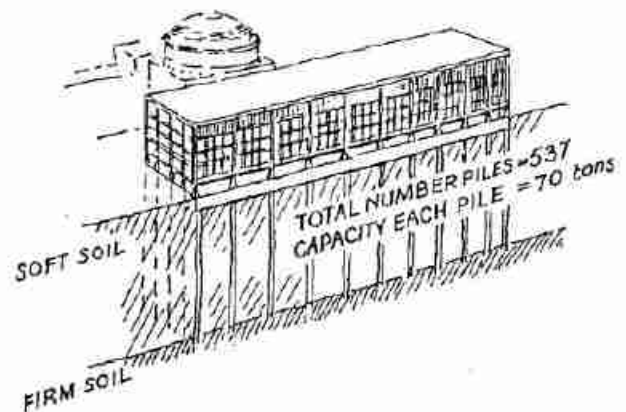


Fig. 1.5 Building on deep pile foundation.

Weight of building	= 15,650 tons
Weight of equipment, books, people, etc.	= 12,200 tons
Maximum total weight	≈ 28,000 tons

Center, and the live load is greater because of the much heavier equipment going into the Materials Building. The three major reasons that the Materials Building was placed on piles to firm soil rather than floated on a mat were:

1. The intended use of the Materials Building was such that floor space below ground surface, i.e., basement space, was not desirable.
2. There was little or no sand and gravel at the site on which to place the mat.
3. There were many underground utilities, especially a large steam tunnel crossing the site, which would have made the construction of a deep basement difficult and expensive.

The foundation selected consisted of 537 piles, each with a capacity of 70 tons. The piles were constructed by boring a hole about three-quarters of the way from ground surface to the firm soil, placing a hollow steel shell of 12½ in. diameter in the bored hole and driving it to the firm soil, and then filling the hollow shell with concrete. (The hollow shell was covered with a steel plate at the tip to prevent soil from entering.) Such a pile is called a *point-bearing pile* (it receives its support at the point, which rests in the firm soil, as opposed to a *friction pile*, which receives its support along a large part of its length from the soil through which it goes) and a *cast-in-place concrete pile* (as opposed to a pile which is *precast* and then driven). Soil was removed by augering for three-quarters of the length of the pile in order to reduce the net volume increase below ground surface due to the introduction of the piles. Had *preaugering* not been employed, the surface of the ground at the building site would have risen almost 1 ft because of the volume of the 537 piles. The rise of the ground surface would have been objectionable because it would have raised piles that had already been driven, and it would have been dangerous because of possible disturbance of the nearby dome shown in the background in Fig. 1.5.

Among the questions faced by the soil engineer in the design and construction of the pile foundation were:

1. What type of pile should be used?
2. What was the maximum allowable load for a pile?
3. At what spacing should the piles be driven?
4. How should the piles be driven?
5. How much variation from the vertical should be permitted in a pile?
6. What was the optimum sequence for driving piles?
7. Would the driving of piles have an influence on adjacent structures?

Example of Embankment on Soft Soil

Figure 1.6 shows a 35-ft embankment of earth placed on a 32-ft layer of soft soil. The original plan was to

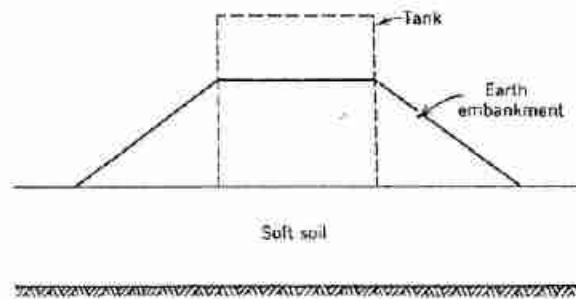


Fig. 1.6 Embankment on soft soil.

place a tank, shown by dashed lines in Figure 1.6, 50 ft in diameter and 56 ft high, at the site. Had the tank been placed on the soft foundation soil with no special foundation, a settlement in excess of 5 ft would have occurred. Even though a steel storage tank is a flexible structure, a settlement of 5 ft is too large to be tolerated.

Soil engineering studies showed that a very economical solution to the tank foundation problem consisted of building an earth embankment at the site to compress the soft soil, removing the embankment, and finally placing the tank on the prepared foundation soil. Such a technique is termed *preloading*.

Since the preload was to be removed just prior to the construction of the tank, and the tank pad brought to the correct elevation, the magnitude which the preload settled was of no particular importance. The only concern was that the fill not be so high that a shear rupture of the soil would occur. If the placed fill caused *shear stresses* in the foundation which exceeded the *shear strength*, a rupture of the foundation could occur. Such a rupture would be accompanied by large movements of earth with probably serious disturbance to the soft foundation soil and possible damage to nearby tanks. Among the questions that had to be answered on this project were the following ones.

1. How high a fill could be placed?
2. How fast could the fill be placed?
3. What were the maximum slopes for the fill?
4. Could the fill be placed without employing special techniques to contain or drain the soft foundation soil?
5. How much would the fill settle?
6. How long should the fill be left in place in order that the foundation be compressed enough to permit construction and use of the tank?

Example of Foundation Heave

The foundation engineer faces not only problems involving settlement but also problems involving the upward movement (heave) of structures. Heave problems arise when the foundation soil is one that expands

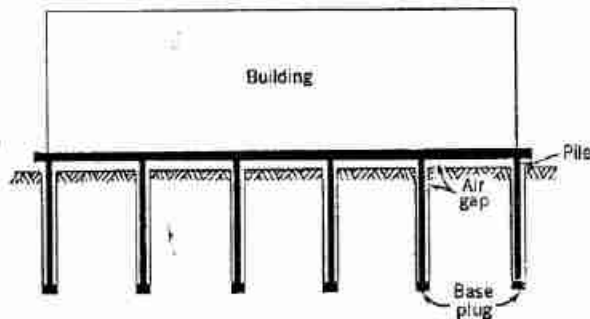


Fig. 1.7 Building on expansive soil.

when the confining pressure is reduced and/or the water content of the soil is increased. Certain soils, termed *expansive soils*, display heaving characteristics to a relatively high degree.

Heave problems are particularly common and economically important in those parts of the world with arid regions, e.g., Egypt, Israel, South Africa, Spain, Southwestern United States, and Venezuela. In such areas the soils dry and shrink during the arid weather and then expand when moisture becomes available. Water can become available from rainfall, or drainage, or from capillarity when an impervious surface is placed on the surface of the soil, thereby preventing evaporation. Obviously, the lighter a structure, the more the expanding soil will raise it. Thus heave problems are commonly associated with light structures such as small buildings (especially dwellings), dam spillways, and road pavements.

Figure 1.7 shows a light structure built in Coro, Venezuela. In the Coro area the soil is very expansive, containing the mineral *montmorillonite*. A number of buildings in Coro have been damaged by heave. For example, the floor slab and entry slab of a local hotel, resting on the ground surface, have heaved extensively, thus cracking badly and becoming very irregular. The building in Fig. 1.7 employs a scheme that avoids heave troubles but clearly is much more expensive than a simple shallow mat. First, holes were augered into the soil, steel shells were placed, and then concrete base plugs and piles were poured. Under the building and around the piles was left an air gap, which served both to reduce the amount of heave of the soil (by permitting evaporation) and to allow room for such heave without disturbing the building.

The main question for the soil engineer was in selecting the size, capacity, length, and spacing of the piles. The

piles were made long enough to extend below the depth of soil that would expand if given access to moisture. The depth selected was such that the confining pressure from the soil overburden plus minimum load was sufficient to prevent expansion.

1.2 SOIL AS A CONSTRUCTION MATERIAL

Soil is the most plentiful construction material in the world and in many regions it is essentially the only locally available construction material. From the days of neolithic man, earth has been used for the construction of monuments, tombs, dwellings, transportation facilities, and water retention structures. This section describes three structures built of earth.

When the civil engineer uses soil as a construction material, he must select the proper type of soil and the method of placement, and then control the actual placement. Man-placed soil is called *fill*, and the process of placing it is termed *filling*. One of the most common problems of earth construction is the wide variability of the source soil, termed *borrow*. An essential part of the engineer's task is to see that the properties of the placed material correspond to those assumed in the design, or to change the design during construction to allow for any difference between the properties of the constructed fill and those employed in the design.

Example of an Earth Dam

Figure 1.8 is a vertical cross section of an earth dam built to retain a reservoir of water. The two main zones of the dam are the *clay core* and the *rock toe*: the core with its impermeable clay keeps leakage low; and the heavy, highly permeable rock toe adds considerable stability to the dam. Between these zones is placed a



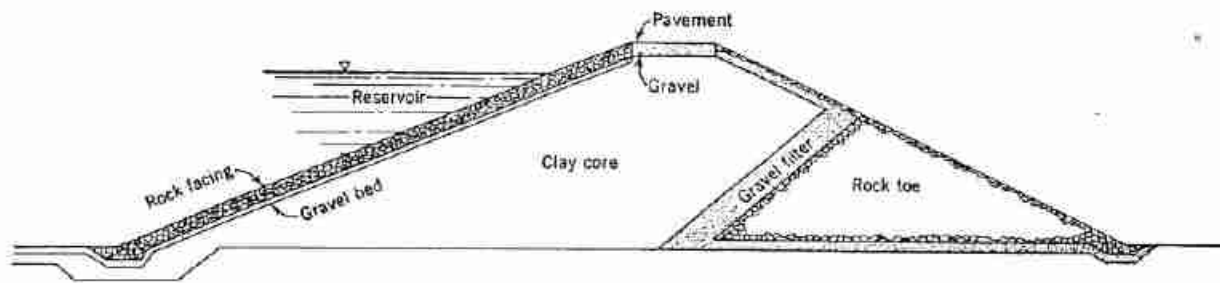


Fig. 1.8 Earth dam.

gravel filter to prevent washing of soil particles from the core into the voids of the rock toe. Between the core and the reservoir is a rock facing placed on a gravel bed. The rock facing prevents erosion of the core by rain or water in the reservoir. The gravel bed prevents large rocks on the face from sinking into the clay. This type of dam is called a *zoned earth dam* to differentiate it from a *homogeneous earth dam* in which the same type of material is used throughout the cross section.

The popularity of earth dams compared to concrete dams is increasing steadily for two major reasons. First, the earth dam can withstand foundation and abutment movements better than can the more rigid concrete structure. Second, the cost of earth construction per unit volume has remained approximately constant for the last 50 years (the increased cost of labor has been offset by the improvements in earth-handling equipment), whereas the cost of concrete per unit volume has steadily increased. One would thus expect earth dams to become increasingly popular.

The relative sizes of the zones in an earth dam and the types of material in each zone depend very much on the earth materials available at the site of the dam. At the site of the dam shown in Fig. 1.8, excavation for the reservoir yielded clay and rock in about the proportions used in the dam. Thus none of the excavated material was wasted. The only scarce material was the gravel used for the filter and the bed. This material was obtained from stream beds some distance from the site and transported to the dam by trucks.

Dam construction was carried out for the full length and the full width of the dam at the same time; i.e., an attempt was made to keep the surface of the dam approximately horizontal at any stage of construction. The toe, consisting of rock varying in size from 6 in. to 3 ft, was *end-dumped* from trucks and washed as dumped with water under high pressure. The clay and gravel were placed in horizontal lifts of 6 in. to 1 ft in thickness, then brought to a selected moisture content, and finally *compacted* by rolling compaction equipment over the surface.

The following questions were faced by the civil engineer during the design and construction of the earth dam.

1. What should be the dimensions of the dam to give the most economical, safe structure?
2. What is the minimum safe thickness for the gravel layers?
3. How thick a layer of gravel and rock facing is necessary to keep any swelling of the clay core to a tolerable amount?
4. What moisture content and compaction technique should be employed to place the gravel and clay materials?
5. What are the strength and permeability characteristics of the constructed dam?
6. How would the strength and permeability of the dam vary with time and depth of water in the reservoir?
7. How much leakage would occur under and through the dam?
8. What, if any, special restrictions on the operation of the reservoir are necessary?

Example of a Reclamation Structure

There are many parts of the world where good building sites are no longer available. This is particularly true of harbor and terminal facilities, which obviously need to be on the waterfront. To overcome this shortage, there is an increasingly large number of reclamation projects wherein large sites are built by filling. The soil for such projects is usually obtained by dredging it from the bottom of the adjacent river, lake, or ocean and placing it at the location desired. This process is *hydraulic filling*.

Figures 1.9 and 1.10 show a successful reclamation project built in Lake Maracaibo, Venezuela. The island was constructed by driving a wall of concrete piles enclosing an area 850 m long by 600 m wide. Soil was then dredged from the bottom of Lake Maracaibo and pumped into the sheet pile enclosure until the level of the hydraulic fill reached the desired elevation. Three factors—the lack of available land onshore, the deep water

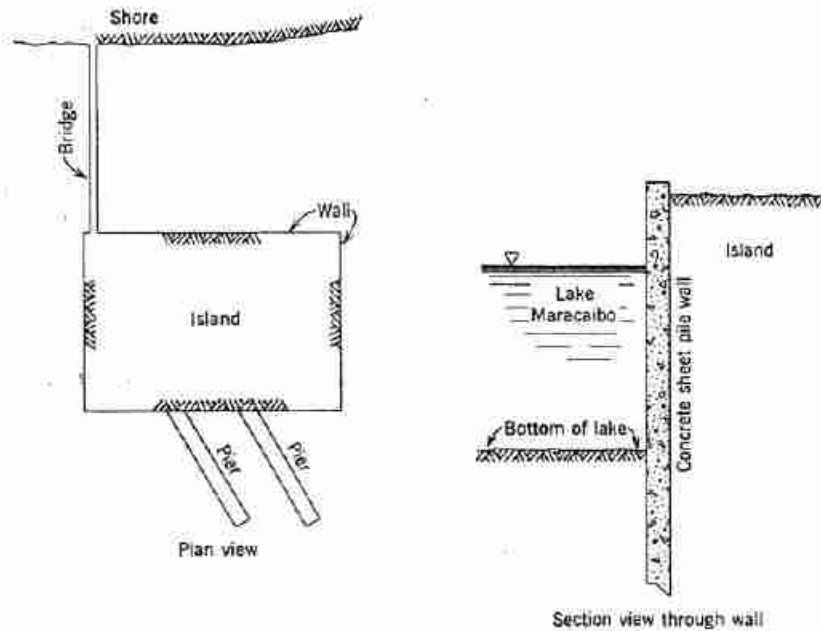


Fig. 1.9 Marine terminal built of hydraulic fill.

needed for large ships to come near the terminal, and the need to dredge a channel in the lake—combined to make the construction of this man-made island an excellent solution to the need of terminal facilities at this location.

On the island, storage tanks for various petroleum products were constructed. The products are brought by pipelines from shore to the tanks on the island and then pumped from the tanks to tankers docked at the two piers shown in Fig. 1.9.

Many exploratory borings were made in the area to be dredged in order to permit the soil engineer to estimate the type of fill that would be pumped onto the island. This fill consisted primarily of clay in the form of hard chunks varying in size from 1 to 6 in. plus a thin slurry of water with silt and clay particles in suspension. Upon coming out of the dredge pipe on the island, the large particles settled first, and the finer particles were transported a considerable distance from the pipe exit. At one corner of the island was a spillway to permit the excess water from the dredging operation to re-enter the lake.

Following are some questions faced by the civil engineer on this terminal project.

1. How deep should the sheet pile wall penetrate the foundation soil?
2. How should these piles be braced laterally?
3. What is the most desirable pattern of fill placement—i.e., how should the exit of the dredge pipe be located in order to get the firmer part of the fill at the locations where the maximum foundation loads would be placed?

4. What design strength and compressibility of the hydraulic fill should be used for selecting foundations for the tanks, buildings, and pumping facilities to be placed on the island?
5. Where did the soil fines in the dirty effluent which went out of the island over the spillway ultimately settle?

Example of Highway Pavement

One of the most common and widespread uses of soil as a construction material is in the pavements of roads and airfields. Pavements are either flexible or rigid. The primary function of a flexible pavement is to spread the



Fig. 1.10 La Salina Marine Terminal (compliments of the Creole Petroleum Corporation).

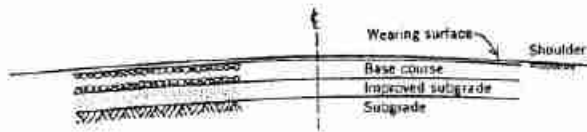


Fig. 1.11 Highway pavement.

concentrated wheel loads over a sufficiently large area of the foundation soil to prevent overstressing it. The rigid pavement constructed of reinforced concrete possesses sufficient flexural strength to bridge soft spots in the foundation. Which pavement is better for a given problem depends on the nature of the foundation, availability of construction materials, and the use to be made of the pavement.

Figure 1.11 shows a highway flexible pavement designed for 100 passes per lane per day of a vehicle having a maximum wheel load of 15,000 lb. The selected pavement consisted of an *improved subgrade* made by compacting the top 6 in. of the *in situ* soil; a *base course* consisting of a 6-in. layer of soil from the site, mixed with 7% by soil weight of portland cement, brought to proper moisture content, mixed and then compacted; and a *wearing surface* consisting of a 2-in.-thick layer of hot-mixed sand-asphalt.

Commonly, the base course of a pavement consists of gravel or crushed stone. In the desert, where the pavement shown in Fig. 1.11 was built, there was a shortage of gravel but an abundance of desert sand. Under these circumstances, it was more economical to improve the properties of the local sand (*soil stabilization*) than to haul gravel or crushed stone over large distances. The most economical soil stabilizer and the method of preparing the stabilized base were chosen on the basis of a program of laboratory tests involving various possible stabilizers and construction techniques.

Among the questions faced by the engineer on the design and construction of this road were the following ones.

1. How thick should the various components of the pavement be to carry the expected loads?
2. What is the optimum mixture of additives for stabilizing the desert sand?
3. Is the desert sand acceptable for the construction of the wearing surface?
4. What grade and weight of available asphalt make the most economical, satisfactory wearing surface?
5. What type and how much compaction should be used?

1.3 SLOPES AND EXCAVATIONS

When a soil surface is not horizontal there is a component of gravity tending to move the soil downward, as

illustrated by the force diagram in Fig. 1.12a. If along a potential slip surface in the soil the shear stress from gravity or any other source (such as moving water, weight of an overlying structure, or an earthquake) exceeds the strength of the soil along the surface, a shear rupture and movement can occur. There are many circumstances in natural slopes, compacted embankments, and excavations where the civil engineer must investigate the stability of a slope by comparing the shear stress with the shear strength along a potential slip surface—i.e., he must make a *stability analysis*.

Figure 1.12a shows a natural slope on which a building has been constructed. The increased shear stress from the building and the possible decrease of soil shear strength from water wasted from the building can cause a failure of the slope, which may have been stable for many years before construction. Such slides are common in the Los Angeles area.

The earth dam shown in Fig. 1.8 has a compacted earth slope which had to be investigated for stability. During the design of this dam, the civil engineer compared the shear stress with the shear strength for a number of potential slip surfaces running through the clay core.

Figures 1.12b and c illustrate excavations for a building and a pipe. The building excavation is a *braced excavation* and that for the pipe is an *unbraced excavation*.² A designing engineer must be sure that the shear strength of the slope is not exceeded, for this would result in a cave-in.

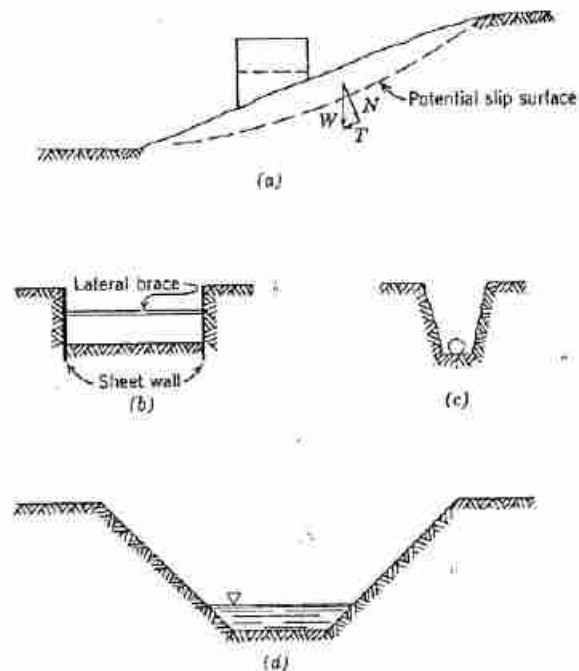


Fig. 1.12 Slopes and excavations. (a) Natural slope. (b) Excavation for building. (c) Excavation for pipe. (d) Canal.



Fig. 1.13 Landslide in a quick clay (compliments of Laurits Hjerrum).

Figure 1.12*d* shows a sketch of a canal. Canals usually are built by excavating through natural materials, but sometimes they are built by compacting fill. The slopes of the canal must be safe both against a shear failure, as described previously, and against the effects of moving water. If protection against moving water is not furnished the canal banks may erode, requiring continuous removal of eroded earth from the canal and possibly triggering a general shear failure of the canal sides.

Figure 1.13 shows a dramatic landslide of a natural slope of *quick clay*. Quick clay is a very sensitive clay deposited in marine water and later leached by ground water. The removal of the salt in the soil pores results in a soil that loses much of its strength when disturbed. The soil in the landslide zone in Fig. 1.13 had been leached for thousands of years until it became too weak to support the natural slope. Some excavation at the toe of the slope or added load may have triggered the slide. Landslides of this type are common in Scandinavia and Canada.

Panama Canal

Figure 1.14 shows one of the world's most famous canals—the Panama Canal. Excavation on the Panama Canal was started in February 1883 by a French company that intended to construct a sea level canal across the Isthmus of Panama joining the Atlantic and Pacific oceans. Excavation proceeded slowly until the end of 1899 when work ceased because of a number of engineering problems and the unhealthy working conditions.

In 1903, the United States signed a treaty with Colombia granting the United States rights for the construction, operation, and control of the Panama Canal. This treaty was later rejected by the Colombian Government. Following a revolt and secession of Panama from Colombia, the United States signed a treaty with Panama in 1903 for control of the Canal Zone in perpetuity.

Engineers studying the canal project developed two schemes: (a) a canal with locks estimated to cost \$147,000,000 and requiring 8 years to build; and (b) a sea level canal costing \$250,000,000 and requiring 12–15 years to build. Congress chose the high level lock canal, and construction was started in 1907 and finished in 1914. The actual construction cost was \$380,000,000.

The canal is 51.2 miles from deep water to deep water and required a total excavation of 413,900,000 cubic yards of which 168,300,000 cubic yards came from the Gaillard cut shown in Fig. 1.14. The minimum width of the canal was originally 300 ft (through the Gaillard cut) and it was later widened to approximately 500 ft. The minimum depth of the canal is 37 ft (in Balboa Harbor at low tide).

Many shear slides occurred during construction, especially in the Cucaracha formation, a notoriously soft shale. (The slides contributed to the high construction cost.) The canal was opened to traffic in August 1914; however, landslides closed the canal on several occasions for periods of a few days to 7 months. The last closure was in 1931, although constrictions have occurred on several occasions since then. Removal of soil from slides and erosion now requires continuous maintenance by

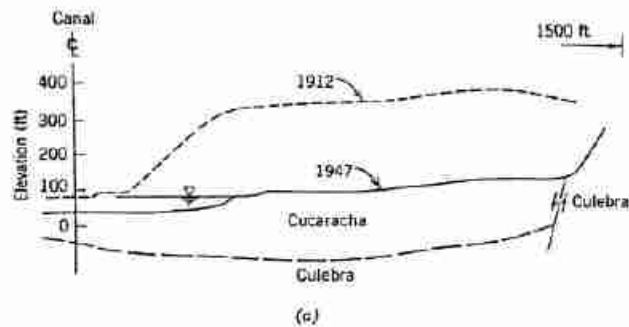


Fig. 1.14 The Panama Canal. (a) Cross section through East Culebra Slide. (b) Cucaracha Slide of August 1913. (c) Ship in Canal in 1965.

canal dredges. At one location the side slopes are even today moving into the canal at the rate of 28 ft per year.

The long-term strength characteristics of soft shales, such as those lining parts of the Panama Canal, are a perplexing problem to the soil engineer. Since the slides along the canal appear to be related to cracks in the rocks and special geologic features, the analysis of slopes in these materials cannot be done solely on the basis of theoretical considerations and laboratory test results. The solution of this type of problem depends very much on an understanding of geology, and illustrates the importance geology can have to the successful practice of civil engineering.

1.4 UNDERGROUND AND EARTH RETAINING STRUCTURES

Any structure built below ground surface has forces applied to it by the soil in contact with the structure. The design and construction of underground (subterranean) and earth retaining structures constitute an important phase of civil engineering. The preceding pages have already presented examples of such structures; they include the pipe shells that were driven for the foundation shown in Fig. 1.2, the basement walls of the buildings shown in Figs. 1.4 and 1.5, the concrete sheet pile wall

encircling the island shown in Fig. 1.9, and the bracing for the excavation shown in Fig. 1.12b. Other common examples of underground structures include tunnels for railways or vehicles, underground buildings like powerhouses, drainage structures, earth retaining structures, and pipelines.

The determination of forces exerted on an underground structure by the surrounding soil cannot be correctly made either from a consideration of the structure alone or from a consideration of the surrounding soil alone, since the behavior of one depends on the behavior of the other. The civil engineer therefore must be knowledgeable in *soil-structure interaction* to design properly structures subjected to soil loadings.

Example of Earth Retaining Structure

A common type of earth retaining structure is the *anchored bulkhead*, as illustrated in Fig. 1.15. Unlike a *gravity retaining wall*, which has a large base in contact with the foundation soil and enough mass for friction between the soil and the wall base to prevent excessive lateral movement of the wall, the anchored bulkhead receives its lateral support from penetration into the foundation soil and from an anchoring system near the top of the wall.

The bulkhead shown in Fig. 1.15 was built as part of a

ship-loading dock. Ships are brought alongside the bulkhead and are loaded with cargo stored on the land side of the wall. The loading is done by a crane moving on rails parallel to the bulkhead.

To determine the proper cross section and length of the bulkhead wall, the engineer must compute the stresses exerted by the soil against the wall (*lateral soil stresses*). The distribution of these stresses along the wall depends very much on the lateral movements that occur in the soil adjacent to the wall, and these strains in turn depend on the rigidity of the wall—a problem in soil-structure interaction.

The selection of the length and section of the bulkhead and the design of the anchoring system was only part of the problem. Consideration had to be given to the stability of the entire system against a shear rupture in which the slip surface passed through the backfill and through the soil below the tip of the bulkhead. This type of overall stability can be a much more serious problem with anchored bulkheads than is the actual design of the bulkhead itself.

The following questions had to be answered in planning the design of the anchored bulkhead.

1. What type of wall (material and cross section) should be used?
2. How deep must the wall penetrate the foundation soil in order to prevent the wall from kicking out to the left at its base?

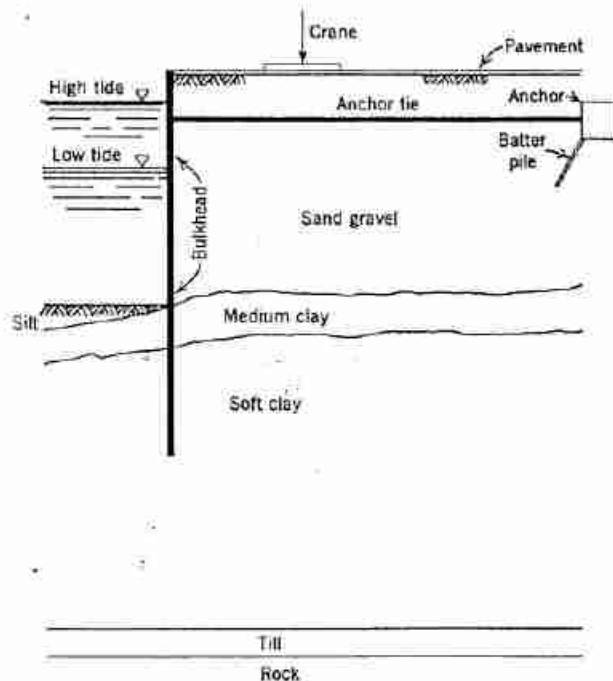


Fig. 1.15 Anchored bulkhead.

3. At what height on the wall should the anchor tie be located?
4. How far from the wall should the anchor tie extend?
5. What type of anchoring system should be employed at the onshore end of the anchor tie? (One way to anchor the wall is to use a large mass of concrete, i.e., *deadman*. Another way is to use a system of piles including some driven at a slope with the vertical; such a sloping pile is termed a *batter pile*.)
6. What was the distribution of stresses acting on the wall?
7. What type of drainage system should be installed to prevent a large differential water pressure from developing on the inside of the wall?
8. How close to the wall should the loaded crane (130,000 lb when fully loaded) be permitted?
9. What restrictions, if any, are necessary on the storage of cargo on the area back of the wall?

Example of Buried Pipeline

Frequently a pipe must be buried under a high embankment, railway, or roadway. The rapid growth of the pipeline industry and the construction of superhighways have greatly increased the frequency of buried pipe installations. Buried pipes are usually thin-wall metal or plastic pipes, called *flexible pipes*, or thick-wall reinforced concrete pipes, called *rigid pipes*.

There have been very few recorded cases of buried pipes being crushed by externally applied loads. Most of the failures that have occurred have been associated with: (a) faulty construction; (b) construction loads in excess of design loads; and (c) pipe sag due to foundation settlement or failure. Faced with the impressive performance record of the many thousands of buried pipes, we are forced to conclude that the design and construction procedures commonly used result in safe installations. There is little published information, however, indicating just how safe these installations are and whether or not they are far overdesigned, thus resulting in a great waste of money.

Figure 1.16 shows an installation of two steel pipes, each 30 in. in diameter with a wall thickness of $\frac{3}{4}$ in., buried under an embankment 80 ft high at its center line. Use of the commonly employed analytical method yielded a value for the maximum pipe deflection of 7½ in. Current practice suggests a value of 5% of the pipe diameter, 1½ in. for the 30-in. diameter pipe, as the maximum allowable safe deflection.

At this stage in the job, laboratory soil tests and field experimentation with installations were carried out. Use of the soil data obtained from these tests resulted in a computed pipe deflection of 0.32 in., a safe value. The maximum value of pipe deflection actually measured in the installation was only 0.17 in. These stated deflections indicate the merit of a controlled installation (and also

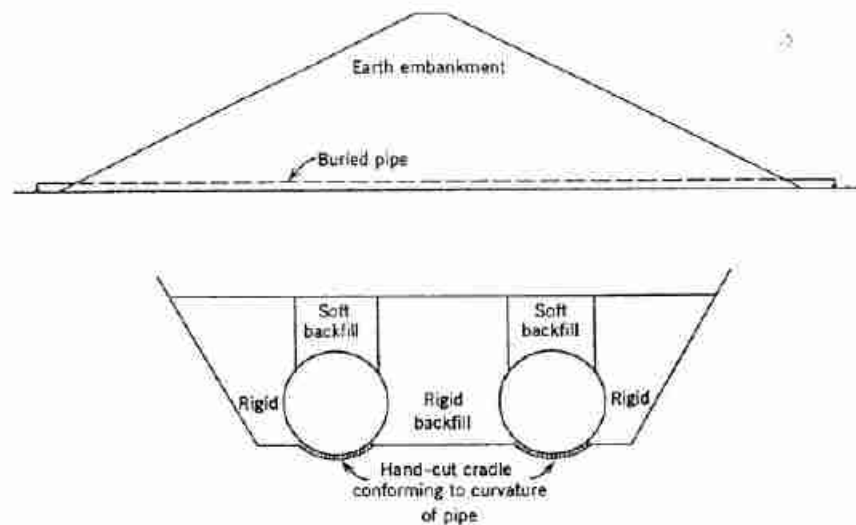


Fig. 1.16 Buried pipes.

the inaccuracy of commonly employed techniques to estimate the deflection of buried pipes).

The method of pipe installation employed is indicated in Fig. 1.16 and consisted of the following: carrying the fill elevation above the elevation of the tops of the pipes; cutting a trench for the pipes; shaping by hand a cradle for each pipe conforming to the curvature of the pipe; backfilling under carefully controlled conditions to get a rigid backfill on the sides of the pipes and a soft spot on top of each pipe.

The rigid side fills were to give strong lateral support to the pipes and thus reduce their lateral expansion. The soft spots were to encourage the fill directly over the pipes to tend to settle more than the rest of the fill, thus throwing some of the vertical load to the soil outside the zone of the pipes; this phenomenon is called *arching*.

Since the vertical load on the two pipes is related to the height of the fill, one would expect the settlement of the pipes to be the maximum at the midpoint of the embankment. Such was the case with 17 cm of settlement occurring at the center of the embankment and about 1 cm at the two toes of the embankment. The flexible steel pipes, more than 100 m in length, could easily withstand the 16 cm sag.

The civil engineer on this project had to select the thickness of the pipe wall, and work out and supervise the installation of the pipes.

1.5 SPECIAL SOIL ENGINEERING PROBLEMS

The preceding sections have discussed and illustrated some common civil engineering problems that involve soil mechanics. There are, in addition, many other types of soil problems that are less common but still important.

Some of these are noted in this section in order to give a more complete picture of the range of problems in which soil mechanics is useful.

Vibrations

Certain granular soils can be readily densified by vibrations. Buildings resting on such soils may undergo significant settlement due to the vibration of their equipment, such as large compressors and turbines. The effects of a vibration can be particularly severe when the frequency of the vibration coincides with the natural frequency of the soil foundation. Upon deciding that vibrations can cause deleterious settlement in a particular structure, the engineer has the choice of several means of preventing it. He can increase the mass of the foundation, thus changing its frequency, or densify or inject the soil, thereby altering its natural frequency and/or compressibility.

Explosions and Earthquakes

Civil engineers have long been concerned with the effects on buildings of earth waves caused by quarry blasting and other blasting for construction purposes. The ground through which such waves pass has been found to influence greatly the vibrations that reach nearby buildings.

This problem has received an entirely new dimension as the result of the advent of nuclear explosives. The military has become increasingly interested in the design of underground facilities that can survive a very nearby nuclear explosion. The Atomic Energy Commission has established the Plowshare program to consider the peaceful uses of nuclear explosions, such as the excavation of canals or highway cuts. The possibility of excavating a sea level Panama Canal by such means has received



Fig. 1.17 Oil storage reservoir (compliments of the Creole Petroleum Corporation).

special attention and raises a whole new set of questions, such as the stability of slopes formed by a cratering process.

Similar problems arise as the result of earthquakes. The type of soil on which a building rests and the type of foundation used for the building influence the damage to a building by an earthquake. The possible effects of earthquakes on large dams have recently received much attention. The 1964 earthquake in Alaska caused one of the largest earth slides ever recorded.

The Storage of Industrial Fluids in Earth Reservoirs

Section 1.2 describes an earth structure for the retention of water. Because earth is such a common and cheap construction material, it has considerable utility for the construction of reservoirs and containers to store industrial fluids. One of the most successful applications of this technique is the earth reservoir for the storage of fuel oil shown in Fig. 1.17. This structure, with a capacity of 11,000,000 barrels, was built at one-tenth the cost of conventional steel tankage and resulted in a saving of approximately \$20,000,000. Because of the interfacial tension between water and certain industrial fluids, compacted, fine-grained, wet soil can be used to store such fluids with no leakage.

Another example of this special application is the use of reservoirs for the storage of refrigerated liquefied gas. Earth reservoirs have been built for the retention of liquefied propane at -44°F and for liquefied natural gas at -260°F . Introducing a liquid at such low temperatures into a water-wet soil freezes the pore water in the soil. If the soil has enough water so that there are not continuous air channels in the soil, it will become impervious to both liquid and gas upon freezing of the pore water.

Frost

Because certain soils under certain conditions expand on freezing, the engineer may be faced with *frost heave* problems. When *frost susceptible* soils are in contact with moisture and subjected to freezing temperatures, they can

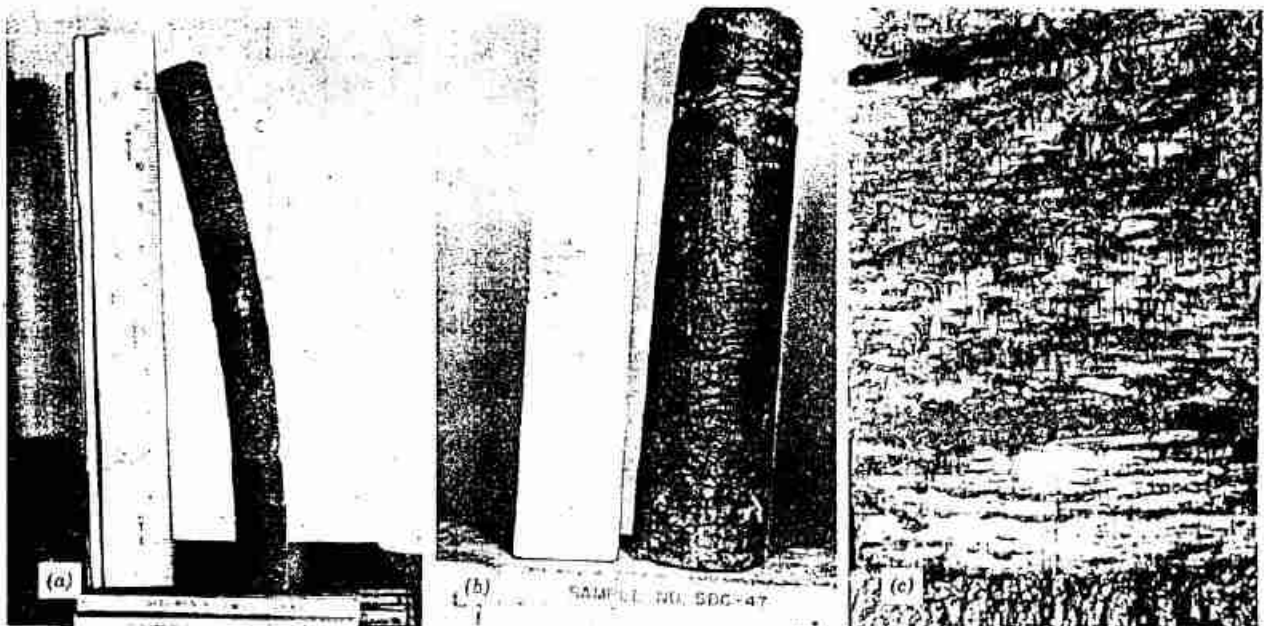


Fig. 1.18 Frost heave. (a) Soil sample which heaved from 3.1 to 12.6 in. on freezing. (b) Soil sample which heaved from 6 to 12 in. on freezing. (c) A close view of frozen soil. (Photographs compliments of C. W. Kaplar of U.S. Army CRREL.)

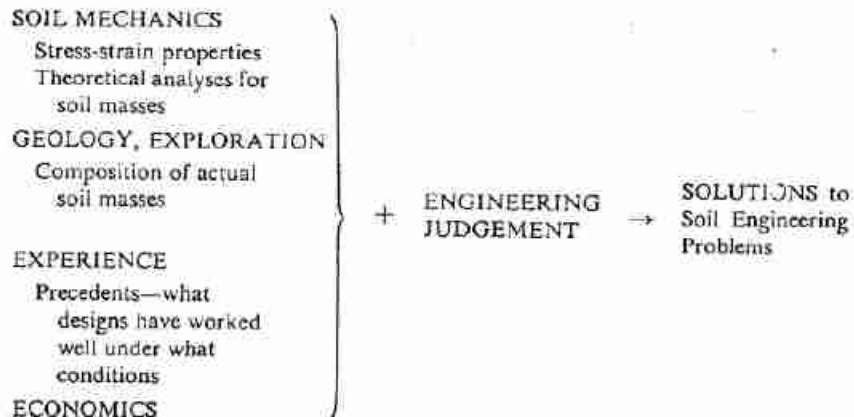


Fig. 1.19 The solution of soil engineering problems.

imbibe water and undergo a very large expansion. Figure 1.18 dramatically illustrates the magnitude a soil can heave under ideal conditions. Such heave exerts forces large enough to move and crack adjacent structures, and can cause serious problems on thawing because of the excess moisture. The thawing of frozen soil usually proceeds from the top downward. The melt water cannot drain into the frozen subsoil, thus becomes trapped, greatly weakening the soil. The movement of icehouses and ice-skating rinks is an interesting example of this phenomenon, but nowhere nearly as important and widespread as the damage to highway pavements in those areas of the world that have freezing temperatures. Frost heaves and potholes, which develop when the frost thaws, are sources of great inconvenience and cost to many northern U.S. areas, such as New England.

The civil engineer designing highway and airfield pavements in frost areas must either select a combination of base soil and drainage that precludes frost heave, or design his pavement to withstand the weak soil that occurs in the spring when the frost melts.

Regional Subsidence

Large-scale pumping of oil and water from the ground can cause major settlements over a large area. For example, a 16 square mile area of Long Beach, California, has settled as the result of oil pumping, with a maximum settlement to date of 25 ft. As a result, the Naval Shipyard adjacent to the settled area has had to construct special sea walls to keep out the ocean, and has had to reconstruct dry docks. Mexico City has settled as much as 30 ft since the beginning of the twentieth century as the result of pumping water for domestic and industrial use. The first step in minimizing such regional subsidence is to locate the earth materials that are compressing as the fluid is removed, and then consider methods of replacing the lost fluid.

1.6 THE SOLUTION OF SOIL ENGINEERING PROBLEMS

Thus far this chapter has described some of the problems the civil engineer encounters with construction on soil, in soil, and of soil. The successful solution of each problem nearly always involves a combination of soil mechanics and one or more of the components noted in Fig. 1.19.

Geology aids the soil engineer because the method of forming a mass influences its size, shape, and behavior. Exploration helps establish the boundaries of a deposit and enables the engineer to select samples for laboratory testing.

Experience, as the term is used here, does not mean merely *doing* but the *doing* coupled with an *evaluation* of results of the act. Thus, when the civil engineer makes a design or solves a soil problem and then evaluates the outcome on the basis of measured field performance, he is gaining experience. Too much emphasis is usually placed on the *doing* component of experience and too little emphasis on the *evaluation* of the outcome of the act. The competent soil engineer must continue to improve his reservoir of experience by comparing the predicted behavior of a structure with its measured performance.

Economics is an important ingredient in the selection of the *best* solution from among the possible ones. Although a detailed economic evaluation of a particular earth structure depends on the unit costs at the site of a planned project, certain economic advantages of one scheme over another may be obvious from the characteristics of the schemes.

This book is limited to one component of the solution of soil engineering problems—*soil mechanics*: the science underlying the solution of the problem. The reader must remember that science alone cannot solve these problems.

Nearly all soil problems are statically indeterminate to a high degree. Even more important is the fact that natural soil deposits possess five complicating characteristics:

1. Soil does not possess a linear or unique stress-strain relationship.
2. Soil behavior depends on pressure, time, and environment.
3. The soil at essentially every location is different.
4. In nearly all cases the mass of soil involved is underground and cannot be seen in its entirety but must be evaluated on the basis of small samples obtained from isolated locations.
5. Most soils are very sensitive to disturbance from sampling, and thus the behavior measured by a laboratory test may be unlike that of the *in situ* soil.

These factors combine to make nearly every soil problem unique and, for all practical purposes, impossible of an exact solution.

Soil mechanics can provide a solution to a mathematical model. Because of the nature and the variability of soil and because of unknown boundary conditions, the mathematical model may not represent closely the actual problem. As construction proceeds and more information becomes available, soil properties and boundary

conditions must often be re-evaluated and the problem solution modified accordingly.

The interpretation of insufficient and conflicting data, the selection of soil parameters, the modification of a solution, etc., require experience and a high degree of intuition—i.e., *engineering judgment*. While a sound knowledge of soil mechanics is essential for the successful soil engineer, *engineering judgment* is usually the characteristic that distinguishes the outstanding soil engineer.

PROBLEMS

1.1 List three events of national and/or international importance that involve soil mechanics (e.g., the extensive damage from the 1964 Alaskan earthquake).

1.2 Note the type of foundation employed in a building constructed recently in your area. List obvious reasons why this type of foundation was selected.

1.3 On the basis of your personal experience, describe briefly an engineering project that was significantly influenced by the nature of the soil encountered at the site of the project.

1.4 Note several subsoil and building characteristics that would make a pile foundation preferable to a spread foundation.

1.5 List difficulties you would expect to result from the large settlement of the Palacio de las Bellas Artes shown in Fig. 1.3.

1.6 Note desirable and undesirable features of building flotation.

CHAPTER 2

A Preview of Soil Behavior

This chapter presents a preliminary and intuitive glimpse of the behavior of homogeneous soil. This preview is intended to give the reader a general picture of the way in which the behavior of soil differs from the behavior of other materials which he has already studied in solid and fluid mechanics, and also to indicate the basis for the organization of this book. To present clearly the broad picture of soil behavior, this chapter leaves to later chapters a consideration of exceptions to, and details of, this picture.

2.1 THE PARTICULATE NATURE OF SOIL

If we examine a handful of beach sand the naked eye notices that the sand is composed of discrete particles. The same can be said of all soils, although many soil particles are so small that the most refined microscopic techniques are needed to discern the particles. The discrete particles that make up soil are not strongly bonded together in the way that the crystals of a metal are, and hence the soil particles are relatively free to move with respect to one another. The soil particles are solid and cannot move relative to each other as easily as the elements in a fluid. Thus soil is inherently a *particulate system*.¹ It is this basic fact that distinguishes soil mechanics from solid mechanics and fluid mechanics. Indeed, the science that treats the stress-strain behavior of soil may well be thought of as *particulate mechanics*.

The next sections examine the consequences of the particulate nature of soil.

2.2 NATURE OF SOIL DEFORMATION

Figure 2.1 shows a cross section through a box filled with dry soil, together with a piston through which a vertical load can be applied to the soil. By enlarging a portion of this cross section to see the individual particles,

¹ The word "particulate" means "of or pertaining to a system of particles."

we are able to envision the manner in which the applied force is transmitted through the soil: contact forces develop between adjacent particles. For convenience, these contact forces have been resolved into components normal N and tangential T to the contact surfaces.

The individual particles, of course, deform as the result of these contact forces. The most usual type of deformation is an elastic or plastic strain in the immediate vicinity of the contact points. Particle crushing can be important in certain situations (as later chapters discuss). These deformations lead to an enlargement of the contact area between the particles, as shown in Fig. 2.2a, and thus permit the centers of the particles to come closer together. If platelike particles are present, these particles will bend,

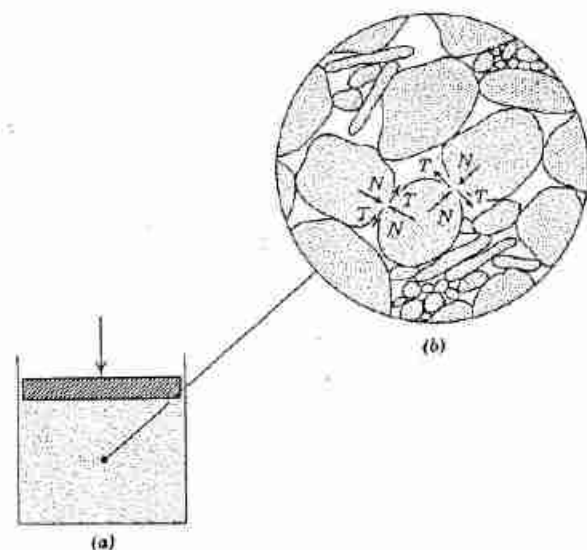


Fig. 2.1 Schematic representation of force transmission through soil. (a) Cross section through box filled with soil. (b) Enlargement through portion of cross section showing forces at two of the contact points.

as in Fig. 2.2*b*, thus allowing relative movements between the adjacent particles. In addition, once the shear force at a contact becomes larger than the shear resistance at the contact, there will be relative sliding between the particles (Fig. 2.2*c*). The overall strain of a soil mass will be partly the result of deformation of individual particles and partly the result of relative sliding between particles. However, experience has shown that interparticle sliding, with the resultant rearrangement of the particles, generally makes by far the most important contribution to overall strain. The *mineral skeleton* of soil usually is quite deformable, due to interparticle sliding and rearrangement, even though the individual particles are very rigid.

Thus we see the first consequence of the particulate nature of soil: *the deformation of a mass of soil is controlled by interactions between individual particles, especially by sliding between particles.* Because sliding is a nonlinear and irreversible deformation, we must expect that the stress-strain behavior of soil will be strongly nonlinear and irreversible.² Moreover, a study of phenomena at the contact points will be fundamental to the study of soils, and we shall inevitably be concerned with concepts such as friction and adhesion between particles.

There are, of course, a fantastically large number of individual contact points within a soil mass. For example, there will be on the order of 5 million contacts within just 1 cm³ of a fine sand. Hence it is impossible to build up a stress-strain law for soil by considering the behavior at each contact in turn even if we could describe exactly what happens at each contact. Rather it is necessary to rely upon the direct experimental measurement of the properties of a system involving a large number of particles. Nonetheless, study of the behavior at typical contact points still plays an important role; it serves as a guide to the understanding and interpretation of the direct experimental measurements. This situation may be likened to the study of metals: knowledge of the behavior of a single crystal, and the interactions between crystals, guides understanding the behavior of the overall metal and how the properties of the metal may be improved.

If the box in Fig. 2.1 has rigid side walls, the soil will normally decrease in volume as the load is increased. This volume decrease comes about because individual particles nestle closer and closer together. There are shear failures (sliding) at the many individual contact points, but there is no overall shear failure of the soil mass. The vertical load can be increased without limit. Such a process is volumetric *compression*. If the applied load is removed, the soil mass will increase in volume through a reverse process again involving rearrangement of the particles. This process of volume increase is called *expansion*, or in some contexts, *swell*.

² This statement means that a plot of stress-strain is not a straight line and is not unique for load-unload cycles.

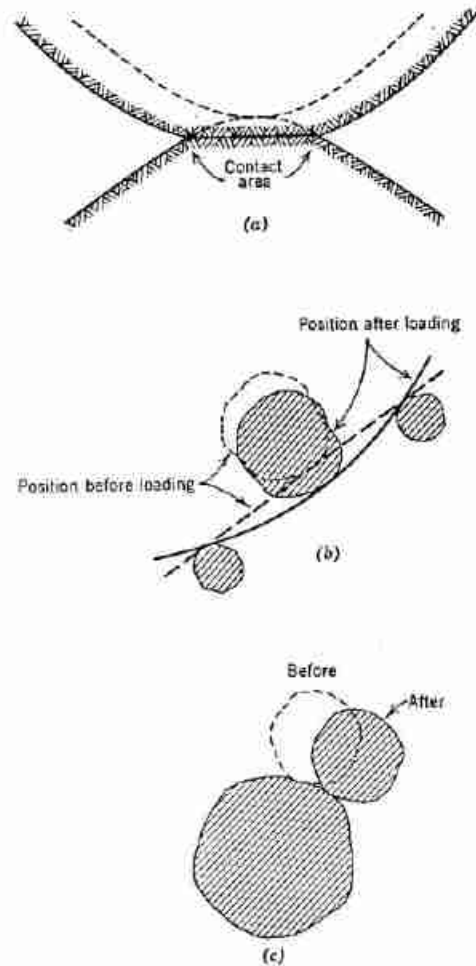


Fig. 2.2 Causes of relative motions among soil particles. (a) Motion of particles due to deformation of contacts. Solid lines show surfaces of particles after loading (the lower particle was assumed not to move); dashed lines show surfaces before loading. (b) Relative motion of particles due to bending of platelike particles. (c) Relative motion of particles due to interparticle sliding.

If, on the other hand, the box has flexible side walls, an overall shear failure can take place. The vertical load at which this failure occurs is related to the *shear strength* of the soil. This shear strength is determined by the resistance to sliding between particles that are trying to move laterally past each other.

The properties of compressibility, expansibility, and shear strength will be studied in detail in later chapters.

2.3 ROLE OF PORE PHASE: CHEMICAL INTERACTION

The spaces among the soil particles are called *pore spaces*. These pore spaces are usually filled with air

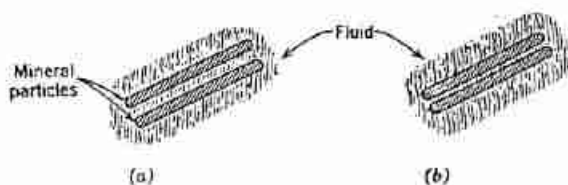


Fig. 2.3 Fluid films surrounding very small soil particles. (a) Before load. (b) Particles squeezed close together by load.

and/or water (with or without dissolved materials). Thus soil is inherently a *multiphase system* consisting of a mineral phase, called the *mineral skeleton*, plus a fluid phase, called the *pore fluid*.

The nature of the pore fluid will influence the magnitude of the shear resistance existing between two particles by introducing chemical matter to the surface of contact. Indeed, in the case of very tiny soil particles, the pore fluid may completely intrude between the particles (see Fig. 2.3). Although these particles are no longer in contact in the usual sense, they still remain in close proximity and can transmit normal and possibly also tangential forces. The spacing of these particles will increase or decrease as the transmitted compressive forces decrease or increase. Hence a new source of overall strain in the soil mass is introduced.

Thus we have a second consequence of the particulate nature of soil: *soil is inherently multiphase, and the constituents of the pore phase will influence the nature of the mineral surfaces and hence affect the processes of force transmission at the particle contacts*. This interaction between the phases is called *chemical interaction*.

2.4 ROLE OF PORE PHASE: PHYSICAL INTERACTION

Let us now return to our box of soil, but now consider a soil whose pore spaces are completely filled with water—a *saturated soil*.

First we assume that the water pressure is hydrostatic; i.e., the pressure in the pore water at any point equals the unit weight of water times the depth of the point below the water surface. For such a condition there will be no flow of water (see Fig. 2.4a).

Next we suppose that the water pressure at the base of the box is increased while the overflows hold the level of the water surface constant (Fig. 2.4b). Now there must be an upward flow of water. The amount of water that flows will be related to the amount of excess pressure added to the bottom and to a soil property called *permeability*. The more *permeable* a soil, the more water will flow for a given excess of pressure. Later parts of this book consider the factors that determine the permeability of a soil.

If the excess water pressure at the base is increased, a pressure will be reached where the sand is made to boil by the upward flowing water (Fig. 2.4c). We say that a *quick condition* is created. Obviously, there has been a *physical interaction* between the mineral skeleton and the pore fluid.

At this stage, the soil will occupy a somewhat greater volume than initially, and clearly the soil has less shear strength in the quick condition than in the normal condition. These changes have occurred even though the total weights of sand and water pressing down have remained unchanged. But we have seen that changes in volume and shear strength come about through changes in the forces at contacts between particles. Hence these contact forces must have been altered by the changes in pressure in the pore phase; that is, these contact forces must be related

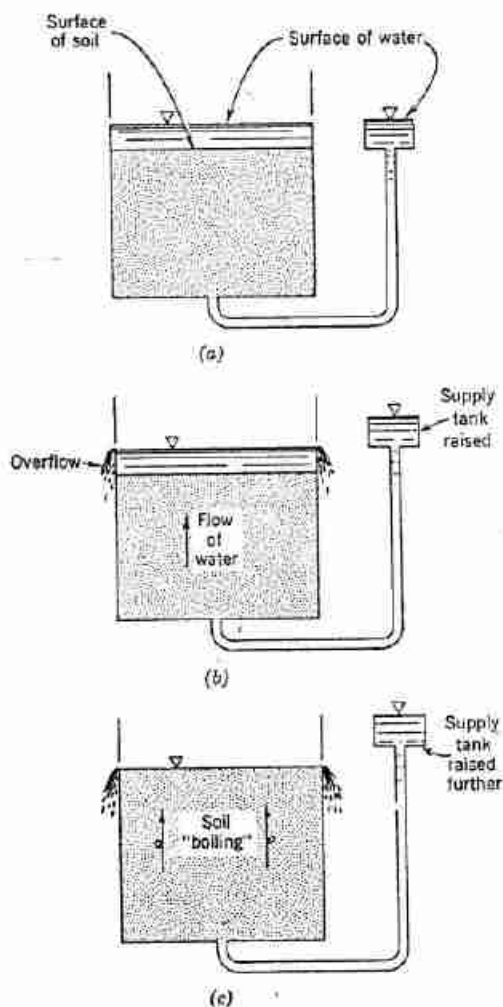


Fig. 2.4 Physical interaction between mineral and pore phases. (a) Hydrostatic condition: no flow. (b) Small flow of water. (c) Quick condition.

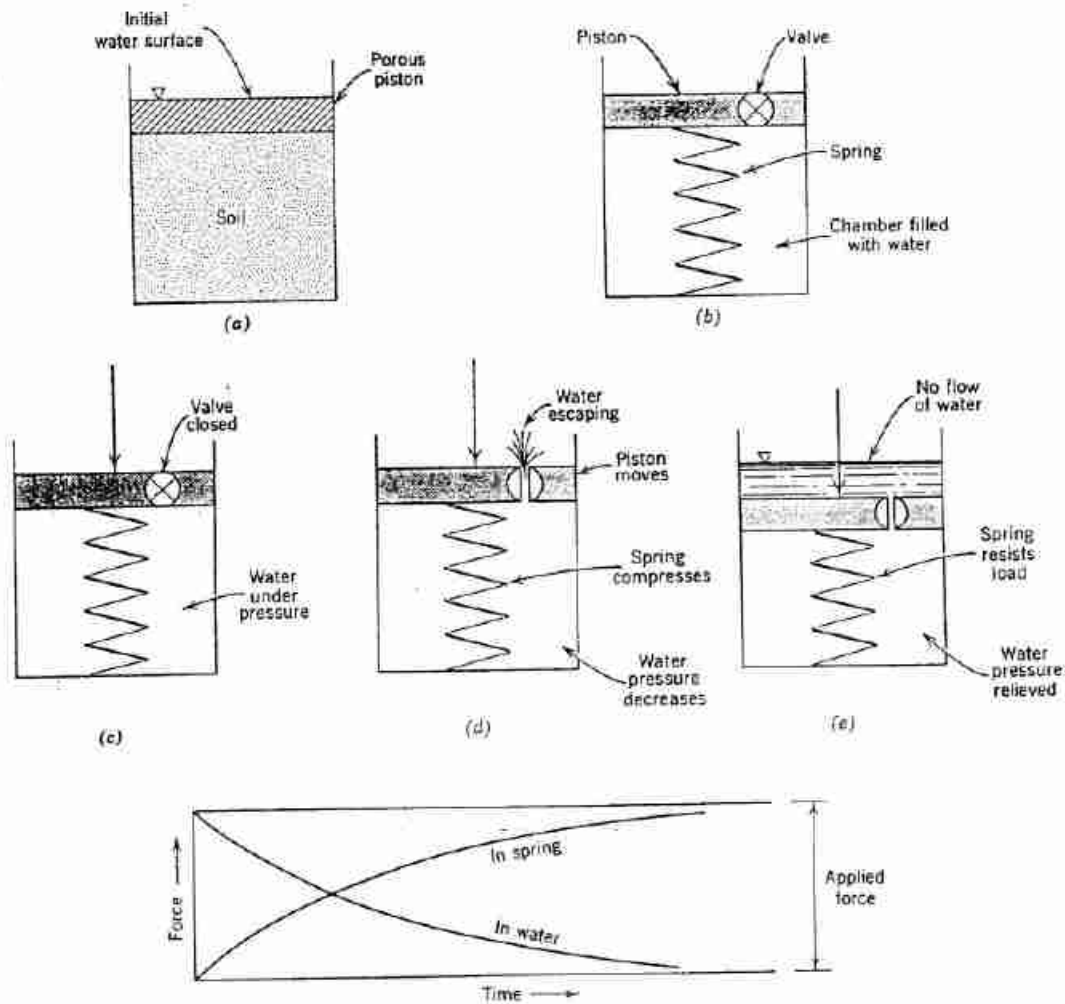


Fig. 2.5 Hydromechanical analogy for load-sharing and consolidation. (a) Physical example. (b) Hydromechanical analog; initial condition. (c) Load applied with valve closed. (d) Piston moves as water escapes. (e) Equilibrium with no further flow. (f) Gradual transfer of load.

to the difference between the stress pressing downward (the *total stress*) and the *pore pressure*. These observations form the basis for the very important concept of *effective stress*.

We have now seen the third consequence of the particulate nature of soil: *water can flow through soil and thus interact with the mineral skeleton, altering the magnitude of the forces at the contacts between particles and influencing the compression and shear resistance of the soil.*

2.5 ROLE OF PORE PHASE: SHARING THE LOAD

Finally, because soil is a multiphase system, it may be expected that a load applied to a soil mass would be carried in part by the mineral skeleton and in part by

the pore fluid. This "sharing of the load" is analogous to partial pressures in gases.

The sketches in Fig. 2.5 help us to understand load sharing. Figure 2.5a shows a cylinder of saturated soil. The porous piston permits load to be applied to the soil and yet permits escape of the fluid from the pores of the soil. Part (b) shows a hydromechanical analog in which the properties of the soil have been "lumped": the resistance of the mineral skeleton to compression is represented by a spring; the resistance to the flow of water through the soil is represented by a valve in an otherwise impermeable piston.

Now suppose a load is applied to the piston of the hydromechanical analog but that the valve is kept closed. The piston load is apportioned by the water and the spring in relation to the stiffness of each. The piston in our

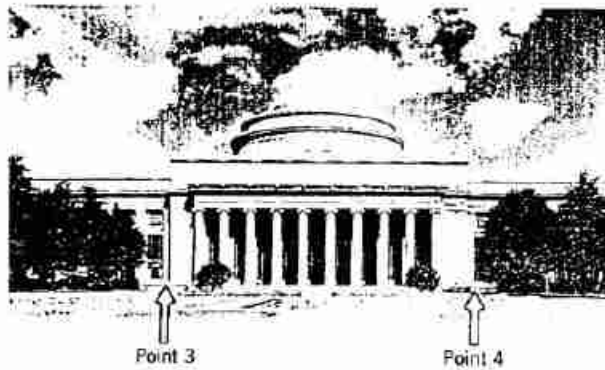
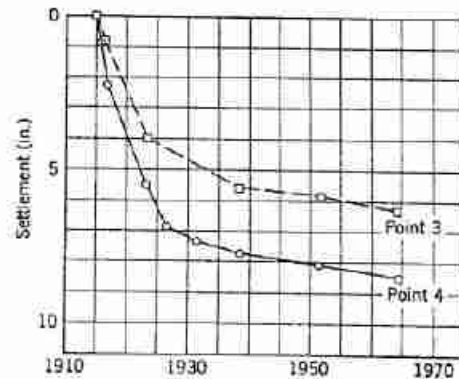


Fig. 2.6 Settlement of Building 10 at M.I.T.



hydromechanical analogy will move very little when the load is applied because the water is relatively incompressible. Since the spring only shortens slightly it will carry very little of the load. Essentially all of the applied load is resisted by an increase in the fluid pressure within the chamber. The conditions at this stage are represented in Fig. 2.5c.

Next we open the valve. The fluid pressure within the chamber will force water through this valve (Fig. 2.5d). As water escapes the spring shortens and begins to carry a significant fraction of the applied load. There must be a corresponding decrease in the pressure within the chamber fluid. Eventually a condition is reached (Fig. 2.5e) in which all of the applied load is carried by the spring and the pressure in the water has returned to the original hydrostatic condition. Once this stage is reached there is no further flow of water.

Only a limited amount of water can flow out through the valve during any interval of time. Hence the process of transferring load from the water to the spring must take place gradually. This gradual change in the way that the load is shared is illustrated in Fig. 2.5f.

Sharing the load between the mineral and pore phases also occurs in the physical example and in actual soil problems, although the pore fluid will not always carry all of the applied load initially. We shall return to this subject in detail in Chapter 26. Moreover, in actual problems there will be the same process of a gradual change in the way that the load is shared. This process of gradual squeezing out of water is called *consolidation*, and the time interval involved is the *hydrodynamic time lag*. The amount of compression that has occurred at any time is related not only to the applied load but also to the amount of stress transmitted at the particle contacts, i.e., to the difference between the applied stress and the pore pressure. This difference is called *effective stress*. Consolidation and the reverse process of swelling (which occurs when water is sucked into a soil following load removal) are treated in several chapters.

Here then is the fourth consequence of the particulate nature of soil: *when the load applied to a soil is suddenly changed, this change is carried jointly by the pore fluid and by the mineral skeleton. The change in pore pressure will cause water to move through the soil, hence the properties of the soil will change with time.*

This last consequence was discovered by Karl Terzaghi around 1920. This discovery marked the beginning of modern soil engineering. It was the first of many contributions by Terzaghi, who is truly the "father of soil mechanics."

The most important effect of the hydrodynamic time lag is to cause delayed settlement of structures. That is, the settlement continues for many years after the structure has been completed. Figure 2.6 shows the time-settlement record of two points on Building 10 on the campus of the Massachusetts Institute of Technology. The settlement of this building during the first decade after its completion was the cause of considerable alarm. Terzaghi examined the building when he first came to the United States in 1925, and he correctly predicted that the rate of settlement would decrease with time.

A further look at consolidation. At this stage it is essential that the student have a general appreciation of the duration of the hydrodynamic time lag in various typical soil deposits. For this purpose it is useful to make an intuitive analysis of the consolidation process to learn which soil properties affect the time lag and how they affect it. (Chapter 27 presents a precise derivation and solution for the consolidation process.)

The time required for the consolidation process should be related to two factors:

1. The time should be directly proportional to the volume of water which must be squeezed out of the soil. This volume of water must in turn be related to the product of the stress change, the compressibility of the mineral skeleton, and the volume of the soil.
2. The time should be inversely proportional to how

fast the water can flow through the soil. From fluid mechanics we know that velocity of flow is related to the product of the permeability and the hydraulic gradient, and that the gradient is proportional to the fluid pressure lost within the soil divided by the distance through which the pore fluid must flow.

These considerations can be expressed by the relation

$$t \sim \frac{(\Delta\sigma)(m)(H)}{(k)(\Delta\sigma/H)} \quad (2.1)$$

where

- t = the time required to complete some percentage of the consolidation process
- $\Delta\sigma$ = the change in the applied stress
- m = the compressibility of the mineral skeleton
- H = the thickness of the soil mass (per drainage surface)
- k = the permeability of the soil

Hence the time required to reach a specified stage in the consolidation process is

$$t \sim \frac{mH^2}{k} \quad (2.2)$$

This relation tells us that the consolidation time:

1. Increases with increasing compressibility.
2. Decreases with increasing permeability.
3. Increases rapidly with increasing size of soil mass.
4. Is independent of the magnitude of the stress change.

The application of this relation is illustrated by Examples 2.1 and 2.2.

► **Example 2.1**

A stratum of sand and a stratum of clay are each 10 ft thick. The compressibility of the sand is $\frac{1}{5}$ the compressibility of the clay and the permeability of the sand is 10,000 times that of the clay. What is the ratio of the consolidation time for the clay to the consolidation time of the sand?

Solution.

$$\frac{t_{\text{clay}}}{t_{\text{sand}}} = \frac{1}{1/5} \frac{10,000}{1} = 50,000$$

► **Example 2.2**

A stratum of clay 10 ft thick will be 90% consolidated in 10 years. How much time will be required to achieve 90% consolidation in a 40-ft-thick stratum of this same clay?

Solution.

$$t \text{ for 40 foot stratum} = 10 \text{ years} \times \frac{40^2}{10^2} = 160 \text{ years}$$

Soils with a significant clay content will require long times for consolidation—from one year to many hundreds of years. Coarse granular soils, on the other hand, will consolidate very quickly, usually in a matter of minutes. As we shall see, this difference in consolidation time is one of the main distinctions among different soils.

2.6 ORGANIZATION OF BOOK

This chapter has described the important consequences of soil being particulate and hence multiphase. As shown in Table 2.1, these consequences are used as the basis for organizing this book.

Part II will study individual particles, the way that they are put together, and the chemical interaction between

Table 2.1 Soil Is a Different Type of Material because It Is Particulate, and Hence Multiphase

Consequence	Example of Importance	Discussed in Part	Concepts Needed from Previous Studies
Stress-strain behavior of mineral skeleton determined by interactions between discrete particles	Great compressibility of soil Strength is frictional in nature, and related to density	II, III	Stress and strain; continuity; limiting equilibrium; Mohr circle
There are chemical interactions between pore fluid and mineral particles	Affects density (and hence strength) which soil will attain under given stress Quick clays	III	Principles of chemical bonding
There are physical interactions between pore fluid and mineral skeleton	Quicksands Slope instabilities affected by ground water	IV	Fluid mechanics: potential flow, laminar flow
Loads applied to soil masses are "shared" by mineral skeleton and pore phase	Consolidation time-lag Delayed failure of slopes	V	

these particles and the pore phase. Part III will study the processes of volume change and shear strength in situations where there is no physical interaction between the phases, i.e., in dry soils. Part IV will then analyze the consequences of the physical interaction between the phases in the cases where the flow of water is governed by natural ground water conditions. Part V will study the transient phenomena that occur after a change in load is applied to a soil.

PROBLEMS

2.1 Cite at least three passages from Chapter 1 that refer to

physical interaction between the mineral skeleton and pore phase.

2.2 Cite at least one passage from Chapter 1 that refers to the hydrodynamic time-lag or consolidation effect.

2.3 The time for a clay layer to achieve 99% consolidation is 10 years. What time would be required to achieve 99% consolidation if the layer were twice as thick, five times more permeable, and three times more compressible?

2.4 List the possible components of soil deformation.

2.5 Which component listed in the answer to Problem 2.4 would be most important in each of the following situations:

a. loading a loose array of steel balls;

b. loading an array of parallel plates;

c. unloading a dense sample of mica plates and quartz sand.

ARTHUR CASAGRANDE



Arthur Casagrande was born (August 28, 1902) and educated in Austria. He immigrated to the United States in 1926. There he accepted a research assistantship with the Bureau of Public Roads to work under Terzaghi at M.I.T. While at M.I.T. Professor Casagrande worked on soil classification, shear testing, and frost action in soils. In 1932 he initiated a program in soil mechanics at Harvard University.

Professor Casagrande's work on soil classification, seepage through earth structures and shear strength has had major influence on soil mechanics. Professor Casagrande has been a very active consultant and has participated in many important jobs throughout the world. His most important influence on soil mechanics, however, has been through his teaching at Harvard. Many of the leaders in soil mechanics were inspired while students of his at Harvard.

Professor Casagrande served as President of the International Society of Soil Mechanics and Foundation Engineering during the period 1961 through 1965. He has been the Rankine Lecturer of the Institution of Civil Engineers and the Terzaghi Lecturer of the American Society of Civil Engineers. He was the first recipient of the Karl Terzaghi Award from the ASCE.

PART II

The Nature of Soil

Part II, consisting of Chapters 3 to 7, examines the nature of soil. Chapter 3 considers an assemblage of soil particles. This chapter is placed at the start of Part II because the student must master the definitions and terms relating the phases in a soil mass before he proceeds with his study of soil mechanics. Chapter 4 looks closely at

the individual particles that make up a soil mass. Chapters 5 and 6 consider stress transmission between soil particles on a microscopic scale and the influence of water on these stresses. Part II closes with a treatment (Chapter 7) of the natural soil profile.

CHAPTER 3

Description of an Assemblage of Particles

This chapter considers the description of an assemblage of particles. It presents relationships among the different phases in the assemblage, and discusses particle size distribution and degree of plasticity of the assemblage. The phase relationships are used considerably in soil mechanics to compute stresses. The phase relationships, particle size characteristics, and Atterberg limits are employed to group soils and thus facilitate their study.

3.1 PHASE RELATIONSHIPS

By being a particulate system, an element of soil is inherently "multiphase." Figure 3.1 shows a typical element of soil containing three distinct phases: *solid* (mineral particles), *gas*, and *liquid* (usually water). Figure 3.1a represents the three phases as they would typically exist in an element of natural soil. In Part (b) the phases have been separated one from the others in order to facilitate the development of the phase relationships. The phases are dimensioned with volumes on the left and weights on the right side of the sketch.

Below the soil elements in Fig. 3.1 are given expressions that relate the various phases. There are three important relationships of volume: *porosity*, *void ratio*, and *degree of saturation*. *Porosity* is the ratio of void volume to total volume and *void ratio* is the ratio of void volume to solid volume. Porosity is usually multiplied by 100% and thus the values are given in percent. Void ratio is expressed in a decimal value, such as a void ratio of 0.55, and can run to values greater than unity. Both porosity and void ratio indicate the relative portion of void volume in a soil sample. This void volume is filled with fluid, either gas or liquid, usually water. Although both terms are employed in soil mechanics, void ratio is the more useful¹

¹ During a typical compression of a soil element, both the numerator and the denominator of the porosity decrease, whereas only the numerator of the void ratio decreases. This fact results in void ratio being more useful than porosity for studying soil compression.

of the two. Two relationships between porosity n and void ratio e are

$$n = \frac{e}{1 + e} \quad \text{and} \quad e = \frac{n}{1 - n}$$

The degree of saturation indicates the percentage of the void volume which is filled with water. Thus a value of $S = 0$ indicates a dry soil, $S = 100\%$ indicates a saturated soil, and a value between 0 and 100% indicates a partially saturated soil.

The most useful relationship between phase weights is *water content*, which is the weight of water divided by the weight of solid in a soil element. The water content of a soil sample is readily obtained by: weighing the natural soil; drying it in an oven; weighing the dry soil; and, finally, computing the water content as the difference in initial and dry weights divided by the dry weight. This procedure assumes that all of the volatiles are water, an acceptable assumption except when working with organic soils or soils containing additives such as asphalt. For a saturated soil the water content and void ratio are uniquely related, as one can see by examining the expressions for the two terms. Since it is much easier to obtain weights than to obtain volumes, the soil engineer makes considerable use of changes in water content of a saturated soil to measure volumetric strain.

The lower part of Fig. 3.1 gives expressions for various unit weights, i.e., the weight of a given volume. The *total unit weight* γ_t is, for example, the weight of the entire soil element divided by the volume of the entire element.² The *dry unit weight*, often called *dry density*, is the weight of mineral matter divided by the volume of the entire element. Unit weights appear in units of weight per volume such as pounds per cubic foot, grams per cubic centimeter, and tons per cubic meter.

² The symbol γ is also used for total unit weight.

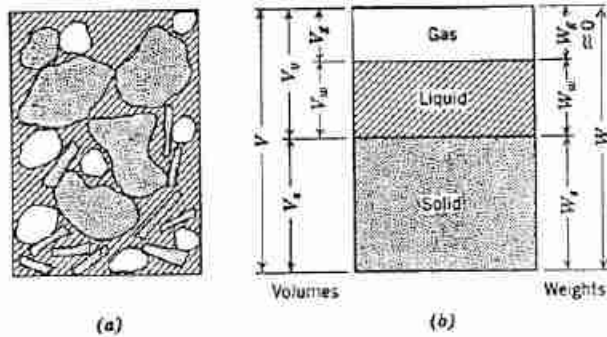


Fig. 3.1 Relationships among soil phases. (a) Element of natural soil. (b) Element separated into phases.

Volume

Porosity:

$$n = \frac{V_v}{V}$$

Void ratio:

$$e = \frac{V_v}{V_s}$$

Degree of saturation:

$$S = \frac{V_w}{V_v}$$

$$n = \frac{e}{1 + e}; \quad e = \frac{n}{1 - n}$$

Weight

Water content:

$$w = \frac{W_w}{W_s}$$

Specific Gravity

Mass:

$$G_m = \frac{\gamma_t}{\gamma_0}$$

Water:

$$G_w = \frac{\gamma_w}{\gamma_0}$$

Solids:

$$G = \frac{\gamma_s}{\gamma_0}$$

γ_0 = Unit weight of water at 4°C $\approx \gamma_w$

Note that $G_w = S_e$

Unit Weight

Total:

$$\gamma_t = \frac{W}{V} = \frac{G + Se}{1 + e} \gamma_w = \frac{1 + w}{1 + e} G \gamma_w$$

Solids:

$$\gamma_s = \frac{W_s}{V_s}$$

Water:

$$\gamma_w = \frac{W_w}{V_w}$$

Dry:

$$\gamma_d = \frac{W_s}{V} = \frac{G}{1 + e} \gamma_w = \frac{G \gamma_w}{1 + wG/S} = \frac{\gamma_t}{1 + w}$$

Submerged (buoyant):

$$\gamma_b = \gamma_t - \gamma_w = \frac{G - 1 - e(1 - S)}{1 + e} \gamma_w$$

Submerged (saturated soil):

$$\gamma_b = \gamma_t - \gamma_w = \frac{G - 1}{1 + e} \gamma_w$$

Specific gravity is the unit weight divided by the unit weight of water. Values of specific gravity of solids G for a selected group of minerals³ are given in Table 3.1.

Table 3.1 Specific Gravities of Minerals

Quartz	2.65
K-Feldspars	2.54-2.57
Na-Ca-Feldspars	2.62-2.76
Calcite	2.72
Dolomite	2.85
Muscovite	2.7-3.1
Biotite	2.8-3.2
Chlorite	2.6-2.9
Pyrophyllite	2.84
Serpentine	2.2-2.7
Kaolinite	2.61 ^a
	2.64 ± 0.02
Halloysite (2 H ₂ O)	2.55
Illite	2.84 ^a
	2.60-2.86
Montmorillonite	2.74 ^a
	2.75-2.78
Attapulgite	2.30

^a Calculated from crystal structure.

The expression $G_w = S_e$ is useful to check computations of the various relationships.

The student in soil mechanics must understand the meanings of the relationships in Fig. 3.1, convince himself once and for all that they are correct, and add these terms to his active vocabulary. These relationships are basic to most computations in soil mechanics and thus are an essential part of soil mechanics.

Typical Values of Phase Relationships for Granular Soils

Figure 3.2 shows two of the many possible ways that a system of equal-sized spheres can be packed. The dense packings represent the densest possible state for such a system. Looser systems than the simple cubic packing can be obtained by carefully constructing arches within the packing, but the simple cubic packing is the loosest of the stable arrangements. The void ratio and porosity of

³ Chapter 4 discusses the common soil minerals.

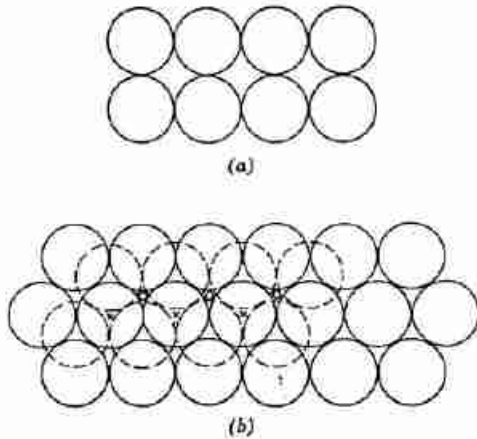


Fig. 3.2 Arrangements of uniform spheres. (a) Plan and elevation view: simple cubic packing. (b) Plan view: dense packing. Solid circles, first layer; dashed circles, second layer; o, location of sphere centers in third layer: face-centered cubic array; x, location of sphere centers in third layer: close-packed hexagonal array. (From Deresiewicz, 1958.)

these simple packings can be computed from the geometry of the packings, and the results are given in Table 3.2.

This table also gives densities for some typical granular soils in both the "dense" and "loose" states. A variety of tests have been proposed to measure the maximum and

Table 3.2 Maximum and Minimum Densities for Granular Soils

Description	Void Ratio		Porosity (%)		Dry Unit Weight (pcf)	
	e_{max}	e_{min}	n_{max}	n_{min}	γ_{dmin}	γ_{dmax}
Uniform spheres	0.92	0.35	47.6	26.0	—	—
Standard Ottawa sand	0.80	0.50	44	33	92	110
Clean uniform sand	1.0	0.40	50	29	83	118
Uniform inorganic silt	1.1	0.40	52	29	80	118
Silty sand	0.90	0.30	47	23	87	127
Fine to coarse sand	0.95	0.20	49	17	85	138
Micaceous sand	1.2	0.40	55	29	76	120
Silty sand and gravel	0.85	0.14	46	12	89	146

B. K. Hough, *Basic Soils Engineering*. Copyright © 1957, The Ronald Press Company, New York.

minimum void ratios (Kolbuszewski, 1948). The test to determine the maximum density usually involves some form of vibration. The test to determine minimum density usually involves pouring oven-dried soil into a container. Unfortunately, the details of these tests have

not been entirely standardized, and values of the maximum density and minimum density for a given granular soil depend on the procedure used to determine them. By using special measures, one can obtain densities greater than the so-called maximum density. Densities considerably less than the so-called minimum density can be obtained, especially with very fine sands and silts, by slowly sedimenting the soil into water or by fluffing the soil with just a little moisture present.

The smaller the range of particle sizes present (i.e., the more nearly uniform the soil), the smaller the particles, and the more angular the particles, the smaller the minimum density (i.e., the greater the opportunity for building a loose arrangement of particles). The greater the range of particle sizes present, the greater the maximum density (i.e., the voids among the larger particles can be filled with smaller particles).

A useful way to characterize the density of a natural granular soil is with *relative density* D_r , defined as

$$D_r = \frac{e_{max} - e}{e_{max} - e_{min}} \times 100\% = \frac{\gamma_{dmax}}{\gamma_d} \times \frac{\gamma_d - \gamma_{dmin}}{\gamma_{dmax} - \gamma_{dmin}} \times 100\% \quad (3.1)$$

where

- e_{min} = void ratio of soil in densest condition
- e_{max} = void ratio of soil in loosest condition
- e = in-place void ratio
- γ_{dmax} = dry unit weight of soil in densest condition
- γ_{dmin} = dry unit weight of soil in loosest condition
- γ_d = in-place dry unit weight

Table 3.3 characterizes the density of granular soils on the basis of relative density.

Table 3.3 Density Description

Relative Density (%)	Descriptive Term
0-15	Very loose
15-35	Loose
35-65	Medium
65-85	Dense
85-100	Very dense

Values of water content for natural granular soils vary from less than 0.1% for air-dry sands to more than 40% for saturated, loose sand.

Typical Values of Phase Relationships for Cohesive Soils

The range of values of phase relationships for cohesive soils is much larger than for granular soils. Saturated sodium montmorillonite at low confining pressure can exist at a void ratio of more than 25; saturated clays

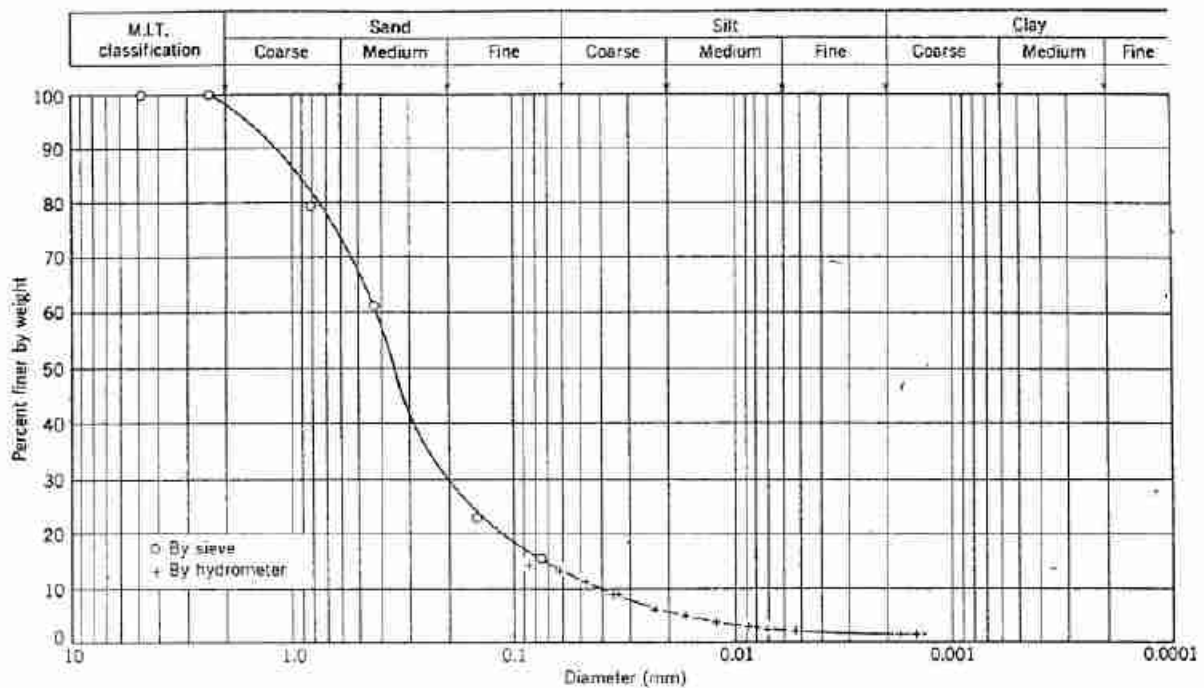


Fig. 3.3 Particle size distribution curve (From Lambe, 1951).

compressed under the high stresses (e.g., 10,000 psi) that exist at great depths in the ground can have void ratios less than 0.2.

Using the expression $G_w = S_e$ (Fig. 3.1), we can compute the water contents corresponding to these quoted values of void ratio:

Sodium montmorillonite	900%
Clay under high pressure	7%

If a sample of oven-dry Mexico City clay sits in the laboratory (temperature = 70°F, relative humidity = 50%), it will absorb enough moisture from the atmosphere for its water content to rise to 2½% or more. Under similar conditions, montmorillonite can get to a water content of 20%.

3.2 PARTICLE SIZE CHARACTERISTICS

The particle size distribution of an assemblage of soil particles is expressed by a plot of percent finer by weight versus diameter in millimeters, as shown in Fig. 3.3. Using the definition for sand, silt, and clay noted at the top of this figure⁴ we can estimate the make-up of the soil sample as:

Gravel	2%
Sand	85%
Silt	12%
Clay	1%

⁴ This set of particle size definitions is convenient and widely used. A slightly different set is given in Tables 3.5 and 3.6.

The uniformity of a soil can be expressed by the *uniformity coefficient*, which is the ratio of D_{60} to D_{10} , where D_{60} is the soil diameter at which 60% of the soil weight is finer and D_{10} is the corresponding value at 10% finer. A soil having a uniformity coefficient smaller than about 2 is considered "uniform." The uniformity of the soil whose distribution curve is shown in Fig. 3.3 is 10. This soil would be termed a "well-graded silty sand."

There are many reasons, both practical and theoretical, why the particle size distribution curve of a soil is only approximate. As discussed in Chapter 4, the definition of particle size is different for the coarse particles and the fine particles.

The accuracy of the distribution curves for fine-grained soils is more questionable than the accuracy of the curves for coarse soils. The chemical and mechanical treatments given natural soils prior to the performance of a particle size analysis—especially for a hydrometer analysis—usually result in effective particle sizes that are quite different from those existing in the natural soil. Even if an exact particle size curve were obtained, it would be of only limited value. Although the behavior of a cohesionless soil can often be related to particle size distribution, the behavior of a cohesive soil usually depends much more on geological history and structure than on particle size.

In spite of their serious limitations, particle size curves, particularly those of sands and silts, do have practical value. Both theory and laboratory experiments show

Table 3.4 Atterberg Limits of Clay Minerals

Mineral	Exchangeable Ion	Liquid Limit (%)	Plastic Limit (%)	Plasticity Index (%)	Shrinkage Limit (%)
Montmorillonite	Na	710	54	656	9.9
	K	660	98	562	9.3
	Ca	510	81	429	10.5
	Mg	410	60	350	14.7
	Fe	290	75	215	10.3
	Fe*	140	73	67	—
Illite	Na	120	53	67	15.4
	K	120	60	60	17.5
	Ca	100	45	55	16.8
	Mg	95	46	49	14.7
	Fe	110	49	61	15.3
	Fe*	79	46	33	—
Kaolinite	Na	53	32	21	26.8
	K	49	29	20	—
	Ca	38	27	11	24.5
	Mg	54	31	23	28.7
	Fe	59	37	22	29.2
Attapulgite	Fe*	36	35	21	—
	H	270	150	120	7.6

Data from Cornell, 1951.
* After five cycles of wetting and drying.

that soil permeability and capillarity are related to some effective particle diameter. These relationships are discussed later in the book.

The method of designing inverted filters for dams, levees, etc., uses the particle size distribution curves of the soils involved. This method is based on the relationship of particle size to permeability, along with experimental data on the particle size distribution required to prevent the migration of particles when water flows through the soil. Also, the most common criterion for establishing the susceptibility of soils to frost damage is based on particle size.

3.3 ATTERBERG LIMITS

Largely through the work of A. Atterberg and A. Casagrande (1948), the Atterberg limits and related indices have become very useful characteristics of assemblages of soil particles. The limits are based on the concept that a fine-grained soil can exist in any of four states depending on its water content. Thus a soil is *solid* when dry, and upon the addition of water proceeds through the *semisolid*, *plastic*, and finally *liquid* states, as shown in Fig. 3.4. The water contents at the boundaries between adjacent states are termed *shrinkage limit*, *plastic limit*, and *liquid limit*. The four indices noted in Fig. 3.4 are computed from these limits.

The liquid limit is determined by measuring the water content and the number of blows required to close a specific width groove for a specified length in a standard liquid limit device. The plastic limit is determined by measuring the water content of the soil when threads of

the soil $\frac{1}{8}$ in. in diameter begin to crumble. The shrinkage limit is determined as the water content after just enough water is added to fill all the voids of a dry pat of soil. The detailed procedures for determining these three limits are given in Lambe (1951). Table 3.4 gives Atterberg limits for some common clay minerals.

Physical Significance of the Atterberg Limits

The concept of a soil existing in various states, depending on its moisture content, is a sound one. The greater the amount of water a soil contains, the less interaction there will be between adjacent particles and the more the soil should behave like a liquid.

In a very general way, we may expect that the water that is attracted to surfaces of the soil particles should not behave as a liquid. Thus, if we compare two soils *A* and *B*, and if soil *A* has a greater tendency to attract water to the particle surfaces, then we should expect that the water content at which the two soils begin to behave as a liquid will be greater for soil *A* than for soil *B*. That is, soil *A* should have a larger liquid limit than soil *B*. We might expect that the same reasoning would apply to the plastic limit, and hence to the plasticity index.

However, the limits between the various states have

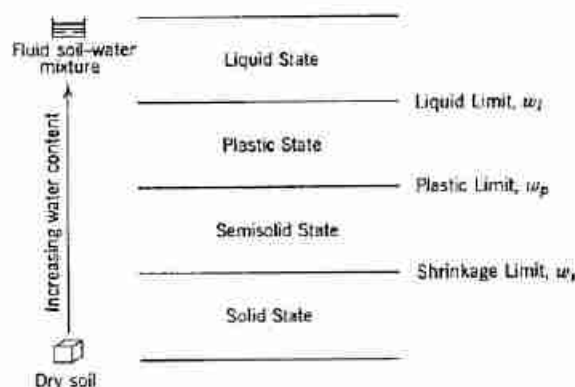


Fig. 3.4 Atterberg limits and related indices.

Plasticity Index:

$$I_p \text{ or } PI = w_l - w_p$$

Flow Index:

I_f = Slope of flow curve (flow curve is plot of water content vs number of blows, log scale)

Toughness Index:

$$I_t = \frac{I_p}{I_f}$$

$$\left. \begin{array}{l} \text{Water-plasticity Ratio } B \\ \text{Liquidity Index } LI \text{ or } I_L \end{array} \right\} = \frac{w_n - w_p}{w_l - w_p}$$

w_n = natural water content

been set arbitrarily, and thus it is unlikely that the limits *per se* can be completely interpreted fundamentally. That is, it is unlikely that the magnitude of the liquid limit for a particular soil can be tied quantitatively to the thickness of the adsorbed water layer.

The difficulty of interpreting fundamentally the Atterberg limits should not deter their use. The student should think of them as approximate boundaries between the states in which fine-grained soils can exist, and not worry too much about attaching significance to the exact value of the arbitrarily determined limits.

Relationship of Atterberg Limits to Composition of Soil

Let us make further use of the concept that the Atterberg limits for a soil are related to the amount of water that is attracted to the surfaces of the soil particles. Because of the great increase in surface area per mass with decreasing particle size (as discussed in Chapter 5), it may be expected that the amount of attracted water will be largely influenced by the amount of clay that is present in the soil. On the basis of this reasoning, Skempton (1953) defined a quantity he called activity:

$$\text{Activity of a clay} = \frac{\text{plasticity index}}{\% \text{ by weight finer than } 2 \mu} \quad (3.2)$$

Figure 3.5 shows some results obtained on prepared mixtures of various percentages of particles less than and greater than 2μ . In Part (a) several natural soils were separated into fractions greater and less than 2μ and then the two fractions were recombined as desired. The results in the right diagram were obtained on clay minerals mixed with quartz sand.

Engineering Use of Atterberg Limits

The Atterberg limits and related indices have proved to be very useful for soil identification and classification, as shown in the next section. The limits are often used directly in specifications for controlling soil for use in fill and in semiempirical methods of design.

The plasticity index, indicating the magnitude of water content range over which the soil remains plastic, and the liquidity index, indicating the nearness of a natural soil to the liquid limit, are particularly useful characteristics of soil. One must realize, however, that all of the limits and indices with the exception of the shrinkage limit are determined on soils that have been thoroughly worked into a uniform soil-water mixture. The limits therefore give no indication of particle fabric or residual bonds between particles which may have been developed in the natural soil but are destroyed in preparing the specimen for the determinations of the limits.

3.4 SOIL CLASSIFICATION

The direct approach to the solution of a soil engineering problem consists of first measuring the soil property needed and then employing this measured value in some rational expression to determine the answer to the problem. Examples of this approach are:

1. To determine the rate of water flowing through a sample of soil, measure the permeability of the soil, and use this value together with a flow net and Darcy's law to determine the flow.
2. To determine the settlement of a building, measure the compressibility of the soil, and use this value in

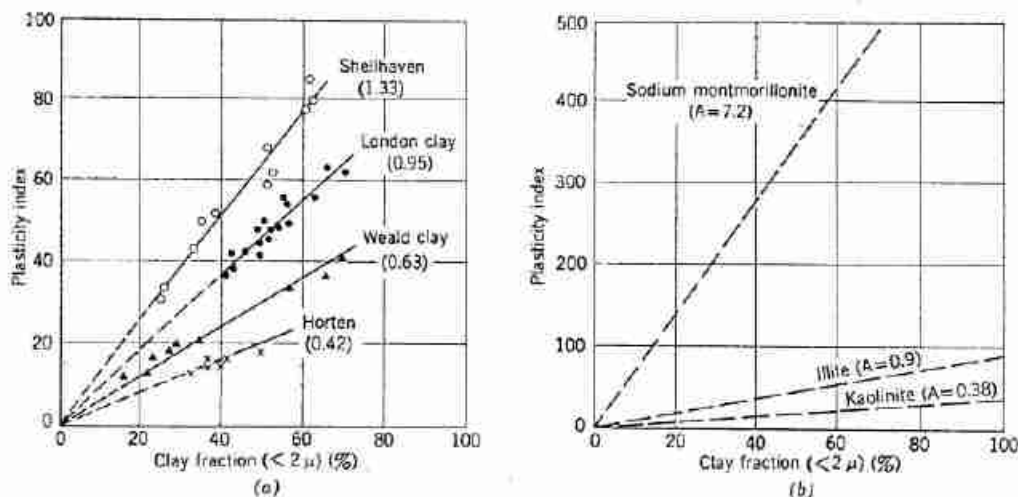


Fig. 3.5 Relation between plasticity index and clay fraction. Figures in parentheses are the "activities" of the clays. (From Skempton, 1953.)

TABLE 2.5 UNIFIED SOIL CLASSIFICATION

Field Identification Procedures (Excluding particles larger than 3 in. and basting fraction on estimated weights)	Group Symbol	Typical Mixtures	Information Required for Describing Soils	Laboratory Classification Criteria
<p>Clayey More than half of coarse fraction is larger than No. 4 sieve size</p> <p>Graels More than half of coarse fraction is smaller than No. 4 sieve size</p> <p>Clayey More than half of coarse fraction is smaller than No. 4 sieve size</p> <p>Graels More than half of coarse fraction is larger than No. 4 sieve size</p>	<p>GI¹</p> <p>GI²</p> <p>GM</p> <p>GC</p> <p>SW</p> <p>SP</p> <p>SM</p> <p>SC</p>	<p>Well graded sands, gravel-sand mixture, little or no fines</p> <p>Poorly graded sands, gravel-sand mixtures, little or no fines</p> <p>Silty sands, poorly graded gravel-sand-silt mixtures</p> <p>Clayey sands, poorly graded gravel-sand-clay mixtures</p> <p>Well graded sands, gravelly sands, little or no fines</p> <p>Poorly graded sands, gravelly sands, little or no fines</p> <p>Silty sands, poorly graded sand-silt mixtures</p> <p>Clayey sands, poorly graded sand-clay mixtures</p>	<p>Give typical name; indicate approximate percentages of sand, gravel, maximum size, sphericity, surface condition, and hardness of the coarse grains; local or geologic name and other pertinent descriptive information; and symbol in parentheses</p> <p>For undisturbed soils add information on stratification, degree of compaction, consolidation, moisture conditions, and drainage characteristics</p> <p>Example: Silty sand, gravelly; about 20% hard, angular gravel particles < 1/8 in. maximum size, rounded and subangular sand grains coarse to fine, about 15% non-plastic, poorly sorted, well-compacted and moist in place, alluvial sand, (SM)</p>	<p>Determine percentages of gravel and sand from grain size curve 200 sieve sizes coarse, graded soils are classified as follows: Less than 5% GM, GC, SM, SP More than 12% SW, SP 5% to 12% GI, GI¹, GI², GP, GM, GC, SM, SP</p> <p>Use grain size curve in identifying the fractions as given under field identification</p>
<p>Clayey More than half of coarse fraction is smaller than No. 200 sieve size</p> <p>Clayey More than half of coarse fraction is larger than No. 200 sieve size</p> <p>Clayey More than half of coarse fraction is smaller than No. 200 sieve size</p> <p>Clayey More than half of coarse fraction is larger than No. 200 sieve size</p>	<p>ML</p> <p>CL</p> <p>OL</p> <p>MH</p> <p>CH</p> <p>OH</p> <p>PT</p>	<p>Inorganic silts and very fine sands, rock flour, silt or clayey fine sands with slight plasticity</p> <p>Inorganic silts of low to medium plasticity, gravelly clays, sandy clays, silty clays, lean clays</p> <p>Organic silts and organic silts of low plasticity</p> <p>Inorganic silts, noncohesive or diatomaceous fine sandy or silty soils, elastic silts</p> <p>Inorganic clays of high plasticity, fat clays</p> <p>Organic clays of medium to high plasticity</p> <p>Peat and other highly organic soils</p>	<p>Give typical name; indicate degree and character of plasticity, amount and maximum size of coarse grains; colour in wet condition, odour if any, local or geologic name; and other pertinent descriptive information, and symbol in parentheses</p> <p>For undisturbed soils add information on structure, stratification, consistency in undisturbed and remoulded states, moisture and drainage conditions</p> <p>Example: Clayey ML, brown; slightly plastic; small percentage of fine sand; numerous vertical root holes; firm and dry in place; loess; (ML)</p>	<p>Plasticity index</p> <p>Liquid limit</p> <p>Plasticity chart for laboratory classification of fine grained soils</p>

From Wagner, 1957.

a. Secondary classification. Soils possessing characteristics of two groups are designated by combinations of group symbols. For example GI¹-GC, well graded gravel-sand mixture with clay binder.

b. All sieve sizes on this chart are U.S. standard.

This procedure is to be performed on the minus No. 40 sieve size particles, approximately 1/4 in. For field classification purposes, increasing is not intended; simply remove by hand the coarse particles that interfere with the tests.

Dilatancy (Reaction to shaking).
After removing particles larger than No. 40 sieve size, prepare a pat of moist soil with a volume of about one-half cubic inch. Add enough water if necessary to make the soil soft but not sticky. Place the pat in the open palm of one hand and shake horizontally, striking vigorously against the other hand several times. A positive reaction consists of the appearance of water on the surface of the pat which changes to a heavy consistency and becomes glossy. When the sample is squeezed between the fingers, the water and gloss disappear from the surface, the pat stiffens and finally cracks or crumbles. The rapidity of appearance of water during shaking and of its disappearance during squeezing assist in identifying the character of the fines in a soil. Very fine clean sands give the quickest and most distinct reaction whereas a plastic clay has no reaction. Inorganic silts, such as a typical rock flour, show a moderately quick reaction.

Field Identification Procedure for Fine Grained Soils or Fractions
Soils possessing characteristics of two groups are designated by combinations of group symbols. For example GI¹-GC, well graded gravel-sand mixture with clay binder.

Dry Strength (Crushing characteristics).
After removing particles larger than No. 40 sieve size, mould a pat of soil to the consistency of putty, adding water if necessary. Allow the pat to dry completely by oven, sun or air drying, and then test its strength by breaking and crumbling between the fingers. This strength is a measure of the character and quantity of the colloidal fraction contained in the soil. The dry strength increases with increasing plasticity. High dry strength is characteristic for clays of the CH group. A typical inorganic silt possesses only very slight dry strength. Silty fine sands and silts have about the same slight dry strength, but can be distinguished by the feel when powdering the dried specimen. Fine sand feels gritty whereas a typical silt has the smooth feel of flour.

Table 3.6 Soil Components and Fractions

Soil	Soil Component	Symbol	Grain Size Range and Description	Significant Properties	
Coarse-grained components	Boulder	None	Rounded to angular, bulky, hard, rock particle, average diameter more than 12 in.	Boulders and cobbles are very stable components, used for fills, ballast, and to stabilize slopes (riprap). Because of size and weight, their occurrence in natural deposits tends to improve the stability of foundations. Angularity of particles increases stability.	
	Cobble	None	Rounded to angular, bulky, hard, rock particle, average diameter smaller than 12 in. but larger than 6 in.		
	Gravel	G	Rounded to angular bulky, hard, rock particle, passing 3-in. sieve (76.2 mm) retained on No. 4 sieve (4.76 mm)	Gravel and sand have essentially same engineering properties differing mainly in degree. The No. 4 sieve is arbitrary division, and does not correspond to significant change in properties. They are easy to compact, little affected by moisture, not subject to frost action. Gravels are generally more perviously stable, resistant to erosion and piping than are sands. The well-graded sands and gravels are generally less pervious and more stable than those which are poorly graded (uniform gradation). Irregularity of particles increases the stability slightly. Finer, uniform sand approaches the characteristics of silt: i.e., decrease in permeability and reduction in stability with increase in moisture.	
			Coarse		3- to 1-in.
			Fine		1-in. to No. 4
	Sand	S	Rounded to angular, bulky, hard, rock particle, passing No. 4 sieve (4.76 mm) retained on No.200 sieve (0.074 mm)		
			Coarse		No. 4 to 10 sieves
			Medium		No. 10 to 40 sieves
Fine			No. 40 to 200 sieves		
Fine-grained components	Silt	M	Particles smaller than No. 200 sieve (0.074 mm) identified by behavior; that is, slightly or non-plastic regardless of moisture and exhibits little or no strength when air dried		Silt is inherently unstable, particularly when moisture is increased, with a tendency to become quick when saturated. It is relatively impervious, difficult to compact, highly susceptible to frost heave, easily erodible and subject to piping and boiling. Bulky grains reduce compressibility; flaky grains, i.e., mica, diatoms, increase compressibility, produce an "elastic" silt.
	Clay	C	Particles smaller than No. 200 sieve (0.074 mm) identified by behavior; that is, it can be made to exhibit plastic properties within a certain range of moisture and exhibits considerable strength when air dried	The distinguishing characteristic of clay is cohesion or cohesive strength, which increases with decrease in moisture. The permeability of clay is very low, it is difficult to compact when wet and impossible to drain by ordinary means, when compacted is resistant to erosion and piping, is not susceptible to frost heave, is subject to expansion and shrinkage with changes in moisture. The properties are influenced not only by the size and shape (flat, plate-like particles) but also by their mineral composition; i.e., the type of clay-mineral, and chemical environment or base exchange capacity. In general, the montmorillonite clay mineral has greatest, illite and kaolinite the least, adverse effect on the properties.	
	Organic matter	O	Organic matter in various sizes and stages of decomposition	Organic matter present even in moderate amounts increases the compressibility and reduces the stability of the fine-grained components. It may decay causing voids or by chemical alteration change the properties of a soil, hence organic soils are not desirable for engineering uses.	

From Wagner, 1957.

Note. The symbols and fractions were developed for the Unified Classification System. For field identification, 1/2 in. is assumed equivalent to the No. 4, and the No. 200 is defined as "about the smallest particle visible to the unaided eye." The sand fractions are not equal divisions on a logarithmic plot; the No. 10 was selected because of the significance attached to that size by some investigators. The No. 40 was chosen because the "Atterberg limits" tests are performed on the fraction of soil finer than the No. 40.

Table 3.7 Engineering Use Chart

Typical Names of Soil Groups	Group Symbols	Important Properties				Relative Desirability for Various Uses								
		Permeability when Compacted	Shearing Strength when Compacted and Saturated	Compressibility when Compacted and Saturated	Workability as a Construction Material	Rolled Earth Dams		Canal Sections		Foundations		Roadways		
						Core	Shell	Erosion Resistance	Com-pacted Earth Lining	Seepage Im-portant	Seepage not Im-portant	Frost Heave not Possible	Frost Heave Possible	Sur-facing
Well-graded gravels, gravel-sand mixtures, little or no fines	GW	pervious	excellent	negligible	excellent	—	1	1	—	1	1	1	1	3
Poorly graded gravels, gravel-sand mixtures, little or no fines	GP	very pervious	good	negligible	good	—	2	2	—	3	3	3	3	—
Silty gravels, poorly graded gravel-sand-silt mixtures	GM	semipervious to impervious	good	negligible	good	2	4	4	4	1	4	4	9	5
Clayey gravels, poorly graded gravel-sand-clay mixtures	GC	impervious	good to fair	very low	good	1	—	3	1	2	6	5	5	1
Well-graded sands, gravelly sands, little or no fines	SW	pervious	excellent	negligible	excellent	—	—	3 if gravelly	6	—	2	2	2	4
Poorly graded sands, gravelly sands, little or no fines	SP	pervious	good	very low	fair	—	—	4 if gravelly	7 if gravelly	—	5	6	4	—
Silty sands, poorly graded sand-silt mixtures	SM	semipervious to impervious	good	low	fair	4	5	—	5 if gravelly	3	7	8	10	6
Clayey sands, poorly graded sand-clay mixtures	SC	impervious	good to fair	low	good	3	2	—	5	4	8	7	6	2
Inorganic silts and very fine sands, rock flour, silty or clayey fine sands with slight plasticity	ML	semipervious to impervious	fair	medium	fair	6	6	—	—	6	9	10	11	—
Inorganic clays of low to medium plasticity, gravelly clays, sandy clays, silty clays, lean clays	CL	impervious	fair	medium	good to fair	5	3	—	9	5	10	9	7	7
Organic silts and organic silt-clays of low plasticity	OL	semipervious to impervious	poor	medium	fair	8	8	—	—	7	11	11	12	—
Inorganic silts, micaceous or diatomaceous fine sandy or silty soils, clastic silts	MH	semipervious to impervious	fair to poor	high	poor	9	9	—	—	8	12	12	13	—
Inorganic clays of high plasticity, fat clays	CH	impervious	poor	high	poor	7	7	—	10	9	13	13	8	—
Organic clays of medium to high plasticity	OH	impervious	poor	high	poor	10	10	—	—	10	14	14	14	—
Fat and other highly organic soils	PI	—	—	—	—	—	—	—	—	—	—	—	—	—

From Wagner, 1957.

settlement equations based on Terzaghi's theory of consolidation.

3. To evaluate the stability of a slope, measure the shear strength of the soil and substitute this value in an expression based on the laws of statics.

To measure fundamental soil properties like permeability, compressibility, and strength can be difficult, time consuming, and expensive. In many soil engineering problems, such as pavement design, there are no rational expressions available for the analysis for the solution. For these reasons, sorting soils into groups showing similar behavior may be very helpful. Such sorting is *soil classification*.

Soil classification is thus the placing of a soil into a group of soils all of which exhibit similar behavior. The correlation of behavior with a group in a soil classification system is usually an empirical one developed through considerable experience. Soil classification permits us to solve many types of simple soil problems and guide the test program if the difficulty and importance of the problem dictate further investigation.

Most soil classifications employ very simple index-type tests to obtain the characteristics of the soil needed to place it in a given group. Clearly a soil classification loses its value if the index tests become more complicated than the test to measure directly the fundamental property needed. The most commonly used characteristics are particle size and plasticity.

Since soil classifications are developed as an attempt to aid in the solution of problems, classifications for many types of problems have grown. Thus, for use in flow problems, soils are described as having degrees of permeability such as high, medium, low, very low, practically impermeable. The Corps of Engineers has developed a frost susceptibility classification in which, on the basis of particle size, we can classify soil in categories of similar frost behavior. The Bureau of Public Roads developed a classification for soils in highway construction. The Corps of Engineers and FAA each developed a classification for airfield construction. In 1952 the Bureau of Reclamation and the Corps of Engineers developed a "unified system" intended for use in all engineering problems involving soils. This classification is presented in Tables 3.5 and 3.6. Table 3.7 gives a general indication of the permeability, strength, and compressibility of the various soil groups along with an indication of the relative desirability of each group for use in earth dams, canal sections, foundations, and runways.

Soil classification has proved to be a valuable tool to the soil engineer. It helps the engineer by giving him general guidance through making available in an empirical manner the results of field experience. The soil engineer must be cautious, however, in his use of soil

classification. Solving flow, compression, and stability problems merely on the basis of soil classification can lead to disastrous results. As this book will show in subsequent chapters, empirical correlations between index properties and fundamental soil behavior have many large deviations.

3.5 SUMMARY OF MAIN POINTS

1. There are a number of terms (given in Fig. 3.1) used to express the phase relationships in an element of soil. These terms are an essential component of soil mechanics.
2. The looseness of a sand is expressed by its relative density, which is a most reliable indicator of the behavior of the sand.
3. The particle size distribution and the Atterberg limits are useful index tests for classifying soils. Since the conduct of these tests inherently involves disturbance of the soil, they may not give a good indication of the behavior of the *in situ*, undisturbed soil.

PROBLEMS

3.1 Four soil samples, each having a void ratio of 0.76 and a specific gravity of 2.74, have degrees of saturation of 85, 90, 95, and 100%. Determine the unit weight for each of the four samples.

3.2 A cubic foot of soil in its natural state weighs 113 lb; after being dried it weighs 96 lb. The specific gravity of the soil is 2.70. Determine the degree of saturation, void ratio, porosity, and water content for the soil as it existed in its natural state.

3.3 A container of saturated soil weighed 113.27 g before it was placed in an oven and 100.06 g after it remained in the oven overnight. The container alone weighs 49.31 g; the specific gravity of the soil is 2.80. Determine the void ratio, porosity, and water content of the original soil sample.

3.4 A saturated soil has a unit weight of 120 pcf and a water content of 32.5%. Determine the void ratio and specific gravity of the soil.

3.5 A sample of dry sand having a unit weight of 105 pcf and a specific gravity of 2.70 is placed in the rain. During the rain the volume of the sample remains constant but the degree of saturation increases to 40%. Determine the unit weight and water content of the soil after being in the rain.

3.6 Determine the submerged unit weight of each of the following chunks of saturated soil:

- a. A silty sand, total unit weight = 131 pcf;
- b. A lean clay, total unit weight = 122 pcf;
- c. A very plastic clay, total unit weight = 106 pcf. Assume reasonable values for any additional data which you need.

3.7 For a soil with a specific gravity of 2.70 prepare a chart in which total unit weight (units of gm/cm³, range of 1.0-2.5) is plotted as ordinate and void ratio (range of 0.2-1.8) is plotted as abscissa. Plot for the three percentages of saturation of 0, 50, and 100%.

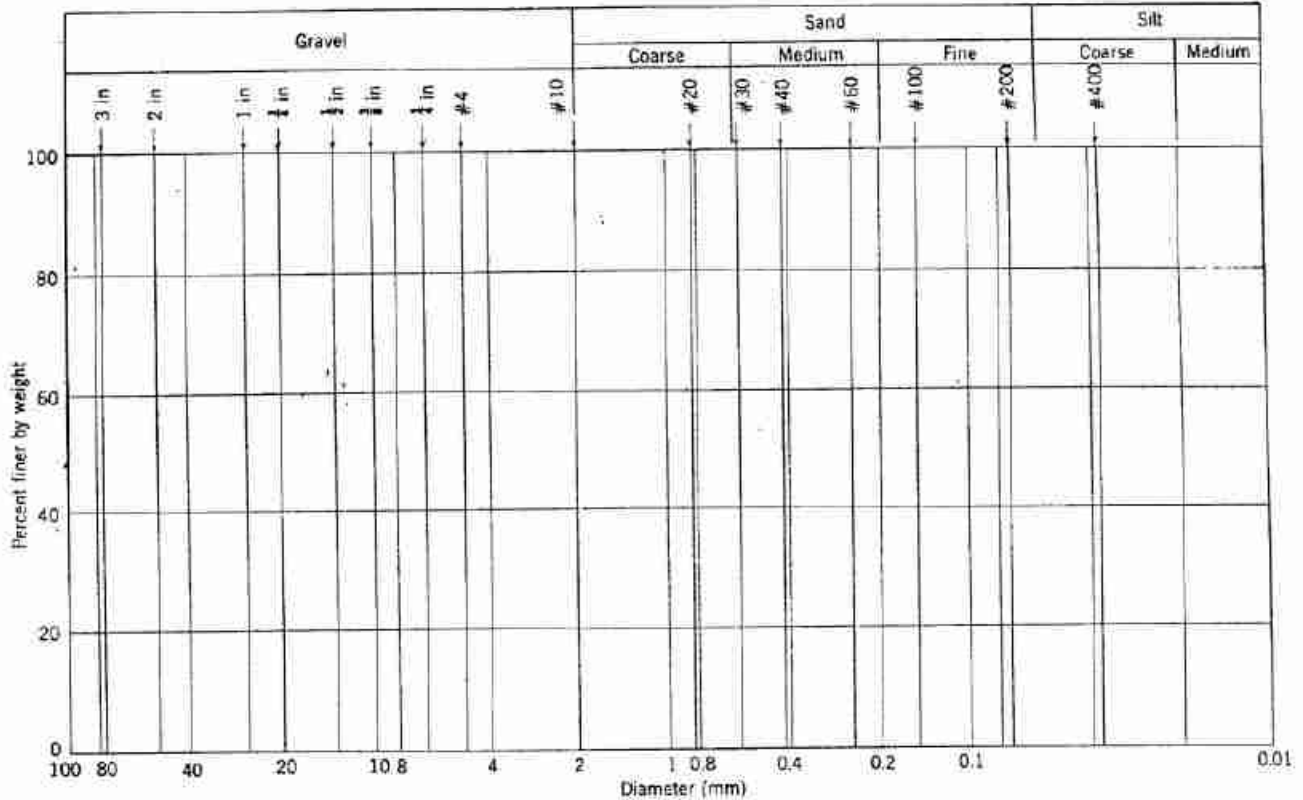


Fig. P3.10

3.8 Prove $G_w = S_e$

3.9 A sample of parallel kaolinite particles (all have the size shown in Fig. 5.6) is saturated. The water content is 30%. What is the average particle spacing?

3.10 A sieve analysis on a soil yields the following results:

Sieve	3 in.	2 in.	1 in.	$\frac{1}{2}$ in.	#4	#10
Percentage passing	100	95	84	74	62	55
Sieve	#20	#40	#60	#100	#200	
Percentage passing	44	32	24	16	9	

a. Plot the particle size distribution of this soil on Fig. P3.10 and classify the soil on the basis of the scale shown in the figure.

b. Comment on the suitability of this soil as drainage material behind a concrete retaining wall.

Hints. (a) Use Tables 3.5–3.7 to predict whether or not soil will be pervious, easy to work as construction material, etc. (b) A common guide for frost susceptibility is percentage finer than 0.02 mm must be less than 3% for material to be nonfrost susceptible.

3.11 Prove that the identity given by Eq. 3.1 is correct.

CHAPTER 4

Description of an Individual Soil Particle

A sample of soil consists of an assemblage of many individual soil particles with air and/or liquid filling the voids among the particles. This chapter examines the individual soil particle.

4.1 APPEARANCE OF A SOIL PARTICLE

Particle Size

The size of a particle, other than a sphere or cube, cannot be uniquely defined by a single linear dimension. The meaning of "particle size" therefore depends on the dimension that was recorded and how it was obtained. Two common ways of determining particle size are a *sieve analysis*¹ for particles larger than approximately 0.06 mm and a *hydrometer analysis*¹ for smaller particles. In the sieve analysis, the soil particles are shaken on a sieve with square openings of specified size. Thus the "size" of a particle larger than 0.06 mm is based on the side dimension of a square hole in a screen. In the hydrometer analysis, the "size" of a particle is the diameter of a sphere which settles in water at the same velocity as the particle.

Soil particles vary in size from 1×10^{-6} mm, i.e., 10 Å, up to large rocks several meters in thickness, a range of one to more than a billion. The tremendous magnitude of this range can be better grasped by noting that the size range between a moth ball or child's marble and our earth is also a one to a billion.

In describing the size of a soil particle, we can cite either a dimension or a name that has been arbitrarily assigned to a certain size range. Table 4.1 gives such a set of names with their corresponding particle size ranges. (Noted in Table 4.1 in parentheses are other numerical values which are also used.) The word "clay" is also used to describe a fine-grained soil having plasticity, as was discussed in Chapter 3. We can avoid confusion by

¹ The detailed procedures for these analyses are given in Lambe (1951).

Table 4.1 Particle Size¹

Boulder	>12 in.
Cobble	6 to 12 in.
Gravel	2.0 mm (or 4.76 mm) to 6 in.
Sand	0.06 (or 0.076 mm) to 2.0 mm (or 4.76 mm)
Silt	0.002 to 0.06 mm (or 0.074 mm)
Clay	< 0.002 mm

employing "clay size" rather than merely "clay" to denote a particle smaller than 2 μ .

In Fig. 4.1 are plotted the sizes of various particles and the ranges of some methods of detecting particle size. A widely used soil particle size classification is shown at the top of Fig. 4.1. A study of this figure will give perspective to particle size and its determination.

Particle Shape

The preceding discussion noted that the size of a particle could be given by a single number only when the particle was equidimensional, as a cube or sphere. This situation is not too far from true for soil particles in the silt range and coarser, but it is far from true for particles in the clay size range. This is illustrated in Figs. 4.2 and 4.3, which show sand particles, and in Fig. 4.4, which shows clay particles. Sheetlike particles, such as mica, do occur in the silt and larger size portions of soil, and particles having shapes such as those shown in Figs. 4.2 and 4.3 do occur in the clay size range. In general, however, most of the particles in the silt range and coarser are approximately equidimensional and most of those in the clay size are far from equidimensional. The most common shape for clay size particles is platey, as are the kaolinite particle and illite particle shown in Fig. 4.4. Rods and laths, however, are found in soils, generally in the clay size fraction.

Geologists working with rocks describe particle shapes using such terms as disk, sphere, blade, and rod on the basis of dimension ratios. The civil engineer generally

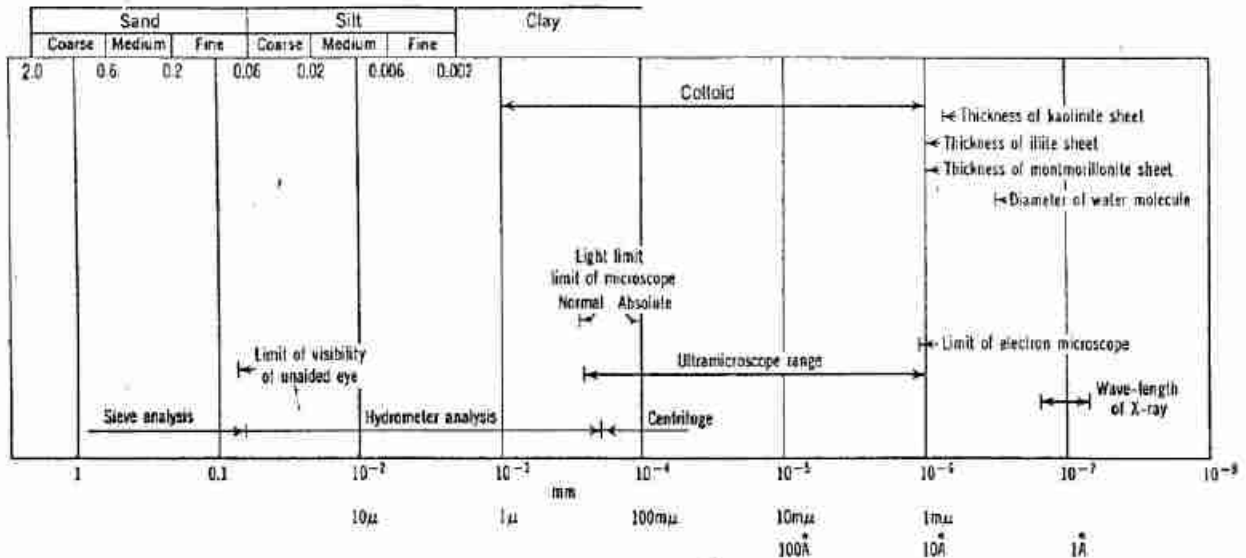


Fig. 4.1 Size.

finds it impractical to characterize numerically particle shape because of the small-sized particles with which he normally works.

Degree of Roundness, Surface Texture, and Color

The degree of roundness refers to the sharpness of the edges and corners of a particle. Figure 4.5 shows five levels of degree of roundness.

Minor features of a surface of a particle, independent of size, shape, or degree of roundness, are termed "surface texture" of the particle. Some terms used to describe surface texture are dull or polished, smooth or rough, striated, frosted, etched, or pitted.

Color is a useful particle characteristic to the geologist working in mining, but it is of little value to the soil engineer. The soil engineer does, however, frequently use color to describe an assemblage of particles, e.g., Boston blue clay. He must use color descriptions with caution, since the color of a soil mass can change with a change in moisture content or chemical composition.

The soil particles in Figs. 4.2, 4.3, and 4.4 illustrate several features of particle appearance. The Ottawa sand and Raguba particles are well rounded and frosted. The particles of sand formed by crushing large mineral chunks (Fig. 4.2d, e, and f) have sharp edges and corners, and their surfaces are not striated, frosted, or etched. The photographs of the Venezuelan sand show that compression to high pressures may cause considerable crushing of particles. The natural Venezuelan sand (Fig. 4.2h) had 4% of its particles finer than 0.074 mm, whereas after compression (Fig. 4.2i) it had 20% of its particles finer than 0.074 mm.

All of the Libyan sands shown except the Raguba sand

are from near the Mediterranean Sea and are 70-90% carbonate minerals. The Raguba sand came from the desert 100 miles away from the sea and is 98% quartz. The carbonate sands, especially those in Fig. 4.3a, have a high degree of aggregation (i.e., joining together of particles by cementation), as can be seen. This aggregation inevitably affects the behavior of the soil. For example, tests on undisturbed specimens of the aggregated sand displayed a significant time dependency of the stress-strain behavior. However, tests on reconstituted specimens in which the aggregation has been disintegrated show less time dependency.

The kaolinite particle in Fig. 4.4 is about 1μ across and 0.08μ thick. Two smaller kaolinite particles can be seen on top of the large one. The surface of the kaolinite particle appears to be smooth to a scale of probably 100 Å. The smallest clay particles, montmorillonite, can and do commonly exist in platelets as thin as 10 Å and are smooth to within an angstrom.

4.2 COMPOSITION OF A SOIL PARTICLE

The beginning student in soil mechanics usually reasons with apparent logic that the composition of the individual particles in an element of soil is an important characteristic of soil. This belief is false since there are few useful, general relationships between soil composition and soil behavior. On the other hand, this belief is true as far as a fundamental understanding of soil behavior is concerned. The nature and arrangement of the atoms in a soil particle—i.e., composition—have a significant influence on permeability, compressibility, strength, and stress transmission in soils, especially in fine-grained soils. There

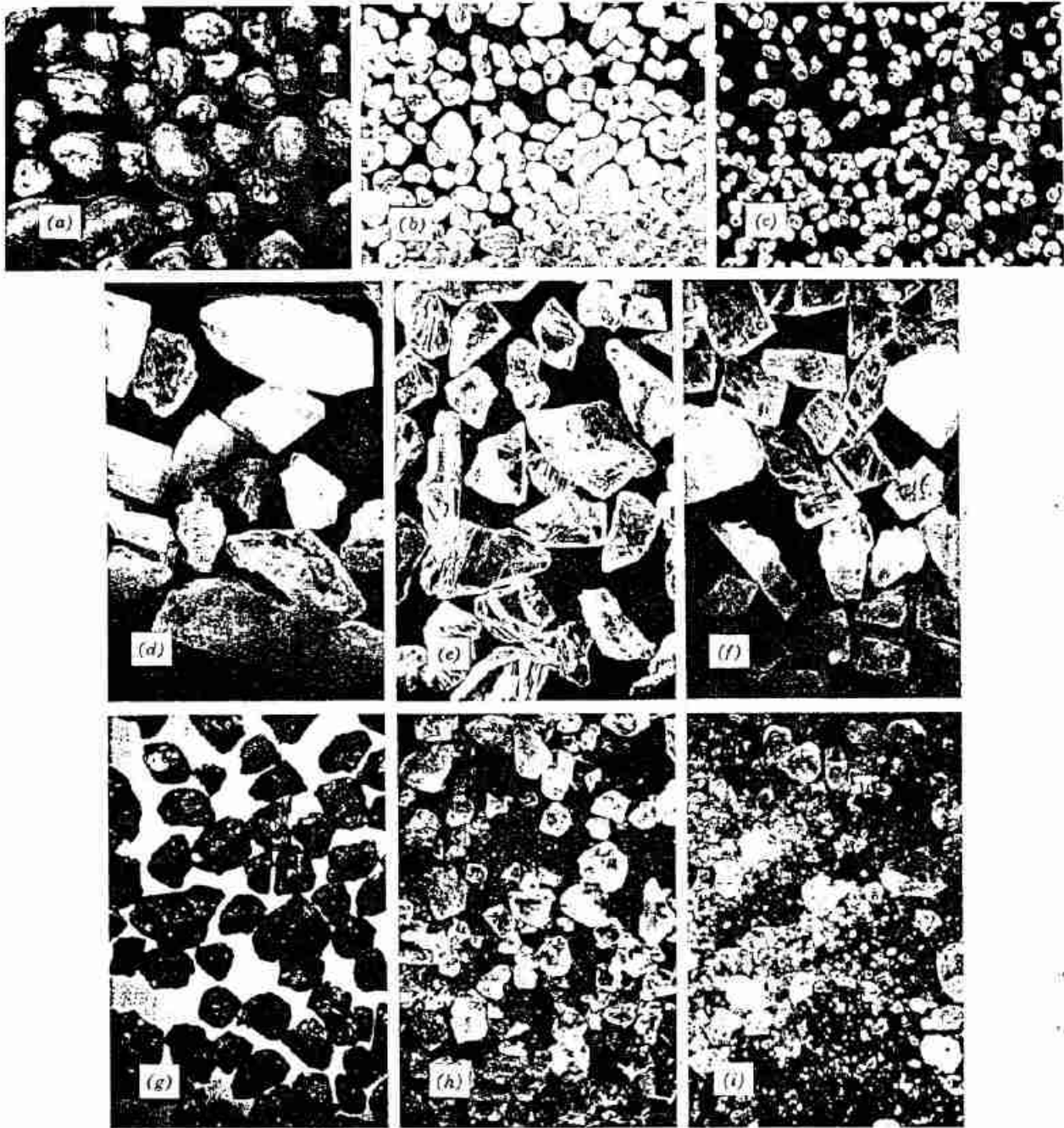


Fig. 4.2 Sand particles. (a) Ottawa sand, 0.42 to 0.84 mm. (b) Ottawa sand, 0.19 to 0.42 mm. (c) Ottawa sand, 0.11 to 0.19 mm. (d) Ground feldspar, 0.19 to 0.42 mm. (e) Ground quartz, 0.19 to 0.42 mm. (f) Ground dolomite, 0.19 to 0.42 mm. (g) Hawaiian beach sand. (h) Venezuelan sand. (i) Venezuelan sand (sand #1 after compression to 20,000 psi). (From Roberts, 1964.)

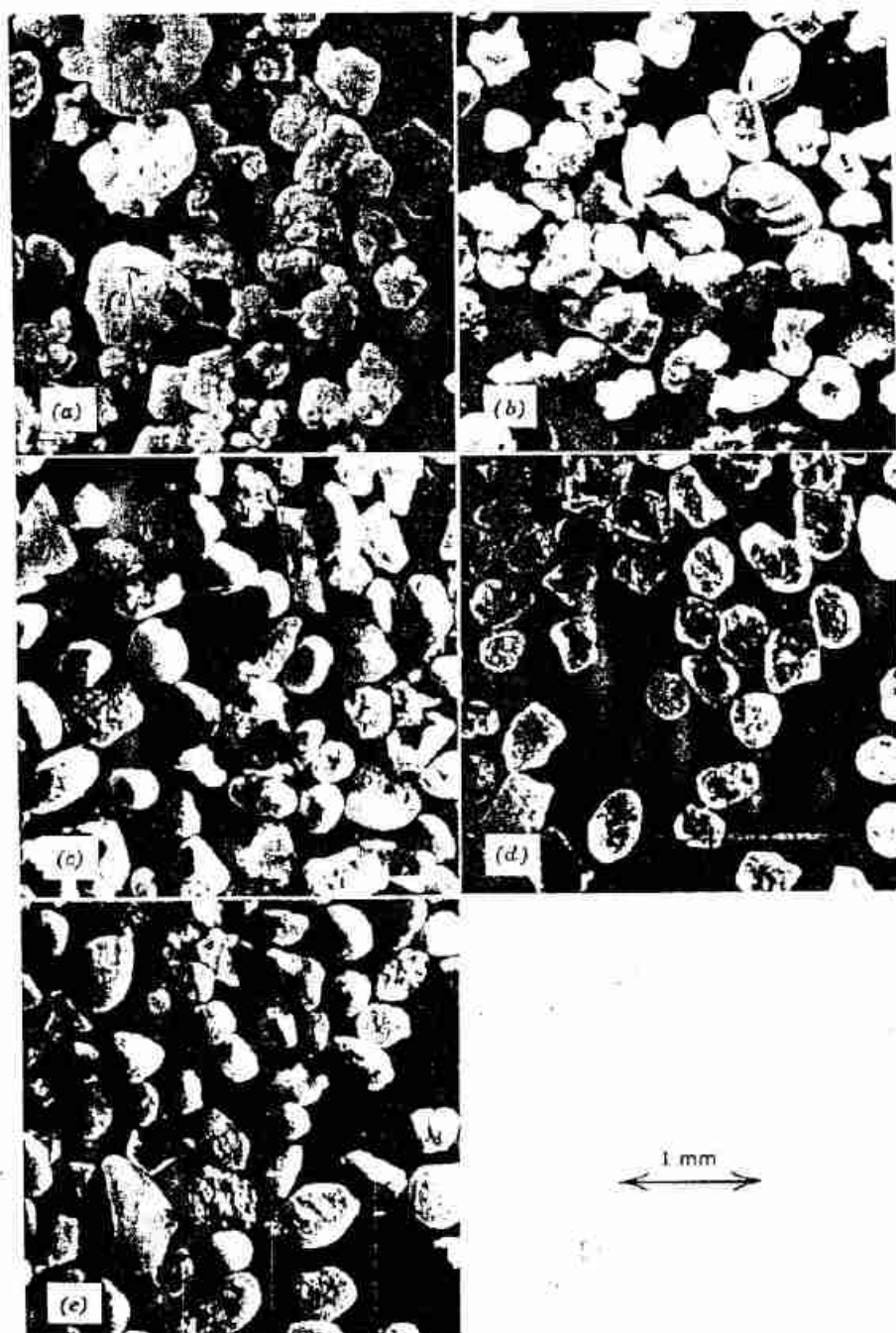


Fig. 4.3 Sands from Libya (0.15 to 0.25 mm fraction). (a) Plant site, Brega. (b) Harbor bottom, Brega. (c) Gas plant, Brega. (d) Raguba. (e) Crude tank farm, Brega. (Sands supplied by ESSO Libya: Photos by R. T. Martin, M.I.T.)

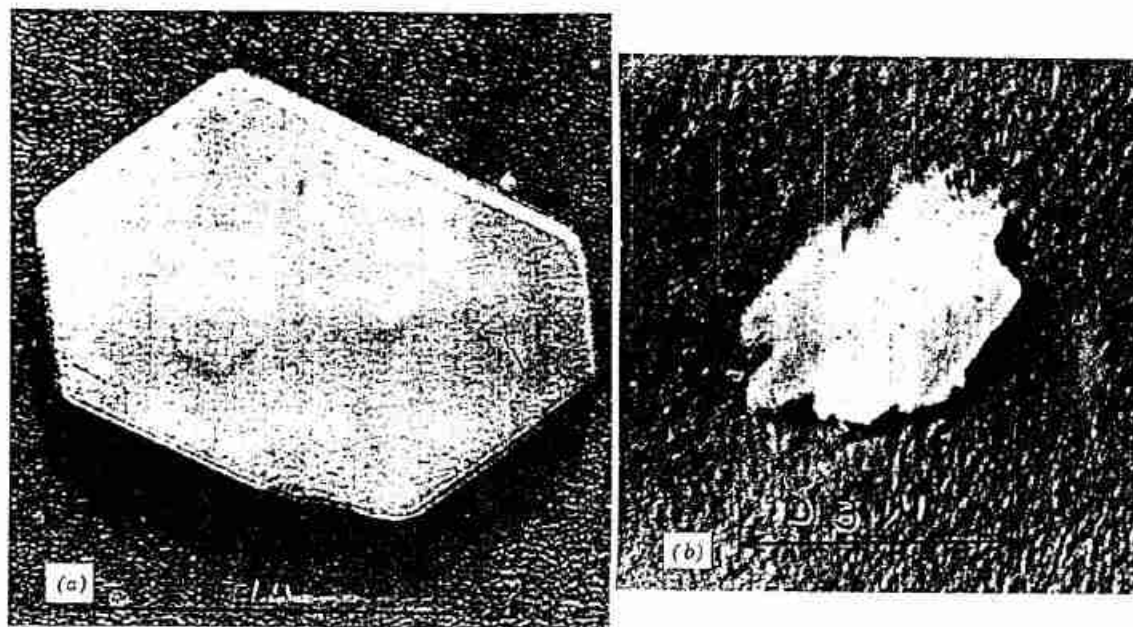


Fig. 4.4 Clay particles. (a) Kaolinite (From Lambe, 1951). (b) Illite (by R. T. Martin, M.I.T.).

are certain minerals that can give a soil containing them unusual properties. Two examples are montmorillonite and halloysite. Montmorillonite can cause a soil to be highly expansive and halloysite can cause soil to have a very low unit weight. These and other relationships between composition and behavior are noted in later chapters. Thus the student needs to study soil composition if he is to understand the fundamentals of clay behavior and particularly the dependence of this behavior on time, pressure, and environment. In explaining soil behavior, later chapters in this book will make use of the material presented in the remaining part of this chapter on soil composition.

A soil particle may be either *organic* or *inorganic*. Little is known about the composition of organic soil; in fact, at the present state of knowledge, the engineer makes little attempt to identify the actual organic compounds in soil. There are soils that are composed entirely of organic particles, such as peat or muskeg,² and there are soils that contain some organic particles and some inorganic particles, such as "organic silt."

An inorganic soil particle may be either a mineral or a rock. A *mineral* is a naturally occurring chemical element or compound (i.e., has a chemical composition expressible by a formula) formed by a geologic process. A *rock*

is the solid material which comprises the outer shell of the earth and is an aggregate of one or more minerals or glasses.

The rest of this chapter presents certain principles of mineralogy and describes a few minerals of interest to the soil engineer. The intent of this presentation is to give the reader some understanding of the nature and arrangement of atoms in soil particles so that he can then grasp why certain particles are small plates that are chemically active and other particles are large, approximately equidimensional chunks that are relatively inactive. For a detailed consideration of mineralogy the reader should see books devoted entirely to this subject, such as Grim (1953), Dana (1949), and *Proceedings of National Conference on Clays and Clay Minerals*.³

Minerals have been classified on the basis of both the nature of the atoms and the arrangement of the atoms. The first classification has headings such as carbonates, phosphates, oxides, and silicates. This classification is of limited value to the civil engineer since the most abundant and important minerals are silicates. In fact, if all of the soil in the world were placed in one pile, over 90% of the weight of the pile would be silicate minerals.

Table 4.2 (p. 50) is a classification of silicates based on the arrangement of atoms in the mineral. This classification has merit for several reasons. First, it is a

² The National Research Council of Canada has had a group studying muskeg for a number of years. The various proceedings of Muskeg Research Conferences sponsored by NRC are an excellent source of information on muskeg.

³ Available from the Publications Office of the National Academy of Sciences, National Research Council, 2101 Constitution Avenue, Washington 25, D.C.

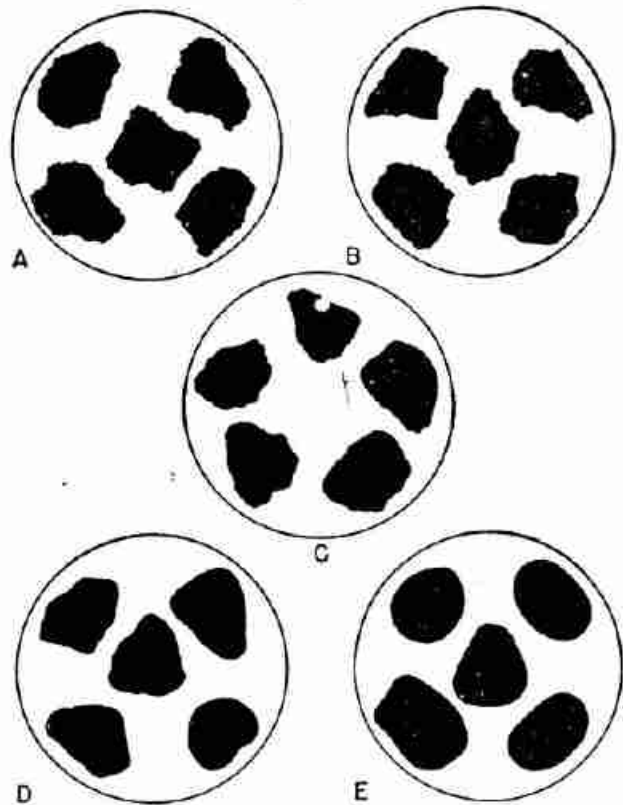


Chart to show roundness classes. A, angular; B, subangular; C, subrounded; D, rounded; E, well rounded.

Fig. 4.5 Degree of particle roundness [Fig. 24 *Sedimentary Rocks* (1949) by F. J. Pettijohn, by permission of Harper & Row, Publishers.]

definite grouping since there is only one known silicate (vesuvianite) that falls into more than one group. Second, there is a relationship between the atomic arrangement in a mineral and its physical, optical, and chemical properties.

Soils are usually the products of rock weathering and thus the most abundant soil minerals are common rock-forming minerals and those that are most resistant to chemical and physical weathering. The sheet and framework silicate minerals are therefore the most abundant and common soil minerals.

Basic Structural Units

The study of the silicate mineral structures may be facilitated by "building" a mineral out of basic structural units. This approach is an educational technique and not necessarily the method whereby the mineral is actually formed by nature. The structures presented in this chapter are idealized. The typical crystal in a clay is a complex structure similar to the idealized arrangement but usually having irregular substitutions and interlayering. Figure 4.6 shows a group of basic silicate units.

The silicon-oxygen tetrahedron consists of four oxygens nestled around a silicon atom to form the unit shown in Fig. 4.6a. The atoms are drawn to scale on the basis of the radii in units of angstroms given in Fig. 4.6h. The table at the right of each unit gives the valences.

Figure 4.6e shows the aluminum-oxygen octahedron and Fig. 4.6d the magnesium-oxygen octahedron. Combining the silicon-oxygen tetrahedrons gives the silica sheet shown in Fig. 4.6e. Combining the aluminum-oxygen octahedrons gives gibbsite (Fig. 4.6f), and combining the magnesium-oxygen octahedrons gives brucite (Fig. 4.6g). A study of the valences in Fig. 4.6 shows that the tetrahedron and two octahedrons are not electrically neutral and therefore do not exist as isolated units. Gibbsite and brucite are, however, electrically neutral and exist in nature as such.

Two-Layer Sheet

If we stack a brucite unit on top of a silicate unit we get serpentine, as shown in Fig. 4.7. This figure shows both the atomic structure and the symbolic structure. Combining in a similar way gibbsite and silica gives the mineral kaolinite shown in Fig. 4.8.

The actual mineral particle does not usually consist of only a few basic layers as suggested by the symbolic structures in Figs. 4.7 and 4.8. Instead, a number of sheets are stacked one on top of another to form an actual crystal—the kaolinite particle shown in Fig. 4.4 contains about 115 of the two-layer units. The linkage between the basic two-layer units consists of hydrogen bonding and secondary valence forces.

In the actual formation of the sheet silicate minerals the phenomenon of *isomorphous substitution* frequently occurs. Isomorphous (meaning "same form") substitution consists of the substitution of one kind of atom for another. For example, one of the sites filled with a silicon atom in the structure in Fig. 4.8 could be occupied by an aluminum. Such an example of isomorphous substitution could occur if an aluminum atom were more readily available at the site than a silicon atom during the formation of the mineral; furthermore, aluminum has coordinating characteristics somewhat similar to silicon, thus it can fit in the silicon position in the crystal lattice. Substituting the aluminum with its +3 valence for silicon with its +4 valence has two important effects:

1. A net unit charge deficiency results per substitution.
2. A slight distortion of the crystal lattice occurs since the ions are not of identical size.

The significance of the charge deficiency is discussed in Chapter 5. The distortion tends to restrict crystal growth and thus limits the size of the crystals.

In the kaolinite mineral there is a very small amount of isomorphous substitution, one possibility being one aluminum replacing one silicon in the silica sheet of the

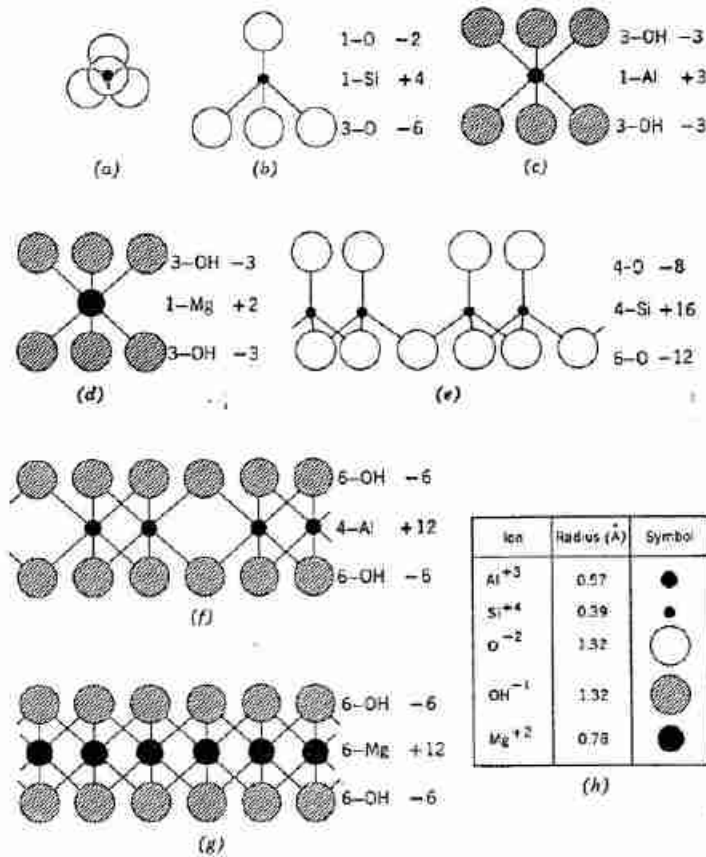


Fig. 4.6 Basic silicate units. (a) and (b) Silicon tetrahedron. (c) Aluminum octahedron. (d) Magnesium octahedron. (e) Silica. (f) Gibbsite. (g) Brucite.

mineral. The amount of this substitution needed to explain the charge on kaolinite is one substitution for every four hundredth silicon ion.

Since the basic structure of kaolinite consists of a layer of gibbsite on top of a layer of silicate, this mineral is called a "two-layer" mineral. Kaolinite is the most important and most common two-layer mineral encountered by the engineer. Halloysite, having essentially the same composition and structure as kaolinite, is an interesting and not uncommon member of the two-layer silicate group. The main difference between halloysite and kaolinite is the presence of water between the basic sheets of halloysite, which results in halloysite existing in tubular particles.

Three-Layer Sheets

The three-layer sheet minerals are formed by placing one silica on the top and one on the bottom of either a gibbsite or brucite sheet. Figure 4.9 shows the mineral pyrophyllite made of a gibbsite sandwiched between two

silica sheets. Figure 4.10 shows the structure of the mineral muscovite, which is similar to pyrophyllite except that there has been isomorphous substitution of aluminum for silicon in muscovite. The net charge created by this substitution is balanced by potassium ions, which serve to link the three-layer sandwiches together, as indicated in the symbolic structure in Fig. 4.10.

The two most common three-layer structures in soil are montmorillonite and illite type minerals. Montmorillonite has a structure similar to pyrophyllite with the exception that there has been isomorphous substitution of magnesium for aluminum in the gibbsite sheet.

Figure 4.11 gives a summary of the sheet silicate minerals of importance to the civil engineer.

Frameworks

Quartz, a framework silicate structure, has a very low ratio of oxygen to silicon (2:1), as noted in Table 4.2. It is thus one of the most weather resistant minerals. The feldspars have higher oxygen to silicon ratios (2.7 to 4.0)

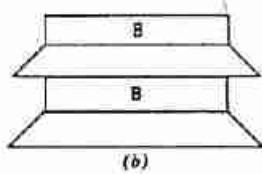
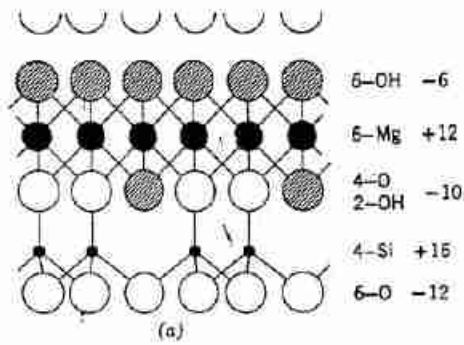


Fig. 4.7 The structure of serpentine. (a) Atomic structure. (b) Symbolic structure.

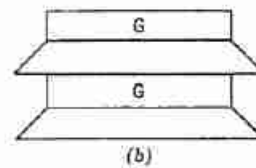
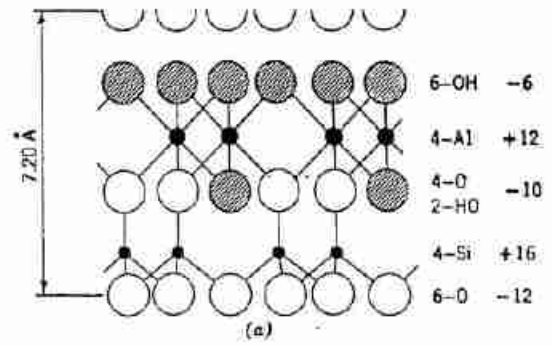


Fig. 4.8 The structure of kaolinite. (a) Atomic structure. (b) Symbolic structure.

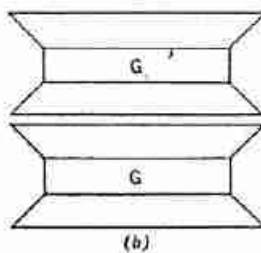
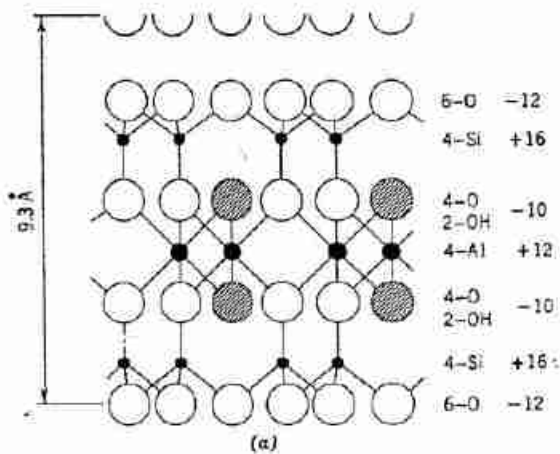


Fig. 4.9 The structure of pyrophyllite. (a) Atomic structure. (b) Symbolic structure.

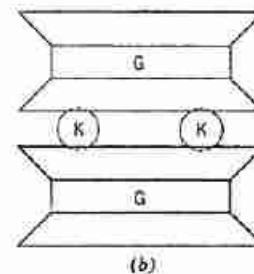
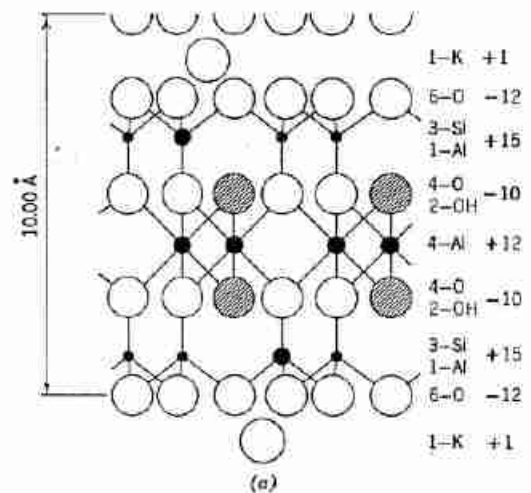


Fig. 4.10 The structure of muscovite. (a) Atomic structure. (b) Symbolic structure.



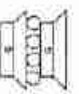
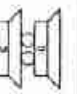


Mineral	Structure Symbol	Isomorphous Substitution (nature and amount)	Linkage between Sheets (type and strength)	Specific Surface (m^2/g)	$\frac{1}{\text{Charge Density}} (\text{\AA}^2/\text{ion})$	Potential Exchange Capacity (me/100 g)	Actual Exchange Capacity (me/100 g)	Particle Shape	Particle Size
Serpentine		none	H-bonding + secondary valence			1	1	Platy or fibrous	
Kaolinite		Al for Si 1 in 400	H-bonding + secondary valence	10-20	83	3	3	Platy	$d = 0.3 \text{ to } 3 \mu$ thickness $= \frac{1}{2} \text{ to } \frac{1}{10} d$
Halloysite ($4H_2O$)		Al for Si 1 in 100	Secondary valence	40	55	12	12	Hollow rod	OD = 0.07 μ ID = 0.04 μ $L = 0.5 \mu$
Halloysite ($2H_2O$)		Al for Si 1 in 100	Secondary valence	40	55	12	12	Hollow rod	OD = 0.07 μ ID = 0.04 μ $L = 0.5 \mu$
Talc		none	Secondary valence			1	1	Platy	
Pyrophyllite		none	Secondary valence			1	1	Platy	

Fig. 4.11 Sheet silicate minerals.


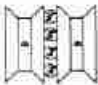
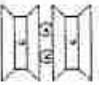
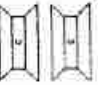
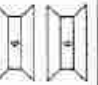
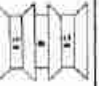

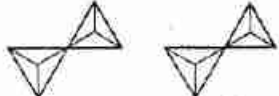
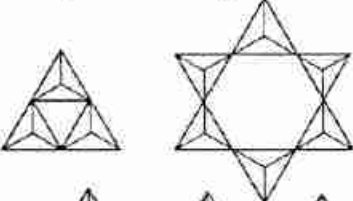
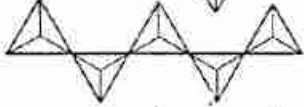
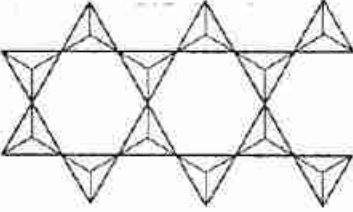
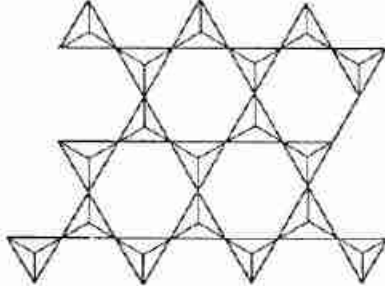
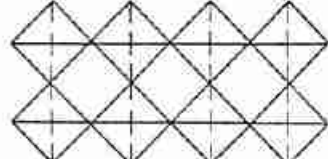
Muscovite		Al for Si, 1 in 4	Secondary valence + K linkage		250	5-20	Platy	$r = \frac{1}{10}d$ to $\frac{1}{20}d$
Vermiculite		Al, Fe, for Mg Al for Si	Secondary valence + Mg linkage	5-400	150	150	Platy	$d = 0.1$ to 2μ $r = \frac{1}{10}d$
Illite		Al for Si, 1 in 7 Mg, Fe for Al Fe, Al for Mg	Secondary valence + K linkage	80-100	150	25	Platy	$d = 0.1$ to 1μ $r = \frac{1}{10}d$
Montmorillonite		Mg for Al, 1 in 6	Secondary valence + exchangeable ion linkage	800	100	100	Platy	$d = 0.1$ to 1μ $r = \frac{1}{10}d$
Nontronite		Al for Si, 1 in 6	Secondary valence + exchangeable ion linkage	800	100	100	Lath	$d = 0.4$ to 2μ $r = \frac{1}{10}d$
Chlorite		Al for Si, Fe, Al for Mg	Secondary valence + brucite linkage	5-50	20	20	Platy	

Fig. 4.11 Sheet silicate minerals.

Table 4.2 The Silicate Structures

Structural Group	Diagrammatic Representation	No. Shared Oxygens per Silicon	Oxygen to Silicon Ratio	Si-O Unit and Charge	Example
Independent tetrahedrons		0	4:1	$(\text{SiO}_4)^{-4}$	Zircon ZrSiO_4
Double tetrahedrons		1	7:2	$(\text{Si}_2\text{O}_7)^{-3}$	Akermanite $\text{Ca}_2\text{Mg}(\text{Si}_2\text{O}_7)$
Rings		2	3:1	$(\text{SiO}_3)^{-2}$	Beryl $\text{Be}_3\text{Al}_2\text{Si}_6\text{O}_{18}$
Chains Single		2	3:1	$(\text{SiO}_3)^{-2}$	Enstatite MgSiO_3
Double		$2\frac{1}{2}$	11:4	$(\text{SiO}_3)^{-2}$ and $(\text{SiO}_2)^{-1}$	Tremolite $\text{Ca}_2\text{Mg}_5\text{Si}_8\text{O}_{22}(\text{OH})_2$
Sheets		3	5:2	$(\text{SiO}_2)^{-1}$	Pyrophyllite $\text{Al}_2\text{Si}_4\text{O}_{10}(\text{OH})_2$
Frameworks		4	2:1	$(\text{SiO}_2)^0$	Quartz SiO_2

and can change through weathering into clay minerals. Because they are very common rock-forming minerals, the frameworks, especially quartz and feldspars, are very abundant in soils. While these minerals sometimes occur in clay size particles, they are most common in silt size and larger. Because of the nature of their structure, particles of the framework minerals tend to exist in shapes that are approximately equidimensional.

4.3 SUMMARY OF MAIN POINTS

This chapter gives a very condensed and selected treatment of an extensive and complex body of knowledge. The significant points in this treatment are the following:

1. Soil particles range in size from very small to very large.
2. Generally, sand and silt particles are approximately equidimensional, but clay particles are plate-shaped or, less commonly, lath-shaped or rod-shaped.

3. Particle size, shape, and activity can be explained in terms of crystal chemistry of the particle.
4. Isomorphous substitution, common in the sheet minerals, tends to retard crystal growth and gives the crystal a net electrical charge.

PROBLEMS

4.1 Would you expect the sand shown in Fig. 4.3a to exhibit a particle size distribution dependent on the treatment given the sand prior to sieving? Why?

4.2 Would you disaggregate the sand (Fig. 4.3a) prior to sieving if the purpose of the particle size testing was an attempt to relate particle size and permeability? Why?

4.3 Draw the atomic structure of montmorillonite. [Hint. Alter the pyrophyllite structure (Fig. 4.9) in accordance with the isomorphous substitution noted in Fig. 4.11.]

4.4 Using Fig. 4.5 as a guide, classify the sands shown in Fig. 4.2 as to roundness.

CHAPTER 5

Normal Stress between Soil Particles

Chapter 4 considered soil particles as individual, isolated units. This chapter examines the interaction of adjacent soil particles; i.e., the stresses that develop between adjacent soil particles and the way in which these stresses affect the way that adjacent particles fit together. This presentation deals primarily with the normal stresses acting between small particles which are not in contact. Chapter 6 treats shear stresses and normal stresses between particles in contact with each other.

In a highly schematic way, the types of forces that exist between two adjacent soil particles are (see Fig. 5.1):

- F_m = the force where the contact is mineral-mineral
- F_a = the force where the contact is air-mineral or air-air
- F_w = the force where the contact is water-mineral or water-water
- R = the electrical repulsion between the particles
- A = the electrical attraction between the particles

5.1 THE ELECTRICAL CHARGE ON A SOIL PARTICLE

Every soil particle carries an electrical charge. This fact can readily be demonstrated by mixing a fine-grained soil with water in a beaker and then inserting at different locations in the beaker two electrodes which are components of an electrical circuit containing a battery and an ammeter. The ammeter will indicate that the electrical charge in the circuit is transmitted through the soil-water mixture. Although theoretically a soil particle can carry either a net negative or a net positive charge, only negative charges have been measured. This net electrical charge may arise from any one or a combination of the five following factors:

1. Isomorphous substitution.
2. Surface disassociation of hydroxyl ions.
3. Absence of cations in the crystal lattice.

4. Adsorption of anions.
5. Presence of organic matter.

Of these five possible causes the first—*isomorphous substitution*—is the most important.

In addition to a net charge, a soil particle can carry a distribution charge because the seat of the positive charge and the seat of the negative charge do not coincide. Similarly, the crystal bonding in a soil particle results in local charges.

Since the magnitude of the electrical charge is directly related to the particle surface area, the influence of this charge on the behavior of the particle relative to the influence of mass forces (i.e., the weight of the particle) will be directly related to the surface area per mass of

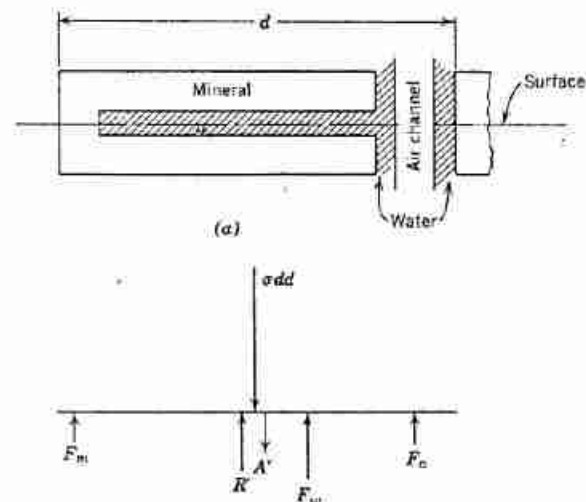


Fig. 5.1 Forces between particles. (a) Adjacent soil particles. (b) Forces across surface.

particles. The magnitude of the surface area per mass, *specific surface*,¹ is therefore a good indication of the relative influence of electrical forces on the behavior of the particle. The term *colloid* is used to describe a particle whose behavior is controlled by the surface-derived forces rather than mass-derived forces.

A clay particle is a colloid because of its small size and irregular shape. The smaller a particle size the larger its specific surface, as can be seen in Table 5.1. From this

Table 5.1

Length of Cube Side (cm)	Number of Particles	Total Volume (cm ³)	Total Surface Area (cm ²)	Surface Area ÷ Volume ($\frac{1}{\text{cm}}$)
1	1	1	6	6
1 μ = 10 ⁻⁴	10 ¹²	1	60,000	60,000
1 m μ = 10 ⁻⁷	10 ²¹	1	60,000,000	60,000,000

table we can see that the specific surface goes up directly as the particle size goes down. As a matter of fact, the surface area per volume of a cube is 6/L and of a sphere is 6/L.

The size range of colloids has been more or less arbitrarily set as 1 m μ to 1 μ , as noted in Fig. 4.1. Below 1 m μ lie the diameters of atoms and molecules. Most particles larger than approximately 1 μ are predominantly influenced by forces of mass. A specific surface of 25 m²/g has also been suggested as the lower limit of the colloidal range. The principles of colloidal chemistry are helpful in the understanding of clay behavior.

Particles silt size and larger have specific surface values of less than 1 m²/g, i.e., considerably smaller than the lower limit of the colloidal range. The "specific surface" column in Fig. 4.11 gives typical values of specific surface for clay particles. Note particularly the large difference in specific surface between kaolinite (10 to 20 m²/g) and montmorillonite (800 m²/g). The tremendous surface area of montmorillonite can be visualized when one realizes that 6 g of montmorillonite has approximately the same surface area as an entire football field—or only 12 g of montmorillonite would be needed to cover an entire football field (to cover the field requires 2 × 6 g since the area on both faces of the clay particles contribute to the specific surface).

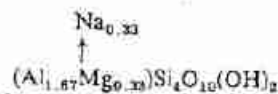


Fig. 5.2 Montmorillonite formula.

¹ Specific surface is sometimes defined as surface area per volume.

Unit Weight;

Al:	1.67 × 26.97 =	45.0
Mg:	0.33 × 24.32 =	8.0
Na:	0.33 × 23.0 =	7.6
Si:	4 × 28.06 =	112.4
O:	12 × 16.00 =	192.0
H:	2 × 1.00 =	2.0
	Total	367.0

Charge Deficiency = $\frac{1}{3}$ electrical equivalent per 367 gram-mol-weights.

$$= \frac{0.333}{367} = 0.091 \frac{\text{equivalents}}{100 \text{ grams}}$$

$$= 91 \text{ me}/100 \text{ g}$$

Fig. 5.3 Computation of net charge.

A soil particle in nature attracts ions to neutralize its net charge. Since these attracted ions are usually weakly held on the particle surface and can be readily replaced by other ions, they are termed *exchangeable ions*. The soil particle with its exchangeable ions is neutral.

As an illustration of the net charge on a soil particle, let us consider a montmorillonite crystal approximately 1000 Å in lateral dimension and one basic three-layer-unit thick. Figure 5.2 gives the structural formula for montmorillonite. The net negative charge of one-third of a unit charge is shown as being balanced by an exchangeable sodium. It is a common convention to represent the exchangeable ion as sodium in a structural formula, although any one or a combination of a large number of cations can exist in the exchangeable positions. Calcium is a very common exchangeable ion in soil.

Figure 5.3 shows the computation for the formula weight of montmorillonite. The formula weight of 367 g and the charge deficiency of one-third per formula can be expressed in terms of milliequivalents per 100 g of clay, abbreviated as me/100 g. The computation yields 91 me/100 g as the theoretical charge deficiency, or *ion exchange capacity*, of montmorillonite. The measured exchange capacity for montmorillonite is close to the theoretical value of 91.

We can also make theoretical calculations of the specific surface and the surface area per charge of a soil crystal. Figures 5.4 and 5.5 show these computations for a

$$\begin{aligned} \text{Surface area per unit} &= 92.6 \text{ \AA}^2 \\ \text{Volume per unit} &= \frac{92.6}{2} \text{ \AA}^2 \times 10 \text{ \AA} = 463 \text{ \AA}^3 \\ \text{Weight per unit} &= 463 \text{ \AA}^3 \times 10^{-24} \text{ cm}^3/\text{\AA}^3 \times 2.76 \text{ g/cm}^3 \\ &= 1278 \times 10^{-24} \text{ g} \\ \text{Surface area per gram} &= \frac{92.6 \text{ \AA}^2 \times 10^{-20} \text{ m}^2/\text{\AA}^2}{1278 \times 10^{-24} \text{ g}} \\ &= 725 \text{ m}^2/\text{g} \end{aligned}$$

Fig. 5.4 Computation of specific surface.

Charge deficiency = $\frac{1}{2}$ per 2 cations in gibbsite
 \therefore Charge deficiency = $\frac{2}{4}$ per 4 cations—i.e., unit in Fig. 4.9
 Surface area for unit is:

$$2(\text{top and bottom surfaces}) \times 8.9 \text{ \AA} \times 5.2 \text{ \AA} = 92.6 \text{ \AA}^2$$

(8.9 and 5.2 are dimensions of unit as determined from atomic structure)

Surface area per unit charge deficiency:

$$92.6 \text{ \AA}^2 \times \frac{2}{1} = 139 \text{ \AA}^2$$

Thus one net charge per surface area of 139 \AA^2

Fig. 5.5 Computation of surface area per charge.

montmorillonite unit with four cations in the gibbsite sheet. The computed value of $725 \text{ m}^3/\text{g}$ is close to the experimental value given in Fig. 4.11 of $800 \text{ m}^3/\text{g}$. (The value of $800 \text{ m}^3/\text{g}$ was obtained from a laboratory test in which the mineral was permitted to adsorb a monomolecular thickness of adsorbate.) The value of net charge per surface area, given in units of $1/\text{\AA}^2$, is the "charge density" of the mineral. The theoretical value of 139 from Fig. 5.5 compares well with the measured value (133) given in Fig. 4.11.

5.2 PARTICLE WITH WATER AND IONS

Let us now consider the nature of a soil particle in water since this is the state in which the civil engineer is nearly always interested. To give perspective to this consideration two typical clay particles will be employed. Figure 5.6a shows a typical particle of montmorillonite, which is one of the smallest and most water sensitive minerals encountered in clay; Fig. 5.6b shows a typical kaolinite particle, one of the larger and less water sensitive minerals encountered in clay. Figure 5.7 shows a portion of the lateral surface of each of these clay particles with the sites of the exchangeable ions.

The two typical clay particles contain about 14,000 exchangeable monovalent ions on the montmorillonite and 4,000,000 monovalent ions per kaolinite particle. Figure 5.8 shows the computation of the number of

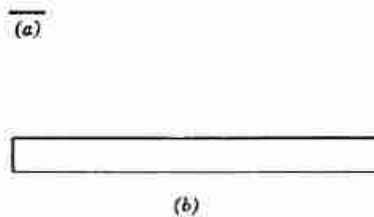


Fig. 5.6 Typical clay particles. (a) Montmorillonite, 1000 \AA by 10 \AA thick. (b) Kaolinite, $10,000 \text{ \AA}$ by 1000 \AA thick.

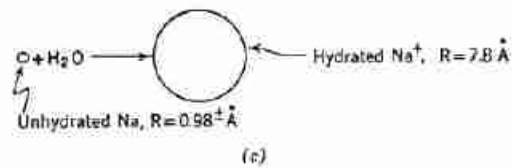
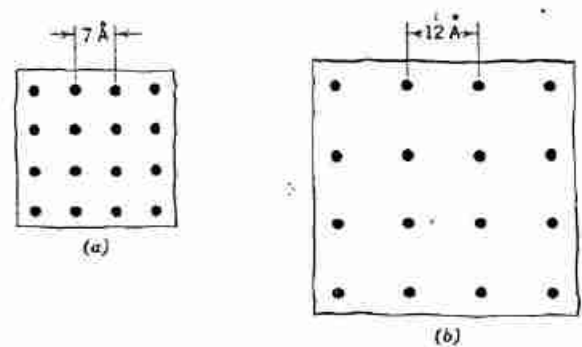


Fig. 5.7 Soil surface with exchangeable ions. (a) Surface of dry kaolinite + sodium ions. (b) Surface of dry montmorillonite + sodium ions. (c) Hydration of sodium ion.

charge deficiencies or sites for monovalent exchangeable ions on the montmorillonite particle. In this discussion, sodium has been chosen as the exchangeable ion for illustrative purposes. Thus the montmorillonite particle in Fig. 5.6 would carry 14,000 sodium ions and the kaolinite particle 4,000,000 sodium ions.

If the individual clay particles are now dropped into water, both the mineral surfaces and the exchangeable ions pick up water, i.e., hydrate. Upon hydration, the sodium ion grows about sevenfold, as is illustrated in Fig. 5.7. As the scaled drawings indicate, the hydrated sodium ions are too large to fit into a monoionic layer on the mineral particles even if they wanted to. Actually, the exchangeable ions with their shells of water move away from the mineral surfaces to positions of equilibrium. The ions are attracted to the mineral surface to satisfy the negative charge existing within the surface; they also desire to move away from each other because of their thermal energies; the actual positions they occupy are compromises between these two types of forces. Thus,

For montmorillonite particle $0.1 \mu \times 0.1 \mu \times 10 \text{ \AA}$
 Surface area of particle:

$$1000 \text{ \AA} \times 1000 \text{ \AA} \times 2 = 2 \times 10^6 \text{ \AA}^2$$

Number of charge deficiencies:

$$2 \times 10^6 \text{ \AA}^2 \times \frac{1 \text{ charge}}{139 \text{ \AA}^2} = 14,400$$

Fig. 5.8 Number of charges on montmorillonite particle.

when the individual particles are dropped into water the ions move away from the surface to form what is termed the *double layer*.² In Fig. 5.9 the clay particles are shown with the fully developed double layers they would have in pure water. Figure 5.10 shows in three dimensions the same surface sections presented in Fig. 5.7. From Fig. 5.10, we can get some idea of the approximate spacings of the hydrated ions in the double layer. These spacings represent a maximum since the pore fluid in this case is distilled water. Figure 5.11 shows the double layers of the sodium kaolinite particle and the sodium montmorillonite particle to the same scale as in Fig. 5.10. In Fig. 5.11a the ions around our selected surface sections are shown as point charges. Figure 5.11b shows plots of the concentration of sodium ions versus distance from the particle surface. At a distance of approximately 400 Å, which is the thickness of the double layer, the concentration of sodium ions has become equal to that in the "pore" or "free" water. In Fig. 5.11c plots of electrical potential versus distance from the surface are shown. Electrical potential is the work required to move a unit charge from infinity to the point in question and is negative for clay surfaces. The double-layer thickness is thus the distance from the surface required to neutralize the net charge on the particle, i.e., the distance over which there is an electrical potential.

The water in the double layer is under an attractive force to the soil particle since this water is attached to the exchangeable ions which are in turn attracted to the soil surface. Water is also attracted to the mineral surface by other forces (the force between the polar water and the stray electrical charges on the mineral surface,

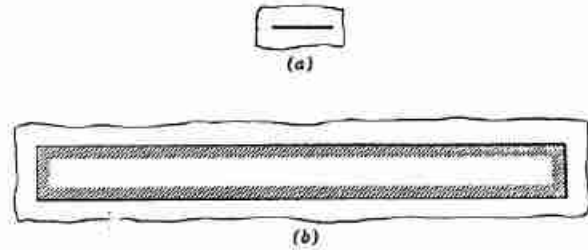


Fig. 5.9 Soil particles with water and ions. (a) Sodium montmorillonite. (b) Sodium kaolinite.

hydrogen bonding, and van der Waals forces). Although there is controversy as to the exact nature of the water immediately next to the mineral surface, it is generally recognized that at least the first few molecular layers of water around the soil particle are strongly attracted to the particle.

In order to illustrate the importance of this adsorbed or attracted water, let us calculate for typical soil particles the water content corresponding to a 5 Å layer (about two water molecules thick).

Table 5.2, which is highly approximate and intended only to show trends, illustrates the great importance of particle size on the amount of water which can be bound to a particle. To illustrate the significance of these results

Table 5.2

Particle	Specific Surface (m ² /g)	Water Content ^a (for 5 Å layer) (%)
0.1 mm sand	0.03	1.5 × 10 ⁻⁴
Kaolinite	10	0.5
Illite	100	5
Montmorillonite	1000	50

^a The water content was calculated as:

$$\text{Water content} = (\text{specific surface}) \times (\text{thickness of layer of water}) \times (\text{unit weight of water})$$

For kaolinite,

$$\text{Water content} = (10 \text{ m}^2/\text{g}) \times (5 \times 10^{-10} \text{ m}) \times (10^6 \text{ g/m}^3) = 5 \times 10^{-3} \text{ or } 0.5\%$$

² The Gouy Chapman double layer theory can be used to calculate the distribution of ions in the double layer (Verwey and Overbeek, 1948).

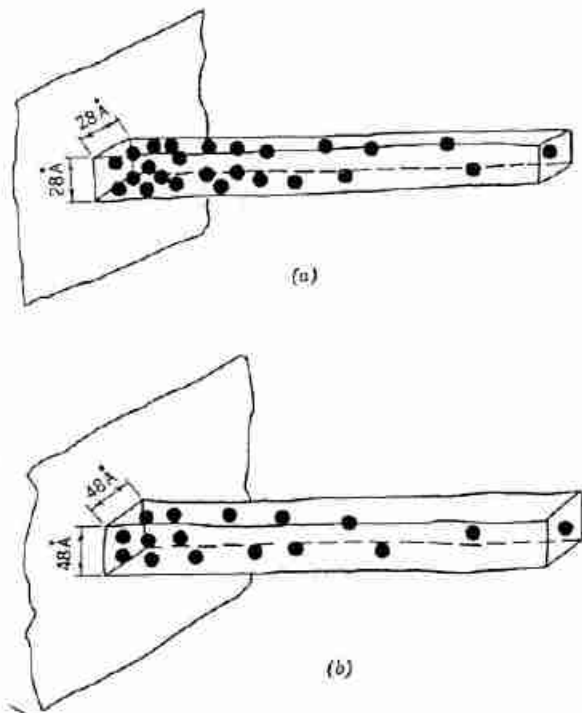


Fig. 5.10 Particle surfaces with water and ions. (a) Sodium kaolinite. (b) Sodium montmorillonite.

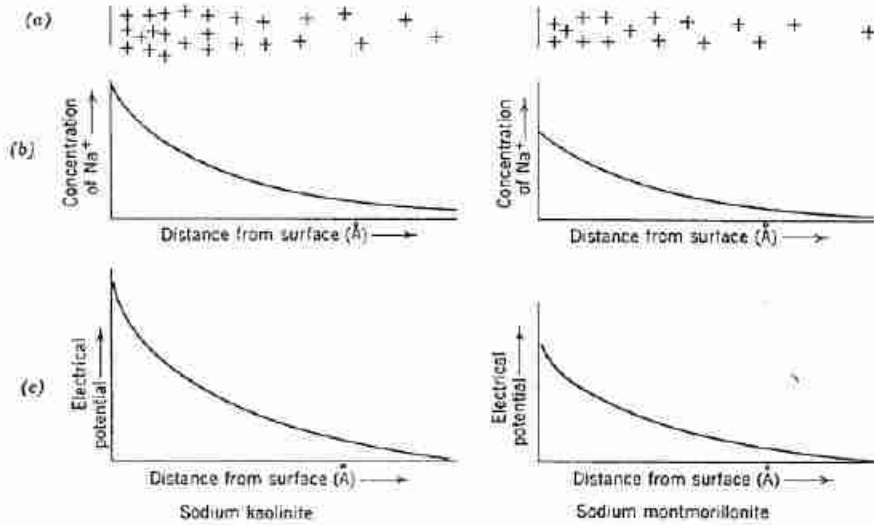


Fig. 5.11. Particles with double layers.

a typical illitic clay in nature may have a water content of 50%. From our calculation, we see that almost all of this water is "free"; i.e., not strongly attracted to the mineral skeleton and thus really constituting a separate phase. On the other hand, in many highly montmorillonitic clays, it may be quite difficult to separate the mineral and pore phases.

There are certain soil minerals that have the ability to immobilize a relatively large amount of water. The most common such mineral is halloysite, which has a crystal structure similar to kaolinite, as indicated in Fig. 4.11. Because of the ability of halloysite to adsorb water between the sheets, soils containing this mineral can exist at a high water content and a low density. Clays containing halloysite have successfully been used for dam cores even though they showed compacted dry densities of 50-60 lb/ft³ (half of that for normal clays) and water contents of 30-50% (two or more times the usual compaction water content for clay). Several examples of this unusual behavior are given by Lambe and Martin (1953-1957).

In the preceding discussion, sodium has been selected as the exchangeable ion. The ions adsorbed on soil particles can readily be exchanged, as illustrated in the

symbolic reaction shown in Fig. 5.12. The addition of calcium chloride to a soil-water system results in the replacement of sodium by calcium. The nature of the exchangeable ion on the soil particle has an important influence on the behavior of the soil system. Note from Table 3.4, for example, how much the Atterberg limits of clay can depend on the nature of the exchangeable ion.

A reaction, such as that shown in Fig. 5.12, results in a depression of the double layer around the soil particle, i.e., the thickness of the ion-water layer around the soil particle reduces. This reduction of particle double layer results in a change of the properties of a mass of particles. There are general principles that control the rate and direction of exchange reactions. These principles involve the valence of the exchanged cations, concentration of cations, etc.

5.3 THE FORCES R' AND A'

If we take two clay particles in water which are far apart and then bring them toward each other, they will reach an interparticle spacing at which they begin to exert forces on each other. Since each particle carries a net negative charge, the two particles repel each other

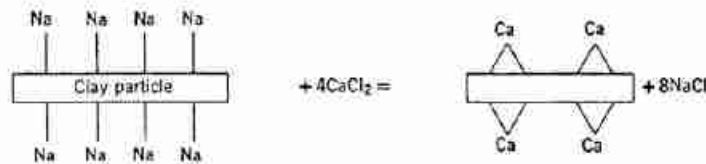


Fig. 5.12 Ion exchange reaction.

because of the Coulombic electrical force between like charges. This is the force R' . This repulsion of the approaching clay particles is like that between two bar magnets when the negative poles are pushed toward each other (or the positive poles are pushed toward each other).

Since the negative charge on a clay particle is balanced by the cations in the double layer, the two advancing particles begin to repel each other when their double layers come into contact with one another. The repulsive force between the adjacent particles for any given spacing is therefore directly related to the sizes of the double layers on the two particles, and any change in the characteristics of the soil-water system that reduces the thickness of the double layers reduces this repulsive force for the same interparticle spacing. Figure 5.13 illustrates the influences of various characteristics of the system on the electrical potential ψ , and therefore R' , at any given distance x from the particle surface.

In addition to a repulsive force between the approaching clay particles, there is also a component of attractive force A' between the two particles. This attractive force is the van der Waals' force, or secondary bonding force, which acts between all adjacent pieces of matter. This attractive force between the clay particles is essentially independent of the characteristics of the fluid between the particles.

At this stage, it is convenient to distinguish two cases: (a) the case where the total force between particles is very small, i.e., equivalent to the weight of soil contained in an ordinary beaker; and (b) the case where the total force is equivalent to the weight of a building or to the weight of ten or more feet of overburden.

The first case is encountered as a sedimentary soil is first formed, and a study of this case leads to an understanding of how particles may be arranged within a sedimentary soil. This case is studied in Section 5.4. It suffices to consider R' and A' only in qualitative terms.

The second case is typical of that encountered in engineering practice, and a study of this case (see Section 5.5) leads to an understanding of just how forces are transmitted between particles. In this study it will be necessary to treat R' and A' in quantitative terms.

5.4 FLOCCULATION AND DISPERSION

If the net effect of the attractive and repulsive forces between the two clay particles is attractive, the two particles will tend to move toward each other and become attached—*flocculate*. If the net influence is repulsive they tend to move away—*disperse*. Since the repulsive force component is highly dependent on the characteristics of the system and the attractive component of force is not strongly influenced by the characteristics of the system, a tendency toward flocculation or dispersion may be caused by an alteration in the system characteristics,

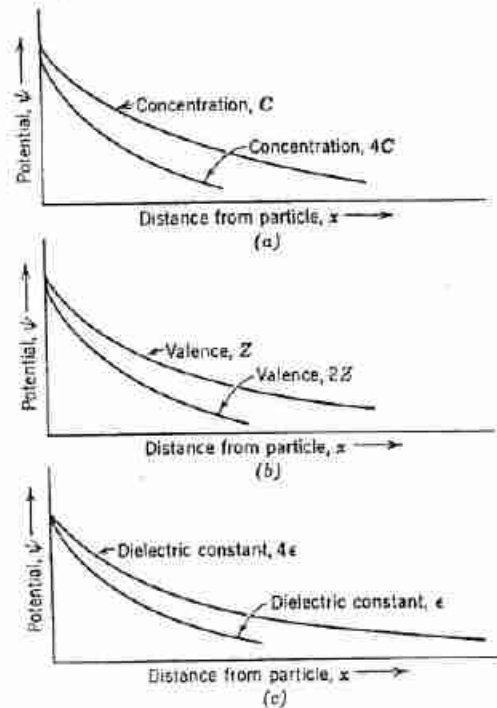


Fig. 5.13 The effects of changes in system properties on double layers: (a) Concentration only variable. (b) Valence only variable. (c) Dielectric constant only variable.

which alters the double-layer thickness. A tendency toward flocculation is usually caused by increasing one or more of the following:

- Electrolyte concentration
- Ion valence
- Temperature

or decreasing one or more of the following:

- Dielectric constant
- Size of hydrated ion
- pH
- Anion adsorption

Most of the effects of varying the characteristics of the soil-water system on the tendency toward flocculation or dispersion can be demonstrated with a soil-water suspension in a test tube. In each demonstration the same weight of soil particles is employed. These are illustrated in Fig. 5.14.

The two types of interparticle forces discussed so far have two important characteristics:

1. They originate from within the mineral crystal.
2. They can act over relatively large distances, i.e., several hundred angstroms.

These are the only two types of forces considered by colloidal theories. There is convincing evidence that there

are other electrical forces which can become very important when the spacing between clay particles decreases to very small distances such as are typical in the deposit with which the civil engineer usually works. The most important force not considered by the colloidal theories is that arising from the net positive charge at the edges of the soil particles. This net charge is small relative to the net

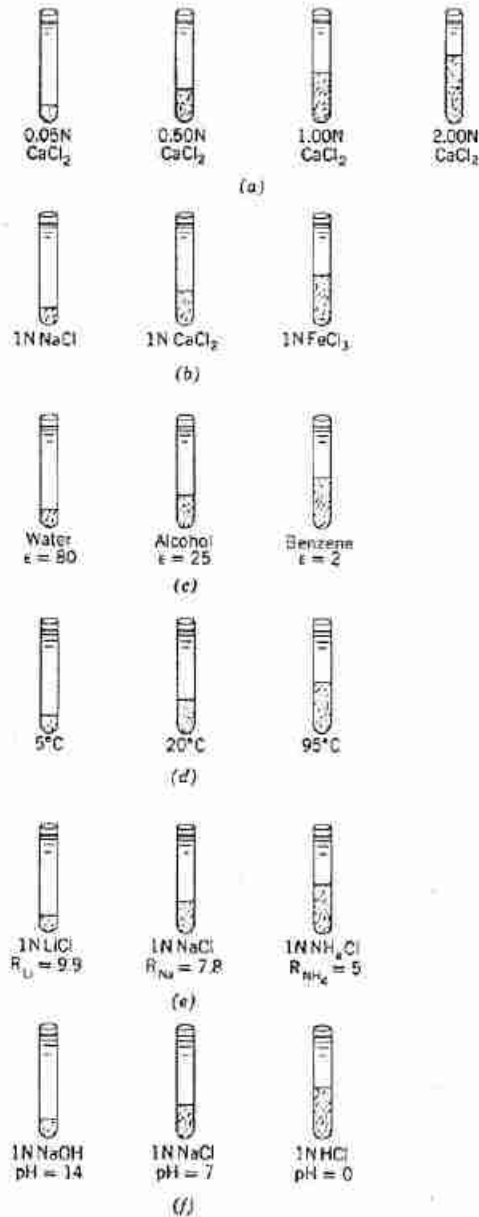


Fig. 5.14 Effects of system characteristics on soil sediment. (a) Effect of electrolyte concentration. (b) Effect of ion valence. (c) Effect of dielectric constant. (d) Effect of temperature. (e) Effect of size of hydrated ion. (f) Effect of pH. Each tube has same concentration of soil in liquid.

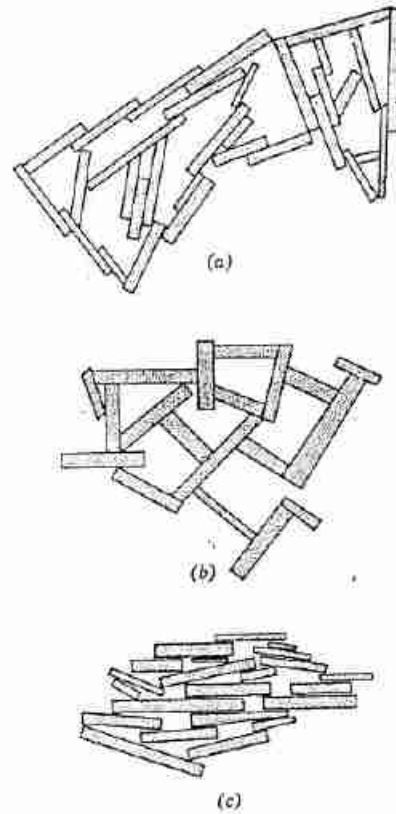


Fig. 5.15 Sediment structures. (a) Salt flocculation. (b) Nonsalt flocculation. (c) Dispersion.

negative charge on the particle arising from isomorphous substitution and thus plays a minor role when adjacent particles are hundreds of angstroms apart. When, however, the particles are very close together, this edge charge can participate in an edge-to-face linkage between particles of an electrostatic type.

In the demonstrations illustrated in Fig. 5.14, the flocculated sediments consisted of particles attracted to one another to form loose arrays. The particles in the sediment which repelled each other could stack in efficient arrays much like playing cards in a deck. Figure 5.15 illustrates particle arrangements in the soil sediments. Where there is salt-type flocculation (that treated by the colloidal theories), there is a measurable degree of parallelism between adjacent particles since the attraction between the particles is of the secondary valence type. In the edge-to-face or nonsalt-type flocculation, the particles tend to be perpendicular to each other since the attraction is an electrostatic one between the edge of one particle and the face of another. As shown in Fig. 5.15c, the dispersed sediment tends to have particles that are in a parallel array.

5.5 THE TRANSMISSION OF FORCE THROUGH SOIL

Figure 5.16 shows two parallel platens to which a normal force of 14.7 lb is applied. Each platen is square, 1 in. on a side, thus having an area of 1 in.². The normal stress between the two platens is the total force 14.7 divided by the area of 1 in.² and thus equals 14.7 lb/in.².

Each platen is now coated with a layer of wet sodium montmorillonite particles oriented parallel to the platens. For a system of parallel sodium montmorillonite particles Bolt (1956) obtained experimentally the curve of spacing versus stress shown in Fig. 5.16b. Since the parallel clay particles cover essentially all of the area of the platens facing each other, the stress between particles is 14.7 lb/in.² and, from Bolt's data, are at a spacing of about 115 Å. In other words, the stress carried by the clay particles is essentially the same as that carried by the platens. Further, the particle spacing and interparticle stress are related such that the greater the stress between the particles the smaller the spacing. A stress of about 80,000 lb/in.² is required to force the two montmorillonite particles into mineral-mineral contact, thereby squeezing out the adsorbed water between them.

Next the platens are coated with sand particles, as shown in Fig. 5.16c. Each particle has a diameter of approximately 0.06 mm. For such a parallel array of particles between the platens, the stress at points of contact between the sand particles is equal to the force divided by the actual contact area. Measurements of this contact area show that typically it is approximately 0.03% of the total area. Thus contact stress is equal to 14.7 divided by 0.0003 in.², which equals approximately 49,000 lb/in.². This contact stress is high enough to extrude the adsorbed water.

The example in Fig. 5.16 illustrates the fact that normal stress can be transmitted through a highly dispersed clay system by long-range electrical stresses, and there is no direct mineral-mineral contact between the particles. On the other hand, in a flocculated soil, such as that shown in Fig. 5.15a or 5.15b, the particles are effectively in mineral-mineral contact and the normal stresses are transmitted in a fashion similar to that for the sand system shown in Fig. 5.16c.

The particles in a natural soil are not the same size and shape as the colloidal theories assume. Nearly all natural soils contain particles of many shapes and many sizes, and almost all soils contain particles of different compositions and impurities. Silt-sized particles occur in most natural clays and these nonplate-shaped particles affect the arrangements of the plate-shaped particles. Moreover, even the plate-shaped clay particles do not in general have perfectly smooth surfaces. For example, irregularities can be seen on the surface of the kaolinite particle shown in Fig. 4.4a. Such irregularities may be 100 Å high, which

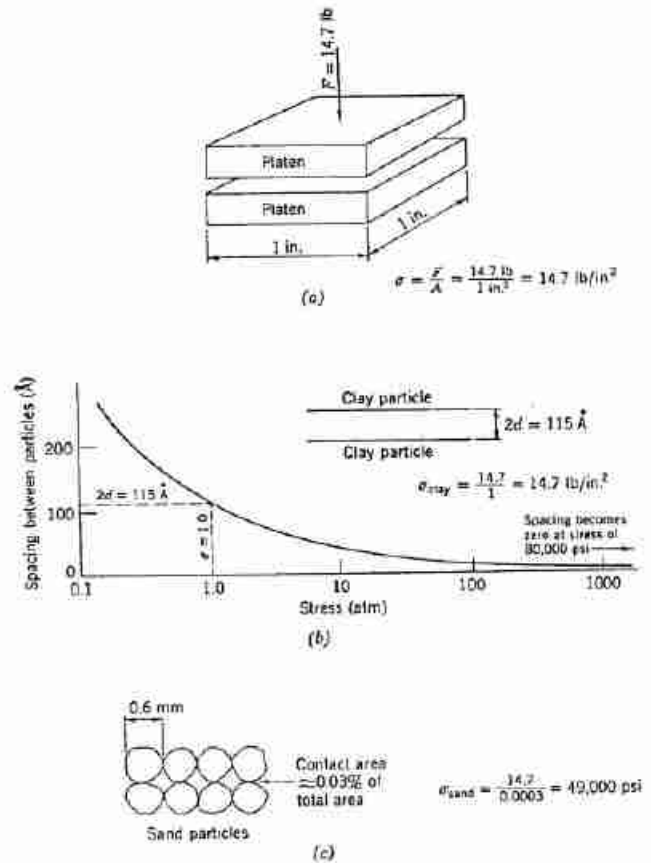


Fig. 5.16 Stress transmission through soil.

is equal to the distance over which significant long-range electrical forces can act.

Thus the mechanism of stress transmission between soil particles in natural clays must lie between the extreme situations of equidimensional particles and of parallel clay particles. The behavior in general is nearer to that of soils with equidimensional particles.

Because of these difficulties, and because the theories neglect certain forces which probably are important when the particle spacing is less than 100 Å, the principles of colloidal chemistry have been of very little quantitative help in the study of clay behavior. The colloidal principles are, however, very useful to the civil engineer in helping to give an understanding of the fundamental behavior of fine-grained soils.

5.6 SUMMARY OF MAIN POINTS

1. Every soil particle carries an electrical charge on its surface and therefore attracts ions to this surface in order to achieve overall electrical neutrality.
2. These ions in turn attract molecules of water and, in addition, water is attracted directly to the surfaces

of soil particles. Hence all soil particles tend to be surrounded by a layer of water.

3. Forces of attraction and repulsion act between all soil particles, but again are more important (with respect to the weight of the particles) in fine-grained soils. These forces affect the way in which particles are arranged during sedimentation and can cause fine-grained soils to have a very open mineral skeleton of low unit weight.
4. Factors such as temperature and ion concentration in the pore water have an influence on the forces of attraction and repulsion between particles, and hence the environment of deposition can have an influence on the way that the particles are arranged during deposition.
5. In soils composed of equidimensional particles, stress is transmitted through the soil by means of mineral-mineral contact forces. In soils composed solely of small clay platelets oriented face-to-face, stress is transmitted through long-range electrical stresses, and particles may be separated by distances of 100 \AA or even more. Stress transmission through

natural clay soils lies between these extreme situations.

PROBLEMS

5.1 Estimate the specific surface in units of square meters per gram for the sand in Fig. 4.2a. Take the specific gravity equal to 2.65.

5.2 Compute the ion exchange capacity in units of me/100 g for kaolinite having isomorphous substitution of one Al for every four hundredth Si.

5.3 For the kaolinite particle shown in Fig. 4.4a compute:

- a. The total surface area.
- b. The specific surface in m^2/g .
- c. The surface area (in \AA^2) per unit charge from isomorphous substitution.
- d. The number of sodium ions required to satisfy the ion exchange computed in Problem 5.2.

The specific gravity of kaolinite is 2.62.

5.4 If calcium chloride were added to the wet clay in Fig. 5.16b, would the platens move together or apart? Why?

5.5 If the contact stress required to crush quartz is 1,000,000 psi, what force would have to be applied to the platens in Fig. 5.16c to crush quartz sand?

CHAPTER 6

Shear Resistance between Soil Particles

This chapter considers the fundamental nature of shear resistance between soil particles. Section 6.1 discusses the mechanism of shear resistance in general terms and indicates its typical magnitude. Sections 6.2 to 6.5 present a more detailed treatment for those who wish to delve more deeply into the subject.

6.1 GENERAL DISCUSSION OF SHEAR RESISTANCE BETWEEN PARTICLES

Chapter 2 stated that relative sliding between particles is the most important mechanism of deformation within a soil mass. Hence the resistance of soil to deformation is influenced strongly by the shear resistance at contacts between particles. A knowledge of the possible magnitude of this shear resistance, and of the factors that influence this resistance, is basic to the mastery of soil mechanics.

It must be emphasized that the shear resistance between mineral surfaces is only part of the resistance of a soil mass to shear or compression. Also very important is the interlocking of particles, which is largely a function of packing density. Interlocking is treated in Part III. The fundamental considerations of this chapter, however, apply no matter how the particles are packed.

Mechanism of Shear Resistance

The shear resistance between two particles is the force that must be applied to cause a relative movement between the particles. The source of the shear resistance is the attractive forces that act among the surface atoms of the particles. These attractive forces lead to chemical bond formation at points of contact of the surfaces. Thus the frictional resistance between two particles is fundamentally of the same nature as the shear resistance of a block of solid, intact material such as steel.

The strength and the number of bonds that form at the interface between two particles are influenced very much by the physical and chemical nature of the surfaces of the

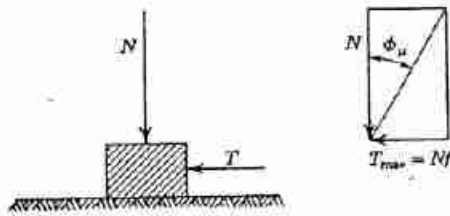
particles. Hence an understanding of the magnitude of the shear resistance between particles involves an understanding of the factors that influence the interaction between the two surfaces at their points of contact. A detailed explanation of this interaction effect is presented in the later sections of this chapter. However, we can summarize the interaction effect by saying that the total shear resistance (the product of the strength of each bond and the total number of bonds) is proportional to the normal force that is pushing the two particles together. If this normal force decreases, either the strength or the number of bonds decreases, and thus the total shear resistance decreases. Hence we say that interparticle shear resistance is *frictional* in nature.

There are some situations in which part of the total shear resistance between particles is independent of the normal force pushing the particles together; i.e., even if the normal force is decreased to zero there is still a measurable shear resistance. In such cases, we say that there is *true cohesion* between particles. True cohesion can develop between soil particles that have remained in stationary contact over a long period of time. In some cases this true cohesion can be very important, as when cementation turns sand into sandstone. Generally, however, the magnitude of true cohesion between particles is very small, and its contribution to the strength of a soil is also very small. Later chapters of this book will discuss a few of the situations in which true cohesion between particles is important. The reader should regard frictional behavior as the normal situation for soils and cohesive behavior as the exception.

Two alternative ways of expressing frictional resistance are in common use. The first is to use the coefficient of friction f . Thus, if N is the normal force across a surface, the maximum shear force on this surface is $T_{\max} = Nf$. The second is to use a friction angle ϕ_μ defined such that

$$\tan \phi_\mu = f$$

The geometric interpretation of ϕ_μ is shown in Fig. 6.1.

Fig. 6.1 Definition of friction angle ϕ_μ .

6.2 FUNDAMENTALS OF FRICTIONAL BEHAVIOR

Basic Laws of Friction

There are two basic laws of frictional behavior:

1. The shear resistance between two bodies is proportional to the normal force between the bodies.
2. The shear resistance between two bodies is independent of the dimensions of the two bodies.

The second law can be illustrated by pulling a brick over a flat surface. The pulling force will be the same whether the brick rests on a face or on an edge.

As is the case with many of the "laws" of science, the "laws of friction" merely state the result of many empirical observations. Exceptions to these rules are easy to find. Nevertheless, they remain a good starting point for understanding frictional behavior. These laws were first stated by Leonardo da Vinci in the late 1400s, largely forgotten, and then rediscovered by the French engineer Amontons in 1699. They are often called Amontons' laws.

Mechanism of Friction

The basic explanation of the friction process is embodied in the following statements:

1. On a submicroscopic scale most surfaces (even carefully polished ones) are actually rough, hence two solids will be in contact only where the high points (termed *asperities*) touch one another; i.e., actual contact is a very small fraction of the apparent contact area (see Fig. 6.2).
2. Because contact occurs at discrete sites, the normal stresses across these contacts will be extremely high and even under light loading will reach the yield strength of the material at these sites. Thus the actual area of contact A_c will be

$$A_c = \frac{N}{q_u} \quad (6.1)$$

where N is the normal load and q_u is the normal stress required to cause yielding (i.e., plastic flow). Since q_u is fixed in magnitude, an increase in total

normal load between the bodies must mean a proportional increase in the area of actual contact. This increase is a result of plastic flow of the asperities.

3. The high contact stresses cause the two surfaces to adhere at the points of actual contact; i.e., the two bodies are joined by chemical bonds. Shear resistance is provided by the adhesive strength of these points. Thus the maximum possible shear force T_{max} is

$$T_{max} = sA_c \quad (6.2)$$

where s is the shear strength of the adhered junctions and A_c is the actual area of contact.¹ For the moment, we will not say whether or not s is equal to the shear strength s_m of the material composing the particles.

Combining these ideas leads to the relation

$$T_{max} = N \frac{s}{q_u} \quad (6.3)$$

Since s and q_u are material properties, T_{max} is proportional to N . The friction factor f should equal the ratio s/q_u .

Terzaghi (1925) stated this hypothesis in his pioneering book on soil mechanics,² but his ideas on this subject were overlooked for many years. The hypothesis was independently stated and shown to describe the frictional behavior of a wide variety of materials by Bowden, Tabor, and their colleagues starting in the late 1930s [see, for example, Bowden and Tabor (1950) and (1964)]. It is called the Adhesion Theory of Friction and now serves as the starting point for essentially all friction studies. The following paragraphs will discuss its applicability to the friction of soil minerals.

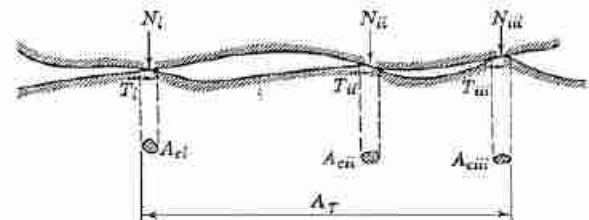


Fig. 6.2 Microscopic view of frictional resistance.

$$\begin{aligned} N &= \sum N_i = \sum A_{ci} q_u \\ T &= \sum T_i = \sum A_{ci} \tau_m \\ \mu &= \frac{T}{N} = \frac{\tau_m}{q_u} \end{aligned}$$

¹ A_c is the area of mineral-mineral contact. The term A_m is also used for this area.

² An English version of this section of *Erdbaumechanik* is in Terzaghi (1960).

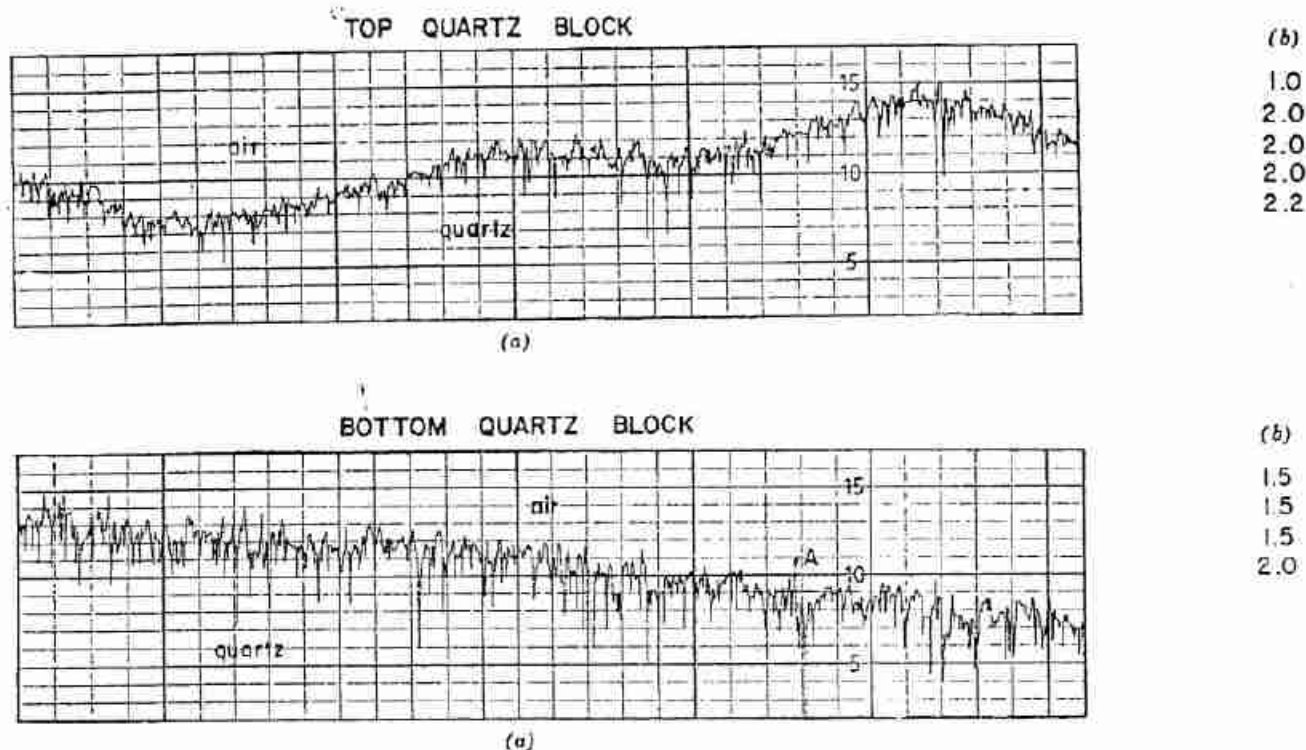


Fig. 6.3 Profile of "smooth" quartz surfaces. (a) Surface traces. Scale: vertical, 1 division = 2×10^{-3} in.; horizontal, 1 division = 2×10^{-3} in. (b) Center line average roughness in 10^{-6} in. (From Dickey, 1966.)

Surface Roughness

Various techniques can be used to measure the roughness of a surface. For example, a sharp diamond stylus, called a "profilometer", may be slid across the surface and measurements made of the up and down movement of the stylus. Figure 6.3 shows the trace made by such an instrument as it moved across two "smooth" quartz surfaces (Dickey, 1966). The surfaces had been ground with a very fine diamond wheel (600 grit) and appeared to be mirror smooth. However, the profilometer shows the surfaces to be composed of peaks and valleys having an average height of $2 \mu\text{in.}$ (about 500 \AA).

It should be noted that the horizontal sensitivity of the profilometer is 1000 times less than the vertical and therefore the asperities were not really jagged, as the trace seems to indicate. Rather, they were very flat, as shown in Fig. 6.4, which is a true-scale drawing of one of the asperities. Figure 6.4 also shows a typical asperity from a "rough" quartz surface, prepared by grinding with a No. 220 grit diamond wheel. The average roughness of this surface was about $20 \mu\text{in.}$ The asperities were sharper than for the smooth surface, but they were still quite gentle, having an average included angle of about 120° . Both of these surfaces are probably smoother than the surfaces of most granular soil particles.

Magnitude of Contact Stress

When two surfaces are brought into contact they will be supported initially on the summits of the highest asperities. As the normal load is increased, the "bearing capacity" of the contacting asperities will be exceeded and they will deform plastically. The magnitude of stress required to cause plastic flow is termed q_0 . It can be determined by indentation hardness measurements.³

For quartz, with a hardness of about 1100 kg/mm^2 (Brace, 1963), the stress on an asperity must exceed $1,500,000 \text{ psi}$ to produce plastic deformation. Whether or not this stress is reached for a significant number of asperities in a granular soil mass is not known, but it seems likely that it is. If q_0 is not reached, the asperities deform *elastically*, and then the behavior becomes quite different. According to the Hertz contact theory (see Bowden and Tabor, 1964) the contact area A_0 increases as $N^{2/3}$. Thus the coefficient of friction will probably *decrease* with increasing load. Such behavior has been

³ Indentation hardness is measured by pushing a suitably shaped indenter into a flat test surface. The high confining stresses that develop around the tip of the indenter inhibit brittle fracture in a material such as quartz. The analogy between this test and the asperity contacts between two surfaces is evident. The indentation hardness is defined as the normal load on the indenter divided by the residual deformed area after the indenter is removed.

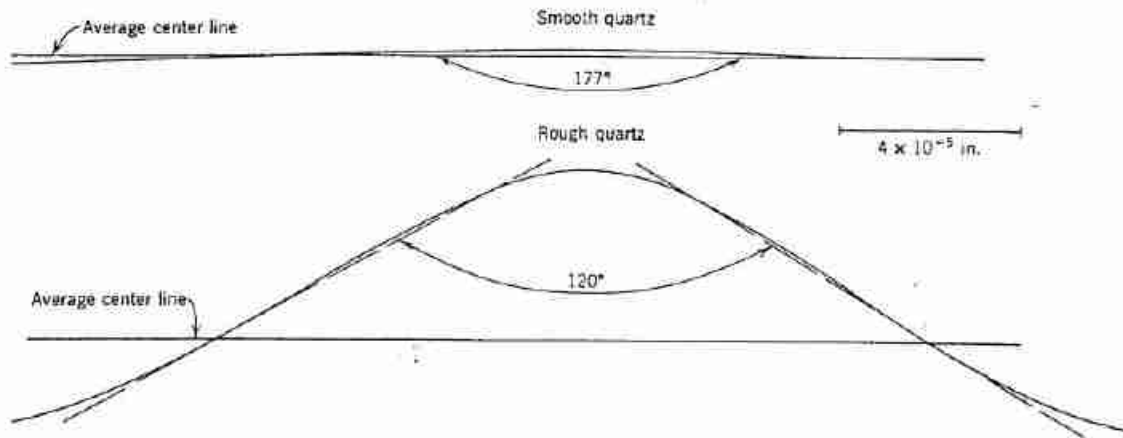


Fig. 6.4 Typical asperities on quartz surfaces.

observed for a diamond stylus on a flat diamond plate. Diamond is elastic even under the very large stresses developed at asperity contacts (q_u for diamond is estimated to be greater than 15,000,000 psi). However, the complex contact conditions between two surfaces that have a very large number of asperities *can* lead to a nearly constant value of f even though the individual asperities are deforming elastically (e.g., see Archard, 1957).

Shear Resistance at Points of Contact

In Chapter 5 it was pointed out that water and other materials are attracted to the surfaces of minerals, where they are adsorbed and act as a contaminating layer. When two such contaminated surfaces are put together, the amount of actual solid-to-solid contact will be influenced by the type and amount of adsorbed material, as shown in Fig. 6.5.

The most important influence of the surface contaminants is to make the junctions weaker in shear than is the bulk solid. If the surface contaminants are removed, e.g., by heating the surfaces in a high vacuum chamber, the shear strength of the junctions approaches that of the bulk solid. This causes the coefficient of friction to increase. Under these conditions, ductile metals undergo a process known as junction growth, whereby the contacting asperities undergo large-scale plastic deformations. This leads to the phenomenon known as cold welding, which produces extremely high coefficients of friction ($f \gg 1$). Minerals and other brittle materials do not exhibit the large-scale plastic flow under shear stresses that is required for junction growth and hence do not cold-weld.

Effect of Surface Roughness

The Adhesion Theory implies that friction is independent of surface roughness. For metals this is found to be

the case over a wide range of surface finishes. However, as surfaces become very rough, asperity interlocking may increase the value of f . It is difficult to define exactly what is "very rough". The frosted appearance of most granular soil particles indicates that they are rough. Electron photomicrographs indicate that many sheet

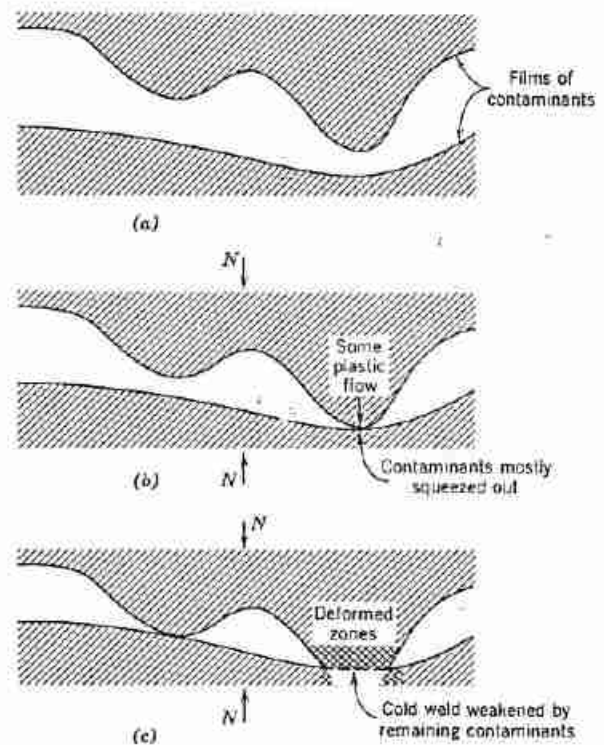


Fig. 6.5 The development of junctions. (a) Unloaded condition. (b) Light normal load. (c) Increased normal load; plastic flow at contact with constant normal stress.

minerals, on the other hand, have "supersmooth" surfaces. By assuming an average slope of angle θ for the asperities, the effect of surface roughness on the value of f can be estimated (see Problem 6.4).

Because the contact situation between two real surfaces is so complex, generally it is not possible to determine a value of θ to use for predicting f . Hence the relationship between friction and surface roughness must be determined experimentally.

Static Versus Kinetic Friction

The shear force required to initiate sliding between two surfaces is often greater than the force required to maintain motion (see Fig. 6.6a). That is, the static friction exceeds the kinetic (sliding) friction. This behavior is usually explained by assuming that bond formation at the junctions is time-dependent, either because creep causes gradual increases in the contact area or because the surface contaminants are gradually squeezed out from within the junction.

The difference between the static and the kinetic friction often leads to the phenomenon known as *stick-slip* (Fig. 6.6b). When sliding begins, part of the stored elastic energy in the loading mechanism is released, accelerating the slider and causing the measured shear force to drop below that required to maintain motion. The slider then stops and the shear force must be increased to the value associated with the static friction to induce sliding again. When sliding begins the whole procedure of intermittent motion is repeated. Under these conditions, one cannot determine accurately the value of the kinetic coefficient of friction.

Rolling Friction

When one body is rolled over another, junctions form at the contact points just as when two bodies are pressed together. As the rolling body moves on, these junctions are broken in tension, not in shear. Due to elastic rebound as the normal force goes to zero, the strength of the junctions in tension is usually almost zero. This explains why the adhesion between two surfaces that are pressed together is not generally observed—it only acts when the surfaces are under a compressive load. Hence rolling friction is generally quite small ($f \ll 0.1$) compared to static and sliding friction, and is essentially independent of surface cleanliness.

Summary

Section 6.2 has presented the fundamentals of frictional behavior; emphasis has been given to the following concepts, which are necessary in order to develop a quantitative explanation of observed frictional behavior:

1. The roughness and irregularity of apparently smooth surfaces.

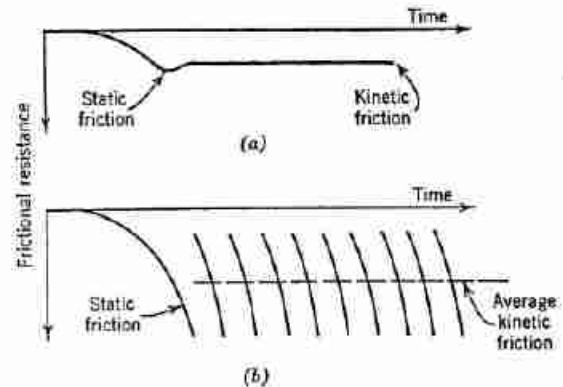


Fig. 6.6 Starting and kinetic friction. (a) Smooth sliding. (b) Slip-stick. *Note.* Shear displacement applied at constant rate through load cell with some flexibility; surfaces move at constant rate only during smooth sliding.

2. The very low ratio of actual contact area to apparent contact area.
3. The plastic flow that occurs at actual contact points.
4. The adhesion that occurs between two surfaces at the actual contact points.
5. The weakening influence of surface contaminants on the strength of this welded junction.

These concepts will now be used to explain the observed frictional behavior of soil minerals.

6.3 FRICTION BETWEEN MINERALS IN GRANULAR FORM

This section will treat friction between nonsheet minerals such as quartz, the feldspars, and calcite—those minerals that make up granular particles of silt size and larger. The following section will treat the behavior of sheet minerals. The friction of minerals has not been studied nearly as intensively as has the friction of metals. Therefore much of what follows is based on limited data and must be considered speculative.

General Nature of Contact

Particles of coarse silt have a minimum diameter of 0.002 cm (20 μ or 200,000 Å). The diameters of these and larger particles are clearly larger than the height of the asperities (about 1000–10,000 Å) that may be expected on the surfaces of these particles. Consequently, we would expect that each apparent point of contact between particles actually involves many minute contacts.

The surfaces of these soil particles are, of course, contaminated with water molecules and various ions and possibly other materials. These contaminants are largely squeezed out from between the actual points of contact, although some small quantity of contaminants remains to influence the shear strength of the junctions.

The minimum diameter of fine silt particles is 2μ or 20,000 Å. Such small particles have dimensions of the same order as the height of the asperities on larger particles. For these small particles it makes more sense to talk about "corners" rather than asperities. Although the general nature of the frictional resistance is the same for either large or small granular particles, an apparent contact between very small granular particles may, in fact, consist of only one actual contact point.

The testing systems shown in Fig. 6.7 have been used to determine the frictional resistance for minerals. When fixed buttons or sliding blocks are used (Fig. 6.7a) the results give the static (and perhaps kinetic) coefficient of friction. When many sand particles are pulled over a flat surface (Fig. 6.7b), the results generally reflect some combination of sliding and rolling friction. Hence the friction factor as measured by the second type of test involving many particles may be different from the value measured by the first type of test.

Effect of Surface Water and Surface Roughness

Figure 6.8 summarizes the friction factors observed for quartz under varying conditions of surface cleanliness, humidity, and surface roughness. The results show that the friction of smooth quartz varies from about $f = 0.2$

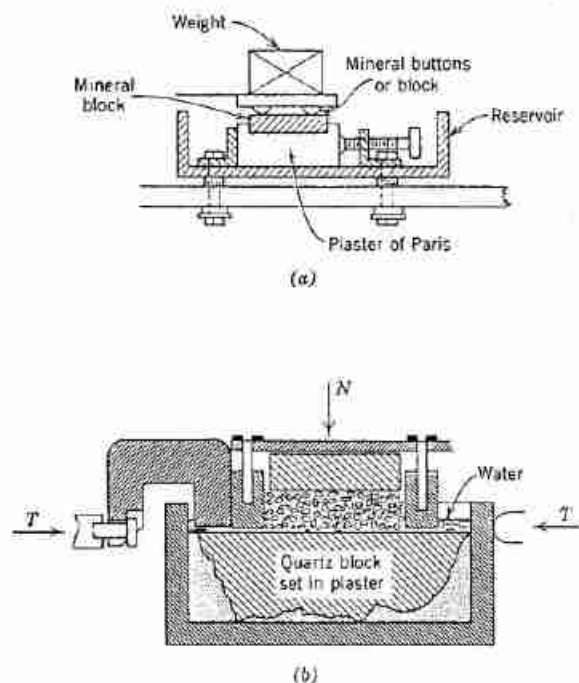


Fig. 6.7 Devices for measuring friction factor of mineral surfaces: (a) Sliding on buttons or on block. (b) Sliding of many particles.

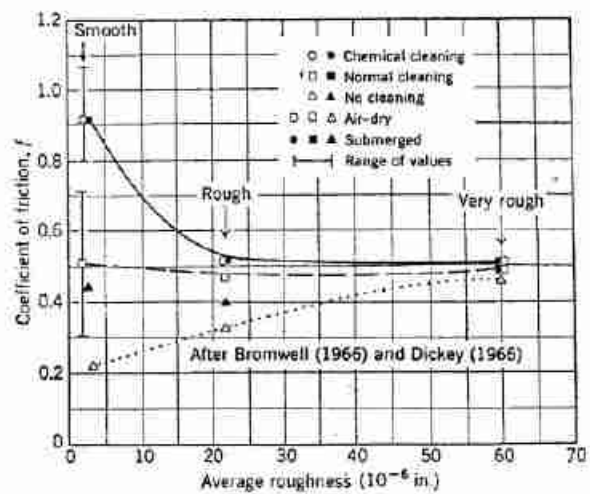


Fig. 6.8 Friction of quartz [after Bromwell (1966) and Dickey (1966)].

to $f = 1.0$ depending on the surface cleanliness.⁴ For the more contaminated surfaces, water increases the friction; i.e., it acts as an antilubricant. However, for carefully cleaned surfaces, water has no effect. This indicates that water is intrinsically neutral on quartz. But if there is a contaminating layer (probably a thin film of organic material) the water disrupts this layer, reduces its effectiveness as a lubricant, and thereby increases the friction.

As the surfaces get rougher the effects of cleaning procedure on friction decrease, so that a "very rough" surface of $60 \mu\text{in.}$ (about 15,000 Å) gives essentially the same value of f independent of surface cleanliness. This indicates that the ability of the contaminating layer to lubricate the surfaces decreases as the surface roughness increases. This is what we would expect for a thin lubricating layer which acts as a boundary lubricant (Bowden and Tabor, 1964).

The fact that the rougher surfaces do not give higher values of friction when they are carefully cleaned is more difficult to explain. The evidence seems to indicate that the rougher surfaces cannot be cleaned as effectively as smooth surfaces, although the reason for this is not clear.

From a practical point of view, the essentially constant value of $f = 0.5$ ($\phi_s = 26^\circ$) for very rough quartz surfaces is of great significance, since essentially all quartz particles in natural soils have rough surfaces.

Values of friction for other nonsheet minerals are summarized in Table 6.1. The low values of f for these minerals in the air-dry condition probably have no

⁴ These results were obtained on ground surfaces [Bromwell (1966) and Dickey (1966)]. However, the trend of the results generally supports the data and conclusions of previous tests, which were usually run on polished surfaces [see, for example, Horn and Deere (1962)].

Table 6.1 Friction of Nonsheet Minerals

Mineral	Conditions of Surface Moisture		
	Oven-Dried	Oven-Dried;	
		Air-Equilibrated	Saturated
Quartz ^a	0.13	0.13	0.45
Feldspar	0.12	0.12	0.77
Calcite	0.14	0.14	0.68

Notes. Tests run on highly polished surfaces. Data from Horn and Deere (1962).

^a For effects of surface cleanliness and surface roughness on the friction of quartz, see Fig. 6.8.

practical significance, since they represent ineffective cleaning of smooth, polished surfaces. Much more data are needed for these other minerals before one can confidently choose f values.

Effect of Normal Load

The measured friction factors for nonsheet minerals have been found to be independent of normal load. Based on tests in which the normal load per contact varied by a factor of 50, Rowe (1962) reported that the friction angle ϕ_μ remained constant within $\pm 1^\circ$.

On the other hand, Rowe's results show that the friction angle ϕ_μ is affected by the size of the particle involved in the test (Fig. 6.9). Rowe used the test procedure shown in Fig. 6.7b. For a given total normal load, the normal load per contact increases as the particle size increases. However, since the particle diameter in this case also increases, the average contact stress (N/A_c) did not change. Therefore arguments involving elastic deformation do not appear adequate to explain these data. One possible explanation is that the larger particles are able to roll more easily than the smaller particles, perhaps as a result of their center of gravity being further away from the plane of shear. Hence the measured friction angle, which involves both rolling and sliding components, is smaller for the larger particles.

6.4 FRICTION BETWEEN SHEET MINERALS

We are interested in minerals such as mica primarily because the frictional behavior of such minerals may be similar to the frictional behavior of clay-size particles.⁵

General Nature of Contact

Surfaces of mica do show irregularities, but in the form of mesas and plateaus rather than in the form of asperities. Moreover, the scale of these irregularities is quite

⁵ Data from M.I.T. and from the Norwegian Geotechnical Institute have been obtained on the friction angle ϕ_μ between clay particles. Values as low as 3° have been recorded.

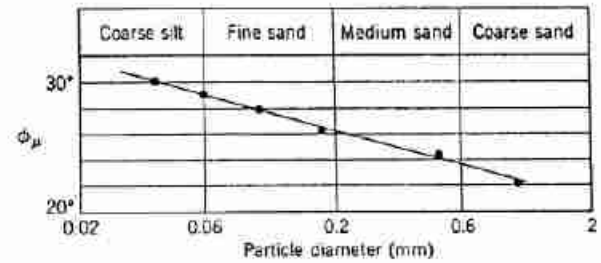


Fig. 6.9 Friction angle of quartz sands as function of grain size (after Rowe, 1962).

different from that existing on the surfaces of granular particles. On fresh cleavage surfaces, the "steps" are only as high as the thickness of several repeating sheet units (about 10–100 Å). In the words of Bowden and Tabor (1964), the cleavage surfaces "... are molecularly smooth over large areas." Compared to the surfaces of smooth quartz particles, fresh cleavage surfaces are "supersmooth". There are reasons to believe that the surfaces of clay particles are similar. Unfortunately, the fundamentals of frictional resistance between super-smooth surfaces have received relatively little study, and hence the following explanations are still largely speculative.

Two cleavage faces of mica give quite a different contact than do surfaces with asperities. Mica, and presumably clay, surfaces should come into close proximity over almost their entire area, but they may not actually come into direct contact. The contaminants on the surfaces, including adsorbed water, are not squeezed out from between the surfaces unless the normal stress exceeds about 80,000 psi. Rather, these contaminants participate in the transmission of the normal stress, as described in Chapter 5.

A more normal situation for clay particles is probably some sort of edge-to-face orientation. This type of contact is more nearly similar to the asperity contacts discussed for granular particles, except that in the case of clays, each contact probably consists of only one "asperity".

It still remains to discuss whether the shear resistance between very smooth surfaces is greater or less than the resistance between rough surfaces. To answer this, we must turn to experimental data.⁶

Effect of Surface Water

The data in Table 6.2 show that the water acts as a lubricant. A possible explanation for this behavior is as follows. In the oven-dried condition the surface ions are not completely hydrated. The actual mineral surfaces come close together, and the bonding is strong. As water is introduced, the ions hydrate and become less strongly

⁶ These data come primarily from Horn and Deere (1962).

attached to the mineral surfaces. Hence the shear resistance drops as water is introduced.

It is important to contrast the role of the contaminants for the cases of very smooth and rough surfaces. With rough surfaces the contaminants serve to weaken the crystalline bond, and increasing the mobility of the contaminants with water helps get them out of the way and hence minimizes their adverse influence. With very smooth surfaces the contaminants are actually part of the

Table 6.2 Friction Factors for Several-Layer Lattice Materials Under Varying Conditions of Humidity

Mineral	Condition of Surface Moisture		
	Oven-Dried	Oven-Dried; Air-Equilibrated	Saturated
Muscovite mica	0.43	0.30	0.23
Phlogopite mica	0.31	0.25	0.15
Biotite mica	0.31	0.26	0.13
Chlorite	0.53	0.35	0.22

Notes: Starting and moving friction identical. Data from Horn and Deere (1962).

mineral, and increasing their mobility decreases the shear resistance.

In the saturated condition the friction angle between sheet minerals can be low. Since clay minerals are always surrounded by water in practical situations, it is important to test these minerals in the saturated condition.

Static and Kinetic Friction

The kinetic friction of the sheet minerals is greater than 90% of the static friction and usually equals it. The slip-stick phenomenon has not been observed with these minerals. The friction factors of mica increase about 25% when the rate of sliding is increased from 0.7 to 6.0 in./min. Because the adhesive bonding is relatively weak in the case of these minerals, and the ions through which the bonding occurs are relatively free to move, this relatively small time effect is to be expected.⁷

Variation of Friction Angle with Normal Load

For the usual range of normal loads used, the friction angle of these minerals appears to be constant. However, nothing is known concerning the possible variation with very large changes in the normal load.

⁷ Mitchell (1964), by invoking rate process theory, has provided an excellent description of the mechanisms underlying this time-dependent behavior of clay minerals.

6.5 MISCELLANEOUS CONCEPTS CONCERNING SHEAR RESISTANCE BETWEEN MINERAL SURFACES

At the present time, we are still not sure of the extent to which the theory in Section 6.4 may apply to shear resistance between clay particles. However, it is shown in Part IV that many natural clay soils, especially those in which montmorillonite and illite are important constituents, have shear resistances that are compatible with this theory.

The larger a particle, the greater the likelihood that there will be surface irregularities of any consequence. For example, cleavage steps can be seen on the surface of kaolinite platelets, as shown in Fig. 4.4a, which are on the order of 100 Å in height. Hence, when platelets of kaolinite are in a face-to-face configuration, it is certain that actual "contact" occurs only over part of the apparent contact surface, and unless the platelets are perfectly aligned it seems likely that contact is confined to relatively small zones right at the cleavage steps. As this situation develops, it is likely that the mechanism of shear resistance, and even the magnitude of shear resistance, becomes more and more analogous to the behavior of granular particles. The same would be true when particles come together in edge-to-face orientation.

Present knowledge regarding interparticle friction in soils can be summarized as follows:

1. The frictional behavior between granular particles is reasonably well understood.
2. The theory for sliding between ideal clay platelets probably applies to the smallest of clay particles in face-to-face array.
3. The mechanism of shear resistance in natural clay lies between the two extremes of granular particles and parallel clay platelets, often nearer to that of the granular particles.

True Cohesion between Clay Particles

Our study of the fundamentals of frictional behavior has helped us to understand the possibility of a true cohesion developing between clay particles. If clay platelets are in edge-to-face contact, there is a good chance that a true cohesion will develop, especially if a bonding has been developed over almost all of the area of the contact.

The discussion in Chapter 5 has already suggested that clay platelets in face-to-face contact may be pushed together so tightly that they will not move apart when the load is removed. Such an occurrence certainly represents true cohesion, and a new and thicker particle has in effect been created by this process. Time, weathering, and desiccation contribute to true cohesion.

6.6 SUMMARY OF MAIN POINTS

The foregoing discussion shows that it is very difficult to say just what the particle-to-particle friction factor will be for any particular case. Hence the main results of this chapter can be summarized in terms of some general principles and a range of possible shear resistances.

1. The shear resistance between particles is provided by adhesive bonding at the points of contact.
2. The shear resistance is determined primarily by the magnitude of the current normal load, so that the overall behavior is frictional in nature.
3. For quartz the friction angle ϕ_μ is generally in the range of 26° to 30° . Because the surfaces of such particles are rough, the presence or absence of water has little or no effect on the frictional resistance. The friction of other nonsheet minerals has received less study and typical values cannot be given.
4. For parallel clay particles whose faces are "super-smooth", the friction angle may be below 8° and may typically be about 13° . The bonding occurs over a rather large area but is relatively weak and may be somewhat time-dependent.
5. For most natural clays the frictional resistance is probably nearer that of granular particles than of parallel colloidal particles.
6. True cohesion can develop between particle surfaces. The true cohesion at any one contact is generally small, so that the overall effect is important only when there are many contacts—as in clay soils. Such bonds are most likely to develop at edge-to-face contacts and can be broken by very small strains.
7. The particle-to-particle friction angle ϕ_μ is but one of the factors which contribute to the strength of an actual soil. Other factors such as interlocking of particles will be discussed in later chapters.

PROBLEMS

6.1 Derive the equations that lead to the following results:

- a. f is independent of N for materials that deform plastically.
 - b. f is a function of normal load for elastic materials.
- State the necessary assumptions for each equation.

6.2 The diameter of the contact area between two elastic solids (Fig. P6.2-1) is given by

$$d = \left[\frac{12(1 - \nu^2)}{E} N \frac{R_1 R_2}{R_1 + R_2} \right]^{1/3}$$

- ν = Poisson's ratio = 0.31 for quartz
- E = Young's modulus = 11×10^{11} psi for quartz
- N = normal load
- R_1, R_2 = radii of curvature

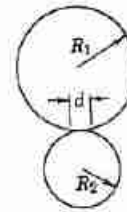


Fig. P6.2-1

- a. Develop a relationship for the average contact stress (N/A) between two quartz spheres of equal radius.
- b. Consider a system of dry silt-sized material. If the particles are perfect quartz spheres of radius 0.005 mm in a cubic array (see Fig. P6.2-2a), what all-around confining stress must be applied to cause plastic yielding? (Plastic yielding for quartz occurs at a normal stress of 1,500,000 psi.)
Hint. Consider a horizontal plane through the system (see Fig. P6.2-2b) and calculate the contact area on this plane for various values of confining stress.
- c. If each sphere in part (b) is not perfectly smooth but contacts its neighbors on one asperity which has a tip radius of 1000 Å, what must the confining stress be to cause plastic deformation?
- d. An actual silt may be expected to give plastic deformation at the contacts at some value of confining stress between the values given by parts (b) and (c). Why?
- e. Would the stress required to cause some plastic yielding be greater for a loose or a dense silt? Explain.

6.3 Consider a flocculated clay made up of platelike particles 1μ long \times 0.1μ wide \times 0.01μ thick. The void ratio is 2.0 and $G_s = 2.70$.

- a. Calculate the number of particles per unit volume.
- b. The number of particles contacting a unit area may be assumed equal to $(\text{no./unit volume})^{2/3}$. If each particle makes two stress-carrying contacts on a horizontal plane, what is the number of contacts per unit area?
- c. If each particle-particle contact is assumed to be an edge-to-face contact with the edge taken as a spherical indenter with radius 0.01μ , what effective confining stress must be applied to the clay to cause plastic yielding? Use same elastic constants as for quartz, but assume plastic flow starts at $N/A = 1,000,000$ psi.

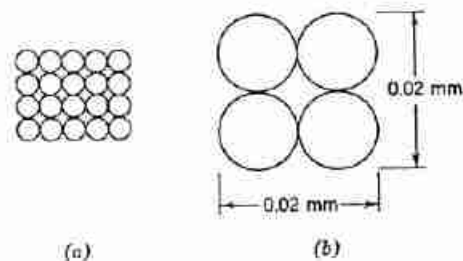


Fig. P6.2-2

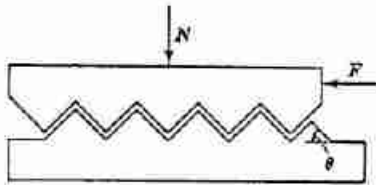


Fig. P6.4

6.4 The asperities on the idealized surface shown in Fig. P6-4 are inclined at an angle θ to the direction of sliding.

a. Derive a relationship for the horizontal force F required to initiate motion. Express F in terms of N , θ , and ϕ_μ (the friction angle for a surface with $\theta = 0$).

b. Calculate the coefficient of friction for the surfaces shown in Fig. P6-4 if $\phi_\mu = 15^\circ$ for a quartz surface with $\theta = 0$. Discuss the validity of this calculation.

6.5 Three clay-water mixtures composed of flocculated platelike particles have the particle dimensions and void ratio given in following table:

Mixture	Particle Dimensions (μ)	Void Ratio
A	$10 \times 10 \times 1$	1
B	$1 \times 1 \times 0.05$	2
C	$0.1 \times 0.1 \times 0.001$	5

If the net attractive stress at particle contacts under zero normal load were equal to F where

$$F \text{ (dynes)} = 10^{-6} \text{ particle thickness } (\text{\AA})$$

compute the cohesion (tensile stress) which must be overcome in order to pull apart the three mixtures. *Note:* Use the approach in Problem 6.3 to obtain the number of contacts per unit area.

Answer:

System	c (kg/cm^2)
A	0.06
B	0.36
C	1.32

CHAPTER 7

Soil Formation

Based on its method of formation, a soil is *sedimentary*, *residual*, or *fill*. In sedimentary soil the individual particles were created at one location, transported, and finally deposited at another location. A residual soil is one formed in place by the weathering of the rock at the location, with little or no movement of the individual soil particles. Fill is a man-made soil deposit. These three types of soil are discussed in order in this chapter. Preceding this discussion is a consideration of the concept of "structure", which will be used in the presentation of the soil types.

7.1 SOIL STRUCTURE

The term *soil structure* refers to the orientation and distribution of particles in a soil mass (also called "fabric" and "architecture") and the forces between adjacent soil particles. This discussion is limited primarily to small, plate-shaped particles and to the orientation of individual particles. The arrangement of larger particles is considered in later chapters. The force component of soil structure refers primarily to those forces that are generated within the particles themselves—electrochemical forces.

The two extremes in soil structure, as illustrated in Fig. 7-1, are *flocculated* structure and *dispersed* structure. In the flocculated structure the soil particles are edge to face and attract each other. A dispersed structure, on the other hand, has parallel particles which tend to repel each other. Between the two extremes there is an infinite number of intermediate stages. At the present development of knowledge and of techniques for measuring orientations and interparticle forces, there seems little justification in attempting to define structures between the two extremes. Thus the terms *flocculated* and *dispersed* are used in a general sense to describe soil elements which have the structures approaching those shown in Fig. 7.1.

Chapter 5 discussed the electrical forces between particles and introduced the concepts of flocculated and

dispersed. No attempt is made to distinguish between the two types of flocculation suggested in Fig. 5.15.

A given soil structure can be significantly altered by introducing displacements between particles. Generally, displacements tend to break down the bonds between particles and to move particles toward a parallel array. If the flocculated structure in Fig. 7.1a were subjected to a horizontal shear displacement, the particles would tend to line up as shown in the dispersed structure on the right. A compression tends to cause adjacent particles to move toward a parallel array, probably resulting in small zones of approximately parallel particles, with an unlike orientation between zones. Physically working an element of soil until it becomes homogeneous (termed "remolding") tends to align adjacent particles and to destroy bonds between the particles.

The engineering behavior of a soil element depends very much on the existing structure. In general, an element of flocculated soil has a higher strength, lower compressibility, and higher permeability than the same element of soil at the same void ratio put in a dispersed state. The higher strength and lower compressibility in the flocculated state result from the interparticle attraction and the greater difficulty of displacing particles when they are in a disorderly array. The higher permeability in the flocculated soil results from the larger channels available for flow. Whereas a flocculated element and a dispersed element at the same void ratio have approximately the same total cross-sectional area available for

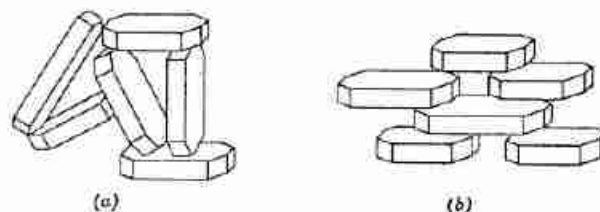


Fig. 7.1 Types of soil structure. (a) Flocculated. (b) Dispersed.

Table 7.1 Effects of Transportation on Sediments

	Water	Air	Ice	Gravity	Organisms
Size	Reduction through solution, little abrasion in suspended load, some abrasion and impact in traction load	Considerable reduction	Considerable grinding and impact	Considerable impact	Minor abrasion effects from direct organic transportation
Shape and roundness	Rounding of sand and gravel	High degree of rounding	Angular, soled particles (◻)	Angular, non-spherical	
Surface texture	Sand: smooth, polished, shiny Silt: little effect	Impact produces frosted surfaces	Striated surfaces	Striated surfaces	
Sorting	Considerable sorting	Very considerable sorting (progressive)	Very little sorting	No sorting	Limited sorting

flow, in the flocculated soil the flow channels are fewer in number and larger in size. Thus there is less resistance to flow through a flocculated soil than through a dispersed soil.

7.2 SEDIMENTARY SOIL

The formation of sedimentary soils can best be presented by considering sediment formation, sediment transportation, and sediment deposition, respectively.

Sediment Formation

The most important manner of forming sediments is by the physical and chemical weathering of rocks on the surface of the earth. Generally silt-, sand-, and gravel-sized particles are formed by the physical weathering of rocks and clay-sized particles are formed by the chemical weathering of rocks. The formation of clay particles from rocks can take place either by the build-up of the mineral particles from components in solution, or by the chemical breakdown of other minerals.

Sediment Transportation

Sediments can be transported by any of five agents: water, air, ice, gravity, and organisms. Transportation affects sediments in two major ways: (a) it alters particle shape, size, and texture by abrasion, grinding, impact, and solution; (b) it sorts the particles. Table 7.1 summarizes some of the effects of the five transporting agents on sediments.

Sediment Deposition

After soil particles have been formed and transported they are deposited to form a sedimentary soil. The three main causes of deposition in water are velocity reduction, solubility decrease, and electrolyte increase. When a stream reaches a lake, ocean, or other large body of water it loses most of its velocity. The competency of the stream thus decreases and sedimentation results. A

change in water temperature or chemical nature can result in a reduction in the solubility of the stream, with a resulting precipitation of some of the dissolved load. Figure 7.2 suggests the soil structure that might result from a sedimentary soil formed in salt water compared with one formed in fresh water. As was shown in Fig. 5.14, the soil deposited in salt water will be more highly flocculated and will thus have a much larger void ratio and water content.

7.3 RESIDUAL SOIL

Residual soil results when the products of rock weathering are not transported as sediments but accumulate in place. If the rate of rock decomposition exceeds the rate of removal of the products of decomposition, an accumulation of residual soil results. Among the factors influencing the rate of weathering and the nature of the products of weathering are climate (temperature and rainfall), time, type of source rock, vegetation, drainage, and bacterial activity.

The residual soil profile may be divided into three zones: (a) the *upper zone* where there is a high degree of weathering and removal of material; (b) the *intermediate zone* where there is some weathering at the top part of the zone, but also some deposition toward the bottom part of the zone; and (c) the *partially weathered zone* where there is the transition from the weathered material to the unweathered parent rock.

Temperature and other factors have been favorable to the development of significant thicknesses of residual soils in many parts of the world, particularly Southern Asia, Africa, Southeastern North America, Central America, the islands of the Caribbean, and South America. As we can infer from this distribution, residual soils tend to be more abundant in humid, warm regions that are favorable to chemical weathering of rock, and have sufficient vegetation to keep the weathering products from being easily transported as sediments. Even

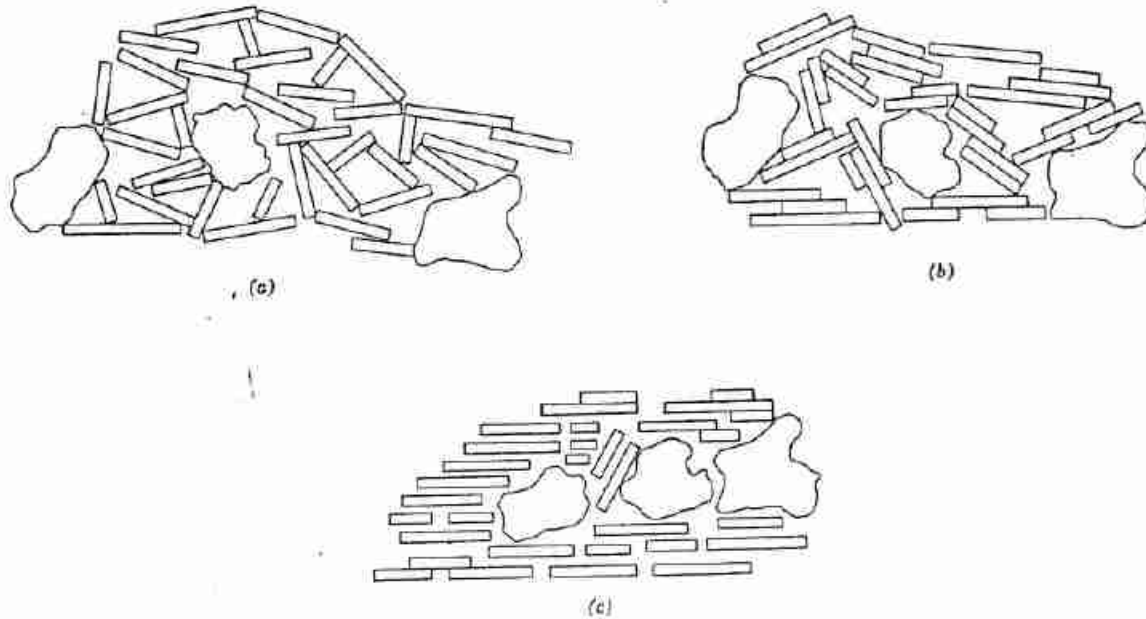


Fig. 7.2 Structure of natural soil (a) Undisturbed salt water deposit. (b) Undisturbed fresh water deposit. (c) Remoulded.

though residual soils are widely spread throughout the world, they have received relatively little study from soil mechanics experts because these soils are generally located in areas of undeveloped economies, as contrasted to the sedimentary soils which exist in most centers of population and industry.

Sowers (1963) gives the following typical depths of residual soils:

Southeastern United States	20 to 75 ft
Angola	25 ft
South India	25 to 50 ft
South Africa	30 to 60 ft
West Africa	33 to 66 ft
Brazil	33 to 83 ft

7.4 FILL

The two preceding sections considered the formation of soil deposits by nature. A man-made soil deposit is called a *fill* and the process of forming the deposit is called *filling*. A fill is actually a "sedimentary" deposit for which man carried out all of the formation processes. Soil, termed *borrow*, is obtained from a source or made by blasting, transported by land vehicle (such as truck, scraper, pan, or bulldozer) or water vehicle (barge) or pipe, and deposited by dumping. The fill can be left as dumped, such as the rock toe in the earth dam shown in Fig. 1.8 and the hydraulic fill shown in the terminal in Fig. 1.9, or can be processed and densified—*compacted*—

as for the core in the dam shown in Fig. 1.8 or the highway pavement shown in Fig. 1.11. The principles of compaction and the properties of compacted soils are treated in Chapter 34.

7.5 ALTERATIONS OF SOIL AFTER FORMATION

The civil engineer working with soil must design his structure not only for the properties of the soil as it exists at the start of the project but also for the entire design-life of the structure. He thus needs to know both the properties of the soil at the start of the project and how these properties will vary during the design-life. Both the size and shape of a given deposit and the engineering properties of the soil in the deposit may change very significantly. Many of these changes occur independent of man's activity, whereas others are brought about by the construction activity itself.

The significant changes in engineering behavior that can and do occur during the life of a soil make soil engineering both difficult and interesting. The engineer soon learns that soil is not inert but rather very much alive and sensitive to its environment. Table 7.2 lists the factors with the greatest influence on the behavior of soil.

Stress

In general, an increase in stress on a soil element causes an increase in shear strength, a decrease in compressibility,

Table 7.2 Factors Influencing Soil Behavior

Factors Influencing Behavior of As-Formed Deposit	Factors Contributing to Changes in Soil Behavior
Sedimentary soil	
Nature of sediments	Stress
Methods of transportation and deposition	Time
Nature of deposition environment	Water
Compacted soil	
Nature of soil	Environment
Amount of molding water	
Amount and type of compaction	Disturbance

and a decrease in permeability; a reduction in stress causes the reverse. The changes brought about by a stress reduction are usually less than those caused by a stress increase of equal magnitude.

During the formation of a sedimentary soil the total stress at any given elevation continues to build up as the height of soil over the point increases. Thus the properties at any given elevation in a sedimentary soil are continuously changing as the deposit is formed. The removal of soil overburden, e.g., by erosion, results in a reduction of stress. A soil element that is at equilibrium under the maximum stress it has ever experienced is *normally consolidated*, whereas a soil at equilibrium under a stress less than that to which it was once consolidated is *overconsolidated*.

There are construction activities that result in an increase of the confining stress on soil and there are activities that result in a reduction of stress. For example, the embankment shown in Fig. 1.6 caused a very great increase of vertical stress on the soils underneath the embankment. When equilibrium was reached under this embankment load, the soil underneath the embankment had become much stronger. On the other hand, the excavation for the Panama Canal (Fig. 1.14) resulted in considerable unloading of the soil in the canal and immediately adjacent to it. This unloading resulted in a decrease in the strength of the shale immediately adjacent to the canal and contributed to the slides that occurred along the canal.

Time

Time is a dependent variable for the other factors contributing to change in soil behavior (especially stress, water, and environment). As noted in Chapter 2, for the full effects of a stress change to be felt, water usually must be extruded or imbibed in the soil element. Because

of the relatively low permeability of fine-grained soil, time is required for this water to flow into or out of this type of soil. Time is an obvious factor in chemical reactions such as those occurring during weathering.

Water

As was discussed in Chapter 2, water can have two deleterious effects on soil. First, the mere presence of water causes the attractive forces between clay particles to decrease. Second, pore water can carry applied stress and thus influence soil behavior. A sample of clay which may have a strength approaching that of a weak concrete when it has been dried can become mud when immersed in water. Thus increasing the water content of a soil generally reduces the strength of the soil.

The activities of both nature and man serve to alter pore water conditions. In many parts of the world, there is a very marked variation in water conditions during the year. During the hot, dry season, there is a lack of rain and the ground water level drops; during the wet season, there is surface water and a general rising of the ground water. This seasonal variation in water conditions causes a marked change in soil properties through the year.

There are many construction operations that alter ground water conditions. For example, the dam shown in Fig. 1.8 impounded a reservoir, which subjected the foundation soils to a great increase in pore water pressure. Not only were the foundation soils given an increase in pore pressure, but many dry soils which had never been inundated were submerged with water from the reservoir. Construction for the two buildings shown in Figs. 1.4 and 1.5 required a lowering of the water table. This lowering caused a change in the properties of the subsoils.

Environment

There are several characteristics of the environment of a soil which may influence its behavior. The two considered here are the nature of the pore fluid and temperature. A sedimentary clay or compacted clay can be formed with a pore fluid of a certain composition, and at a certain temperature both of these can change during the life of the deposit. One example is a marine clay laid down in water high in salt, 35 g of salt/liter of water for a typical marine environment. A marine clay is frequently uplifted so that it is above the level of the sea, and the ground waters percolating through the clay are of much lower salt content than the sea water. Thus during the life of the sedimentary clay there can occur a gradual removal of the salt in the pore fluid so that, after many thousands of years of leaching, the pore fluid can be quite different from that at time of sediment formation. As discussed in Chapter 5, reducing the electrolyte content of the water around soil particles can reduce the net

attraction between them. In other words, leaching of the salt in the pore fluid can cause a reduction in shear strength.

The most dramatic example of a reduction in shear strength brought about from pore water leaching is exhibited in the "quick clays". These marine clays were deposited in a highly flocculated condition. Despite the resulting high water content, these clays developed a moderately large strength because of the bonds that formed at the edge-to-face contacts. These clays then had most of the electrolyte in their pore fluid removed by years of leaching. For this new environmental condition, the clay would tend to be in a dispersed condition (see Fig. 7.2c), and for the same water content it would have very little strength. However, this change does not show up fully until the clay is subjected to enough disturbance to break the bonds built up by years of confining stress. Upon disturbance, the clay may lose all of its strength and become a soil-water slurry with zero shear strength. These quick clays have caused many engineering problems in the Scandinavian countries and in Canada where they are widespread. The landslide shown in Fig. 1.13 occurred in a quick clay.

The change in temperature from time of deposit formation to a given time under consideration can result in a change of soil behavior. Thus a clay deposited in a glacial lake undergoes a general warming during its life. Further, a soil existing at great depth in the ground, sampled and brought into the laboratory for testing, may undergo property changes due to the difference in temperature between the ground and the laboratory. Increasing the temperature of a cohesive soil normally causes an expansion of the soil as well as causing some of the air dissolved in the pore fluid to come out of solution.

The engineer can see from the discussion in this section that he must give thought to how the properties of the soil might change during the life of his structure, and not expect to make a proper design solely on the basis of the properties of the soil as it exists prior to construction. He could be faced with a disastrous failure if he designed his earth dam on the basis of the strengths of the soil which exist prior to the construction of the dam. Later chapters in this book will treat the principles needed to select the proper values of strength, permeability, and compressibility to be used in a given soil problem.

7.6 SOIL INVESTIGATION

Table 7.3 lists some of the methods of soil investigation¹ in general use. The proper program of soil investigation for a given project depends on the type of project, the importance of the project, and the nature of

¹ The reader is referred to Terzaghi and Peck (1967) for a more detailed treatment of soil investigation.

the subsoils involved. For example, a large dam project would usually require a more thorough subsoil investigation than would a highway project. A further example is soft clays, which usually require more investigation than do gravels.

The first four methods of soil investigation listed in Table 7.3 normally cover a large area and are intended to give the engineer a general picture of the entire site. Geophysical techniques make possible the detection of

Table 7.3 Methods of Soil Investigation

Reconnaissance
Visual inspection
Airphotos
Geologic reports and maps
Records of past construction
Exploration
Geophysical
Electrical
Pits—sampling and testing
Borings—sampling and testing
Field tests
Penetration tests
Vane tests
Water table—pore pressure tests
Pumping tests
Load tests
Compaction tests

markedly different strata in the subsoils. These techniques permit a relatively large volume of subsoil to be explored in a given period of time.

Sampling either from pits or from borings followed by laboratory testing is widely used in soil investigation, especially for important structures and relatively uniform subsoils. The investigator can obtain high-quality undisturbed samples from open pits, but obviously pits can be advanced only to relatively shallow depths. Pits or trenches can be dug by hand or by power equipment such as a back hoe or dozer. Borings can be made by augers either with or without a casing.

There are difficulties in obtaining high-quality undisturbed soil samples, especially from considerable depths. The sampling operation, sample transportation, and specimen preparation require that the soil be subjected to stresses which are quite different from those that existed in the ground. This inherent change of stress system alters the behavior of the soil. Further, the sampling, transportation and preparation operation usually subjects the specimen to strains that alter the soil structure. For these reasons the determination of *in situ* properties by laboratory tests can be most difficult. Later chapters in this book discuss laboratory testing and

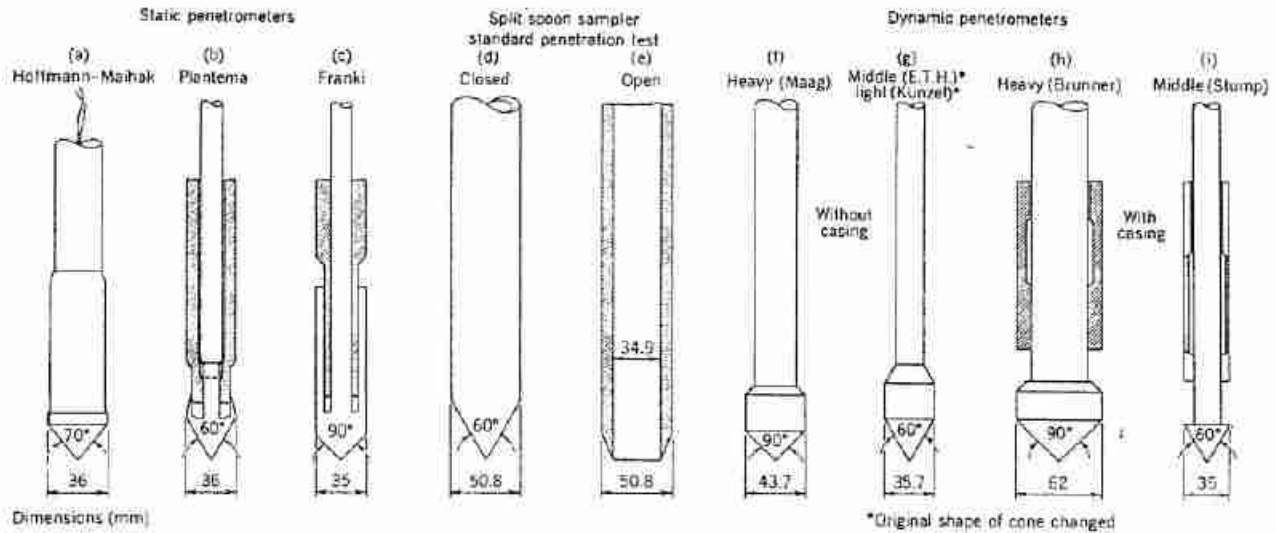


Fig. 7.3 Penetrometers (From Schultze and Knäusenberger, 1957).

point out some of the significant influences of sample disturbance.

Field tests take on an increased importance in soils which are sensitive to disturbance and in subsoil conditions where the soils vary laterally and/or vertically. The most widely used field test method is penetration testing. Figure 7.3 shows some of the penetrometers that have been used for soil investigation. These penetrometers are driven or pushed into the ground and the resistance to penetration is recorded. The most widely used penetration test is the "standard penetration test", which consists of driving the spoon, shown in Fig. 7.4, into the ground by dropping a 140-lb weight from a height of 30 in. The penetration resistance is reported in number of blows of the weight to drive the spoon 1 ft.

Table 7.4 presents a correlation of standard penetration resistance with relative density for sand and a correlation of penetration resistance with unconfined compressive strength for clay. The standard penetration test is a very valuable method of soil investigation. It should, however, be used only as a guide, because there

are many reasons why the results are only approximate.

Figure 7.5 presents the results of some penetration tests run in a large tank in the laboratory. These test data show that the penetration resistance depends on factors other than relative density. As can be seen, the penetration resistance depends on the confining stress and on the type of sand. Further, the figures show that the test data scatter considerably. The influence of sand type on penetration resistance is particularly large at low densities—those of most interest. Another factor that may have a marked influence on the penetration resistance of a sand is the pore pressure conditions during the measuring operation. If the level of water in the drill hole is lowered prior to penetration measurement, a lowered resistance can result.

Experience has shown that the determination of the shear strength of a clay from the penetration test can be very unreliable.

The standard penetration test should be used only as an approximation or in conjunction with other methods of exploration.

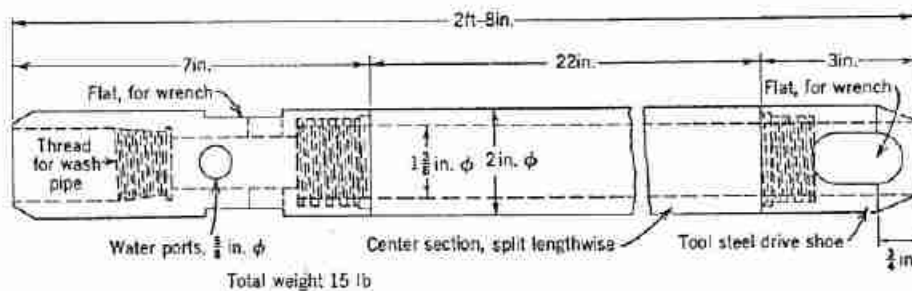


Fig. 7.4 Spoon for standard penetration test (From Terzaghi and Peck, 1967).

Table 7.4 Standard Penetration Test

Relative Density of Sand		Strength of Clay		
Penetration Resistance N (blows/ft)	Relative Density	Penetration Resistance N (blows/ft)	Unconfined Compressive Strength (tons/ft ²)	Consistency
0-4	Very loose	<2	<0.25	Very soft
4-10	Loose	2-4	0.25-0.50	Soft
10-30	Medium	4-8	0.50-1.00	Medium
30-50	Dense	8-15	1.00-2.00	Stiff
>50	Very dense	15-30	2.00-4.00	Very stiff
		>30	>4.00	Hard

From Terzaghi and Peck, 1948.

In certain countries, such as Holland, subsoil conditions are such that penetration testing has proved to be a relatively reliable technique. More sophisticated techniques [such as the friction jacket cone (Begemann, 1953)] have been widely used.

The vane test has proved to be a very useful method of determining the shear strength of soft clays and silts. Figure 7.6 shows various sizes and shapes of vanes which have been used for field testing. The vane is forced into the ground and then the torque required to rotate the vane is measured. The shear strength is determined from the torque required to shear the soil along the vertical and horizontal edges of the vane.

As later chapters in this book will show, a proper subsoil investigation should include the determination of water pressure at various depths within the subsoil. Methods of determining pore water pressure are discussed in Part IV. Part IV also notes how the permeability of a subsoil can be estimated from pumping tests.

Various load tests and field compaction tests may be highly desirable in important soil projects. In this type of test, a small portion of the subsoil to be loaded by the prototype is subjected to a stress condition in the field which approximates that under the completed structure. The engineer extrapolates the results of the field tests to predict the behavior of the prototype.

7.7 SUBSOIL PROFILES

Figures 7.7 to 7.17 present a group of subsoil profiles and Table 7.5 gives some information on the geological history of the various profiles. The purposes of presenting these profiles are to:

1. Indicate how geological history influences soil characteristics.
2. Give typical values of soil properties.

3. Show dramatically the large variability in soil behavior with depth.
4. Illustrate how engineers have presented subsoil data.

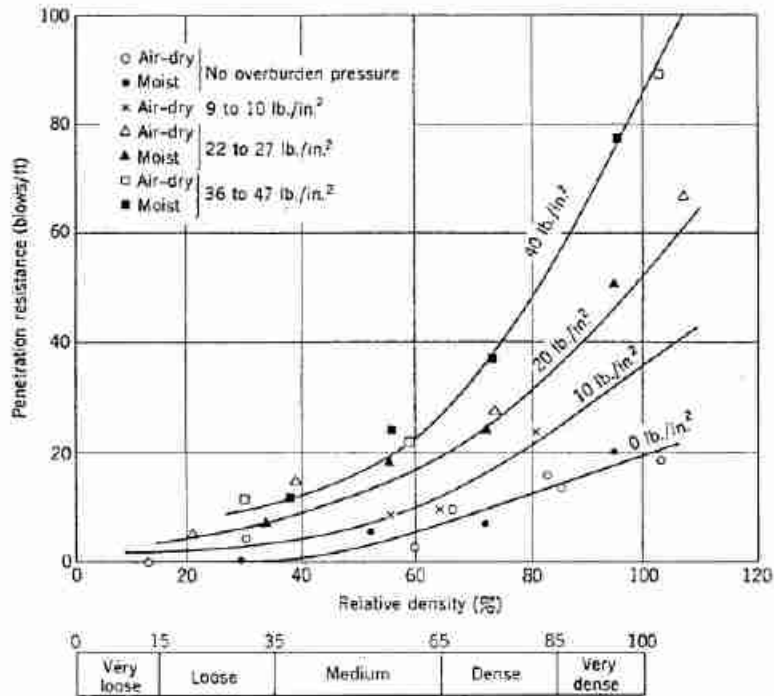
Three considerations were used in the selection of the profiles: first, examples were chosen with different types of geological history; second, most of the profiles are ones for which there are excellent references giving considerably more detail on the characteristics of the soil and engineering problems involved with the particular profile; and finally, most of the profiles selected have been involved in interesting and/or important soil engineering projects.

Some of the soil characteristics shown in the profiles have already been described in this book. These characteristics include water content, unit weight, void ratio, porosity, Atterberg limits, and particle size. Other characteristics, particularly those referring to strength and compressibility, will be discussed in detail in later portions of this book. Reference will then be made back to these profiles.

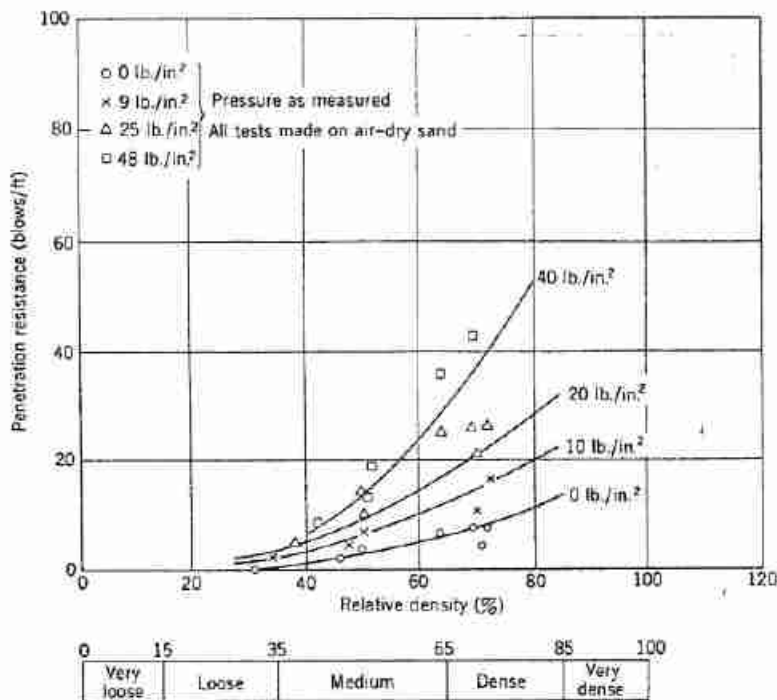
The profiles illustrate many concepts presented in the preceding parts of this book; some of them are discussed in the remaining part of this section.

Stress History

In a normally consolidated sedimentary soil both the void ratio and water content decrease with depth in the profile, and the strength therefore increases. This characteristic is illustrated in several of the profiles, e.g., the Norwegian marine clay (Fig. 7.7), the Thames Estuary clay (Fig. 7.10), and the Canadian clay (Fig. 7.11). The London clay is overconsolidated since it was compressed by a greater overburden than now exists. Erosion removed some of the original overburden. As would be expected, the overconsolidated London clay does not



(a)



(b)

Fig. 7.5 Results of standard penetration tests. (a) Coarse sand. (b) Fine sand. (From Gibbs and Holtz, 1957.)

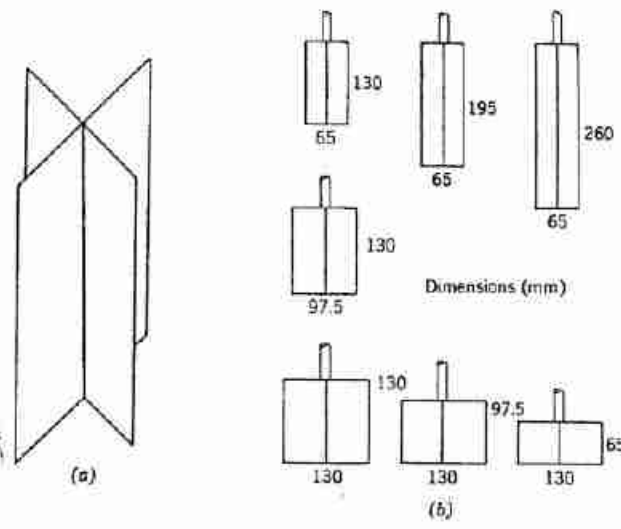


Fig. 7.6 Vanes. (a) Vane. (b) Vanes studied by Aas (1965).

Table 7.5 Subsoil Profiles

Number	Profile	Formation	Post Deposition	Comments	References
1	Norwegian marine clay	Sediments transported by rivers of melted glaciers of Pleistocene and deposited in sea	Sediments uplifted and leached. Surface dried and weathered	Normally consolidated below surface crust	Bjerrum, 1954
2	London clay	Deposited under marine conditions during the Eocene, roughly 30 million years ago	Uplift and erosion removed the overlying deposits and $\frac{1}{2}$ to $\frac{3}{4}$ of London clay	Overconsolidated to maximum past pressure $\approx 20T/ft^2$	Skempton and Henkel, 1957 Ward, Samuels and Butler, 1959
3	Boston blue clay	Sediments transported by streams of melted glaciers of Pleistocene and deposited in the quiet marine waters of Boston Basin	Clay uplifted, submerged, and re-uplifted	Overconsolidated at top, normally consolidated at bottom	Horn and Lambe, 1964 Skempton, 1948
4	Thames Estuary clay	Sediments transported by streams and deposited in an estuary during post-glacial time		Normally consolidated below surface crust	Skempton and Henkel, 1953
5	Canadian varved clay	Sediments transported by streams from melting glaciers and deposited in cold lakes		Light, silt layer laid down in spring, summer; dark "clay" layer, in winter	Milligan, Soderman and Rutka, 1962 Eden and Bozozuk, 1962
6	Mexico City clay	Sediments of volcanic origin deposited in lake in valley of Mexico during late Pleistocene	Pumping from water wells has lowered water table	In some parts of city clay is normally consolidated, other parts overconsolidated	Marsal, 1957 Lo, 1962 Zeevaert, 1953
7	Chicago clay and sand	Clay deposited as till sheets by glaciers, during both advancing and receding stages, and deposited in glacial lakes	Clay surface desiccated, giving crust usually 3-6 ft thick		Peck and Reed, 1954
8	South African clay				Jennings, 1953
9	Brazilian residual clay	Formed in place by weathering of rock			Vargas, 1953
10	Volga River sand	Alluvial sand of the Volga river		Data in Fig. 7.17 obtained on frozen samples from pits	Durante, Kozan, Ferronsky, and Nosal, 1957
11	Kawasaki subsoils	Alluvial deposits of the Holocene Epoch. Top 4 m hydraulic fill		Profile shown in Part IV	

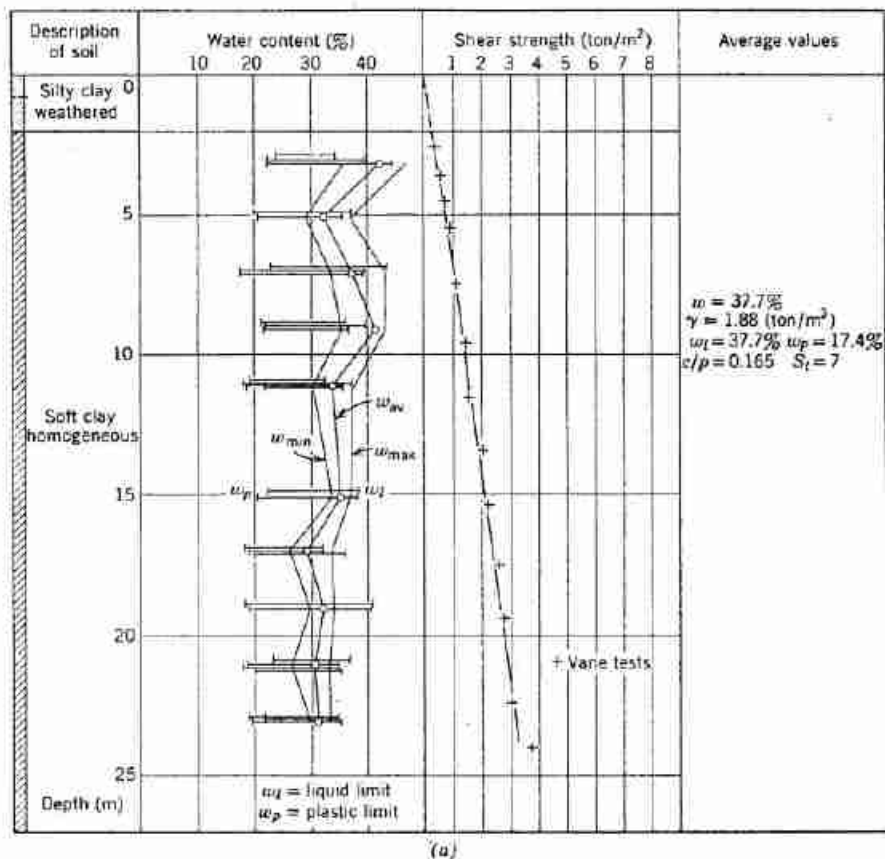


Fig. 7.7 Norwegian marine clay. (a) Results of a boring in Drammen. (b) Results of a boring at Manglerud in Oslo. (From Bjerrum, 1954.)

show a marked reduction in water content or increase in strength with depth.

The surfaces of most of the soil profiles contain crusts resulting from desiccation and weathering. Drying causes pore water tensions, which increase the stress between soil particles and overconsolidate the clay. Desiccation also encourages chemical weathering, especially oxidation, which gives the soil an apparent overconsolidation.

In both the Mexico City clay and London clay the pore water pressure in the soil is less than the static pressure. The importance of this reduced water pressure is discussed in detail in Parts IV and V of this book.

The Brazilian residual clay (Fig. 7.16) shows evidence of overconsolidation in the upper half of the stratum and normal consolidation in the lower half. It is doubtful that one should use the terms "overconsolidated" and "normally consolidated" in reference to residual soils, however.

Sensitivity

Time and changes in stress and environment since the time of formation may result in a soil having a higher strength in the undisturbed state than it does in the remolded state (after the soil has been thoroughly worked as was done prior to the liquid limit test described in Chapter 3). The term *sensitivity* is used to describe this difference in strength and is determined by the ratio of the strength in the undisturbed state to that in the remolded state. Sensitivity is related to liquidity index, since the greatest loss of strength should occur in a highly flocculated soil whose water content is very large compared to its liquid limit as measured using remolded soil. As discussed in the preceding section, sedimentary soils laid down in a marine environment and then leached after deposition tend to have high sensitivity. Any soil with a sensitivity equal to or greater than eight is termed "quick". The Manglerud clay (Fig. 7.7) is an extreme

example of a quick clay, having a sensitivity ranging to above 500. The Canadian clay (Fig. 7.11) is also quick.

Variability in Soil

The profiles offer many examples of variability in soils, over both large and small distances. In the Manglerud clay and Thames Estuary clay, distinct strata of many feet of thickness can be detected. In the sedimentary clays there often exists a large variation in soil properties over distances of less than an inch. Such variations over small distances are dramatically shown in the Canadian varved clay (Fig. 7.12). Figure 7.12 shows the great differences in water content and plasticity between the dark ("clay") and light ("silt") layers.

Plasticity

The plasticity of the clay shown in the various profiles varies tremendously. The glacial clays, generally containing a significant amount of the clay mineral illite, tend to have relatively low plasticity. Values of plasticity index of 15 to 20 are shown for the glacial clays, e.g., the

Norwegian marine clay—however, they can have much higher values, as indicated by the data on the Canadian varved clay, especially the dark layers.

The Mexico City clay, containing the clay mineral montmorillonite and volcanic ash, is one of the most plastic clays encountered by the soil engineer. As can be seen in Fig. 7.13, this clay can have values of PI in excess of 400. The South African soils (Fig. 7.15) can have high values of PI and fall above the *A* line on the plasticity chart. This characteristic is common of soils which present heave problems as do some of the South African clays.

7.8 SUMMARY OF MAIN POINTS

1. The determination of the soil profile is an essential step in almost all soil mechanics problems.
2. The properties of the soils in a profile depend on (a) the nature of soil components, (b) the method of profile formation, and (c) the alteration of the profile after formation.

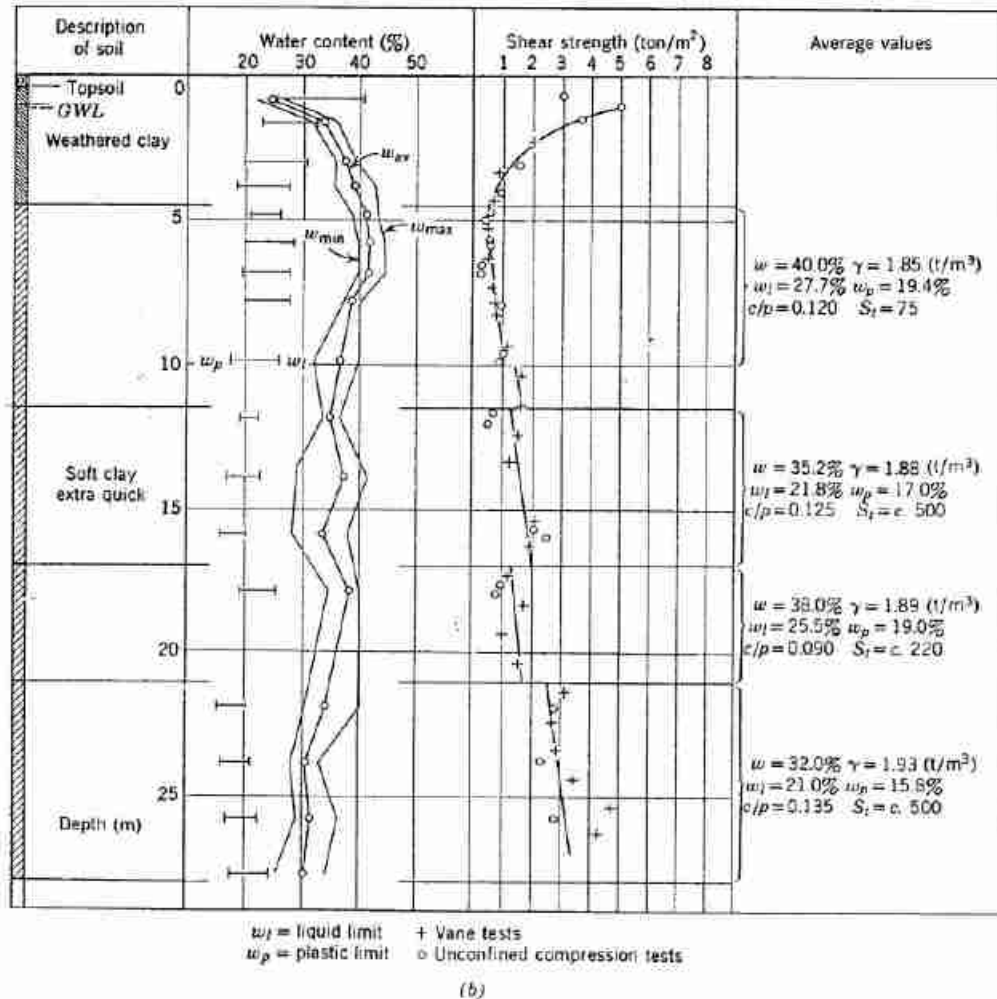


Fig. 7.7 (continued)

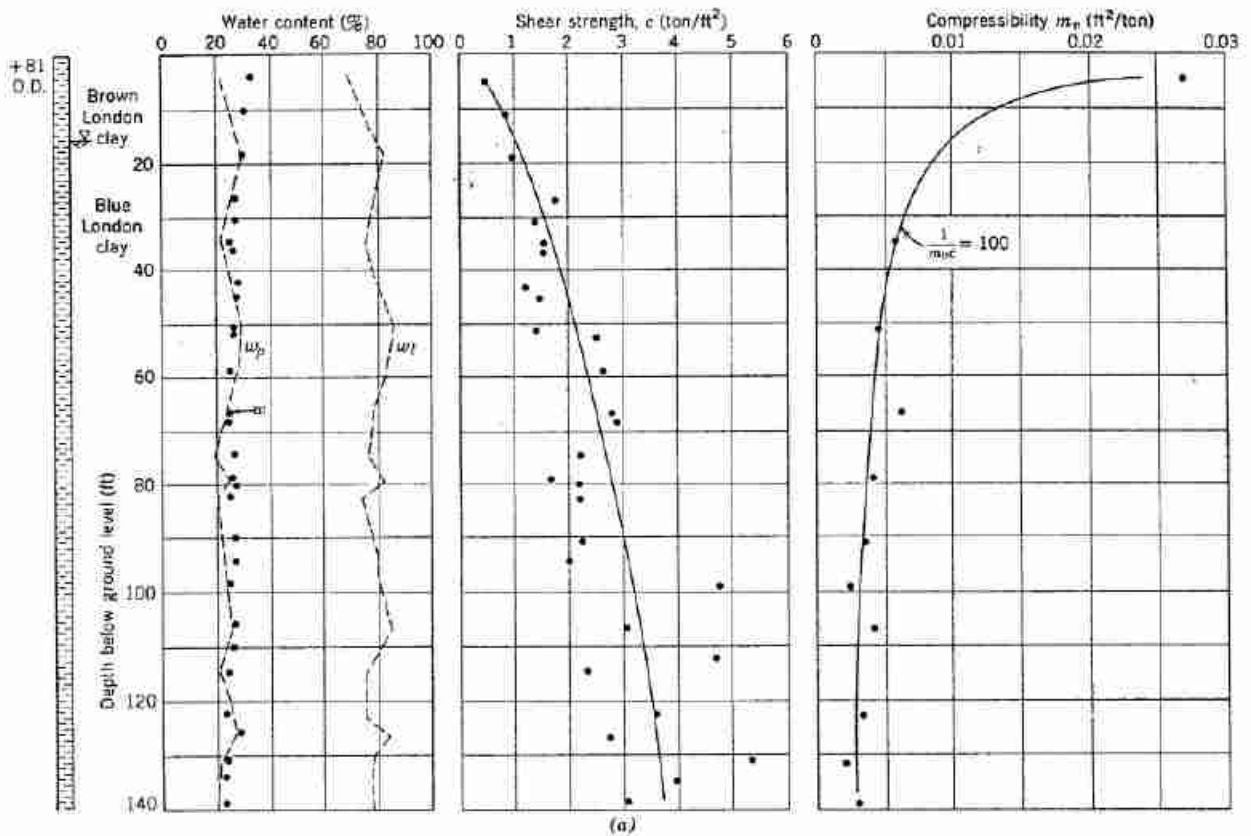
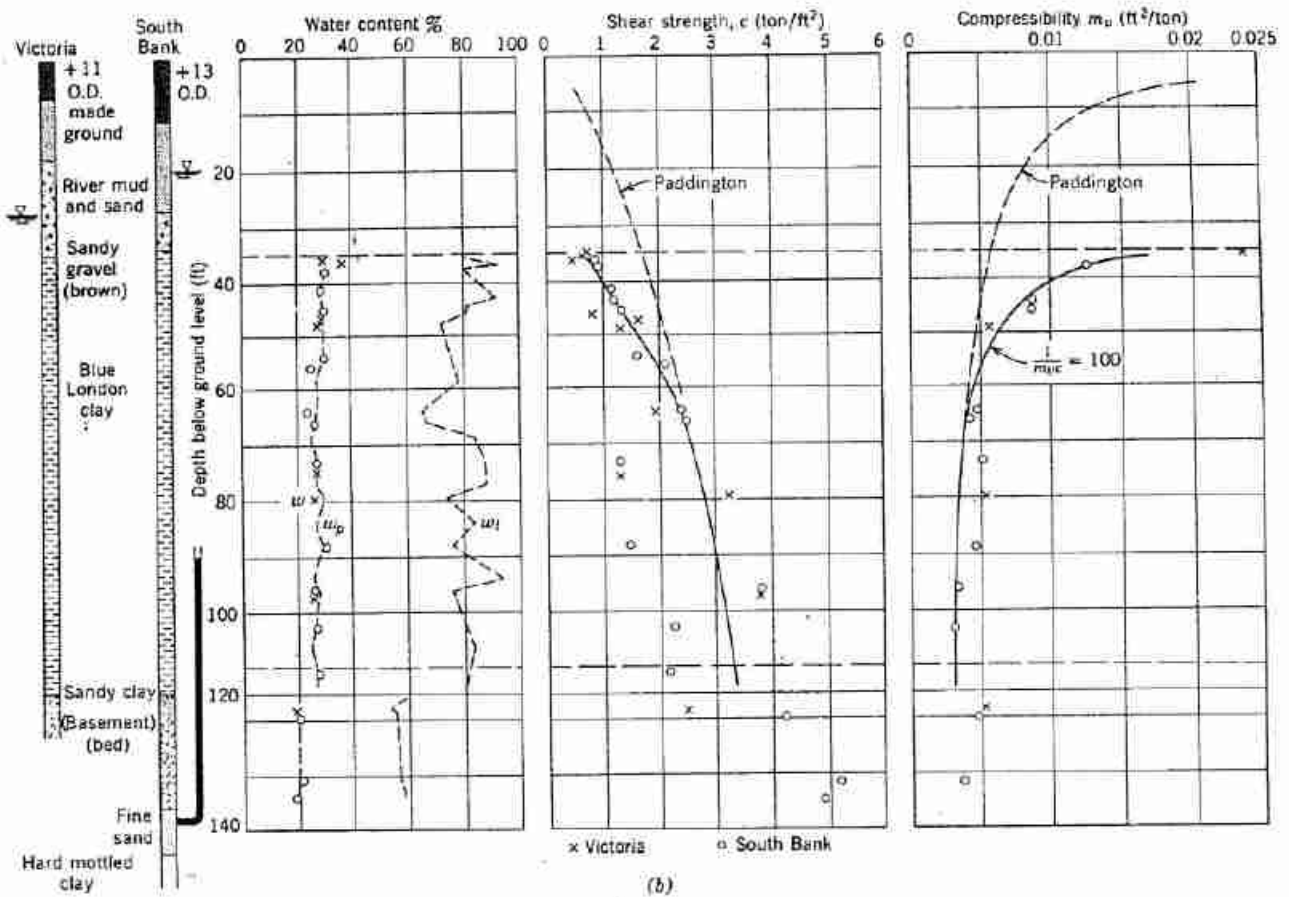


Fig. 7.8 London clay. (a) Test results at Paddington. (b) Test results at Victoria and South Bank. (From Skempton and Henkel, 1957.)



(b)

Fig. 7.8 (continued)

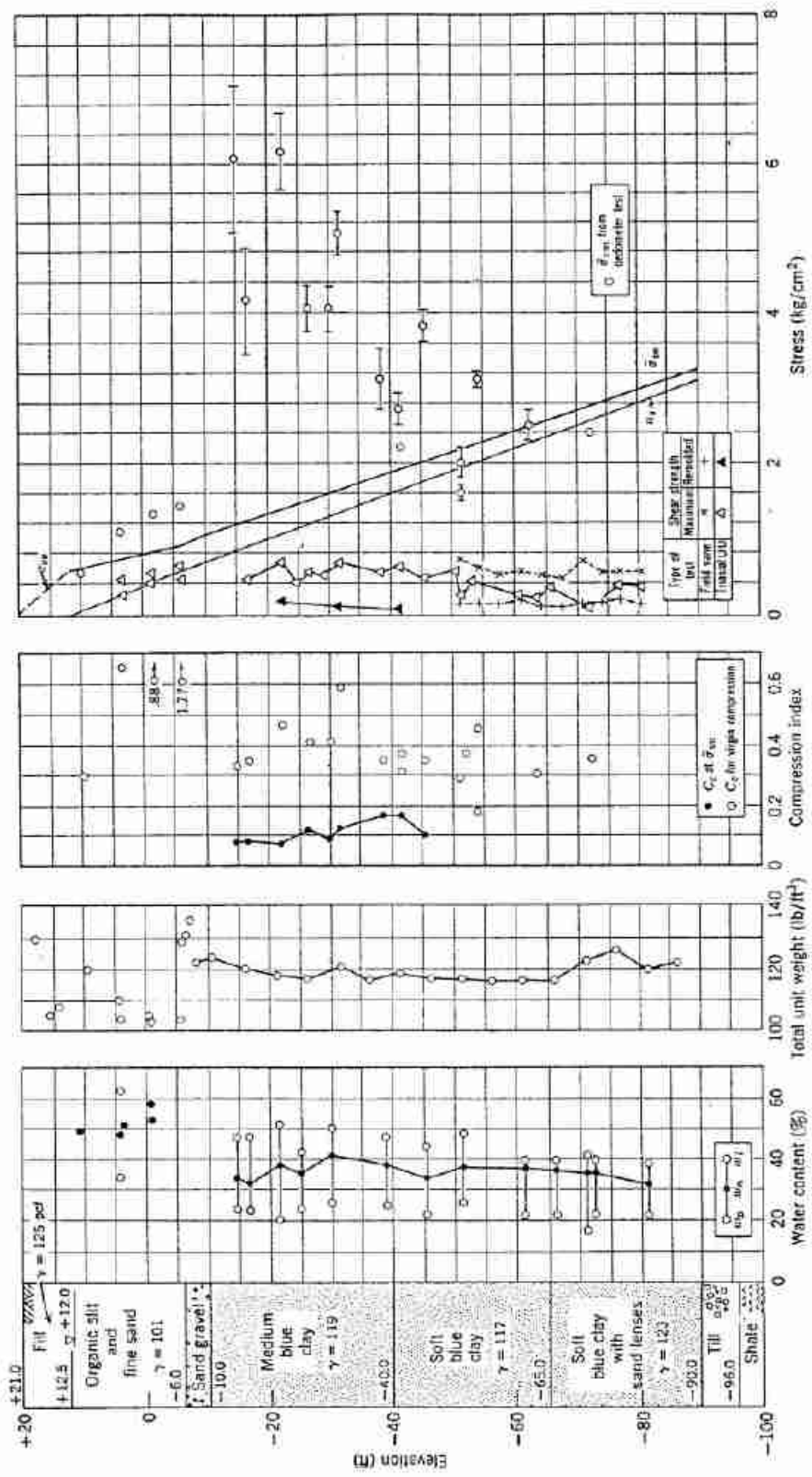
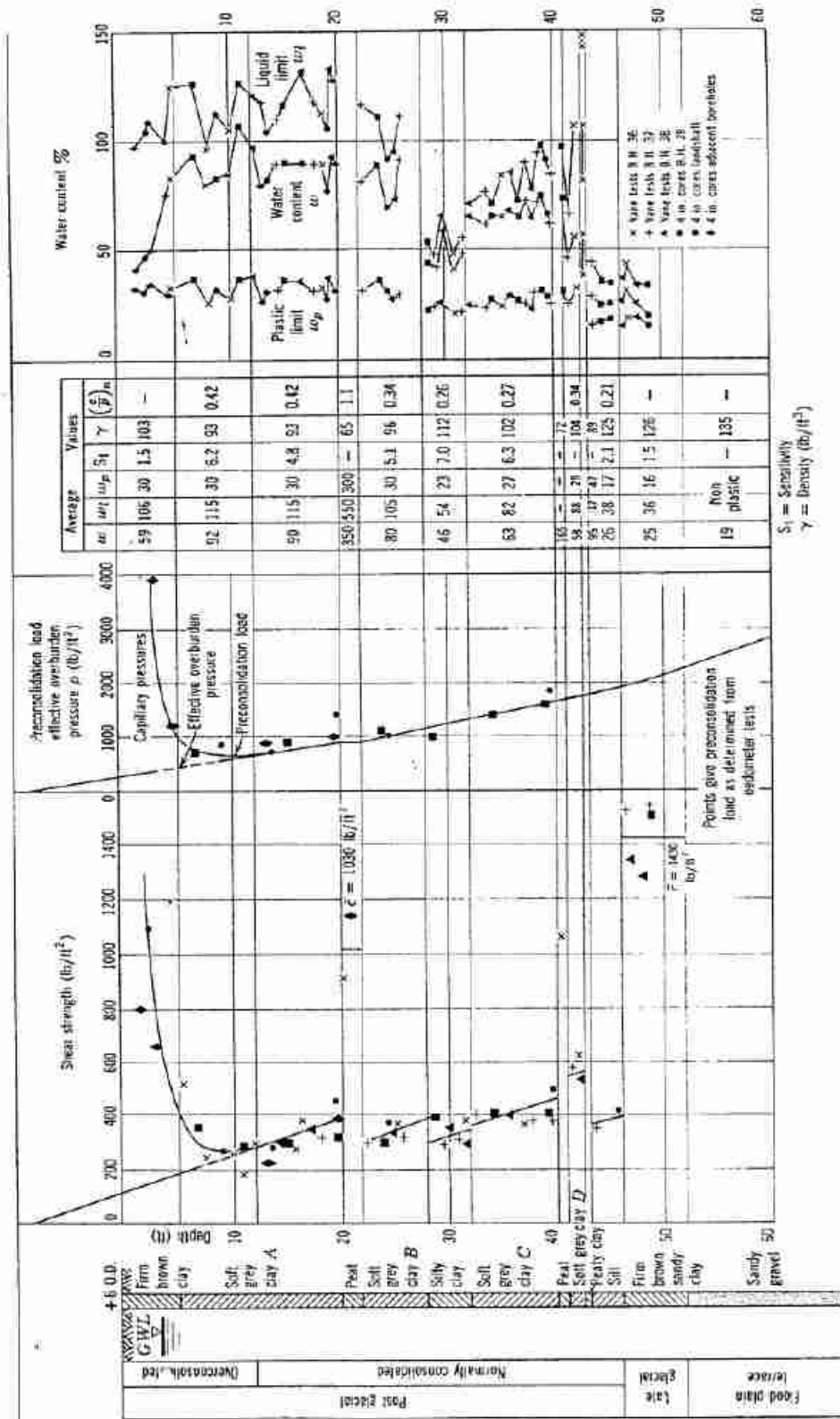


Fig. 7.9 Profile at M.I.T. Advanced Engineering Center.



Swelhaven test results

Fig. 7.10 Thames Estuary clay (From Skempton and Henkel, 1953)

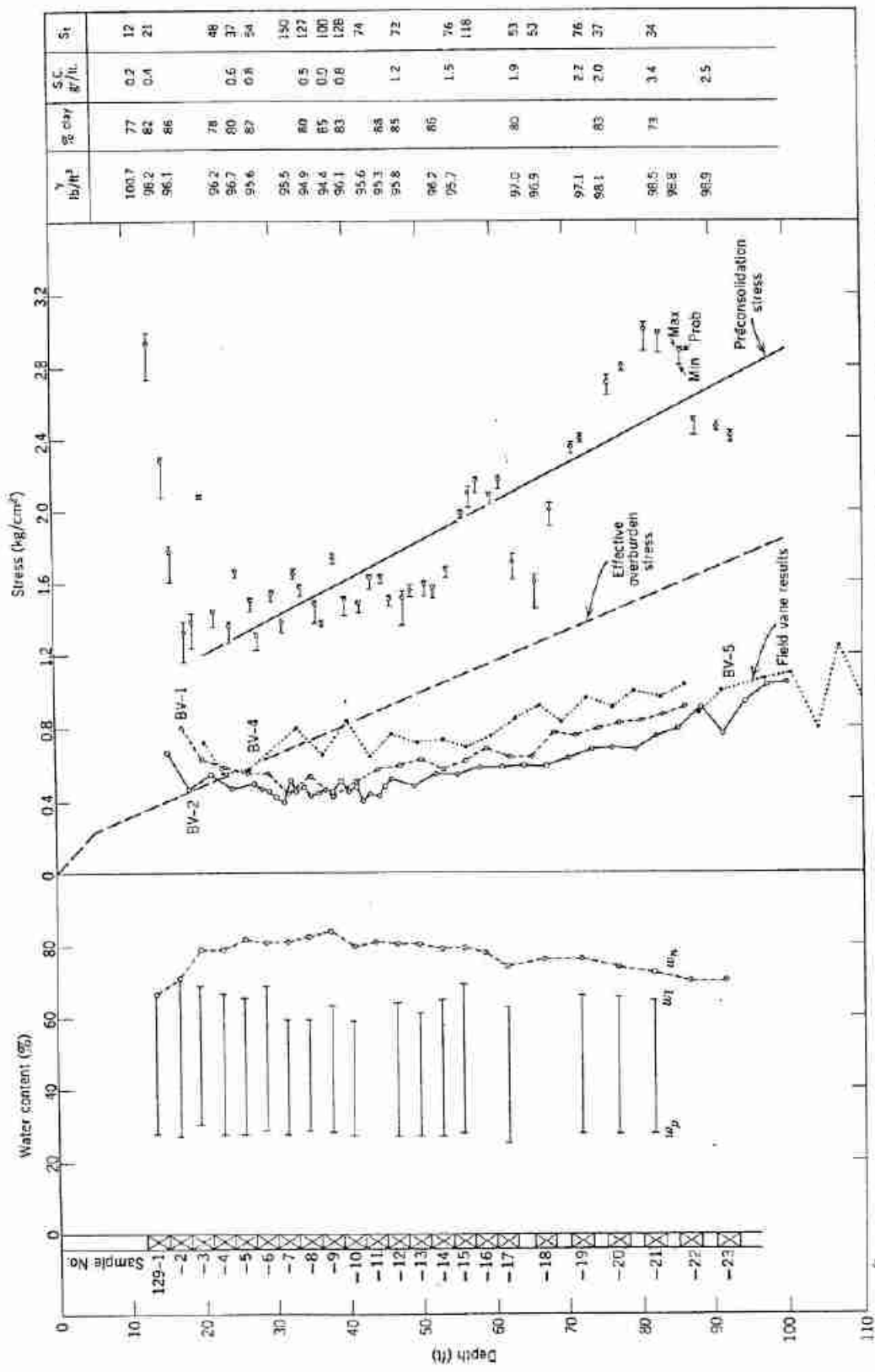


Fig. 7.11 Canadian clay (private communication, Div. of Building Research, National Research Council of Canada, Ottawa).

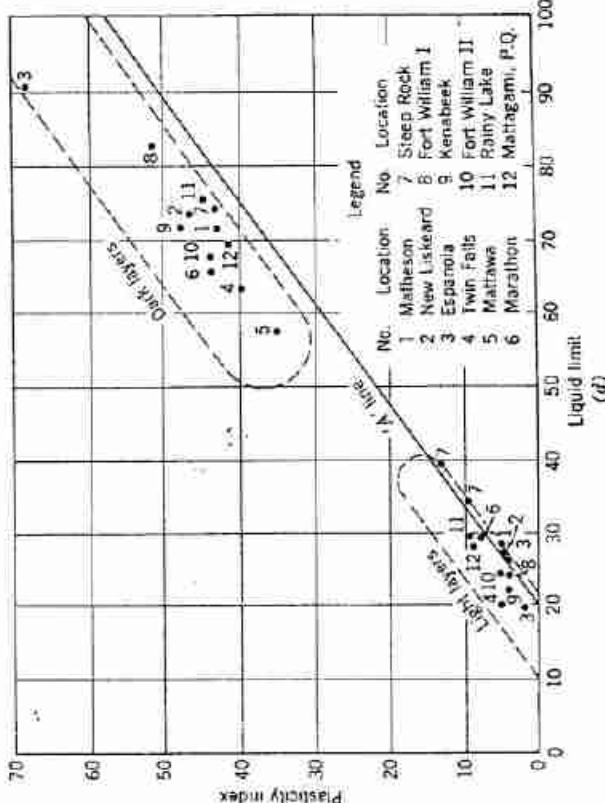
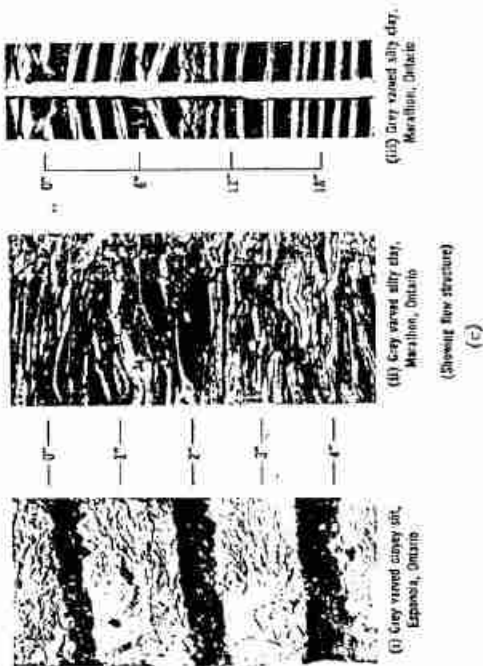
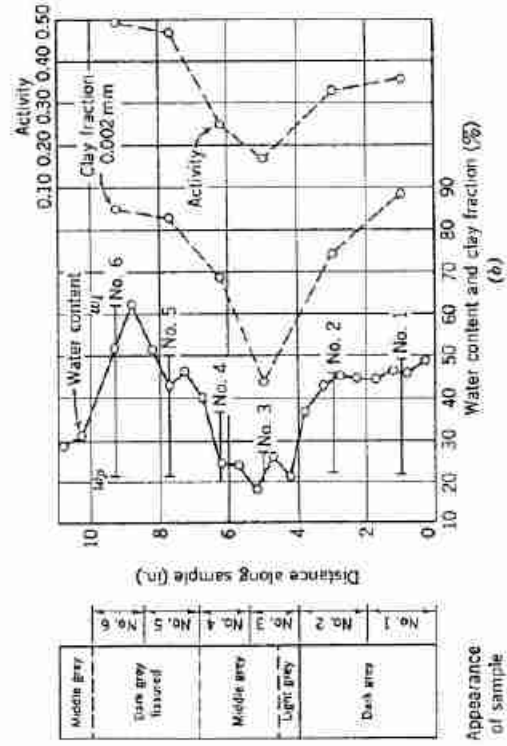
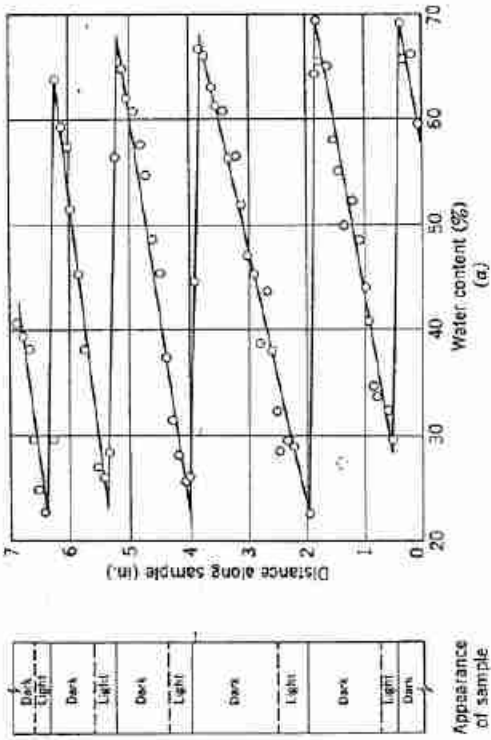


Fig. 7.12 Canadian varved clays. (a) Water content variation in a sample of varved clay (after De Lory, 1960). (b) Water content and activity variation in a sample of varved clay (after De Lory, 1960). (c) Varved clay samples. (d) Casagrande classification chart for some varved clays. (From Milligan, Soderman, and Ruika, 1962.)

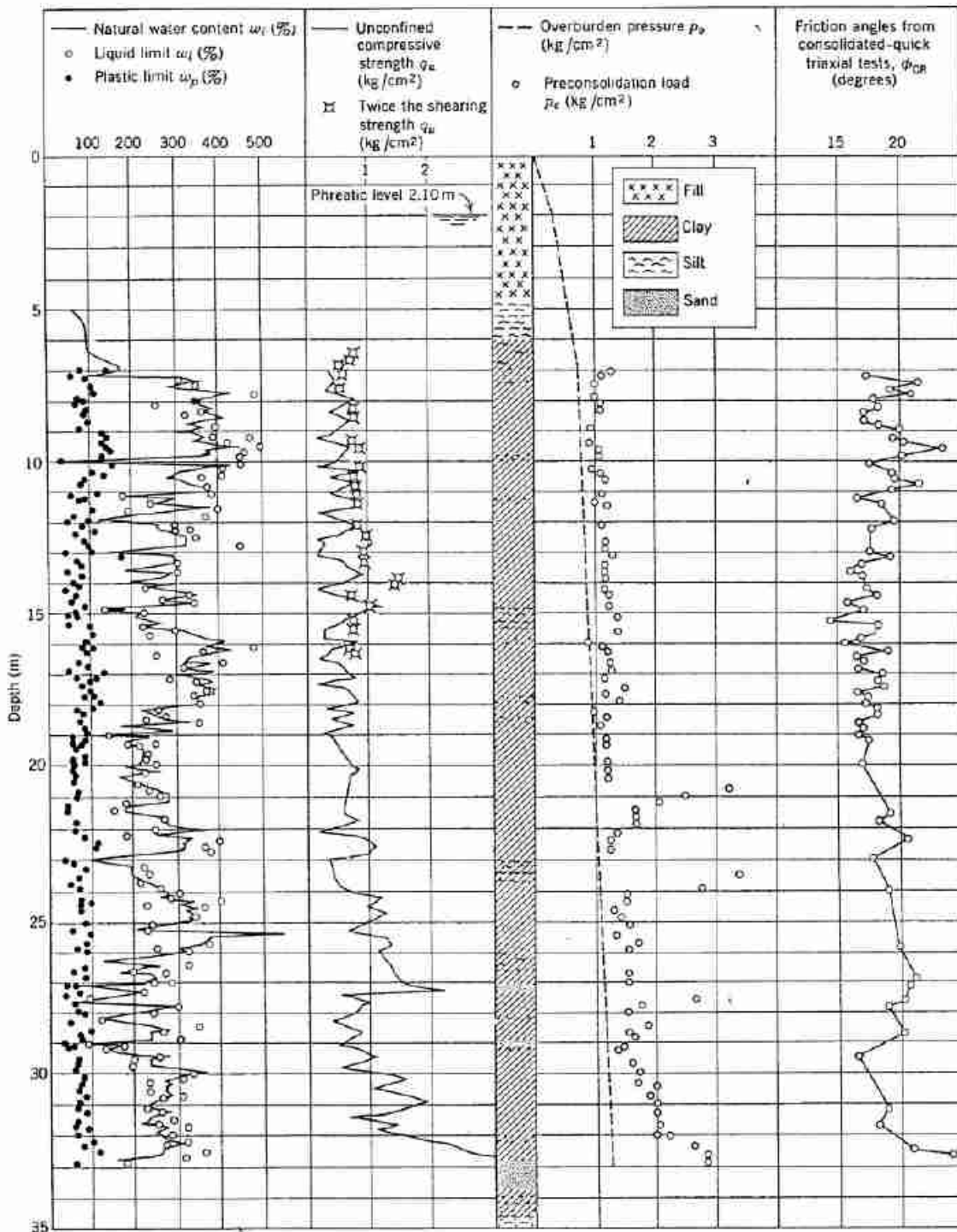
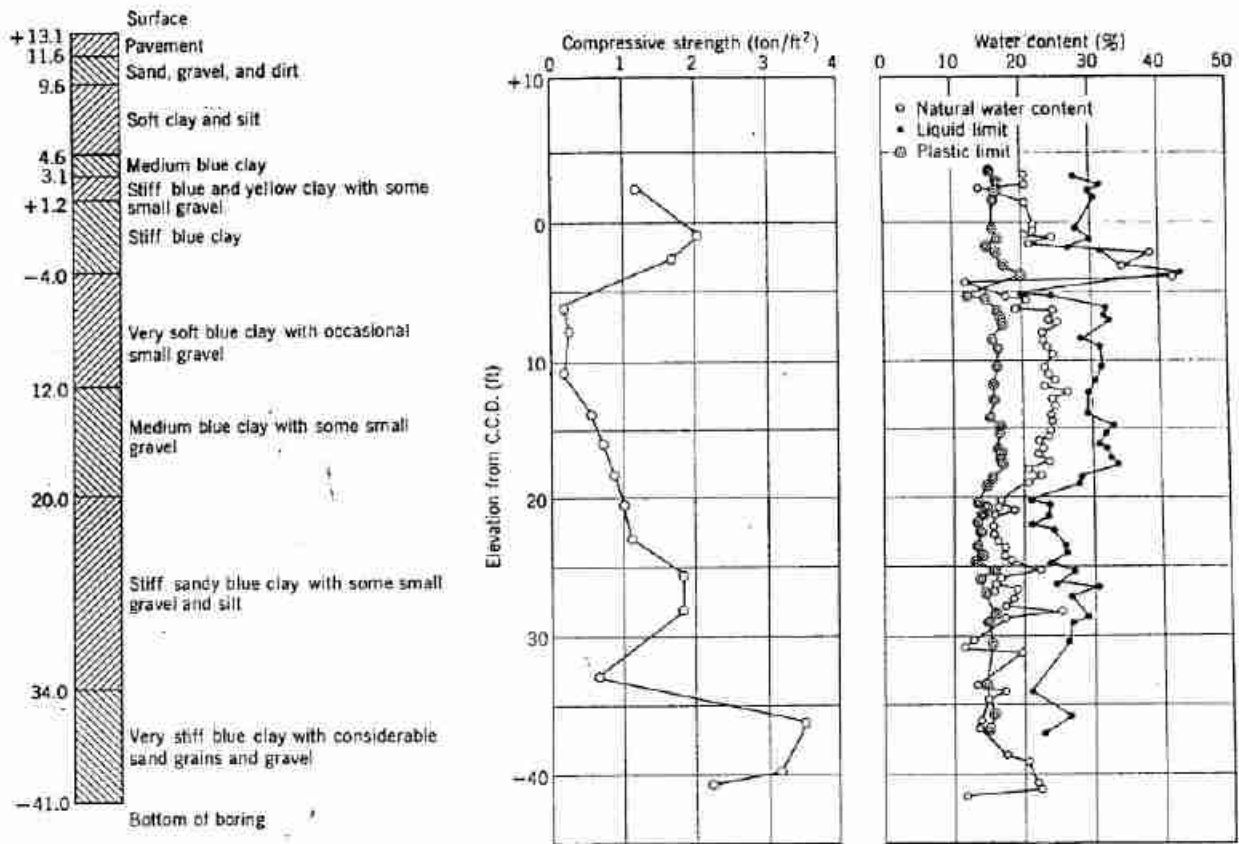
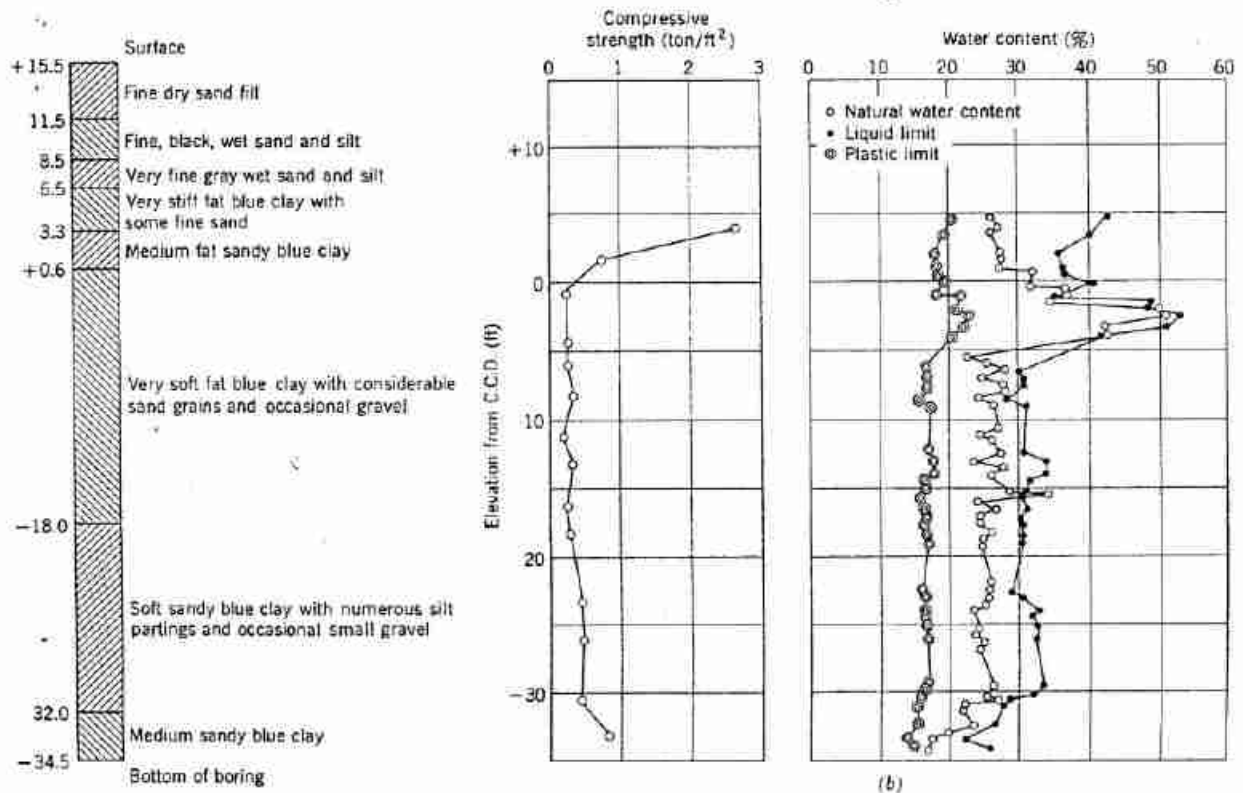


Fig. 7.13 Mechanical properties of clays of the Valley of Mexico at a typical spot of the City (From Marsal, 1957).



(a)



(b)

Fig. 7.14 Chicago subsoils. (a) Boring on Division Street near Milwaukee Avenue (1200N, 1600W). (b) Boring at Congress Street and Racine Avenue (500S, 1200W). (From Peck and Reed, 1954.)

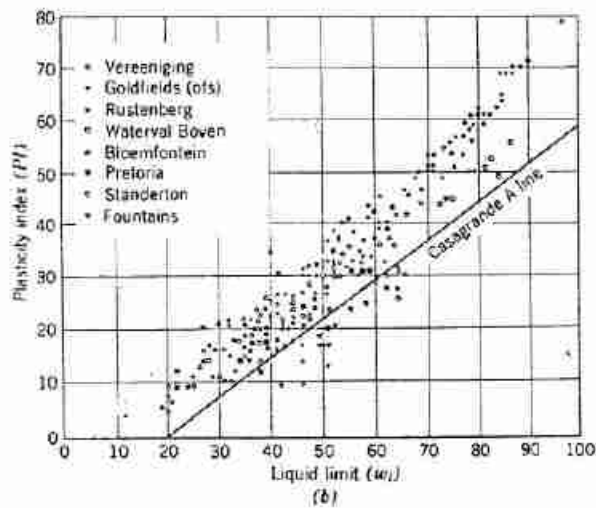
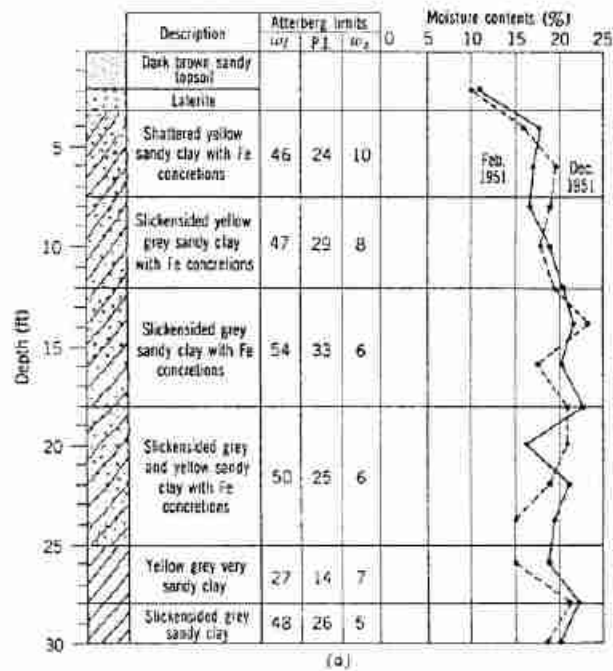


Fig. 7.15 South African clays. (a) Variations of direct measurements of moisture content in the soil under an impermeable slab. (b) Results of indicator tests on South African soils where heaving conditions have been observed. (From Jennings, 1953.)

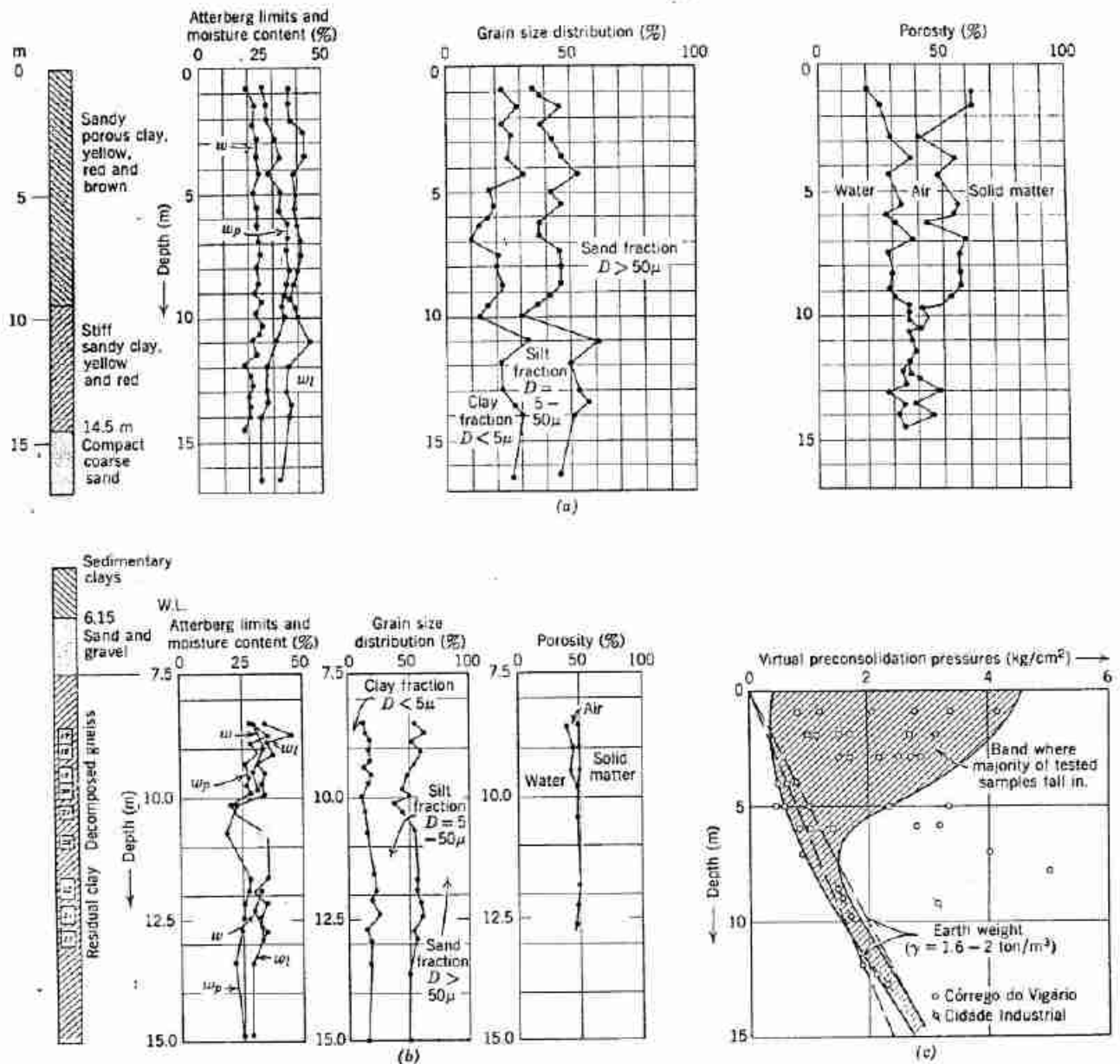
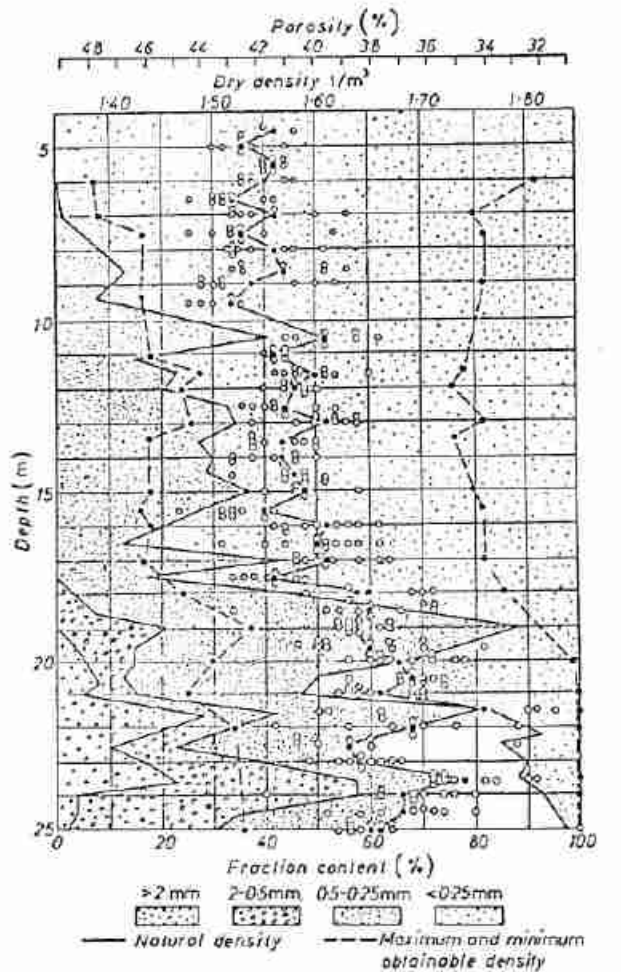


Fig. 7.16 Brazilian residual clay. (a) Porous residual clay (Campinas) from decomposition of a clayey sandstone. Variation of consistency, grain-size distribution, and porosity with depth. (b) Residual clay (Belo Horizonte) from decomposition of gneiss. Variation of consistency, grain-size distribution, and porosity with depth. (c) Virtual preconsolidation pressures against depth of samples. (From Vargas, 1953.)



Natural density and grading of alluvial sands (vertical section of pit)
 Fig. 7.17 Volga River sand (From Durante et al., 1957).

3. There are many methods available for investigating subsoils. The standard penetration test is very useful for giving an approximate, general portrayal of the subsoil profile. Sampling and laboratory and field testing are usually necessary to obtain design data.
4. Experience—as illustrated by the actual profiles shown in Figs. 7.7 to 7.17—emphasizes the importance of stress history and the great variability of soil properties in a given profile.

PROBLEMS

7.1 Suggest soil investigation methods for each of the following situations:

- a. Dwelling house on sand.
 - b. Highway section on rock.
 - c. 100-ft-high embankment on 20-ft deep deposit of soft clay.
 - d. Large compressor foundation on 10-ft hydraulic sand fill.
- 7.2 Plot depth (ordinate) versus liquidity index (abscissa) for:

- a. Mangerud clay (Fig. 7.7).
- b. Paddington clay (Fig. 7.8).
- c. Chicago clay (Fig. 7.14).

Comment on any relationship between liquidity index and geological history for each clay.

7.3 Plot sensitivity (ordinate) versus liquidity index (abscissa) using data from the following soils:

- a. Drammen clay and Mangerud clay (Fig. 7.7).
- b. Boston blue clay (Fig. 7.9).

Comment on any relationship between sensitivity and liquidity index.

7.4 Compute the activity of Boston blue clay, a Canadian varved clay, and a Brazilian residual clay.

7.5 For the Volga River sand (Fig. 7.17) plot relative density (abscissa) versus depth (ordinate).

RALPH B. PECK



Dr. Ralph Peck was born in Winnipeg, Canada, on June 23, 1912 and received his education at Rensselaer Polytechnic Institute and Harvard University. At Harvard in 1939, Dr. Peck began a long association with Dr. Terzaghi. As Dr. Terzaghi's representative during the initial construction of the Chicago subways, Dr. Peck was in charge of the soil laboratory and of the program of field measurements on one of the earliest large construction projects in which modern soil mechanics played a major role.

Dr. Peck has devoted his efforts primarily to the application of soil mechanics to design and construction, and to the evaluation and the presentation of the results of research in form suitable for ready use by the practicing engineer. Dr. Peck is one of the most respected consulting soil engineers in the world. An excellent lecturer, Dr. Peck has left his imprint on the many students he has had at the University of Illinois. His textbook, jointly authored with Dr. Terzaghi, *Soil Mechanics in Engineering Practice*, is a widely used book, both by students and by practicing engineers.

Dr. Peck has been the recipient of the Norman Medal and Wellington Prize of the ASCE, and has been a Terzaghi Lecturer.

PART III

Dry Soil

Part III establishes certain basic principles concerning the stress-strain behavior of the skeleton of the soil by considering cases (i.e., dry soils) in which there are no important interactions between the skeleton and the pore fluid. The principles concerning the properties of dry soils will be of the greatest value to the study of soils containing water in Parts IV and V.

When we talk about dry soil in Part III, we mean an

air-dried soil. Even an air-dried sand actually contains a small amount of water (perhaps a water content as much as 1%). However, as long as the particle size is that of a coarse silt or larger, this small amount of moisture has little or no effect upon the mechanical properties of the soil. The principles established in Part III apply to a wide variety of dry soils including coarse silts, sands, and gravels.

CHAPTER 8

Stresses within a Soil Mass

Part II dealt with the forces that act between individual soil particles. In an actual soil it obviously is impossible to keep track of the forces at each individual contact point. Rather, it is necessary to use the concept of *stress*.

This chapter introduces the concept of stress as it applies to soils, discusses the stresses that exist within a soil as a result of its own weight and as a result of applied forces, and, finally, presents some useful geometric representations for the state of stress at a point within a soil.

8.1 CONCEPT OF STRESS FOR A PARTICULATE SYSTEM

Figure 8.1a shows a hypothetical small measuring device (Element *A*) buried within a mass of soil. We imagine that this measuring device has been installed in

such a way that no soil particles have been moved. The sketches in Fig. 8.1*b, c* depict the horizontal and vertical faces of Element *A*, with soil particles pushing against these faces. These particles generally exert both a normal force and a shear force on these faces. If each face is square, with dimension *a* on each side, then we can define the stresses acting upon the device as

$$\sigma_v = \frac{N_v}{a^2}, \quad \sigma_h = \frac{N_h}{a^2}, \quad \tau_h = \frac{T_h}{a^2}, \quad \tau_v = \frac{T_v}{a^2} \quad (8.1)$$

where N_v and N_h , respectively, represent the normal forces in the vertical and horizontal directions; T_h and T_v , respectively, represent the shear forces in the vertical and horizontal directions; and σ_v , σ_h , τ_v , and τ_h represent the corresponding stresses. Thus we have defined four stresses which can, at least theoretically, be readily visualized and measured.

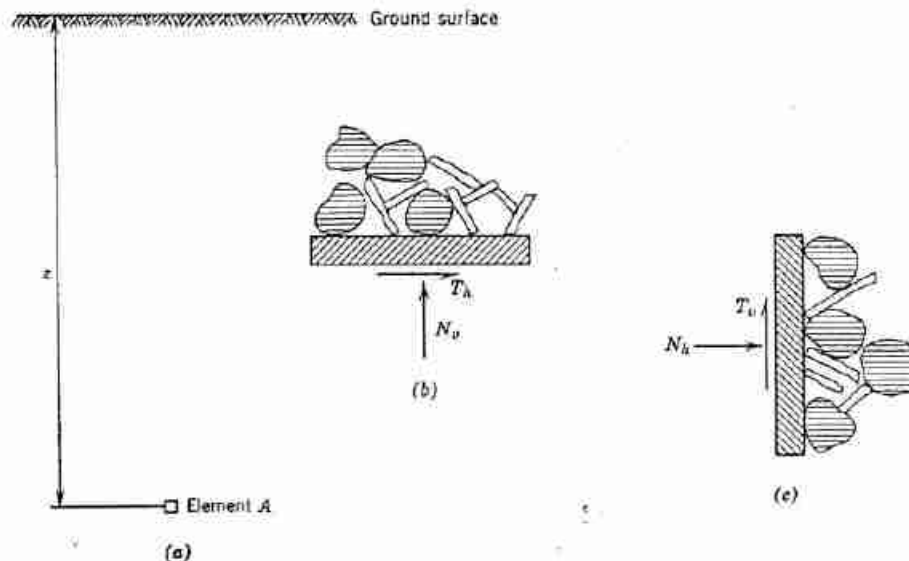


Fig. 8.1 Sketches for definition of stress. (a) Soil profile. (b) and (c) Forces at element *A*.

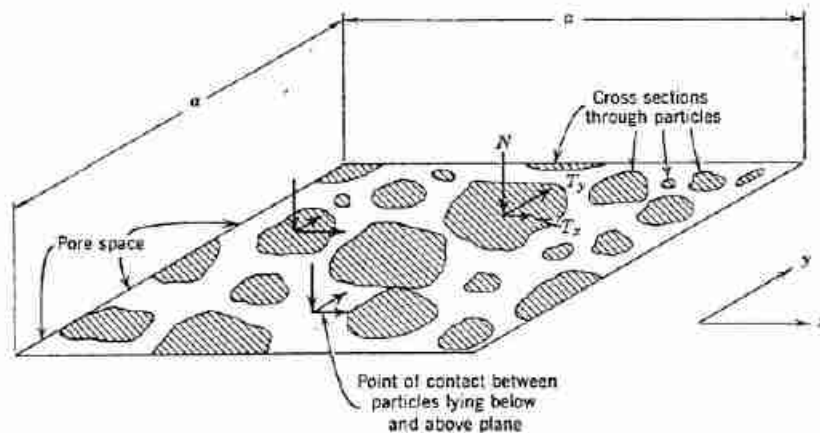


Fig. 8.2. Definition of stress in a particulate system.

$$\sigma = \frac{\Sigma N}{a \times a} \quad \tau_x = \frac{\Sigma T_x}{a \times a} \quad \tau_y = \frac{\Sigma T_y}{a \times a}$$

In Part III, except as noted, it will be assumed that the pressure within the pore phase of the soil is zero; i.e., equal to atmospheric pressure. Hence the forces N , N_x , T_x , and T_y arise entirely from force that is being transmitted through the mineral skeleton. In dry soil, stress may be thought of as the *force in the mineral skeleton per unit area of soil*.

Actually, it is quite difficult to measure accurately the stresses within a soil mass, primarily because the presence of a stress gage disrupts the stress field that would otherwise exist if the gage were not present. Hamilton (1960) discusses soil stress gages and the problems associated with them. In order to make our definition of stress apply independently of a stress gage, we pass an imaginary plane through soil, as shown in Fig. 8.2. This plane will pass in part through mineral matter and in part through pore space. It can even happen that this plane passes through one or more contact points between particles. At each point where this plane passes through mineral matter, the force transmitted through the mineral skeleton can be broken up into components normal and tangential to the plane. The tangential components can further be resolved into components lying along a pair of coordinate axes. These various components are depicted in Fig. 8.2. The summation over the plane of the normal components of all forces, divided by the area of the plane, is the *normal stress* σ acting upon the plane. Similarly, the summation over the plane of the tangential components in, say, the x -direction, divided by the area of this plane, is the *shear stress* τ_x in the x -direction.

There is still another picture which is often used when defining stress. One imagines a "wavy" plane which is warped just enough so that it passes through mineral matter only at points of contact between particles. Stress

is then the sum of the contact forces divided by the area of the wavy plane. The summation of all the contact areas will be a very small portion of the total area of the plane, certainly less than 1%. Thus stress as defined in this section is numerically much different from the stress at the points of contact.

In this book, when we use the word "stress" we mean the macroscopic stress; i.e., force/total area, the stress that we have just defined with the aid of Figs. 8.1 and 8.2. When we have occasion to talk about the stresses at the contacts between particles, we shall use a qualifying phrase such as "contact stresses". As was discussed in Chapter 5, the contact stresses between soil particles will be very large (on the order of 100,000 psi). The macroscopic stress as defined in this chapter will typically range from 1 to 1000 psi for most actual problems.

The concept of stress is closely associated with the concept of a continuum. Thus when we speak of the stress acting at a point, we envision the forces against the sides of an infinitesimally small cube which is composed of some homogeneous material. At first sight we may therefore wonder whether it makes sense to apply the concept of stress to a particulate system such as soil. However, the concept of stress as applied to soil is no more abstract than the same concept applied to metals. A metal is actually composed of many small crystals, and on the submicroscopic scale the magnitude of the forces between crystals varies randomly from crystal to crystal. For any material, the inside of the "infinitesimally small cube" is thus only statistically homogeneous. In a sense all matter is particulate, and it is meaningful to talk about macroscopic stress only if this stress varies little over distances which are of the order of magnitude of the size of the largest particle. When we talk about the stresses

at a "point" within a soil, we often must envision a rather large "point".

Returning to Fig. 8.1, we note that the forces N_c , etc., are the sums of the normal and tangential components of the forces at each contact point between the soil particles and the faces. The smaller the size of the particle, the greater the number of contact points with a face of dimension a . Thus for a given value of macroscopic stress, a decreasing particle size means a smaller force per contact. For example, Table 8.1 gives typical values for the force per contact for different values of stress and different particle sizes (see Marsal, 1963).

Table 8.1 Typical Values for Average Contact Forces within Granular Soils

Particle Description	Particle Diameter (mm)	Average Contact Force (lb) for Macroscopic Stress (psi)		
		1	10	100
Gravel	60	3	30	300
	2.0	0.003	0.03	0.3
Sand	0.06	3×10^{-4}	3×10^{-3}	0.0003
	0.002	3×10^{-9}	3×10^{-8}	3×10^{-7}

8.2 GEOSTATIC STRESSES

Stresses within soil are caused by the external loads applied to the soil and by the weight of the soil. The pattern of stresses caused by applied loads is usually quite complicated. The pattern of stresses caused by the soil's own weight can also be complicated. However, there is one common situation in which the weight of soil gives rise to a very simple pattern of stresses: when the ground surface is horizontal and when the nature of the soil varies but little in the horizontal directions. This situation frequently exists, especially in sedimentary soils. In such a situation, the stresses are called *geostatic stresses*.

Vertical Geostatic Stress

In the situation just described, there are no shear stresses upon vertical and horizontal planes within the soil. Hence the vertical geostatic stress at any depth can be computed simply by considering the weight of soil above that depth.

Thus, if the unit weight of the soil is constant with

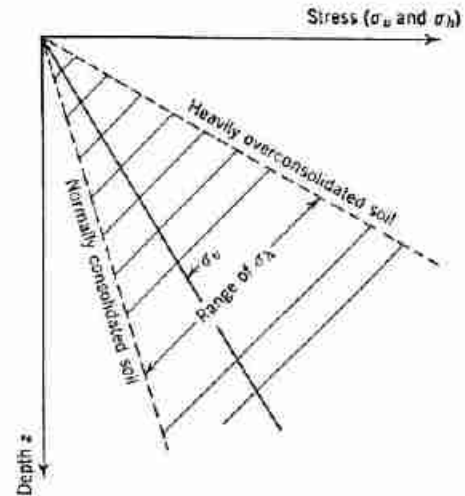


Fig. 8.3 Geostatic stresses in soil with horizontal surface.

depth,

$$\sigma_v = z\gamma \tag{8.2}$$

where z is the depth and γ is the total unit weight of the soil. In this case, the vertical stress will vary linearly with depth, as shown in Fig. 8.3. A typical unit weight for a dry soil is 100 pcf. Using this unit weight, Eq. 8.2 can be converted into the useful set of formulas listed in Table 8.2.¹

Table 8.2 Formulas for Computing Vertical Geostatic Stress

Units for σ_v	Units for z	Formula for σ_v
psf	feet	100z
psi	feet	0.694z
kg/cm ²	meters	0.158z
atmospheres	feet	0.0473z

Note. Based upon $\gamma = 100$ pcf. For any other unit weight, multiply by $\gamma/100$.

Of course the unit weight is seldom constant with depth. Usually a soil will become denser with depth because of the compression caused by the geostatic stress. If the unit weight of the soil varies continuously with depth, the vertical stress can be evaluated by means of the integral

$$\sigma_v = \int_0^z \gamma dz \tag{8.3}$$

¹ A complete list of factors for converting one set of units to others is given in the Appendix.

If the soil is stratified and the unit weight is different for each stratum, then the vertical stress can conveniently be computed by means of the summation

$$\sigma_v = \sum \gamma \Delta z \quad (8.4)$$

Example 8.1 illustrates the computation of vertical geostatic stress for a case in which the unit weight is a function of the geostatic stress.

► Example 8.1

Given. The relationship between vertical stress and unit weight

$$\gamma = 95 + 0.0007\sigma_v$$

where γ is in pcf and σ_v is in psf.

Find. The vertical stress at a depth of 100 feet for a geostatic stress condition.

Solution Using Calculus. From Eq. 8.3:

$$\sigma_v = \int_0^z (95 + 0.0007\sigma_v) dz \quad (z \text{ in feet})$$

or

$$\frac{d\sigma_v}{dz} = 95 + 0.0007\sigma_v$$

The solution of this differential equation is:

$$\sigma_v = 135,800(e^{0.0007z} - 1)$$

For $z = 100$ ft:

$$\sigma_v = 135,800(1.0725 - 1) = 9840 \text{ psf}$$

Alternative Approximate Solution by Trial and Error.

First trial: assume average unit weight from $z = 0$ to $z = 100$ ft is 100 pcf. Then σ_v at $z = 100$ ft would be 10,000 psf. Actual unit weight at that depth would be 102 pcf, and average unit weight (assuming linear variation of γ with depth) would be 98.5 pcf.

Second trial: assume average unit weight of 98.5 pcf. Then at $z = 100$ ft, $\sigma_v = 9850$ psf and $\gamma = 111.9$ pcf. Average unit weight is 98.45 pcf, which is practically the same as for the previous trial.

The slight discrepancy between the two answers occurs because the unit weight actually does not quite vary linearly with depth as assumed in the second solution. The discrepancy can be larger when γ is more sensitive to σ_v . The solution using calculus is more accurate, but the user easily can make mistakes regarding units. The accuracy of the trial solution can be improved by breaking the 100-ft depth into layers and assuming a uniform variation of unit weight through each layer. ◀

Horizontal Geostatic Stress

The ratio of horizontal to vertical stress is expressed by a factor called the *coefficient of lateral stress* or *lateral*

stress ratio, and is denoted by the symbol K :

$$K = \frac{\sigma_h}{\sigma_v} \quad (8.5)$$

This definition of K is used whether or not the stresses are geostatic.

Even when the stresses are geostatic, the value of K can vary over a rather wide range depending on whether the ground has been stretched or compressed in the horizontal direction by either the forces of nature or the works of man. The possible range of the value of K will be discussed in some detail in Chapter 11.

Often we are interested in the magnitude of the horizontal geostatic stress in the special case where there has been no lateral strain within the ground. In the special case, we speak of the *coefficient of lateral stress at rest*² (or *lateral stress ratio at rest*) and use the symbol K_0 .

As discussed in Chapter 7, a sedimentary soil is built up by an accumulation of sediments from above. As this build-up of overburden continues, there is vertical compression of soil at any given elevation because of the increase in vertical stress. As the sedimentation takes place, generally over a large lateral area, there is no reason why there should be significant horizontal compression during sedimentation. From this, one could logically reason that in such sedimentary soil the horizontal total stress should be less than the vertical stress. For a sand deposit formed in this way, K_0 will typically have a value between 0.4 and 0.5.

On the other hand, there is evidence that the horizontal stress can exceed the vertical stress if a soil deposit has been heavily preloaded in the past. In effect, the horizontal stresses were "locked-in" when the soil was previously loaded by additional overburden, and did not disappear when this loading was removed. For this case, K_0 may well reach a value of 3.

The range of horizontal stresses for the at rest condition have been depicted in Fig. 8.3.

8.3 STRESSES INDUCED BY APPLIED LOADS

Results from the theory of elasticity are often used to compute the stresses induced within soil masses by externally applied loads. The assumption of this theory is that stress is proportional to strain. Most of the useful solutions from this theory also assume that soil is *homogeneous* (its properties are constant from point to point) and *isotropic* (its properties are the same in each direction through a point). Soil seldom if ever exactly fulfills, and often seriously violates, these assumptions. Yet the soil engineer has little choice but to use the results of this theory together with engineering judgment.

² The phrase *coefficient of lateral pressure* is also used, but in classical mechanics the word pressure is used in connection with a fluid that cannot transmit shear.

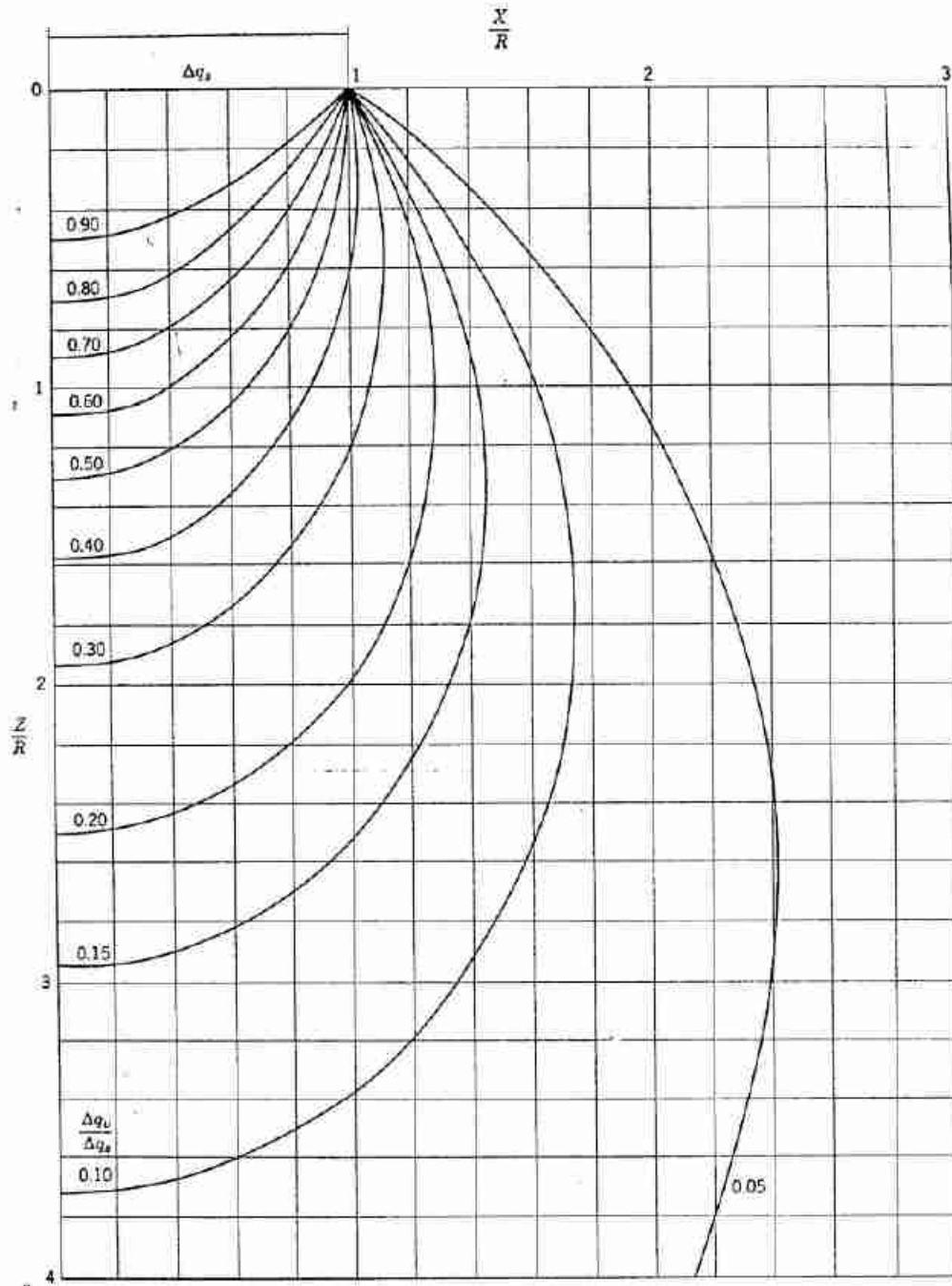


Fig. 8.4 Vertical stresses induced by uniform load on circular area.

It is a very tedious matter to obtain the elastic solution for a given loading and set of boundary conditions. In this book, we are concerned not with how to obtain solutions but rather with how to use these solutions. This section presents several solutions in graphical form.

Uniform load over a circular area. Figures 8.4 and 8.5 give the stresses caused by a uniformly distributed normal stress Δq_s acting over a circular area of radius R on the

surface of an elastic half-space.³ These stresses must be added to the initial geostatic stresses. Figure 8.4 gives

³ In general, the stresses computed from the theory of elasticity are functions of Poisson's ratio μ . This quantity will be defined in Chapter 12. However, vertical stresses resulting from normal stresses applied to the surface are always independent of μ , and stresses caused by a strip load are also independent of μ . Thus of the charts presented in this chapter only those in Fig. 8.5 depend upon μ , and are for $\mu = 0.45$.

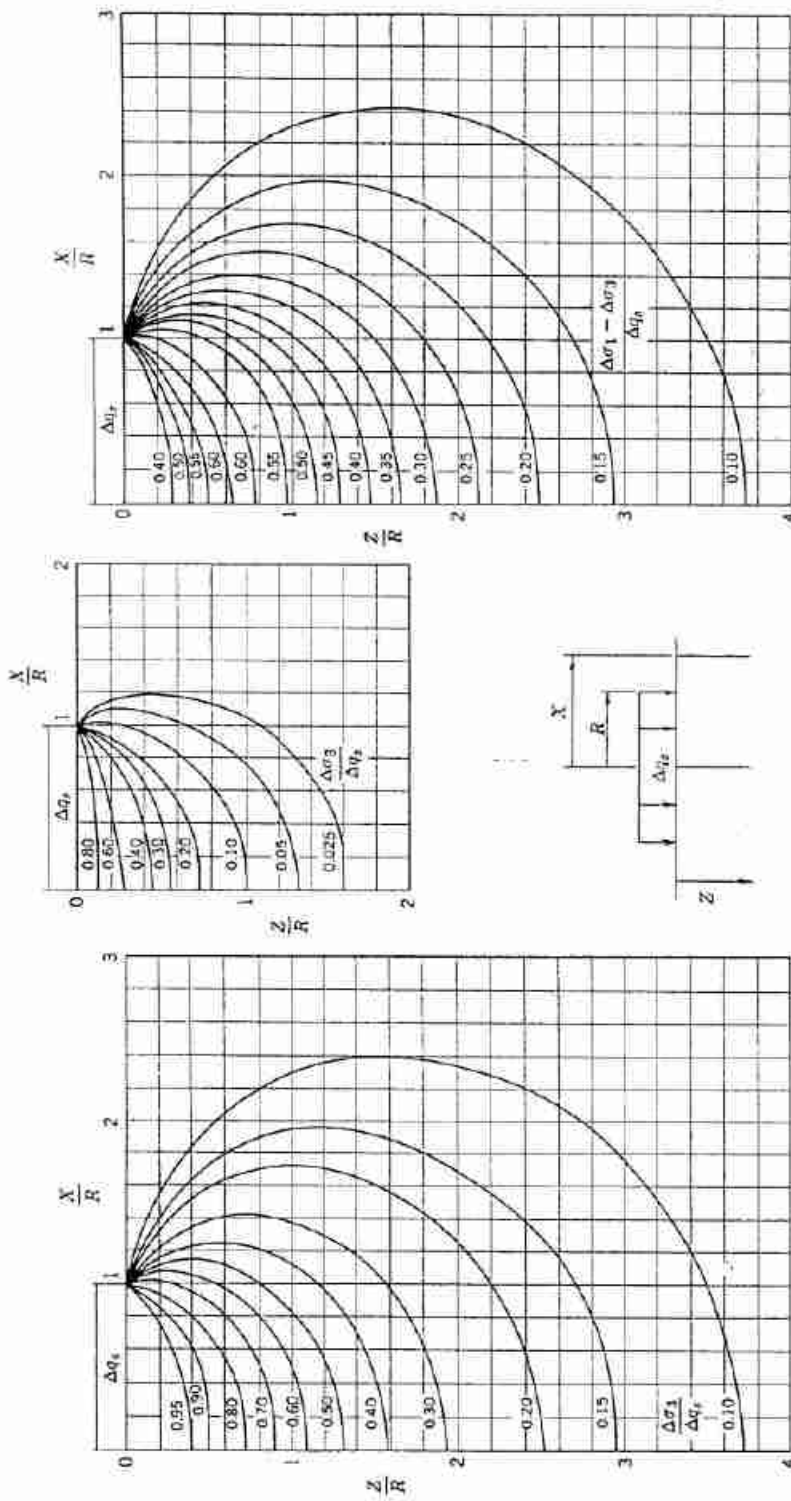


Fig. 8.5 Stresses under uniform load on circular area.

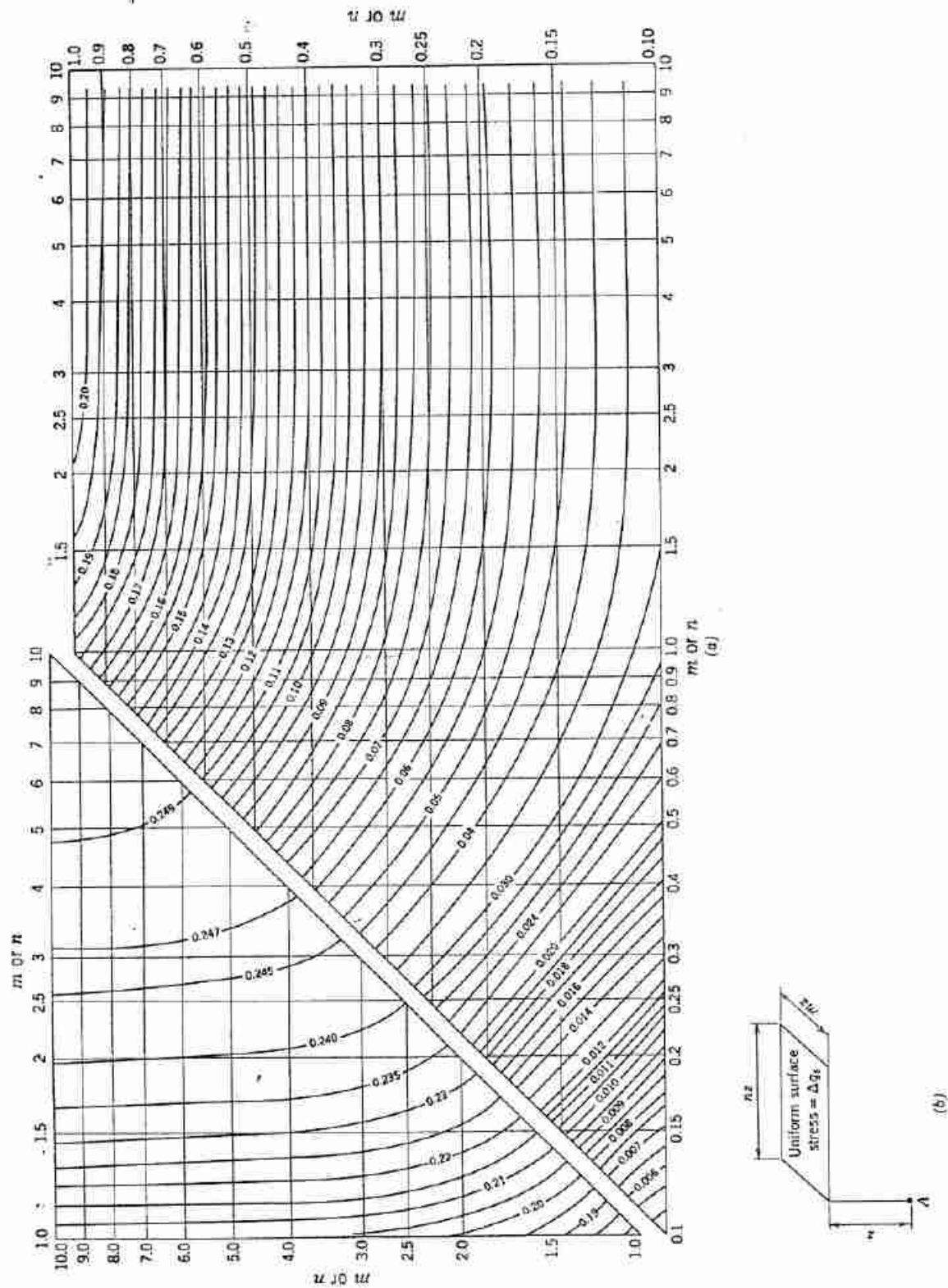


Fig. 8.6 (a) Chart for use in determining vertical stresses below corners of loaded rectangular surface areas on elastic, isotropic material. Chart gives $f(m, n)$. (b) At point A , $\Delta\sigma_v = \Delta q_0 \times f(m, n)$. (From Newmark, 1942)

the vertical stresses. The significance of $\Delta\sigma_1$ and $\Delta\sigma_3$, given in Fig. 8.5, will be discussed in Section 8.4. For the moment it suffices to know that along the vertical center line

$$\Delta\sigma_1 = \Delta\sigma_v \quad \text{and} \quad \Delta\sigma_3 = \Delta\sigma_h$$

Example 8.2 illustrates the use of these charts. The stresses induced by a surface loading must be added to the geostatic stresses in order to obtain the final stresses after a loading.

Charts such as these give the user a feel for the spread of stresses through a soil mass. For example, the zone under a loaded area wherein the vertical stresses are significant is frequently termed the "bulb" of stresses. For a circular loaded area, the vertical stresses are less than $0.15\Delta q_s$ at a depth of $3R$ and less than $0.10\Delta q_s$ at a depth of $4R$. Usually the stress bulb is considered to be the volume within the contour for $0.1\Delta q_s$, but this choice is strictly arbitrary.

Uniform load over rectangular area. The chart in Fig. 8.6 may be used to find the vertical stresses beneath the corner of a rectangularly loaded area. Example 8.3 illustrates the way in which this chart may be used to find the stresses at points not lying below the corner of a load. Problems involving surface loads which are not uniformly distributed or which are distributed over an irregularly shaped area can be handled by breaking the load up into pieces involving uniformly distributed loads over rectangular areas.

Strip loads. Figures 8.7 and 8.8 give stresses caused by strip loadings; i.e., loadings which are infinitely long in the direction normal to the paper. Two cases are shown: load uniformly distributed over the strip and load distributed in a triangular pattern. Again, $\Delta\sigma_1 = \Delta\sigma_v$ and $\Delta\sigma_3 = \Delta\sigma_h$ along the center line.

Other solutions. Solutions are also available in chart form for other loading conditions, for layered elastic bodies, and for elastic bodies which are rigid in the horizontal directions but can strain in the vertical direction. With the digital computer, the engineer can readily

► **Example 8.2**

Given. Soil with $\gamma = 105$ pcf and $K_0 = 0.5$, loaded by $\Delta q_s = 5000$ psf over a circular area 20 ft in diameter.

Find. The vertical and horizontal stresses at a depth of 10 ft. under the center of the loaded area.

Solution.

	Vertical Stress (psf)	Horizontal Stress (psf)
Initial stresses	$\gamma z = 1050$	$K_0 \gamma z = 525$
Stress increments	Fig. 8.4 $(0.64)(5000) = 3200$	Fig. 8.5b $(0.10)(5000) = 500$
Final stresses	4250	1025

► **Example 8.3**

Given. The plan view of a loading shown in Fig. E8.3-1.

Find. The vertical stress at a depth of 10 ft below point *A*.

Solution. The given loading is equivalent to the sum of the four loadings shown in Fig. E8.3-2.

Loading	<i>m</i>	<i>n</i>	Coefficient	$\Delta\sigma_v - \text{ksf}$
I	1.5	2	0.223	0.223
II	0.5	2	0.135	-0.135
III	1.5	0.5	0.131	-0.131
IV	0.5	0.5	0.085	0.085
				0.042 ksf

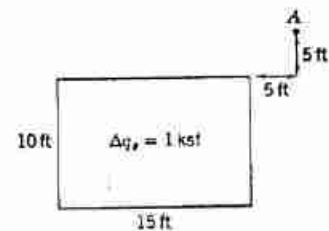


Fig. E8.3-1

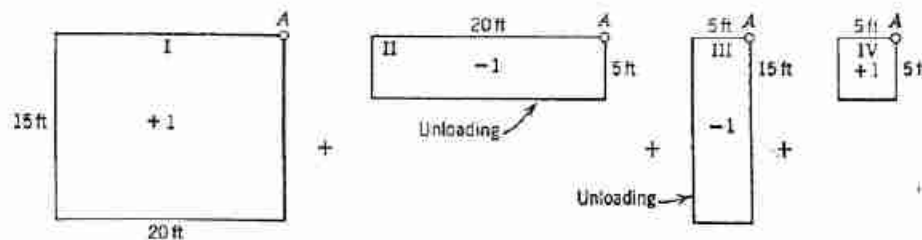


Fig. E8.3-2

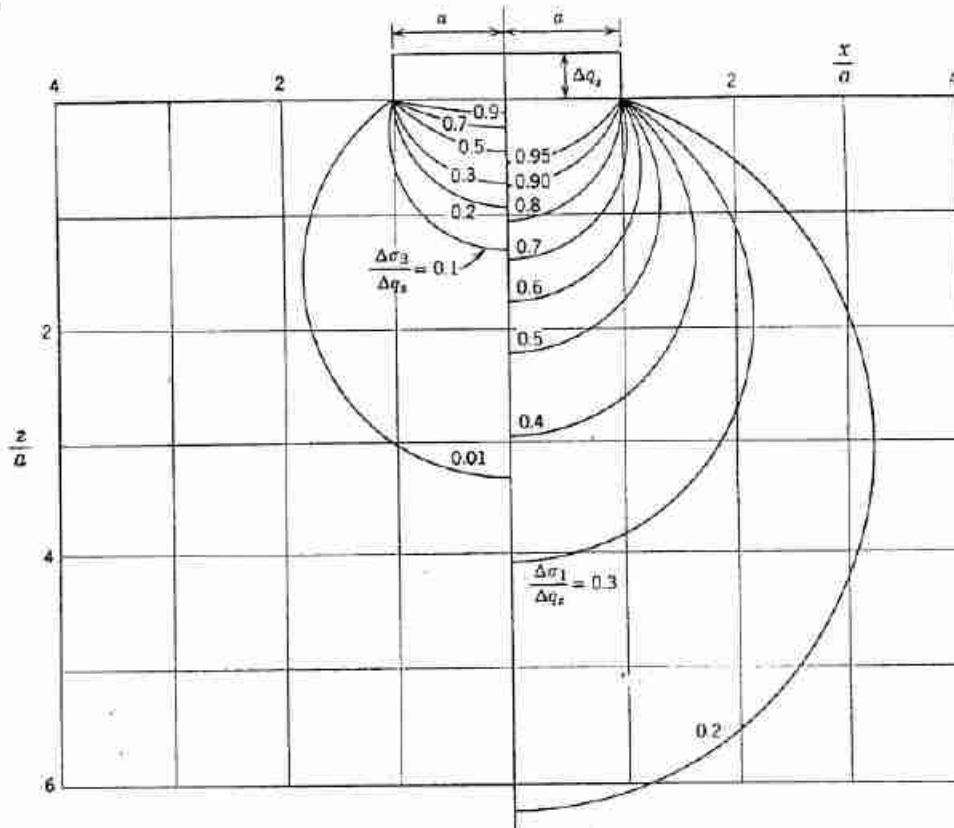


Fig. 8.7 Principal stresses under strip load.

obtain elastic stress distributions for almost any loading and boundary conditions. Charts such as those given here are useful for preliminary analysis of a problem or when the computer is not available.

Accuracy of calculated values of induced stresses. A critical question is: How accurate are the values of induced stresses as calculated from stress distribution theories? This question can be answered only by comparing calculated with actual stress increments for a number of field situations. Unfortunately, there are very few reliable sets of measured stress increments within soil masses (see Taylor, 1945 and Turnbull, Maxwell, and Ahlvin, 1961).

The relatively few good comparisons of calculated with measured stress increments indicate a surprisingly good agreement, especially in the case of vertical stresses. A great number of such comparisons are needed to establish the degree of reliability of calculated stress increments. At the present stage of knowledge, the soil engineer must continue to use stress distribution theories based on the theory of elasticity for lack of better techniques. He should realize, however, that his computed stress values may be in error by as much as $\pm 25\%$ or more.

8.4 PRINCIPAL STRESSES AND MOHR CIRCLE

As in any other material, the normal stress at a point within a soil mass is generally a function of the orientation of the plane chosen to define the stress. It is meaningless to talk of *the* normal stress or *the* shear stress at a point. Thus subscripts will usually be attached to the symbols σ and τ to qualify just how this stress is defined. More generally, of course, we should talk of the *stress tensor*, which provides a complete description for the state of stress at a point. This matter is discussed in textbooks on elementary mechanics, such as Crandall and Dahl (1959). The following paragraphs will state the essential concepts and definitions.

Principal Stresses

There exist at any stressed point three orthogonal (i.e., mutually perpendicular) planes on which there are zero shear stresses. These planes are called the *principal stress planes*. The normal stresses that act on these three planes are called the *principal stresses*. The largest of these three

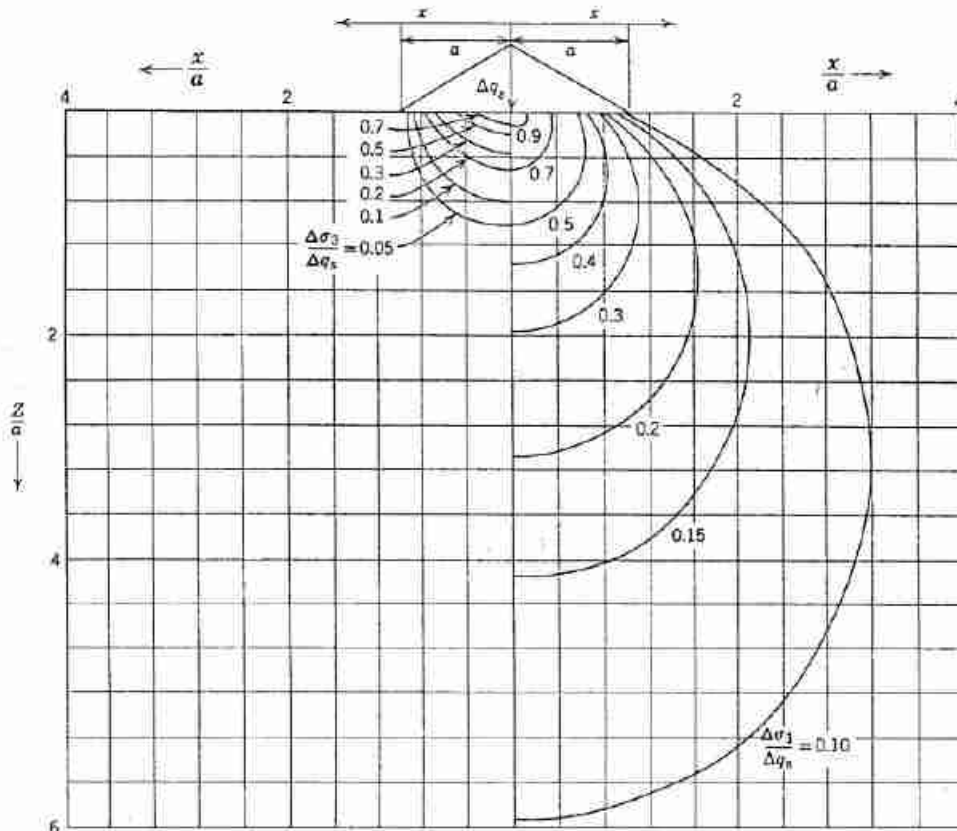


Fig. 8.8 Principal stresses under triangular strip load.

stresses is called the *major principal stress* σ_1 , the smallest is called the *minor principal stress* σ_3 , and the third is called the *intermediate principal stress* σ_2 .

When the stresses in the ground are geostatic, the horizontal plane through a point is a principal plane and so too are all vertical planes through the point. When $K < 1$, $\sigma_x = \sigma_1$, $\sigma_h = \sigma_2$, and $\sigma_z = \sigma_3 = \sigma_h$. When $K > 1$ the situation is reversed: $\sigma_h = \sigma_1$, $\sigma_x = \sigma_3$, and $\sigma_z = \sigma_2 = \sigma_h$. When $K = 1$, $\sigma_x = \sigma_h = \sigma_1 = \sigma_2 = \sigma_3$ and the state of stress is *isotropic*.

We should also recall that the shear stresses on any two orthogonal planes (planes meeting at right angles) must be numerically equal. Returning to the definition of stresses given in Section 8.1, we must have $\tau_u = \tau_v$.

Mohr circle. Throughout most of this book, we shall be concerned only with the stresses existing in two dimensions rather than those in three dimensions.⁴ More

⁴The intermediate principal stress unquestionably has some influence upon the strength and stress-strain properties of soil. However, this influence is not well understood. Until this effect has been clarified, it seems best to work primarily in terms of σ_1 and σ_3 .

specifically, we shall be interested in the state of stress in the plane that contains the major and minor principal stresses, σ_1 and σ_3 . Stresses will be considered positive when compressive. The remainder of the sign conventions are given in Fig. 8.9. The quantity $(\sigma_1 - \sigma_3)$ is called the *deviator stress* or *stress difference*.

Given the magnitude and direction of σ_1 and σ_3 , it is possible to compute normal and shear stresses in any other direction using the equations developed from statics and shown in Fig. 8.9.⁵ These equations, which provide a complete (in two dimensions) description for the state of stress, describe a circle. Any point on the circle, such as *A*, represents the stress on a plane whose normal is oriented at angle θ to the direction of the major principal stress. This graphical representation of the state of stress is known as the *Mohr circle* and is of the greatest importance in soil mechanics.

Given σ_1 and σ_3 and their directions, it is possible to find the stresses in any other direction by graphical

⁵Equations 8.6 and 8.7 are derived in most mechanics texts; e.g., see Crandall and Dahl (1959), pp. 130-138.

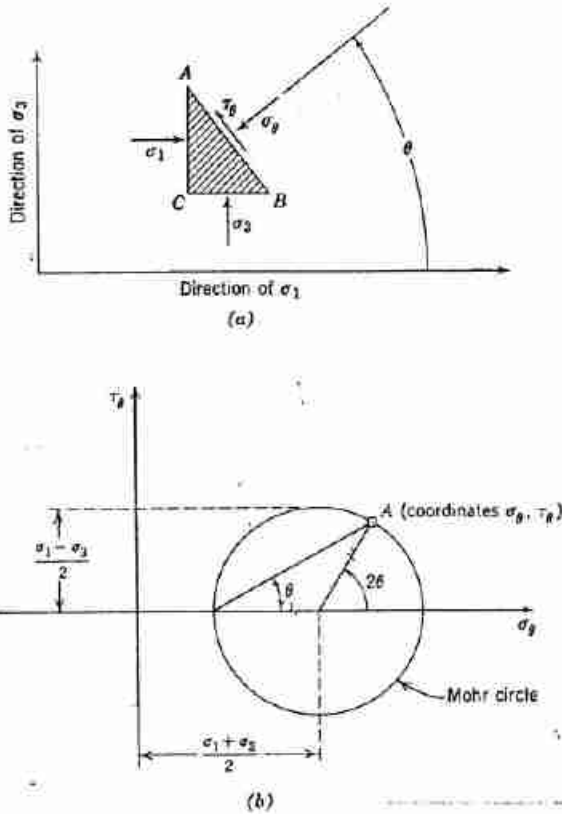


Fig. 8.9 Representation of stress by the Mohr circle. (a) Equations for state of stress at a point. (b) Mohr diagram for state of stress at a point. τ is positive when counterclockwise; θ is measured counter clockwise from the direction of σ_1 .

$$\sigma_\theta = \sigma_1 \cos^2 \theta + \sigma_3 \sin^2 \theta = \frac{\sigma_1 + \sigma_3}{2} + \frac{\sigma_1 - \sigma_3}{2} \cos 2\theta \quad (8.6)$$

$$\tau_\theta = (\sigma_1 - \sigma_3) \sin \theta \cos \theta = \frac{\sigma_1 - \sigma_3}{2} \sin 2\theta \quad (8.7)$$

construction using the Mohr circle. Or, given the σ_θ and τ_θ that act on any two planes, the magnitude and direction of the principal stresses can be found. The notion of the *origin of planes* is especially useful in such constructions. The origin of planes is a point on the Mohr circle, denoted by O_p , with the following property: a line through O_p and any point A of the Mohr circle will be parallel to the plane on which the stresses given by point A act. Examples 8.4 to 8.7 illustrate the use of the Mohr circle and of the origin of planes. The reader should study these examples very carefully.

The maximum shear stress at a point, τ_{max} , is always equal to $(\sigma_1 - \sigma_3)/2$; i.e., the maximum shear stress equals the radius of the Mohr circle. This maximum

shear stress occurs on planes lying at $\pm 45^\circ$ to the major principal stress direction.

If the stress condition is geostatic, the largest shear stress will be found upon planes lying at 45° to the horizontal. The magnitude of the maximum shear stress will be

$$\text{if } K < 1, \quad \tau_{max} = \frac{\sigma_v}{2} (1 - K)$$

$$\text{if } K > 1, \quad \tau_{max} = \frac{\sigma_v}{2} (K - 1)$$

$$\text{if } K = 1, \quad \tau_{max} = 0$$

8.5 p-q DIAGRAMS

In many problems it is desirable to represent, on a single diagram, many states of stress for a given specimen of soil. In other problems, states of stress for many different specimens are represented on one such diagram. In such cases it becomes cumbersome to plot Mohr circles, and even more difficult to see what is on the diagram once all circles are plotted.

An alternative scheme for plotting the state of stress is to plot a *stress point* whose coordinates are

$$p = \frac{\sigma_1 + \sigma_3}{2}$$

$$q = \pm \frac{\sigma_1 - \sigma_3}{2} \begin{cases} + \text{ if } \sigma_1 \text{ is inclined equal to or} \\ \text{less than } \pm 45^\circ \text{ to the vertical} \\ - \text{ if } \sigma_1 \text{ is inclined less than} \\ \pm 45^\circ \text{ to the horizontal} \end{cases} \quad (8.8)$$

In most cases for which the stress point representation is used, the principal stresses act on vertical and horizontal planes. Then Eq. (8.8) simplifies to

$$p = \frac{\sigma_v + \sigma_h}{2}, \quad q = \frac{\sigma_v - \sigma_h}{2} \quad (8.9)$$

Plotting a stress point is equivalent to plotting one single point of a Mohr circle: the uppermost point if q is positive or the bottom-most point if q is negative. Numerically, q equals one-half of the deviator stress.

Example 8.8 shows stress points corresponding to the state of stress worked out in Examples 8.4 to 8.6. Knowing the values of p and q for some state of stress, one has all of the information needed to plot the corresponding Mohr circle. However, the use of a p - q diagram is no substitute for the use of the Mohr circle construction to determine the magnitude of these principal stresses from a given state-of-stress.

► Example 8.4

Given. Figure E8.4-1.

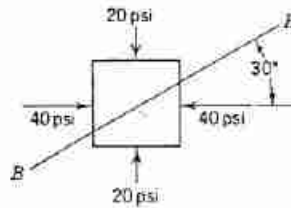


Fig. E8.4-1

Find. Stresses on plane B-B.

Solution. Use Fig. E8.4-2.

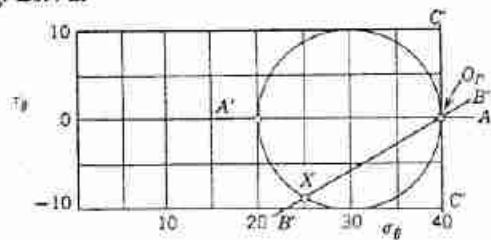


Fig. E8.4-2

1. Locate points with co-ordinates (40, 0) and (20, 0).
2. Draw circle, using these points to define diameter.
3. Draw line A'A' through point (20, 0) and parallel to plane on which stress (20, 0) acts.
4. Intersection of A'A' with Mohr circle at point (40, 0) is the origin of planes.
5. Draw line B'B' through O_P parallel to BB.
6. Read coordinates of point X where B'B' intersects Mohr circle.

Answer. See Fig. E8.4-3.

$$\text{on } BB \quad \begin{cases} \sigma = 25 \text{ psi} \\ \tau = -8.7 \text{ psi} \end{cases}$$

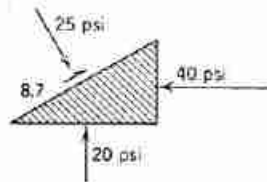


Fig. 8.4-3

Alternate Solution. Steps 1 and 2 same as above.

3. Draw line C'C' through (40, 0) parallel to plane on which stress (40, 0) acts. C'C' is vertical.

4. C'C' intersects Mohr circle only at (40, 0), so this point is O_P. Steps 5 and 6 same as above.

Solution Using Eqs. 8.6 and 8.7.

$$\sigma_1 = 40 \text{ psi} \quad \sigma_2 = 20 \text{ psi} \quad \theta = 120^\circ$$

$$\sigma_\theta = \frac{40 + 20}{2} + \frac{40 - 20}{2} \cos 240^\circ = 30 - 10 \cos 60^\circ = 25 \text{ psi}$$

$$\tau_\theta = \frac{40 - 20}{2} \sin 240^\circ = -10 \sin 60^\circ = -8.66 \text{ psi}$$

(Questions for student. Why is $\theta = 120^\circ$? Would result be different if $\theta = 300^\circ$?)

► Example 8.5

Given. Figure E8.5-1.

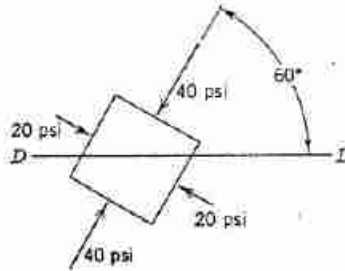


Fig. E8.5-1

Find. Stresses on horizontal plane *DD*.

Solution.

1. Locate points (40, 0) and (20, 0) on Mohr diagram (Fig. E8.5-2).

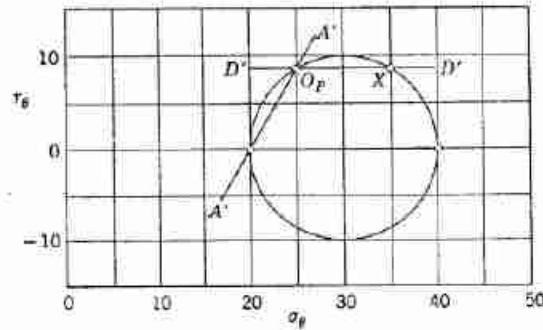


Fig. E8.5-2

2. Draw Mohr circle.
3. Draw line *A'A''* through (20, 0) parallel to plane upon which stress (20, 0) acts.
4. Intersection of *A'A''* with Mohr circle gives O_{21} .
5. Draw line *D'D'* parallel to plane *DD*.
6. Intersection *X'* gives desired stresses

Answer. See Fig. E8.5-3.

$$\text{on } DD \quad \begin{cases} \sigma = 35 \text{ psi} \\ \tau = 8.7 \text{ psi} \end{cases}$$

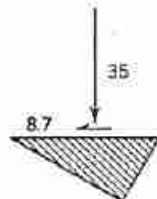


Fig. E8.5-3

Example 8.6

Given. Figure E8.6-1.

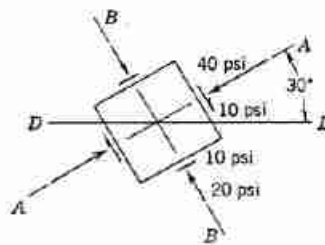


Fig. E8.6-1

Find. Magnitude and direction of the principal stresses.

Solution. Use Fig. E8.6-2.

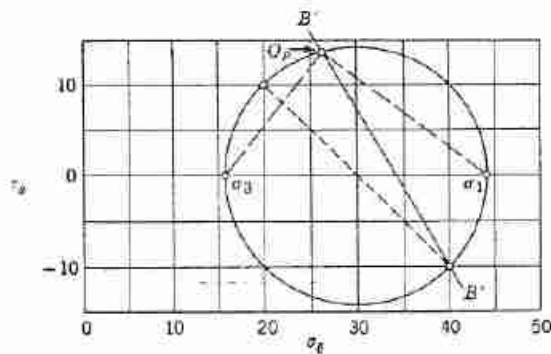


Fig. E8.6-2

1. Locate points (40, -10) and (20, 10).
2. Erect diameter and draw Mohr circle.
3. Draw $B'B'$ through (40, -10) parallel to BB .
4. Intersection of $B'B'$ with circle gives O_p .
5. Read σ_1 and σ_3 from graph.
6. Line through O_p and σ_3 gives plane on which σ_3 acts, etc. (see Fig. E8.6-3).

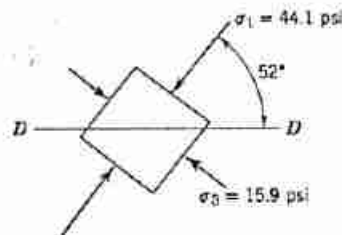


Fig. E8.6-3

Solution by Equations.

1. First make use of fact that sum of normal stresses is a constant:

$$\frac{\sigma_1 + \sigma_3}{2} = \frac{\Sigma \sigma_n}{2} = \frac{40 + 20}{2} = 30 \text{ psi}$$

2. Use relation

$$\left(\frac{\sigma_1 - \sigma_3}{2}\right) = \sqrt{\left[\sigma_\theta - \left(\frac{\sigma_1 + \sigma_3}{2}\right)\right]^2 + [\tau_\theta]^2}$$

with either pair of given stresses

$$\left(\frac{\sigma_1 - \sigma_3}{2}\right) = \sqrt{[20 - 30]^2 + [10]^2} = \sqrt{200} = 14.14 \text{ psi}$$

$$3. \quad \sigma_1 = \left(\frac{\sigma_1 + \sigma_3}{2}\right) + \left(\frac{\sigma_1 - \sigma_3}{2}\right) = 44.14 \text{ psi}$$

$$\sigma_3 = \left(\frac{\sigma_1 + \sigma_3}{2}\right) - \left(\frac{\sigma_1 - \sigma_3}{2}\right) = 15.86 \text{ psi}$$

4. Use stress pair in which σ_θ is largest; i.e. (40, -10)

$$\sin 2\theta = \frac{2\tau_\theta}{\sigma_1 - \sigma_3} = \frac{-20}{28.28} = -0.707$$

$$2\theta = -45^\circ$$

$$\theta = -22\frac{1}{2}^\circ$$

5. Angle from horizontal to major principal stress direction = $30^\circ - \theta = 52\frac{1}{2}^\circ$ ◀

► Example 8.7

Given. A load of 5000 psf uniformly distributed over a circular area with a radius of 100 ft.

Find. At 100-ft depth under the edge of the loaded area, find the horizontal stress increment and the directions of the major and minor principal stress increments.

Solution. Figures 8.4 and 8.5 can be used to find $\Delta\sigma_v$, $\Delta\sigma_1$, and $\Delta\sigma_3$. These are plotted and the Mohr circle is constructed. The origin of planes is located by drawing a horizontal line through the point representing the vertical stress, and the problem is then completed.

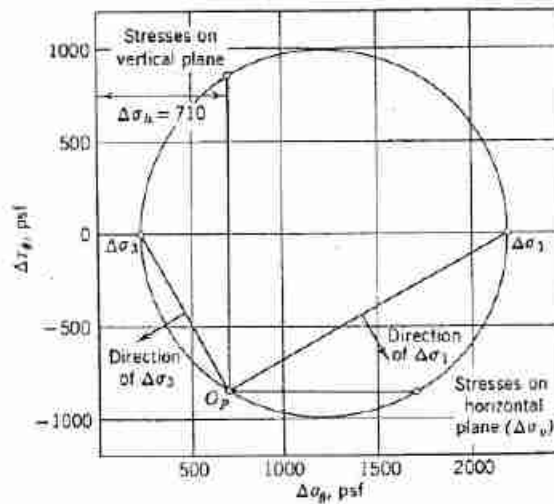


Fig. E8.7

Question for student. In order to construct the diagram, it was necessary to assume that the shear stress was negative on the horizontal plane. One way to test this assumption is to ask whether the directions of the principal stress increments are reasonable. Are they? ◀

► Example 8.8

On a p - q diagram, represent the states of stress given in Examples 8.4 to 8.6.

Solution. See Fig. E8.8.

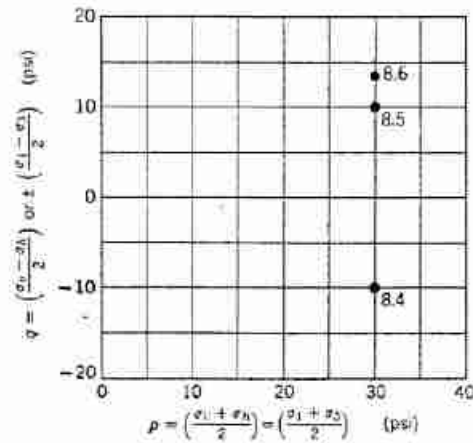


Fig. E8.8

8.6 STRESS PATHS

We shall often wish to depict the successive states of stress that exist in a specimen as the specimen is loaded. One way to do this is to draw a series of Mohr circles. For example, Fig. 8.10a shows successive states as σ_1 is increased with σ_3 constant. However, a diagram with many circles can become quite confusing, especially if the results of several tests are plotted on the same diagram. A more satisfactory arrangement is to plot a series of stress points, and to connect these points with a line or curve (Fig. 8.10b). Such a line or curve is called a *stress path*. Just as a Mohr circle or a stress point represents a state of stress, a stress path gives a continuous

representation of successive states of stress.⁶ Figure 8.11 shows a variety of stress paths that will be of interest to us in following chapters.

Figure 8.11a shows stress paths starting from a condition where $\sigma_v = \sigma_h$. This is a common initial condition in many types of laboratory tests. From this initial condition, we commonly either change σ_v and σ_h by the same amount ($\Delta\sigma_v = \Delta\sigma_h$), or else change one of the principal stresses while holding the other principal stress constant ($\Delta\sigma_v$ positive while $\Delta\sigma_h = 0$, or $\Delta\sigma_h$ negative while $\Delta\sigma_v = 0$). Of course many other stress paths are

⁶The terms *stress trajectory* and *vector curve* are also used to denote curves depicting successive states of stress, but the definitions of these other curves are somewhat different.

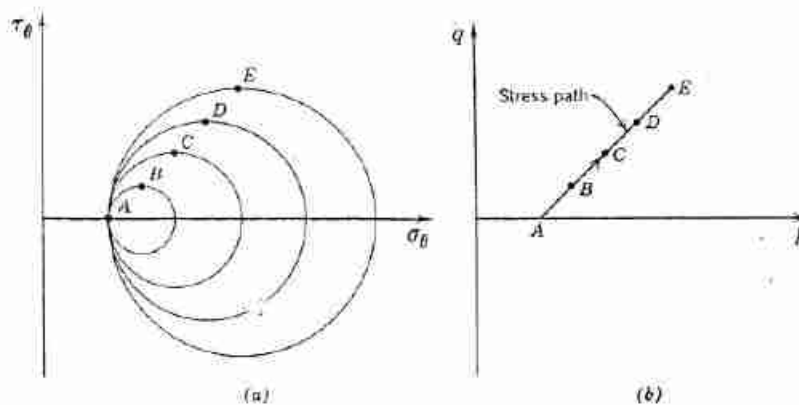


Fig. 8.10 Representation of successive states of stress as σ_1 increases with σ_3 constant. Points A , B , etc., represent the same stress conditions in both diagrams. (a) Mohr circles. (b) p - q diagram.

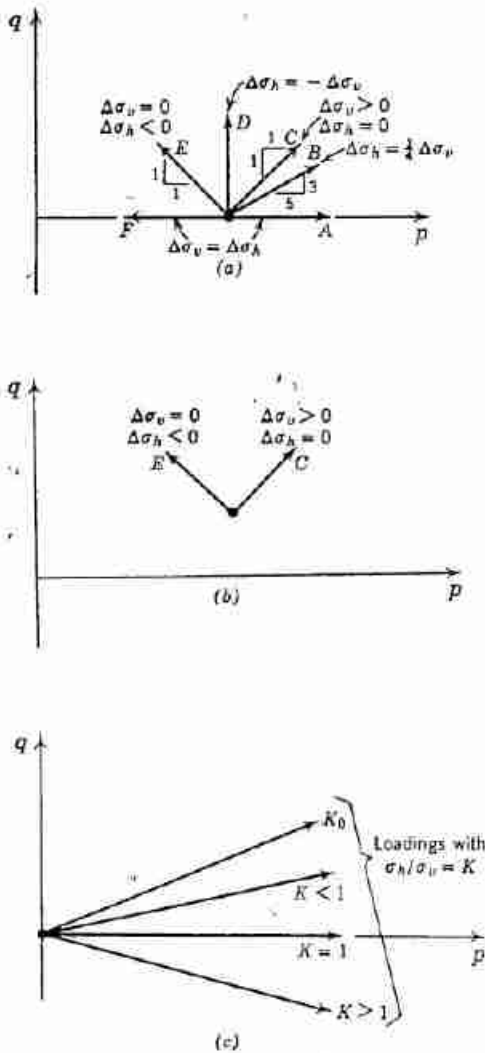


Fig. 8.11 Examples of stress paths. (a) $\sigma_v = \sigma_h$ initially. (b) $\sigma_v > \sigma_h > 0$ initially. (c) $\sigma_v = \sigma_h = 0$ initially.

► Example 8.9

Given. Loading and soil conditions as shown in Fig. E8.9-1.

Find. Stress paths for points A to H.

Solution. Use Figs. 8.4 and 8.5 to find stresses. Stress paths are given in the following table and in Fig. E8.9-2.

Point	Initial				Increment		Final			
	σ_v	σ_h	p	q	$\Delta\sigma_v$	$\Delta\sigma_h$	σ_v	σ_h	p	q
A	3.22	1.29	2.26	0.97	5.34	2.83	8.56	4.12	6.34	2.22
B	6.45	2.58	4.51	1.93	4.60	1.32	11.05	3.90	7.48	3.58
C	9.68	3.87	6.76	2.90	3.62	0.59	13.30	4.46	8.88	4.42
D	12.90	5.16	9.02	3.87	2.75	0.27	15.65	5.43	10.54	5.11
E	19.37	7.74	13.53	5.80	1.62	0.07	20.99	7.81	14.40	6.59
F	25.80	10.32	18.04	7.74	1.02	0.02	26.82	10.34	18.58	8.24
G	32.25	12.90	22.55	9.67	0.69	0	32.94	12.90	22.92	10.02
H	38.70	15.48	27.06	11.61	0.50	0	39.20	15.48	27.34	11.86

possible; we may increase both $\Delta\sigma_1$ and $\Delta\sigma_3$ in such a way that $\Delta\sigma_3 = \Delta\sigma_1/4$.

A more common initial condition is to have σ_v and σ_h both greater than zero, but $\sigma_v \neq \sigma_h$. Part (b) of Fig. 8.11 depicts several stress paths starting from such an initial condition.

We are also interested in loadings that start from $\sigma_1 = \sigma_3 = 0$ and during which σ_1 and σ_3 increase in constant ratio (Fig. 8.11c). For this type of loading

$$\frac{q}{p} = \frac{1 - K}{1 + K} \quad (8.10)$$

where K is the coefficient of lateral stress as defined in Section 8.2. The stress path $K=1$ corresponds to isotropic compression without shear stresses. The stress path K_0 indicates the way in which the stresses within a normally consolidated soil increase during the sedimentation process. The slope of the stress path K_0 is denoted as β ; i.e., for a K_0 loading,

$$\frac{q}{p} = \tan \beta \quad (8.11)$$

Combining Eqs. 8.10 and 8.11, we find

$$K_0 = \frac{1 - \tan \beta}{1 + \tan \beta} \quad (8.12)$$

A stress path need not be a straight line. For example, we might specify that the stresses are applied in such a way that $\Delta\sigma_v = \frac{1}{2}(\Delta\sigma_h)^2$. A stress path might well consist of a series of straight lines joined together. Two different loadings might follow just the same curve in p - q space, but one of these loadings might involve increasing stresses and the other decreasing stresses. To avoid any ambiguity, each stress path should carry an arrowhead to indicate the sense of the loading.

Example 8.9 shows stress paths for several points on

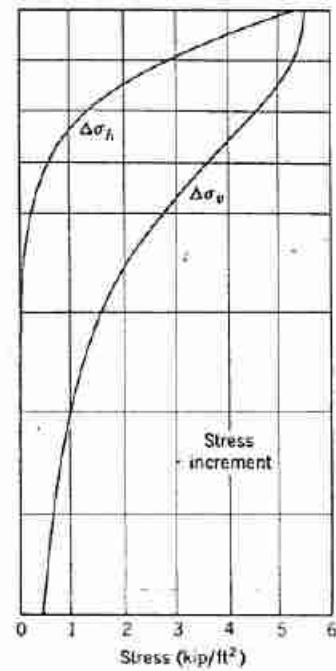
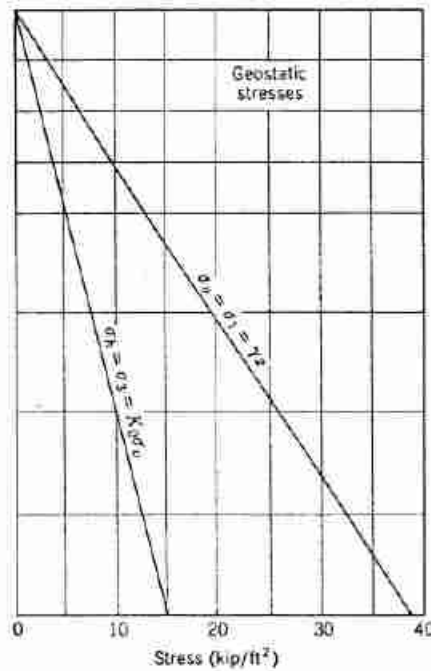
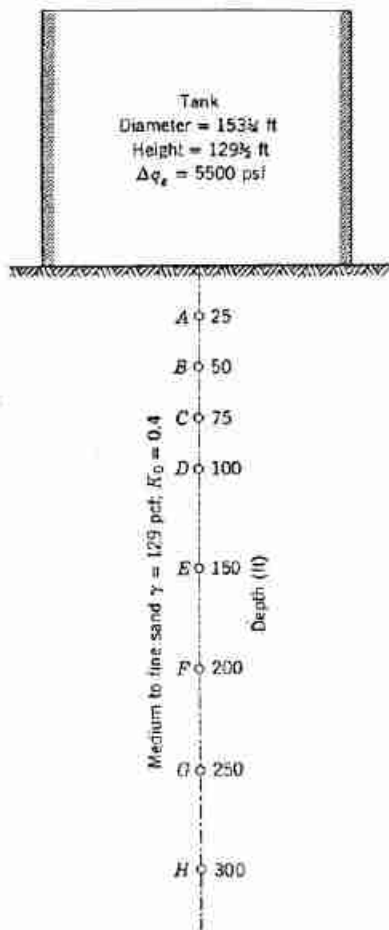


Fig. E8.9-1

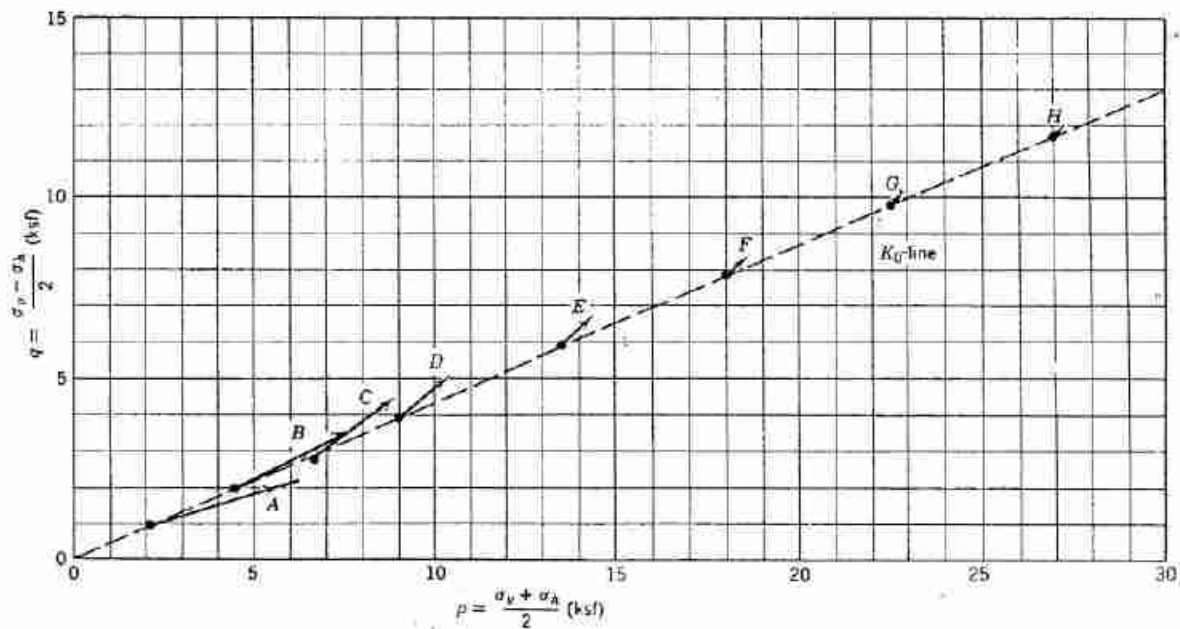


Fig. E8.9-2

the center line below a circular loaded area. The usefulness of the stress path for depicting the stress changes is evident in this example.

8.7 SUMMARY OF MAIN POINTS

1. The traditional concept of stress can be applied to a particulate system, provided that the stress changes only very slightly over distances which are of the order of magnitude of the largest particle.
2. The Mohr circle representation for the state of stress at a point is extremely useful in soil mechanics.
3. The p - q diagram is also a useful means for representing the state of stress at a point, and the stress path is a useful way to represent a change of stress.
4. When the surface of a soil deposit is level and the unit weight is constant with depth, the vertical and horizontal geostatic stresses increase linearly with depth.
5. Elastic theory provides a convenient means for estimating the stresses induced within a soil mass by applied loads.

Since soil is not elastic, and for other reasons cited in this chapter, the engineer should use the stress distribution charts herein with judgment and caution. Many cases in which calculated and field measured stresses are compared are needed in order for the accuracy of calculated stresses to be assessed.

PROBLEMS

8.1 A soil has a unit weight of 110 pcf and a lateral stress coefficient at rest of 0.45. Assuming that the stress condition is geostatic, draw a plot showing the vertical and horizontal stresses from ground surface to 50-ft depth.

8.2 A soil has the following profile:

0-10 ft	$\gamma_t = 110$ pcf
10-25 ft	$\gamma_t = 95$ pcf
25-50 ft	$\gamma_t = 113$ pcf

Assuming that the stress condition is geostatic, what is the vertical stress at 40-ft depth?

8.3 The relationship between vertical stress and unit weight is:

$$\gamma_t = 80 + 0.003\sigma_v$$

where γ_t is expressed in pcf and σ_v is expressed in psf. What is the vertical stress at a depth of 100 ft in a deposit of this soil, assuming that the stress condition is geostatic?

8.4 Consider the results shown in Example 8.4. Take horizontal and vertical components of the stresses on the inclined face and (considering the relative area of the three faces) show that the free body really is in equilibrium.

8.5 Consider Example 8.5.

a. Rework the problem, but in step 3 construct a line parallel to the plane on which σ_1 acts. Show that you get the same O_p .

b. Compute the stresses on the horizontal plane using Eqs. 8.6 and 8.7 (see Fig. 8.9).

8.6 Consider Example 8.6.

a. Rework the problem, but in step 3 construct a line parallel to AA .

b. Find the stresses on a horizontal plane, and show the stresses acting upon the free body.



Fig. P8.6

8.7 Given the following stresses, find the magnitude and orientation of the principal stresses.

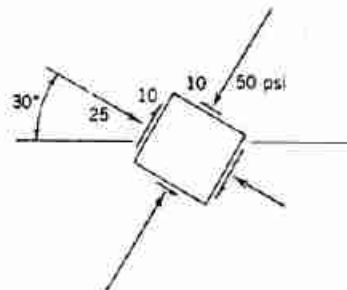


Fig. P8.7

8.8 Draw stress paths for the following loading conditions on a p - q diagram.

a. Initial condition $\sigma_h = \sigma_v = 20$ psi. σ_h remains constant while σ_v increases to 60 psi.

b. Initial condition $\sigma_h = \sigma_v = 20$ psi. σ_v remains constant while σ_h increases to 60 psi.

c. Initial condition $\sigma_h = \sigma_v = 20$ psi. σ_v remains constant while σ_h decreases to 10 psi.

d. Initial condition $\sigma_h = \sigma_v = 20$ psi. σ_v and σ_h both increase with $\Delta\sigma_h = \Delta\sigma_v/3$.

e. Initial condition $\sigma_v = 20$ psi, $\sigma_h = 10$ psi. σ_v remains constant while σ_h decreases to 7 psi.

f. Initial condition $\sigma_v = 20$ psi, $\sigma_h = 10$ psi. σ_v remains constant while σ_h increases to 60 psi.

8.9 The surface of an elastic body is loaded by a uniform load of 1000 psf over an area 20 ft by 40 ft. Find:

a. The vertical stress at a depth of 10 ft below a corner of the loaded area.

b. The vertical stress at a depth of 20 ft below the center of the loaded area.

8.10 A uniform load of 2000 psf is applied over a circular area 15 ft in diameter on the surface of an elastic body. The elastic body has $\gamma = 110$ pcf and $K_0 = 0.45$. Find the following stresses at the center line at a depth of 10 ft, both before and after loading.

a. The vertical stress.

b. The horizontal stress.

c. The maximum shear stress.

Plot the stress path for the loading.

CHAPTER 9

Tests to Measure Stress-Strain Properties

If soil were isotropic and linearly elastic it would be possible to determine the elastic constants E (Young's modulus) and μ (Poisson's ratio) from a single simple test¹ and then to use these constants to compute the relationship between stress and strain for other types of tests. With soils such a simple approach is generally not possible. Hence several different tests have come into common use, each designed to study stress-strain behavior during a specific type of loading. Figure 9.1 depicts four of the most common tests used to study the stress-strain behavior of soil. The apparatus required for triaxial compression tests also permits isotropic compression tests; indeed, isotropic compression is the first stage of a triaxial test.

This chapter describes the key features of the apparatus and procedures of these tests. Very careful testing technique, with painstaking attention to detail, is necessary to obtain good test results. Lambe (1951) describes the necessary apparatus and techniques in more detail. Bishop and Henkel (1962) give a good treatment of the triaxial test.

9.1 OEDOMETER TEST

In the oedometer test, stress is applied to the soil specimen along the vertical axis, while strain in the horizontal directions is prevented. Thus the axial strain is exactly equal to the volumetric strain. Figure 9.2 shows cross-sectional views through two common types of oedometers. Other names for this test are the *one-dimensional compression test*, the *confined compression test*, and the *consolidation test*. The last name is applied because this form of test was first used extensively to study the consolidation phenomenon (see Chapters 2 and 27).

In this test the ratio of the lateral stress to the vertical stress is K_0 , the *coefficient of lateral stress at rest* (see

¹ This procedure is discussed in Chapter 12.

Section 8.2). The stress path for this test is shown in Fig. 9.1, and previously has been given in Fig. 8.11c. Shear stresses and shear strains as well as compressive stresses and volume changes occur in this test, but since the soil is prevented from failing in shear, compression is the dominant source of strain. The test is popular because it is relatively simple to perform and because the strain condition is approximately similar to one frequently encountered in actual problems.

The major experimental difficulty with the oedometer test is side friction: shear forces develop along the cylindrical surface of the specimen as vertical strains occur. The presence of side friction disturbs the one-dimensional state of strain and prevents some of the axial force from reaching the bottom portions of the specimen. To minimize the effect of these side friction forces the thickness-diameter ratio of the specimen is kept as small as practicable, usually 1:3 to 1:4. Use of the floating ring container (Fig. 9.2b) also helps to minimize the effects of side friction. Many attempts have been made to minimize side friction through use of lubricants and plastic liners, and these techniques have proved to be of some value. Apparatus compressibility may also be a difficulty when testing the relatively incompressible soils, and special devices are then necessary (Whitman, Miller, and Moore, 1964).

In the common form of oedometer the lateral stress developed during the test is not measured. Figure 9.3 shows a special oedometer that permits the measurement of the lateral stress. Strain gages mounted on the metal ring sense any lateral straining of this ring, and the lateral pressure is then adjusted to give zero lateral strain. By a similar arrangement it is possible to carry out a one-dimensional compression test using a triaxial form of apparatus; i.e., a narrow ring placed around the membrane senses lateral strain and the chamber pressure is adjusted to make this strain zero. The problem of side friction is thereby eliminated.

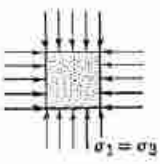
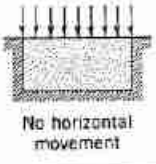
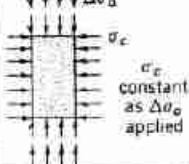
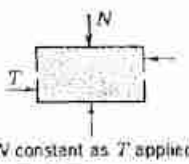


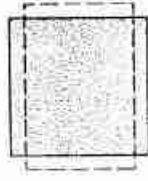

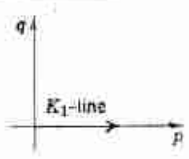
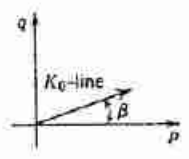
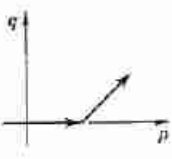
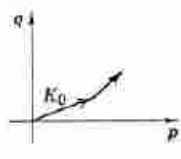
Test	Isotropic compression	Confined compression (oedometer)	Triaxial compression	Direct shear
Basic conditions				
Type of deformation	Volumetric 	Primarily volumetric but some distortion 	Distortion and volumetric 	Primarily distortion, but some volumetric 
Stress path				
Uses	For study of purely volumetric strains	Very simple; approximates certain field conditions	Most common test for studying stress-strain and strength properties	Simple test for measuring strength

Fig. 9.1 Common types of stress-strain tests.

9.2 TRIAXIAL TEST

Figure 9.4 shows the basic idea of the *triaxial test*, the most common and versatile test used to determine the stress-strain properties of soil. A cylindrical specimen of soil is first subjected to a confining pressure σ_c which equally stresses all surfaces of the specimen. Then the axial stress is increased $\Delta\sigma_a$ until the specimen fails. Since there are no shearing stresses on the sides of the cylindrical specimen, the axial stress $\sigma_c + \Delta\sigma_a$ and the confining stress σ_c are the major and minor principal stresses, σ_1 and σ_3 , respectively. The increment of axial stress, $\Delta\sigma_a = \sigma_1 - \sigma_3$, is the *deviator stress*.

The triaxial test is simply a special version of the cylindrical compression test that is used to determine the mechanical properties of many materials, such as concrete. Usually there is no confining pressure during a test on concrete, although a confining pressure may be

employed in some very special tests. However, a confining pressure is usually essential when testing soil. The reader will already be well aware that a specimen of dry sand will not stand without confinement. In following chapters we shall see that the confining pressure has an important influence on the stress-strain behavior of soil.

Size of Specimen

The soil cylinder is commonly about 1.5 in. in diameter and from 5 to 4 in. in length. Specimens about 3 in. in diameter and from 6 to 8 in. long are also encountered frequently. Much larger specimens are used in the testing of soils containing gravel.

Confining Pressure

The pressure vessel is usually composed of a transparent plastic cylinder with metal end pieces. Typical

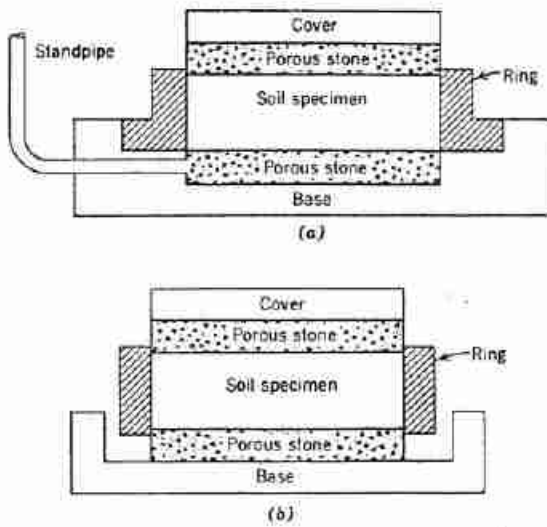


Fig. 9.2 Common forms of oedometers. (a) Fixed-ring container. (b) Floating-ring container. (From Lambe, 1951.)

arrangements are shown in Fig. 9.5. Either gas or liquid under pressure is used to apply the confining pressure, although the use of a liquid (usually de-aired water) is preferable. For confining pressures greater than 100 to 150 psi, metal reinforcing bands must be placed around the lucite, or the lucite replaced by a metal cylinder.

The soil is encased by a flexible *membrane* or *jacket* and two end caps. Thus the confining fluid does not penetrate into the pore spaces.

Axial Loading

In the common form of triaxial test (herein termed *standard triaxial test*) the soil is failed by increasing the axial stress while holding the confining stress constant. Thus the stress path during the loading is that shown in Fig. 8.10. Axial force is applied to the loading piston either by means of dead weights (*controlled stress test*) or by a geared or hydraulic loading press (*controlled strain test*). When testing dry soils the rate of loading is limited solely by the time required to observe and record the data. Usually 5–30 min. elapse from the time that additional axial force is first applied until the peak resistance is reached.

Control of Pressure in Pore Spaces

If a dry soil specimen is completely sealed, and if the volume of the soil changes during loading, there must be some change in the volume and pressure of the air occupying the pores of the soil. A drainage system, consisting of a porous stone plus a passage to the outside of the pressure vessel, is usually provided so that air can move into or out of the soil and thereby prevent the pressure change. The drainage provision will prove to

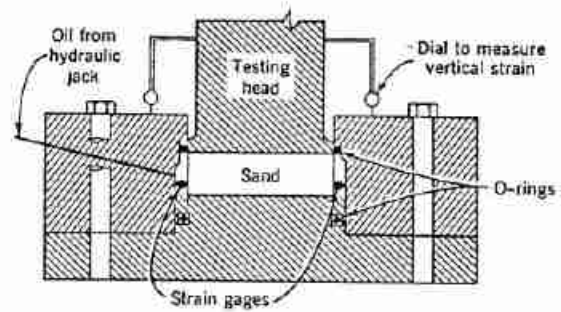


Fig. 9.3 Special oedometer permitting measurement of lateral stress (From Hendron, 1963).

be of great importance during tests on soils containing water, as will be discussed in Parts IV and V.

The drainage feature can also be used to accomplish a special form of triaxial test: the *vacuum triaxial test*. If air is evacuated from the pores of the soil, a confining pressure is caused by the difference between the atmospheric pressure acting against the outside of the specimen and the reduced pressure in the pores of the specimen. A pressure vessel is not needed for this form of test, but of course the confining pressure cannot be made greater than 1 atm.

Measurement of Volume Changes

It is not easy to make accurate measurements of the changes in the volume of a dry soil, either as the confining

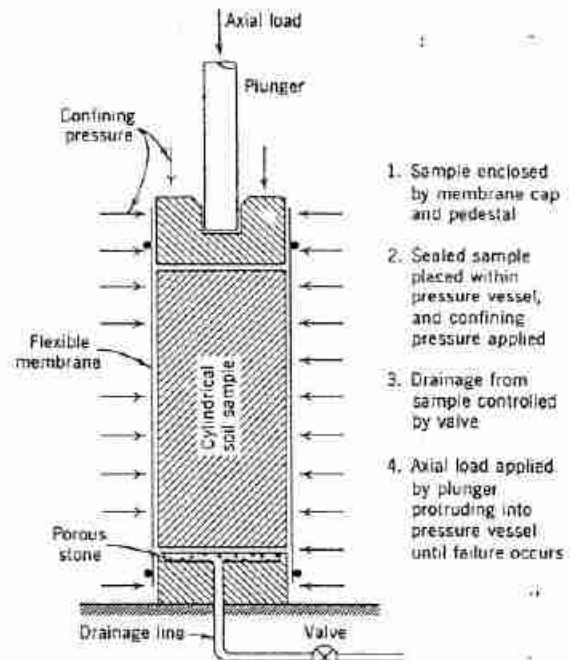


Fig. 9.4 Essential features of a triaxial cell.

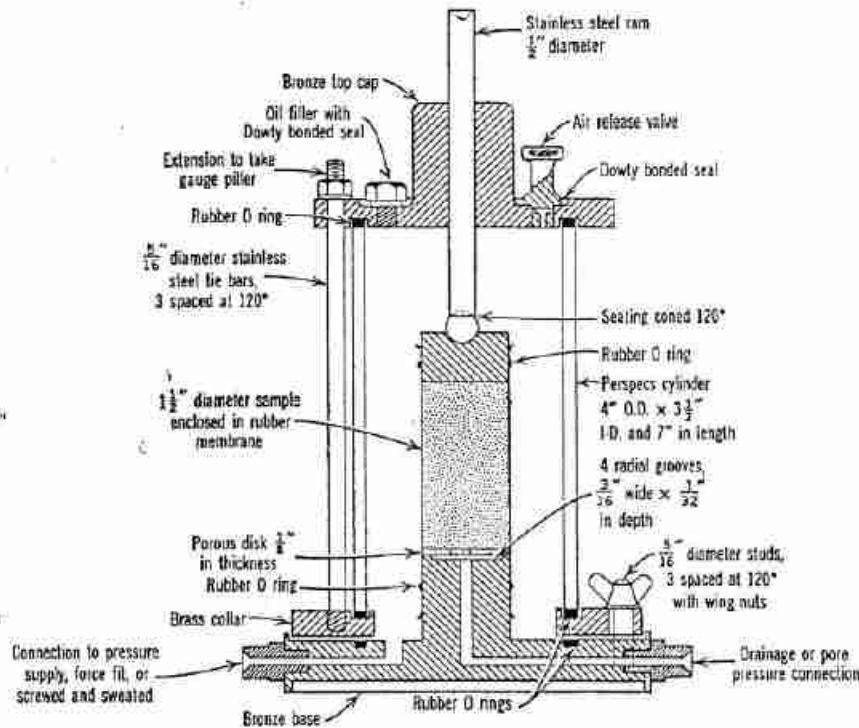


Fig. 9.5 Cross section of a typical triaxial cell. (From Bishop and Henkel, 1962.)

pressure or the additional axial stress is applied. When a soil is saturated with water, its change in volume during a triaxial test can be determined by measuring the volume of water that flows into or out of the specimen. Fortunately, as we shall see in Part IV, the stress-strain behavior of dry and saturated granular soil is similar, provided that the pore fluid can flow freely into or out of the pores. Some of the test results presented in Chapters 9 to 12 were actually obtained using saturated specimens.

Even with saturated specimens it is difficult to make very accurate measurements of volume changes occurring within coarse soils. This is one of the reasons why the oedometer test is often used to study volumetric strains.

Deformed Shapes of Specimens

Figure 9.6 shows typical shapes of specimens tested in triaxial compression. Distortions such as these give rise to difficulties in the interpretation of test results. The change in the cross-sectional area of a specimen is usually so large that it must be taken into account when computing axial stress from the measured axial force. Distortion of the cylindrical shape, which arises primarily because of the restraints imposed by the rigid end caps, makes it difficult to determine the change in area and otherwise introduces errors and uncertainties into measured stress-strain data. Several schemes have been developed which freely permit lateral motions between

the soil and the end caps, and thus help to minimize distortions (Rowe and Barden, 1964).

9.3 THE DIRECT SHEAR TEST

The oldest form of shear test upon soil is the direct shear test, first used by Coulomb in 1776. The essential elements of the direct shear apparatus are shown by the schematic diagram in Fig. 9.1. The soil is held in a box that is split across its middle. A confining force is applied, and then a shear force is applied so as to cause relative displacement between the two parts of the box. The magnitude of the shear forces is recorded as a function of the shear displacement, and usually the change in thickness of the soil specimen is also recorded.

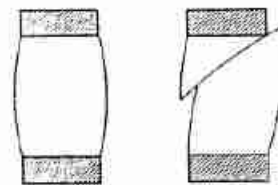


Fig. 9.6 Typical distorted shapes for triaxial specimens tested between rigid end caps.

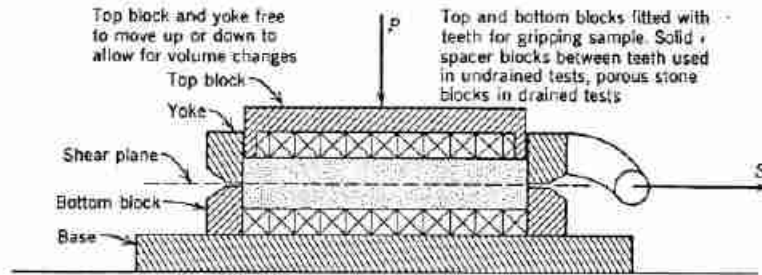


Fig. 9.7 Cross section through direct shear box (B. K. Hough—*Basic Soils Engineering*. Copyright © 1957 The Ronald Press Co. N.Y.).

The shear box may be either square or circular in plan view. Typically the box will be 3–4 in.² and about 1 in. in height. The normal load is applied either by a loading press or by means of dead weights. In most devices the normal stress will range from 0 to about 150 psi. The shear force is applied either by dead weights (*stress controlled test*) or by a motor acting through gears (*strain controlled test*). When testing dry soils the duration of

the direct shear test is similar to that of the triaxial test.

Figure 9.7 shows a cross section through a typical direct shear box. The porous stones shown in this figure are not necessary for tests on dry soils, but are essential for tests on moist or saturated soils, as will be discussed in Part IV. Specific procedures for conducting a direct shear test are presented in Lambe (1951).

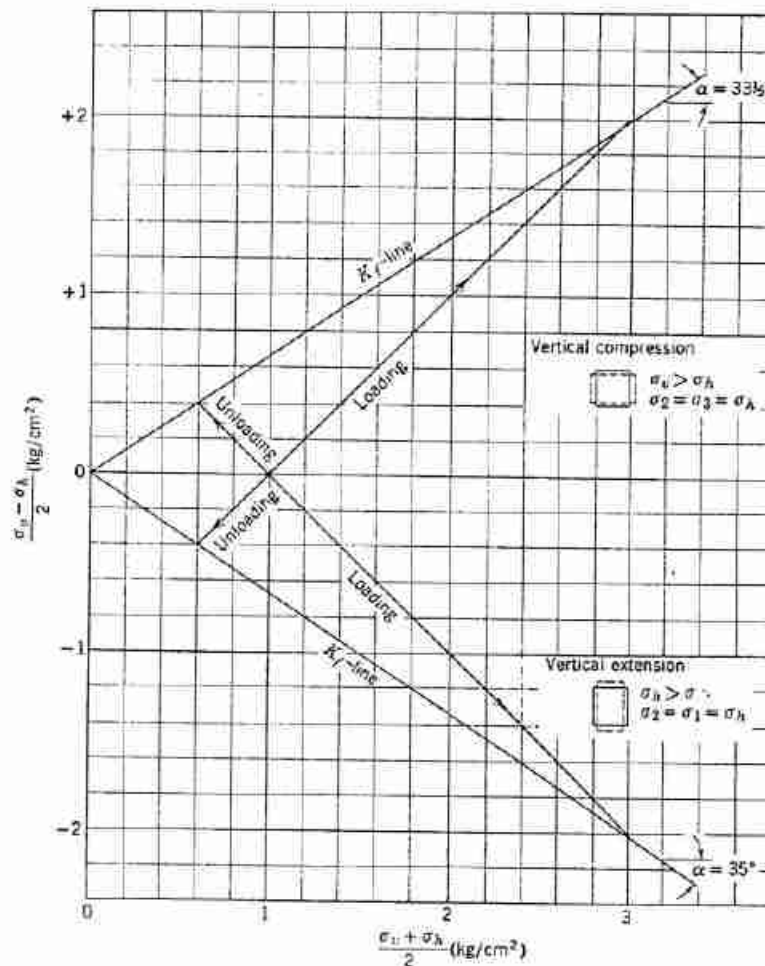


Fig. 9.8 Stress paths for triaxial tests.

Figure 9.1 indicates the stress path for a direct shear test. First there is a K_0 loading as the vertical force is applied. Then application of the shear force causes an increase in q and also an increase in p . The stress path cannot be drawn exactly for such a test; since only the stresses on a horizontal plane are known, the entire state of stress is unknown. A recent, improved version of the direct shear test is described by Bjerrum and Landva (1966).

9.4 OTHER TESTS

Numerous devices have been created to permit special types of tests. There are devices to study stress-strain behavior during dynamic loadings. There are also devices to study stress-strain behavior in plane strain (Bishop, 1966) and in simple shear (Roscoe, 1961).

Any loading condition not involving a rotation of the principal stress directions can be simulated in a triaxial cell. Examples of typical test conditions, together with the nomenclature used, are given in Fig. 9.8. The compression unloading test is accomplished by reducing the chamber pressure while adding force to the loading piston in order to keep the axial stress constant. To accomplish the extension tests it is necessary to pull upward on the loading piston. It also is possible to run a test so that the

sum $\sigma_1 + \sigma_3 = \sigma_v + \sigma_h$ remains constant, i.e., the stress path marked D in Fig. 8.11a.

9.5 SUMMARY OF MAIN POINTS

1. Because soil is such a complex material, no one test suffices for the study of all important aspects of stress-strain behavior.
2. The oedometer test is the easiest test for studying volumetric stress-strain relationships, while the direct shear test is the easiest and oldest test for studying shear strength.
3. The triaxial test provides the best and most versatile method for studying stress-strain properties. A great variety of actual loading conditions can be obtained with this test.

PROBLEMS

9.1 Problem 8.8 describes several types of loading conditions which can be applied in a triaxial cell. Using the nomenclature given in Fig. 9.8, describe each condition a to f as vertical compression loading, etc.

9.2 An oedometer test is run starting from zero stress. When $\sigma_v = 100$ psi it is observed that $\sigma_h = 45$ psi. Draw the stress path for this test, assuming that the ratio σ_h/σ_v is constant throughout. What are K_0 and β for this soil?

CHAPTER 10

General Aspects of Stress-Strain Behavior

This chapter begins our study of the stress-strain properties of soils by illustrating and explaining the deformation of dry granular soils. Because of the particulate nature of the mineral skeleton of soil, the stress-strain behavior of soil is exceedingly complex. In this chapter we shall rely on diagrams to aid us in describing this behavior. Subsequent chapters will present simple, approximate mathematical expressions for specific, limited situations.

Chapter 8 presented the concept of stress for a particulate system. The application to soil of the concept of strain may be understood with the aid of Fig. 10.1. The two particles shown in this figure are separated by a distance L , which is large compared to their size. If these particles move toward each other by an amount ΔL , then the unit compressive strain ϵ_x is defined as $\Delta L/L$.

Like stress, strain is a tensor quantity, and we must be careful to define strain. In this book we shall be concerned with:

- ϵ_x : the unit compressive strain along some specified axis
- γ_{xy} : the unit shear strain referenced to two specified axes
- $\Delta V/V$: the unit volumetric strain

Positive compressive strain is shortening; positive volumetric strain is a volume decrease.

10.1 MECHANISMS OF STRAIN

The strains experienced by an element of soil are the result of strains within and relative motions among the many particles composing the element. At each of the contacts between particles, the local strains may be very large, much larger than the overall strain as defined previously. In order to understand the overall stress-strain behavior of the element, it is necessary to appreciate just what goes on inside the element. Chapter 2 discussed

the mechanisms that contribute to the deformation of soil. Fundamentally there are two mechanisms in granular soils: distortion (and crushing) of individual particles, and relative motion between particles as the result of sliding or rolling. However, these two mechanisms are seldom independent of one another. For example, the array of particles shown in Fig. 10.2 would be stable under the applied forces if the particles were rigid and did not slide relative to each other. Since actual particles are not rigid, deformation of the particles will cause slight movements of the array, leading to collapse of the potentially unstable array. While relative motion between particles causes the large strains often encountered in soil, these motions generally would not be possible if it were not for distortions of particles.

Several simplified models have been proposed to explain the interactions among particles. The theory for two elastic spheres in contact has been used to analyze and predict the strains that would result from elastic distortion of particles. This theory is described in detail by Deresiewicz (1958). Scott (1963), Rowe (1962), and others have developed theories which consider sliding and rolling motions within regular packings of rigid spheres, and this theory has been used to study the strength behavior of granular soils. Still other theories have simultaneously considered sliding within regular packings of deformable spheres (see Hendron, 1963, and Miller, 1963).

The motions within an actual soil are far too complex to be analyzed by any simple model. At any instant during the deformation process, different mechanisms

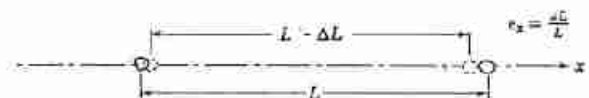


Fig. 10.1 Definition of strain in a particulate system.

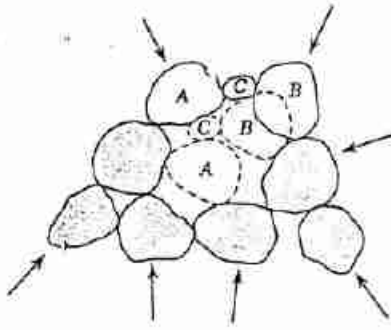


Fig. 10.2 Collapse of an unstable array of particles.

may be acting in different parts of an element of soil. At any one spot within the element, the relative importance of the different mechanisms may change as the deformation process continues. Nonetheless, the simple models serve a very useful role by providing a basis for interpreting experimental results for actual soils. Some of the more important results obtained from these simple models will be noted in the following sections.

10.2 VOLUMETRIC STRAINS DURING ISOTROPIC COMPRESSION

Large volumetric strains can occur during isotropic compression as the result of the collapse of arrays of particles as sketched in Fig. 10.2. Each such collapse causes rolling and sliding between particles, and as a result tangential forces occur at the contact points between particles. However, such tangential forces average out to zero over a surface passed through many contact points. Thus the shear stress on any plane is zero even though large shear forces exist at individual contacts.

The volumetric stress-strain relationships of soils are very similar during both isotropic and confined compression. As observed in Chapter 9, it is easier to perform an oedometer test than an isotropic compression

test. Moreover, confined compression is a common situation in nature; it occurs during formation of a soil by sedimentation and when vertical loads of large lateral extent are applied to soil strata. On the other hand, pure isotropic compression seldom is encountered in nature.

For these reasons, isotropic compression will not be considered in detail. Qualitatively, the stress-strain relations presented in Section 10.3 for confined compression apply to isotropic compression as well. Quantitatively, the relationships are somewhat different. For a given change in σ_1 , the change in the sum of the principal stresses ($\sigma_1 + \sigma_2 + \sigma_3$) is greater during isotropic compression. Hence a given change in σ_1 will cause a greater volumetric strain during isotropic compression.

10.3 STRESS-STRAIN BEHAVIOR DURING CONFINED COMPRESSION

Figure 10.3 shows the stress-strain behavior of a medium to coarse uniform quartz sand during confined compression. Initially the sand was in a dense state. The strain is the vertical strain, equal to the volumetric strain, based on the original thickness of the specimen. The stress is the vertical stress. The data are composite results from several oedometer tests, using conventional equipment for the lower range of stresses and special equipment for the larger stresses. Note that the stress-strain curves are plotted with positive (i.e., compressive) strains downward. This is common practice in soil mechanics since compressive strains are associated with settlement (i.e., downward movement).

Figure 10.3e suggests that the stress-strain behavior of sand should be considered in three stages.

1. For stresses up to about 2000 psi, the stress-strain curves are concave upward. Thus the sand gets stiffer and stiffer as the level of stress increases. This form of stress-strain behavior, called *locking*, is very characteristic of particulate systems. The strains result primarily from the type of action shown in Fig. 10.2. As the stress is increased, first

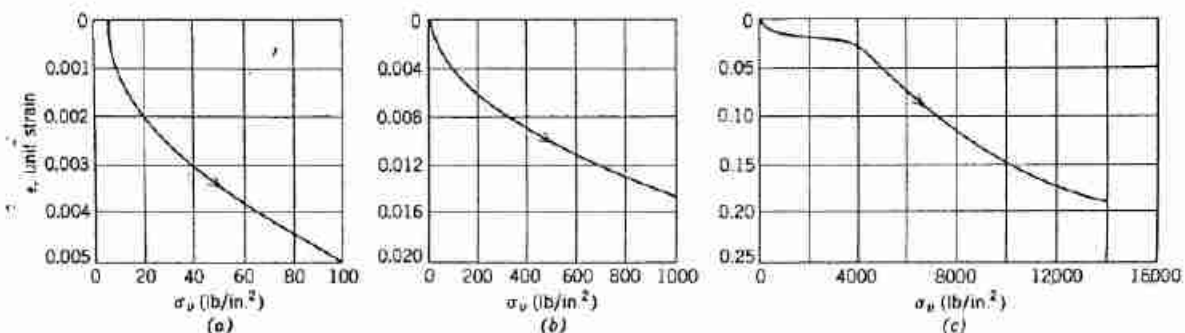


Fig. 10.3 Stress-strain curves for confined compression. Ottawa sand, initial porosity = 0.375.

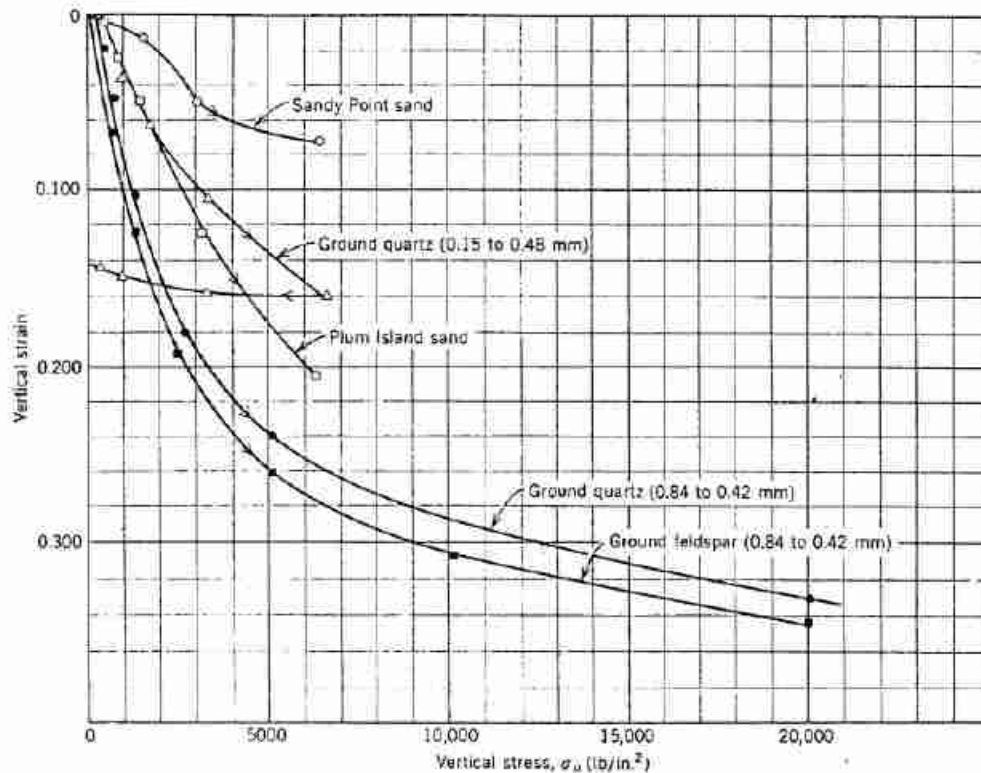


Fig. 10.4 Results of high stress, one-dimensional compression tests on several sands (data from Roberts, 1964).

loose arrays within the soil will collapse, and then the denser arrays will. Each such movement results in a more tightly packed, hence stiffer, arrangement of particles. Finally, a stage is reached in which already dense arrays are being squeezed more tightly together as contact points crush, thus allowing a little more sliding.

- Starting at about 2000 psi, the stress-strain curve begins to develop a reverse curvature and becomes concave to the strain axis. This *yielding* is the result of fracturing of individual sand particles, which permits large relative motions between particles. Distinct popping sounds can be heard at this stage of loading. Microscopic examination and grain size analyses before and after testing show that considerable particle degradation actually occurs (see Figs. 4.2*h* and 4.2*i*).
- Fracturing the particles permits still tighter packing of the new and remaining particles. Since the number of particles has now increased, the average force per contact has actually decreased. Thus the sand once again becomes stiffer and stiffer as the stress increases still further.

These same general processes take place during the compression of all granular soils, although seldom in such distinct stages. Figure 10.4 shows results for several typical natural sands. Sliding between particles is usually present at all stress levels. Crushing and fracturing of particles actually begins in a minor way at very small stresses, but becomes increasingly important when some critical stress is reached. This critical stress is smallest when the particle size is large, the soil is loose, the particles are angular, the strength of the individual mineral particles is low, and the soil has a uniform gradation.

In most engineering problems the stress levels are usually small enough so that particle crushing is relatively unimportant. For these problems, stress-strain curves for confined compression typically are of the locking type, as shown in Figs. 10.3*a* and 10.3*b*. Usually fracturing only becomes important when the stresses exceed 500 psi. Stresses greater than this magnitude are encountered in very high earth dams, and also in problems involving the subsidence of large areas as the result of pumping oil or water from deep strata. In the case of uniform rockfills with very large particle sizes, fracturing

may be very important for stresses as small as 100 psi. The fracturing of particles has been studied by Roberts (1964), Hendron (1963), Marsal (1963), and Lee and Farhoomand (1967).

Behavior During Unloading and Reloading

As shown in Fig. 10.5, only a portion of the strain that occurs during loading is recovered during subsequent unloading. The strains that result from sliding between particles or from fracturing of particles are largely irreversible. The rebound upon unloading is caused by the elastic energy stored within individual particles as the soil was loaded. However, there actually is some reverse sliding between particles during unloading.

Figure 10.5 also illustrates the behavior during reloading of a sand which has been loaded and then unloaded. For stresses smaller than the maximum stress of the first loading, the sand is much stiffer during the reloading than during the first loading, since much of the potential sliding between particles has already occurred during the first loading. When the sand is reloaded to stresses greater than the maximum stress of the first loading, the stress-strain curve is essentially the same as if there never had been any unloading.

Figure 10.6 illustrates the effect of cycling the stress between two fixed limits. During the first 10 to 50 cycles, a small amount of permanent strain results from each cycle. Finally, a stable *hysteresis loop* is obtained, involving little or no additional permanent strain for a cycle of loading (Fig. 10.7a).

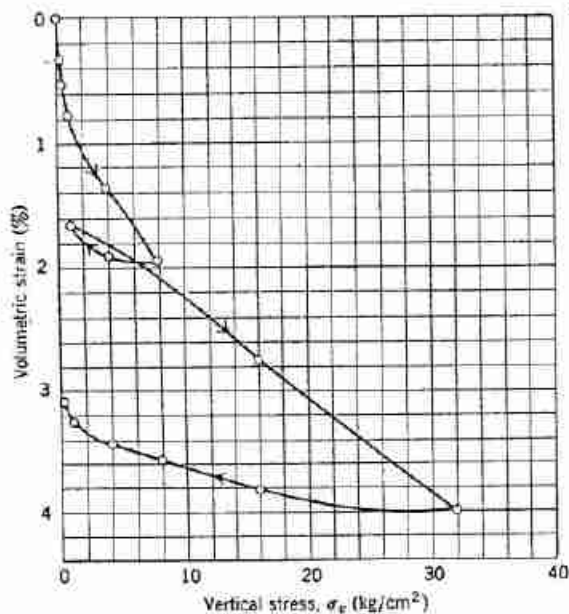


Fig. 10.5 Oedometer test results for a well graded, calcareous sand from Libya.

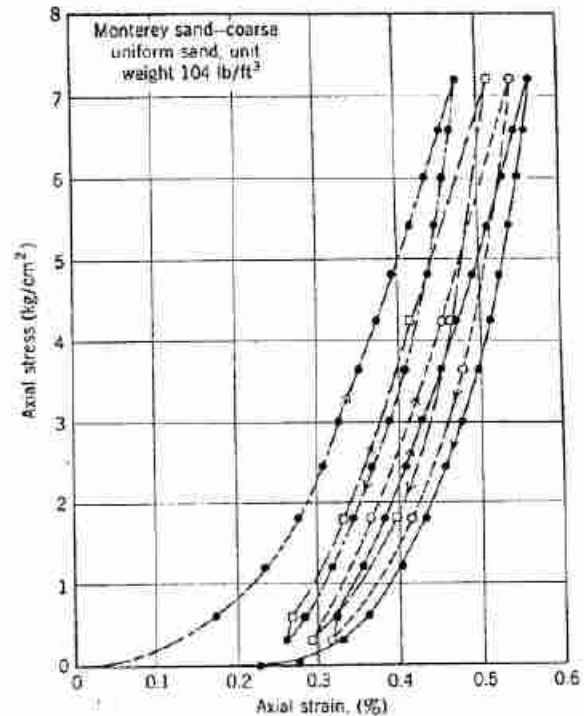


Fig. 10.6 Stress-strain curves during several cycles of loading in oedometer test (From Seaman et al., 1963).

The sequence of events during cyclic loading can be explained by using results from a theoretical study of an ideal packing of elastic spheres (Miller, 1963). It is possible to get one-dimensional straining of such an array, as indicated in Fig. 10.7c. The normal forces at the contacts compress the spheres, but sliding occurs so that the resultant relative motion is purely vertical. Upon unloading, the particles regain their original shape and sliding occurs in the reverse direction. Some small amount of energy is absorbed during each loading cycle. The same general pattern of events must occur in actual soils.

For most engineering problems, time effects during the compression of sands are of no practical importance. Figure 10.8 shows the typical behavior. All but the final few percent of compression takes place within the first few minutes.

For compression at stresses large enough to cause significant fracturing of particles, however, there is a significant time lag, as illustrated by the typical compression versus time curve shown in Fig. 10.9. For most soils, this occurs only for very large stresses. However, for soils consisting of weak particles or of weakly cemented particles, significant time effects may occur at ordinary stresses.

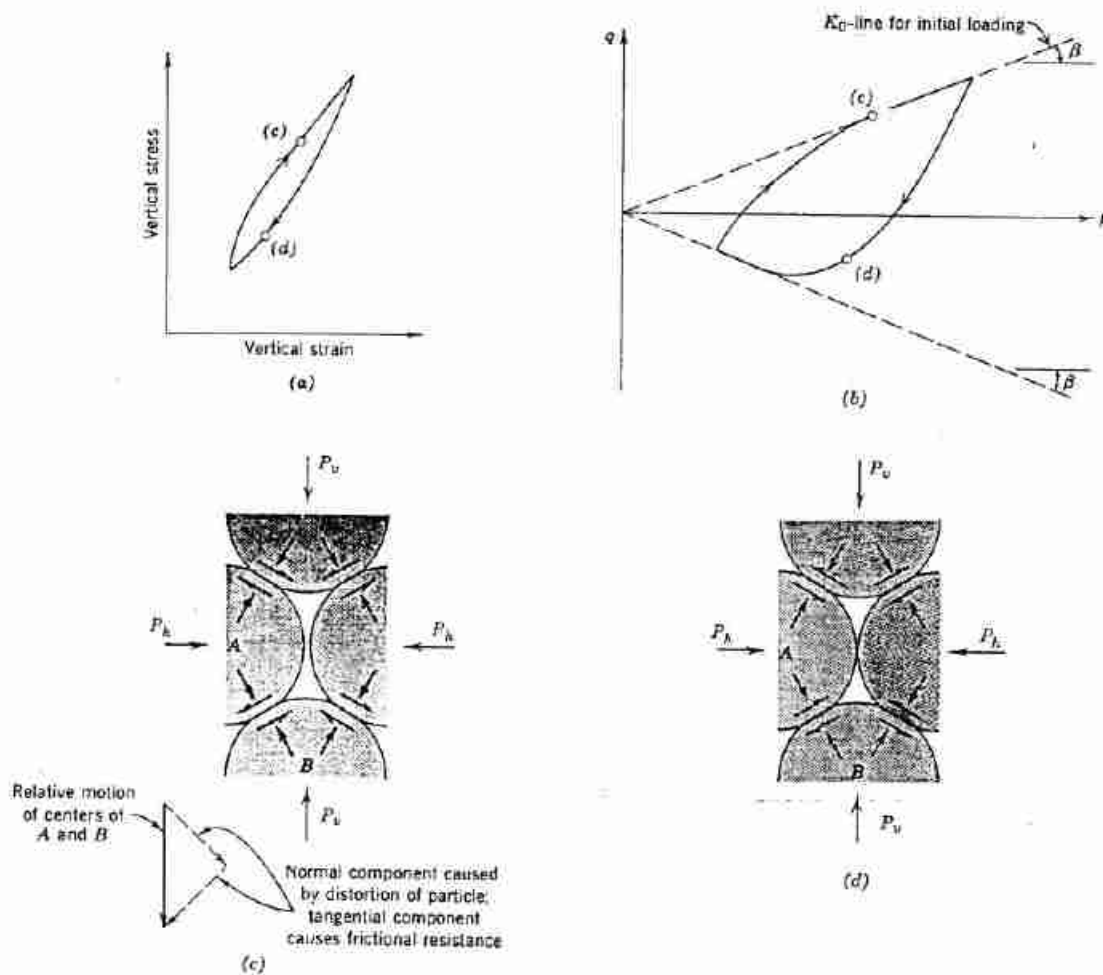


Fig. 10.7 Behavior during cyclic confined compression. (a) Hysteresis loop during cyclic confined compression. (b) Stress path. (c) Increase of vertical strain. The particles deform at the contact points, and move downward with no lateral displacement of their centers. Geometric compatibility requires sliding, and hence frictional forces, in the sense shown. For these conditions, $P_v > P_h$. (d) Decrease of vertical strain. During unloading, the elastic energy stored in the particles caused upward movement of A relative to B. Reverse sliding must develop to maintain the condition of zero lateral displacement. Hence $P_v < P_h$.

Whitman (1963) has discussed the importance of time effects during loadings of very short duration.

Small Increments of Stress Superimposed on an Initial Stress

The stress-strain behavior is shown in Fig. 10.10. Sliding between particles does not begin until the stress increment exceeds some critical level. For smaller increments, strains result only from elastic deformations of individual particles (Whitman, Miller, and Moore, 1964).

The stress required to initiate interparticle sliding increases with increasing initial stress and decreasing void ratio. This critical stress is increased when the soil has been heavily prestressed by previous loadings, and is

larger for rapid loadings than for slow loadings. For most engineering problems this critical stress is probably less than 1 psi and hence is of no practical concern. However, this initial range of stress-strain behavior is important to the study of wave propagation velocities.

Lateral Stresses during Confined Compression

During confined compression, particle motions are, on the average, in one direction only. Thus when the tangential contact forces are summed over the many contacts lying on some surface, there should be a net tangential force; i.e., a net shear stress on the surface. Hence, in general, the horizontal stress will differ from the vertical stress during confined compression. The

ratio of horizontal to vertical stress is, by definition, K_0 , the lateral stress ratio at rest.

When a granular soil is loaded for the first time, the frictional forces at the contacts act in such a direction that σ_h is less than σ_v ; i.e., $K_0 < 1$. The magnitude of K_0 must depend on the amount of frictional resistance mobilized at contact points between particles. Figure 10.11 shows data giving values of K_0 as a function of the friction angle ϕ .¹ For a few soils, such as the Sangamon River sand, the value of K_0 can be predicted by a theoretical equation based upon the study of an idealized packing of elastic spheres. However, experimental values of K_0 are best represented by an expression suggested by Jaky (1944):

$$K_0 = 1 - \sin \phi \quad (10.1)$$

Combining Eq. 10.1 with Eq. 8.12, which defines the slope β of the K_0 stress path, leads to

$$\tan \beta = \frac{\sin \phi}{2 - \sin \phi} \quad (10.2)$$

and

$$\sin \phi = \frac{2 \tan \beta}{1 + \tan \beta} \quad (10.3)$$

As indicated in Fig. 10.7*d*, the direction of the frictional forces at contact points between particles begins to reverse during unloading. For a given vertical stress, the horizontal stress will be larger during unloading than during the original loading. During the later stages of unloading, the horizontal stress may even exceed the vertical stress. This pattern is shown by the experimental data given in Fig. 10.12. During reloading of a soil, the

¹ ϕ will be defined in Chapter 11; it is the peak friction angle.

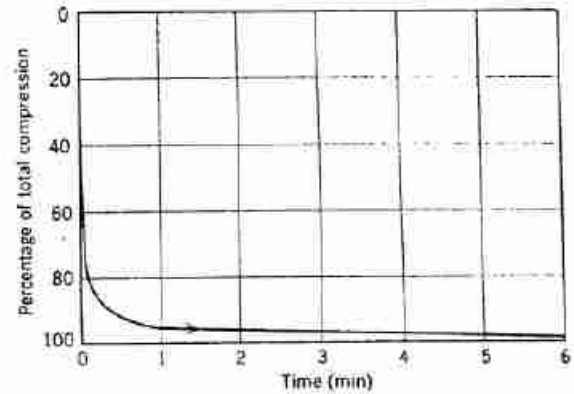


Fig. 10.8 Time curve for a typical load increment on sand (From Taylor, 1948).

lateral stress ratio generally starts out at a value greater than that given by Eq. 10.1, and then decreases to this value as the stress increases. During cyclic loading and unloading, the stress path will be as shown in Fig. 10.7*b*, with the lateral stress ratio alternating approximately between K_0 and $1/K_0$.

10.4 STRESS-STRAIN BEHAVIOR DURING TRIAXIAL COMPRESSION

Figure 10.13 shows a typical set of data from a triaxial test upon a sand. The stress path for this test is given in Fig. 10.14. The specimen was first compressed isotropically to 1 kg/cm² by increasing the chamber pressure. Then the vertical (axial) stress was increased while the horizontal stress (chamber pressure) was held constant.

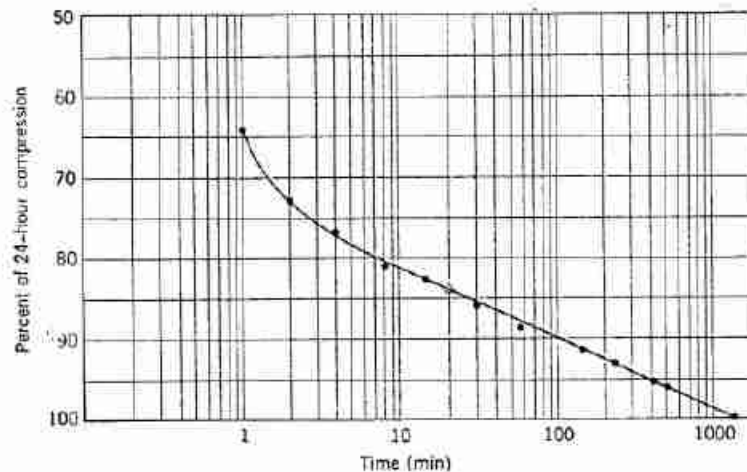


Fig. 10.9 Typical compression-time curve for high-stress test (From Roberts, 1964).

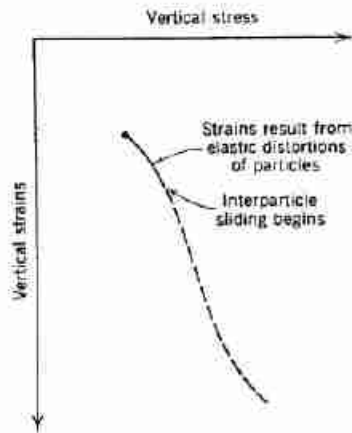


Fig. 10.10 Behavior during small stress increment superimposed upon an initial stress.

Figure 10.13 plots q , equal to one-half the deviator stress, versus the vertical (axial) strain. This stress-strain relation becomes curved at very small strains and achieves a peak at a strain of about 3%. The resistance of the soil then gradually decreases until this test was arbitrarily stopped at a strain of 11.6%. If the test had been carried to larger strains, the stress-strain curve would have leveled off at a constant value of stress. For further discussion of this stress-strain behavior, it is useful to define three stages in the straining process:

1. An initial stage during which strains are very small. For the test shown in Fig. 10.13 this range extends to a strain of about $\frac{1}{4}$ %.
2. A range which begins when the specimen begins to yield and which includes the peak of the curve and the gradual decrease of resistance past the peak.

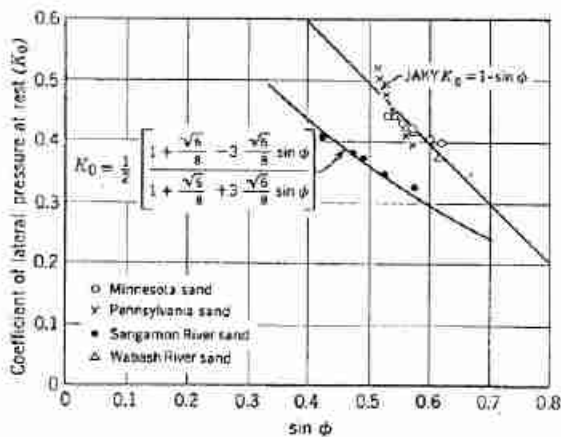


Fig. 10.11 Coefficient of lateral stress at rest for initial loading versus friction angle (from Hendron, 1963).

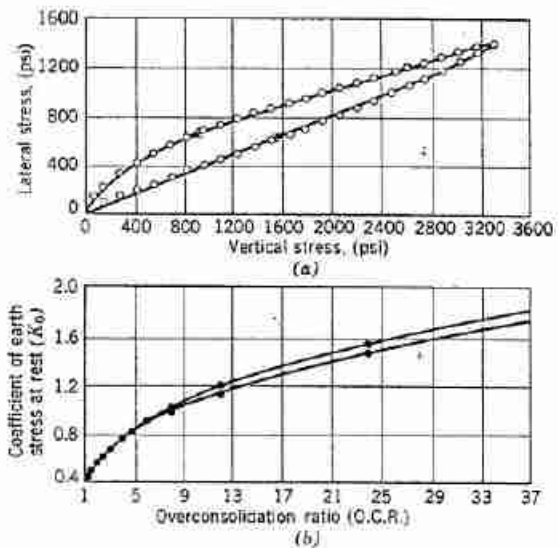


Fig. 10.12 Lateral stress during one-dimensional compression, Minnesota sand; $e_0 = 0.62$, $D_r = 0.34$. (From Hendron, 1963.)

For the test shown, this range extends from $\frac{1}{4}$ % strain until the end of the test.

3. A final range during which the resistance is constant with further straining. This range is called the *ultimate condition*.

Behavior During Initial Range

During the initial range the volume of the specimen decreases slightly, as shown in Fig. 10.13. Part (c) of the figure shows that the specimen is bulging slightly so that the horizontal strain is negative, but numerically the horizontal strain is less than the vertical strain.

This is exactly the pattern of behavior that would be expected when the compressive stresses are increasing. In this stage the particles are being pushed into a denser arrangement. The general behavior is very similar to that during confined or isotropic compression. Figure 10.15 compares the stress-strain behavior during isotropic, confined, and triaxial compression upon identical specimens which initially had the same void ratio and carried the same vertical stress.

Behavior at and near Peak

Within this range the soil fails. The deviator stress at the peak point of the stress-strain curve is called the *compressive strength* of the soil. The value of q at the peak (i.e., half the compressive strength) is related to the *shear strength* of the soil.

The behavior during this stage is quite different from

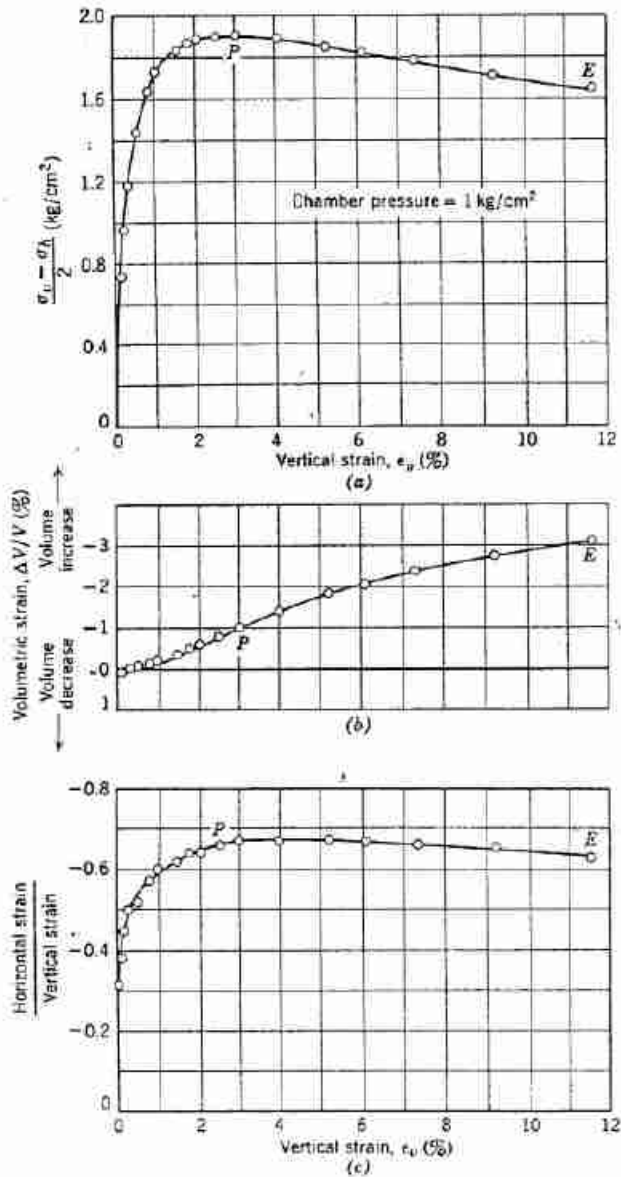


Fig. 10.13. Results of triaxial compression test upon a well graded calcareous sand from Libya.

that during the initial stage, and can be explained by studying the deformation of a planar array of rigid spheres. Figure 10.16d shows a unit element from a densely packed array. When this element is compressed vertically, strains can result only if the spheres C and D move laterally. This pattern of motion *must* be accompanied by an increase in the volume of the array, as can be seen by comparing the void spaces in parts (a) and (b) of the figure. Figure 10.13b shows that just such a volume increase occurs during loading of actual soils. It is a remarkable fact that a dense sand, when compressed in

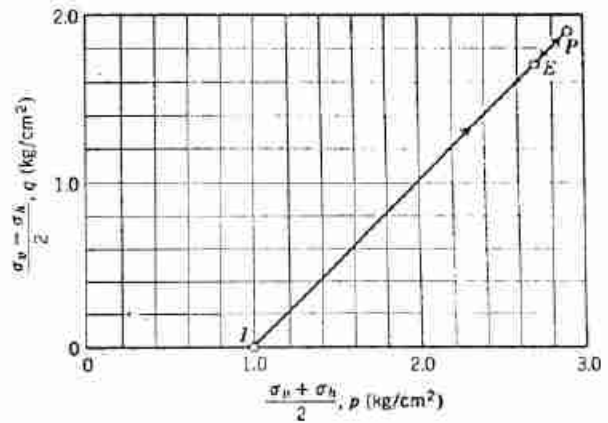


Fig. 10.14 Stress path for standard triaxial test on well graded sand from Libya.

one direction, actually increases in volume. The fact was first observed and investigated by Osbourne Reynolds in 1885. Reynolds applied the name *dilatant* to this volume increase effect.

The planar array of spheres can also be used to study the conditions that exist at the peak of the stress-strain curve and to explain the decrease in strength past the peak (Rowe, 1962). However, these aspects of the behavior can be more readily discussed using the sketches in Fig. 10.17, which illustrate the concept of *interlocking*.

Figure 10.17a shows soil particles sliding over a smooth surface. This is the situation we dealt with in Chapter 6, and for this situation the shear resistance is given by ϕ_m , the mineral-to-mineral friction angle. However, the situation within actual soils is more like that shown in parts (b) and (c) of the figure: soil particles are in contact with other soil particles, and planes through the contact points are inclined to the horizontal. In order to have a

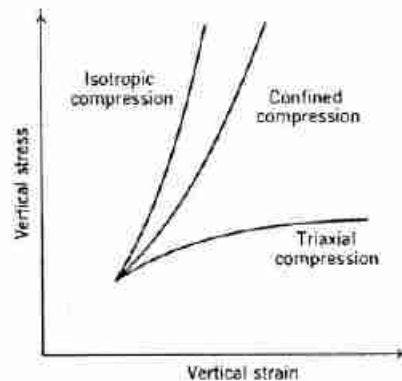


Fig. 10.15 Comparison of stress-strain curves for three types of compression.

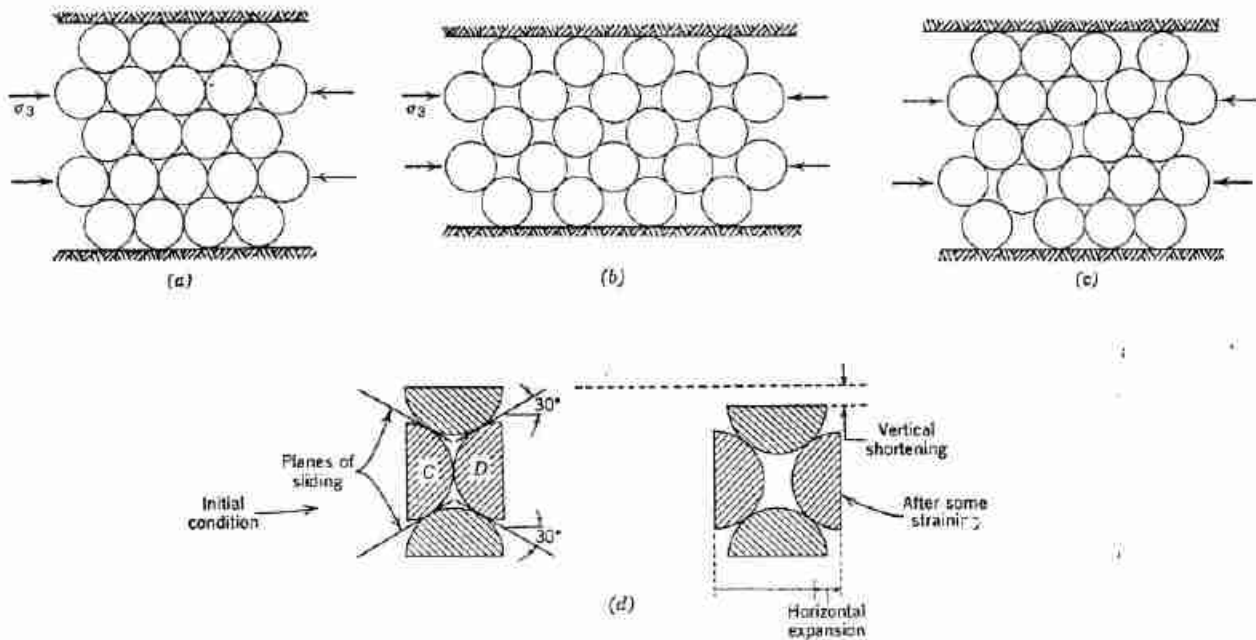


Fig. 10.16 Strains within regular array of spheres. (a) Initially dense array. (b) Loosest condition—uniform strains. (c) Loosest condition—nonuniform strains. (d) Behavior of unit of element.

shear failure between particles, it is therefore not only necessary to overcome the mineral-to-mineral frictional resistance, it is, in addition, necessary to make particles move up and over one another.

Hence the shear resistance of an actual soil mass is made up of two components: (a) one whose magnitude is controlled by ϕ_μ ; and (b) a second component whose magnitude is related to the degree of interlocking. The greater the degree of interlocking, the greater the overall shear resistance. Thus for a given value of normal force N , the shear force T necessary to start sliding will be greatest in the situation shown in Fig. 10.17c and will be least in the situation shown in Fig. 10.17a.

For the situations shown in parts (b) and (c) of Fig. 10.17, the plates must start to move apart just as soon as shear motion between the plates commences. As shear motion continues, the degree of interlocking must decrease, and consequently the shear force necessary to continue the motion must also decrease. Thus, if we start with the highly interlocked arrangement of Fig. 10.17c and cause shear motion to occur, the arrangement will tend to become more and more like the arrangement shown in part (b) of the figure.

If the foregoing concepts regarding dilatancy and interlocking are correct, the initial void ratio should have a great effect upon the stress-strain curves during triaxial compression. The data in Fig. 10.18 show that this is true. For the dense specimen, the curve of deviator

stress versus axial strain shows a pronounced peak and the deviator stress decreases following this peak. On the other hand, the corresponding curve for the loose specimen does not have a peak, and the deviator stress remains essentially constant with further straining once the compressive strength is reached. Furthermore, the dense

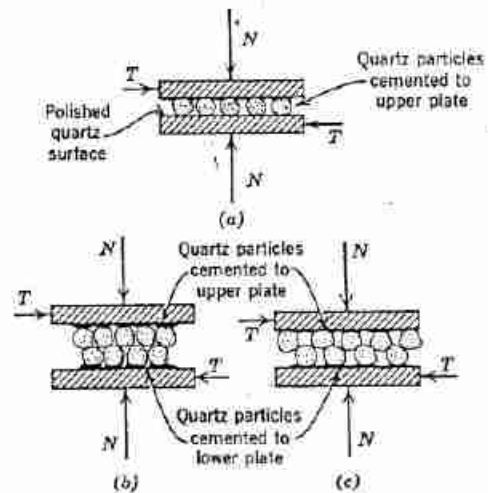


Fig. 10.17 Example of interlocking. (a) Smooth sliding surface. (b) Slightly interlocked surfaces. (c) Highly interlocked surfaces.

specimen expands in volume to a very marked degree as the specimen is strained. On the other hand, the loose specimen first decreases in volume, then expands once again, and finally ends up at almost the volume at which it started.

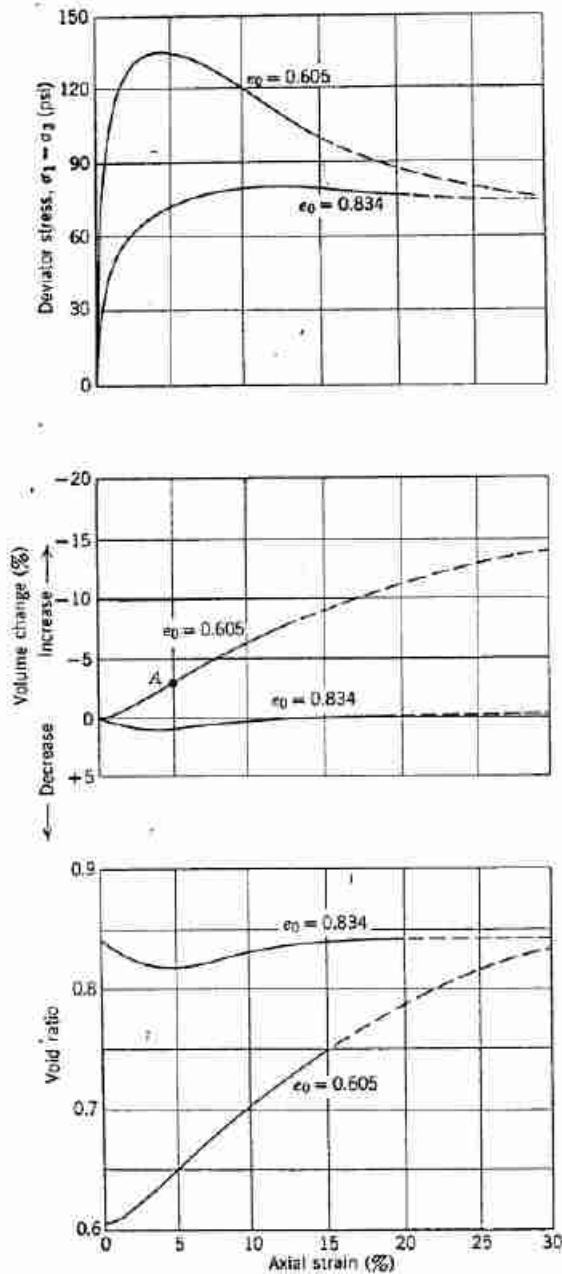


Fig. 10.18 Stress-strain curves for loose and dense specimens. Medium-fine sand. $\sigma_3 = 30 \text{ lb/in.}^2$; $e_0 = 0.605 \approx 100\% D_r$; $e_0 = 0.834 \approx 20\% D_r$. Solid line, actual test data; dashed line, extrapolations based on results of other tests. (After Taylor, 1948.)

The following patterns of behavior are just what would be predicted by the concepts of dilatancy and interlocking:

1. The denser the sand, the greater the interlocking, hence the greater the deviator stress, hence the greater the friction angle.
2. The denser the sand, the greater the volume increase which must occur.

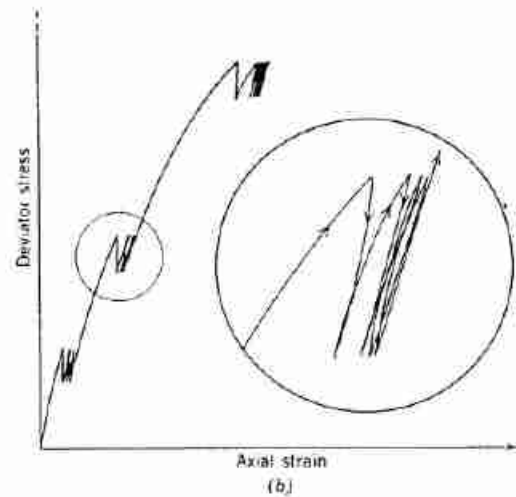
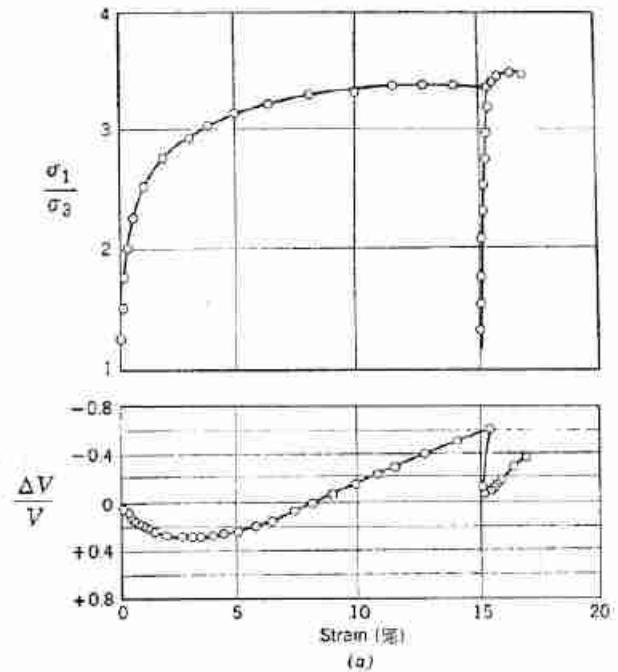


Fig. 10.19 Behavior during repeated loading in triaxial compression. [(a) From Rowe, 1962. (b) From Shannon et al., 1959.]

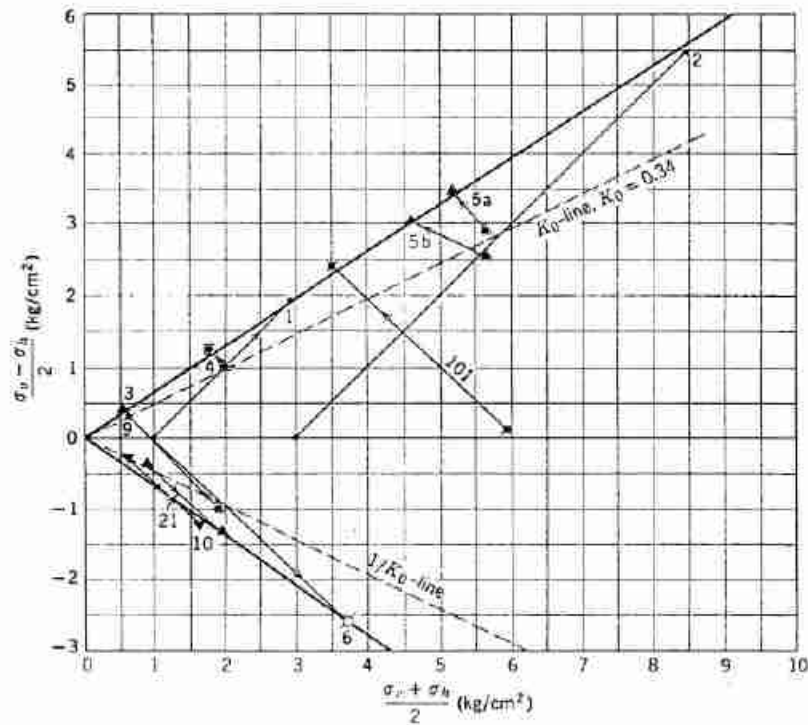


Fig. 10.20 Stress paths for various loadings.

3. As the sand expands, the resistance to straining decreases.
4. This decrease is most marked in the densest specimens.

We shall return to a discussion of these very important facts in Chapter 11.

Ultimate Condition

In the ultimate condition, the interlocking between the soil particles has decreased to the point where continuous shear deformation can continue without further volume change. The void ratio at this stage is independent of the initial void ratio before shearing was commenced.

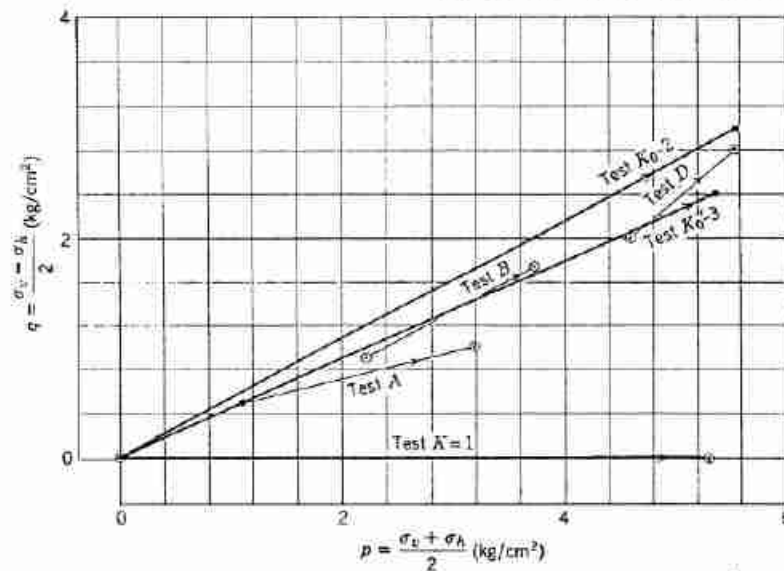


Fig. 10.21 Stress paths for nonfailure loadings.

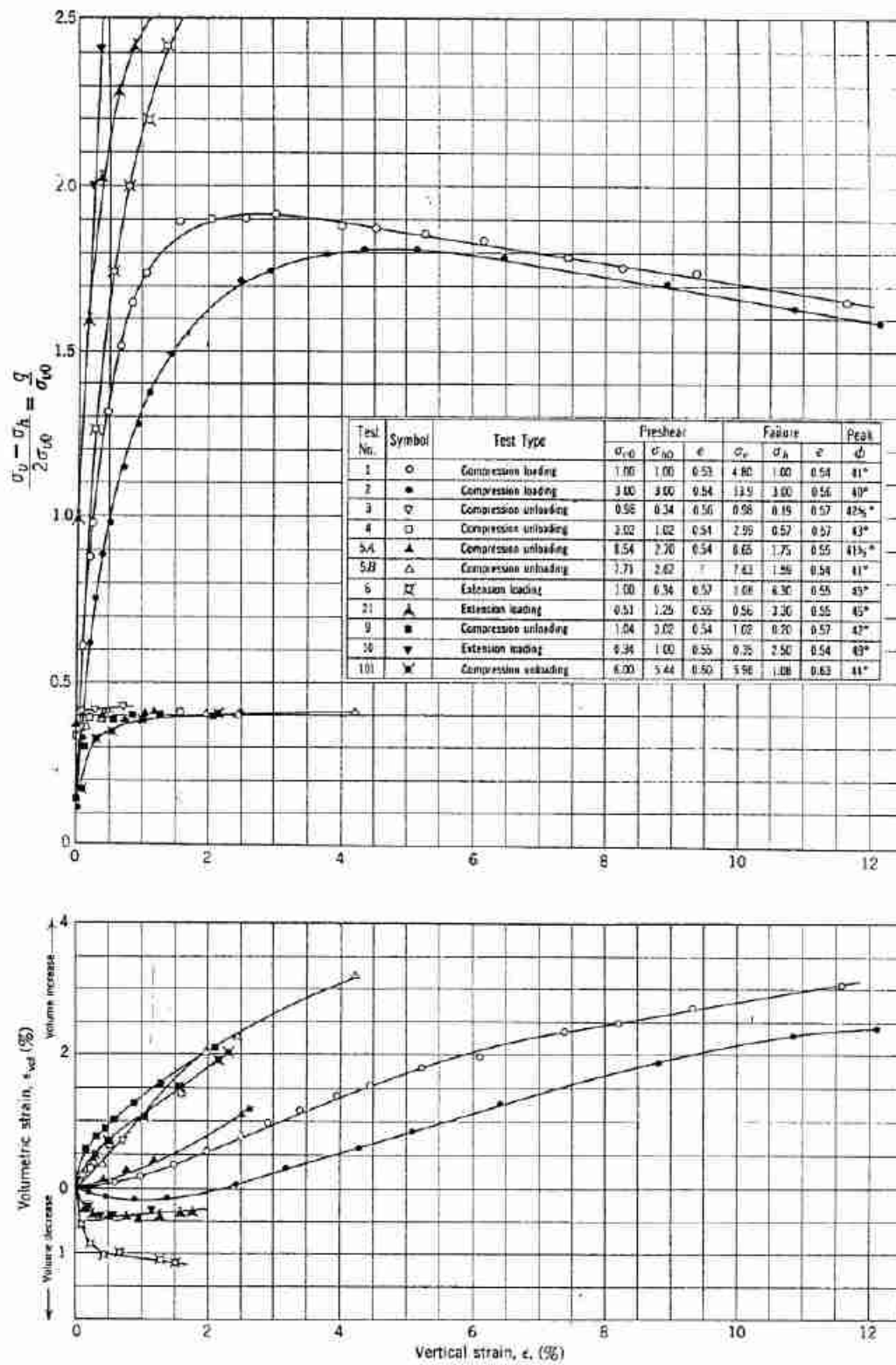


Fig. 10.22 Stress-strain data for various loading conditions.

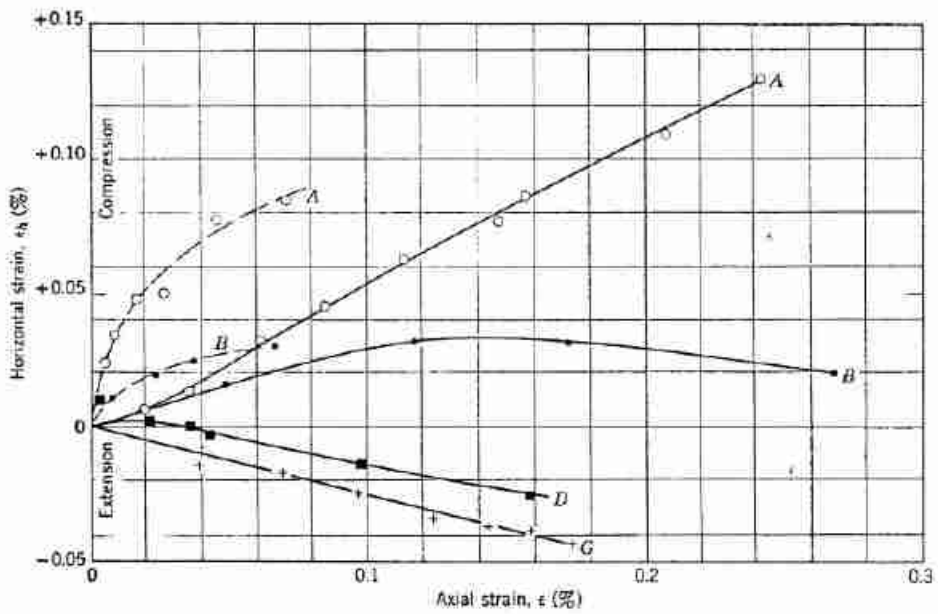
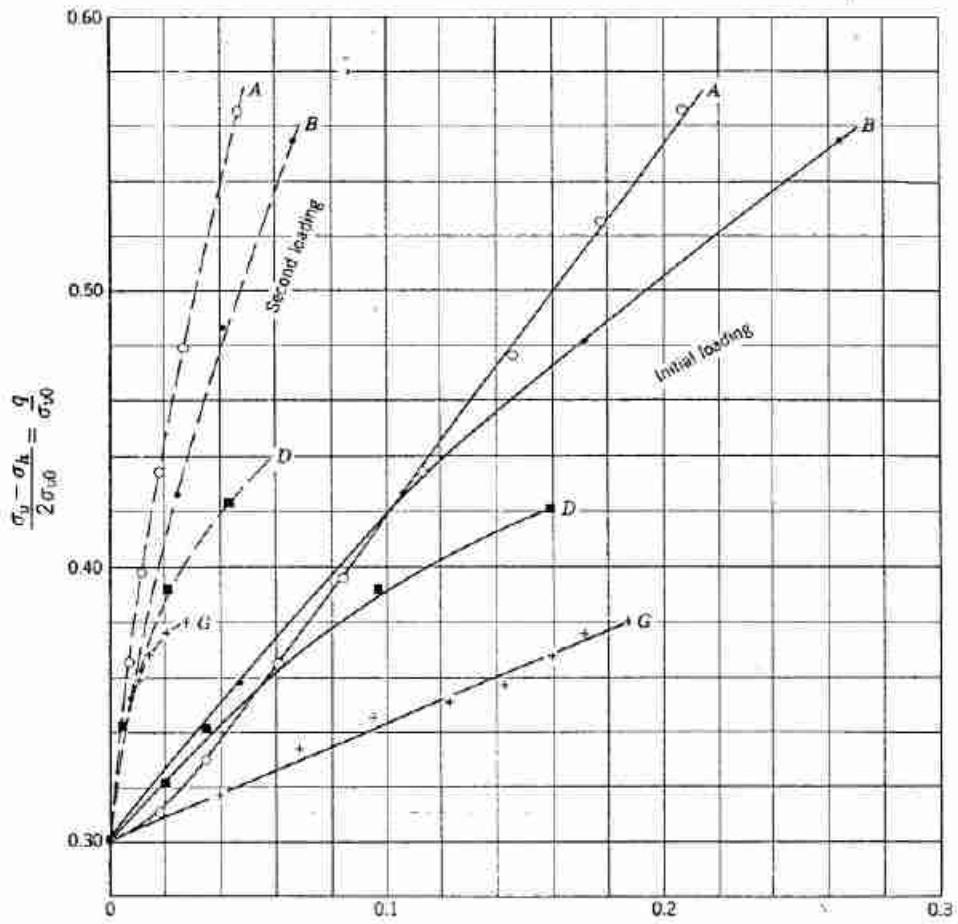


Fig. 10.23 Stress-strain data for nonfailure loadings.

Effect of Unloading and Reloading

Figure 10.19 shows some typical stress-strain curves obtained as a result of successive cycles of loading and unloading. The general features of these curves are similar to those obtained during one-dimensional compression.

10.5 BEHAVIOR DURING OTHER LOADING CONDITIONS

The loadings on typical elements of soil in the ground generally will be neither exactly those for standard triaxial nor those for confined compression. However, study of behavior during confined and triaxial compression has revealed the essential features of the stress-strain relationships in dry granular soils. It usually will be possible to infer the stress-strain features which will occur with the actual loading from those presented in Sections 10.3 and 10.4.

For example, Figs. 10.20 and 10.21 give stress paths for a variety of loading conditions which can be accomplished in a triaxial cell. Figures 10.22 and 10.23 give the resulting stress-strain data. For convenience in plotting, the values of q have been divided by the vertical stress σ_{ve} at the beginning of the test. A careful study of these figures, especially of the data regarding volume changes and horizontal strains, will be rewarding.

Behavior During Direct Shear Test

The general behavior during direct shear tests is exactly similar to that during triaxial compression tests. Figure 10.24 shows a typical set of results from a direct shear test upon a loose sand. Results for a dense sand would show a peaked stress-strain curve and an increase in the thickness of the specimen during shear.

In the usual direct shear test, most of the distortion occurs in a thin zone of unknown thickness. The strain in this zone, which determines the shear resistance, hence is quite different from the displacement between the two parts of the shear box divided by the thickness of the specimen. Therefore it is very difficult to get other than qualitative stress-strain data from the usual direct shear test.

10.6 SUMMARY OF MAIN POINTS

This chapter has explained theoretically and illustrated experimentally both the mechanisms of deformation of granular soils and certain important characteristics of the stress-strain behavior. The main cause of strain, except for very, very small strains, is relative movement (sliding and rolling) between particles. Deformations of particles are also important in that they permit the relative movements to occur. Crushing and fracturing of particles is

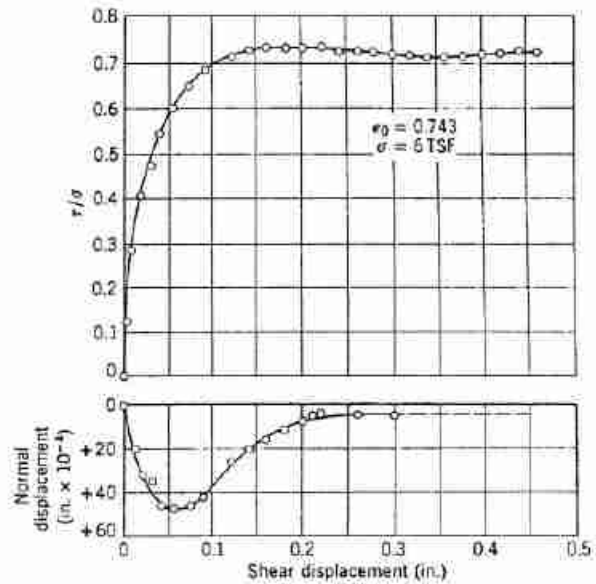


Fig. 10.24 Typical results from a direct shear test on a loose sand.

especially important for stresses greater than 500 psi. For very small strains only elastic deformation of particles occurs.

1. In both confined compression and triaxial compression the following characteristics of stress-strain behavior exist:
 - a. A highly nonlinear stress-strain curve.
 - b. A hysteresis loop in the stress-strain curve.
 - c. A net compressive strain developed by a cycle of loading and unloading.
 - d. An increased stiffness developed by a cycle of loading and unloading.
2. In confined compression the following characteristics exist:
 - a. The stiffness increases with increasing stress (except possibly for very small stress changes).
 - b. K_0 is approximately constant at $1 - \sin \phi$ during initial loading, but increases progressively during unloading.
3. The characteristics of triaxial compression are:
 - a. The stiffness decreases with increasing stress until peak strength is reached.
 - b. Dense sands tend to increase in volume as they are compressed, whereas loose sands experience little volume change.

- c. Dense sands lose strength when strained beyond peak strength, but loose sands do not.

Thus far our discussion of stress-strain behavior has been primarily qualitative. We have avoided saying *how much* strength a soil has or *how large* its stiffness is. In the next two chapters we turn to quantitative consideration of stress-strain, first of strength and then of stiffness.

PROBLEMS

10.1 Plot the stress path for the loading and unloading shown in Fig. 10.12a.

10.2 Using the data in Fig. 10.13 at 4% vertical strain, show that the value of horizontal strain is consistent with the volume change. What would the horizontal strain have been if there were to be zero volume change? (see Eq. 12.5)

10.3 Using the data for loading D in Fig. 10.23, state whether the soil increased or decreased in volume.

CHAPTER 11

Shear Strength of Cohesionless Soil

This chapter discusses the various factors that determine the shear resistance of dry granular soil. These factors fall into two general groups.

The first group includes those factors that affect the shear resistance of a given soil: the void ratio of the soil, the confining stresses, the rate of loading, etc. It is necessary to understand the influence of these factors so that the strength appropriate for a practical problem can be measured. Of these factors, void ratio and confining stress are by far the most important. The effect of void ratio has already been mentioned in Chapter 10. A study of the effect of confining stress will be the starting-point for this chapter.

The second group includes those factors that cause the strength of one soil to differ from the strength of another soil, even for the same confining stress and void ratio: the size, shape, and gradation of the particles making up the soil. Knowledge of the effects of these factors is important when selecting soils for embankments, dams, pavement subgrades, etc.

11.1 EFFECT OF CONFINING STRESS

A typical program of triaxial tests to establish the influence of confining stress on strength involves the following steps: (a) make up two or more cylindrical specimens of a given soil, all having the same void ratio; (b) place the specimens within triaxial cells, and subject each specimen to a different confining stress $\sigma_{v0} = \sigma_{v0}$; and (c) load each specimen axially, recording the resulting vertical strains and volume changes.

The curves in Fig. 10.22, Tests 1 and 2, show typical results from such tests. In order to make clear the influence of the confining stress, the stress-strain curves have been *normalized* with regard to the confining stress; i.e., the value of q at any strain has been divided by σ_{v0} . The normalized curves for these two tests are very similar in shape and magnitude. However, there are some important trends which should be noted.

1. As σ_{v0} increases, the peak normalized stress decreases slightly. There is a slight increase in the strain at which this peak occurs.
2. The normalized stress in the ultimate condition is more-or-less independent of σ_{v0} .
3. The volume increase is less in the case of the test with the larger confining stress.

This pattern of results is explainable by two concepts.

First, granular soil is frictional. The resistance to sliding at each contact point is proportional to the normal force at that contact, and hence the overall resistance increases as the confining stress increases.

Second, interlocking also contributes to the overall resistance. The nature and importance of interlocking were discussed in Chapter 10. Interlocking decreases as the confining stress increases, because the particles become flattened at contact points, sharp corners are crushed, and particles break. Even though these actions result in a denser specimen, they make it easier for shear deformations to occur.

Thus granular soil is a frictional material, but with a deviation from purely frictional behavior because of the effect of confining stress upon interlocking. The soil used to obtain the data shown in Fig. 10.22 was composed of weak carbonate particles with a tendency for crushing and breaking. Thus the deviation from a simple frictional behavior was emphasized. For a sand composed of quartz particles, the normalized stress-strain curves and volume change curves would have been almost identical for the two different confining stresses. The deviation from pure frictional behavior is decreased by using confining stresses which are only slightly different from each other, and increased by using one small and one very large confining stress.

Mohr-Coulomb Failure Law

The strength of a soil is usually defined in terms of the stresses developed at the peak of the stress-strain curve

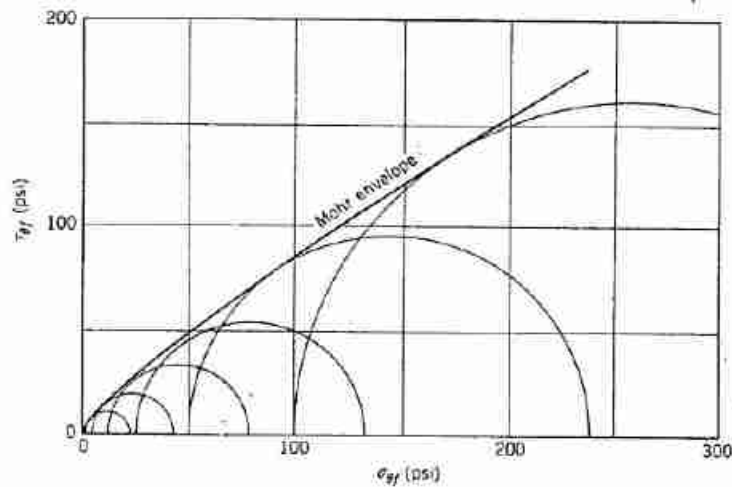


Fig. 11.1 Mohr envelope for a sand-gravel mixture (data from Holtz and Gibbs, 1956).

(point *P* in Fig. 10.13). Figure 11.1 shows one method of representing strength. The data come from six triaxial tests, each at a different confining stress, on a sand-gravel mixture.

First, Mohr circles are drawn to represent the states-of-stress at the peak points of the stress-strain curves.¹ The subscripts *f* denote that this is the failure condition. Then a line is drawn tangent to the Mohr circles. This curve is called the *Mohr failure envelope*, after Otto Mohr, who first wrote about general strength theory in 1882. The physical meaning of the Mohr envelope may be understood from the following statements.

1. If the Mohr circle for a given state of stress lies entirely below the Mohr envelope for a soil, then the soil will be stable for that state of stress.
2. If the Mohr circle is just tangent to the Mohr

envelope, then the full strength of the soil has been reached on some plane through the soil. This situation is shown in Fig. 11.2. The limiting stress condition occurs on a plane inclined at an angle of θ_{cr} to the plane on which the major principle stress is acting. This plane is called the *failure plane*. The stresses on this plane are written as σ_{ff} and τ_{ff} , the normal stress on the failure plane at failure and the shear stress on the failure plane at failure.

3. It is not possible to have within a soil a state-of-stress whose Mohr circle intersects the Mohr envelope for that soil. Any attempt to impose such a state-of-stress would result in unlimited strains, i.e., failure.

The Mohr envelope may be written in functional form as

$$\tau_{ff} = f(\sigma_{ff}) \quad (11.1)$$

The Mohr envelope shown in Fig. 11.1 is a curved line.

¹ For convenience, only the upper half of the Mohr diagram is shown; the whole diagram would be symmetrical about the horizontal axis.

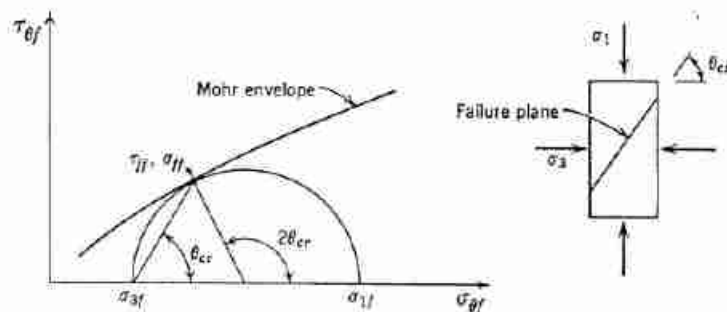


Fig. 11.2 Stresses at failure.

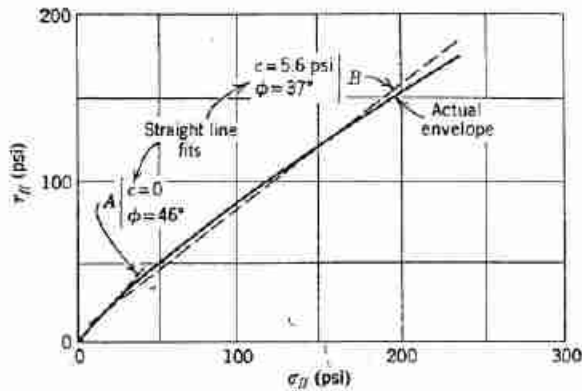


Fig. 11.3 Straight-line approximations to curved Mohr envelopes.

This is generally true for granular soils tested using a wide range of confining stresses. The reasons for this deviation from simple frictional behavior have been discussed earlier in this section. However, for most calculations regarding the stability of a soil mass, it is necessary to use a failure relationship, that is a straight line. Thus the strength is expressed by the *Mohr-Coulomb failure law*:

$$\tau_{ff} = c + \sigma_{ff} \tan \phi \quad (11.2)$$

where c is called the *cohesion* or *cohesion intercept*, and ϕ is called the *friction angle* or *angle of shearing resistance*.

The way in which a straight line is fitted to a Mohr envelope will depend on which range of σ_{ff} is of interest. Figure 11.3 illustrates two ways in which the Mohr envelope of Fig. 11.1 might be fitted by a straight line. Line A is a valid fit for σ_{ff} between 0 and 25 psi, while line B is the best fit for σ_{ff} between 0 and 200 psi. The values of c and ϕ applicable to this sand-gravel mixture also vary with the range of σ_{ff} that is of interest. The actual Mohr envelope for this soil passes through the

origin of the Mohr diagram; the soil will not stand as a cylinder if the confining pressure is zero. In this sense, this sand-gravel mixture is *cohesionless*. However, in order to use Eq. 11.2 over a large range of stresses, it is necessary to use a cohesion intercept.

If the Mohr envelope for a soil were a straight line through the origin rather than a curve, then the failure law could be simplified to

$$\tau_{ff} = \sigma_{ff} \tan \phi \quad (11.3)$$

Equation 11.3 has been applied to granular soils ever since the early studies of Coulomb in 1776. However, it is important to understand that this equation is an approximation which is accurate only for relatively small values of σ_{ff} . For the calcareous sand used to obtain the data in Figs. 10.22 and 10.23, this limit is about 5 kg/cm² (about 75 psi). For a well graded quartz sand, this limit may be as high as 150 psi. The curvature of the Mohr envelope is greatest for dense granular soils, and decreases as a soil becomes looser. The Mohr envelope for the strength in the ultimate condition apparently is quite straight over a large range of stresses.

For most engineering problems, the stresses are small enough that it is reasonable to use Eq. 11.3. However, there are many problems such as high earth dams where the strength of a dry granular soil can be satisfactorily represented only by either a curved Mohr envelope or by Eq. 11.2. Another way to represent the true nonlinear strength relation is to treat ϕ as a variable that depends upon confining pressure, i.e., $\phi = \phi(\sigma_{ff})$. Thus ϕ is computed from the slope of the straight line drawn through the origin and tangent to the Mohr circle representing the stresses at failure (see Fig. 11.4). This method of representing strength is not particularly useful when making stability calculations, but does make it easy to see just to what degree the strength is nonlinear with respect to confining stress.

For those cases where Eq. 11.3 can be used, there are simple useful relationships between ϕ and the various stresses that exist at failure, and between ϕ and σ_{cr} . These

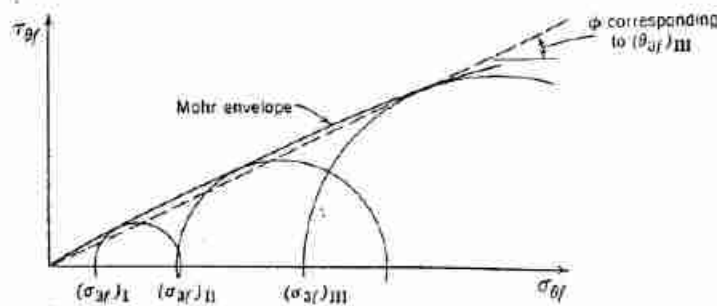


Fig. 11.4 Mohr envelope and friction angle for a large range of confining pressure.

► Example 11.1

Given. Following peak stresses from standard triaxial tests upon a dense, well-graded, coarse quartz sand.

Confining Pressure $\sigma_c = \sigma_{3f}$ (psi)	Peak Axial Stress σ_{1f} (psi)	Peak Value of q $q_f = \left(\frac{\sigma_1 - \sigma_3}{2} \right)_f$ (psi)	Value of p at Time of Peak q_f $p_f = \left(\frac{\sigma_1 + \sigma_3}{2} \right)_f$ (psi)
15	76	30.5	45.5
30	148	59	89
60	312	126	186
120	605	242.5	362.5

Find.

- a. ϕ by constructing Mohr envelope.
- b. ϕ using relationships in Fig. 11.5.
- c. θ_{cr} .

Solution.

- a. See Fig. E11.1.

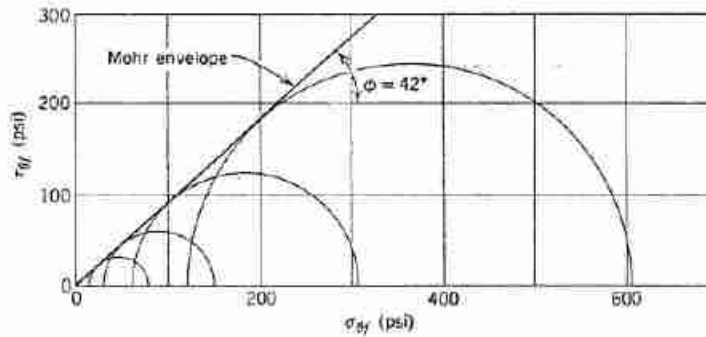


Fig. E11.1

b.

σ_{3f}	$\frac{\sigma_{1f}}{\sigma_{3f}}$	ϕ
15	5.06	42.1°
30	4.93	41.6°
60	5.20	42.7°
120	5.05	42.1°
		ave. 42.1°

c.

$$\theta_{cr} = 45^\circ + \frac{42.1^\circ}{2} = 66^\circ$$

relationships are presented in Fig. 11.5. The quantity $(1 + \sin \phi)/(1 - \sin \phi)$ recurs frequently in soil mechanics and is given a special symbol:

$$N_\phi = \frac{1 + \sin \phi}{1 - \sin \phi} \quad (11.4)$$

N_ϕ is called the *flow factor*. Example 11.1 illustrates the application of these relationships to a set of data which can be fitted quite well by Eq. 11.3. In the remainder of this chapter, we shall use Eq. 11.3 to describe the strength of various granular soils, thus we shall talk only in terms of values of ϕ .

Meaning of Mohr-Coulomb Failure Law

Equation 11.2, or the simple Eq. 11.3 which is generally used for granular soils, is at the same time one of the most widely used and most controversial equations encountered in soil mechanics. There can be no real question of the validity of these equations as useful approximations. This validity is a simple consequence of the way in which c and ϕ were defined and of the way in which they will be used in subsequent chapters. However, the failure plane as defined previously, following the original suggestion of Mohr, may or may not be the plane upon which shear strains become concentrated when the soil fails. The difference between these two planes has occupied the attention of workers such as Rowe (1963).

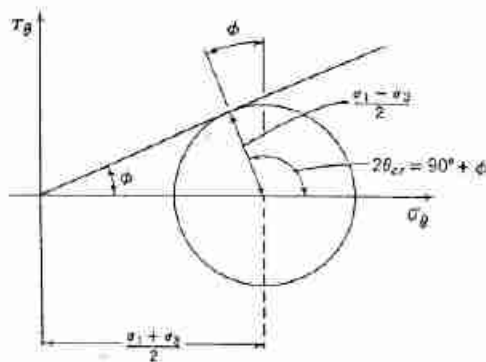


Fig. 11.5 Relations between ϕ and principal stresses at failure.

$$\begin{aligned} \sin \phi &= \frac{(\sigma_1 - \sigma_3)/2}{(\sigma_1 + \sigma_3)/2} = \frac{\sigma_1 - \sigma_3}{\sigma_1 + \sigma_3} = \frac{q}{p} \\ &= \frac{\sigma_1/\sigma_3 - 1}{\sigma_1/\sigma_3 + 1} = \frac{1 - \sigma_3/\sigma_1}{1 + \sigma_3/\sigma_1} \\ \frac{\sigma_1}{\sigma_3} &= \frac{1 + \sin \phi}{1 - \sin \phi} \\ &= \tan^2 (45^\circ + \phi/2) = \tan^2 \theta_{cr} \end{aligned}$$

Note. For convenience, subscript f has been omitted from σ_{1f} and σ_{3f} .

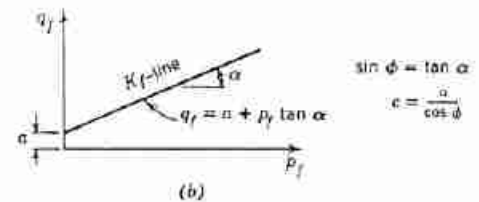
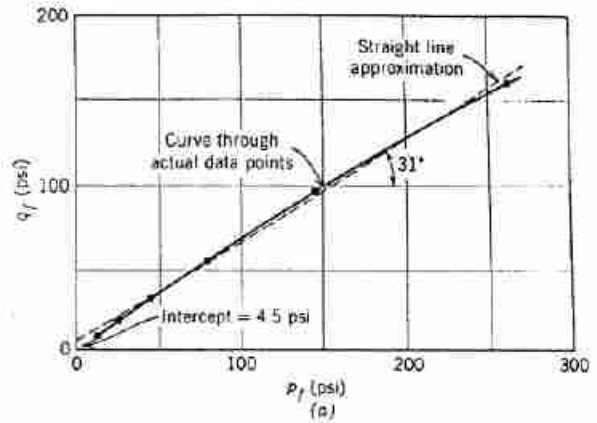


Fig. 11.6 Results of strength tests plotted on p - q diagram. (a) Actual data. (Data for sand-gravel mixture from Holtz and Gibbs, 1956.) (b) Relation of q_f and p_f to Mohr-Coulomb envelope.

To avoid misunderstanding, we shall in the remainder of the book distinguish between two types of failure plane:

1. A *theoretical failure plane*, or *slip line*, which by definition lies at an angle $(45^\circ + \phi/2)$ to the plane upon which the major principal stress acts.
2. An *observed failure plane*, which is the plane upon which the shear strains are observed to be concentrated.

Fortunately, in sands the difference between the orientation of the theoretical and observed failure planes is not great: it is less than 5° . In most problems the engineer can ignore this difference. However, in later chapters we shall encounter problems in which this difference cannot safely be ignored.

Failure often occurs along a curved surface rather than along a plane, and so we often will speak of a *theoretical failure surface* (or *slip surface*) and an *observed failure surface*.

Use of p - q Diagram

Figure 11.6 shows an alternative way to plot the results of a series of triaxial strength tests. The points give the values of p and q corresponding to the peak points of the stress-strain curves. The curve drawn through these points is called the *K_f-line*. Just as the Mohr envelope

for this soil is curved, so is the K_p -line. The K_p -line may be fitted by a straight line over the stress range of interest. For example, the straight-line fit shown in the figure is inclined at an angle $\alpha = 31^\circ$ and intercepts the vertical axis at $a = 4.5$ psi.

Figure 11.6 also gives the simple relationships that exist between α and ϕ and a and c . Note that

$$N_\phi = \frac{1 + \sin \phi}{1 - \sin \phi} = \frac{1 + \tan \alpha}{1 - \tan \alpha} \quad (11.5)$$

For the data given in this figure,

$$\phi = \sin^{-1}(\tan 31^\circ) = \sin^{-1} 0.6 = 37^\circ$$

$$c = \frac{4.5}{\cos 37^\circ} = 5.6 \text{ psi}$$

These are exactly the results found in Fig. 11.3 for line B.

Thus we have two ways to find values of c and ϕ from a series of triaxial tests: (a) construct Mohr circles and draw the Mohr envelope (Fig. 11.1); or (b) plot values of p_j and q_j , draw the K_p -line, and then compute c and ϕ . The choice between these two methods is largely one of personal preference. However, when there are many tests in the series, it will usually be less confusing to plot the results on a p - q diagram, and, further, it will be easier to fit a line through a series of data points than to attempt to pass a line tangent to many circles. For these reasons, this book will usually follow the practice of plotting the results of triaxial tests on a p - q diagram. Example 11.2 provides another illustration of the use of the p - q diagram.

► Example 11.2

Given. The data in Example 11.1.

Find. ϕ by construction of a p - q diagram.

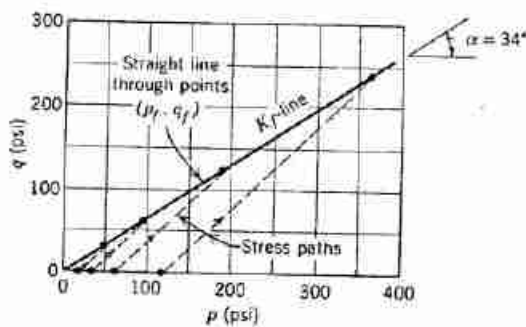


Fig. E11.2

Solution.

$$\sin \phi = \tan \alpha = 0.675$$

$$\phi = 42.5^\circ$$

Obtaining ϕ from Direct Shear Tests

In this form of test, only the normal and shear stresses on a single plane are known. Hence from the test results

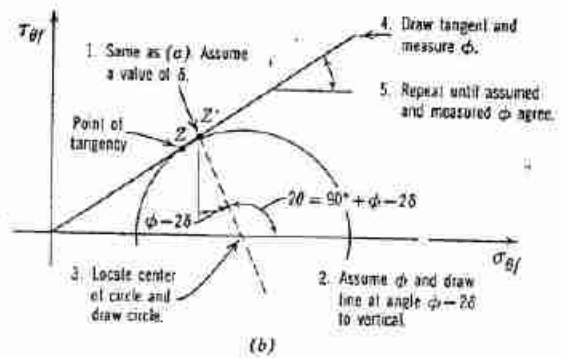
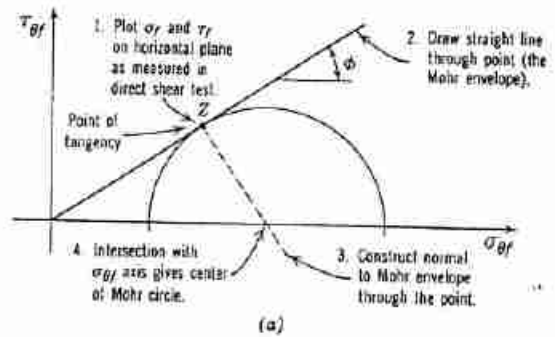


Fig. 11.7 Methods for calculating friction angle from results of direct shear test. (a) Assuming that horizontal plane is theoretical failure plane. (b) Assuming that horizontal plane is observed failure plane.

alone, it is not possible to draw the Mohr circle giving the state of stresses.

However, if we make the assumption that the measured stresses at failure are in the ratio $\tau/\sigma = \tan \phi$, then it is possible to construct the Mohr circle (see Fig. 11.7). In effect, we have assumed that the horizontal plane through the shear box is identical with the theoretical failure plane:

$$\tau = \tau_{II} \quad \text{and} \quad \sigma = \sigma_{II}$$

This assumption has often been questioned. In many ways it makes more sense that the horizontal plane is actually the plane on which shear strains are at a maximum; i.e., it is an observed failure plane. On this basis, it would be more nearly correct to represent the stresses on the horizontal plane by points lying $2\theta = \pm 2(45^\circ + \phi/2 - \delta)$ from the major principal stress, where δ is the difference in orientation between the theoretical and observed failure planes (point Z' in Fig. 11.7b). However, if δ is less than 5° , then the two methods of obtaining ϕ give results that differ by less than 1° . This difference is insignificant in practical engineering work.

Many comparisons have been made between the value of ϕ from triaxial tests (based upon slope of Mohr

envelope) and the value of ϕ from direct shear tests (based upon the construction in Fig. 11.7a). After averaging out experimental errors in the determination of the two quantities, it appears that ϕ from direct shear tests is generally greater (by perhaps 2°) than ϕ from triaxial tests, especially for dense sands (e.g., see Taylor, 1939).

The direct shear test affords the easiest way to measure the friction angle of a sand or other dry soil. It is also very useful, although perhaps not as widely used, for testing soils containing water.

11.2 EFFECT OF INITIAL VOID RATIO

Figure 11.8 shows the relationship between friction angle ϕ and the initial void ratio e_0 for a medium fine sand. The relationship will of course vary from sand to sand, but the trend of higher ϕ for denser soil is always the same.

As was discussed in Chapter 10, the effect of void ratio on ϕ may be explained by the phenomenon of interlocking. Other ways of looking at these same phenomena have also been advanced. For example, the energy that is put into a soil by the external loads is expended in two ways: to overcome the frictional resistance between particles and to expand the soil against the confining stress. The denser the sand, the greater the expansion which tends to take place during shear. Hence more energy (hence more force and a higher friction angle)

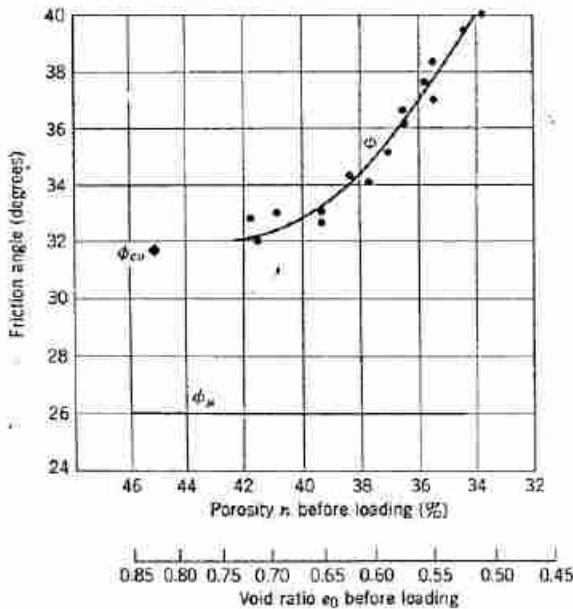


Fig. 11.8 Friction angle versus initial void ratio for medium fine sand (after Rowe, 1962).

must be expended to shear the soil. However, both of these explanations amount to the same thing.²

Strength of a Sand at Constant Volume

Another way to emphasize the important role of interlocking is to answer the question: what will happen if a sand is prevented from changing in volume as it is sheared?

First consider the simple situation shown in Fig. 10.17c. As the shear force is applied, the two plates want to move apart vertically. In order to prevent their moving apart, the normal force N which holds them together must increase. Thus the result of increasing T is to increase N but to cause very little shear displacement. As T is increased further, the contact forces will eventually become so large that the particles will be crushed and fractured, and only then will large shear displacements be possible.

Similarly, we can run a triaxial test in such a way that the volume of the specimen remains constant. The volume of the specimen is monitored, and the confining pressure is adjusted to hold this volume constant. If the sand is dense, it will be necessary to increase the confining pressure by a considerable amount. This of course means that a dense specimen which has been held under constant volume can sustain a much greater axial stress than a specimen which remains under constant confining pressure and which expands during shear. If a very loose specimen is to be held at constant volume during shear, it may be necessary to decrease the confining pressure as the test progresses, and consequently the compressive strength is decreased.

Figure 11.9 shows the results of a constant-volume test on a dense sand. If the same sand at this same initial density were tested at a constant confining pressure of 1 kg/cm², the compressive strength would be only 3.8 kg/cm².

The behavior at constant volume and the behavior with constant confining pressure can be tied together as follows. If a dense sand is to fail in shear, the high degree of interlocking must somehow be overcome. This can happen either (a) by shearing and fracturing of the particles, or (b) by increasing the volume. It will take more energy to cause either of these happenings than will be necessary simply to slide soil particles over a flat surface. If the soil is free to expand, the path of least resistance is

² The additional energy required to overcome interlocking is sometimes referred to as an energy correction (Taylor, 1948; Rowe, 1962). This terminology is rather unfortunate, for there is nothing erroneous or artificial about the large compressive strength of a dense sand. This large strength is quite real and can be relied upon to exist in practical problems. Engineers will have little or no occasion to make use of energy considerations. However, these considerations do play an important role in research aimed at establishing the nature of shear strength. The study by Rowe (1962) of the components of the strength of sands is especially thorough.

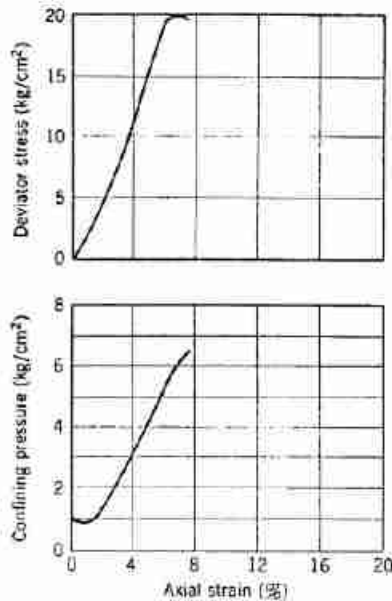


Fig. 11.9 Result of constant volume triaxial test on a sand (fine sand, dense condition.) (after Bjerrum, Kringstad, and Kummeneje, 1961.)

to expand and so to overcome the interlocking in this way. If, however, the soil is impeded from expansion, the path of least resistance may lie in fracturing the soil particles.

The case of shear at constant volume is of little importance when dealing with dry soils. However, this situation will become very important when we deal with the rapid shearing of saturated soils in Part V.

Friction Angle at the Ultimate Condition

After considerable straining of any soil, both the deviator stress and the void ratio achieve values that are independent of the initial void ratio. At this condition,

the sand strains without further volume change and with constant deviator stress. This condition is referred to as the *ultimate* (or *constant volume* or *critical* or *residual*) condition. The deviator stress that exists at this condition can be used to define a friction angle ϕ_{cv} :

$$\sin \phi_{cv} = \frac{(\sigma_1 - \sigma_3)_{cv}}{(\sigma_1 + \sigma_3)_{cv}} \quad (11.6)$$

where the subscript *cv* stands for constant volume.

However, ϕ_{cv} is greater than ϕ_p , the particle-to-particle friction angle as defined in Chapter 6. Figure 11.8 presents a comparison between these two angles. We see that there is still some interlocking when the constant volume condition is reached. Particles must still move up and over (or perhaps mostly around) their neighbors as straining takes place, and on a scale equal to the particle size there must be volume changes—both increases and decreases. The local effects combine in such a way that there is no volume change for the specimen of sand as a whole.

Thus ϕ_{cv} may be thought of as a material property, reflecting the combined effect of ϕ_p plus the degree of interlocking that can occur with zero overall volume change during continued straining. The void ratio at the constant volume condition, e_{cv} , may likewise be considered a material property.

Peak Friction Angle

As already defined, the friction angle ϕ is calculated from the stresses existing at the peak of the stress-strain curve. This friction angle ϕ is not a material property but depends strongly on the void ratio that existed prior to the application of a deviator stress. Actually, some small volume change takes place in the sand before the peak deviator stress is reached, but nonetheless it is customary to plot ϕ as a function of e_0 .

Choice of ϕ for Engineering Practice

In most problems encountered in engineering practice, it is not possible to tolerate large strains within a sand

Table 11.1 Types of Friction Angle to Use in Various Engineering Problems

Problem	Friction Angle	Depends Upon
Internal strength of sand at small strains	Peak friction angle ϕ	Composition of soil; initial void ratio; initial confining stress
Internal strength of sand at very large strains	Ultimate friction angle ϕ_{cv}	Composition of soil; void ratio in ultimate condition
Sliding of sand on smooth surface	Particle-to-particle friction angle ϕ_p	Nature of soil mineral and surface
Sliding of sand on rough surface	Ultimate friction angle ϕ_{cv}	Composition of soil; void ratio in ultimate condition

mass. Thus for most problems the value of ϕ based upon the peak of the stress-strain curve is properly used to represent the strength of the sand. There are some problems in which large strains occur, as when one must evaluate the resistance encountered by a tracked vehicle as it plows its way through a sand mass. For such problems, it would be appropriate to use ϕ_{cr} to represent the strength of the sand.

The foregoing comments apply to the internal strength of a sand. The engineer frequently needs to know the frictional resistance between sand and the surface of some structure, such as a retaining wall or pile. If this surface is very smooth, as in the case of sand sliding on unruled steel, the friction angle is most likely equal to ϕ_u for the sand. If the surface is at all rough, such as a typical concrete surface, then the friction between the surfaces probably approaches ϕ_{cr} .

Table 11.1 summarizes these recommendations concerning the type of friction angle that should be used for various situations. Values of ϕ_u have already been presented in Chapter 6. Typical values for ϕ and ϕ_{cr} appear in this chapter. Subsequent chapters which treat engineering applications in detail will have still more to say about the choice of a friction angle for use in a particular situation.

11.3 EFFECT OF VARIOUS LOADING CONDITIONS

Intermediate Principal Stress

With the normal form of triaxial test (specimen failed by increasing axial stress while holding confining pressure constant), the intermediate principal stress is equal to the minor principal stress: $\sigma_2 = \sigma_3$ (stress path for vertical compression loading in Fig. 9.8). As shown in Fig. 9.8, a specimen can be failed in vertical extension, in which case $\sigma_2 = \sigma_1$.

Numerous investigators have compared the friction angle from compression with that from extension tests, with various results; see Roscoe (1963) et al for a summary. Most investigators have concluded that the friction angle is the same for both cases, but a few have found that ϕ was greater, by several degrees, if $\sigma_2 = \sigma_1$, as compared with the results for $\sigma_2 = \sigma_3$ (as is the case in Figs. 10.20 and 10.22).

Figure 11.10 shows the results of a set of plane-strain tests; these are tests in which the sand can strain only in the axial direction and one lateral direction while its dimension remains fixed in the other lateral direction. The friction angle from these plane-strain tests exceeded the angle as obtained from conventional triaxial tests by as much as 4° for the densest specimens. Little or no difference in ϕ values was observed on loose specimens.

A plane-strain condition is often encountered in engineering practice problems, and for many problems

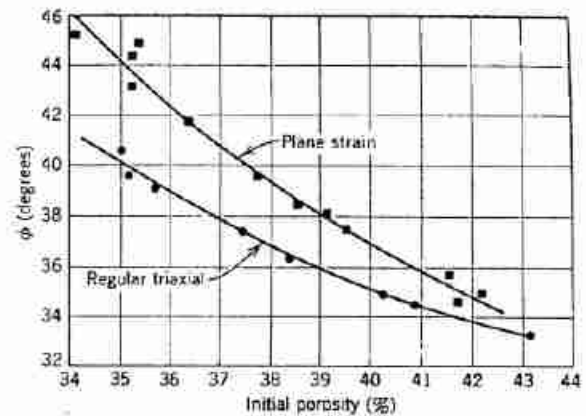


Fig. 11.10 Results of regular and plane-strain triaxial tests (from Cornforth, 1964).

a plane-strain test is more realistic than is the triaxial test. The authors feel that the plane-strain form of triaxial test will become increasingly popular with practicing engineers as well as with researchers.

The reason for the increased resistance in the plane-strain condition presumably comes about because the soil particles are given less freedom in the ways that they can move around their neighbors so as to overcome interlocking. A failure law in three dimensions is now needed. The possible form of such a law has been discussed numerous times (Kirkpatrick, 1957; Haythornthwaite, 1960), but the matter is still unresolved. Special testing devices, which permit greater flexibility in the types of loads that are applied, are needed for use in research to clarify the nature of the three-dimensional failure law.

Failure with Decreasing Stresses

In problems such as retaining walls (under active conditions), the soil fails as the result of decreasing stresses rather than increasing stresses; i.e., the stress path is more like that marked *E* in Fig. 8.11 or that for vertical compression unloading in Fig. 9.8, and those for tests 3, 4, and 5 in Fig. 10.20. As indicated in Fig. 10.22, the friction angle for unloading is virtually the same as for loading.

Rate of Loading

The friction angle of sand, as measured in triaxial compression, is substantially the same whether the sand is loaded to failure in 5 millisecc or 5 min. The increase in $\tan \phi$ from the slower to the faster loading rate is at most 10%, and probably is only 1–2% (see Whitman and Healy, 1963). It is possible that the effect might be somewhat greater if the sand is sheared in plane strain or if the confining pressure is in excess of 100 psi.

Vibrations and Repeated Loadings

Repeated loadings, whether changing slowly or quickly, can cause ϕ to change. A loose sand will densify, with resulting strength increase, and a dense sand can expand, with resulting strength decrease. A stress smaller than the static failure stress can cause very large strains if the load is applied repeatedly (see Seed and Chan, 1961).

Slight Amount of Moisture

Any sand, unless it has just been intentionally dried, possesses a small moisture content. The presence of this moisture can have some effect upon the mineral-to-mineral friction angle (see Chapter 6). However, since both shear tests and most practical situations really involve either air-dry or saturated sand, the presence of this small amount of moisture need seldom be taken into account.

Moisture can also introduce an apparent cohesion between particles by capillarity. In some situations, such as in model tests, this cohesion can be a significant component of strength. In practical problems, this small cohesion is of no consequence.

Testing Errors

Chapter 9 mentioned some of the errors which can develop in triaxial tests and in direct shear tests. The common tests can give rise to an error of as much as 2° in the measurement of the peak friction angle ϕ . Nonetheless, these tests suffice for most engineering purposes. For careful measurement of strength and volume change in research work, it is essential to use the improved devices.

Summary

This section has indicated that many factors have an influence on the friction angle of granular soils. Using the ordinary laboratory test, the measured value of ϕ may differ by several degrees from the friction angle actually available within the ground, even if the initial void ratio has been chosen accurately. If a more accurate evaluation of ϕ is needed, special care must be taken to establish the loading condition actually existing in the ground and to duplicate this condition in the laboratory by means of special tests.

11.4 EFFECT OF COMPOSITION

This section considers the effect of composition on (a) the ϕ versus e_0 relation for a small range of confining stresses, and (b) the change in ϕ over a wide range of confining stresses. Even when confining stresses are limited to conventional magnitudes (less than 100 psi) the ϕ versus e_0 relation falls within a broad band as shown in Fig. 11.11. Since the value of ϕ varies relatively little between various particle sizes or various

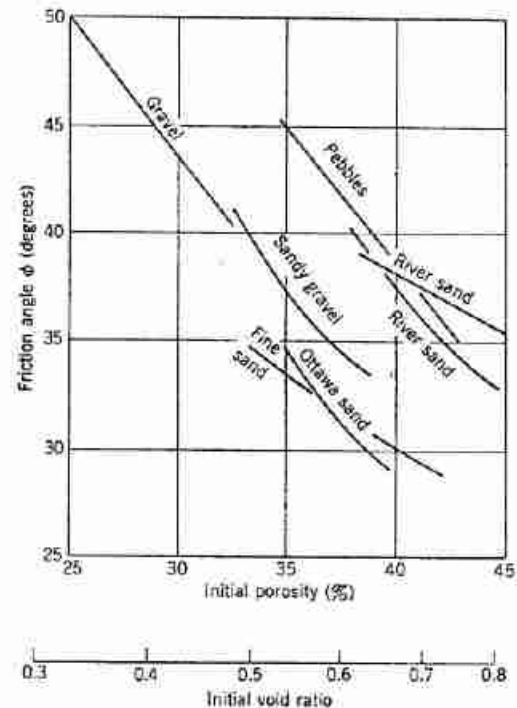


Fig. 11.11 Friction angle versus initial porosity for several granular soils.

minerals, these differences in ϕ for a given e_0 result primarily from different degrees of interlocking.

Composition affects the friction angle of a granular soil in two ways. First it affects the void ratio that is obtained with a given compactive effort, and second it affects the friction angle that is achieved for that void ratio. The effect of composition might be studied either by comparing friction angles at fixed e_0 or at fixed compactive effort. Because the role of composition is most important with regard to embankment construction the comparisons are often made at fixed compactive effort.

Average Particle Size

Figure 11.12b shows data for five soils all having a uniformity coefficient of 3.3, but having different average particle sizes. For a given compactive effort, these sands achieve different void ratios. However, the friction angle was much the same for each sand. The effect of the greater initial interlocking in the sand with the largest particles is compensated by the greater degree of grain crushing and fracturing that occurs with the larger particles because of the greater force per contact.

Crushing of particles, and the consequent curvature of the Mohr envelope, is most important with large particles, especially gravel-sized particles or rock fragments used for rockfills. This is because increasing the

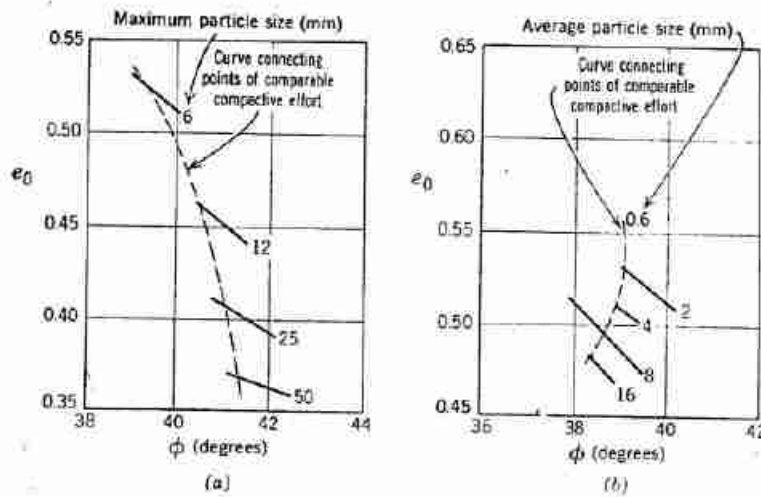


Fig. 11.12: Effect of particle size and gradation on friction angle. (a) Soils with same minimum particle size (0.5 mm). (b) Soils with same uniformity coefficient. Data from Leslie (1963).

particle size increases the load per particle, and hence crushing begins at a smaller confining stress. Spurred by the increasing popularity of rockfill dams, several laboratories have constructed triaxial testing systems which can accommodate specimens as large as 12 in. in diameter. An apparatus that can test specimens 3.7 ft in diameter and 8.2 ft long has been constructed in Mexico (Marsal, 1963).

Grading of the Sand

Figure 11.12a shows data for four soils all having the same minimum particle size but different maximum particle sizes. For comparable compactive efforts, the better graded sand has both a smaller initial void ratio and a larger friction angle. It is apparent that a better distribution of particle sizes produces a better interlocking. This trend is also shown by the data in Table 11.2, and is further confirmed by a series of tests reported by Holtz and Gibbs (1956).

In many soils, a few particles of relatively large size make up a large fraction of the total weight of the soil.

Table 11.2 Effect of Angularity and Grading on Peak Friction Angle.

Shape and Grading	Loose	Dense
Rounded, uniform	30°	37°
Rounded, well graded	34°	40°
Angular, uniform	35°	43°
Angular, well graded	39°	45°

From Sowers and Sowers, 1951.

If these particles are numerous enough so that they interlock with each other, it is important that these large particles be present in the test specimen. However, if these larger particles are just embedded in a matrix of much smaller particles so that the shearing takes place through the matrix, then the large particles can safely be omitted from the specimen. Unfortunately, the profession still is lacking definitive guides as to what constitutes a satisfactory test upon a gravelly soil.

A well-graded soil experiences less breakdown than a uniform soil of the same particle size, since in a well-graded soil there are many interparticle contacts and the load per contact is thus less than in the uniform soil. Figure 11.13 illustrates that the better graded soil suffers less decrease in ϕ with increasing confining pressure.

Angularity of Particles

It would be expected that angular particles would interlock more thoroughly than rounded particles, and hence that sands composed of angular particles would have the larger friction angle. The data for peak friction angle presented in Table 11.2 confirm this prediction. Even when a sand is strained to its ultimate condition, so that no further volume change is taking place and the sand is in a loose condition, the sand with the angular particles has the greater friction angle. In gravels, the effect of angularity is less because of particle crushing.

Mineral Type

Unless a sand contains mica, it makes little difference whether the sand is composed primarily of quartz, one of the feldspars, etc. A micaceous sand will often have a large void ratio, and hence little interlocking and a low

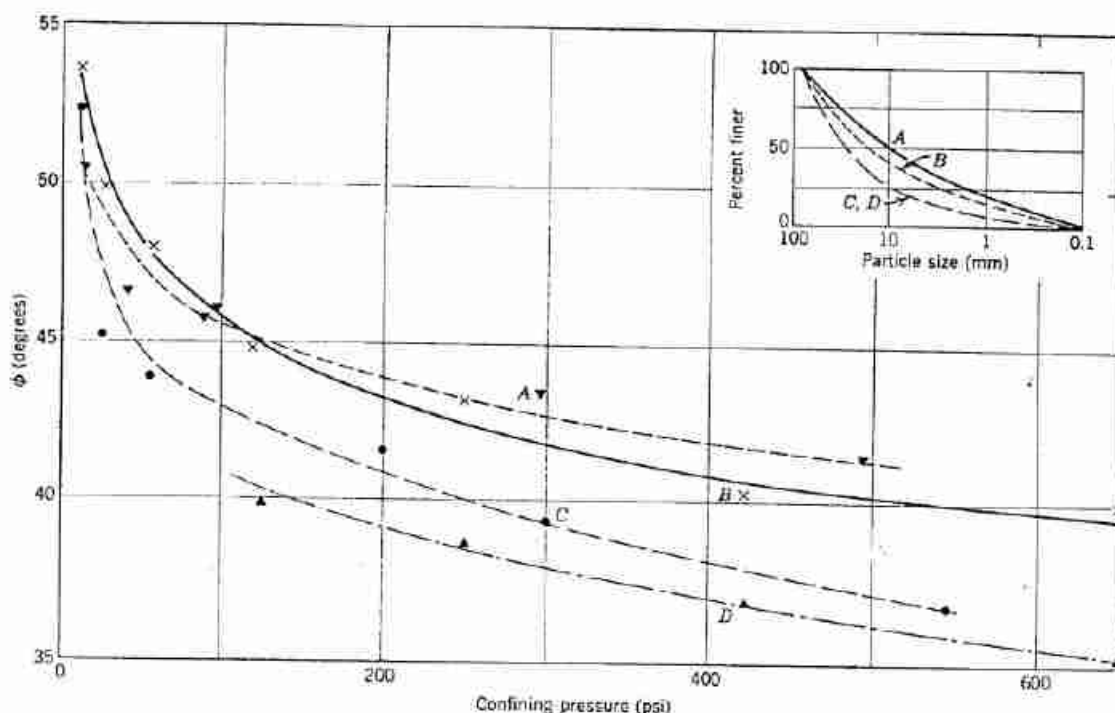


Fig. 11.13 Friction angle versus confining pressure (data from Leslie 1963).

friction angle. The smaller value of ϕ_u for mica compared to that of quartz has relatively little to do with this result.

Tests (Horn and Deere, 1962) have been carried out using powdered mica with care taken to have the mica flakes oriented nearly parallel. The result was a friction angle (ϕ_{cr}) of 16° , compared to $\phi_u = 13\frac{1}{2}^\circ$. There is some small amount of interlocking in such a case.

Where particles of gravel are an important constituent of soil, the origin of the gravel particles can have an important effect. If the gravel particles are relatively soft, crushing of these particles will minimize the interlocking effect and decrease the friction angle as compared to a comparable soil with hard gravel particles.

Summary

The composition of a granular soil can have an important influence upon its friction angle, indirectly by influencing e_0 and directly by influencing the amount of interlocking that occurs for a given e_0 . Table 11.3 provides a summary of data that can be used for preliminary design. However, for final design of an embankment, the actual soil should be tested using the void ratio and stress system that will exist in the field.

11.5 DETERMINATION OF *IN SITU* FRICTION ANGLE

The results presented in the foregoing sections have emphasized the predominant role of the degree of inter-

locking upon magnitude of the friction angle. Thus, if we wish to determine the friction angle of a sand *in situ*, it is not enough to find the nature and shape of the particles composing the sand. It is essential to know how tightly together these particles are packed in their natural state.

It is extremely difficult to obtain samples of a sand without changing the porosity. Thus, except for

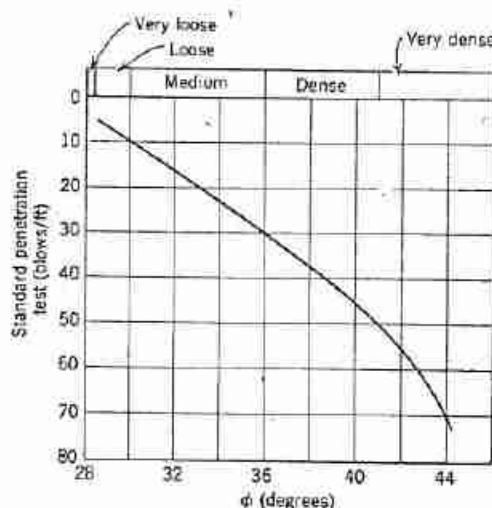


Fig. 11.14 Correlation between friction angle and penetration resistance (From Peck, Hanson, and Thornburn, 1953).

Table 11.3 Summary of Friction Angle Data for Use in Preliminary Design

Classification	Friction Angles							
	Slope Angle of Repose	Slope Angle of Repose	At Ultimate Strength	At Peak Strength				
				Medium Dense	Dense			
$i(^{\circ})$	(vert. to hor.)	$\phi_{cu}(^{\circ})$	$\tan \phi_{cu}$	$\phi(^{\circ})$	$\tan \phi$	$\phi(^{\circ})$	$\tan \phi$	
Silt (nonplastic)	26	1 on 2	26	0.488	28	0.532	30	0.577
	to 30	1 on 1.75	to 30	0.577	to 32	0.625	to 34	0.675
Uniform fine to medium sand	26	1 on 2	26	0.488	30	0.577	32	0.675
	to 30	1 on 1.75	to 30	0.577	to 34	0.675	to 36	0.726
Well-graded sand	30	1 on 1.75	30	0.577	34	0.675	38	0.839
	to 34	1 on 1.50	to 34	0.675	to 40	0.839	to 46	1.030
Sand and gravel	32	1 on 1.60	32	0.625	36	0.726	40	0.900
	to 36	1 on 1.40	to 36	0.726	to 42	0.900	to 48	1.110

From B. K. Hough, *Basic Soils Engineering*. Copyright © 1957, The Ronald Press Company, New York.

Note. Within each range, assign lower values if particles are well rounded or if there is significant soft shale or mica content, higher values for hard, angular particles. Use lower values for high normal pressures than for moderate normal pressure.

problems involving man-made fills, it is difficult to either measure or estimate the friction angle of a sand on the basis of laboratory tests alone. For these reasons, extensive use is made in practice of correlations between the friction angle of a sand and the resistance of the natural sand deposit to penetration.

Figure 11.14 shows an empirical correlation between the resistance offered to the standard penetration spoon (Chapter 7) and the friction angle. Inevitably, any such correlation is crude. The actual friction angle may deviate by $\pm 3^{\circ}$ or more from the value given by the curve. The given relation is intended to apply for depths of overburden up to 40 ft, and is conservative for greater depths.

11.6 SUMMARY OF MAIN POINTS

1. The strength of soil can be represented by a Mohr envelope, which is a plot of τ_{ff} versus σ_{ff} . Generally the Mohr envelope of a granular soil is curved. For stresses less than 100 psi, the envelope usually is almost straight so that

$$\tau_{ff} = \sigma_{ff} \tan \phi$$

where ϕ is the friction angle corresponding to the peak point of the stress-strain curve.

2. The value of ϕ for any soil depends upon ϕ_u and upon the amount of interlocking; i.e., the initial void ratio and σ_{ff} .
3. Where sand is being subjected to very large strains, ϕ_{cu} should be used in the failure law. Unless the sand is very loose, ϕ_{cu} will be less than ϕ . Where the sand is sliding over the surface of a structure, the friction angle will vary from ϕ_u to ϕ_{cu} , depending on the smoothness of the surface.
4. A knowledge of the effect of composition helps guide the selection of materials to be used in man-made fills
5. Materials to be used in man-made fills should be tested using the actual range of confining pressures which will be encountered in the fill.
6. For many practical problems, the friction angle of an *in situ* sand deposit can be determined by indirect means, such as the standard penetration test.

PROBLEMS

- 11.1 Given the following triaxial test data, plot the results (a) in a Mohr diagram and (b) in a p - q diagram, and determine ϕ by each method.

σ_3 (psi)	Peak σ_1 (psi)
10	27.6
20	54.5
30	84.0
40	110.0
50	139.0
60	165.7

11.2 Suppose you had a sample of the sand used to obtain the test results shown in Fig. 10.18. This sand is at a void ratio of 0.7. For $\sigma_3 = 20$ psi, estimate:

- The peak value of σ_1 .
- The ultimate value of σ_1 .
- The void ratio after considerable shearing.

11.3 Draw the stress path for the test on the loose specimen in Fig. 10.18.

11.4 A sand with $\phi = 30^\circ$ is sheared in a triaxial test with $\sigma_1 = \sigma_3 = 20$ psi initially. Both σ_1 and σ_3 are increased, with $\Delta\sigma_3 = \Delta\sigma_1/4$. What is the maximum value of σ_1 reached during the test?

11.5 A sand with a friction angle of 40° is tested in direct shear, using a normal stress of 50 psi. Making the simplest possible assumption concerning the stress condition within

the shear box, determine how much shear stress must be applied before the sand will fail.

11.6 The blow count during a standard penetration-test upon a sand at 20-ft depth is 20 blows/ft. Estimate the friction angle of the sand. Suppose the blow count at 40-ft depth is exactly the same. Is the sand at 40-ft depth looser or denser or the same density as the sand at 20-ft depth? Explain your answer.

11.7 Suppose two sandy soils are compacted with the same compactive effort. Sand *A* is uniform and has rounded particles. Sand *B* is well graded with angular particles

- Which sand will have the larger void ratio?
- Which sand will have the larger friction angle?

11.8 Estimate the value of ϕ for the following soils. Indicate which figures or tables you used to guide your estimate.

- A well-graded sand to be densely compacted for a low embankment.
- A gravel, with less than 20% sand sizes to be used for a rockfill dam 500 ft high.
- A natural deposit of fine sand, of medium density, which is to support a building.

11.9 Derive the relationships given in Fig. 11.6b.

Hint. Draw a Mohr circle and show both the Mohr envelope and K_f -line on this same diagram.

CHAPTER 12

Stress-Strain Relationships

Once an engineer has satisfied himself that a soil mass is not going to fail totally, he generally must then ascertain the amount of movement that will result from the application of loads and decide whether this movement is permissible. To do this, the engineer requires a stress-strain relationship for soil.

From our general study of stress-strain behavior in Chapter 10, we know that this behavior can be very complex. The amount of strain caused by a stress will depend on the composition, void ratio, past stress history of the soil, and manner in which the stress is applied. An equation giving the stress-strain relationship of one sand for any loading with constant direction of principal stresses has been developed by Hansen (1966). However, this expression is extremely complicated. Usually it is preferable to use formulas and data that are adapted to the particular problem at hand.

For many problems, the best approach often is to measure directly the strains produced in a laboratory test using stresses that will occur in the actual soil mass. This approach will be discussed in Chapter 14.

For other problems, it helps greatly to use concepts and formulas from the theory of elasticity. This means that the actual nonlinear stress-strain curves of a soil must be "linearized", i.e., replaced by straight lines. Then one speaks in terms of the *modulus* and *Poisson's ratio* of soil. Obviously, modulus and Poisson's ratio are not constants for a soil, but rather are quantities which approximately describe the behavior of a soil for a particular set of stresses. Different values of modulus and Poisson's ratio will apply for any other set of stresses. Especially when speaking of modulus, one must be very careful to specify what is meant.

The terms *tangent modulus* and *secant modulus* are used frequently. Tangent modulus is the slope of a straight line drawn tangent to a stress-strain curve at a particular point on the curve (see Fig. 12.1). The value of tangent modulus will vary with the point selected. The tangent modulus at the initial point of the curve is the *initial*

tangent modulus. Secant modulus is the slope of a straight line connecting two separate points of the curve. The value of secant modulus will vary with the locations of both points. As the two points come closer together, the secant modulus becomes equal to the tangent modulus. For a truly linear material, all of these values of modulus are one and the same.

12.1 CONCEPTS FROM THE THEORY OF ELASTICITY

If we apply a uniaxial stress σ_z to an elastic¹ cylinder (Fig. 12.1), there will be a vertical compression and a lateral expansion such that

$$\epsilon_z = \frac{\sigma_z}{E} \quad (12.1)$$

$$\epsilon_x = \epsilon_y = -\mu\epsilon_z \quad (12.2)$$

where

$\epsilon_x, \epsilon_y, \epsilon_z$ = strains in the x, y, z directions, respectively (plus when compressive)

E = Young's modulus of elasticity

μ = Poisson's ratio

If shear stresses τ_{zx} are applied to an elastic cube, there will be a shear distortion such that

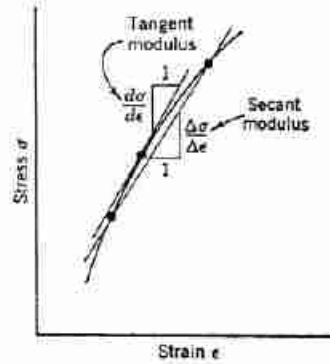
$$\gamma_{zx} = \frac{\tau_{zx}}{G} \quad (12.3)$$

where G = *shear modulus*. Equations 12.1 to 12.3 define the three basic constants of the theory of elasticity: E , G , and μ . Actually only two of these constants are needed, since

$$G = \frac{E}{2(1 + \mu)} \quad (12.4)$$

¹The word "elastic" actually denotes an ability of a material to recover its original size and shape after removal of stress. In this book, we use the word in a more restrictive sense to mean a material having a linear, reversible stress-strain curve.

According to the magnitude of the stress increment



According to the loading condition

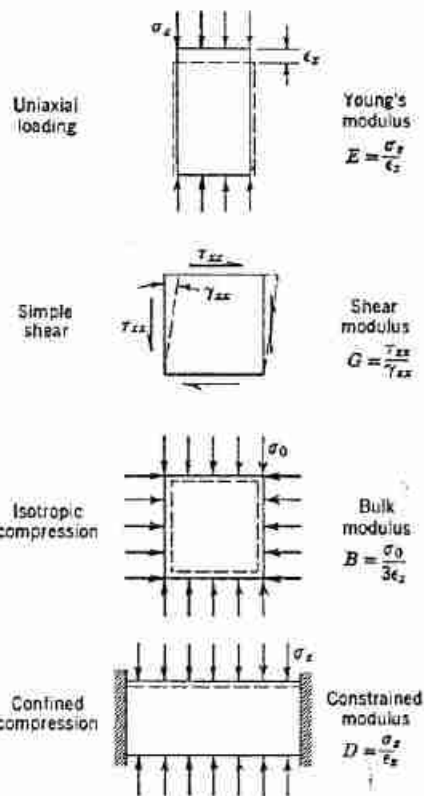
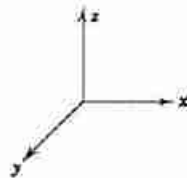


Fig. 12.1 Various types of modulus.

For an elastic material with all stress components acting, we can employ the principle of superposition to obtain

$$\epsilon_x = \frac{1}{E} [\sigma_x - \mu(\sigma_y + \sigma_z)] \quad (12.5a)$$

$$\epsilon_y = \frac{1}{E} [\sigma_y - \mu(\sigma_x + \sigma_z)] \quad (12.5b)$$

$$\epsilon_z = \frac{1}{E} [\sigma_z - \mu(\sigma_x + \sigma_y)] \quad (12.5c)$$

$$\gamma_{xy} = \frac{\tau_{xy}}{G} \quad (12.5d)$$

$$\gamma_{yz} = \frac{\tau_{yz}}{G} \quad (12.5e)$$

$$\gamma_{zx} = \frac{\tau_{zx}}{G} \quad (12.5f)$$

The volumetric strain is

$$\frac{\Delta V}{V} = \epsilon_x + \epsilon_y + \epsilon_z \quad (12.5g)$$

For the special case where $\sigma_x = \sigma_y = \sigma_z = \sigma_0$ and $\tau_{xy} = \tau_{yz} = \tau_{zx} = 0$, the volumetric strain equals

$$\frac{\Delta V}{V} = \frac{3\sigma_0}{E}(1 - 2\mu)$$

The *bulk modulus* B is defined as

$$B = \frac{\sigma_0}{\Delta V/V} = \frac{E}{3(1 - 2\mu)} \quad (12.6)$$

Still another special type of modulus is the *constrained modulus*, D , which is the ratio of axial stress to axial strain for confined compression (Fig. 12.1). This modulus can be computed from Eqs. 12.5 by setting $\epsilon_x = \epsilon_y = 0$. Thus

$$\sigma_x = \sigma_y = \frac{\mu}{1 - \mu} \sigma_z \quad (12.7)$$

$$D = \frac{E(1 - \mu)}{(1 + \mu)(1 - 2\mu)} \quad (12.8)$$

Uniaxial loading and confined compression involve both shear strain and volume change. This important fact is demonstrated in Example 12.1.

► Example 12.1

Find. Volumetric strain ($\Delta V/V$) and maximum shear strain during (a) uniaxial loading, (b) confined compression.
Solution.

Condition	Volumetric	Shear
Uniaxial loading	$\frac{\Delta V}{V} = \epsilon_x + \epsilon_y + \epsilon_z = (1 - 2\mu)\frac{\sigma_x}{E}$	$\tau_{\max} = \frac{\sigma_x}{2}$ $\gamma_{\max} = \frac{\sigma_x}{2G}$
Confined compression	$\frac{\Delta V}{V} = \epsilon_x + \epsilon_y + \epsilon_z = \frac{(1 + \mu)(1 - 2\mu)\sigma_x}{E(1 - \mu)}$	$\tau_{\max} = \frac{\sigma_x(1 - 2\mu)}{2(1 - \mu)}$ $\gamma_{\max} = \frac{\sigma_x(1 - 2\mu)}{2G(1 - \mu)}$

Note. The volumetric strain becomes zero for $\mu = \frac{1}{2}$. τ_{\max} occurs on planes inclined at 45° to the horizontal. γ_{\max} occurs for an element whose sides are at 45° to the horizontal.

For an elastic material, the foregoing equations apply for increments of stress starting from some initial stress, as well as for increments of stress starting from zero stress. Example 12.2 derives equations which may be used to find E and μ from measured strains.

► Example 12.2

Given. Strains $\Delta\epsilon_x = \Delta\epsilon_y$, $\Delta\epsilon_z$ caused by stresses $\Delta\sigma_x = \Delta\sigma_y$, $\Delta\sigma_z$ upon a cylinder of an elastic material.

Find. Expressions for Young's modulus and Poisson's ratio.

Solution. Eqs. 12.5a and 12.5c become

$$E\Delta\epsilon_x = \Delta\sigma_x - \mu(\Delta\sigma_x + \Delta\sigma_z)$$

$$E\Delta\epsilon_z = \Delta\sigma_z - 2\mu\Delta\sigma_x$$

These may be solved to give

$$E = \frac{(\Delta\sigma_x + 2\Delta\sigma_z)(\Delta\sigma_x - \Delta\sigma_z)}{\Delta\sigma_x(\Delta\epsilon_x - 2\Delta\epsilon_z) + \Delta\sigma_z\Delta\epsilon_x}$$

$$\mu = \frac{\Delta\sigma_z\Delta\epsilon_x - \Delta\epsilon_x\Delta\sigma_x}{\Delta\sigma_x(\Delta\epsilon_x - 2\Delta\epsilon_z) + \Delta\sigma_z\Delta\epsilon_x}$$

Wave Velocities

The velocity of wave propagation, or simply *wave velocity*, is defined as the distance moved by a wave in a unit of time (Fig. 12.2). There are several different wave velocities, each corresponding to a wave involving different types of strain:

$$\text{Rod velocity } C_L = \sqrt{E/\rho} \quad (12.9a)$$

$$\text{Shear velocity } C_S = \sqrt{G/\rho} \quad (12.9b)$$

$$\text{Dilatational velocity } C_D = \sqrt{D/\rho} \quad (12.9c)$$

where

ρ = mass density, equal to γ/g

g = acceleration of gravity

C_L and C_D = velocities of compressive waves for uniaxial loading and confined compression, respectively

Because of these simple relationships between modulus and velocity, velocity is often measured and used to evaluate modulus.

12.2 BEHAVIOR DURING CONFINED COMPRESSION

Figure 10.5 gives a typical stress-strain curve for a sand during confined compression. Since there is no lateral strain during this test, the axial strain is exactly equal to the volumetric strain. Example 12.3 gives values of

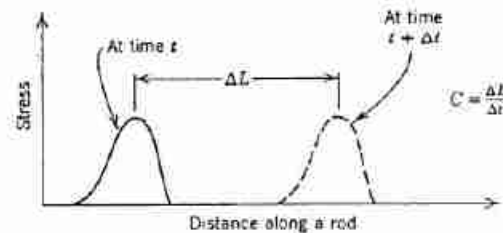


Fig. 12.2 Meaning of wave velocity.

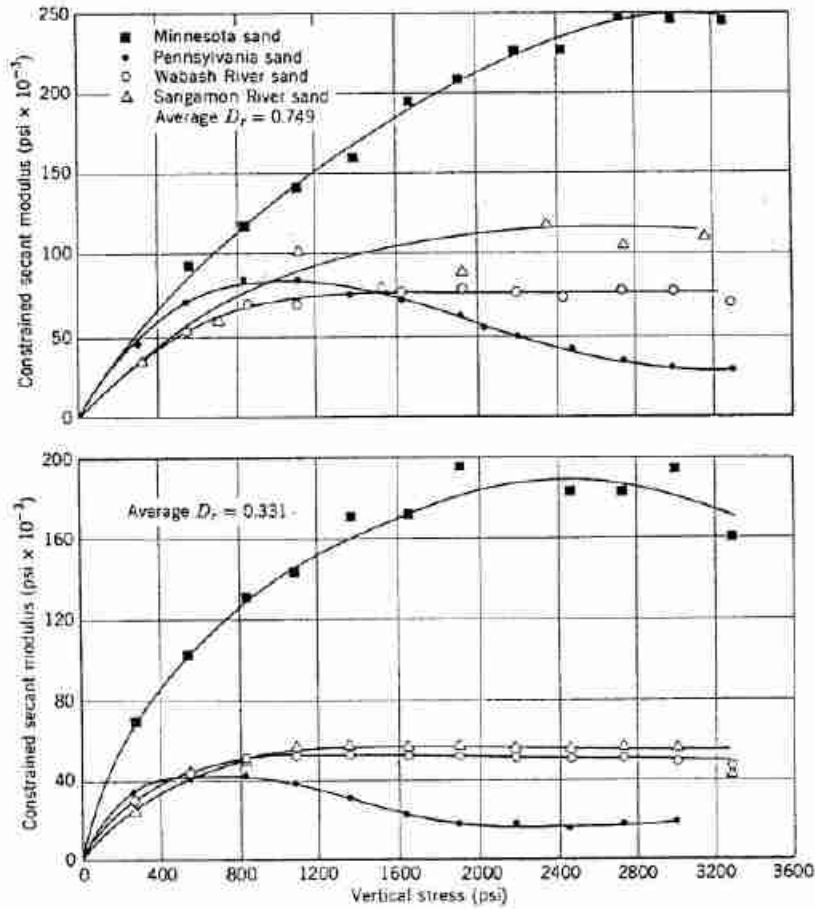


Fig. 12.3 Behavior of several sands during one-dimensional compression. Secant modulus from zero psi to indicated stress. (From Hendron, 1963.)

► Example 12.3

Given. Stress-strain curve in Fig. 10.5.

Find.

- a. Secant modulus from 0 to 1 kg/cm², first loading.
- b. Secant modulus from 1 to 8 kg/cm², first loading.
- c. Secant modulus from 1 to 8 kg/cm², second loading.
- d. Secant modulus from 1 to 8 kg/cm², second unloading.
- e. Tangent modulus at 1 kg/cm², first loading.

Solution.

Case	$\Delta\sigma$ (kg/cm ²)	$\Delta\varepsilon$	Modulus	
			(kg/cm ²)	(psi)
a	1	0.0078	130	1,900
b	7	0.0120	580	8,300
c	7	0.0043	1630	23,000
d	7	0.0031	2300	32,000
e ^a	7	0.0298	230	3,200

^a Measurements made along tangent line, from 1 to 8 kg/cm².

constrained modulus as measured from this curve. The general magnitude of the constrained modulus for a sand should be noted, together with the fact that the sand becomes stiffer as it is loaded and reloaded.

As was discussed in Chapter 10, crushing and breaking of particles become increasingly important for stresses greater than 500 psi. Thus for large stresses the modulus tends to become constant, or may even decrease (Fig. 12.3). The Minnesota sand was composed of hard, rounded particles, whereas the Pennsylvania sand was made up of softer, angular particles. The other two curves illustrate the behavior of well-graded sands.

Initial Relative Density

As would be expected, the looser the soil the smaller the modulus for a given loading increment. This is illustrated by the results given in Table 12.1.

Repeated Loadings

Figure 12.4 illustrates the increase in modulus during successive cycles of loading. The modulus increases

Table 12.1 Secant Constrained Modulus for Several Granular Soils during Virgin Loading

Soil	Relative Density	Modulus (psi × 10 ⁻³)	
		Δσ ₁ from 9 to 15 psi	Δσ ₁ from 29 to 74 psi
Uniform gravel	0	4.4	8.7
1 mm < D < 5 mm	100	17.0	26.0
Well graded sand	0	2.0	3.7
0.02 mm < D < 1 mm	100	7.5	17.6
Uniform fine sand	0	2.1	5.1
0.07 mm < D < 0.3 mm	100	7.4	17.4
Uniform silt	0	0.4	2.5
0.02 mm < D < 0.07 mm	100	5.1	11.0

From Hassib, 1951.

markedly between the first and second loadings. The increase gradually becomes less and less during successive cycles, and after several hundred cycles the stress-strain curve stabilizes.

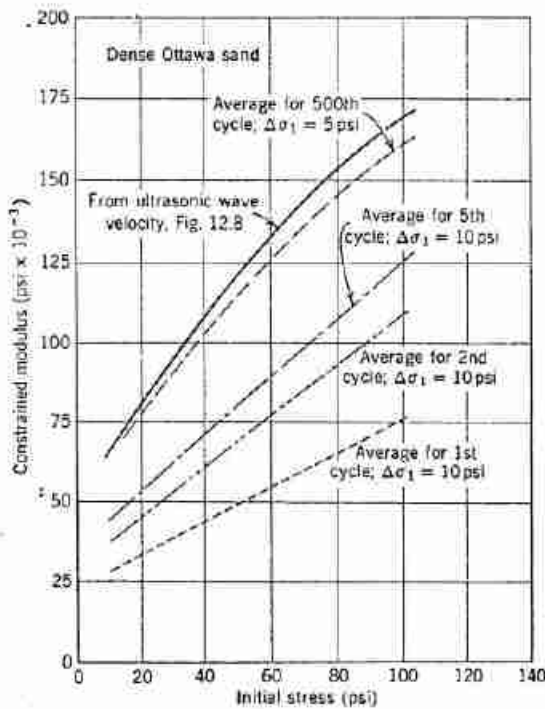


Fig. 12.4 Increase in secant constrained modulus with successive cycles of loading. Note. Average curves have been drawn through scattered data.

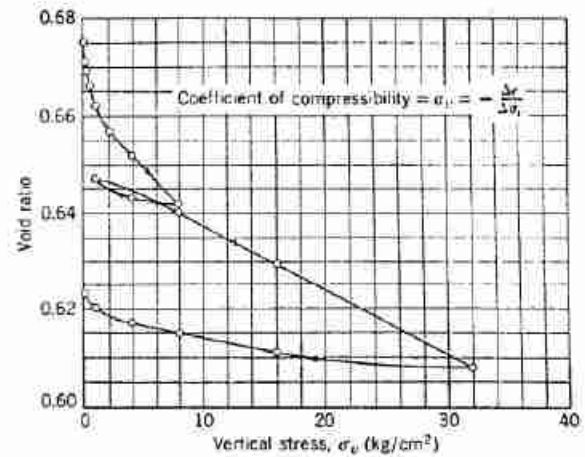


Fig. 12.5 Results of confined compression test plotted as void ratio versus stress on natural scale.

Rate of Compression

For an initial loading on a sand, the modulus is affected by the time required to achieve peak stress. The modulus may double if the loading time is 5 msec instead of the usual several seconds (see Whitman et al., 1964). The influence of the loading time is much less during subsequent cycles of a repeated loading.

Composition

As in the case of friction angle, modulus is affected in two ways by composition: composition affects the void ratio for a given relative density, and then it affects the modulus for that relative density. For a given relative density, the modulus of an angular sand will be less than that of a rounded sand. Table 12.1 indicates the influences of particle size and grading. In general, modulus decreases as the particle size leads to a larger void ratio for a given relative density. The effect of composition tends to disappear at very large stresses and during subsequent cycles of a repeated loading.

Alternate Methods of Protraying Data

In addition to the simple form of stress-strain curve in Fig. 10.5, two other methods of plotting stress-strain data are often used.

Figure 12.5 shows the results of Fig. 10.5 plotted as void ratio versus vertical stress σ_v. The slope of the resulting curve is defined as the *coefficient of compressibility* α_v:

$$\alpha_v = -\frac{de}{d\sigma_v} \quad \text{or} \quad a_p = -\frac{\Delta e}{\Delta \sigma_v} \quad (12.10)$$

Figure 12.6 shows the same results plotted as void ratio versus the logarithm of vertical stress. This form of plot is useful for two reasons: (a) it is convenient for

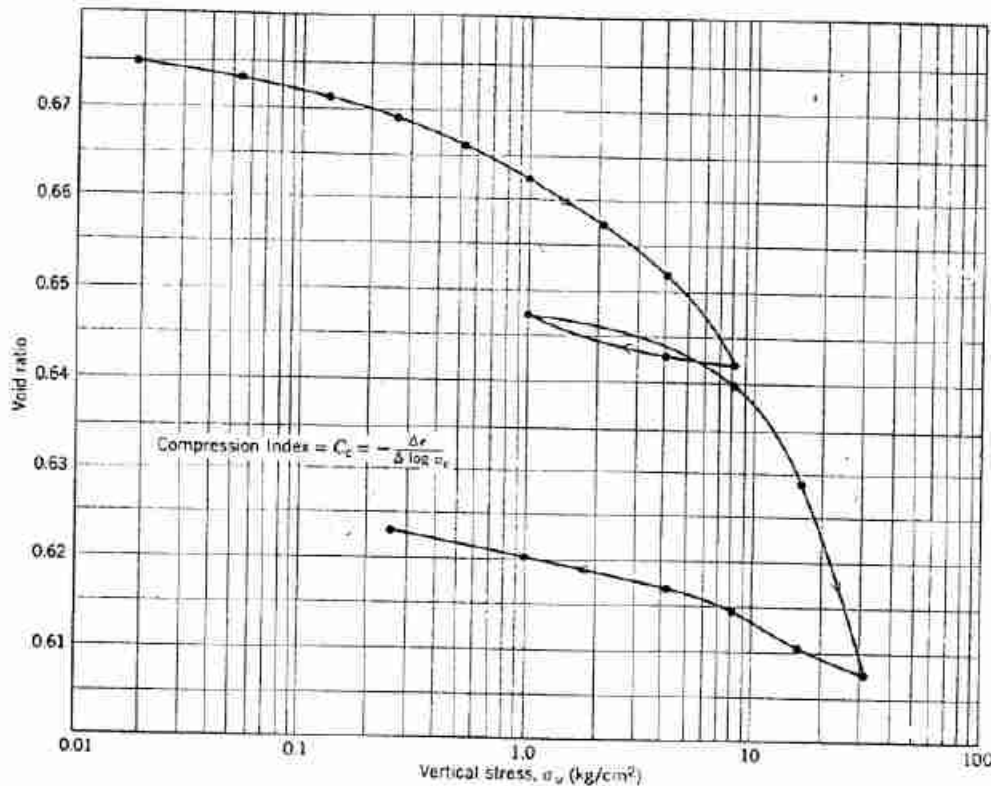


Fig. 12.6 Results of confined compression test plotted as void ratio versus stress on logarithmic scale.

showing stress-strain behavior over a wide range of stresses; and (b) such curves usually become more-or-less straight at large stresses. As will be seen in Part IV, this form of plot is especially useful for clays. Figure 12.7 shows the curves of Fig. 10.4 replotted in this way. At large stresses, the curves for the different sands tend to fall along a common path. The slope of this type of curve is the *compression index* C_c :

$$C_c = -\frac{de}{d(\log \sigma_v)} \quad \text{or} \quad C_c = -\frac{\Delta e}{\Delta(\log \sigma_v)} \quad (12.11)$$

C_c is thus the change in void ratio per logarithmic cycle of stress.

Still another term used to describe stress-strain behavior in confined compression is the *coefficient of volume change* m_v , which is simply the reciprocal of constrained modulus:

$$m_v = \frac{de_v}{d\sigma_v} \quad \text{or} \quad m_v = \frac{\Delta e_v}{\Delta \sigma_v} \quad (12.12)$$

The relationships among D , m_v , a_v , and C_c are given in Table 12.2. The vertical strain during compression equals $\Delta e/(1 + e_0)$, where e_0 is the initial void ratio. Example 12.4 illustrates typical numerical values.

► Example 12.4

Given. Stress-strain curves in Figs. 10.5, 12.5, and 12.6.
Find. Values of m_v , a_v , and C_c for the same stresses used in Example 12.3.

Solution. The values may be scaled from the figures. They may be computed using the equations in Table 12.2, but this computation is inaccurate in the case of secant values of C_c , since the choice of the average stress σ_{av} greatly affects calculated values.

Case	m_v (cm ² /kg)	a_v (cm ² /kg)	C_c
a	0.0078	0.0130	0.0065
b	0.0017	0.0028	0.0225
c	0.0006	0.0010	0.0079
d	0.00045	0.00073	0.0066
e	0.0045	0.0065	0.0140

Note. C_c is dimensionless; a change per logarithmic cycle is the same for any set of units.

Note that the compressibilities a_v and m_v decrease as the stress increases, but that C_c increases. The maximum value of C_c in Fig. 12.6 is 0.07.

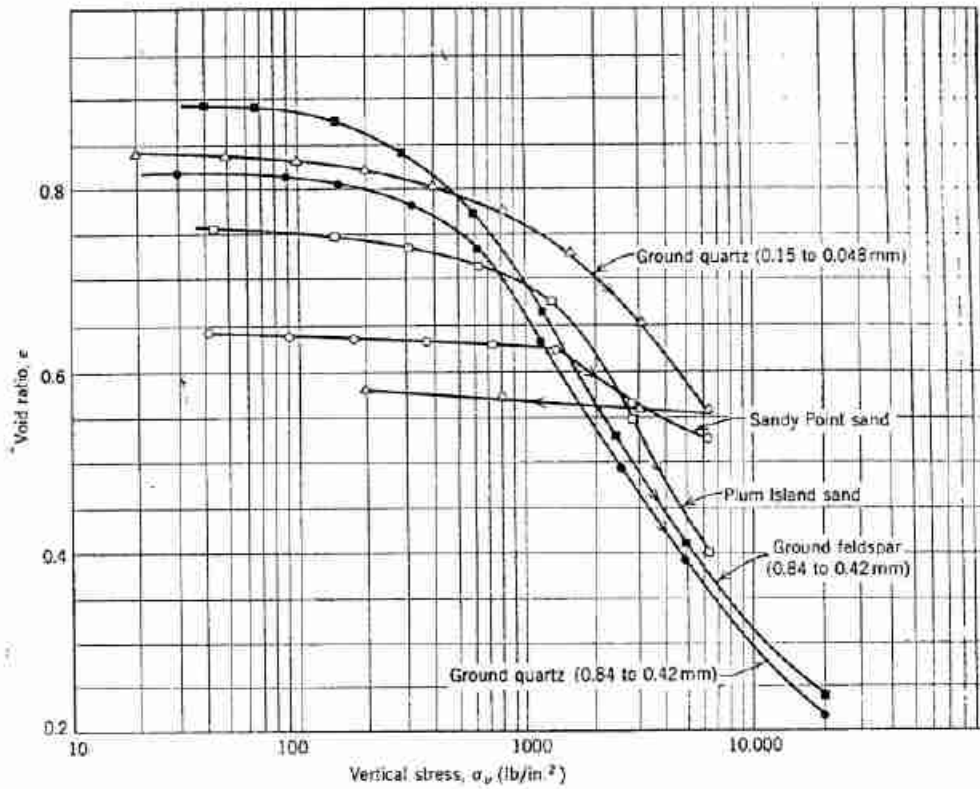


Fig. 12.7 Results of high-stress, confined compression tests on several sands (data from Roberts, 1964).

The stress-strain curve for an initial loading generally resembles a parabola. Hence the stress-strain relationship may be expressed as

$$\sigma_v = C(\epsilon_v)^n \quad (12.13)$$

The coefficient C varies with the type of soil and its initial void ratio. For a wide variety of soils, however, the

exponent n has been found to be very close to 2. For a perfect packing of elastic spheres, this exponent would be 3. The difference between the theoretical and actual values for the exponent is the result of sliding among and rearrangement of the particles within an actual soil. Equation 12.13 implies that both secant modulus from zero stress and the tangent modulus should increase as $\sqrt{\sigma_v}$.

Table 12.2 Relations Between Various Stress-Strain Parameters for Confined Compression

	Constrained Modulus	Coefficient of Volume Change	Coefficient of Compressibility	Compression Index
Constrained modulus	$D = \frac{\Delta \sigma_v}{\Delta \epsilon_v}$	$D = \frac{1}{m_v}$	$D = \frac{1 + e_0}{a_v}$	$D = \frac{(1 + e_0)\sigma_{va}}{0.435C_c}$
Coefficient of volume change	$m_v = \frac{1}{D}$	$m_v = \frac{\Delta \epsilon_v}{\Delta \sigma_v}$	$m_v = \frac{a_v}{1 + e_0}$	$m_v = \frac{0.435C_c}{(1 + e_0)\sigma_{va}}$
Coefficient of compressibility	$a_v = \frac{1 + e_0}{D}$	$a_v = (1 + e_0)m_v$	$a_v = -\frac{\Delta e}{\Delta \sigma_v}$	$a_v = \frac{0.435C_c}{\sigma_{va}}$
Compression index	$C_c = \frac{(1 + e_0)\sigma_{va}}{0.435D}$	$C_c = \frac{(1 + e_0)\sigma_{va}m_v}{0.435}$	$C_c = \frac{a_v\sigma_{va}}{0.435}$	$C_c = -\frac{\Delta e}{\Delta \log \sigma_v}$

Note. e_0 denotes the initial void ratio. σ_{va} denotes the average of the initial and final stresses.

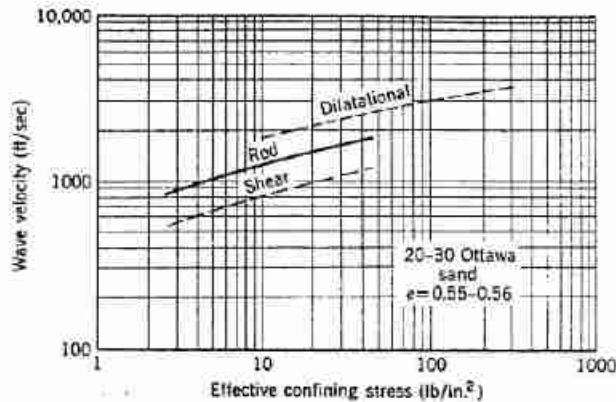


Fig. 12.8 Wave velocities through sand as function of confining stress. Dilatational and shear velocities from Whitman and Lawrence (1963); rod velocities from Hardin and Richart (1963).

Relationship to Wave Velocity

Figure 12.8 shows typical values for dilatational wave velocity through granular soils. The velocity typically increases as $\sigma_v^{0.25}$, which according to Eq. 12.9c means that constrained modulus should increase as $(\sigma_v)^{1/2}$. However, the modulus as computed from measured wave velocity using Eq. 12.9e generally is much larger than the constrained modulus as measured directly in an oedometer. This is illustrated by Example 12.5. The difference

► Example 12.5

Given. Wave velocity versus stress in Fig. 12.8 and modulus versus stress in Fig. 12.4.

Find. Constrained modulus for stress of 20 psi. Compare with modulus as measured directly.

Solution. $C_D = 1900$ ft/sec. Typical value for $\gamma = 105$ pcf, or $\rho = 3.26$ slugs/ft³.

$$D = \rho C_D^2 = 3.26 \times 3.61 \times 10^6 \text{ psf} = 82,000 \text{ psi}$$

versus 30,000 psi as measured directly. ◀

arises because the small stresses associated with a seismic wave mainly cause elastic deformations of particles, whereas the large stresses applied in an oedometer test cause slippage between adjacent particles. This situation has been sketched in Fig. 10.10. If very small stress increments are used in the oedometer, then the modulus as measured directly becomes approximately equal to the modulus as calculated from wave velocity (Whitman et al., 1964). Furthermore, the modulus as measured after many cycles of loading, even using large stress increments, is also about equal to the modulus calculated from wave velocity (Fig. 12.4).

Hence wave velocity is not a useful direct measure of the compressibility of a soil during a single intense loading, but it does indicate the compressibility during

repeated loadings. This appears to be true regardless of the frequency of the repeated loading.

For further discussion of wave velocity, see Hardin and Richart (1963), Whitman (1966).

12.3 BEHAVIOR DURING TRIAXIAL COMPRESSION TEST

The standard triaxial test (i.e., with constant confining stress and increasing axial stress) gives a direct measure of Young's modulus. Modulus decreases with increasing axial stress, and at the peak of the stress-strain curve the tangent modulus becomes zero.

When a value of Young's modulus is quoted for soil, it usually is the secant modulus from zero deviator stress to a deviator stress equal to $\frac{1}{2}$ or $\frac{1}{3}$ of the peak deviator stress. This is a common range of working stresses in actual foundation problems, since typically a safety factor of 2 or 3 is used in these problems. Example 12.6 illustrates

► Example 12.6

Given. Stress-strain curve for test in Fig. 10.13.

Find. Secant Young's modulus for deviator stress equal to $\frac{1}{2}$ of peak stress.

Solution.

$$\begin{aligned} \Delta \sigma_v \text{ at peak} &= 3.8 \text{ kg/cm}^2 \\ \Delta \sigma_v \text{ at } \frac{1}{2} \text{ peak} &= 1.9 \text{ kg/cm}^2 \\ \Delta \epsilon_v &= 0.002 \\ E &= 950 \text{ kg/cm}^2 = 13,500 \text{ psi} \end{aligned}$$

the computation of modulus from a typical stress-strain curve. For the scale to which this curve has been plotted, it is difficult to tell whether or not the curve is linear or curved up to $\frac{1}{2}$ the peak. However, the very precise data given in Fig. 12.9 show that the curve is nonlinear almost from the beginning of loading.

Kondner and Zelasko (1963) suggested that the stress-strain curves of sand in standard triaxial compression can be fitted by a hyperbolic equation of the form

$$\sigma_1 - \sigma_3 = \frac{\epsilon_1}{a + b\epsilon_1} \quad (12.14)$$

where a and b are constants.

Confining Stress

As the confining stress increases, the modulus increases. For the case where the initial stress σ_0 is isotropic, the modulus increases as σ_0^n where n varies from 0.4 to 1.0. A reasonable average value is $n = 0.5$. The larger values of the exponent tend to apply to loose sands.

In most practical problems, the stresses before loading are not isotropic. The effect of the actual state of stress on modulus is not clear, but the best available rule is that modulus depends on the average of the initial principal

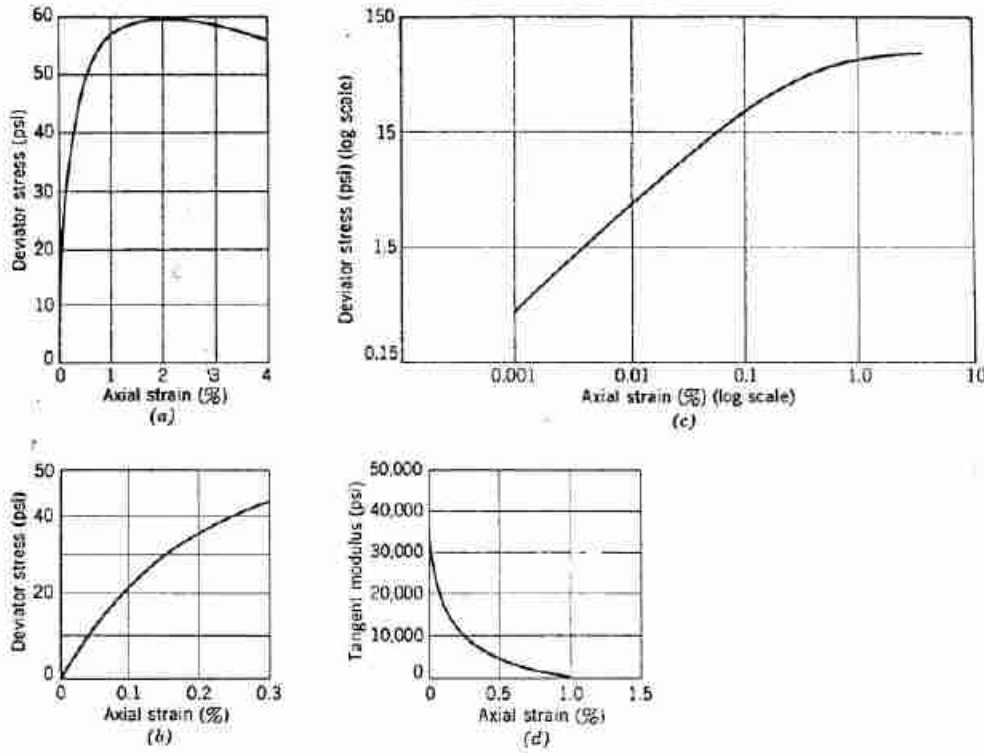


Fig. 12.9 Stress-strain data from a triaxial test. Note. Medium, subangular sand; porosity = 0.39; confining stress = 14.3 lb/in.² (From Chen, 1948.)

stresses; thus

$$E \sim \sqrt{\sigma_v \frac{1 + 2K_0}{3}} \quad (12.15)$$

where K_0 is the coefficient of lateral stress at rest. Equation 12.15 holds only when $\frac{1}{2} < K_0 < 2$ and when the factor of safety against failure is 2 or more.

Various Factors

The effect of void ratio, composition, stress history, and loading rate upon E is the same as their effect upon D . Table 12.3 indicates the general effect of void ratio and composition on E for a first loading to one-half the peak deviator stress. Table 12.4 gives values of E obtained after several cycles of loading. The values in Table 12.4

Table 12.3 Young's Modulus for Initial Loading

	Loose	Dense
Angular, breakable particles	140 kg/cm ² 2000 psi	350 kg/cm ² 5000 psi
Hard, rounded particles	560 kg/cm ² 8000 psi	1050 kg/cm ² 15,000 psi

Note. Secant modulus to $\frac{1}{2}$ peak deviator stress, with 1 atm confining stress.

Table 12.4 Young's Modulus for Repeated Loadings

Soil (1 atm confining pressure)	Young's Modulus (psi)	
	Loose	Dense
Screened crushed quartz, fine angular	17,000	30,000
Screened Ottawa sand, fine rounded	26,000	45,000
Ottawa Standard sand, medium, rounded	30,000	52,000
Screened sand, medium, subangular	20,000	35,000
Screened crushed quartz, medium, angular	18,000	27,000
Well graded sand, coarse, subangular	15,000	28,000

From Chen, 1948.

are also indicative of the initial tangent modulus and of the modulus which is computed from rod wave velocity.

It is of interest to compare these values of E with those for the minerals of which the particles of a granular soil

Table 12.5 Poisson's Ratio and Young's Modulus for Various Materials

Material	Poisson's Ratio	Young's Modulus (psi)
Amphibolite	0.28-0.30	$13.6-17.6 \times 10^6$
Anhydrite	0.30	9.8×10^6
Diabase	0.27-0.30	$12.6-16.9 \times 10^6$
Diorite	0.26-0.29	$10.9-15.6 \times 10^6$
Dolomite	0.30	$16.0-17.6 \times 10^6$
Dunite	0.26-0.28	$21.6-26.5 \times 10^6$
Feldspathic Gneiss	0.15-0.20	$12.0-17.2 \times 10^6$
Gabbro	0.27-0.31	$12.9-18.4 \times 10^6$
Granite	0.23-0.27	$10.6-12.5 \times 10^6$
Ice	0.36	1.03×10^6
Limestone	0.27-0.30	$12.6-15.6 \times 10^6$
Marble	0.27-0.30	$12.6-15.6 \times 10^6$
Mica Schist	0.15-0.20	$11.5-14.7 \times 10^6$
Obsidian	0.12-0.18	$9.4-11.6 \times 10^6$
Oligoclase	0.29	$11.6-12.3 \times 10^6$
Quartzite	0.12-0.15	$11.9-14.0 \times 10^6$
Rock salt	0.25	5.13×10^6
Slate	0.15-0.20	$11.5-16.3 \times 10^6$
Aluminum	0.34-0.36	$8-11 \times 10^6$
Steel	0.28-0.29	29×10^6

Values for rock computed from compressibility measurements by Brace (1966) at confining stresses of 3-5 kilobars. Values for steel and aluminum from Lange (1956).

are composed, and with steel and aluminum (see Table 12.5). The great compressibility of soil, the result of its particulate nature, is evident from this comparison.

Poisson's Ratio

Poisson's ratio may be evaluated from the ratio of the lateral strain to axial strain during a triaxial compression test with axial loading. Figure 10.13 has shown values of this ratio at various stages during a typical test. During the early range of strains for which the concepts from theory of elasticity are of use, the Poisson's ratio is varying with strain. The Poisson's ratio for sand becomes constant only for large strains which imply failure, and then has a value greater than 0.5. Such a value of μ implies expansion of the material during a triaxial test (see Example 12.1). Poisson's ratio is less than 0.5 only during the early stages of such a test where the specimen decreases in volume.

Because of this behavior, it is very difficult to make an exact evaluation of the value of μ for use in any problem. Fortunately, the value of μ usually has a relatively small effect upon engineering predictions. For the early stages of a first loading of a sand, when particle rearrangements

are important, μ typically has values of about 0.1 to 0.2. During cyclic loading μ becomes more of a constant, with values from 0.3 to 0.4. The ratio of two different types of wave velocities is often used to estimate the value of μ applicable to a cyclic loading.

12.4 BEHAVIOR DURING OTHER TESTS

Simple Shear

The shear modulus of soil finds its widest use in connection with foundation vibration problems and is generally evaluated through a measurement of shear wave velocity. Figure 12.8 indicated the typical variation of shear wave velocity with confining stress. Figure 12.10 shows the effect of void ratio. Factors such as composition affect C_s by influencing void ratio. Figure 12.10 can be used for a wide variety of granular soils.

As is the case for constrained and rod modulus, the shear modulus from a static repeated loading is for practical purposes equal to the modulus calculated from the wave velocity for the same initial stress. This is true for stresses much less than those associated with failure. The confining stress may be taken equal to

$$\frac{\sigma_v}{3} (1 + 2K_0)$$

Special Triaxial Tests

In order to duplicate the type of loading expected within an actual mass of soil, both confining stress and axial stress are often varied during a triaxial test. Using the equations developed in Example 12.2, values of E and μ may still be evaluated from such a test. This is illustrated in Example 12.7.

► Example 12.7

Given. Data for Test B, Figs. 10.21 and 10.23.

Find. E and μ at end of first loading.

Solution. The first step is to find the values of $\Delta\sigma_z = \Delta\sigma_x$ and $\Delta\sigma_y = \Delta\sigma_x$.

$$\Delta\sigma_z = \Delta p + \Delta q = 1.52 + 0.81 = 2.33$$

$$\Delta\sigma_y = \Delta p - \Delta q = 1.52 - 0.81 = 0.71$$

The strains from this loading are

$$\Delta\epsilon_z = 0.00268$$

$$\Delta\epsilon_y = 0.00020$$

Then, from Example 12.2,

$$E = \frac{(2.33 + 2 \times 0.71)(1.62)}{0.71(0.00268 - 0.0004) + 2.33(0.00268)}$$

$$= \frac{3.75(1.62)}{0.00162 + 0.00625} = 772 \text{ kg/cm}^2$$

$$\mu = \frac{0.71(0.00268) - 0.00020(2.33)}{0.00787}$$

$$= \frac{0.00189 - 0.00047}{0.00787} = 0.18$$

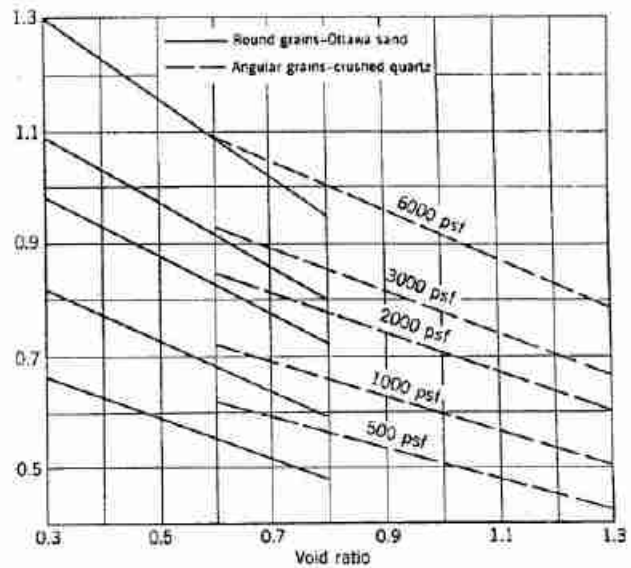
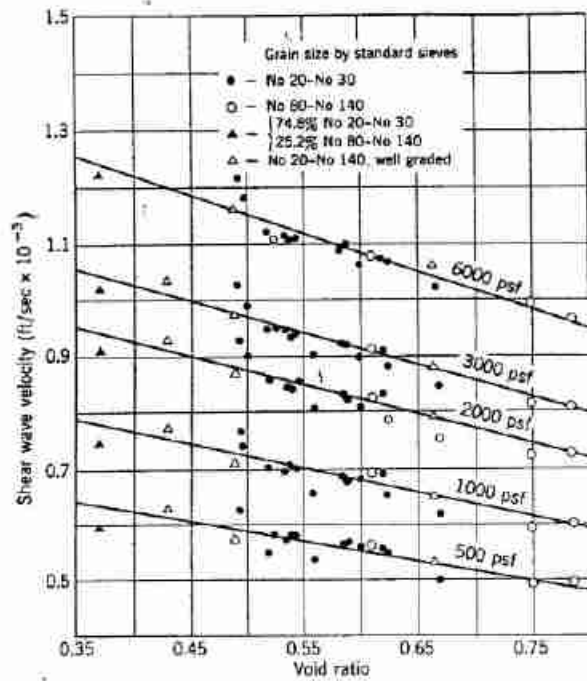


Fig. 12.10 Shear wave velocities through quartz sands (From Hardin and Richart, 1963).

12.5 SUMMARY OF MAIN POINTS

The concepts from the theory of elasticity apply to soil only in a very approximate way. Nonetheless, it is often useful to use these concepts and to use values of modulus and Poisson's ratio which apply approximately for a particular loading. Clearly, good judgment is needed when choosing values for these parameters.

The same factors that affect ϕ also affect modulus. However, the effect upon modulus is more marked. It is difficult to estimate values of modulus with much accuracy, and test data for the particular soil will be necessary whenever an accurate estimate is needed.

Since modulus depends on void ratio, and it is difficult to obtain undisturbed samples of granular soils, it is especially difficult to measure the modulus of granular soils reliably. From experience, it appears that the second cycle of loading during a laboratory test usually gives the best measure of *in situ* modulus. Apparently the effects of sample disturbance are compensated by the effects of the initial loading. There are no reliable correlations between modulus and blow count.

PROBLEMS

12.1 If $E = 16,000$ psi and $\mu = 0.35$, evaluate the constrained modulus D and shear modulus G .

12.2 For the data given in Problem 12.1, compute the dilatational velocity C_D , rod velocity C_L , and shear velocity C_S . Assume a value of ρ which is reasonable for a dense sand.

12.3 K_0 for a sand is found to be 0.45. Assuming that sand is an elastic material, compute Poisson's ratio μ .

12.4 Refer to Figs. 10.21 and 10.23. For Test *D*, initial loading, compute E and μ for (a) the entire stress increment, and (b) the increment to the first data point. First assume that E and μ can be computed as though this were an ordinary triaxial test using Eqs. 12.1 and 12.2. Then use the equations in Example 12.2.

12.5 Repeat Problem 12.4, using the results for Test *A*, second loading.

12.6 Estimate Young's modulus (secant modulus to $\frac{1}{3}$ of failure load for a first loading) for a well-graded, subangular, dense sand located at a depth of 200 ft below ground surface. *Hint.* You will need to estimate several factors in order to arrive at a satisfactory estimate.

12.7 Using the data in Fig. 12.10, estimate the shear modulus at 20-ft depth of a sand having $e = 0.6$, $G = 2.7$, $K_0 = 0.5$.

CHAPTER 13

Earth Retaining Structures and Slopes

Building on preceding chapters, this chapter considers earth retaining structures. Several examples of retaining structures were given in Chapter 1. Figures 1.9 and 1.15 show sheet pile bulkheads and Fig. 1.12*b* shows a braced excavation. Figure 13.1 illustrates an even more common retaining structure: a gravity retaining wall.

When designing retaining structures, an engineer often needs to ensure only that total collapse or failure does not occur. Movements of several inches and even several feet are often of no concern as long as there is assurance that even larger motions will not suddenly occur. Thus the approach to the design of retaining structures generally is to analyze the conditions that would exist at a collapse condition, and to apply suitable safety factors to prevent collapse. This approach is known as *limit design* and requires *limiting equilibrium mechanics*.

The early portions of this chapter present methods used to analyze the stability of structures that retain dry granular soils. There are many practical situations to which these methods can be applied directly. Generally, of course, water and the clay content of a soil are important to a practical problem, but the methods developed for dry granular soils form the basis for the methods (presented in Parts IV and V) used for these more complicated situations.

There are many situations in which the movements of retaining structures must be given serious consideration—situations where consideration of stability only is inadequate for a proper design. These situations arise especially with regard to clayey soils, but they can also arise with sandy soils. The later sections of this chapter consider such situations.

This chapter concludes with a brief discussion of the stability of slopes in dry granular soils.

13.1 APPROACH TO DESIGN OF GRAVITY RETAINING WALLS

A gravity retaining wall is typically used to form the permanent wall of an excavation whenever space require-

ments make it impractical to simply slope the side of the excavation. Such conditions arise, for example, when a roadway or storage area is needed immediately adjacent to an excavation. In order to construct the wall, a temporary slope is formed at the edge of the excavation, the wall is built, and then backfill is dumped into the space between the wall and the temporary slope. In earlier days masonry walls were often used. Today, most such walls are of unreinforced concrete although other special forms of construction are sometimes employed (see Huntington, 1957; Teng, 1962).

Figure 13.2 shows in a general way the forces that act upon a gravity retaining wall. The bearing force resists the weight of the wall plus the vertical components of other forces. The *active thrust*, which develops as the backfill is placed and as any surcharges are placed on the surface of the backfill, acts to push the wall outward. This outward motion is resisted by *sliding resistance* along the base of the wall and by the *passive resistance* of the soil lying above the toe of the wall. The active thrust also tends to overturn the wall around the toe. This overturning is resisted by the weight of the wall and the vertical component of the active thrust. The weight of the wall is thus important in two ways: it resists overturning and it causes frictional sliding resistance at the base of the wall. This is why such a wall is called a *gravity retaining wall*.

A gravity retaining wall, together with the backfill the wall retains and the soil that supports the wall, is a highly *indeterminate* system. The magnitudes of the forces that act upon a wall cannot be determined from statics alone, and these magnitudes will be affected by the sequence of construction and backfilling operations. Hence the design of such a wall is based not on an analysis to determine the expected forces but on analysis of the forces that would exist if the wall started to fail, i.e., to overturn or to slide outwards.

The first step in such an analysis is to envision the pattern of deformations that would accompany such a failure. These patterns have been studied by means of

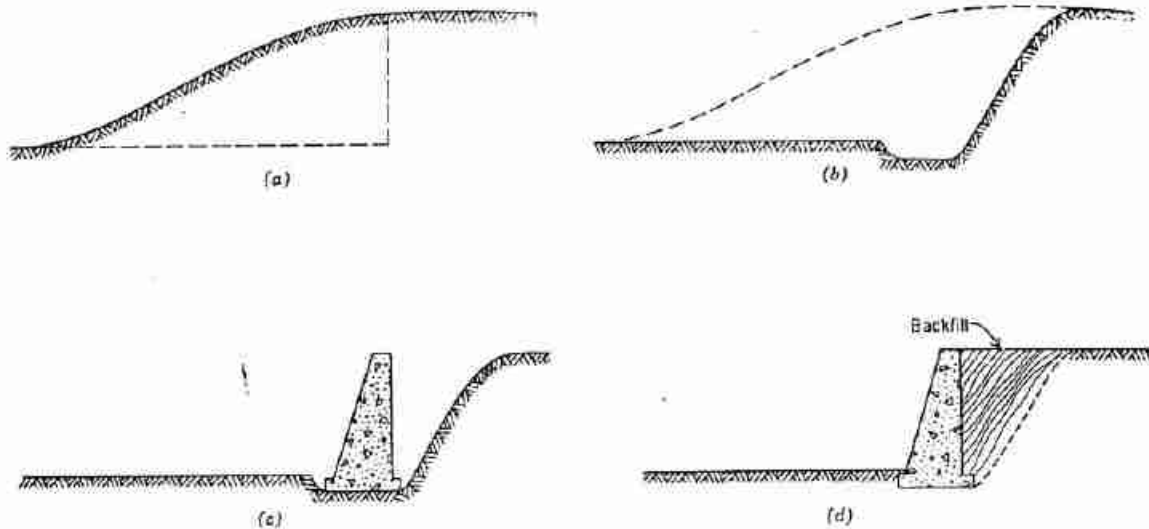


Fig. 13.1 Stages in construction of typical gravity retaining wall. (a) Proposed excavation. (b) Excavation completed. (c) Wall formed and poured. (d) Backfill placed.

small-scale tests which simulate actual retaining walls. Figure 13.3 shows the movements during such a test in which granular soil is simulated by rods.¹ These movements occurred as a support holding the wall was removed. Within the backfill the soil moved toward the wall and downward. These motions indicate that shear failure occurred throughout this *active zone*; i.e., the full frictional resistance was mobilized throughout this zone. A second zone of shear failure (the *passive zone*) developed at the toe of the wall where the wall was pushing against the soil.

Considering these patterns of deformations, an approach to the design of gravity retaining walls can then be stated. First, trial dimensions for the wall are selected. Next, the active thrust against the wall is determined, based on the assumption that shear failure occurs throughout the active zone. Then the resistance offered by the weight of the wall, the shear force at the base of the wall, and the passive zone at the toe of the wall are determined. Finally, the active thrust and total resistance are compared, and the resistance must exceed the active thrust by a suitable safety factor.

¹ There are many variations of this basic technique. There have been tests with sand contained between two glass plates. Use of horizontal metal rods, or even toothpicks, eliminates the need for glass side walls and the problem of friction between these walls and the sand. X-ray techniques have been used to observe the patterns of motion within soil masses (Roscoe et al., 1963).

The frame shown in Fig. 13.3 is used in the M.I.T. laboratories for student experiments and demonstrations (see also Fig. 13.30). The frame is 27 in. long by 29 in. high. The rods are 6 in. long and are of two shapes and sizes (round, $\frac{1}{8}$ and $\frac{1}{4}$ in. diameter; and hexagonal, $\frac{3}{8}$ and $\frac{1}{2}$ in. across flats) to simulate the interlocking which occurs in actual soils. Using this frame, students test their own designs for small-scale retaining structures, thereby gaining experience in the application of theoretical principles to design.

This approach to design will be illustrated in Section 13.6. First, however, we must consider methods for determining active thrust and passive resistance.

13.2 RANKINE ACTIVE AND PASSIVE STATES

As a first step in the evaluation of active thrust and passive resistance, we evaluate the conditions of limiting equilibrium for the geostatic state of stress, which occurs in a soil deposit with a horizontal surface and no shear stresses on horizontal and vertical surfaces.

Suppose that such a soil deposit is stretched in the horizontal direction. Any element of soil will then behave just like a specimen of a triaxial test in which the confining stress is decreased while the axial stress remains constant, as shown by the stress path in Fig. 13.4. When the horizontal stress is decreased to a certain magnitude, the full shear strength of the soil will be mobilized. No further decrease in the horizontal stress is possible. The horizontal stress for this condition is called the *active*

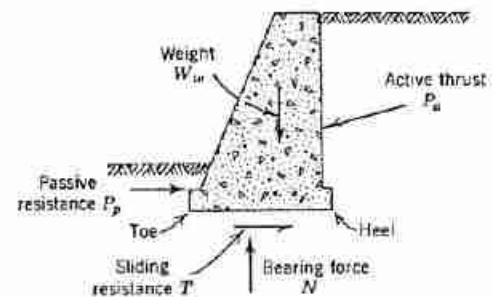


Fig. 13.2 Forces acting on gravity retaining wall.

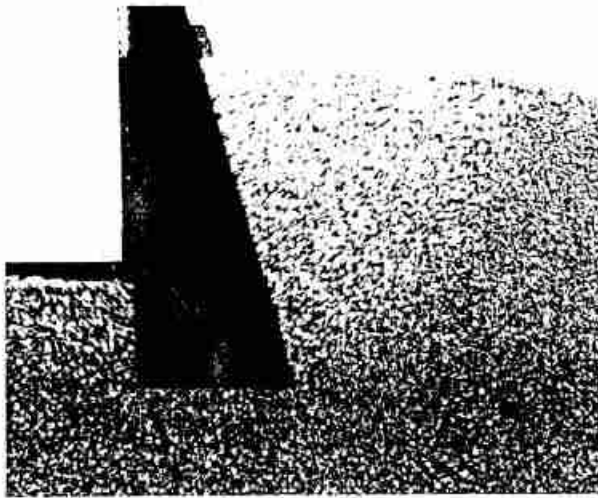


Fig. 13.3 Double exposure showing movements of "soil" surrounding model retaining wall.

stress, and the ratio of horizontal to vertical stress is called the *coefficient of active stress* and is denoted by the symbol K_a .

Figure 13.5 shows the Mohr circle for the active state of stress.² From our analysis of the stresses at failure

² This chapter considers only cases where the failure law is $\tau_{ef} = \sigma_{ef} \tan \phi$. Methods for cases where it is appropriate to use $\tau_{ef} = c + \sigma_{ef} \tan \phi$ are discussed in Part IV.

during a triaxial test (Section 11.1) we already know the ratio of the horizontal and vertical stresses for this case is

$$\begin{aligned} K_a &= \frac{\sigma_{h2}}{\sigma_v} = \frac{\sigma_{3f}}{\sigma_{1f}} = \frac{1 - \sin \phi}{1 + \sin \phi} \\ &= \tan^2 \left(45 - \frac{\phi}{2} \right) = \frac{1 - \tan \alpha}{1 + \tan \alpha} \end{aligned} \quad (13.1)$$

Now let us suppose that the soil is compressed in the horizontal direction. Any element of soil is now in just the condition of a triaxial specimen being failed by increasing the confining pressure while holding the vertical stress constant [or, if we imagine that the triaxial specimen is placed on its side, increasing the axial stress while holding the confining pressure constant (see Fig. 13.4)]. The horizontal stress cannot be increased beyond a certain magnitude called the *passive stress*. The ratio of horizontal to vertical stress is called the *coefficient of passive stress* K_p . Figure 13.5 also shows the Mohr circle for this state of stress, and the magnitude of K_p is given by

$$\begin{aligned} K_p &= \frac{\sigma_{h2}}{\sigma_v} = \frac{\sigma_{1f}}{\sigma_{3f}} = \frac{1 + \sin \phi}{1 - \sin \phi} \\ &= \tan^2 \left(45 + \frac{\phi}{2} \right) = \frac{1 + \tan \alpha}{1 - \tan \alpha} \end{aligned} \quad (13.2)$$

Ignoring any slight difference in ϕ for the two different stress paths (see Chapter 11) we see that $K_p = 1/K_a$.

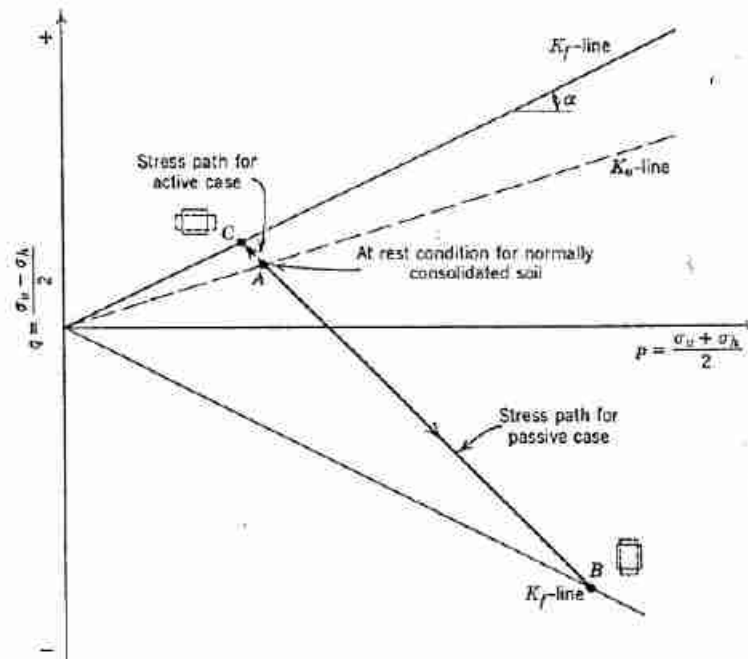


Fig. 13.4 Stress paths for Rankine active and passive conditions.

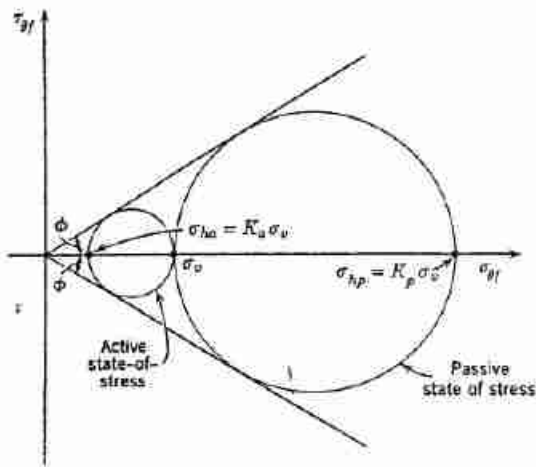


Fig. 13.5 Rankine states of stress for geostatic condition.

Thus for a given vertical geostatic stress σ_v , the horizontal stress can be only between the limits $K_a\sigma_v$ and $K_p\sigma_v$. These two limiting stresses are called *conjugate stresses*. The states of stress at the two extreme situations are called *Rankine states*, after the British engineer Rankine who in 1857 noted the relationship between the active and passive conditions. The inclinations of the slip lines

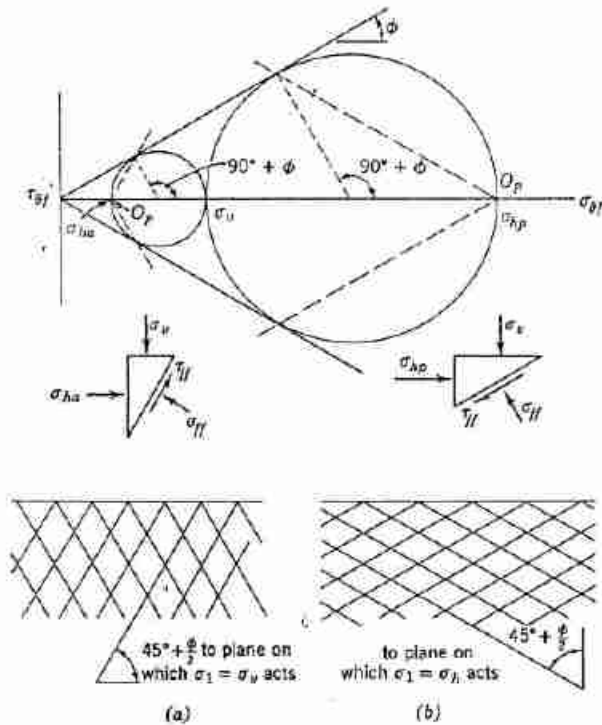


Fig. 13.6 Orientation of slip lines for Rankine states. (a) Active state. (b) Passive state.

for the two limiting cases are sketched in Fig. 13.6, which illustrates the use of the origin of planes to obtain these inclinations. In the active condition the shear stress opposes the effect of gravity. In the passive condition the shear stress acts together with gravity to oppose the large horizontal stress.

Table 13.1 gives typical values for K_a and K_p . If the horizontal stretching or compressing of the soil causes very large strains, the friction angle ϕ_{ov} should be used to determine these coefficients. Generally, however, it is

Table 13.1 Values of K_a and K_p for Rankine States of Geostatic Stress

ϕ	K_a	K_p
10°	0.703	1.42
15°	0.589	1.70
20°	0.490	2.04
25°	0.406	2.46
30°	0.333	3.00
35°	0.271	3.66
40°	0.217	4.60
45°	0.171	5.83

appropriate to use the peak friction angle ϕ . For $\phi = 30^\circ$, the theoretical failure lines will be at 60° to the horizontal for the active case and 30° to the horizontal for the passive case.

Strains Associated With Rankine States

The strains required to achieve active and passive conditions may be inferred from the results of triaxial tests such as those for tests 3 and 6 in Fig. 10.22. These results have been replotted in Fig. 13.7. Part (a) of this figure shows the stress paths and both the horizontal and vertical strains; part (b) shows the horizontal strain versus the stress ratio K . The important conclusions are:

1. Very little horizontal strain, less than -0.5% , is required to reach the active state.
2. Little horizontal compression, about 0.5% , is required to reach one-half of the maximum passive resistance.
3. Much more horizontal compression, about 2% , is required to reach the full maximum passive resistance.

These results are typical for most dense sands. For loose sands the first two conclusions remain valid, but the horizontal compression required to reach full passive resistance may be as large as 15% .

There are two reasons why less strain is required to reach the active condition than to reach the passive condition. First, an unloading (the active state) always

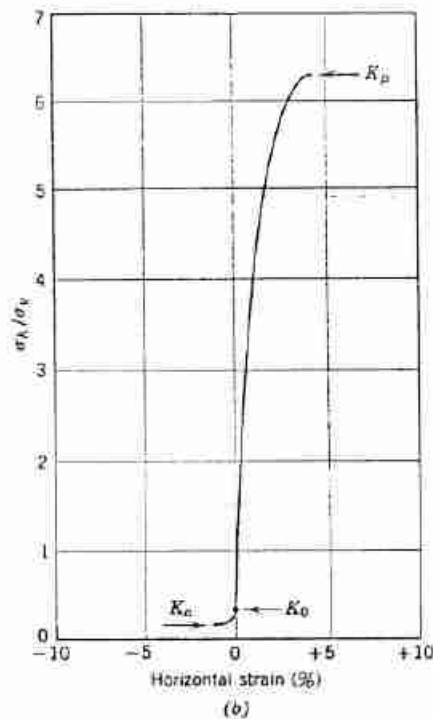
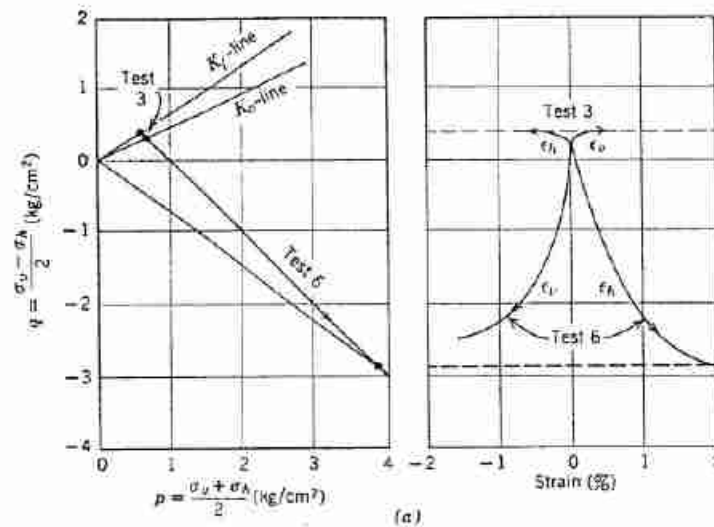


Fig. 13.7 Strains required to reach active and passive states in a dense sand. (a) Stress paths and q versus strain. (b) K versus horizontal strain.

involves less strain than a loading (the passive state). Second, the stress change in passing to the active state is much less than the stress change in passing to the passive state.

The foregoing results apply when the initial condition is a K_0 condition. If initially $\sigma_h/\sigma_v \neq K_0$, then somewhat

different strains will be required to reach the limiting conditions. Furthermore, most field problems involving retaining structures are plane strain situations, and hence the triaxial data just presented are only indicative of those applicable to actual field problems. Data from plane strain tests are more appropriate.

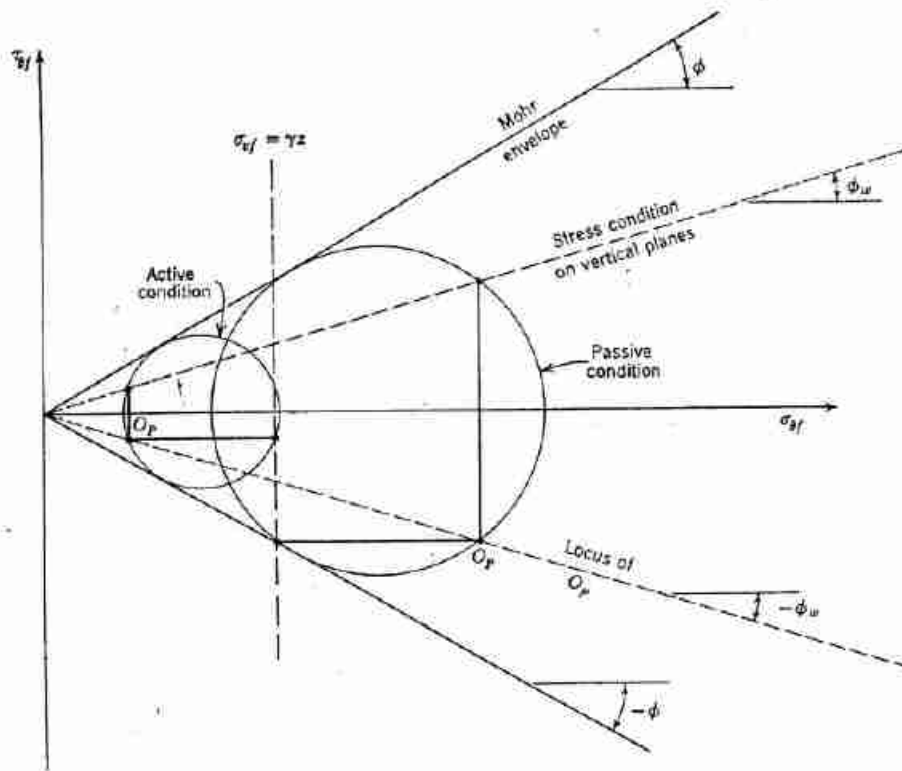


Fig. 13.8 Rankine states of stress for horizontal ground with shear stresses on vertical surfaces.

Other Than Geostatic Condition

The concepts of active and passive stress, and of conjugate stresses, apply to many problems in addition to the problem of horizontal geostatic stresses. For example, consider the case where the ground surface is level but there are equal shear stresses on all vertical planes. These stresses can be represented as $\tau_{vh} = \sigma_h \tan \phi_w$. Figure 13.8 shows the Mohr circle representation for the Rankine active and passive conditions for this case. The Mohr circles must satisfy the following conditions:

1. $\sigma_v = \gamma z$. The shear stresses on vertical planes do not alter this condition, since these shear stresses cancel on opposite sides of a column of soil.
2. The shear stress on a horizontal plane equals the given shear stress on a vertical plane but is of opposite sign.
3. The Mohr circle must pass through the point specified by conditions 1 and 2 and must be tangent to lines at $\pm\phi$.

Careful inspection of the figure will show that the origin of planes must lie along a line inclined at $-\phi_w$. Then a vertical line through the O_p will intersect the line at slope ϕ_w at a point giving the stresses on vertical planes. Example 13.1 illustrates the use of this construction. It

is possible to derive equations giving the conjugate stresses for such situations (see Taylor, 1948). The form of the equations will differ from Eqs. 13.1 and 13.2, but the concepts remain the same.

13.3 SIMPLE RETAINING WALLS WITHOUT WALL FRICTION

Our next step is to consider the case of a simple retaining wall where (a) the backfill has a horizontal surface; (b) the face of the retaining wall in contact with the soil is vertical; and (c) there is no shear stress between the vertical face of the retaining wall and the soil. This simple case will serve to illustrate the concepts and methods needed for the solution of more complex problems. The active case will be considered first.

Active Thrust Using Rankine Zone

One way to evaluate the active thrust for this case is to assume that the active zone is a triangle and that everywhere within the triangle the soil is in the Rankine active condition. The slip lines for this assumed condition are shown in Fig. 13.9. Within the Rankine zone the horizontal stress at any depth z is

$$\sigma_h = K_a \gamma z \quad (13.3)$$

where

- γ = the unit weight of the soil
- z = the depth below ground surface
- K_a = the active stress coefficient, Eq. 13.1

The horizontal stress against the wall increases linearly with depth. Hence the total horizontal thrust against the wall will be

$$P_a = \frac{1}{2} \gamma H^2 K_a \quad (13.4)$$

where

- H = height of the wall
- P_a = active horizontal thrust

The resultant total thrust P_a will act at a point one-third of the distance from the bottom to the top of the wall.

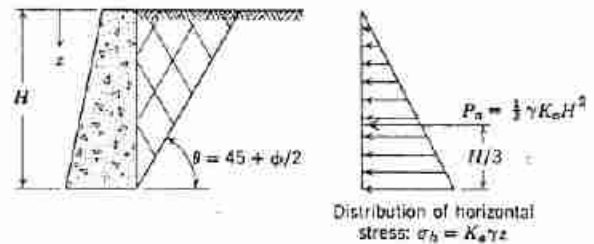


Fig. 13.9 Active thrust for simple Rankine case.

► Example 13.1

Given. Soil with horizontal surface, $\gamma = 110$ pcf, $\phi = 30^\circ$. On vertical planes, $\tau_{vh} = -\sigma_h \tan 30^\circ$.

Find. For active condition at depth of 10 ft: horizontal stress, directions of principal stresses, orientation of slip lines.

Solution. A trial and error solution is necessary. First assume that the shear stress on the horizontal plane is given by point A' in Fig. E13.1. The Mohr circle corresponding to failure conditions is then as shown by the dashed circle. For this circle, the origin of planes is at $O_{p'}$ and the stresses on the vertical plane are given by point B' . This result does not satisfy the requirement that $\tau_{vh} = -\sigma_h \tan 30^\circ$. Further trials show that the given conditions are satisfied only by the Mohr circle drawn as a solid line, with stresses on vertical planes at point A and stresses on horizontal planes at point B .

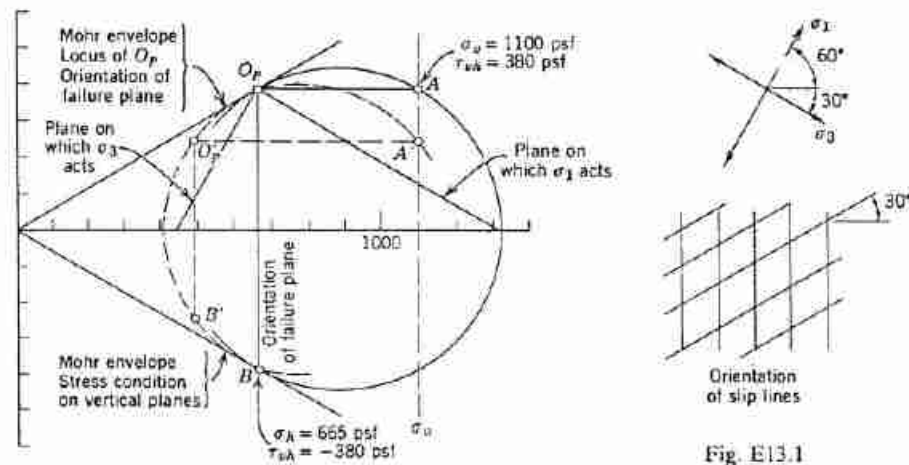


Fig. E13.1

► Example 13.2

Given. Retaining wall as shown in Fig. E13.2.

Find. For the active condition:

- a. Horizontal stress at base of wall.
- b. Total horizontal thrust.
- c. Location of thrust.

Solution. From Table 13.1, find $K_a = 0.333$.

- a. At base, $\sigma_h = (110)(20)(0.333) = 733$ psf
- b. $P_a = \frac{1}{2}(733)(20) = 7330$ lb/ft of wall
- c. Thrust acts $20/3 = 6.7$ ft above base of wall

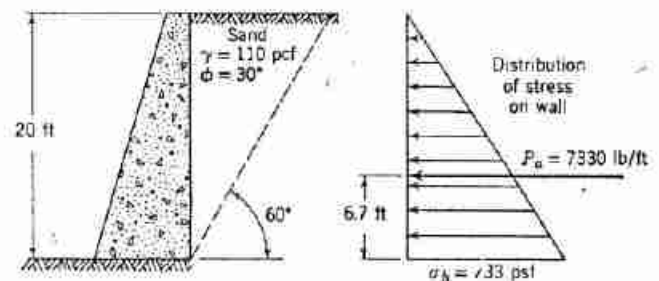


Fig. E13.2

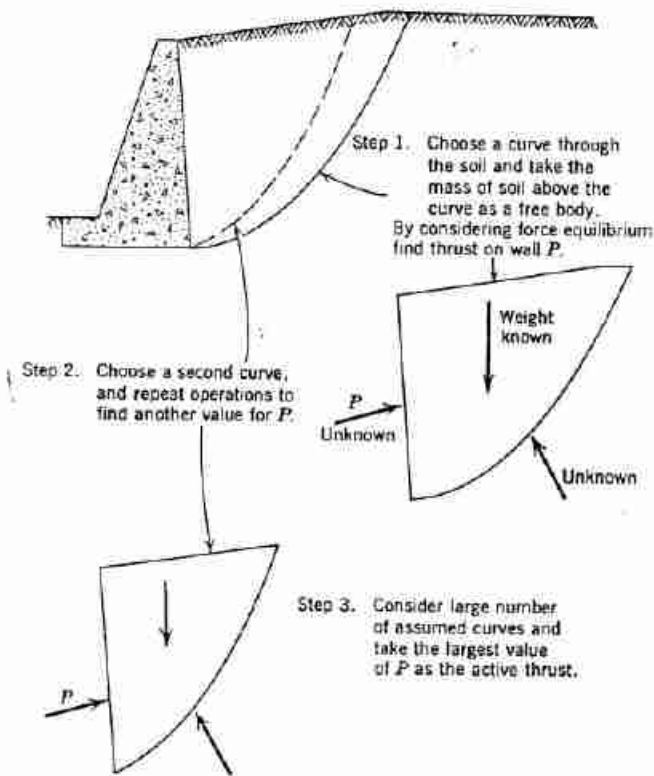


Fig. 13.10 Steps in trial wedge method of stability analysis.

Example 13.2 illustrates the computation of active thrust using these equations. The peak friction angle should be used to evaluate K_a . However, backfills are often in a rather loose condition; thus ϕ typically is about 30° .

This solution is intuitively satisfying. The requirement of equilibrium and the failure condition are fulfilled at each point within the Rankine zone, as are the boundary conditions along the surface of the backfill (no stress) and along the wall (no shear stress). However, this solution is not exact in the mathematical sense. This solution says nothing about the stresses outside of the failure zone; hence there is no complete assurance that the stresses outside the zone satisfy equilibrium without violating the failure law. There are other difficulties which will be discussed in Section 13.5.

Since the usefulness of Eqs. 13.1, 13.3, and 13.4 cannot be proved mathematically, this usefulness can only be demonstrated by comparing the predictions of these equations with actual measurements. Such comparisons have been made by Terzaghi (1934) and these equations have been found to give reasonable predictions for the conditions specified.

Active Thrust by Trial Wedges

The trial wedge method of analysis involves the following steps, which are illustrated in Fig. 13.10:

1. A mass of soil behind the wall is considered as a free body. The force P , which must exist between this free body and the wall, is found by writing the equations of equilibrium for the free body as a whole.
2. A different free body is considered, having a different boundary through the soil. Once again the required force P between the wall and the free body is found.
3. The actual force against the wall will be the *largest* value of P found as the result of considering all possible free bodies.

Even though the active thrust is the minimum possible thrust for which the backfill can be in equilibrium, we must seek the free body that gives the largest value of this thrust consistent with the assumption that the full shear strength of the soil is mobilized.

Figure 13.11 shows the application of the trial wedge method to the problem of a simple retaining wall without friction on the face. Example 13.3 illustrates the computations. Only those free bodies bounded by straight lines through the heel of the wall are considered. There are distributed normal stresses along IJ and JM , and distributed shear stresses along JM , but the desired analysis can be carried out in terms of the resultants P and F of these distributed stresses.

► Example 13.3

Given. Retaining wall and backfill of Example 13.2.

Find. Active thrust by trial wedge method.

Solution. Figure E13.3-1 shows to scale the free bodies and the force polygons for $\theta = 45^\circ$

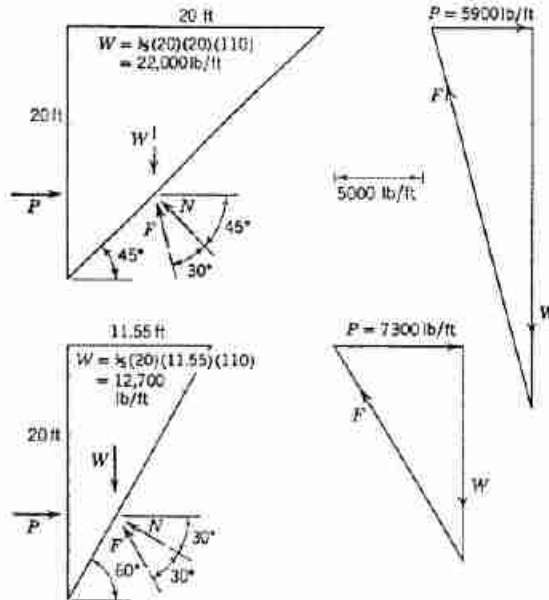


Fig. E13.3-1

and $\theta = 60^\circ$. Equation 13.5 may be used to evaluate P for many values of θ .

θ	$\cot \theta$	$\tan (\theta - 30^\circ)$	Product	P
55°	0.700	0.466	0.328	7210
$57\frac{1}{2}^\circ$	0.637	0.520	0.331	7280
60°	0.577	0.577	0.333	7330
$62\frac{1}{2}^\circ$	0.521	0.637	0.331	7280
65°	0.467	0.700	0.328	7210

The plot in Fig. E13.3-2 shows graphically the manner in which P varies with θ .

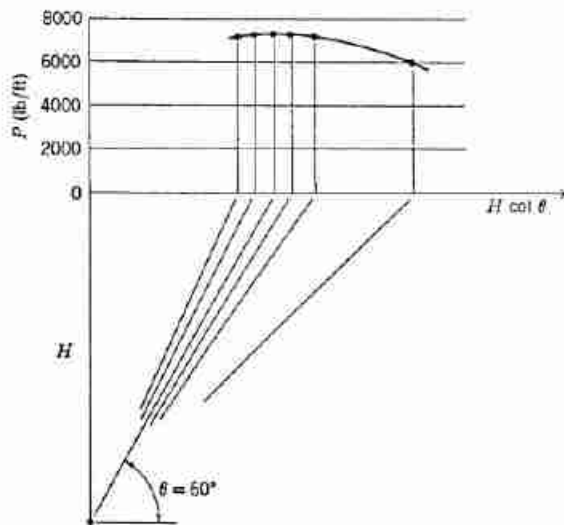


Fig. E13.3-2

Forces acting on the free body:

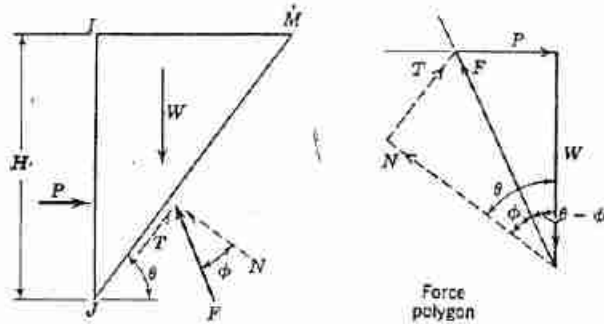
W = weight of soil = $\frac{1}{2}\gamma H^2 \cot \theta$

P = resultant of distributed stresses between soil and wall

N = resultant of normal stresses within soil along assumed plane

T = resultant of shear stresses within soil along assumed plane = $N \tan \phi$

F = resultant of N and T



Equations of equilibrium

$$\begin{aligned} \sum V = 0: \quad F &= \frac{W}{\cos(\theta - \phi)} \\ \sum H = 0: \quad P &= W \tan(\theta - \phi) \\ \therefore P &= \frac{1}{2}\gamma H^2 \cot \theta \tan(\theta - \phi) \quad (13.5) \end{aligned}$$

Fig. 13.11 Equilibrium of trial wedge for simple retaining wall: active case.

Step 1. Place free body in equilibrium. The weight W is known in magnitude and direction. The resultant forces P and F are determined as to direction, but not as to magnitude. Hence there are two unknowns (the magnitudes of P and F) and two equations of force equilibrium. The problem is statically determinate and thus may be solved by statics alone.

In order to solve this equilibrium problem a *force polygon* is useful. The forces acting on the free body are plotted as vectors, with the tail of one vector connected to the head of another vector. In this problem the vector W is first plotted to some convenient scale. Then the directions of P and F are laid off and their intersection gives the closure of the force polygon. The magnitudes of P and F may be scaled from the diagram, or alternatively the force polygon may be used to guide the writing of a pair of equations which are then solved to give the magnitudes of P and F .

Steps 2 and 3. Search for critical free body. There are several ways in which the search for the most critical free body may be performed.

One way is to assume various inclinations of the failure line and determine the value of P corresponding to each inclination. Either Eq. 13.5 may simply be evaluated for several different values of θ , or a force polygon may be constructed for each θ and then P scaled graphically. Example 13.3 illustrates the variation of P with θ and shows a convenient way to plot the results. The thrust P

is greatest when $\theta = 60^\circ$. If P were to be less than the computed value, the backfill would fail along a slope with this inclination.

For this simple case it is possible to carry out the search mathematically (see Example 13.4). The

► Example 13.4

Given. Equation 13.5 (in Fig. 13.11) for P as a function of θ .

Find. Maximum value of P and θ for which this maximum occurs.

Solution.

$$\begin{aligned} \frac{\partial P}{\partial \theta} &= \frac{1}{2}\gamma H^2 \left[-\frac{\tan(\theta - \phi)}{\sin^2 \theta} + \frac{\cot \theta}{\cos^2(\theta - \phi)} \right] \\ &= \frac{1}{2}\gamma H^2 \frac{-\sin(\theta - \phi) \cos(\theta - \phi) + \sin \theta \cos \theta}{[\sin \theta \cos(\theta - \phi)]^2} \\ &\quad - \frac{\sin \theta \cos \theta (\cos^2 \phi - \sin^2 \phi - 1)}{-\sin \phi \cos \phi (\sin^2 \theta - \cos^2 \theta)} \\ &= \frac{1}{2}\gamma H^2 \frac{\sin 2\theta \sin^2 \phi + \sin \phi \cos \phi \cos 2\theta}{[\sin \theta \cos(\theta - \phi)]^2} \\ &= \frac{1}{2}\gamma H^2 \frac{\sin \phi \cos(2\theta - \phi)}{[\sin \theta \cos(\theta - \phi)]^2} \end{aligned}$$

This is zero when $\cos(2\theta - \phi) = 0$ or $2\theta_{cr} - \phi = 90^\circ$ or $\theta_{cr} = 45 + \phi/2$

Substituting in Eq. 13.5,

$$\begin{aligned} P_n &= \frac{1}{2}\gamma H^2 \cot \left(45 + \frac{\phi}{2} \right) \tan \left(45 - \frac{\phi}{2} \right) \\ &= \frac{1}{2}\gamma H^2 \tan^2 \left(45 - \frac{\phi}{2} \right) = \frac{1}{2}\gamma H^2 K_a \quad \blacktriangleleft \end{aligned}$$

equilibrium equation contains the variable θ , which defines the boundary of the free body through the soil. By maximizing the expression for P with respect to θ , the actual thrust as well as the location of the critical thrust plane of sliding can be found. A graphical procedure for finding the critical inclination is also available (see Taylor, 1948, p. 497).

The maximum thrust found by these procedures is the active thrust P_a .

Moment Equilibrium for Trial Wedge

The line of action of the vector W is through the centroid of the trial wedge. One possible location for the vectors P and F is shown in Fig. 13.12: P acts at the third-point of the wall and F acts at the third-point of the failure surface. These locations of P and F are consistent with a linear variation of stress with depth.

Critique of Trial Wedge Method

The trial wedge method does not consider stress conditions either within the trial wedge or outside of the wedge, and again there is no complete assurance that the stresses

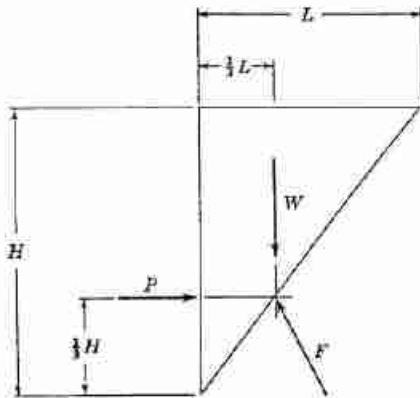


Fig. 13.12 Location of forces so that trial wedge is in moment equilibrium.

within and below the wedge satisfy equilibrium without violating the failure law. Thus, although the solution is intuitively satisfactory, it cannot be mathematically proven to be exact.

For the conditions considered in this section, the trial wedge method gives exactly the same result as does the solution using the Rankine zone. Indeed, for this case the trial wedge method only repeats the steps which led (in Chapter 8) to the equations for the Mohr circle. The difference between the methods becomes greater as we turn to more complex situations.

The trial wedge method was originated by the French engineer Coulomb in 1776, almost a century before Rankine (apparently without knowledge of Coulomb's work) published his analysis. Coulomb can thus be regarded as the founder of the theories for active earth

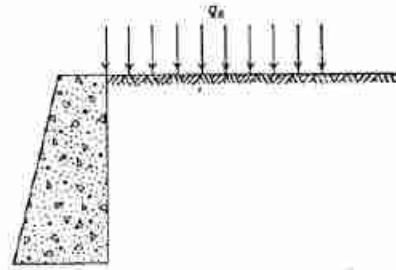


Fig. 13.13 Retaining wall with uniform surcharge.

thrust. The contribution of Rankine was to introduce the concept of passive stress and to tie together the two extreme cases of active and passive stress.

Active Thrust with Uniform Surcharge

The methods of solution presented in the preceding paragraphs can readily be extended to cover situations in which there is a surcharge over the surface of the backfill behind the retaining wall. Such a surcharge might arise from stored material or parked vehicles.

With a uniform surcharge q_s (Fig. 13.13), the vertical stress at any depth is simply³

$$\sigma_v = q_s + \gamma z$$

The horizontal stress is $\sigma_h = K_a \sigma_v$ where K_a is still as given by Eq. 13.1. Hence the horizontal stress at any depth is

$$\sigma_h = (q_s + \gamma z) \frac{1 - \sin \phi}{1 + \sin \phi} = (q_s + \gamma z) K_a \quad (13.6)$$

³ Note that q_s denotes an entirely different quantity than does $q = (\sigma_v - \sigma_h)/2$.

► **Example 13.5**

Given. Retaining wall of Example 13.2, with surcharge of 1000 psf.

Find. Active thrust against wall, and location of this thrust.

Solution. Additional thrust from surcharge (see Fig. E13.5) is

$$(1000)(20)\left(\frac{1}{2}\right) = 6670 \text{ lb/ft}$$

$$P\bar{x} = 6670(10) + 7330(6.67) = 115,6000$$

$$\bar{x} = \frac{115,600}{14,000} = 8.26 \text{ ft}$$

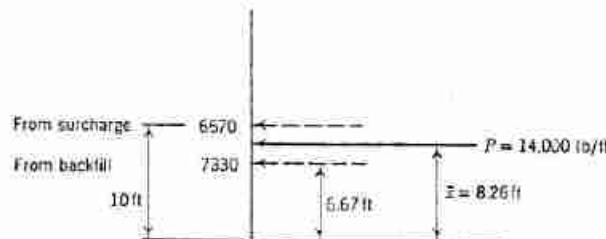


Fig. E13.5

► Example 13.6

Given. Retaining wall and backfill of Example 13.2.

Find. Passive thrust, passive stresses, location of slip line, location of resultant passive thrust.

Solution. See Fig. E13.6:

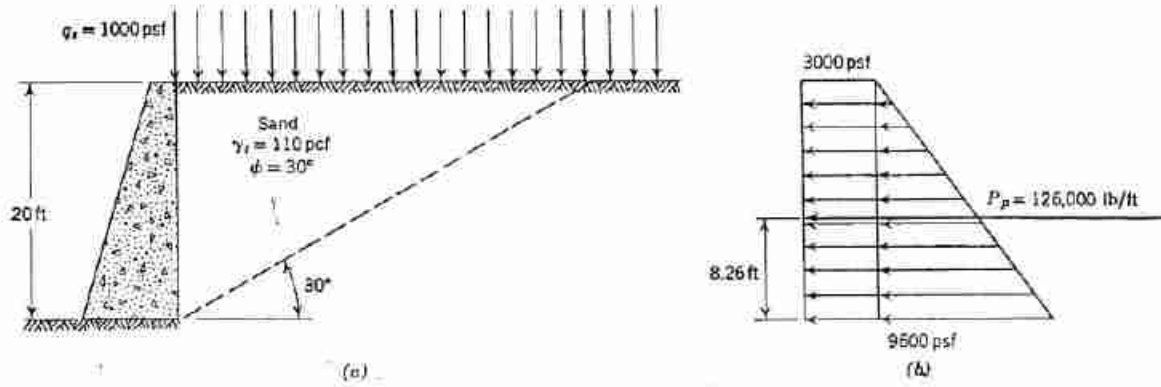


Fig. E13.6

At base: $\sigma_{hp} = [(20)(110) + 1000](3) = [2200 + 1000](3) = 9600 \text{ psf}$

From Fig. E13.6b:

$$P_p = \left[\frac{1}{2}(20)^2(110) + (20)(1000) \right](3) = [22,000 + 20,000](3) = 126,000 \text{ lb/ft}$$

$$\bar{x} = \frac{66,000(20/3) + 60,000(10)}{126,000} = 8.26 \text{ ft}$$

The total active thrust against the wall is then given by

$$P_a = \frac{1}{2}\gamma H^2 K_a + q_s H K_a \quad (13.7)$$

Note that the horizontal stress resulting from the surcharge is distributed uniformly with depth, and hence the resultant force corresponding to the surcharge is located at midheight of the wall. Thus the resultant of the total thrust, reflecting the effects of surcharge and weight of soil, will lie between midheight and the third point. The location of the resultant of the total thrust is found by vectorial addition of the thrusts for each of the two components. This is illustrated in Example 13.5, in which Example 13.2 is extended to include the effects of a surcharge of 1000 lb/ft². The additional thrust of 6670 lb/ft acts at midheight of the wall, or 10.0 ft above the base. The resultant of this thrust plus that from the weight of the soil (see Example 13.5) acts 8.26 ft above the base of the wall.

The trial wedge procedure can be used to obtain the same result. The surcharge causes another force on the free body, but this force simply adds to the weight vector *W*. The location of the critical surface is not affected.

Passive Resistance

Assuming that soil which offers passive resistance is in the passive Rankine condition, the passive stress and

total passive resistance are given by

$$\sigma_h = \gamma z K_p + q_s K_p \quad (13.8)$$

$$P_p = \frac{1}{2}\gamma H^2 K_p + q_s H K_p \quad (13.9)$$

where *K_p* is as given by Eq. 13.2. Here *H* is the depth of the passive zone and *q_s* is the surcharge on the passive zone. The use of these equations is illustrated in Example 13.6.

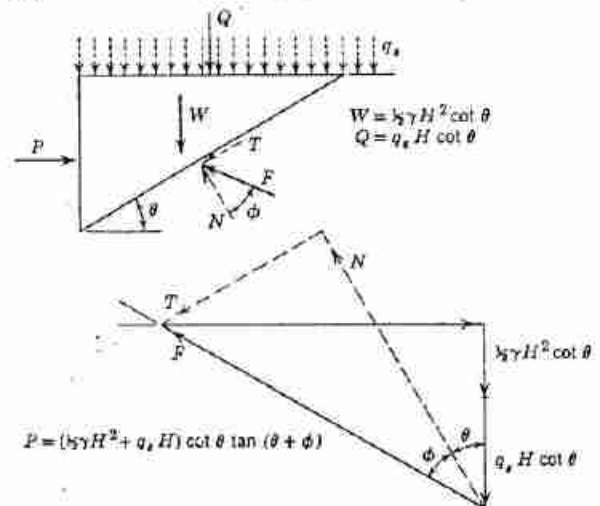


Fig. 13.14 Equilibrium of trial wedge for simple retaining wall: passive case.

► Example 13.7

Given. Retaining wall and backfill of Example 13.6.
Find. Passive thrust by trial wedge method.

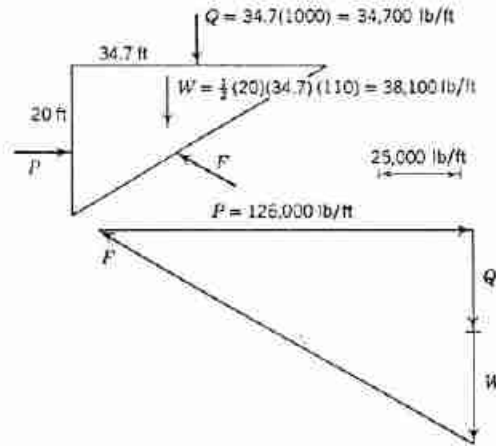


Fig. E13.7

Solution. The force polygon and free body for $\theta = 30^\circ$ are shown in Fig. E13.7. Using equation in Fig. 13.14:

θ	$\cot \theta$	$\tan (\theta + 30^\circ)$	$P/(\frac{1}{2}\gamma H^2 + q, H)$
20°	2.75	1.192	3.28
25°	2.145	1.428	3.06
30°	1.732	1.732	3.00 ←
35°	1.428	2.145	3.06
40°	1.192	2.75	3.28

$$\begin{aligned}
 P_p &= 3\left[\frac{1}{2}(110)(20)^2 + 1000(20)\right] \\
 &= 3[22,000 + 20,000] \\
 &= 126,000 \text{ lb/ft}
 \end{aligned}$$

As in Example 13.6, resultant thrust is located 8.26 ft above base of wall.

The trial wedge method for the passive case is basically similar to that for the active case, with but one significant difference: now the *shear stresses* on the failure surface act *together* with the *weight* of the soil to resist the horizontal thrust from the wall. Thus, even though the passive thrust is the maximum possible thrust for which the soil can be in equilibrium, we must seek the free body that leads to the smallest value for the thrust. If the wall applies a thrust greater than this smallest passive thrust, the soil will not be in equilibrium. Figure 13.14 shows the formulation of the passive problem using straight failure surfaces. Example 13.7 illustrates the method.

As was the case for the active thrust, both methods of solution give the same intuitively satisfying result for the case of a simple wall without wall friction. However, the only true justification for the use of Eqs. 13.2, 13.8, and

13.9 lies in the agreement between the predictions of those equations and actual observed results.

13.4 RETAINING WALLS WITH WALL FRICTION

Generally shear forces develop between the face of a retaining wall and the backfill because of relative motions between the wall and backfill. Figure 13.3 illustrated the typical patterns of motion. In the active zone, the outward stretching leads to downward motion of the soil relative to the wall. Because of friction between the soil and wall, this motion causes a downward shear force on the wall. Such a downward shear upon the wall is called positive wall friction for the active case (see Fig. 13.15). In the passive zone, the horizontal compression must be

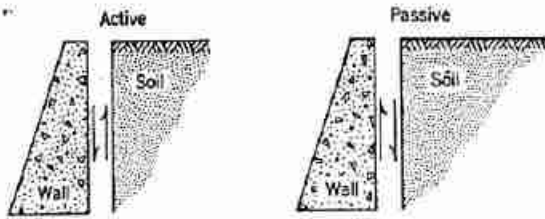


Fig. 13.15 Direction of positive wall friction.

accompanied by an upward bulging of the soil, and hence there tends to be an upward drag on the wall. Such an upward shear on the wall is called positive wall friction for the passive case. In the active case wall friction is almost always positive. Either positive or negative wall friction may develop in the passive case. Whether wall friction is present, and the sign of this friction, must be determined from a study of the motions expected for each problem.

The magnitude of this shear force is controlled by the friction angle ϕ_w between the soil and the wall. As noted in Chapter 11, ϕ_w usually is about equal to ϕ_{cv} and typically has a value of about 30° . For a loose backfill ϕ and ϕ_w will be numerically equal, whereas $\phi_w < \phi$ for a dense backfill.

Solution Using Failure Zone

The conditions that must be fulfilled along the boundaries of the failure zone are sketched in Fig. 13.16. Along the surface of the backfill there are no shear stresses on horizontal and vertical surfaces. Hence at this surface the slip lines must be inclined at $\pm(45 + \phi/2)$ to the horizontal. Along the wall, however, the ratio of shear to normal stresses must equal $\tan \phi_w$. Thus at the wall the stress conditions must be as sketched in Example 13.1, and the slip lines have the inclination shown in Fig. 13.16. Hence different Rankine states apply within different portions of the backfill.

The solution of this boundary value problem now becomes quite complicated. In order that equilibrium be satisfied within the failure zone, the stresses must satisfy the differential equations of equilibrium.⁴

$$\frac{\partial \sigma_x}{\partial z} - \frac{\partial \tau_{xz}}{\partial x} - \gamma = 0 \quad (13.10a)$$

$$\frac{\partial \sigma_h}{\partial x} + \frac{\partial \tau_{xh}}{\partial z} = 0 \quad (13.10b)$$

In addition, the failure condition must be fulfilled throughout the failure zone:

$$\tau_{ij} = \sigma_{ij} \tan \phi \quad (13.11)$$

⁴ See Crandall and Dahl (1959, p. 127) for a derivation of these equations. The special sign convention used in soil mechanics must be taken into account.

Combining Eqs. 13.10 and 13.11 leads to an equation called Kötter's equation. Solution of this equation, for the boundary conditions as shown in Fig. 13.16, gives the orientation of the slip lines together with the stresses at each point of the failure zone (see Sokolovski, 1965; Harr, 1966). A numerical integration technique is necessary in order to obtain this solution.

A complete derivation of Kötter's equation, and the numerical integration technique used for its solution, are beyond the scope of this text. Figure 13.16 illustrates the results by showing the slip-line field construction by this method for the case of $\phi = \phi_w = 30^\circ$. The resulting coefficient of active stress is 0.31. Now K_a is no longer the ratio of vertical to horizontal stress but is the ratio

$$K_a = \frac{\sqrt{\tau_{vh}^2 + \sigma_h^2}}{\gamma z}$$

for stresses at the wall. Note that σ_h is *not* necessarily equal to γz , owing to the curvature of the slip-line field. The active thrust is

$$P_a = \frac{1}{2} \gamma H^2 K_a = 0.31 (\frac{1}{2} \gamma H^2)$$

and is inclined to the horizontal at the angle of the wall friction. Along the wall all components of stress still increase linearly with depth, and so the resultant thrust still acts at the third-point of the wall.

A separate numerical integration must be made for each value of ϕ and ϕ_w . Sokolovski (1965) presents a table giving these results.

Active Thrust by Trial Wedges

Figure 13.17 shows the general formulation of this problem using straight failure surfaces and Example 13.8 illustrates a specific case. The force polygon is modified since P is now inclined instead of horizontal. Otherwise

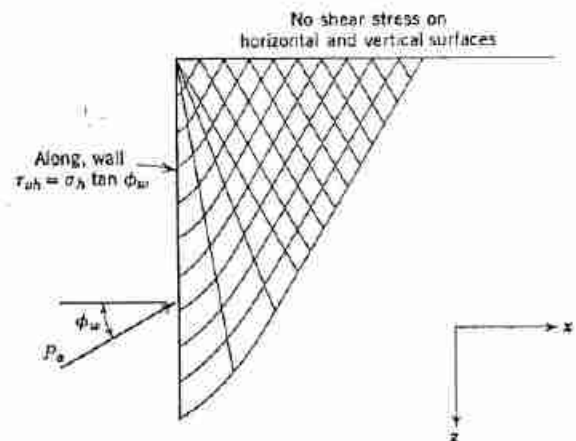


Fig. 13.16 Slip-line field and failure zone for case with wall friction. Slip-line field for $\phi = \phi_w = 30^\circ$ by method of Sokolovski (1965).

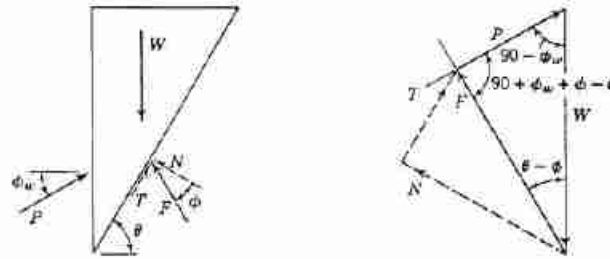


Fig. 13.17 Equilibrium of trial wedge for simple retaining wall with friction.

By law of sines:

$$\begin{aligned}
 P &= W \frac{\sin(\theta - \phi)}{\sin(90 + \phi_w + \phi - \theta)} \\
 &= \frac{1}{2} \gamma H^2 \cot \theta \frac{\tan(\theta - \phi)}{\cos \phi_w + \sin \phi_w \tan(\theta - \phi)}
 \end{aligned}$$

► Example 13.8

Given. Retaining wall and backfill of Example 13.2, except that now there is wall friction $\phi_w = 30^\circ$.

Find. Active thrust by trial wedge method.

Solution. Figure E13.8 shows the free body and force polygon for $\theta = 60^\circ$. The equation in Fig. 13.17 may be used to evaluate P for many values of θ .

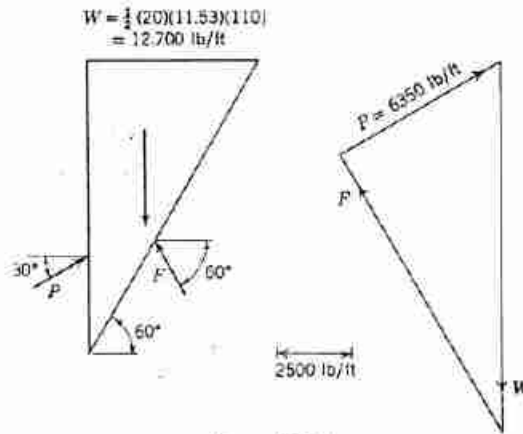


Figure E13.8

θ	$\cot \theta$	$\tan(\theta - 30^\circ)$	$0.866 + \frac{1}{2} \tan(\theta - \phi)$	$\frac{P}{\frac{1}{2} \gamma H^2}$
50	0.839	0.364	1.048	0.292
52½	0.767	0.414	1.073	0.296
55	0.700	0.467	1.100	0.297 ←
57½	0.637	0.520	1.126	0.295
60	0.577	0.577	1.154	0.289

$$P_u = 0.297(\frac{1}{2} \gamma H^2) = 6540 \text{ lb/ft}$$

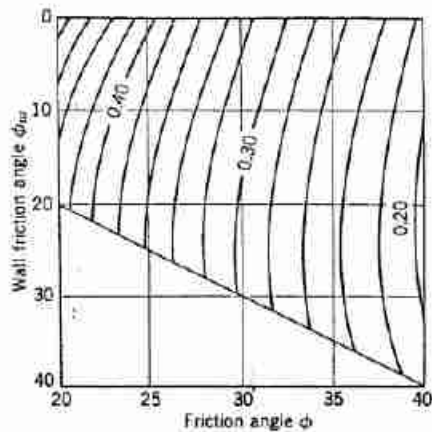


Fig. 13.18 Coefficient of active stress as function of wall friction.

the same general procedure is followed. Moment equilibrium is satisfied with P located at the third-point of the wall, but F is no longer located at the third-point of the failure surface.

The critical straight failure surface found by this method is an approximation to the more exact failure surface indicated in Fig. 13.16. The failure surface of the trial wedge satisfies the boundary conditions neither at the top surface of the backfill nor at the wall. Note that the inclination of this surface is no longer equal to $45 + \phi/2$.

Figure 13.18 gives values of K_a calculated using the trial wedge procedure with straight-line failure surfaces. These values of K_a may be used in Eqs. 13.3 or 13.4 to give the stress against the wall at any depth or the thrust against the wall. The stress thus calculated is $\sqrt{\tau_{vb}^2 + \sigma_v^2}$ rather than just the horizontal stress, and the thrust thus calculated is at the angle ϕ_w to the horizontal rather than the horizontal thrust. Thus wall friction has two effects upon active thrust: (a) on the magnitude of P_a and (b) on the direction of P_a . The second of these effects is usually the more important, as is shown by the comparison in Example 13.9. Wall friction changed the active thrust by only 7%, but decreased the horizontal component of this thrust by 24%.

► Example 13.9

Given. Retaining wall of height H with backfill having $\phi = 35^\circ$ and unit weight γ .

Find. The effect of wall friction ($\phi_w = 35^\circ$) upon (a) the active thrust and (b) the horizontal component of active thrust.

Solution. The difference is that between K_a and $K_a \cos \phi_w$. Fig. 13.18 was used for the following tabulation.

	$\phi_w = 0$	$\phi_w = 35^\circ$	Percent difference
K_a	0.27	0.25	7%
$K_a \cos \phi_w$	0.27	0.204	24%

Use of curved failure surfaces for trial wedges leads to slightly more critical free bodies and to slightly greater values of K_a . However, the differences in K_a are at most a few percent and generally so small they are undetectable in a plot such as Fig. 13.18. The critical curved failure surfaces, and the values of K_a , are almost exactly the same as those found by the method of Sokolovski. However, the important thing is that these results are in reasonable agreement with the few actual measurements which have been made in large-scale tests.

Passive Resistance

For the passive case the trial wedge method using straight failure surfaces significantly overestimates the resistance. That is to say, trial wedge solutions using curved failure surfaces (see Fig. 13.19) give a smaller passive resistance than the passive resistance computed using straight surfaces. The difference increases with increasing wall friction. The technique of solution using the trial wedge method with curved boundaries is described in detail in Terzaghi (1943) and Terzaghi and Peck (1967). Figure 13.20 gives passive stress coefficients obtained in this way. Alternatively, the method of Sokolovski (1965) may be used. Both approaches give essentially the same answer. The thrust computed using the coefficients in Fig. 13.20 is inclined to the horizontal at an angle corresponding to the wall friction.

The theoretical predictions regarding passive resistance with wall friction are not as well confirmed by experiment

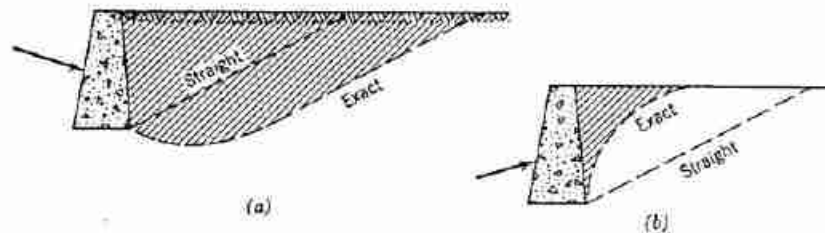


Fig. 13.19 Comparison of passive failure zone predicted by trial wedge method using straight and curved slip lines. (a) Positive wall friction. (b) Negative wall friction.

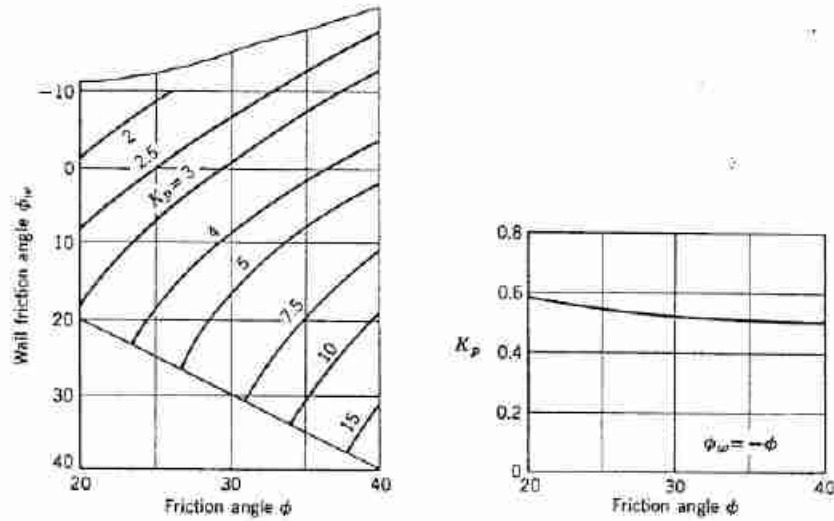


Fig. 13.20 Chart for passive stress coefficient (based on Caquot and Kérisel, 1949).

as the predictions regarding active thrust, and hence cannot be used with as much confidence. Tschebotarioff (1951) reports on the results of a few large-scale laboratory tests.

Surcharge

In general, addition of a surcharge changes somewhat the slip-line field as obtained by the method of Sokolovski or by trial wedges using curved failure surfaces. Hence Eqs. 13.7 and 13.9 do not apply exactly unless simple geostatic conditions exist; i.e., the thrust should be evaluated separately for each different combination of q_s and γ . However, within the accuracy needed for engineering computations (and keeping in mind the uncertainty as to just what is an "exact" solution) Eqs. 13.7 and 13.9 may still be used together with values of K_a or K_p computed for zero surcharge.

13.5 ACTIVE THRUST AND PASSIVE RESISTANCE FOR OTHER CONDITIONS

The foregoing sections have given results which can be applied to simple retaining walls, and, more important, they have illustrated the methods that can be used to handle more complicated situations.

Active thrust from a homogeneous backfill generally can be evaluated with reasonable accuracy using Eq. 13.7. For relatively simple boundary conditions, values of K_a can be obtained from tables, charts, and formulas so that it usually is not necessary to go through a series of trial wedge computations. Figure 13.21 gives a formula (Eq. 13.12) applicable for inclined retaining walls and backfills, including the effect of wall friction. The

coefficient of $\frac{1}{2}\gamma H^2$ in this formula is K_a . The direction of P_a is as indicated in the figure. This formula was derived (by Coulomb in 1776!) by the trial wedge procedure using straight failure surfaces, but the general accuracy of the results has been confirmed by calculations using the method of Sokolovski.

Figure 13.22 gives values of K_a for the special case of zero wall friction. This table can be used to estimate the thrust for the case of wall friction, as is illustrated in Example 13.10. Example 13.11 shows the application of the active stress coefficients to a problem with surcharge. Note that q_s in Eq. 13.7 is the surcharge per horizontal area regardless of the slope of the backfill.

Similarly, Eq. 13.9 may be used to evaluate passive resistance in more complicated problems. The trial

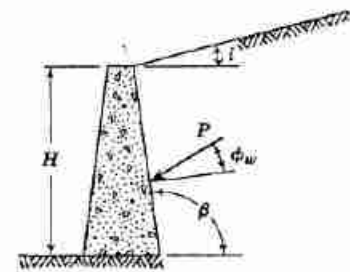


Fig. 13.21 Coulomb equation for sloping backfill and wall friction:

$$P_a = \frac{1}{2}\gamma H^2 \left\{ \frac{\csc \beta \sin (\beta - \phi)}{\sqrt{\sin (\beta + \phi_w) + \frac{\sin (\phi + \phi_w) \sin (\phi - i)}{\sin (\beta - i)}}} \right\}^2 \tag{13.12}$$

$i =$		-30°	-12°	± 0	$+12^\circ$ 1:4.7	$+30^\circ$ 1:1.7
$\phi = 20^\circ$	$\beta' = +20^\circ$		0.57	0.65	0.81	
	$\beta' = +10^\circ$		0.50	0.55	0.68	
	$\beta' = \pm 0^\circ$		0.44	0.49	0.60	
	$\beta' = -10^\circ$		0.38	0.42	0.50	
	$\beta' = -20^\circ$		0.32	0.35	0.40	
$\phi = 30^\circ$	$\beta' = +20^\circ$	0.34	0.43	0.50	0.59	1.17
	$\beta' = +10^\circ$	0.30	0.36	0.41	0.48	0.92
	$\beta' = \pm 0^\circ$	0.26	0.30	0.33	0.38	0.75
	$\beta' = -10^\circ$	0.22	0.25	0.27	0.31	0.61
	$\beta' = -20^\circ$	0.18	0.20	0.21	0.24	0.50
$\phi = 40^\circ$	$\beta' = +20^\circ$	0.27	0.33	0.38	0.43	0.59
	$\beta' = +10^\circ$	0.22	0.26	0.29	0.32	0.43
	$\beta' = \pm 0^\circ$	0.18	0.20	0.22	0.24	0.32
	$\beta' = -10^\circ$	0.13	0.15	0.16	0.17	0.24
	$\beta' = -20^\circ$	0.10	0.10	0.11	0.12	0.16

for $\phi_w = 0$; $\beta' = \beta - 9^\circ$

Fig. 13.22. Coefficient of active stress as function of inclination of wall and backfill.

wedge or Sokolovski method must usually be used to find K_a . These methods may also be employed to find either active thrust of passive resistance for more complicated situations such as stratified backfills, irregularly shaped backfills or walls, nonuniform surcharge, etc. These applications in connection with gravity retaining walls are discussed in Huntington (1957). Application of Kötter's equation to complex problems involving other types of retaining structures is given by Hansen (1953).

General Evaluation of Limiting Equilibrium Solutions

It has already been noted that the methods used to obtain the solutions given in Sections 13.3 and 13.4 are not exact in a mathematical sense. That is, it cannot be proved by mathematics alone that these solutions give a unique solution for the assumed boundary conditions.

A complete, exact solution for an active or passive condition of limiting equilibrium must meet the following five conditions:

1. Each point within the soil mass must be in equilibrium. Hence the pattern of stresses must satisfy the differential equations of equilibrium, Eqs. 13.10.
2. The Mohr-Coulomb failure condition must not be violated at any point; for any plane through any

point,

$$\tau_0 \leq c + \sigma_0 \tan \phi \quad (13.13)$$

3. The strains that occur must be related to the stresses through a stress-strain relationship suitable for the soil.
4. The strains that occur at each point must be compatible with the strains at all surrounding points.
5. The stresses within the soil must be in equilibrium with the stresses applied to the soil.

The requirement of using a suitable stress-strain relationship imposes the greatest obstacle for obtaining an exact solution. It is necessary to consider the strains that occur once the failure condition is reached (such as the volume increase which accompanies shear distortion) as well as the strains for stresses less than failure. Progress has been made in developing methods for handling such complex stress-strain relationships, e.g., Christian (1966). Almost all limiting equilibrium solutions assume that soil is rigid-plastic, which means that there are no strains at any point until the failure condition is fulfilled. Haythornthwaite (1961) discusses the general theory of limiting equilibrium in rigid-plastic materials obeying the Mohr-Coulomb failure law. Upper and lower bound theorems have been developed. However, in view of the uncertainty as to a proper stress-strain relationship, the

► Example 13.10.

Given: Retaining wall and backfill as shown in Fig. E13.10-1.

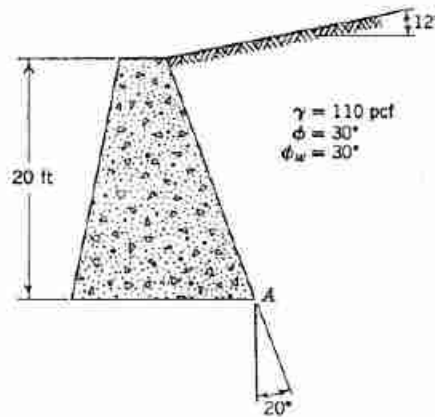


Fig. E13.10-1

Find: Moment of active thrust about point A.

Solution Using Eq. 13.12.

$$i = 12^\circ \quad \beta = 110^\circ$$

$$\csc 110^\circ \sin 80^\circ = \frac{\sin 80^\circ}{\sin 70^\circ} = 1.049$$

$$\sqrt{\sin 140^\circ} = 0.803$$

$$\sqrt{\frac{\sin 60^\circ \sin 28^\circ}{\sin 98^\circ}} = \sqrt{\frac{0.866 \times 0.470}{0.990}} = 0.641$$

$$P_a = \frac{1}{2}(110)(20)^2 \left[\frac{1.049}{0.803 + 0.641} \right]^2 = 22,000(0.528) = 11,600 \text{ lb/ft}$$

Normal component of P_a :

$$P_a \cos 30^\circ = 10,050 \text{ lb/ft}$$

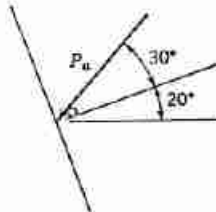


Fig. E13.10-2

P_a acts $\frac{1}{3}$ of way up wall, or at slant distance of 7.1 ft above base (see Fig. E13.10-2).

Moment of P_a about point A = $10,050 \times 7.1 = 71,400 \text{ lb-ft/ft}$.

Approximate Solution Using Fig. 13.22. Use K_a for $\phi_w = 0$, but incline P_a at $\phi_w = 30^\circ$ to normal to wall.

$K_a = 0.59$ instead of 0.528 above, so that moment is overestimated by 12%. ◀

► Example 13.11

Given. Retaining wall and backfill as shown in Fig. E13.11-1. Surcharge = 500 lb/ft² of slope.

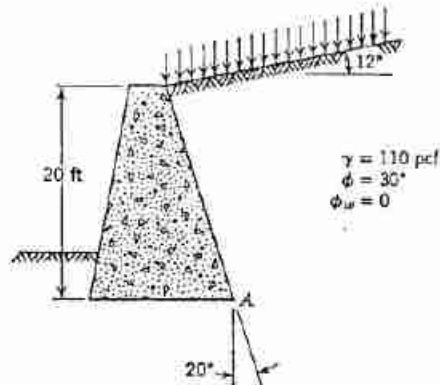


Fig. E13.11-1

Find. Moment of active thrust about point *A*.

Solution. See Fig. E13.11-2.

$$q_s = 500/\cos 12^\circ = 511 \text{ lb/horizontal ft}^2$$

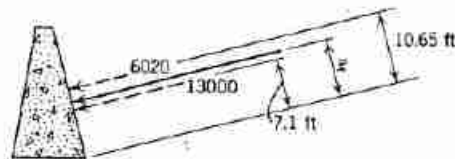


Fig. E13.11-2

From Fig. 13.22

$$K_a = 0.59$$

$$P_a = \frac{1}{2}(0.59)(110)(20)^2 + (0.59)(511)(20) = 13,000 + 6020 = 19,020 \text{ lb/ft of wall}$$

$$\text{Slant height of wall} = \frac{20}{\cos 20^\circ} = 21.3 \text{ ft}$$

$$\bar{x} = \frac{(13,000)(7.1) + (6020)(10.65)}{13,000 + 6020} = 8.23 \text{ ft}$$

$$\text{Moment about point } A = 19,020(8.23) = 157,000 \text{ lb-ft/ft}$$

applicability of these theorems is uncertain. The development of methods for handling more realistic stress-strain relationships deserves much more attention.

Even when a rigid-plastic material is assumed there still are great difficulties. It is difficult to ensure that Eqs. 13.10 and 13.13 are fulfilled throughout the soil mass. Most solutions prove that these conditions are satisfied only in a limited portion of the mass within the failure zone. Even within these zones there is disagreement on the relationship between stress and strain because of the necessity of accounting for the volume changes that

accompany shear strains, and hence there is uncertainty as to whether the strains associated with the stresses are compatible, or *kinematically admissible*.

In addition to these fundamental difficulties, the equations that must be solved (Kötter's equation) are complicated, and contact with physical reality is lost while carrying out the required numerical integrations. Whereas such solutions have received considerable attention in Europe, in the Americas the tendency has been to use the simpler trial wedge method. The solutions of Sokolovski and Hansen, which deserve more attention

► Example 13.12

Given. Retaining wall as shown in Fig. E13.12-1.

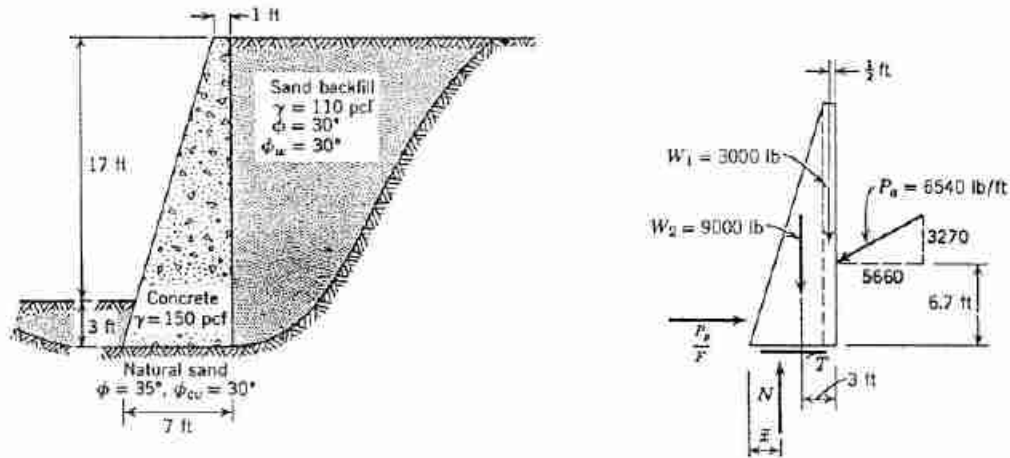


Fig. E13.12-1

Find. Adequacy of wall.

Solution. The first step is to determine the active thrust; see Example 13.8. The next step is to compute the weights:

$$W_1 = (1)(20)(150) = 3000 \text{ lb/ft}$$

$$W_2 = \frac{1}{2}(6)(20)(150) = 9000 \text{ lb/ft}$$

Next N and F are computed:

$$N = 9000 + 3000 + 3270 = 15,270 \text{ lb/ft}$$

$$\text{Overturning moment} = 5660(6.67) - 3270(7) = 37,800 - 22,900 = 14,900$$

$$\text{Moment of weight} = (6.5)(3000) + (4)(9000) = 19,500 + 36,000 = 55,500$$

$$\text{Ratio} = 3.73 \quad \underline{\text{OK}}$$

$$\bar{x} = \frac{55,500 - 14,900}{15,270} = \frac{40,600}{15,270} = 2.66 \text{ ft} \quad \underline{\text{OK}}$$

The location of N shown in Fig. E13.12-2.

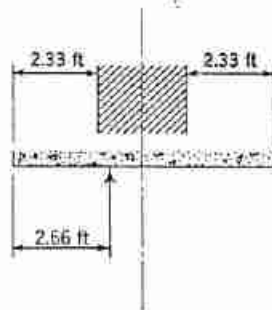


Fig. E13.12-2

Example 13.12 (continued)

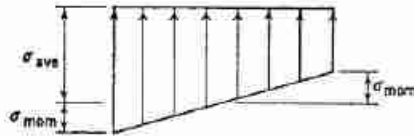


Fig. E13.12-3

Next the bearing stress is computed. The average bearing stress is $15,270/7 = 2180$ psf. Assuming that the bearing stress is distributed linearly, the maximum stress can be found (see Fig. E13.12-3), since

$$\sigma_{\text{mom}} = \frac{M}{S}$$

where

$$M = \text{moment about } \bar{x} = 15,270(3.5 - 2.66) = 12,820 \text{ lb-ft/ft}$$

$$S = \text{section modulus} = \frac{1}{6}B^2 = \frac{1}{6}(7)^2 = 8.17 \text{ ft}^2$$

where B is width of base

$$\sigma_{\text{mom}} = \frac{12,820}{8.17} = 1570 \text{ psf}$$

$$\text{Maximum stress} = 2180 + 1570 = 3750 \text{ psf}$$

Finally, the resistance to horizontal sliding is checked. Assuming passive resistance without wall friction,

$$K_p = 3$$

$$P_p = \frac{1}{2}(110)(3^2)(3) = 1500 \text{ lb/ft}$$

With reduction factor of 2,

$$\frac{P_p}{F} = 750 \text{ lb/ft}$$

$$T = 5660 - 750 = 4910 \text{ lb/ft}$$

$$N \tan 30^\circ = 8810 \text{ lb/ft}$$

$$\frac{N \tan \phi_{\text{av}}}{T} = 1.79 < 2 \quad \underline{\text{not OK}}$$

Ignoring passive resistance

$$T = 5660 \text{ lb/ft}$$

$$\frac{N \tan \phi_{\text{av}}}{T} = 1.55 > 1.5 \quad \underline{\text{OK}}$$

than they have received, are still not exact in the sense that they do not fulfill all of the five conditions previously outlined.

Despite these many theoretical difficulties, the solutions presented in Sections 13.3 to 13.5 are useful in practical work. Their applicability has been verified in a limited number of situations by measurements of stresses and thrusts in large-scale model tests and in actual situations. After being verified by these observations, the results can be used with reason to predict stresses and thrusts in situations for which there are no actual data. For active conditions, the results presented in these sections will give the active thrust within $\pm 10\%$ provided that the friction angle is known accurately. For passive conditions, the uncertainty is greater—perhaps $\pm 20\%$ —especially if wall friction is present.

13.6 EXAMPLE OF DESIGN OF GRAVITY RETAINING WALL

In order to illustrate the design procedure for a gravity retaining wall, let us consider the problem shown in Example 13.12. The following steps should be noted:

1. The active thrust is computed using a value of K_a selected from Fig. 13.18 for the given ϕ and ϕ_{av} . This calculation is made in Example 13.8. This computation, of course, presumes that the failure surface passes entirely through the backfill rather than through the natural sand. It is convenient to break this thrust up into its vertical and horizontal components.
2. The weight of the wall is computed, breaking the

actual geometrical shape up into two simple shapes to facilitate the computation.

3. The bearing force N is computed. The location of the line of action of N is also computed. If \bar{x} were less than zero, obviously the wall would not be stable. That is, such a result would mean that the overturning moment from the active thrust exceeds the resisting moment of the weight. Different engineers use different design rules to guard against such a possibility. One rule which also is used to limit the maximum bearing stress (discussed later) is that N should be within the middle third of the base. An alternate rule is to require that the ratio of resisting to overturning moment should be 1.5 or greater. This second rule is in effect a safety factor against a poor estimate of the active thrust. The wall of the example is adequate by either of these criteria.
4. The next question is: Can the natural sand safely support the vertical force N ? A full answer to this question must wait until after we have studied bearing capacity in Chapter 14. An average bearing stress of 2180 psf (or about 1 TSF) will usually be tolerable. Because the resultant N does not act exactly in the center of the base, the maximum bearing stress at the toe will exceed the average bearing stress. As will be explained in Chapter 14, if N acts within the middle third of the base the maximum stress will be less than twice the average stress and will also be tolerable.
5. Different engineers also use different rules to check for sliding resistance. In one rule the passive resistance is considered, and the combined sliding resistance and passive resistance must exceed the horizontal component of thrust by a safety factor of two or greater. In a second and more common rule the passive resistance is ignored, and it is required that the resistance to sliding be at least 1.5 times the horizontal component of active thrust. The wall is adequate since it fulfills the second of these rules.

In this example, the stated safety factors represent the engineering judgment of engineers regarding the certainty with which the various forces and resistances can be estimated. By these standards the wall is barely adequate. Either smaller or greater safety factors may be required depending upon the circumstances of each individual problem.

The rest of this section discusses further several of the most important points.

Justification for Use of Active Thrust

In earlier sections, it has been pointed out that the active thrust is the minimum possible thrust that the soil may exert against a retaining wall. This question then

arises: Should not such a wall be designed for the possibility that some larger thrust exists?

The first answer to this question is: As long as the backfill is a dry granular soil whose friction angle is known, the thrust against a gravity retaining wall generally does equal the theoretical active thrust. This was demonstrated by the very careful tests by Terzaghi in the 1920s. In these tests, the walls were held against horizontal movement as the backfill was placed and the thrust against the wall was measured. As expected, this thrust was greater than the active thrust. Then the walls were released and permitted to move horizontally or to rotate. After a movement of the top of the wall equal to only 0.001 times the height of the wall, the thrust had dropped to its theoretical active value.⁵ This is a very small amount of movement (the angular rotation is only 0.06°), and it must be expected that a gravity retaining wall will rotate this much as the backfill is placed against it.

Even so, if, for some reason, the thrust against a retaining wall were greater than the active value, it would not mean that the wall potentially was in trouble. On the contrary, it would mean that the earth underlying the wall is much stronger than it need be. Long before a wall can fail, it must move enough to mobilize the shear strength of the soil and to drop the thrust to its active value. In other words, the strength of the backfill behind a retaining wall will be mobilized long before the shear strength of the soil that supports the wall is mobilized. Under such circumstances, it makes great sense to design the wall for the active thrust, and to use a safety factor on the quantity in the design about which the designer knows least: the bearing capacity of the soil supporting the wall.

Having emphasized how small the wall movements are, we now must turn around and emphasize how large they can be. If a retaining wall is 20 ft high, a rotation of 1 in 1000 means a horizontal displacement of $\frac{1}{4}$ in. at the top of the wall. In most situations where gravity retaining walls are used—highway or railway cuts, etc.—this amount of movement (or even several times this amount of movement) literally is of no consequence. However, there are problems where this amount of movement might cause trouble. A classic situation is a wall used for the abutment of a bridge. If the wall has been designed for the active thrust, and if the backfill is placed after the bridge is set in place, then there must be sufficient clearance between the wall and the girders to accommodate the outward movement of the wall.

There are numerous retaining structures that resemble gravity retaining walls, but often these should not be designed on the basis of active thrust. A braced

⁵ In Section 13.2 it was stated that a horizontal strain of about 0.005 is required in passing from the at rest to the active condition. The horizontal width of the failure wedge is $h \cot(45 + \phi/2)$ or about $H/2$. Hence the horizontal displacement of the wall would be $0.0025H$. This behavior of sand during triaxial tests is in good agreement with Terzaghi's results.

excavation (Section 13.7) and sometimes anchored bulkheads (Section 13.8) are examples. The cantilever type of retaining wall shown in Fig. 13.23 is another example. Such walls, which have reinforcing steel, are sometimes used where space restrictions preclude the use of massive gravity walls. If a cantilever wall rests upon very firm soil so that the foundation experiences little or no sliding or rotation, active conditions within the backfill can develop only by bending of the cantilever. The amount of bending necessary to develop the active condition may cause severe cracking of the concrete and yielding of the steel. Cantilever retaining walls are often designed on the basis of K_0 rather than K_a .

The wall surrounding the basement of a building is an example of an unyielding wall. The magnitude of the stresses acting against a foundation wall will depend largely upon the degree of compaction given to the backfill. If a clean sand is dumped against the wall without compaction, the horizontal stresses may be almost as small as the active stresses. If light compaction is used, such as simply running a bulldozer over the several layers of the backfill, the horizontal stresses will likely equal the at-rest stress. With heavy compaction, stresses approaching the passive stresses might be developed. The usual practice is to design foundation walls for the at-rest stress; i.e., for a horizontal stress of approximately one-half the vertical stress. When a wall is designed on this basis, heavy compaction of the backfill must be avoided. Otherwise the foundation wall may be cracked.

Choice of Friction Angle for Backfill

The peak friction angle of the backfill should be used for design computations. If the granular soil is simply dumped into place, this angle will be approximately ϕ_{cr} . Usually, however, backfill is given at least nominal compaction by a bulldozer, so that a medium dense state is generally achieved. The increase in friction angle achieved by moderate compaction will offset the disadvantageous increase in unit weight. However, intense compaction seldom is justified, since there is the danger that large outward wall movements will occur during compaction.

Role of Wall Friction

Wall friction greatly reduces the horizontal thrust and especially the overturning moment against a wall. The wall in Example 13.12 would not be adequate if it were not for wall friction (see Problem 13.8). Generally it is appropriate to take advantage of the beneficial effects of wall friction, since the downward drag will develop as the wall moves outward. However, an engineer must satisfy himself on this point in each case.

Evaluation of Passive Thrust

The horizontal width of the passive failure wedge is $H' \tan(45 + \phi/2)$, or about $2H'$, where H' is the depth

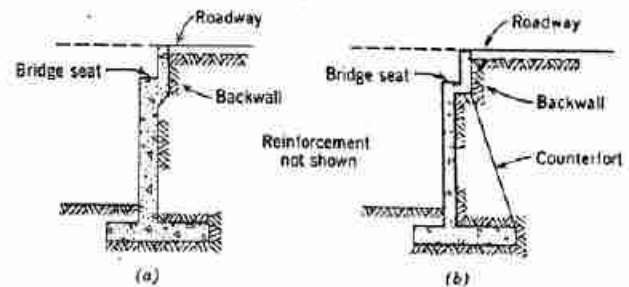


Fig. 13.23 Counterfort and cantilever retaining walls. (a) Cantilever. (b) Counterfort. (From Huntington, 1957.)

to which the wall is embedded. For a loose sand, from 10 to 20% strain might be needed to mobilize full passive resistance. This strain would correspond to a displacement of $0.2H'$ to $0.3H'$. Thus for $H' = 3$ ft, as in our retaining wall example, as much as a foot of horizontal displacement might be necessary in order to mobilize full passive thrust at the toe. This is more base displacement than is desirable, and hence a relatively large safety factor is used whenever passive resistance is taken into consideration. As indicated by the curve in Fig. 13.7, not much displacement is needed to mobilize one-half of the full thrust. Usually wall friction in the passive zone is ignored, thus adding to the conservatism. If wall friction is included, the vertical component of passive thrust will cause a decrease in N , and this effect should be considered.

Some Design Suggestions

The foregoing details have been included to indicate the type of considerations that enter into design. Still other details may be found in Huntington (1957). Clearly the making of an adequate design requires much more "engineering" than simply the calculation of active thrust.

Use of cinders for backfill is sometimes considered as a means of reducing active thrust and economizing on design. Cinders have a small unit weight (50 pcf) and yet have a friction angle as large as sand.

Sloping the wall in contact with the soil leads to a more favorable location of the resultant weight of the wall relative to the outside edge of the wall, and may thus make it possible to use a narrower base and yet keep the resultant N within the middle third of the base. This saving must be compared with the cost of added formwork.

13.7 BRACED EXCAVATIONS

A gravity retaining wall is a permanent structure, used when an excavation is permanent. In many cases, however, an excavation is only temporary. Examples are

excavations for buildings or subways. Here the excavations are filled with a structure which then permanently retains the surrounding earth. If the temporary excavation is made in sand, the walls of the excavation must be supported during construction of the building by a system of bracing, as shown in Fig. 1.12*b*. The design of bracing for excavations will be discussed in some detail to illustrate one situation in which it may not be proper to design on the basis of active thrust.

Figure 13.24 shows two common systems for installing the bracing. In one system, *sheet piling* (a continuous line of piles) is driven in advance of excavation. As excavation proceeds, horizontal members known as *wales* are placed against the sheet piling, and additional

horizontal members called *struts* are placed across the excavation and wedged against the wales. In the second general system, vertical members called *soldier beams* are driven at intervals along the line of excavation. As excavation proceeds, horizontal wooden planks called *lagging* are inserted against the earth and are supported by the soldier beams. Wales are again placed horizontally across several soldier beams, and struts are wedged in place between the opposite walls of the excavation.

There are, of course, many variations on these basic systems, depending on the size of the excavated area and the preferences of the individual contractor. Figure 13.25 shows struts braced against a block in the center of the foundation instead of against the opposite wall. There

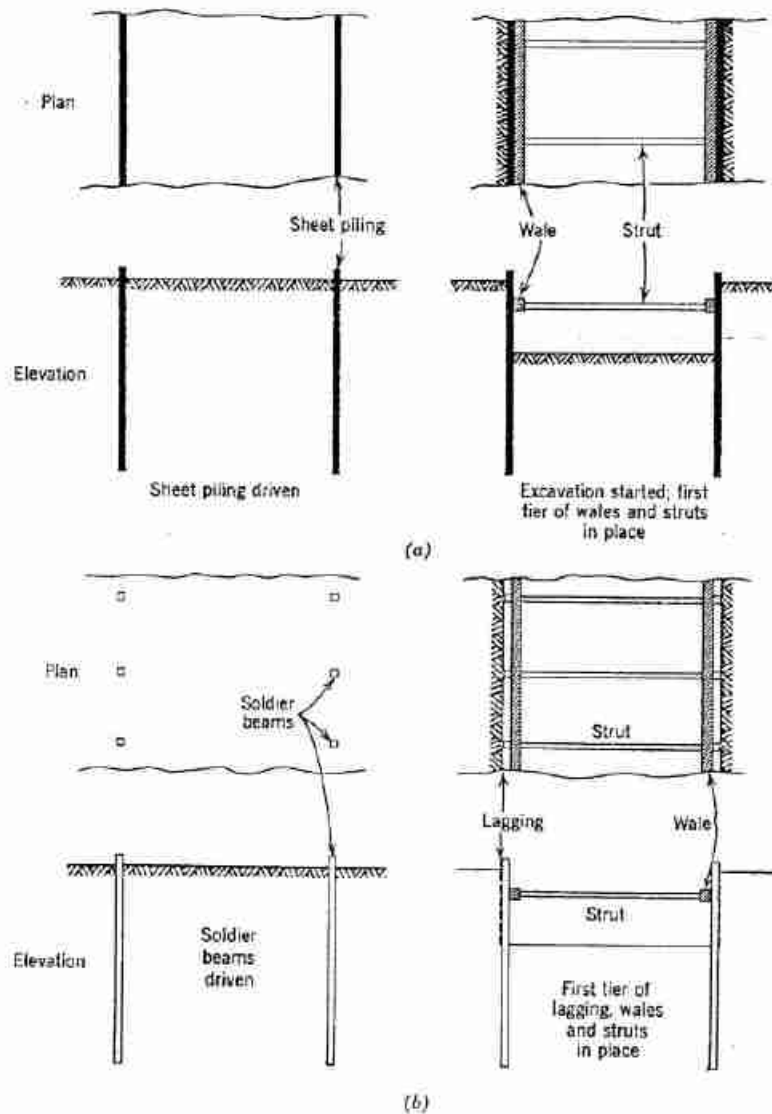


Fig. 13.24 Systems for installing bracing. (a) Braced excavation using sheet piling. (b) Braced excavation using soldier beams and lagging.



Fig. 13.25 Excavation for M.I.T. Center for Advanced Engineering Study.

is increasing use of *tiebacks*, anchors driven through the wall into the earth behind the wall. The use of tiebacks keeps the excavation free of obstacles.

Form and Magnitude of Stress against Bracing

Several field observations⁶ have shown that the stress against the bracing (when the bracing is placed against a sandy soil) has the distribution shown in Fig. 13.26. Note that this distribution is quite different from the active stress distribution. Moreover, measurements have also indicated that the total thrust against the bracing may be somewhat larger than the thrust predicted for the active condition.

The observed pattern of stress may be understood if we examine the way in which the soil deforms as the excavation proceeds (see Fig. 13.27). The topmost strut, once installed and wedged tightly against the wale, will not permit any further appreciable horizontal displacement of the soil at that elevation. As soil is excavated at some lower elevation, the remaining soil at that lower elevation will move toward the excavation until it is in turn supported by a strut. Thus the overall pattern of soil movement is one of rotation about some point near the top of

⁶ Terzaghi and Peck (1967) summarize the results of field measurements from braced excavations.

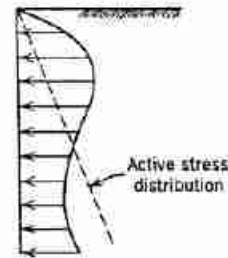


Fig. 13.26 Typical distribution of stress against bracing system.

the bracing. The soil near the top of the bracing is not allowed to move outward as is necessary to mobilize full shear resistance within the soil. Rather, the soil at a lower elevation exerts a drag type of shear force upon the overlying soil. Hence the soil near the top of the wall is more nearly in a passive state of stress than in an active state of stress.

Although the distribution of stress against the bracing is quite different than in the classical active stress situation, it is not necessarily true that the total thrust against the wall differs greatly from that predicted for the active condition. As long as full shear resistance is mobilized along the bottom boundary of the failure wedge, the total thrust exerted against the soil by the retaining structure is much the same whether the retaining structure is a gravity wall or a bracing system. However, the

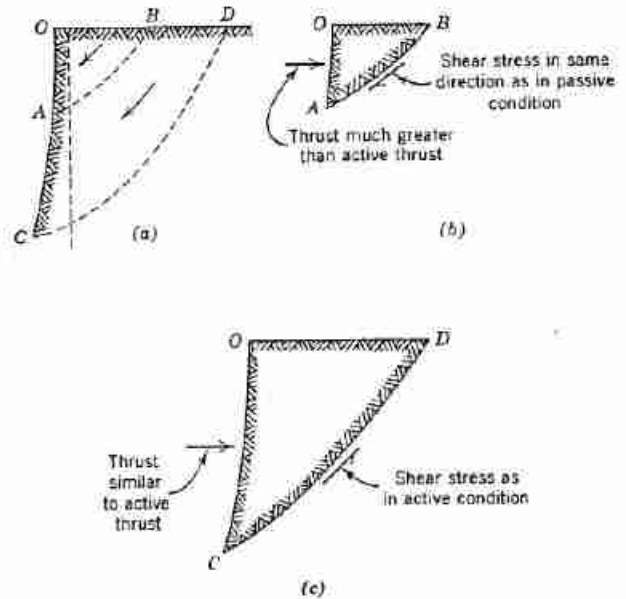


Fig. 13.27 Movements and stresses within soil. (a) Soil movement (greatly exaggerated). (b) Stresses on wedge OAB. (c) Stresses on wedge OCD.

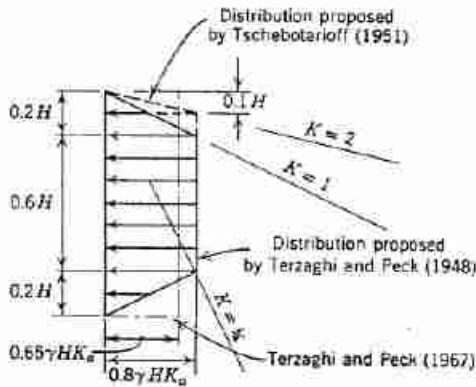


Fig. 13.28 Stress distribution used for design of bracing system.

pattern of deformation of the soil will influence somewhat the location of the critical theoretical failure line, and hence the thrust will change somewhat with the retaining system (Hansen, 1953). The total thrust against a braced wall may be 10–15% greater than that against a gravity wall.

The state of stress in the soil behind a braced cut has often been described as an *arching active* condition.

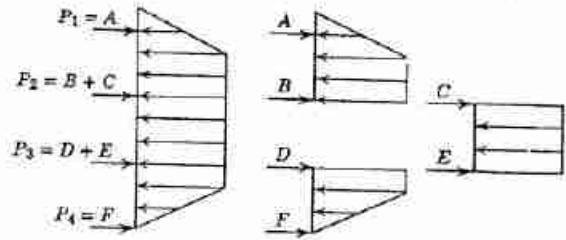


Fig. 13.29 Computation of strut loads.

Design Procedures

For purposes of designing a bracing system it usually is assumed that the distribution of stress against the sheeting or lagging is as shown in Fig. 13.28. The method of computing the strut loads from this distribution is indicated in Fig. 13.29 and is illustrated in Example 13.13.

According to the stress distribution proposed by Terzaghi and Peck (1948), the total thrust is $0.64\gamma H^2 K_a$, or 28% greater than the active thrust. Thus the proposed design stress distribution recognizes that the total thrust may exceed the active thrust. However, there is a second (and more important) reason why the total design thrust exceeds the active thrust. The actual stress distribution

► **Example 13.13**

Given. Excavation and bracing system as shown in Fig. E13.13-1.

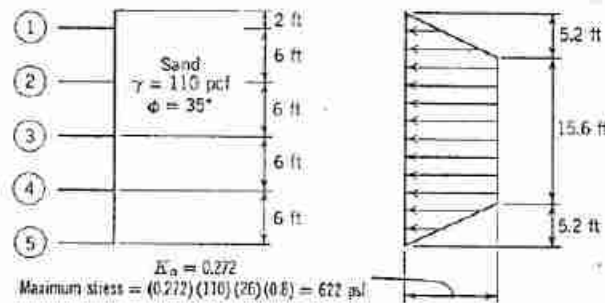


Fig. E13.13-1

Find. Design strut loads.

Solution. From Table 13.1, $K_a = 0.272$. Maximum stress is

$$(0.272)(110)(26)(0.8) = 622 \text{ psf}$$

From Fig. E13.13-2:

$$P_1(6) = 1618(4.53) + (1741)(1.40) = 7320 + 2440 = 9760 \text{ lb}$$

$$P_1 = 1628 \text{ lb/ft}$$

$$B = 1741 + 1618 - 1628 = 1731 \text{ lb/ft}$$

Example 13.13 (continued)

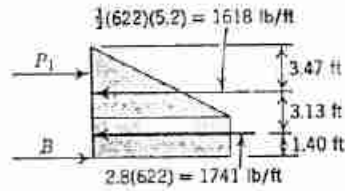


Fig. E13.13-2

From Fig. E13.13-3:

$$C = D = 1865 \text{ lb/ft}$$

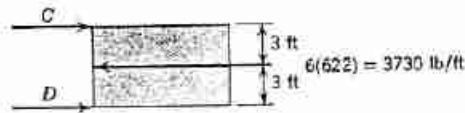


Fig. E13.13-3

From Fig. E13.13-4:

$$P_3(6) = 498(0.4) + (1618)(2.53) = 200 + 4090 = 4290 \text{ lb}$$

$$P_2 = 715 \text{ lb/ft}$$

$$E = 1618 + 498 - 715 = 1401 \text{ lb/ft}$$

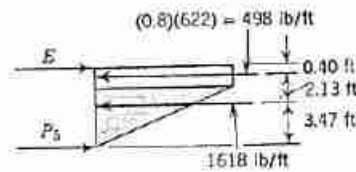


Fig. E13.13-4

Assembling these results:

$$P_1 = 1628 \text{ lb/ft}$$

$$P_2 = 1731 + 1865 = 3596 \text{ lb/ft}$$

$$P_3 = 2(1865) = 3730 \text{ lb/ft}$$

$$P_4 = 1865 + 1401 = 3266 \text{ lb/ft}$$

$$P_5 = 715 \text{ lb/ft}$$

If struts are located at 6-ft intervals along wall, then design strut loads are

$$P_1 = 9800 \text{ lb}$$

$$P_2 = 21,600 \text{ lb}$$

$$P_3 = 22,400 \text{ lb}$$

$$P_4 = 19,600 \text{ lb}$$

$$P_5 = 4300 \text{ lb}$$

Struts should be designed for a safety factor appropriate for the material used for the strut.

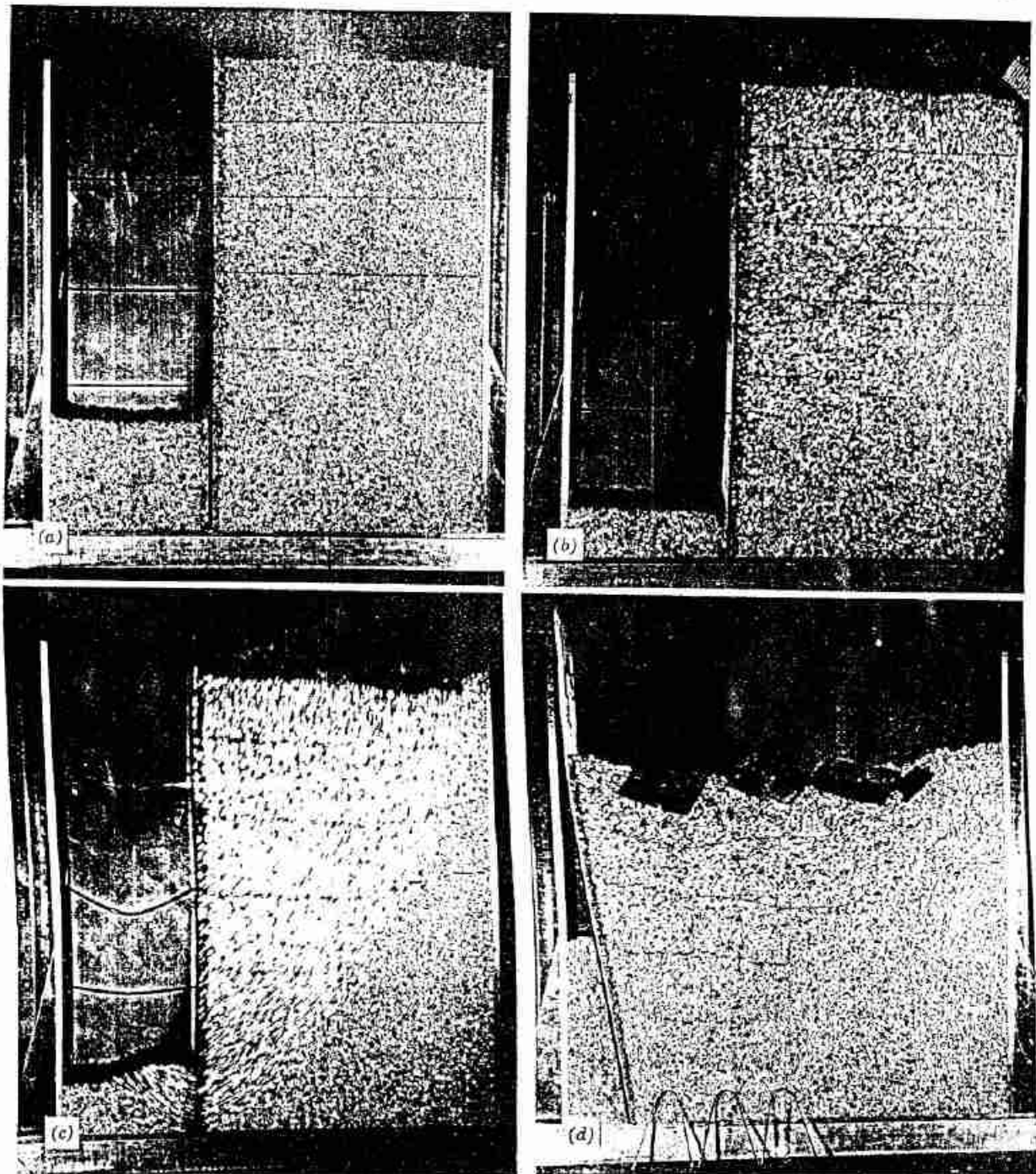


Fig. 13.30 Failure of model of braced excavation. (a) Stable. (b) About to fail. (c) Failing; note motions. (d) After failure.

will change from section to section depending on just how tightly the individual struts are wedged in place. The design stress distribution curve represents an envelope to the various possible actual distributions. Since struts fail in buckling, it is important that no single strut be overstressed. It is not permissible to say that if one strut is overstressed and starts to fail, the overstress will simply be transferred to an adjacent strut. If one strut even starts to buckle, its load-carrying capacity may drop to almost nothing and then the whole bracing system will be in jeopardy. Figure 13.30 illustrates the sudden rapid collapse of a braced excavation as one strut buckles. The use of an envelope to all possible stress distribution curves ensures that each strut will be designed for the largest load which might reach the strut. However, the sum total of the loads in all struts will undoubtedly be less than $0.64\gamma H^2 K_a$.

The two important points with regard to the design of a bracing system are: (a) the uppermost struts⁷ will be subjected to loads much greater than would be predicted from the ordinary active stress distribution; and (b) struts in compression are a brittle system tending to collapse as soon as yielding begins. Limit design is not an appropriate procedure for a brittle system; in contrast, a gravity retaining wall is a ductile system where large foundation movements may occur without loss of foundation strength.

13.8 ANCHORED BULKHEADS

As described and illustrated (Fig. 1.15) in Chapter 1, an anchored bulkhead receives its lateral support from penetration into the foundation soil and from an anchoring system near the top of the wall. The sheet piling must be designed for the shears and bending moments which thus develop. The anchor system must be designed to take the lateral forces required to support the wall.

Anchored bulkheads are often used to form wharves or quays, since the soft soils that usually underlie such waterfront structures are unable to support the weight of massive gravity walls and since the use of anchored bulkheads is generally cheaper than supporting a gravity retaining wall on piles. The design and analysis of anchored bulkheads is a rather complicated subject.

The distribution of stresses from the backfill will depend strongly on the manner in which the wall is constructed. Tschebotarioff (1951) has suggested that we must distinguish among the three cases shown in Fig. 13.31.

1. If backfill is placed after the bulkhead is constructed, the stresses against the bulkhead down to the point of embedment will increase linearly with depth in accordance with the classical theories of active stress.

⁷ The upper struts can receive greater loads at partial excavation than at full excavation.

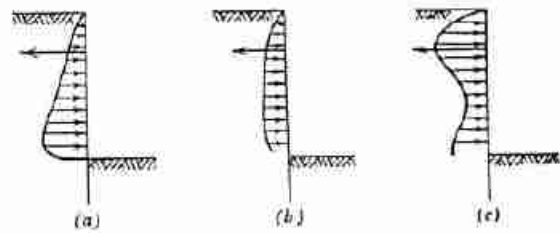


Fig. 13.31 Relation between construction procedure and stress distribution against anchored bulkhead. (a) Backfilling. (b) Dredging with normal yield of anchor. (c) Dredging with unyielding anchor.

2. If the bulkhead is driven into level ground, one side of which is then excavated, the stresses will be more or less uniform with depth—unless the anchor is unusually stiff.
3. If the anchor is unusually stiff, the stress distribution will be similar to that upon a bracing system. This situation might arise if a very heavy member is used for the anchor rod, or if a short rod is attached to a very massive anchor.

Furthermore, the magnitude of the maximum bending moment in the piling is influenced greatly by the distribution of stresses against that part of the piling which is embedded, and the stress conditions in this zone are quite complex. This effect cannot be predicted on the basis of simple theory, although the complex theories of Hansen are useful. Usually, experimental data plus field experience are used as a basis for design. Tschebotarioff (1951) and Rowe (1952) have presented such methods of design.

Often a deadman anchor (Fig. 1.15) is used to support the anchor rod. The design of such an anchor involves an interesting problem in the evaluation of passive resistance.

13.9 STABILITY OF SLOPES

There are many situations in which an earth mass need not be retained by a structure but left as an unretained slope. The inclination of the slope must be flat enough and/or the height low enough for the earth mass to be stable. The same principles of limiting equilibrium mechanics are used to evaluate the stability of an unretained earth mass as for a retained earth mass.

Parts (a) and (b) of Fig. 13.32 show two typical processes by which a slope is formed in a granular soil.⁸ In (a) an embankment is being formed by end dumping from a truck; in (b) ore or sand or some other stockpiled material is dropped from a chute or from the end of a conveyor belt. In both of these situations, the material will tumble down the slope. From time to time during

⁸ A slope can also be formed by excavation, as done for a canal (see, e.g., Fig. 1.14).

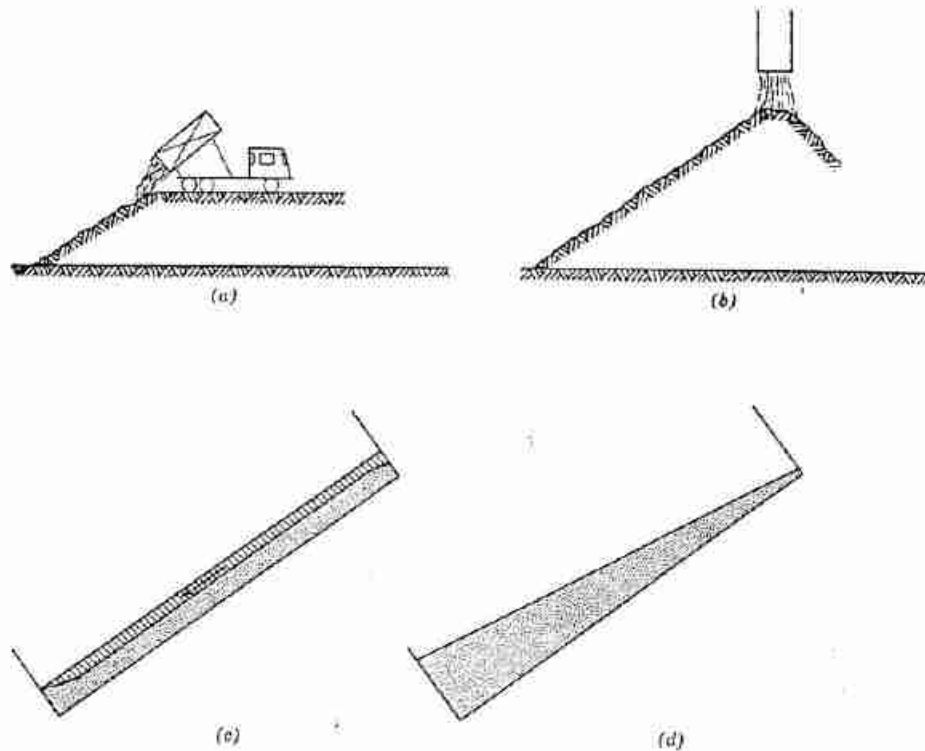


Fig. 13.32 Infinite slope problems. (a) Formation of slope by dumping. (b) Formation of ore pile. (c) Tipping experiment as sliding starts. (d) Tipping experiment after sliding.

dumping, material which has already come to rest on the slope will start moving again; i.e., a mass of material, with a thickness small compared to the height of the slope, will slide down the slope. The inclination of the slope once dumping has ceased—the maximum slope at which the material is stable—is called the *angle of repose*.

The behavior during the tipping experiment depicted in parts (c) and (d) of Fig. 13.32 is similar. As the angle of tipping is gradually increased, individual particles will start to tumble down the slope. Finally, as the angle is increased further, a mass of material will slide as a whole, as indicated in Fig. 13.32c. Once sliding ceases, the slope will have an average inclination roughly equal to the angle of repose for this same sand if dumped.

In all of these situations, the thickness of the unstable moving material is small compared to the height of the slope. In such situations, the slope is called an *infinite slope*. The failure surface is parallel to the slope.

Analysis of Free Body

In order to analyze the stability of this slope, we "cut" a free body element of soil from the slope, as shown in Fig. 13.33. We assume that the slope is very wide in the

direction normal to the cross-section, and consider only the stresses that act in the plane of the cross-section.

In general, there will be stresses on three sides of this free body, as indicated in Fig. 13.33a. However, with an infinite slope it is reasonable to assume that the stresses on the two vertical faces are equal and exactly balance each other. If this were not true, the stresses on vertical faces would change depending on the location along the slope, and such a situation would be inconsistent with the observation that a thin veneer of the whole slope moves as a mass. Thus only the stresses on the face CD , together with the weight of the soil, enter into the equilibrium of the free body.

Part (b) of this figure analyzes the equilibrium of the free body in terms of the total forces T and N acting on the face CD . The result is: when full shear resistance is mobilized and sliding begins, the angle of inclination of the slope should equal the angle of internal friction. According to this analysis, sliding is equally likely to begin at any depth; i.e., the depth of the free body completely cancels out of the result.

Example 13.14 illustrates the computation of the stresses that exist beneath an infinite slope at the angle of repose.

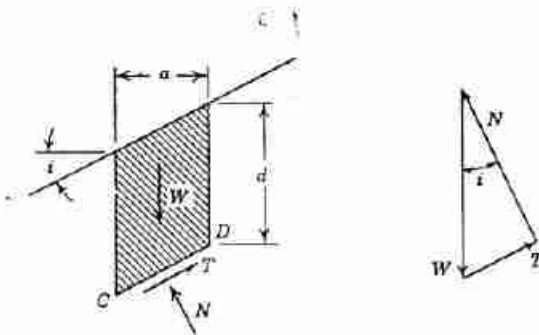
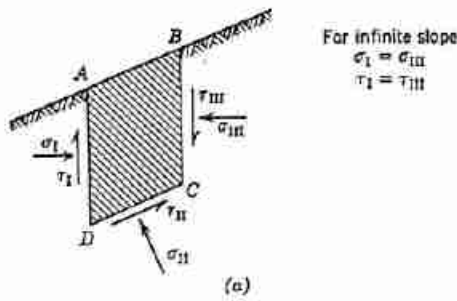


Fig. 13.33 Analysis of infinite slope. (a) Stresses upon element of soil (b) Analysis of equilibrium:

$$\begin{aligned}
 W &= ad\gamma \\
 W - T \sin i - N \cos i &= 0 & N &= W \cos i \\
 T \cos i - N \sin i &= 0 & T &= W \sin i \\
 & & \therefore T &= N \tan i
 \end{aligned}$$

If the full shear resistance is mobilized so that $T = N \tan \phi$, then $i = \phi$.

Note that the vertical stress is not simply equal to the depth multiplied by the unit weight.

Choice of Friction Angle

The slope angle at which sliding commences in the tipping experiment is related to the peak friction angle ϕ^* . Thus the maximum stable slope angle is fundamentally related to the peak friction angle. However, we know that ϕ is very much a function of the void ratio at which the sand exists.

Whenever sand or gravel is dumped the sand generally finds itself in a loose state. For the loose state, ϕ essentially equals ϕ_{lo} . Thus, the angle of repose for dumped sand or gravel is about equal to the angle of internal friction for the loose state, ϕ_{lo} . Typical angles of repose,

² This statement is based on an extrapolation of the results given by Seed and Goodman (1964). In model tests, the small cohesion intercept of a dry soil has some influence on slope stability and determines the actual depth of sliding.

together with the tangents of these angles, have already been listed in Table 11.3.

On the other hand, slopes steeper than the angle of repose can exist in a stable condition. In modern rock fill dams, the fill is carefully compacted as it is dumped in thin layers so as to bring the fill into a dense condition. Hence the friction angle available to resist sliding is greater than the angle of repose.

Safety Factor

The safety factor for an infinite slope usually is defined as

$$FS = \frac{\tan \phi}{\tan i}$$

The only unknown factor in the stability of an infinite slope is the appropriate value for the angle of internal friction. This quantity can be estimated with reasonable accuracy and, furthermore, the consequences of failure of such a slope are slight. Hence the safety factor does not need to be large. Usually an engineer will be conservative in his choice of $\phi = \phi_{lo}$, and will use $FS = 1$.

13.10 SUMMARY OF MAIN POINTS

The main objectives of this chapter have been to illustrate the methods used to calculate active thrust and passive resistance and to illustrate how these calculated forces are used in the design of typical retaining structures. The details of the methods are important, and the student should be competent to carry out an analysis of simple problems by the trial wedge method. In addition, the following concepts should be understood.

1. Limit design can be used for the design of most gravity retaining walls. The active thrust from the backfill is evaluated assuming that full shear resistance is mobilized within the backfill. Resistance is then provided (with an appropriate margin of safety) against the overturning and sliding caused by the active thrust.
2. Compression bracing for excavations should not in general be proportioned by limit design, since such bracing is a brittle system which will fail as soon as any portion becomes overstressed.
3. Other types of retaining structures must be studied carefully to learn how much and what types of movements may occur, and only then should the forces acting on the retaining structures be evaluated.
4. The maximum slope angle in a granular soil is equal to the friction angle of the soil.

PROBLEMS

13.1 A sand backfill has $\gamma = 110$ pcf, $\phi = 30^\circ$, and $K_0 = 0.5$. Construct a p - q diagram showing the K_r and

► Example 13.14

Given. A 30° slope in a sand having $\phi = \phi_{cr} = 30^\circ$. The unit weight is 100 pcf.

Find. The stresses at a depth of 10 ft.

Solution. Referring to Fig. 13.33, the stresses on the failure plane CD are

$$\sigma_{ff} = \frac{N}{a/\cos i} = \gamma d \cos^2 i = 750 \text{ psf}$$

$$\tau_{ff} = \frac{T}{a/\cos i} = \gamma d \sin i \cos i = 433 \text{ psf}$$

The Mohr circle for this condition is shown in Fig. E13.14.

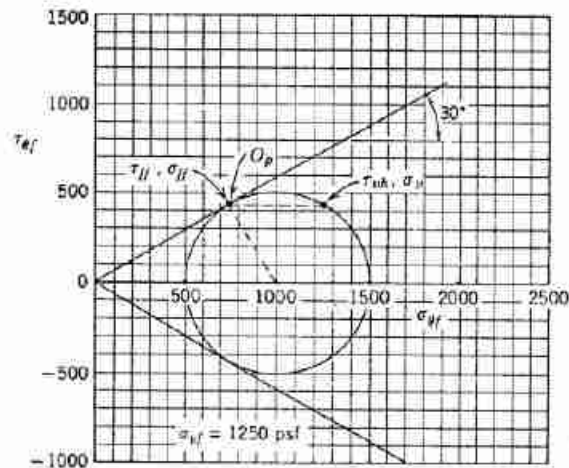


Fig. E13.14

K_0 -lines, and the stress paths for an element of soil at 10 ft depth for:

- Stressing to the active condition.
- Stressing to the passive condition.

Assume that there is zero shear stress on vertical planes.

13.2 From the results for Problem 13.1, what are the horizontal stresses for the active and passive conditions? How do these stresses compare with the average active (Example 13.2) and passive (Example 13.6, ignoring surcharge) stresses for a wall 20 ft high?

13.3 Design a gravity retaining wall, 15 ft high, to retain a backfill with $\gamma = 105$ pcf and $\phi = 40^\circ$ and having a horizontal surface. Assume that $\phi_w = 30^\circ$ and that the coefficient of friction on the base of the wall is 0.5. Neglect passive resistance at the toe, and make the resultant force fall within the middle third of the base.

13.4 Draw the Mohr circles for the active and passive conditions of Problem 13.1.

13.5 Referring to Example 13.5, construct the force polygon for $\theta = 65^\circ$.

13.6 Referring to Example 13.7, construct the force polygons for $\theta = 25^\circ$ and 35° .

13.7 Referring to Example 13.8, construct the force polygon for $\theta = 55^\circ$.

13.8 Evaluate the adequacy of the wall in Example 13.12, assuming $\phi_w = 0$.

13.9 A wall, which supports a horizontal backfill with $\gamma = 110$ pcf and $\phi = 35^\circ$, is to be used to provide a reaction for a horizontal load of 10,000 lb per ft of wall. If the wall is to have a safety factor of 2 against failure, how high must the wall be? At what depth below the top of the wall should the load be placed?

13.10 A braced cut, holding back soil with $\gamma = 105$ pcf and $\phi = 30^\circ$, is 20 ft high. Struts, on 6 ft centers horizontally, are located at depths of 2 ft, 8 ft, 14 ft, and 20 ft. Compute the strut loads.

13.11 Repeat Problem 13.3 for a case where the backfill is sloped at 1 vertical on 3 horizontal.

13.12 Repeat Problem 13.3 for a case where the backfill carries a surcharge of 400 psf.

13.13 A sand having $\phi = 35^\circ$ is sloped at 35° . Find the normal and shear stresses on horizontal and vertical planes at a depth of 15 ft (measured vertically) beneath the slope. Are either of these planes failure planes?

13.14 What should the design slope be for the sand whose friction angle behavior is given in Fig. 10.18, if the sand is to be poorly compacted?

CHAPTER 14

Shallow Foundations

14.1 GENERAL BEHAVIOR OF SHALLOW FOUNDATIONS

As described in Chapter 1, the term "shallow foundation" refers to a structure that is supported by the soil lying immediately beneath the structure. *Individual footings*, usually rectangular in plan view, are the most common shallow foundations for columns, whereas *strip footings* are used to support walls. In some instances structures are supported by *mats*.

The design of foundations is a trial-and-error procedure. A type of foundation and trial dimensions are selected. Analyses are then made to ascertain the adequacy of the proposed foundation. The foundation may be found to be adequate, in which case a check should be made to determine whether a cheaper foundation might also be adequate. If the proposed foundation is found to be inadequate, a larger foundation is considered. In some cases it may be impossible to design an adequate shallow foundation upon the given soil, in which case either deep foundations (Chapter 33) or improvement of soil (Chapter 34) must be considered.

The selection of a trial foundation and trial dimensions is often guided by tables of allowable bearing stresses. Most building codes contain such tables, based upon general experience with soils in the area to which the code applies. These allowable stresses usually lead to conservative designs for low buildings supported on spread footings, but they may lead to unconservative designs for unusual or large structures. In many cases a careful study will show that bearing stresses larger than those given by codes can be safely used.

This chapter discusses the "adequacy" of a foundation. The same general principles that apply to the analysis of settlement and stability of shallow foundations for structures also apply to embankments and dams on soft foundations. For a discussion of the many practical details and economic considerations involved in the design of a foundation the reader is referred to Teng (1962) and

U.S. Navy (1962), and for a discussion of foundation construction to Carson (1965).

This chapter does not consider shallow foundations subjected to dynamic loads; they are treated in Chapter 15.

Behavior of Footing on Elastoplastic Material

To help understand the general behavior of shallow foundations, consider the situation shown in Fig. 14.1, where a stress increment Δq_s is applied to the surface of an idealized material.¹ This material is assumed to be elastic until the maximum shear stress τ_{max} reaches the value c . Once this condition is reached, further shear distortion can occur at constant shear stress. This material is assumed to be perfectly elastic with regard to volume change.

As Δq_s is increased the whole body first behaves elastically, and the stresses and settlements can be predicted

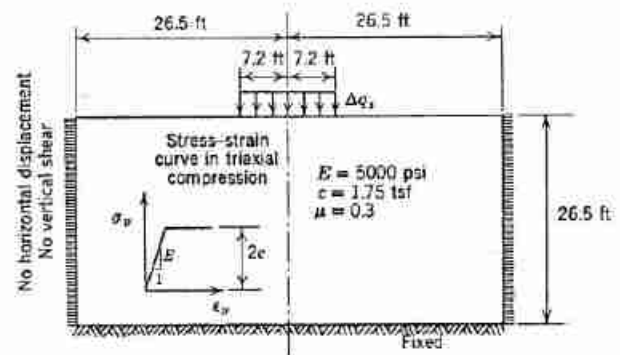


Fig. 14.1 Uniform strip load on hypothetical elastoplastic material.

¹ The results presented here were calculated with a digital computer using a finite difference technique (Whitman and Hoeg, 1966). The procedure has been extended to incorporate other stress-strain relations which are more similar to those of actual soils (Christian, 1966). Note that Δq_s or q_s as used in this chapter denotes applied surface stress and not $(\sigma_v - \sigma_h)/2$.

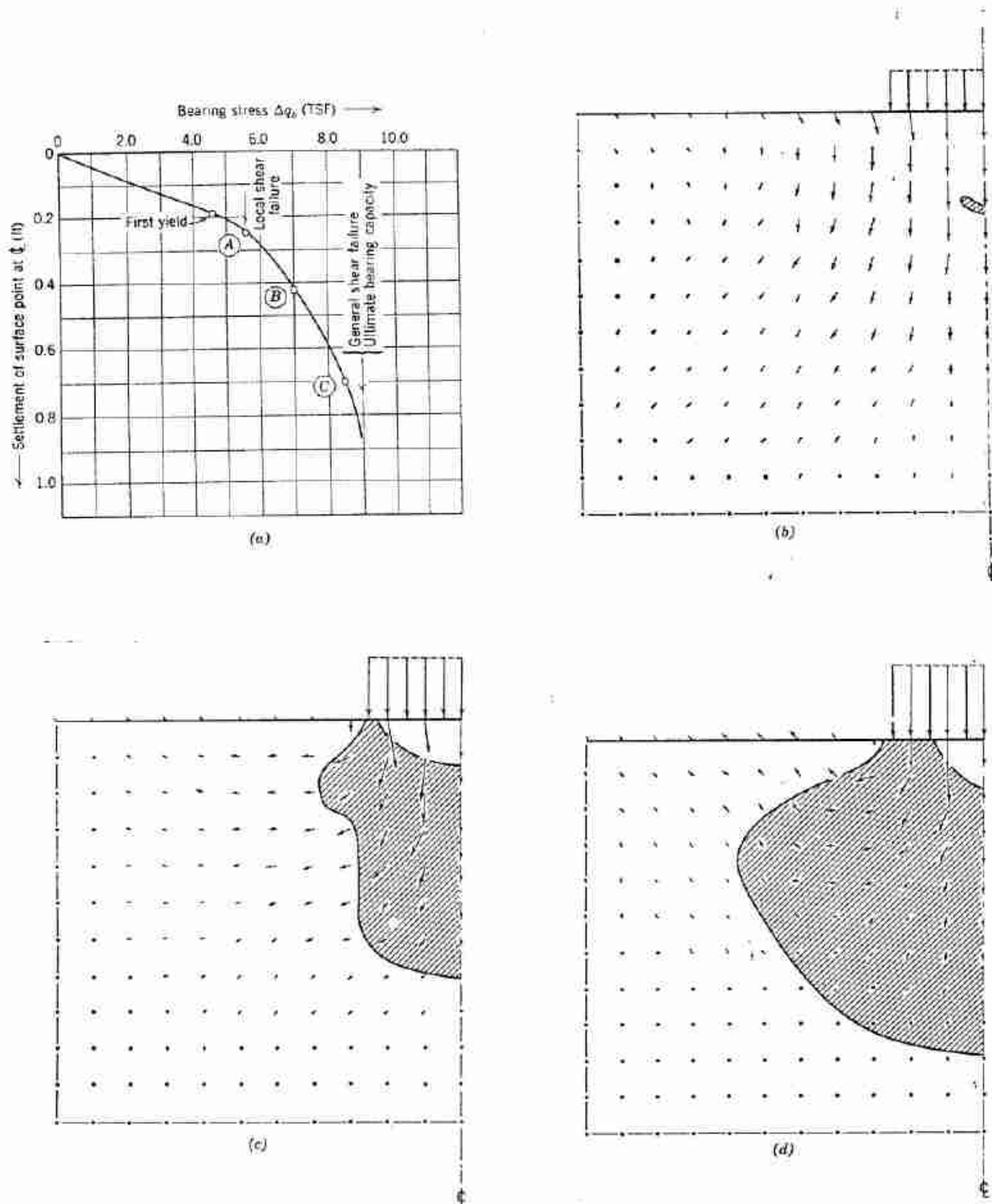


Fig. 14.2 (a) Load-settlement curve at centerline of hypothetical problem. (b) Displacements and first yielded point at load of 4.52 TSF. (c) Extent of yielded zone and motion field at load of 7.0 TSF. (d) Extent of yielded zone and motion field at load of 8.5 TSF.

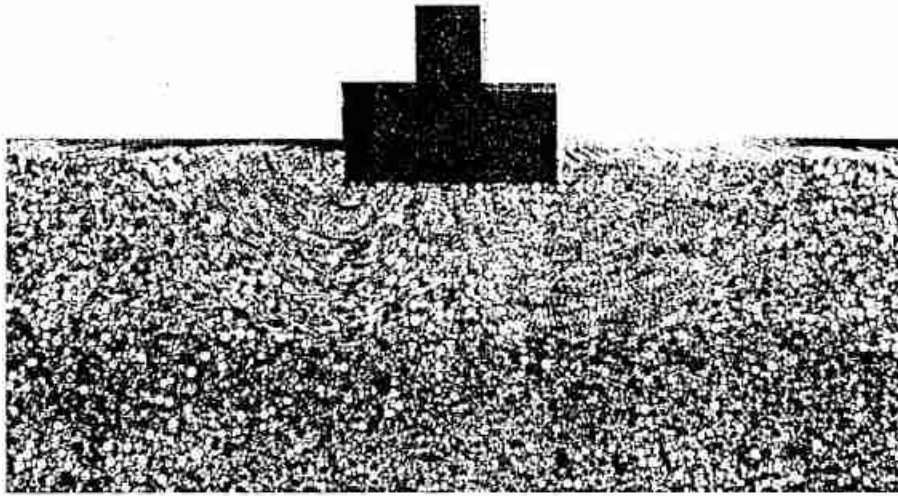


Fig. 14.3 Failure zones under footing.

using elastic theory, as discussed in Chapter 8. As long as $\tau_{\max} < c$ at all points, the settlement is proportional to Δq_s . For any value of Δq_s , the largest value of τ_{\max} occurs along the center line at a depth roughly equal to one-half of the width of the loaded area. When $\Delta q_s = 4.52$ tsf, $\tau_{\max} = c$ at this critical point, and this point yields. However, nothing catastrophic occurs at this stage because this yielded point is fully surrounded by material which can carry additional stress. A further increase in Δq_s causes *contained plastic flow* of the yielded point and additional elastic deformation of the surrounding points. Gradually the surrounding points also yield and the plastic zone grows.

Figure 14.2 shows *load-settlement curve* and the growth of the plastic zone. (Strictly speaking this should be called a "stress-settlement curve", but we shall use the common phrase here.) Shortly after yielding first begins, the load-settlement curve steepens (point A). This condition is called a *local shear failure*. The load-settlement curve steepens gradually until the plastic zone spreads beyond the loaded area (point C). Once this happens, the settlement increases rapidly and, finally, a condition is reached where it is not possible to increase Δq_s without very large settlement. This occurs at $\Delta q_s = 9.0$ tsf. The condition at this stage is called a *general shear failure*, and the value of Δq_s at this condition is called the *ultimate bearing capacity*.

The arrows in Fig. 14.2b show the direction and relative magnitude of the motions of various points during the application of a small increment of load. During the elastic portion of the loading, points on the surface outside the loaded area move downward and toward the load. However, once yielding occurs these points begin to move upward and outward. The inset for the ultimate

load shows the flow of soil from under the load, thence sideways and upwards. As would be expected, these motions are greatest within the zone that has yielded.

Behavior of Footings on Actual Soils

Figure 14.3 shows the pattern of motion at failure within a stack of rods loaded by a rigid punch. As discussed in Chapter 13, pictures such as this provide the basis for understanding the development of failure in granular soils. Note how the "soil" is pushed out from beneath the "footing" and the surface of the surrounding soil heaves. The pattern of motion is quite similar to that computed for the hypothetical material, as shown in Fig. 14.2d.

Figure 14.4 shows load-settlement curves observed during tests of circular plates from 2 to 8 in. in diameter resting on a dry sand. The curve for a medium dense sand (Fig. 14.4b) is very similar to that in Fig. 14.2 for the hypothetical material. There is a well-defined break-point or "knee" in the curve corresponding to a local shear failure. Beyond this point the curve becomes steeper and erratic until a general shear failure occurs. This actual load-settlement curve shows a gradually increasing resistance even after the general shear failure. As the footing penetrates, the soil above the base of the footing acts as a surcharge and increases the shear resistance of the soil.

For very loose sands the shear zones at the sides of the footing never become well-defined and little if any surface heave occurs. This behavior, which is simply an extreme case of the behavior described in the preceding paragraph, is termed a *punching failure*.

A footing on a very dense sand shows a somewhat different behavior. Here the load causing general shear

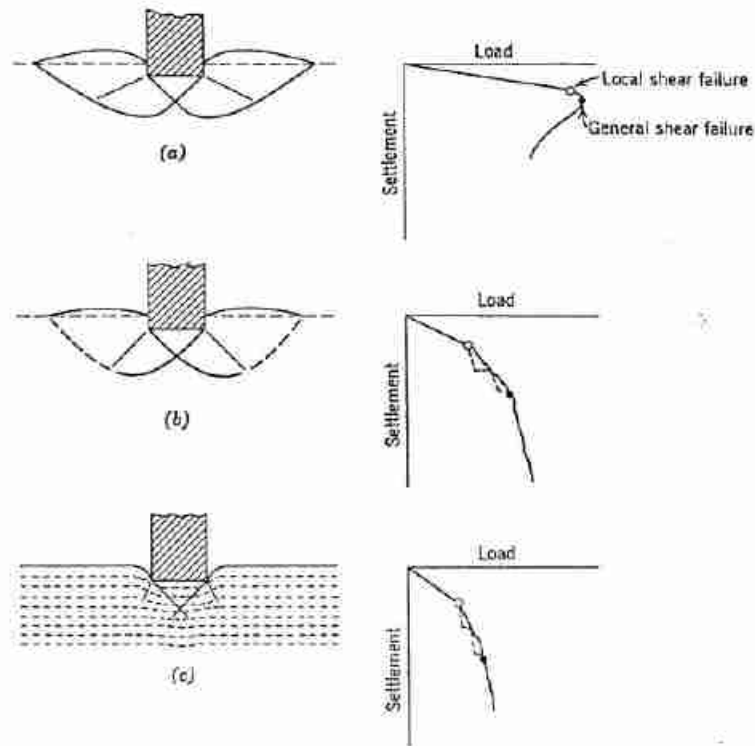


Fig. 14.4 Load-settlement curves and shear zones observed during model tests on sand. (a) Dense sand. (b) Medium dense sand. (c) Very loose sand. (After Vesic, 1963.)

failure is only slightly greater than the load causing local shear failure. Very sharply defined failure surfaces develop. Following the general shear failure, the resistance decreases because of the loss of interlocking resistance past the peak of the stress-strain curve for a dense sand. Although not shown, the resistance will eventually increase again because of the surcharge effect that develops once the footing has penetrated to considerable depth.

The behavior of actual foundations on natural soils appears to be similar to that observed in these small-scale tests, although there have been very few well-documented total failures of foundations resting on sand.

Design Criteria

The basic criterion governing the design of foundations is that the settlement must not exceed some permissible value. This value will vary from structure to structure, as discussed in Section 14.2. In order to ensure that this basic criterion is met, an engineer must make two considerations. First, for any foundation there is some value of the applied stress at which the settlements start to become very large and difficult to predict. This load is called the *bearing capacity*. The foundation must be

designed so that the actual bearing stress is less than the bearing capacity, with an appropriate margin of safety to cover uncertainties in the estimate of both the bearing stress and the bearing capacity. The meaning of the terms "very large settlements" and "difficult to predict" involves judgment on the part of the engineer. Generally, the bearing capacity is taken as the bearing stress causing local shear failure; i.e., the stress corresponding to the "knee" of the stress-settlement curve. In a few problems, an engineer may feel that a larger load better fits the definition of bearing capacity. Clearly, however, the load that causes a general shear failure (i.e., the ultimate bearing capacity) is an upper limit for the bearing capacity.

Second, after determining the bearing capacity and ensuring that the bearing capacity exceeds the expected applied bearing stress with an adequate margin of safety, an engineer must estimate the settlement that will occur under the expected load and compare this estimated settlement with the permissible value.

Thus the three key steps in evaluating foundation design are:

1. Selection of the required factor of safety against a shear failure and the permissible settlement.

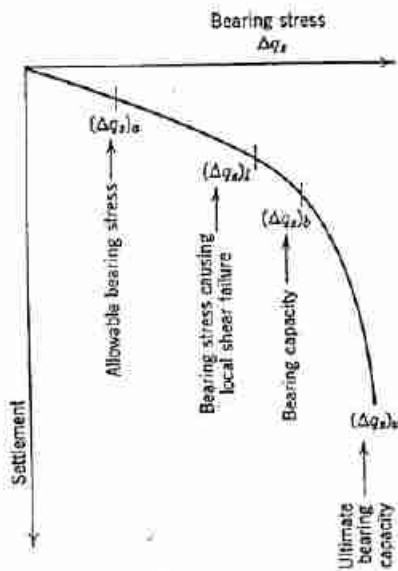


Fig. 14.5 Relationship between bearing stresses and bearing capacities.

2. Determination of the bearing capacity and the actual factor of safety under the expected load.
3. Estimation of the settlement and comparison with the permissible settlement.

In the foregoing discussion, the terms "bearing capacity" and "bearing stress" have been used in several different senses. The meaning of each of the various terms is summarized below and in Fig. 14.5.

Bearing stress Δq_s . This is the stress actually applied to the soil. In an actual foundation Δq_s must be no greater than the:

Allowable bearing stress $(\Delta q_s)_a$. The allowable bearing stress is selected after consideration of safety against instability, permissible settlement, and economy. Often $(\Delta q_s)_a$ is obtained by dividing a safety factor F into the:

Bearing capacity $(\Delta q_s)_b$. The bearing stress at which settlements begin to become very large and unpredictable because of a shear failure is the bearing capacity. Usually, $(\Delta q_s)_b$ is taken equal to the:

Bearing stress causing local shear failure $(\Delta q_s)_l$. This is the bearing stress at which the first major nonlinearity appears in the stress-settlement curve. In some carefully analyzed problems $(\Delta q_s)_b$ may exceed $(\Delta q_s)_l$. However, in any case $(\Delta q_s)_b$ must not exceed the:

Ultimate bearing capacity $(\Delta q_s)_u$. The ultimate bearing capacity is the bearing stress which causes a sudden catastrophic settlement of the foundation.

There are many problems in which $(\Delta q_s)_a$ must be less than $(\Delta q_s)_b$, owing to limitations upon settlement.

14.2 ALLOWABLE SETTLEMENT

Settlement can be important, even though no rupture is imminent, for three reasons: appearance of the structure; utility of the structure; and damage to the structure.

Settlement can detract from the appearance of a building by causing cracks in exterior masonry walls and/or the interior plaster walls. It can also cause a structure to tilt enough for the tilt to be detected by the human eye.

Settlement can interfere with the function of a structure in a number of ways, e.g., cranes and other such equipment may not operate correctly; pumps, compressors, etc., may get out of line; and tracking units such as radar become inaccurate.

Settlement can cause a structure to fail structurally and collapse even though the factor of safety against a shear failure in the foundation is high.

Some of the various types of settlement are illustrated in Fig. 14.6. Figure 14.6a shows *uniform settlement*. A building with a very rigid structural mat undergoes uniform settlement. Figure 14.6b shows a *uniform tilt*, where the entire structure rotates. Figure 14.6c shows a very common situation of *nonuniform settlement*,

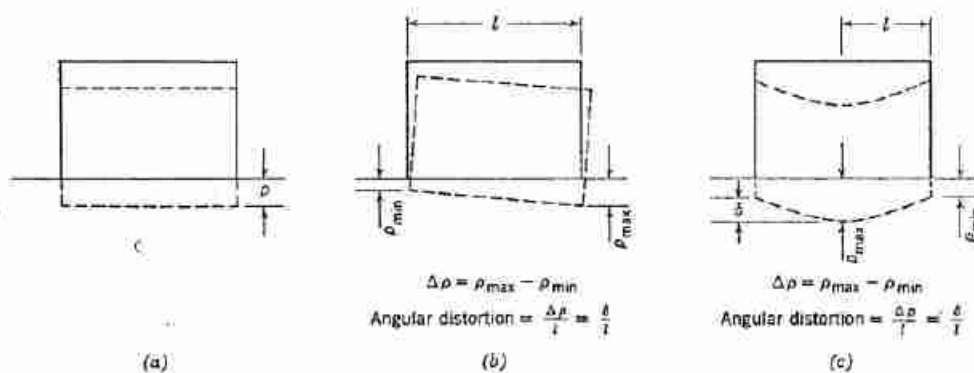


Fig. 14.6 Types of settlement. (a) Uniform settlement. (b) Tilt. (c) Nonuniform settlement.

Table 14.1 Allowable Settlement

Type of Movement	Limiting Factor	Maximum Settlement	
Total settlement	Drainage	6-12 in.	
	Access	12-24 in.	
	Probability of nonuniform settlement:		
	Masonry walled structure	1-2 in.	
	Framed structures	2-4 in.	
Tilting	Smokestacks, silos, mats	3-12 in.	
	Stability against overturning	Depends on height and width	
	Tilting of smokestacks, towers	0.004 <i>l</i>	
	Rolling of trucks, etc.	0.01 <i>l</i>	
	Stacking of goods	0.01 <i>l</i>	
	Machine operation-cotton loom	0.003 <i>l</i>	
	Machine operation-turbogenerator	0.0002 <i>l</i>	
	Crane rails	0.003 <i>l</i>	
	Drainage of floors	0.01-0.02 <i>l</i>	
	Differential movement	High continuous brick walls	0.0005-0.001 <i>l</i>
		One-story brick mill building, wall cracking	0.001-0.002 <i>l</i>
Plaster cracking (gypsum)		0.001 <i>l</i>	
Reinforced-concrete building frame		0.0025-0.004 <i>l</i>	
Reinforced-concrete building curtain walls		0.003 <i>l</i>	
Steel frame, continuous		0.002 <i>l</i>	
Simple steel frame		0.005 <i>l</i>	

From Sowers, 1962.

Note. l = distance between adjacent columns that settle different amounts, or between any two points that settle differently. Higher values are for regular settlements and more tolerant structures. Lower values are for irregular settlements and critical structures.

"dishing." Nonuniform settlement can result from: (a) uniform stress acting upon a homogeneous soil; or (b) nonuniform bearing stress; or (c) nonhomogeneous subsoil conditions.

As shown in Fig. 14.6, p_{max} denotes the maximum settlement and p_{min} denotes the minimum settlement. The differential settlement Δp between two points is the larger settlement minus the smaller. Differential settlement is also characterized by *angular distortion* δ/l , which is the differential settlement between two points divided by the horizontal distance between them.

The amount of settlement a structure can tolerate—the *allowable settlement* or *permissible settlement*—depends on many factors including the type, size, location, and intended use of the structure, and the pattern, rate, cause, and source of settlement. Table 14.1 gives one indication of allowable settlements. It might seem that the engineer designing a foundation would have the permissible settlement specified for him by the engineer who designed the structure. However, this is

seldom the case and the foundation engineer frequently finds himself "in the middle" between the structural engineer who wants no settlement and the client who wants an economical foundation. Thus a foundation engineer must understand allowable settlements.

In the following paragraphs some of the salient aspects of allowable settlement are discussed and illustrated. The last portion of this section presents general guides for estimating the allowable settlement for a particular situation.

Total Settlement

Generally the magnitude of total settlement is not a critical factor but primarily a question of convenience. If the total settlement of a structure exceeds 6 to 12 in. there can be trouble with pipes (for gas, water, or sewage) connected to the structure. Connections can, however, be designed for structure settlement. Figure 1.3 shows a classic example of a building that has undergone large settlements and yet remained in service. However,

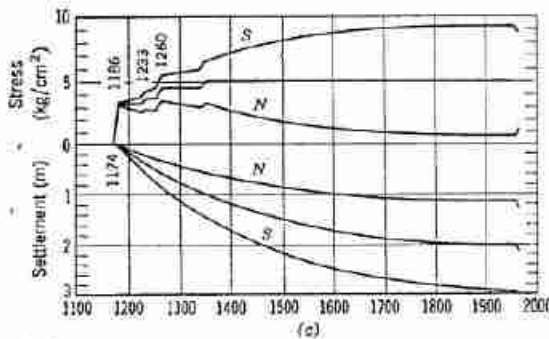
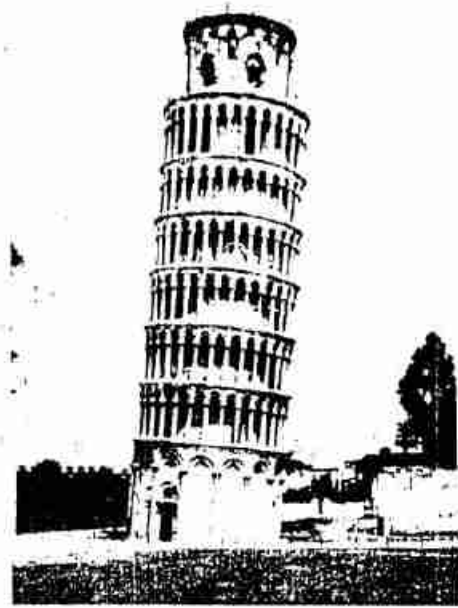
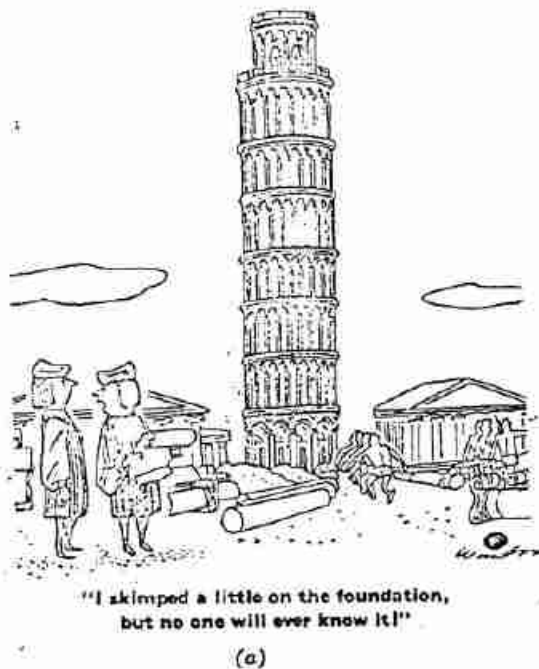


Fig. 14.7 The Leaning Tower of Pisa. (a) From 1964 ASCE Settlement Conference. (b) and (c) From Terracina, 1962.

there are situations where large total settlements can cause serious problems; e.g., a tank on soft clay near a waterfront can settle below water level.

Tilt

The classic case of tilt is the Leaning Tower of Pisa (Fig. 14.7). As can be seen from the time-settlement curve, the north side of the tower has settled a little over 1 m, whereas the south side has settled nearly 3 m, giving a differential settlement of 1.8 m. The tilt causes the bearing stress to increase on the south side of the tower, thus aggravating the situation. This much tilt in a tall building represents a potentially unstable, dangerous situation. Engineers are now studying methods to prevent further tilt (Terracina, 1962).

Nonuniform Settlement

The allowable angular distortion in buildings has been studied by theoretical analyses, by tests on large models of structural frames, and by field observations. Figure 14.8 gives a compilation of results from such studies. An extreme case is precision tracking radars where a tilt as small as $\delta/l = 1/50,000$ can destroy the usefulness of the radar system.

A steel tank for the storage of fluids is a particularly interesting structure. Most of the load is from the stored fluid, and owing to the flexibility of the tank's bottom the bearing stress has a uniform distribution. The flexibility also means that tanks can tolerate large differential settlements without damage, and owners of such tanks are seldom concerned by their appearance. Yet there is amazing disagreement among engineers, builders, and owners as to the allowable settlement of such tanks. A survey of this subject by Aldrich and Goldberg (unpublished) has revealed the following facts:

1. Tanks have settled more than 60 in. and remained in service.
2. Tanks have failed structurally as the result of settlements as small as 7 in.
3. Allowable settlements commonly used for the design of tank foundations vary from 1 to 18 in.

The wide disparity of observed results and views as to allowable settlements illustrates vividly the difficulty faced by a soil engineer in establishing an allowable settlement. Although Table 14.1 and Fig. 14.8 give good

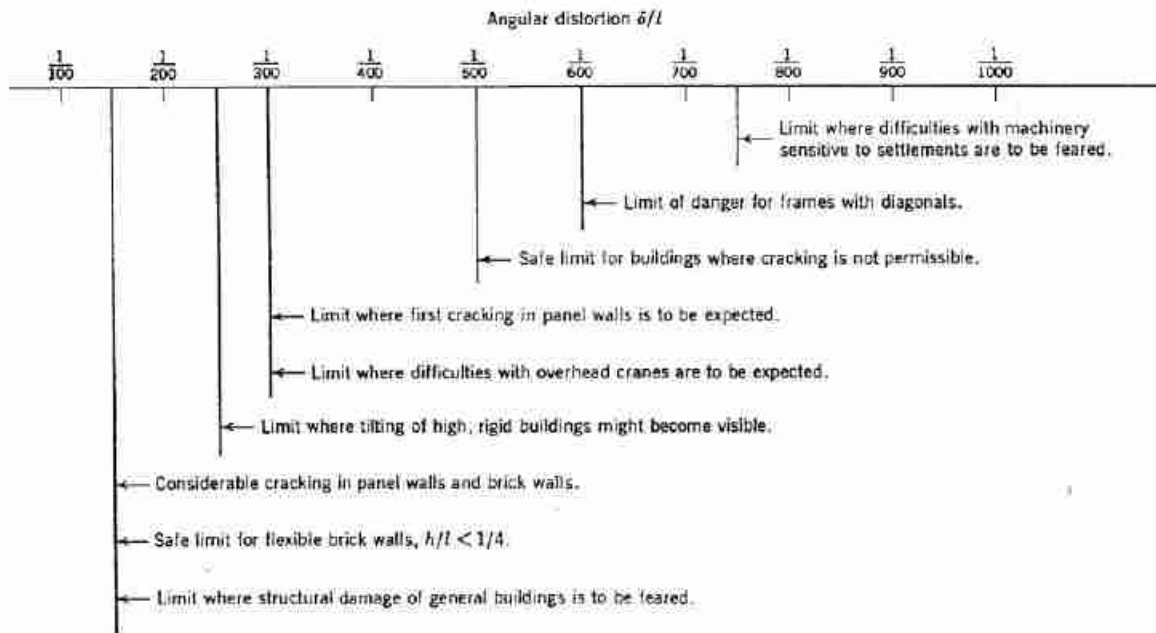


Fig. 14.8 Limiting angular distortions (From Bjerrum, 1963a).

general guidance that will suffice for routine jobs, each large project must receive additional careful study.

Relation of Total and Differential Settlement

As stated previously, it usually is the differential settlement (rather than the total settlement) that is of concern in the designing of a foundation. On the other hand, it is much more difficult to estimate differential settlement than it is to estimate the maximum settlement. This is because the magnitude of differential settlement is affected greatly by the nonhomogeneity of natural soil deposits, and also by the ability of structures to bridge over soft spots in the foundation. On a very important job, it usually is worthwhile to make a very detailed study of the subsoil to locate stronger and weaker zones, and to investigate comprehensively the relation between foundation movements and forces in the structures. On a less important job, it may suffice to use an empirical relationship between total settlement and differential settlement, and to state the design criterion in terms of an allowable total settlement.

Figure 14.9 presents results from actual buildings resting on granular soils. Part (a) gives observed values of angular distortion δ/l versus maximum differential settlement. Whereas δ/l is determined by the differential settlement between adjacent columns, the maximum differential settlement may well be between two columns which are far apart. The curve drawn on the figure gives the average for the observed points. Part (b) shows the relationship between maximum differential settlement

and maximum settlement. The line drawn as an upper envelope indicates that the maximum differential settlement can be equal to the maximum settlement; i.e., there may well be one column which has almost no settlement. Generally, the maximum differential settlement is less than the maximum settlement.²

The use of these relationships is illustrated in Example 14.1. From the nature of the building a permissible δ/l is

► Example 14.1

Given. A one-story reinforced concrete building with brick curtain walls.

Find. Allowable total settlement which will ensure no cracking of the brick walls.

Solution. From Fig. 14.8, maximum $\delta/l = 1/500 = 0.002$.

Table 14.1 would give 0.003. Use $\delta/l = 0.002$.

From Fig. 14.9a, maximum allowable differential settlement is 2.5 cm.

From Fig. 14.9b, using the upper bound, the allowable total settlement is also 2.5 cm or 1 in.

chosen. Then the curves are used to find first the maximum differential settlement and then the maximum permissible total settlement. The settlement as predicted by the methods discussed in Sections 14.8 through 14.10 should then be less than this allowable settlement. An allowable total settlement of 1 in. is a typical specification for commercial buildings.

² Maximum differential settlement greater than maximum total settlement can result when one portion of the structure heaves while another settles. This situation is not uncommon in tanks on sand.

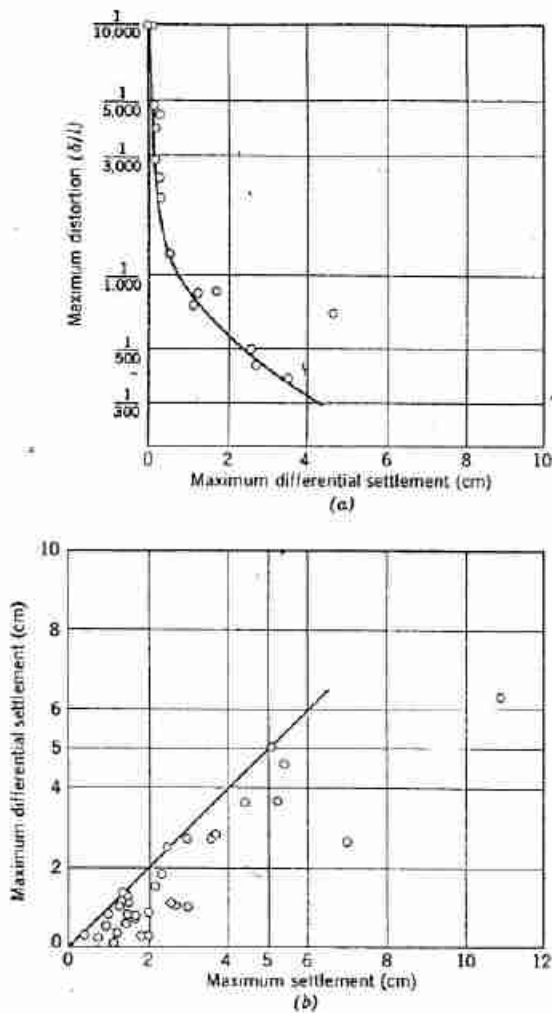


Fig. 14.9 Settlement of structures on sand (From Bjerrum, 1963a and 1963b).

14.3 ULTIMATE BEARING CAPACITY OF STRIP FOOTINGS

As a first step in our study of methods for establishing the bearing capacity of foundations, we shall study the ultimate bearing capacity $(\Delta q_u)_u$ of a footing which is very long compared to its width. This type of footing occurs under retaining walls and under building walls. Methods have been developed for predicting the ultimate bearing capacity of such footings. Subsequent sections will discuss how the theoretical results are modified by judgment and experience to account for the effects of local shear failure and for different shapes of footings.

A typical strip footing is depicted in Fig. 14.10. Because the footing is very long in comparison to its width, the problem is one of plane strain; i.e., the

problem is two-dimensional. There are several reasons why the footing is generally located below ground surface rather than at the very surface: (a) to avoid having to raise the first-floor level well above ground surface; (b) to permit removal of the surface layer of organic soil; (c) to gain the additional bearing capacity that comes from partial embedment (see later portions of this section); and (d) to place the footing below the zone of soil which experiences volume changes because of frost action or other seasonal effects. In Boston, for example, the building code requires that exterior footings be 4 ft or deeper below ground surface.

For purposes of analysis, the actual situation shown in Fig. 14.10a is usually replaced by the situation shown in Fig. 14.10b: the soil above the base of the footing is replaced by a uniform surcharge of intensity $q_s = \gamma d$, where

- γ = the unit weight of the soil
- d = the depth of the base of the footing below ground surface

The effect of the weight of the soil above the footing base is thus taken into consideration, but the shear resistance of this soil is neglected. The accuracy of this approximation will be discussed later in this section.

Solution Based on Rankine Wedges

We shall begin with an analysis which is much too approximate for practical use, but which illustrates in a simple way the factors that must be considered in a more accurate analysis. It is assumed that the failure zone is made up of two separate wedges, as shown in Fig. 14.11: a Rankine active wedge I, which is pushed downward and outward, and a Rankine passive wedge II, which is pushed outward and upward. There are corresponding patterns of motion on the other side of the center line.

The analysis begins with consideration of wedge II. Using Eq. 13.9, we can write an expression for the maximum thrust P (i.e., passive thrust) which can be applied to this wedge along the vertical face AA' (note $N_s = K_p$). Equation 14.1 includes the resistance resulting from friction and surcharge. This thrust P is also the maximum thrust available to hold the active wedge I in equilibrium under the application of the loading Q_{ult}/B . The value of this loading may therefore be found by using Eq. 13.7 for the active thrust.

Equation 14.3 may be written in the form³

$$\frac{Q_{ult}}{B} = (\Delta q_u)_u = \frac{\gamma B}{2} N_\gamma + q_s N_q \quad (14.4)$$

where N_γ and N_q are dimensionless factors that depend only on the friction angle of the soil. Based on this

³ The reason for writing $\gamma B/2$ is purely historical; i.e., this is the way it was first written.

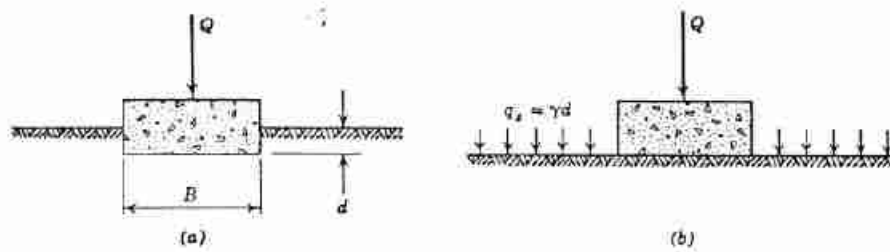


Fig. 14.10 Shallow strip footing under a vertical load. (a) Actual situation. (b) Assumed situation.

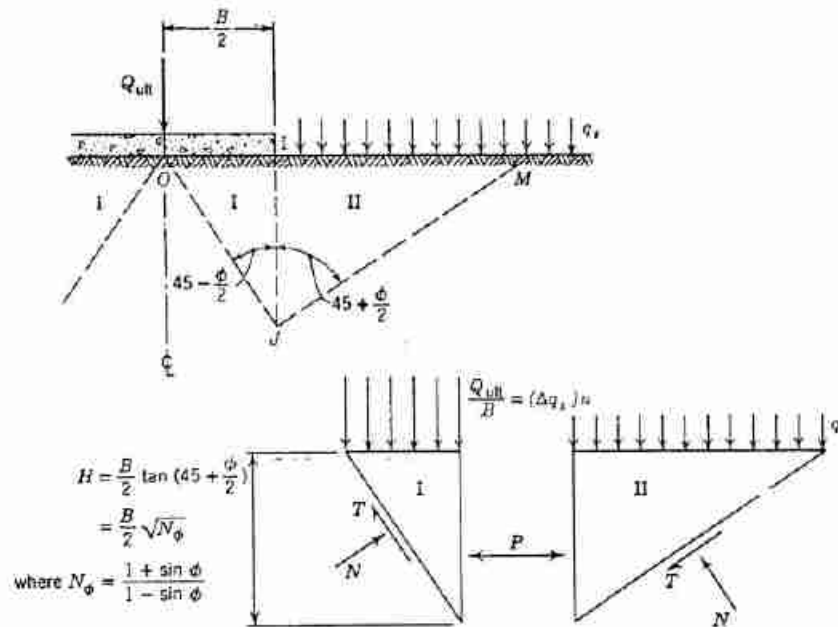


Fig. 14.11 Derivation of bearing capacity based on Rankine wedges.

Maximum force P that can be applied to passive wedge II

From Eq. 13.9:

$$P = q_s H N_\phi + \frac{1}{2} \gamma H^2 N_\phi$$

$$P = q_s \frac{B}{2} N_\phi^{3/2} + \frac{1}{8} \gamma B^2 N_\phi^2 \quad (14.1)$$

Maximum surcharge Q_{ult}/B that can be applied to active wedge I

From Eq. 13.7:

$$P = \frac{Q_{ult}}{B} \frac{H}{N_\phi} + \frac{1}{2} \gamma H^2 \frac{1}{N_\phi}$$

$$\frac{Q_{ult}}{B} = \frac{P}{H} N_\phi - \frac{1}{2} \gamma H$$

$$= \left(\frac{2P}{B} - \frac{1}{4} \gamma B \right) \sqrt{N_\phi}$$

$$\frac{Q_{ult}}{B} = q_s N_\phi^{3/2} + \frac{1}{4} \gamma B N_\phi^{5/2} - \frac{1}{4} \gamma B N_\phi^{1/2} \quad (14.2)$$

$$\frac{Q_{ult}}{B} = \frac{\gamma B}{4} (N_\phi^{3/2} - N_\phi^{1/2}) + q_s N_\phi^{3/2} \quad (14.3)$$

solution involving Rankine wedges, N_γ and N_c have the values

$$\begin{aligned} N_\gamma &= \frac{1}{2}(N_\phi^{3/2} - N_\phi^{1/2}) \\ N_c &= N_\phi^2 = K_p^2 \end{aligned} \quad (14.5)$$

where

$$N_\phi = K_p = \frac{1 + \sin \phi}{1 - \sin \phi}$$

Thus, according to Eq. 14.4, the ultimate bearing capacity of a strip footing can be written as the sum of the two terms. The first term depends on the unit weight of the soil and the width of the footing. The second term depends on the surcharge. By introducing the relation between the depth of embedment and the surcharge (Fig. 14.10),

$$\frac{Q_{ult}}{B} = (\Delta q_s)_u = \frac{\gamma B}{2} N_\gamma + \gamma d N_c \quad (14.6)$$

The dimensionless factors N_γ and N_c are called *bearing capacity factors* and depend only on ϕ .

The use of the foregoing results is illustrated by Examples 14.2 to 14.4. As mentioned earlier, the results obtained using the Rankine wedges are too approximate (too low) for use in practice, but the results do serve to illustrate the following important points which are also true of the more accurate solutions:

1. An important increase in ultimate bearing capacity comes about as the result of partial embedment.
2. There is a sharp increase in bearing capacity as the friction angle increases. The footing load, which of course causes the stresses that shear the soil, also causes normal stresses which act to increase the shear resistance. Figure 14.12 shows stress paths for points at mid-depth within the passive and active zones, assuming that initially the stresses are geostatic with $K_p = 1.4$. The stress path for the point under the footing rises at a slope less than 45° . With increasing friction angle for the soil, a larger and larger footing load is required to make the stress path "catch up" with the failure line.

Note also that the bearing capacity of a footing on sand would be zero if the soil were weightless.

Other Solutions

There are two basic shortcomings to the foregoing solution based on simple Rankine wedges. First, the actual failure zone (see Fig. 14.4) is bounded by curves rather than by two straight surfaces. Second, the foregoing solution has neglected the shear stresses which

⁴ In drawing the stress path for point R , we assume that the force P increases uniformly as the load is applied. The actual variation of P with load is discussed in Section 14.4, and actual stress paths for point R are curved rather than straight.

► Example 14.2

Given. Footing shown in Fig. E14.2.

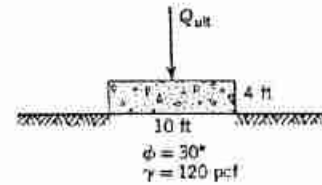


Fig. E14.2

Find. Q_{ult} .

Solution.

$$N_\phi = \frac{1 + \sin \phi}{1 - \sin \phi} = 3$$

$$N_\gamma = \frac{1}{2}(15.60 - 1.73) = 6.94$$

$$N_c = 3^2 = 9$$

$$\frac{Q_{ult}}{B} = (\Delta q_s)_u = (120)(10) \left(\frac{6.94}{2} \right) = 4160 \text{ psf}$$

$$Q_{ult} = 41,600 \text{ lb/ft of wall}$$

► Example 14.3

Given. Footing shown in Fig. E14.3.

Find. Q_{ult} .

Solution.

$$\frac{Q_{ult}}{B} = (\Delta q_s)_u = 4160 + (120)(4)(9)$$

$$= 4160 + 4320 = 8480 \text{ psf}$$

$$Q_{ult} = 84,800 \text{ lb/ft of wall}$$

► Example 14.4

Given. Same as Example 14.3, but with $\phi = 40^\circ$.

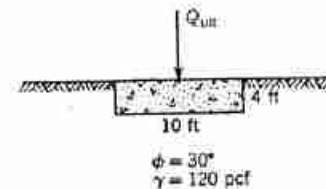


Fig. E14.3

Find. Q_{ult} .

Solution.

$$N_\phi = 4.61$$

$$N_\gamma = \frac{1}{2}(45.8 - 2.15) = 21.6$$

$$N_c = 21.2$$

$$\frac{Q_{ult}}{B} = (\Delta q_s)_u = (120)(10) \left(\frac{21.6}{2} \right) + (120)(4)(21.2)$$

$$= 12,960 + 10,180$$

$$= 23,140 \text{ psf}$$

$$Q_{ult} = 231,000 \text{ lb/ft of wall}$$

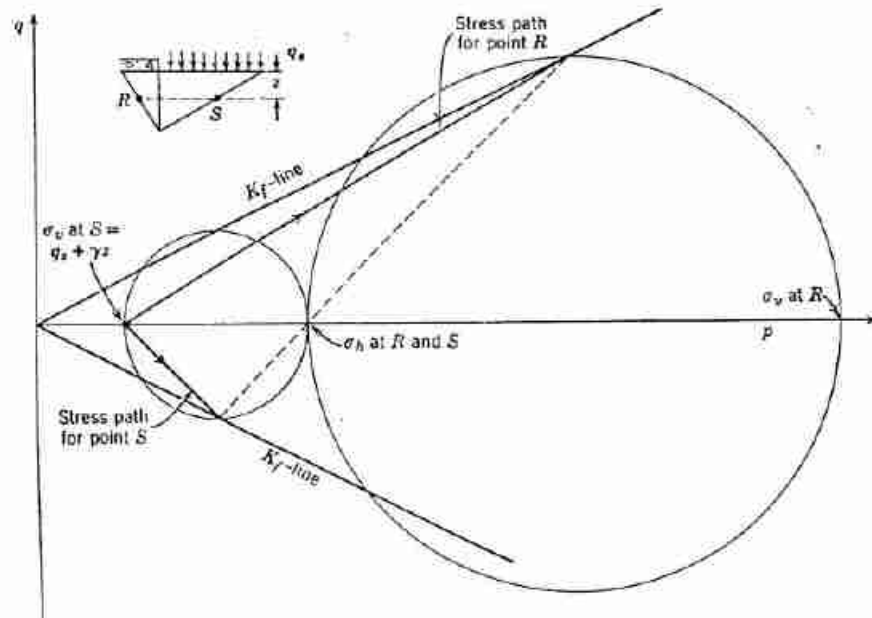


Fig. 14.12 Stress paths at points below foundation.

must act upon the line *W* in Fig. 14.11. Because of the second shortcoming the solution grossly underestimates the actual bearing capacity.

Many different types of solutions have been made in an attempt to overcome satisfactorily these shortcomings. Trial wedge solutions have been made using free bodies bounded by various combinations of straight lines, circles, and logarithmic spirals (Hansen, 1966). Solutions have been made by numerical integration of Kötter's equation (Sokolovski, 1965; Harr, 1966). Most of these solutions involve some degree of approximation and, as discussed in Chapter 13, it still is not clear just what is meant by an exact solution to a limiting equilibrium problem involving soil.

The most commonly used solution is that developed by Terzaghi (1943). This solution assumes that Eq. 14.6 is applicable; i.e., the resistance offered by the weight of the soil and by the surcharge can be evaluated independently of each other. This is not strictly true, since the location of the theoretical failure surface is somewhat different for each combination of ϕ , γ , and Δq_s . However, it has been shown that this assumption leads to a conservative result—to an underestimate of the bearing capacity. Having made this assumption, Terzaghi then evaluated N_c and N_q by the trial wedge method using free bodies of the type shown in Fig. 14.13a. Values applicable to a rough footing, which is the typical case encountered in practice, are plotted versus ϕ in Fig. 14.13b. Values for smooth bases are also available. Examples 14.5 to 14.7 repeat the earlier examples, but

use Terzaghi's values of N_c and N_q and thereby obtain much larger estimates for the bearing capacity.

Table 14.2 compares values of N_c and N_q as calculated by Terzaghi with average values deduced from small-scale footing tests. There was considerable scatter in the

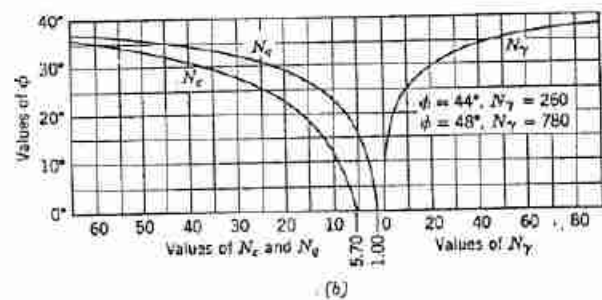
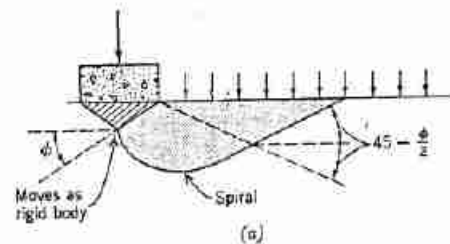


Fig. 14.13 (a) Shapes of failure surfaces for Terzaghi solution. (b) Bearing capacity factors according to Terzaghi (for footing with rough base).

► Example 14.5

Repeat Example 14.2, using Terzaghi's bearing capacity factors

$$N_y = 20$$

$$(\Delta q_s)_u = (120)(10)\left(\frac{20}{2}\right) = 12,000 \text{ psf} \quad \blacktriangleleft$$

► Example 14.6

Repeat Example 14.3, using Terzaghi's bearing capacity factors

$$N_q = 22$$

$$(\Delta q_s)_u = 12,000 + (120)(4)(22)$$

$$= 12,000 + 10,700 = 22,700 \text{ psf} \quad \blacktriangleleft$$

► Example 14.7

Repeat Example 14.4, using Terzaghi's bearing capacity factors

$$\left. \begin{matrix} N_y = 130 \\ N_q = 80 \end{matrix} \right\} \text{ see Table 14.2}$$

$$(\Delta q_s)_u = (120)(10)\left(\frac{130}{2}\right) + (120)(4)(80)$$

$$= 78,000 + 38,000 = 116,000 \text{ psf} \quad \blacktriangleleft$$

experimental data. These results indicate that Terzaghi's factors are conservative with regard to the average experimental results, especially for large friction angles. The value of ϕ as measured in conventional triaxial tests was used to deduce N_q and N_y from the footing tests. Since a strip footing is a situation in plane strain, ϕ should have been assumed somewhat larger (see Section 11.4.). Assuming a larger ϕ would cause one to deduce smaller values of N_q and N_y in order to give the observed bearing capacity, and thus would lead to better agreement between Terzaghi's values and the experimental values.

None of the other solutions has given appreciably better agreement between theoretical and measured bearing capacities, and hence the Terzaghi solution continues to be used.

A Further Look at Effect of Embedment

Equation 14.6 may be rearranged to read

$$\frac{Q_{ult}}{B} = (\Delta q_s)_u = \frac{\gamma B}{2} N_y \left(1 + 2 \frac{d}{B} \frac{N_q}{N_y}\right)$$

Examination of the results in Table 14.2 indicates that, for ϕ equal to 30° , the ratio N_q/N_y is approximately equal

Table 14.2 Comparison of Theoretical and Actual Bearing Capacity Factors

Factor	$\phi = 30^\circ$	$\phi = 40^\circ$
N_q —Terzaghi	22	80
experimental	23	400
N_y —Terzaghi	20	130
experimental	33	170–210

to unity, although the value of the ratio may drop to 0.6 for denser sands. Several experimenters have reported values of from 0.7 to 1.0 for this ratio. As an approximation, we can assign a value of unity to this ratio and thus obtain the following approximate expression:

$$(\Delta q_s)_u = \frac{\gamma B}{2} N_y \left(1 + 2 \frac{d}{B}\right) \quad (14.7)$$

Meyerhof (1951) has investigated the importance of the shear resistance of the soil lying above the base of the footing. For $d < B$, he found that the rules derived above (based on consideration only of the weight of this soil) were reasonably accurate. For deeper footings and for friction piles, it is necessary to take the resistance of this soil into account.

14.4 EFFECT OF LOCAL SHEAR FAILURE ON BEARING CAPACITY

There is no strictly theoretical method for estimating the load at which local shear failure occurs. In this section, we first examine the factors that make local shear failure more important in some soils than in others. Then we present semiempirical methods for estimating bearing capacity.

When the load equals the ultimate bearing capacity a general shear failure occurs: the full shear resistance of the soil is mobilized all along a failure surface which starts beneath the footing and extends to the surface of the soil beyond the footing. As explained in Section 14.1, at some smaller load there will be a local shear failure, at which time the shear resistance is reached along only a part of the ultimate failure surface. It was also noted that local shear failure increases in importance as a soil becomes looser. Figure 14.14 indicates the range of relative densities for which the several types of failure

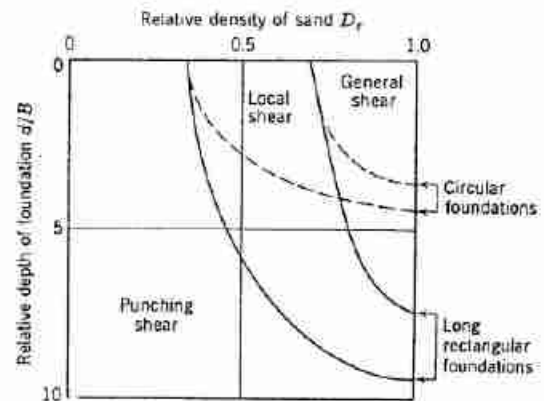


Fig. 14.14 Controlling type of failure as function of relative density and depth of embedment (From Vesic, 1963).

determine the load at which the load-settlement curve shows major yielding.

In order to understand the relationship between ultimate bearing capacity and the load causing local shear failure, it is necessary to consider: (a) the ratio of horizontal to vertical stress before loading, i.e., K_0 ; and (b) the way in which strains develop during loading. Representation of the failure zone by two Rankine wedges (Fig. 14.11) and of stress conditions by stress paths for two typical points (Fig. 14.12) provides a convenient basis for an approximate discussion of these two factors.

Loose Sand

Point O in Fig. 14.15a shows the stress conditions at the two typical points R and S before loading.

During the initial stage of loading, while the soil is still more-or-less elastic, there is relatively little change in σ_h at point R (see, for example, point C in Example 8.9). Thus during this early stage, the stress path for point R rises essentially as in an ordinary triaxial test (path OL in Fig. 14.15a) while the stresses at point S remain essentially unchanged. This situation continues until the stress path for point R reaches the failure line, at which time local shear failure occurs.

As the load is increased further, σ_h increases at both points R and S . The stress path for point S is ON in Fig. 14.15a and loading continues until this stress path reaches the failure line at N , at which time the ultimate bearing capacity is reached. Meanwhile, the stress path for point R runs along the failure line from L to M .

The load causing local shear failure may be computed using the derivation in Fig. 14.11. The assumption that σ_h remains constant during the early part of the loading means that the horizontal force P on surface IJ will be $\frac{3}{2}\gamma H^2 K_0$. Using the expression immediately preceding Eq. 14.2, the load causing local shear failure is

$$(\Delta q_s)_l = \frac{3}{2}\gamma H(K_0 N_\phi - 1)$$

Dividing by the corresponding expression for $(\Delta q_s)_u$ gives

$$\frac{(\Delta q_s)_l}{(\Delta q_s)_u} = \frac{K_0 N_\phi - 1}{N_\phi^2 - 1} \tag{14.8}$$

Using typical values of $K_0 = 0.6$ and $N_\phi = 3$, the ratio is 0.1. While this analysis is too crude for practical use, it shows clearly that in a loose sand local shear failure will occur at a load much smaller than the ultimate bearing capacity.

During the early stage of loading, the soil immediately beneath the footing strains much as in an ordinary triaxial test starting from the K_0 condition. Since the sand is loose, there is relatively little horizontal strain when failure occurs in such a test. Hence there is very

³ For this derivation the surcharge q_s is taken as zero.

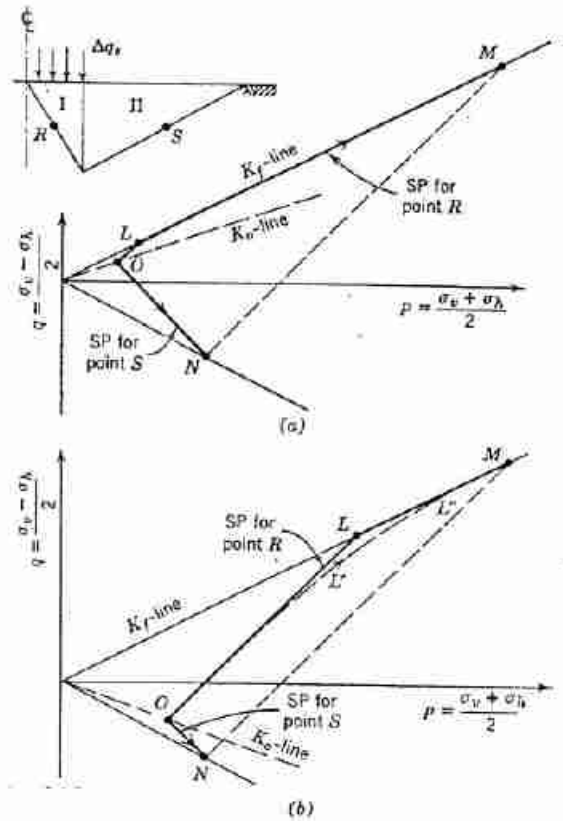


Fig. 14.15 Effect of density of sand on stress paths at two points under foundation. (a) Loose sand. (b) Dense sand.

little outward push against the loose sand in zone II (Fig. 14.15) and thus σ_h stays essentially constant at points R and S . Once local failure occurs in zone I, then large horizontal strains occur in zone I as the load is increased farther and this outward push causes shear resistance to be developed in zone II.

Dense Sand

Figure 14.15b shows the corresponding stress paths for a dense sand, again assuming that the horizontal stresses remain constant until local shear failure occurs at point R . Using $K_0 = 2$ and $N_\phi = 4$, the ratio in Eq. 14.8 is 0.47; this is much greater than for a loose sand.

Actually the stress path for point R is more like $OL'L'M$. Since it is dense, the sand within zone I will begin to dilate before local shear failure can occur. The resulting horizontal strains cause an outward push against zone II, and since the sand is dense relatively little push is necessary to develop significant shear resistance in zone II. Thus the ratio of $(\Delta q_s)_l$ to $(\Delta q_s)_u$ is greater than given by Eq. 14.8.

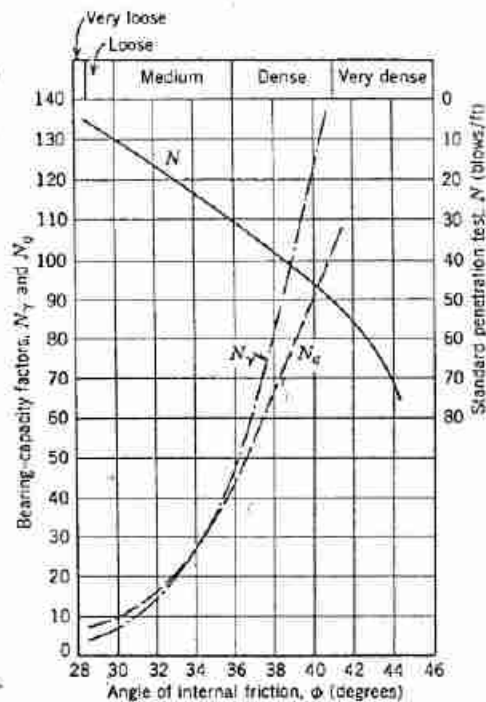


Fig. 14.16 Bearing capacity factors which automatically incorporate allowance for local shear failure (From Peck, Hansen, and Thornburn, 1953).

Combined Effect

These findings can be restated as follows. The soil which supports a footing begins to yield $(\Delta q_s)_i$ when the full shear resistance has been mobilized directly underneath the footing, but does not reach the ultimate bearing capacity $(\Delta q_s)_u$ until full resistance is reached all along the boundary of the failure wedge. For a dense sand, full resistance is mobilized almost simultaneously along all parts of the boundary. However, for a loose sand considerable footing movement is necessary before full resistance is reached along the outermost portions of the boundary. This difference occurs because of the differences in the initial stress conditions and compressibility of loose and dense sands. An accurate analysis of the development of local and general shear failures in loose and dense sands is given by Christian (1966) using finite difference techniques.

Empirical Solution for Bearing Capacity

Figure 14.16 gives factors N_y and N_q , which may be used to estimate bearing capacity $(\Delta q_s)_b$ according to the equation

$$(\Delta q_s)_b = \frac{\gamma B}{2} N_y + \gamma d N_q \quad (14.10)$$

In this figure ϕ denotes the peak friction angle of the soil. These factors, which take into account local shear, were obtained as follows. For $\phi \geq 38^\circ$, the curves are the same as for the ultimate bearing capacity (Fig. 14.13). For $\phi \leq 28^\circ$, the N_y and N_q are equal to the values in Fig. 14.13 at $\phi = \tan^{-1}(\frac{2}{3} \tan \phi)$. Thus N_y in Fig. 14.16 for $\phi = 28^\circ$ equals N_y in Fig. 14.13 for $\phi = 19.5^\circ$. This strictly empirical correction to account for local shear in loose soils was suggested by Terzaghi from an analysis of experimental data. For $28^\circ < \phi < 38^\circ$, smooth transition curves were drawn.

14.5 FOOTING DESIGN

The bearing capacity results given in Sections 14.3 and 14.4 may be applied directly to the design of foundations for walls, as illustrated in Example 14.8.

► Example 14.8

Given. A wall which is 7 ft wide at the base, and which rests 3 ft below the surface of a sand with $\phi = 35^\circ$ and $\gamma = 110$ pcf.

Find. Bearing capacity.

Solution. From Fig. 14.16 we find

$$N_y = 35$$

$$N_q = 34$$

Hence,

$$\begin{aligned} (\Delta q_s)_b B &= \frac{1}{2}(110)(7)^2(35) + 3(110)(7)(34) \\ &= 94,000 + 78,000 \\ &= 172,000 \text{ lb/ft of wall} \end{aligned}$$

This wall and its supporting soil have the same properties as the wall and supporting soil in Example 13.12. In that example, the vertical component of the force on the supporting soil was 15,270 lb/ft of wall, less than one-tenth of the bearing capacity just computed. Strictly speaking, of course, one should check for the effects of inclination and eccentricity of the actual loading upon the base of a retaining wall (see Section 14.7). However, with such a large factor of safety against bearing capacity failure, and considering that the resultant lies within the middle third of the base and that the wall checks for resistance to sliding, most designers would consider the wall of Example 13.12 safe. ◀

In such foundation design problems, it usually is necessary to rely upon the results of penetration tests to provide an estimate of the friction angle (see Section 11.5). Figure 14.16 can be used to relate blow count directly to bearing capacity factors. The fact that the proper value of ϕ is usually uncertain whenever blow count must be used is one reason why a rather liberal factor of safety (at least 3) should be used when checking the bearing capacity of foundations. A small uncertainty in ϕ causes a large uncertainty in the values for the bearing capacity factors. For example, the bearing capacity (172,000 lb/ft of wall) in Example 14.8 would only be 75,000 lb/ft if ϕ were reduced from 35° to 32° .

At this point the reader may well ask: Why did we study all the theory and then revert to crude empirical equations with a large safety factor? The reasons are simple. The theory has served an indispensable function. It has indicated how the bearing capacity should vary with such factors as the unit weight of soil and the width of the foundation. Moreover, the theory has provided numerical results for the ultimate bearing capacity. However, the theory is inadequate to provide accurate numerical values for the bearing capacity, taking into account the effects of local shear. Data from model tests and field experience must be used to fill this gap. Such experience has been incorporated in Fig. 14.16. Used together with a liberal safety factor, this approach will provide a conservative answer for any practical problem. If conservatism must be avoided, then alternative methods, such as a loading test on the site, must be used to evaluate the bearing capacity. Since such a load test can seldom be performed using a full-scale foundation, theory must be used to extrapolate from the actual loading test to the full-scale foundation (see Example 14.9).

► Example 14.9

Given. A plate bearing test shows a bearing capacity failure at a bearing stress of 3.6 tons/ft². The plate is 1 ft square and bears 3 ft below the ground surface. The unit weight of the soil is estimated at 100 pcf.

Find. Bearing capacity for a footing 6 ft square, to be founded 3 ft below ground surface.

Solution. The first step is to find a value of ϕ which will satisfy Eq. 14.12:

$$2000(3.6)\text{psf} = \frac{1}{2}(100)(1)(0.7)N_y + 3(100)(1.2)N_q$$

After several trials, it is found that $\phi = 32.5^\circ$, giving $N_y = 16\frac{1}{2}$ and $N_q = 18\frac{1}{2}$, satisfies the equation. Now these values of N_y and N_q can be applied to the actual footing:

$$\begin{aligned} (\Delta q_s)_b &= \frac{1}{2}(100)(6)(0.7)(16\frac{1}{2}) + 3(100)(1.2)(18\frac{1}{2}) \\ &= 10,100 \text{ psf or } 5.05 \text{ tsf} \end{aligned}$$

14.6 ROUND AND RECTANGULAR FOOTINGS

Several very approximate theoretical analyses have been made for the bearing capacity of round footings. However, there are no theoretical analyses that give the ultimate bearing capacity of square or rectangular footings. There have been numerous model studies aimed at evaluating the ultimate bearing capacity of round, square, or rectangular footings but, unfortunately, the data from these tests are often conflicting. Data for surface footings by Vesic (1963) are shown in Fig. 14.17.

Many equations have been proposed for use in estimating the bearing capacity of round and rectangular footings. All are based on theoretical considerations

plus experimental data, and from the practical standpoint the differences in the predictions are slight. The following are recommended:

Round footings:

$$\frac{Q_b}{(\pi/4)D^2} = (\Delta q_s)_b = (0.6)\frac{1}{2}\gamma DN_y + \gamma dN_q \quad (14.11)$$

where D is the diameter (Terzaghi, 1943).

Rectangular and square footings:

$$\frac{Q_b}{BL} = (\Delta q_s)_b = \frac{1}{2}\gamma BN_y \left(1 - 0.3 \frac{B}{L}\right) + \gamma dN_q \left(1 + 0.2 \frac{B}{L}\right) \quad (14.12)$$

where L is the length of the footing (Hansen, 1966). The values of N_y and N_q are taken from Figs. 14.13 or 14.16 as appropriate. Example 14.10 illustrates the use of such equations.

► Example 14.10

Given. A footing 6 ft by 12 ft is to be founded 4 ft below the surface of a sand with $\phi = 40^\circ$ and $\gamma = 115$ pcf.

Find. Bearing capacity.

Solution. Equation 14.12 becomes

$$(\Delta q_s)_b = (0.85)\frac{1}{2}\gamma BN_y + (1.1)\gamma dN_q$$

Using either Fig. 14.13 or Fig. 14.16 we find

$$N_y = 120$$

$$N_q = 90$$

Consequently,

$$\begin{aligned} (BL)(\Delta q_s)_b &= (6)(12)\left[\frac{1}{2}(0.85)(115)(6)(120)\right. \\ &\quad \left.+ (1.1)(115)(4)(90)\right] \\ &= (72)[36,000 + 45,000] \\ &= 5,830,000 \text{ lb} = 2,910 \text{ tons} \end{aligned}$$

Figure 14.17 compares results predicted using these equations with failure loads observed in model tests. Note that there is considerable scatter in the experimental results. Except for dense sand with very large friction angles the equations adequately predict the general shear failures. Use of Fig. 14.16 overestimates the loads at which local shear failure occurs, primarily because this sand has a very high friction angle for a given relative density. The need for a large safety factor when using these equations is clear.

14.7 BEARING CAPACITY UNDER INCLINED AND ECCENTRIC LOADS

Meyerhof (1953) has suggested the following relation be used whenever strip footing loads are inclined and/or

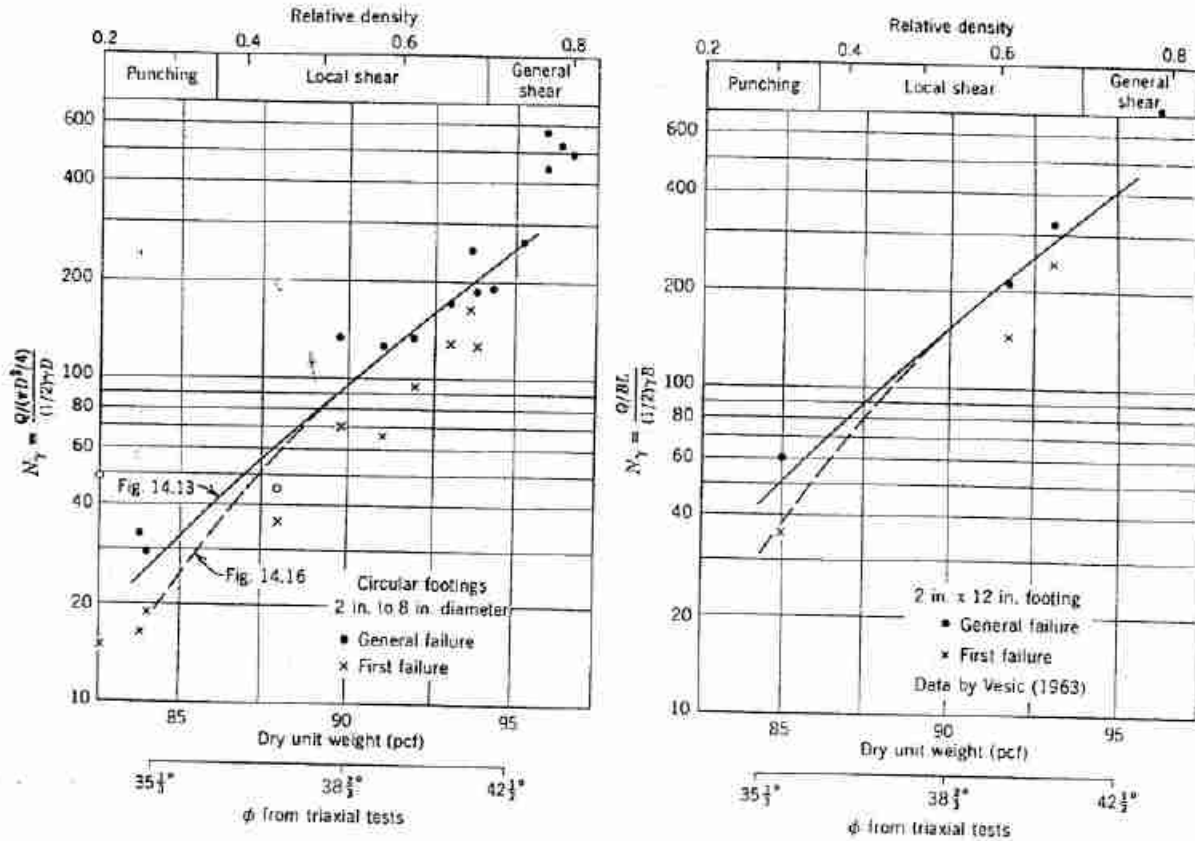


Fig. 14.17 Comparison of predicted and measured N_y .

eccentric to the centroid of the footing (see Fig. 14.18):

$$(\Delta q_s)_s = \frac{Q_b}{B} = \left(1 - \frac{2e}{B}\right) \left(1 - \frac{\alpha}{90^\circ}\right)^2 \gamma d N_c + \left(1 - \frac{2e}{B}\right)^2 \left(1 - \frac{\alpha}{\phi}\right)^2 \frac{1}{2} \gamma B N_y \quad (14.13)$$

where

Q_b = limiting value for the vertical component of the load

N_y and N_c = bearing capacity factors for vertical loading

e = the distance between the centroid of the base and the point of action of the resultant force on the base

α = the angle of inclination of the resultant force with respect to the vertical

Meyerhof developed Eq. 14.13 partly on rough theoretical grounds and partly on the basis of fitting a conservative envelope to experimental results. The equation no doubt is quite conservative. Note that the friction angle of the soil supporting the footing, rather than the friction angle between the soil and the footing, is used in this equation.

Example 14.11 illustrates the use of this equation. Comparing the results in Examples 14.9 and 14.11, we see that consideration of inclination and eccentricity leads to a large reduction in bearing capacity. Equation 14.13 should be used with a safety factor of 3 or more. On this basis the wall in Example 13.12 is still safe, since the safety factor is $51.0/15.3 = 3.3$.

For a rectangular footing Eq. 14.13 may be used by including the correction factors appearing in Eq. 14.12.

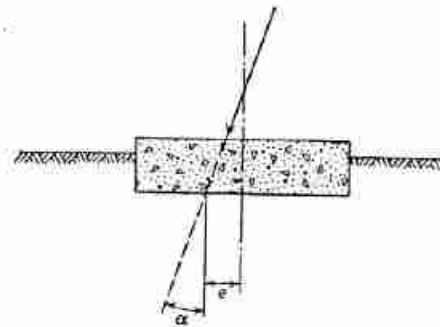


Fig. 14.18 Footing with eccentric and inclined load.

provided that the eccentricity is in the narrow direction of the footing. For the more general case of eccentric loads on rectangular footings see Harr (1966).

► Example 14.11

Given. Retaining wall in Example 13.12.

Find. Bearing capacity, considering eccentricity and inclination of force on base.

Solution. Eccentricity:

$$e = 0.84 \text{ ft}$$

Inclination: horizontal component of active thrust – passive resistance = 4910 lb/ft

$$\tan \alpha = \frac{4910}{15,270} = 0.32; \quad \alpha = 18^\circ$$

Eq. 14.13:

$$\begin{aligned} Q_b &= \left(1 - \frac{1.68}{7}\right) \left(1 - \frac{18}{90}\right)^2 \gamma B d N_q + \left(1 - \frac{1.68}{7}\right)^2 \\ &\quad \times \left(1 - \frac{18}{35}\right)^2 \frac{1}{2} \gamma B^2 N_\gamma \\ &= (0.760)(0.640)(78,000) + (0.578)(0.235)(94,000) \\ &= (38,000 + 13,000) = 51,000 \text{ lb/ft of wall} \end{aligned}$$

14.8 SETTLEMENTS AS PREDICTED BY ELASTIC THEORIES

Figure 14.19 shows the magnitude of the settlement, in ratio to footing width, at which ultimate bearing capacity was recorded in small-scale footing tests. For example, for a relative density of 0.7, the average settlement at failure for a round footing is 10% of the diameter. For a diameter of 10 ft, the settlement would be 1 ft. If the working load is one-third of the ultimate bearing capacity, i.e., a factor of safety of 3, the settlement at the working load would be about $\frac{1}{3}$ to $\frac{1}{2}$ ft (3 to 4 in.). This amount of settlement would generally be unacceptable. Hence in foundation design it usually is not sufficient merely to determine the bearing capacity and apply a safety factor. The settlement under the working load must be determined and the foundation designed to make this settlement less than the permissible value.

If soil were elastic, homogeneous, and isotropic there would be no difficulty in predicting the settlement that would take place as a result of a surface loading. For such a simple situation there are formulas from the theory of elasticity giving the relationship between load and settlement. In actuality, however, it is very difficult to predict the magnitudes of settlements of footings on real soils. Not only are actual soils nonhomogeneous and nonisotropic, with the modulus generally increasing with depth, but there is the added difficulty of evaluating the *in situ* stress-strain properties.

Despite these complications, however, elastic theory

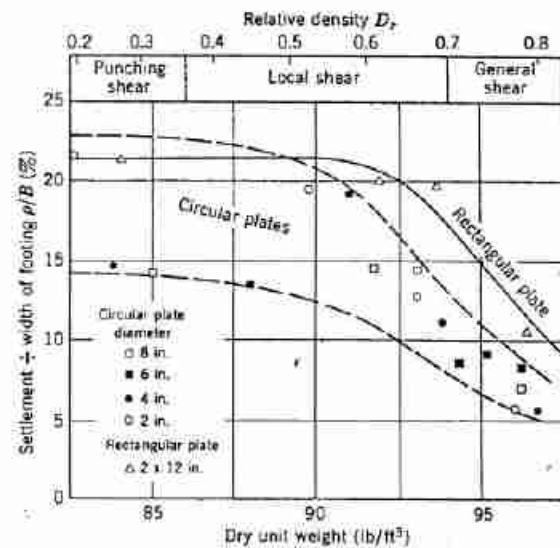


Fig. 14.19 Settlements of model footings at ultimate failure (From Vesic, 1963).

plays a key role in settlement predictions. With judgment, results from the theory of elasticity can be used to give useful estimates of settlement. More important, results from the theory provide an understanding of the settlement phenomenon, which then provides the basis for establishing approximate methods for predicting settlements for practical work.

Hence our discussion of predicting settlements begins with the study of elastic theory. In this section we are concerned with concepts and principles. The problem of using these results in practice, and the all important question of selecting a modulus for use in these results, will be considered in Section 14.9.

Elastic Theory for Settlement under a Uniform Circular Load

Chapter 8 discussed the use of elastic theory to compute the stress increments developed within an elastic body as a result of a uniform stress applied over a circular area on the surface of an elastic material. An example of the calculation of these stresses was given in Example 8.9. Knowing these stresses, and using the equations presented in Chapter 12, we can compute the strains. For example, the strains corresponding to Example 8.9 are shown in Example 14.12, based upon assumed values of E and μ .⁶

By adding up the strains along any vertical line the settlement of the surface can be computed. In the case of an elastic body with a simple surface loading, this

⁶ The choice of E is discussed in Section 14.9. μ is taken as 0.45 to be consistent with the stress distribution charts given in Chapter 8.

► Example 14.12

Given. The tank loading and subsoil of Example 8.9.

$$E = 2000 \text{ kips/ft}^2$$

$$\mu = 0.45$$

Find. The vertical and horizontal strains as a function of depth in the subsoil.

Solution. From Equation 12.5 we get

$$\epsilon_v = \frac{1}{E} (\Delta\sigma_v - 2\mu\Delta\sigma_h)$$

and

$$\epsilon_h = \frac{1}{E} [(1 - \mu)\Delta\sigma_h - \mu\Delta\sigma_v]$$

ϵ_v and ϵ_h versus depth are given in Example 8.9.

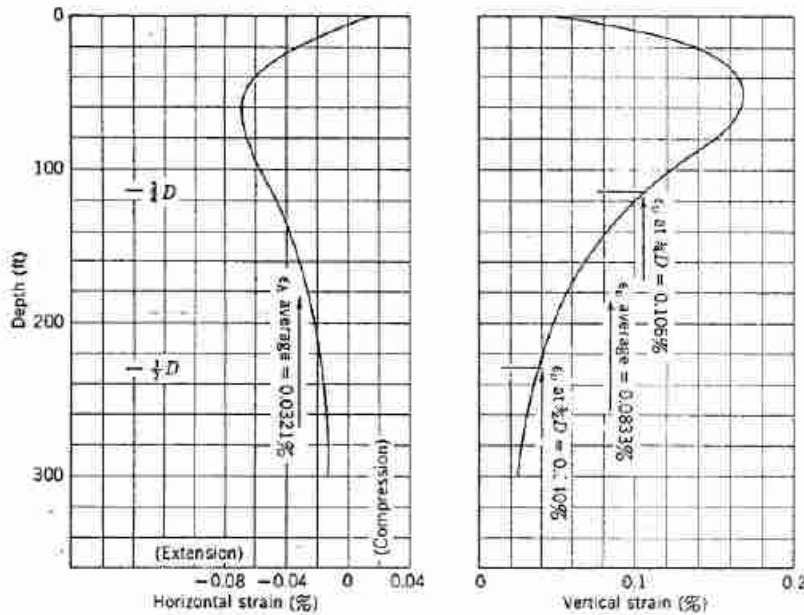


Fig. E14.12

ϵ_v and ϵ_h have been computed for every 12½ ft from depth zero to 300 ft and plotted as shown in Fig. E14.12. The significance of the average strains will be discussed in Example 14.13.

result can be obtained by direct integration of the equations for strain at a point:

$$\rho = \int_0^Z \epsilon_v dz$$

where

- ρ = settlement
- ϵ_v = vertical strain
- z = depth measured from surface
- Z = depth over which strains are to be summed

If the elastic body is of infinite depth, $Z = \infty$, the surface settlement may be expressed as

$$\rho = \Delta q_s \frac{R}{E} I_p \tag{14.14}$$

where

- R = radius of the loaded area
- I_p = an influence coefficient, which depends on Poisson's ratio μ and the radius to the point at which the settlement is being evaluated

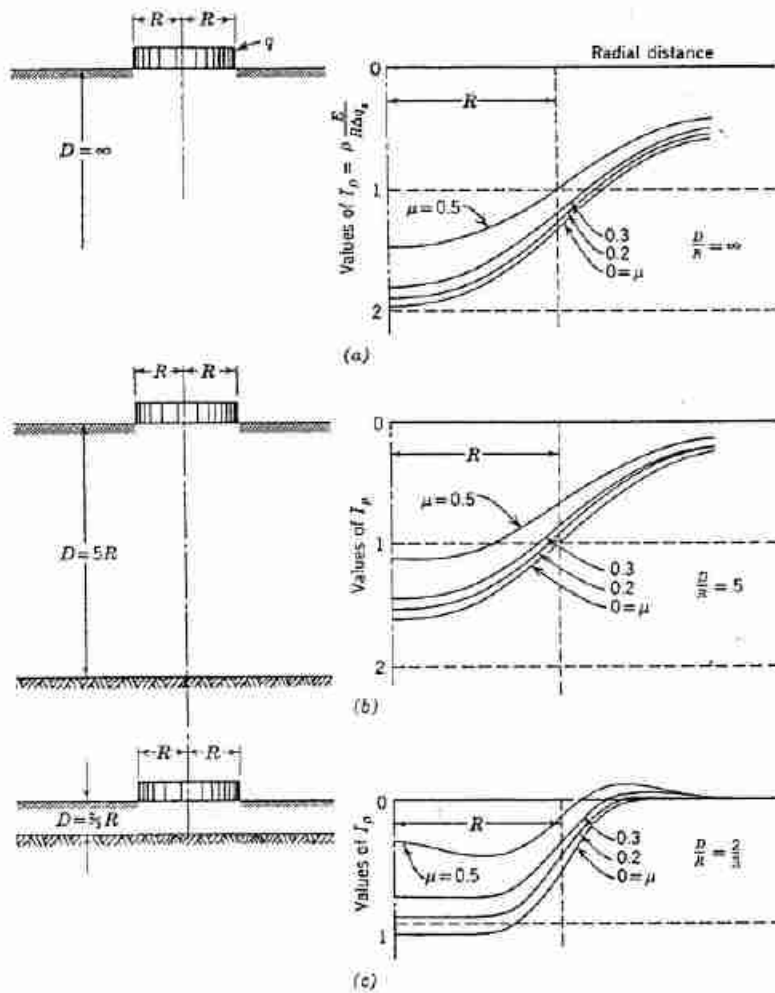


Fig. 14.20 Influence coefficients for settlement under uniform load over circular area (From Terzaghi, 1943).

Figure 14.20a gives values of this influence coefficient. Not only does the loaded area itself settle downward, but points on the surface outside of the loaded area also settle. The settlement at the edge of the loaded area is approximately 70% of that at the center line. A simple expression can be written for the settlement at the center line:

$$p = \Delta q, \frac{R}{E} 2(1 - \mu^2) \quad (14.15)$$

Strains at considerable depth, although small, still contribute to the settlement of the surface. This is shown in Fig. 14.21, which indicates the error in the calculated settlement if strains below any depth are ignored. For example, strains within a depth of $4R$ account for only about 75% of the total settlement.

Example 14.13 illustrates the application of Eq. 14.15 to the computation of settlement. The example further

shows that a reasonable estimate for the settlement can be obtained by (a) defining the bulb of stresses as being $3R$ deep, (b) finding the vertical strain at mid-depth of the bulb, $3R/2$, and (c) multiplying this "average" strain times the depth of the bulb. This procedure is useful for making approximate settlement estimates.

As may be seen in Example 14.12, the relative importance of horizontal and vertical strains changes markedly with depth. At most depths, the change in horizontal stress is small compared to the change in vertical stress, as is true in the standard triaxial compression test. Thus at most depths the horizontal strain is tensile and points move outward (see Fig. 14.2). On the other hand, at the surface under the loaded area the change in horizontal stress approximately equals the change in vertical stress, as in an isotropic compression test. Here the horizontal strain is compressive, and points on the surface must move toward the center line of the load. Outside of the

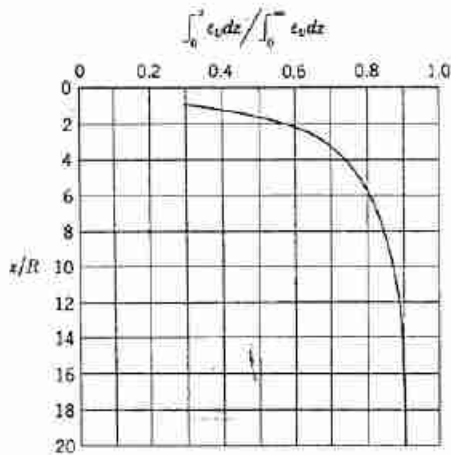


Fig. 14.21 Effect upon I_p of considering only a limited depth of strains.

► Example 14.13

Given. The tank loading and subsoil shown in Example 8.9.

$$E = 2000 \text{ kips/ft}^2$$

$$\mu = 0.45$$

Find. The settlement at the center of the tank for the condition of homogeneous, isotropic soil of infinite depth.

Solution.

$$\rho \Delta = \Delta q_s \frac{R}{E} 2(1 - \mu^2) \quad \text{Eq. 14.15}$$

$$\left. \begin{aligned} \Delta q_s &= 5.50 \text{ kips/ft}^2 \\ R &= \frac{D}{\gamma} = \frac{153\frac{1}{2} \text{ ft}}{2} \end{aligned} \right\} \text{ given in Example 8.9}$$

$$\rho \Delta = \frac{5.50 \text{ kips/ft}^2 \times \frac{153\frac{1}{2} \text{ ft}}{2} \times 2(1 - 0.45^2)}{2000 \text{ kips/ft}^2}$$

$$= \underline{\underline{0.346 \text{ ft} = 4 \text{ in.}}}$$

Settlement may be estimated by multiplying an average strain times the depth of the bulb of stresses. The following tabulation shows several ways in which this might be done.

Assumed Depth of Bulb	Average Strain	Settlement (in.)
$3R = 230 \text{ ft}$	Use strain at depth of $3R/2$: $\epsilon_x = 0.00106$	3.0
$4R = 306 \text{ ft}$	Use strain at depth of $2R$: $\epsilon_x = 0.00076$	2.8

The first method, using a bulb of depth $3R$, gives a closer estimate to the actual result of 4 in. ◀

loaded area the horizontal strains at the surface must be tensile, and this can happen only if the horizontal stress increments are tensile. Circular tension cracks are often observed around heavy loads resting on the surface of grounds. This general pattern of horizontal strains is somewhat similar to that in a fixed-end beam carrying a concentrated load at midspan.

Equation 14.14 may also be used when the elastic body is of limited depth. However, a different value of I_p must be used. Figure 14.20 gives values of I_p for two cases of an elastic stratum of limited depth. As would be expected, decreasing the depth of the elastic body decreases the settlement. When the elastic body is thin in comparison to the dimensions of the load, points outside of the loaded area may heave instead of settling. Burmister (1956) has compiled charts and tables that are especially useful when dealing with settlements of strata of limited thickness.

Elastic Theory for Settlement under Other Uniform Loads

The settlement at the corner of a rectangular area carrying a uniform stress Δq_s may be calculated from

$$\rho = \Delta q_s \frac{B(1 - \mu^2)}{E} I_p \quad (14.16)$$

where

- B = the width (least dimension) of the rectangle
- L = the length (greatest dimension) of the rectangle
- I_p = an influence coefficient given by Fig. 14.22

Settlements for points other than the corner of a rectangular area, and for any shape of loaded area that can be divided into rectangles, can be obtained using the method of superposition, as explained in Chapter 8 in connection with computing stresses (see Example 8.3). In particular, the settlement at the center of a square loaded area is

$$\rho = \Delta q_s \frac{B}{E} 1.12(1 - \mu^2) \quad (14.17)$$

As L/B becomes very great (i.e., for a strip footing), I_p gradually increases beyond all bounds. Thus a strip footing resting on an elastic body of infinite depth would experience an infinite settlement. In real problems, of course, soil strata are not infinite in depth and strip footings are not infinite in length. For a rectangular loaded area on an elastic stratum of thickness D overlying a rigid body, the approximate settlement at the corner of the area may be computed using Eq. 14.16 and

$$I_p = (1 - \mu^2)F_1 + (1 - \mu - 2\mu^2)F_2 \quad (14.18)$$

where the functions F_1 and F_2 may be read from Fig. 14.23. Burmister (1956) also presents useful charts for such problems.

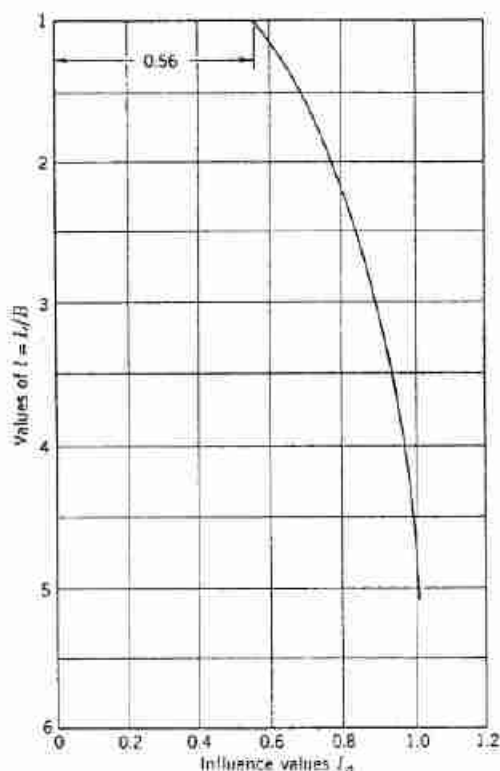


Fig. 14.22 Influence coefficient for settlement of rectangular loaded area (From Terzaghi, 1943).

Solutions have also been obtained for many other types of loading conditions, including loading by shear stresses. Scott (1963) gives a useful summary. With computer techniques, numerical values applicable to specific cases can be obtained.

Elastic Theory for Settlement under Rigid Footings

The condition of a uniformly distributed load occurs in practical problems, such as steel tanks for the storage of fluids. In many practical problems, however, the structural member (such as a footing) in contact with the soil will be quite rigid, and the settlement is more or less uniform over the area of contact between the footing and the soil. Since a uniform stress causes a dish-shaped pattern of settlement, in order to produce a uniform settlement the contact stresses must increase on the outside of the loaded area and decrease near the center line. The curves in Fig. 14.24 marked $K_r = \infty$ show the theoretical distribution of contact stress for the case of a truly rigid foundation. At the edge of the loaded area the contact stress theoretically is infinite.

A change in the distribution of stress over the contact area means a change in the relationship between load and

settlement. For a circular rigid loaded area this becomes

$$p = \Delta q_s \frac{R}{E} \frac{\pi}{2} (1 - \mu^2) \quad (14.19)$$

where Δq_s = average stress over the loaded area. Comparing Eq. 14.19 with Eq. 14.15, we see that the settlement of a rigid footing is 21% less than the center line settlement under a uniform load. Whitman and Richart (1967) present load-settlement relationships for rigid rectangular footings with various types of loading.

In some problems the structural member in contact with the soil cannot be considered perfectly flexible or perfectly rigid. Figure 14.24 can be used to estimate the contact stresses for intermediate conditions.

14.9 THEORETICAL PROCEDURES FOR USE WITH SOILS

As was discussed in Chapters 10 and 12, a mass of soil does not behave as an elastic, homogeneous, and isotropic material. Nonelasticity influences (a) the distribution of stress increments caused by these loads, and (b) the strains resulting from these stress increments. At present there are no theoretical procedures that consider both these difficulties, although such procedures are under development. Fortunately, experience has shown that useful predictions of settlement can be made by using the distribution of stress increments predicted by elastic theory, but employing special procedures to determine the resulting strains.

Stress Path Method

As applied to estimating the settlements, the stress path method consists of the following four steps:

1. Select one or more points within the soil under the proposed structure.
2. Estimate for each point the stress path for the loading to be imposed by the structure.
3. Perform laboratory tests which follow the estimated stress paths.
4. Use the strains measured in these tests to estimate the settlement of the proposed structure.

This same general approach, which is a powerful aid to understanding and solving deformation and stability problems, has already been used in Chapter 13.

Example 14.14 illustrates the application of this approach to the tank foundation of Example 8.9. Stress paths for selected points have already been given in Example 8.9. Figure 10.23 presents stress-strain results from triaxial tests following the stress paths for points A, B, D, and G. The vertical and horizontal strains as measured in these tests have been plotted in Example 14.14. Integration of these strains over a depth of 300

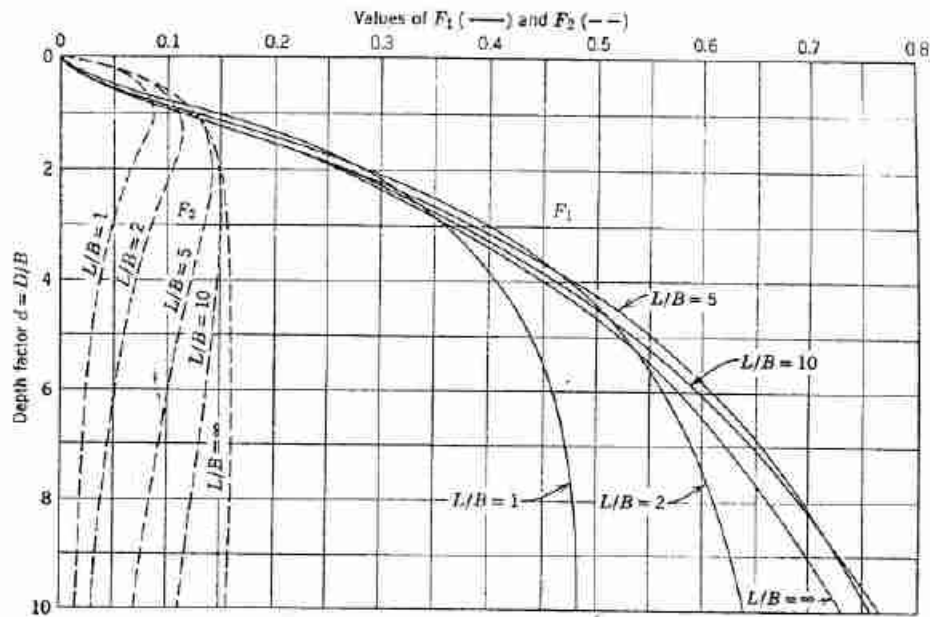


Fig. 14.23 Chart for factors in Eq. 14.18 (After Steinbrenner, 1934).

ft gives a center line settlement of $4\frac{1}{2}$ in. for the initial loading and $\frac{3}{4}$ in. for the second loading. There are strains below a depth of 300 ft. An estimate for the additional contribution of these deep-seated strains can be obtained from Fig. 14.21.

Stress Path Method Based on Average Point

A simple, and usually adequate, form of the stress path method involves use of a single "average point"

together with the concept of a bulb of stresses. According to the discussion in Section 14.8, the bulb may be taken as $3R$ deep with the average point at a depth of $3R/2$. As can be seen in Example 8.9, the laboratory test run for point D closely represents the conditions at the average point under the tank. The vertical strains in this test were 0.14% for the first loading and 0.027% for the second loading. Multiplying these strains by $3R = 230$ ft gives settlements of 3.9 and 0.75 in, respectively.

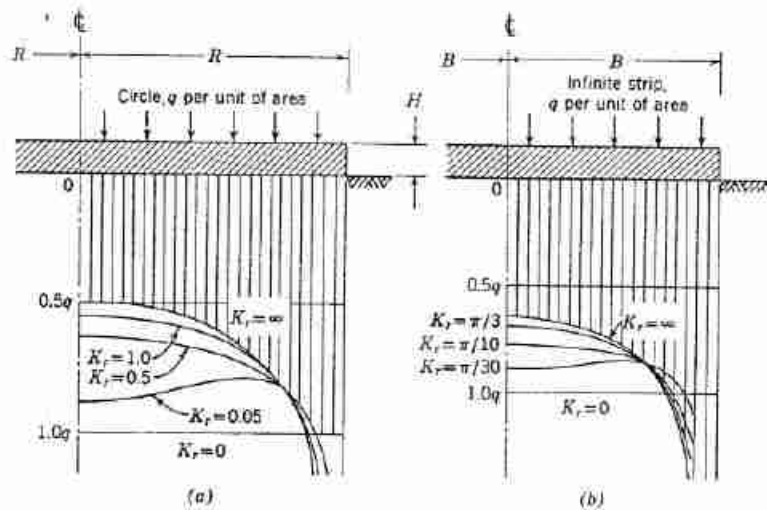


Fig. 14.24 Stress distributions under circular footings of varying rigidity (After Borowicka, 1936 and 1938).

► Example 14.14

Given. The same tank loading and subsoil as in Examples 8.9, 14.12, and 14.13.

Find. The settlement and distribution of subsoil strains by the stress path method.

Solution. A series of points (*A* to *H*) are selected and stress paths for them are drawn (Example 8.9).

Triaxial tests are run along paths *A*, *B*, *D*, and *G*; test results are plotted in Fig. 10.23. The vertical and horizontal strains measured in the laboratory tests are plotted as shown in Fig. E14.14.

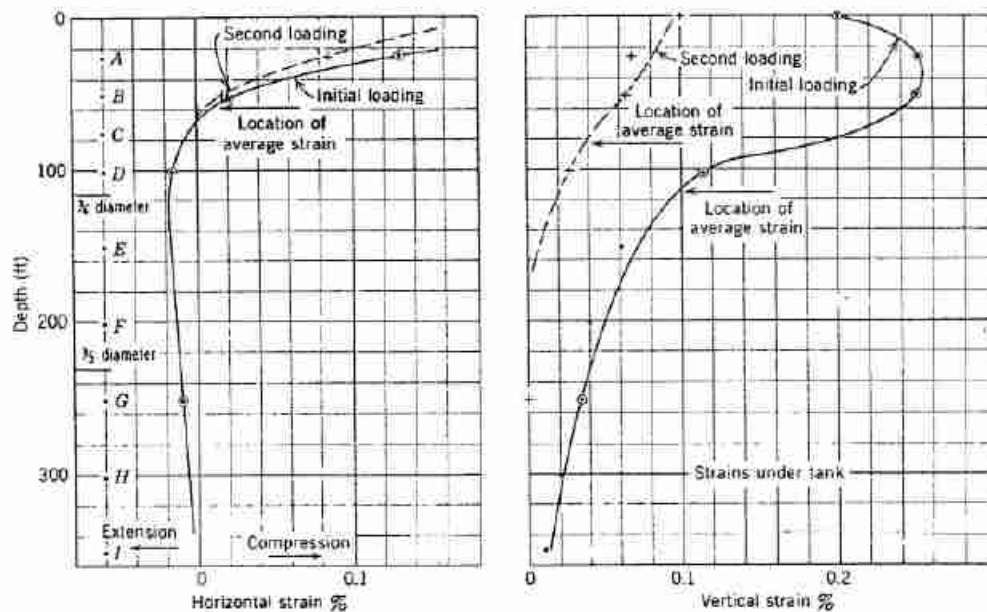


Fig. E14.14

The settlement under the center of the tank, found by the mechanical integration of strain-depth plot is:

$$\text{Initial loading: } \rho\delta = 4\frac{1}{2} \text{ in.}$$

$$\text{Second loading: } \rho\delta = \frac{3}{4} \text{ in.}$$

Use of Stress Path Method to Determine Modulus

An alternate procedure is to determine a value of E from the stress path test for the average point, and then to compute settlement from an equation such as Eq. 14.15. The procedure illustrated in Example 12.7 may be used to determine the modulus E from the stress path test. In the case of test *D*, the change in horizontal stress is so small (i.e., this test is so much like a standard triaxial compression test) that it suffices to obtain E by dividing change in axial stress by change in axial strain. This gives $E = 2000$ kips/ft² for the first loading and $E = 7500$ kips/ft² for the second loading. The settlement for the first loading has already been computed in Example 14.13 as 4 in.; the settlement corresponding to the second loading is 1.1 in.

Discussion of Methods

Figure 14.25 compares the strains as predicted by elastic theory (Example 14.12) with those predicted by the stress path method (Example 14.14). The stress path method gives larger strains near ground surface but gives smaller strains at depth. This is because the stress path method takes into account the increase in stiffness of the soil with depth. At shallow depths, the initial stress and hence the stiffness are small and relatively large strains occur. Conversely, at greater depth the stiffness is greater than the average stiffness at point *D*, and hence the strains at depth are smaller than those computed from an average modulus. Figure 14.25 shows that the predicted pattern of strain under the tanks agrees generally with those measured under a model footing.

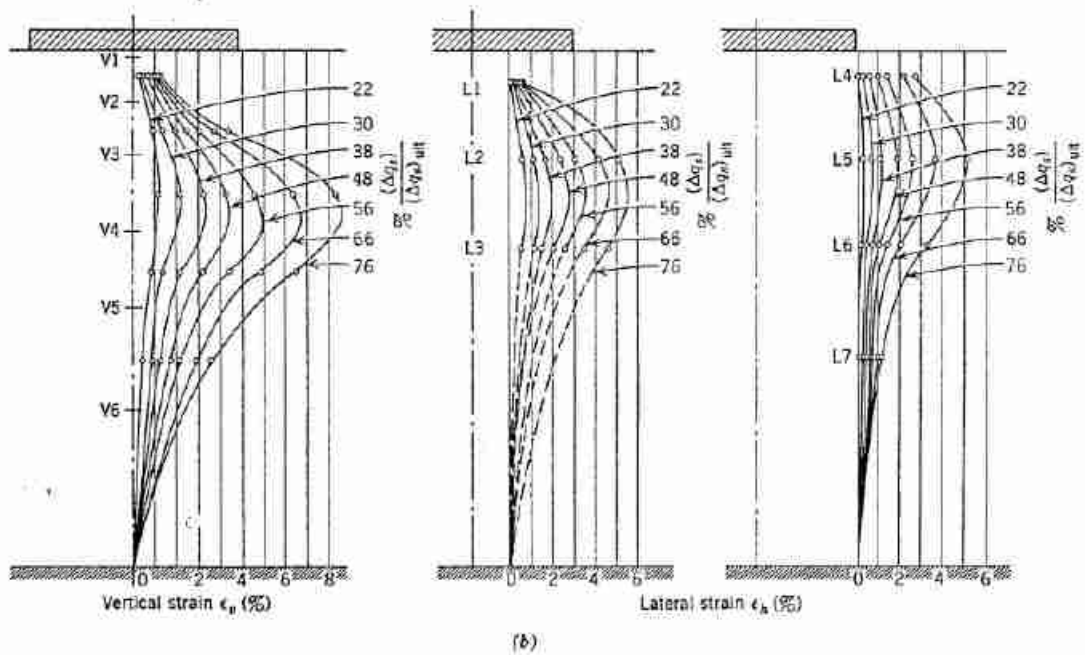
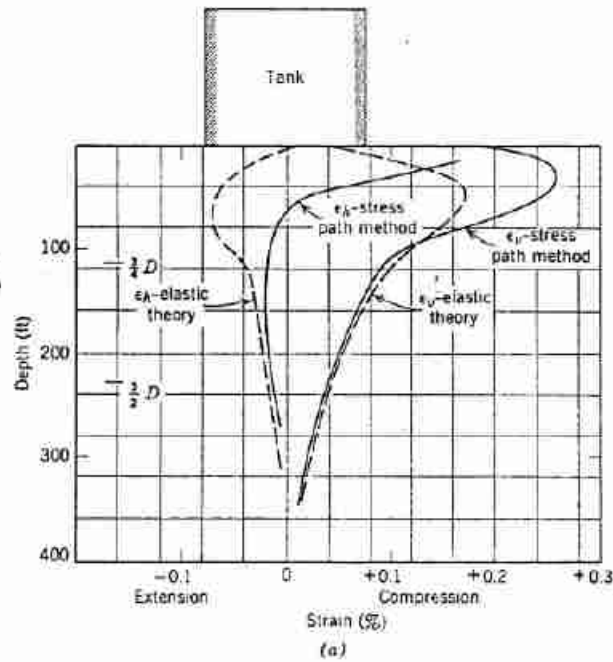


Fig. 14.25 Strains in subsoil [(b) From Eggestad, 1963.]

Each of the three methods involves approximations and each has its advantages. The stress path method involving several points best accounts for the many factors that affect the stiffness of soil, but must neglect the strains below some depth. The stress path method with a single average point is very simple, but involves several assumptions. The elastic method, using an average modulus from an average point, also involves doubtful assumptions, but is especially useful when the settlement must be known at many points other than just at the center line. The choice among the methods will depend upon the circumstances of each problem.

A major difficulty in making theoretical estimates of settlements is obtaining representative samples of the soil. Usually the process of sampling tends to decrease the stiffness of the sample compared to the *in situ* stiffness. Settlements estimated in the foregoing examples from the second loading ($\frac{3}{4}$ to 1 in.) are reasonable in view of the settlement actually measured under similar tanks in the same area, but the estimates based on the first loading are unreasonably large. Considerable evidence of this type suggests that stress-strain data from a second loading should be used when estimating the settlement of structures to be founded on sands.

In summary, any theoretical estimate of settlement is an approximation. At the present time, the best estimates can be obtained by the stress path method which (a) uses elastic theories to estimate stresses, (b) obtains strains or moduli from tests that duplicate the initial stresses and

expected stress increments, and (c) relies upon experience to indicate how best to compensate for the effects of sample disturbance.

14.10 EMPIRICAL METHODS FOR PREDICTING SETTLEMENT

Because of the difficulties with a strictly theoretical approach, an engineer should always study the settlement experience of existing structures nearby. Empirical approaches, based on a large number of case studies, may also be used to supplement theoretical analyses or for crude preliminary estimates. The two most widely used empirical, or semiempirical, methods are the *load test* and the *penetration test*.

Load Test

In the load test the soil is subjected to a load increased in stages with the settlement under each increment of load being measured. The measured load-settlement data are then used to predict the behavior of the actual footing. Although a full-size footing can be used for the loading test, the normal practice is to employ a small plate of the order of 1–3 ft in diameter. The use of larger test footings is usually impractical because of the expense and difficulty in obtaining large loads. The results from the load test are then extrapolated from the test footing to the prototype footing.

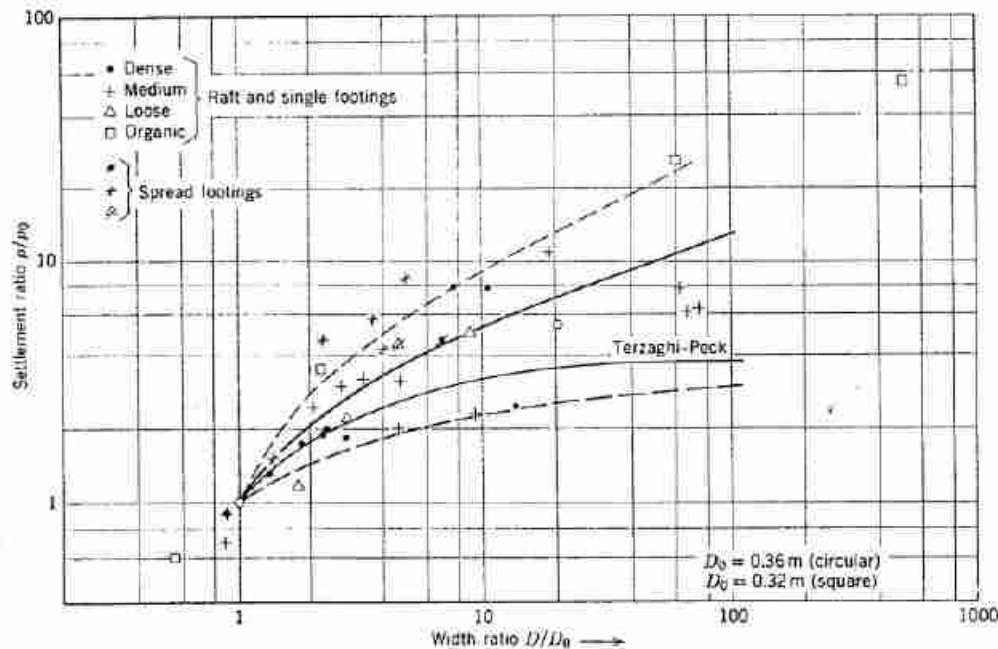


Fig. 14.26 Comparison between settlement and dimension of loaded area as derived from collected case records (From Bjerrum and Eggstad, 1963).

A widely used relation between settlement on sands and footing size is the empirical one developed by Terzaghi and Peck (1967):

$$\frac{\rho}{\rho_0} = \frac{4}{(1 + D_0/D)^2} \quad (14.20)$$

where

- ρ = the settlement of the prototype
- ρ_0 = the settlement of the test footing
- D = the smallest dimension of the prototype
- D_0 = the smallest dimension of the test footing

Figure 14.26 shows a plot prepared by Bjerrum and Eggstad (1963) from 14 sets of load-settlement data along with a plot of Eq. 14.20. This figure shows that the settlement of Eq. 14.20 is approximately correct, but that there is considerable scatter.

To get dependable results from a load test we must be sure that the soil under the test plate is not disturbed, and that the soil at the site is homogeneous for a depth which is large relative to the size of the actual footing. Figure 14.27, for example, shows a subsoil situation in which the results of the load test may be very misleading. The settlements under the test plate are due primarily to strains occurring within soil *A*, whereas under the actual footing the settlements are due primarily to strains occurring in soil *B*. If soils *A* and *B* have different stress-strain properties, the settlement predicted from the load test can bear little resemblance to what will actually occur under the prototype footing.

Penetration Tests

Various penetration tests—standard penetration tests, Dutch deep sounding tests, and a radio-isotropic probe (see Meigh and Nixon, 1961, for a comparison of these penetration tests)—have been used to predict the settlement of foundations on sand. The one most widely used, especially in the United States, is the standard penetration test described in Chapter 7.

Figure 14.28 gives the surface stress Δq_s required to cause a settlement of 1 in. for a footing resting on sand

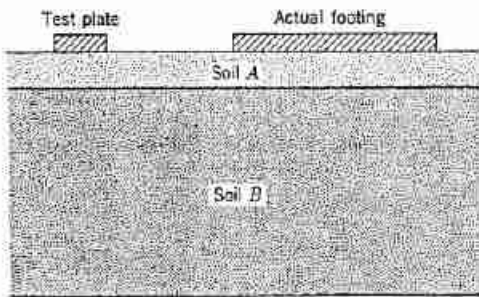


Fig. 14.27 Situation where load test results can be misleading.

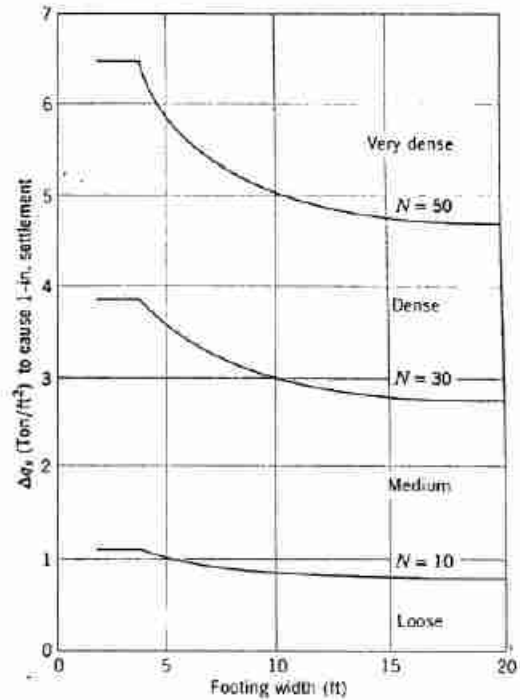


Fig. 14.28 Settlement of footing from standard penetration resistance *N*. (From Terzaghi and Peck, 1948).

as a function of the standard penetration resistance *N* and the footing width *B*. Another relation, proposed by Meyerhof (1965), gives,

$$\begin{aligned} \Delta q_s &= \frac{N\rho}{8} & B \leq 4 \text{ ft} \\ \Delta q_s &= \frac{N\rho}{12} \left(\frac{B+1}{B}\right)^2 & B > 4 \text{ ft} \end{aligned} \quad (14.21)$$

where Δq_s is in tons/ft², *B* in feet, and ρ in in. Figure 14.29 (Meyerhof, 1965) shows a comparison of predicted and observed settlements for footings on sand and on gravel. It shows that the predicted settlements for the actual structure studied by Meyerhof are greater than the observed ones, and that there does not appear to be any significantly superior performance of either the standard penetration or the static cone penetration test.

14.11 THE INFLUENCE OF FOOTING SIZE ON BEARING CAPACITY AND SETTLEMENT

The preceding sections have shown that the bearing capacity and settlement of a footing resting on sand depend on the properties of the sand and on the size, shape, and embedment of the footing. Bearing capacity

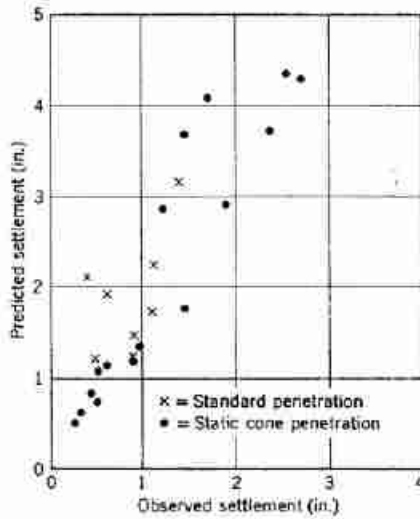


Fig. 14.29 Comparison of predicted and observed settlements of footing on sand and gravel (From Meyerhof, 1965).

depends significantly on the friction angle ϕ and on the relative density of the sand. The soil property which most significantly influences the settlement of a footing is the stress-strain modulus E . The rest of this section considers primarily the influence of footing size on bearing capacity and settlement, in an attempt to pull together some of the many concepts already presented and to leave the student with a simple, general picture of the behavior of footings on sand.

The bearing capacity equations show that, for footings on the surface of sand, the bearing capacity is directly proportional to the size of the footing. Further, the

► Example 14.15

Given. A round footing resting on sand with: $\phi = 34\frac{1}{2}^\circ$ and $\gamma = 100 \text{ lb/ft}^3$.

Find. The bearing capacity for:

- a. $D = 3 \text{ ft}, d = 0$.
- b. $D = 3 \text{ ft}, d = 2 \text{ ft}$.
- c. $D = 6 \text{ ft}, d = 0$.
- d. $D = 6 \text{ ft}, d = 2 \text{ ft}$.

Solution.

$$(\Delta q_s)_b = (0.6)\frac{1}{2}\gamma DN_f + \gamma d N_q \quad (14.11)$$

From Fig. 14.16, $N_f = N_q = 30$.

- a. $(\Delta q_s)_b = (0.6)(\frac{1}{2})(100)(3)(30) = 2.7 \text{ kips/ft}^2$
- b. $(\Delta q_s)_b = (0.6)(\frac{1}{2})(100)(3)(30) + (100)(2)(30) = 8.7 \text{ kips/ft}^2$
- c. $(\Delta q_s)_b = (0.6)(\frac{1}{2})(100)(6)(30) = 5.4 \text{ kips/ft}^2$
- d. $(\Delta q_s)_b = (0.6)(\frac{1}{2})(100)(6)(30) + (100)(2)(30) = 10.4 \text{ kips/ft}^2$

bearing capacity goes up significantly as the depth of the footing below the surface increases. The importance of these two variables (footing size and depth below the surface) is illustrated in Example 14.15.

► Example 14.16

Given. A 48-ft-high tank is built on an infinite deposit of sand with:

$$\gamma = 129 \text{ pcf}$$

$$\mu = 0.45$$

Find. The settlement of the center of the tank when filled with water for the following conditions:

- a. $D = 100 \text{ ft}$; E constant and equals 4000 kips/ft^2 .
- b. $D = 200 \text{ ft}$; E constant and equals 4000 kips/ft^2 .
- c. $D = 100 \text{ ft}$; E varies as σ_{v0} and equals to 4000 kips/ft^2 at $d = 75 \text{ ft}$.
- d. $D = 200 \text{ ft}$; E varies as σ_{v0} and equals 4000 kips/ft^2 at $d = 75 \text{ ft}$.
- e. $D = 100 \text{ ft}$; E varies as $\sqrt{\sigma_{v0}}$ and equals 4000 kips/ft^2 at $d = 75 \text{ ft}$.
- f. $D = 200 \text{ ft}$; E varies as $\sqrt{\sigma_{v0}}$ and equals 4000 kips/ft^2 at $d = 75 \text{ ft}$.

Solution.

$$\rho = \Delta q_s \frac{R}{E} 2(1 - \mu^2) \quad (14.15)$$

$$\Delta q_s = 48 \text{ ft} \times 62.4 \text{ lb/ft}^3 = 3.0 \text{ kips/ft}^2$$

$$2(1 - \mu^2) = 2(1 - 0.45^2) = 1.60$$

$$a. \rho = 3.0 \text{ kips/ft}^2 \times \frac{50 \text{ ft} \times 1.60}{4000 \text{ kips/ft}^2} = 0.60 \text{ ft}$$

$$b. \rho = \frac{3.0 \times 100 \times 1.60}{4000} = 1.20 \text{ ft}$$

c. Since E varies as σ_{v0} and σ_{v0} varies as depth, E varies as depth. Take "average point" at depth = $\frac{1}{2}D$

$$E_{(D/2)} = E_{75} = 4000 \text{ kips/ft}^2$$

ρ for case c same as for case a, i.e., $\rho = 0.60 \text{ ft}$.

d. Now $E_{(D/2)} = E_{150}$, and hence the modulus is twice as large as in c. The radius R is also twice as large.

$$\rho = \frac{(3.0)(100)(1.60)}{2 \times 4000} = 0.60 \text{ ft}$$

e. ρ same as ρ for case a, i.e., $\rho = 0.60 \text{ ft}$

$$f. \rho = \frac{(3.0)(100)(1.60)}{\sqrt{\frac{150}{75}} \times \frac{\gamma}{\gamma} \times E \text{ at } 75} = \frac{(30)(100)(1.60)}{\sqrt{2} \times 4000} = 0.85 \text{ ft}$$

Example 14.16 illustrates the influence of foundation size and the nature of variation of the modulus E with depth on settlement. The modulus at a depth of 75 ft is given. This is the "average point" for the 100-ft foundation. Different rules are used to extrapolate the given

modulus to the average point for the larger foundation. Assuming modulus E is constant with depth, settlement is directly proportional to foundation size. If the modulus E varies directly with the vertical confining stress, the settlement is independent of foundation size.

► Example 14.17

Given. A round, rigid footing resting on sand with

$$\begin{aligned}\phi &= 34\frac{1}{2}^\circ \\ \gamma &= 100 \text{ lb/ft}^3 \\ \mu &= 0.45\end{aligned}$$

Find. Relationship among D (varying from 1 to 10 ft), ρ , and $(\Delta q_s)_b$ for

- $E = 200 \text{ kips/ft}^2$.
- $E = 200 \text{ kips/ft}^2$ at depth 10 ft and varying as σ_{v0} .
- $E = 200 \text{ kips/ft}^2$ at depth 10 ft and varying as $\sqrt{\sigma_{v0}}$.

Solution. Bearing capacity

$$(\Delta q_s)_b = (0.6)\frac{1}{2}\gamma DN_y \quad (14.11)$$

From Fig. 14.16,

$$N_y = 30$$

$$\therefore (\Delta q_s)_b = (0.6)\left(\frac{1}{2}\right)(100)D(30) = 0.9 D \text{ in kips/ft}^2$$

Settlement:

$$\rho = \Delta q_s \frac{R}{E} \frac{\pi}{2} (1 - \mu^2) \quad (14.19)$$

$$\frac{\pi}{2} (1 - 0.45)^2 = \left(\frac{\pi}{2}\right)(0.797) = 1.25$$

$$a. \quad \rho = \Delta q_s R \frac{1.25}{200} = \Delta q_s R (6.25 \times 10^{-3})$$

$$b. \quad \rho = \Delta q_s R \frac{1.25}{(200/10)(3R/2)} = \Delta q_s (4.17 \times 10^{-3})$$

$$c. \quad \rho = \Delta q_s R \frac{1.25}{(200/\sqrt{10})\sqrt{\frac{3}{2}}R} = \Delta q_s \sqrt{R} (1.62 \times 10^{-3})$$

These equations are used to compute the following results

	$D = 5 \text{ ft}$	$D = 10 \text{ ft}$
$(\Delta q_s)_b$	4.5 kips/ft ²	9.0 kips/ft ²
a. ρ for $\Delta q_s = 3$	—	0.0938 ft
ρ for $\Delta q_s = 1\frac{1}{2}$	0.0235 ft	0.0469 ft
b. ρ for $\Delta q_s = 3$	—	0.125 ft
ρ for $\Delta q_s = 1\frac{1}{2}$	0.063 ft	0.063 ft
c. ρ for $\Delta q_s = 3$	—	0.109 ft
ρ for $\Delta q_s = 1\frac{1}{2}$	0.038 ft	0.054 ft

These results are plotted in Fig. E14.7.

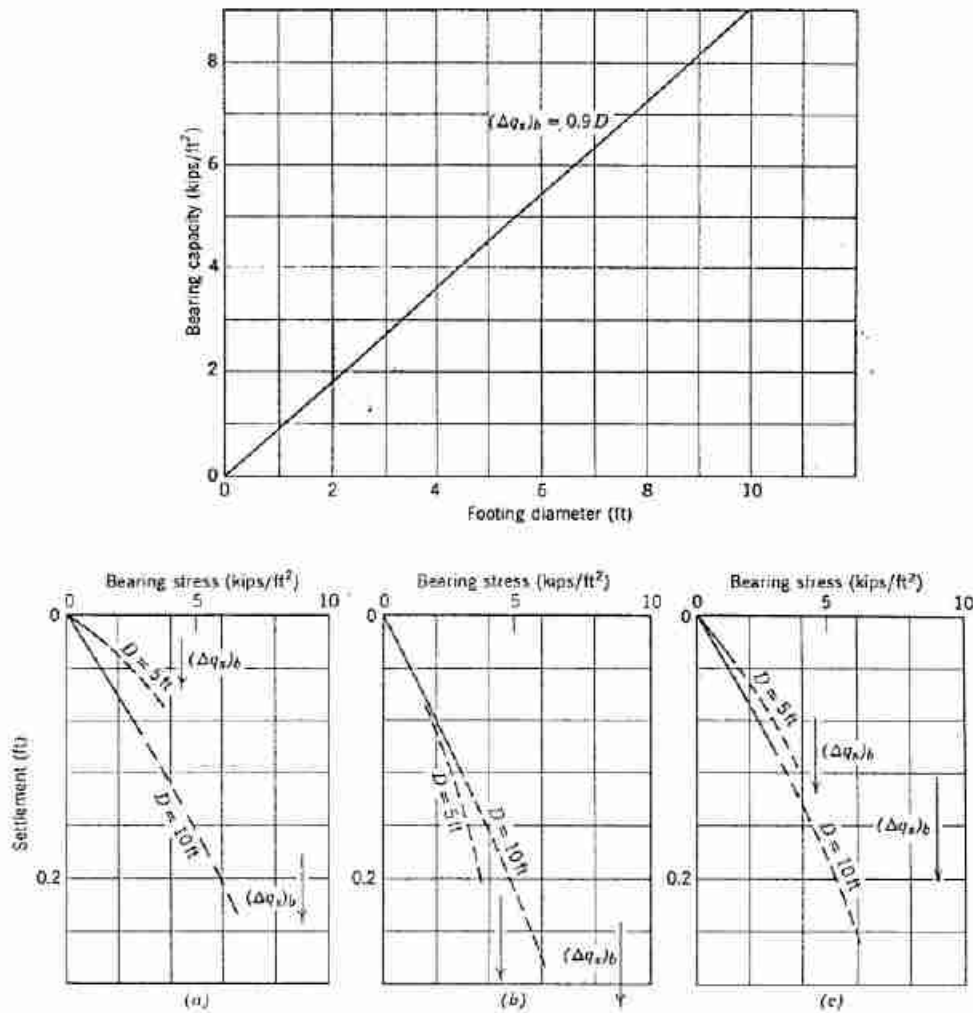


Fig. E14.17 (a) Constant E . (b) E varies as σ_{v0} . (c) E varies as $\sqrt{\sigma_{v0}}$.

If the modulus E varies as the square root of the confining stress—probably the best general relationship between E and confining stress—the result is intermediate.

Example 14.17 combines most of the variables of Examples 14.15 and 14.16 to show the relationship among footing size, settlement, and bearing stress. As illustrated in Fig. E14.17, the bearing capacity is directly related to the footing diameter and is equal to 0.9 of the diameter of the footing. The lower part of Fig. E14.17 shows the settlements versus bearing stress plots for footings of diameters of 5 and 10 ft for the three conditions of modulus E . The situation shown in *c* is that which best represents the general relationship between stress and settlement for footings on sand.

It should be emphasized that the settlement equations, such as Eq. 14.14, hold only for bearing stresses which

are small relative to the bearing capacity, e.g., factors of safety of 3 or greater. As the bearing stress approaches the bearing capacity, the settlements increase in an unpredictable fashion. This important fact is accounted for in Fig. E14.17 by showing the early portion of the stress-settlement curve as a solid line and that portion past the factor of safety of 3 as a dashed line.

14.12 SUMMARY OF MAIN POINTS

1. For a footing to be properly designed it must meet two conditions:
 - a. The bearing stress Δq , must be less than the bearing capacity $(\Delta q_s)_h$, which is the bearing stress that causes a shear failure within the foundation soil.

- b. The settlement must be less than the *allowable settlement*.
- As a footing is loaded to failure the foundation soil first reaches *local shear* and then *general shear*.
 - Local shear occurs when the strength of the soil in a zone is reached and the zone becomes plastic. General shear occurs when all the soil along a slip surface is at failure.
 - In a loose sand, local shear occurs at a much lower bearing stress than does general shear. In a dense sand, local shear occurs at a bearing stress only slightly less than that which causes general shear.
 - Bearing capacity is seldom a controlling factor in the design of footings on sand other than small footings—less than 3 ft—because the bearing capacity is usually far in excess of the bearing stress which causes the settlement to exceed the allowable settlement.
 - The allowable settlement is the maximum settlement a structure can tolerate and still perform properly.
 - It is usually the *differential settlement* or *angular distortion* between two points which is more serious to the structure than the total settlement. The allowable settlement is expressed as a function of total settlement rather than differential settlement or distortion because:
 - The differential settlement is much more difficult to predict than the total settlement.
 - There generally exists an empirical relationship between differential settlement and maximum settlement.
 - Available for predicting settlement are two theoretical methods—*elastic formulas* and *summation of strains*—and two empirical or semiempirical methods—*load test* and *penetration test*. Theoretical methods should be used in conjunction with empirical methods, since empirical methods reflect field experience.
 - Recommended for predicting settlement is the *stress path method*, either to help pick the modulus E for an elastic solution or to get measured strain for a direct summation of strains.
 - The inadequacy of methods for predicting settlement are due to:
 - Difficulty in obtaining correct stresses in soil.
 - Difficulty in obtaining appropriate *in situ* stress-strain data from laboratory tests (trouble caused primarily by sample disturbance).
 - Soil is not a linearly-elastic, homogeneous, isotropic material.
 - Soil varies considerably both in horizontal and vertical directions.

- Bearing capacity and settlement of a footing on sand are related both to soil properties and to footing size and depth of embedment. Bearing capacity increases significantly with increased footing size and depth of embedment. Settlement increases somewhat with increasing footing size.

PROBLEMS

14.1 A footing 8 ft square bears at 3 ft depth in a sand with a friction angle of 36° . Find the bearing capacity and the ultimate bearing capacity. The sand weighs 115 pcf.

14.2 The soil profile at a given site is as follows:

0–4 ft cinders, with $\phi = 30^\circ$ and $\gamma = 55$ pcf

4–50 ft sandy gravel, with $\phi = 38^\circ$ and $\gamma = 120$ pcf

Find the bearing capacity for a 10 ft square footing bearing on top of the sandy gravel.

14.3 A load test was made on a square plate 1 ft by 1 ft on a dense sand having a unit weight of 115 lb/ft³. The bearing plate was enclosed in a box surrounded by a surcharge of the same soil 1 ft deep. Failure occurred at a load of 7000 lb. What would be the failure load per unit of area of the base of a footing 5 ft square located at the same depth in the same material?

14.4 Assume that the footing in Problem 14.3 supports a light building frame which exerts not only a vertical load V but also a horizontal component $H = 0.15V$ and a moment $M = 0.5V$ (i.e., eccentricity 0.5 ft). What is the allowable load V if a safety factor of 3 is used?

14.5 A foundation 50 ft by 100 ft rests upon a soil with an average E of 10,000 psi. The average bearing stress is 6 tsf. Calculate the settlement at the corners and center of the foundation. Assume $\mu = 0.3$.

14.6 Repeat Problem 14.5, assuming that the sand is only 25 ft thick and is underlain by rock.

14.7 A standard load test (1 ft square plate) on a dense dry sand ($\gamma = 120$ pcf) gives the following data:

Load (TSF)	Settlement (ft)
0.75	0.01
1.50	0.02
2.25	0.04
3.00	0.08
3.75	0.25 (failure)

Another load test is run on the same soil but with the following differences:

Width = 5 ft

Length = 50 ft

Predict:

- The ultimate bearing capacity.
- The settlement at a load of 2 tsf.

14.8 Using the data of Problem 14.7, determine the allowable bearing stress for a 8 ft square footing if the permissible settlement is 1 in.

14.9 A sand has an average blow count of 20 blows/ft. Design a footing to carry a load of 200 tons with a maximum settlement of 2 in. and a minimum safety factor of 3 against a shear failure.

14.10 The soil at the site of the tank in Example 14.12 has a standard penetration resistance varying between 15 and 25 blows/ft. Predict the tank settlement on the basis of (a) Eq. 14.21; and (b) Fig. 14.28.

14.11 On the basis of Figs. 14.8 and 14.9 select the maximum allowable settlement for a factory building to house equipment very sensitive to differential settlement.

14.12 A 6-ft-wide strip footing rests 3 ft below the surface of sand having $\phi = 32^\circ$ and $\gamma = 130 \text{ lb/ft}^3$. Compute the ultimate bearing capacity from: (a) Eqs. 14.4 and 14.5; and (b) Eq. 14.6 and Fig. 14.16. Which value is more nearly correct? Explain.

CHAPTER 15

Dynamic Loading of Soil

If the loads applied to a mass of soil change rapidly enough so that inertia forces become significant in comparison to static forces, special calculations become necessary in order to estimate the deformation of the soil. Typical problems of this type include machine foundations, slope stability during earthquakes, pile driving, and vibratory compaction. This chapter introduces some of the basic concepts from the important field of soil dynamics.

The rate of loading at which a problem "becomes dynamic" depends very much upon the size of the mass of soil involved. With the typical specimen used for laboratory tests, inertial forces generally do not become significant until the frequency of loading exceeds 25 cycles per second (cps). On the other hand, a large earth dam may experience significant inertial forces with frequencies as low as 0.5 cps.

15.1 FOUNDATIONS SUBJECTED TO DYNAMIC LOADS

The most common problem involving dynamic loading is that of foundations for machinery. Reciprocating machines and poorly balanced rotating equipment cause periodic dynamic forces Q :

$$Q = Q_0 \sin 2\pi ft \quad (15.1)$$

where

$$\begin{aligned} Q_0 &= \text{maximum amplitude of dynamic force} \\ f &= \text{operating frequency} \\ t &= \text{time} \end{aligned}$$

Typical operating frequencies range from 200 cycles/min for large reciprocating air compressors to about 12,000 cycles/min for turbines and high-speed rotary compressors. Punch presses and forging hammers also apply intermittent, dynamic loads to foundations. A recent problem is that of providing foundations for precision tracking radars. The principles used to analyze the

response of foundations to such applied loads may also be used to analyze the response of foundations to ground motions, such as those imposed by earthquakes, blasting, and nearby machinery.

As in the case of foundations subjected to static loadings, the basic criterion governing the design of machine foundations is permissible motion. In general, there is a prescribed limit for the dynamic motions to be permitted during operation, and also a prescribed limit upon the settlement that may develop during an extended period of operation.

Usually it is necessary to perform a dynamic analysis in order to assure that these criteria are met. In order to make such an analysis, the machine-foundation-soil system can be represented by an equivalent lumped mass-spring-dashpot system, which will vary from problem to problem (see Fig. 15.1) depending on the number of modes of motion which the actual system can experience. This section, which is based upon Whitman and Richart (1967), discusses systems having a single degree of freedom, usually vertical motion. For a fuller discussion of the problem, together with methods for handling more complicated types of problems, the reader may consult Barkan (1962). Field tests demonstrating the validity of these methods are described by Richart and Whitman (1967) and Whitman (1966).

Permissible Dynamic Motions

A foundation subjected to a periodic dynamic load will experience a dynamic motion p_d at the same frequency as the applied force. The peak velocities and accelerations of the foundation may be expressed in terms of the maximum motion and frequency as follows:

$$\dot{p}_d = 2\pi f p_d \quad (15.2a)$$

$$\ddot{p}_d = (2\pi f)^2 p_d \quad (15.2b)$$

where dots indicate differentiation with respect to time. To avoid damage to machines or machine foundations,

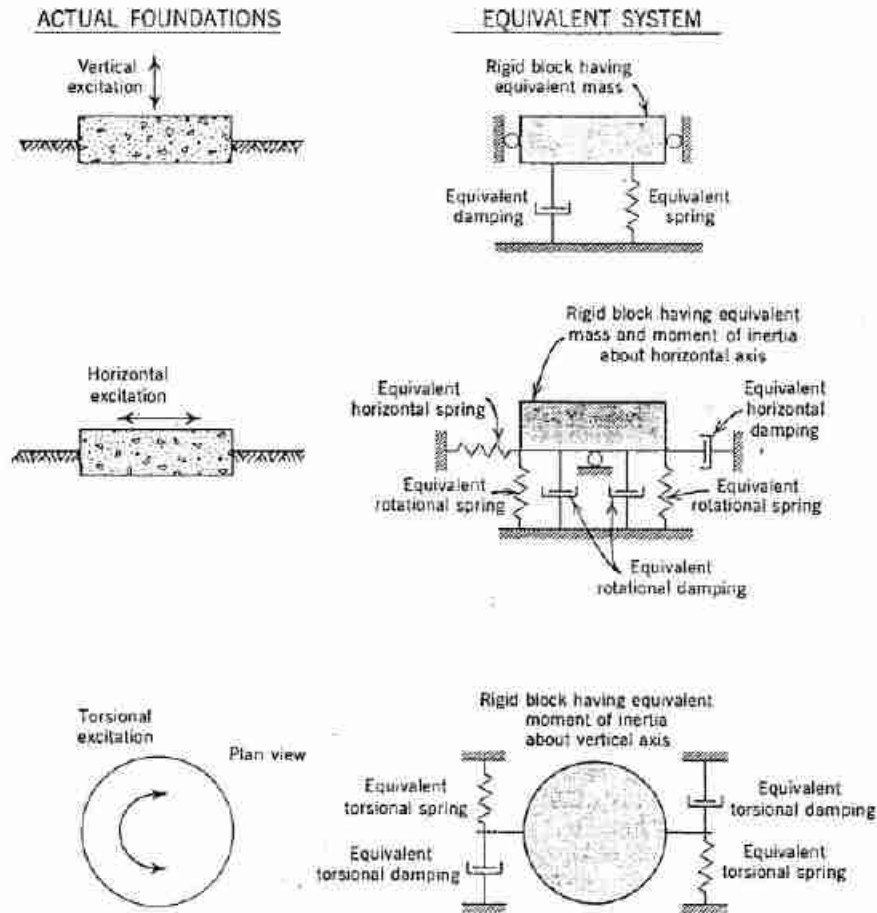


Fig. 15.1 Typical equivalent lumped systems.

the maximum velocity of vibration should not exceed 1 in./sec. However, if people are to work near the equipment, even stricter requirements may be necessary. Vibrations begin to be troublesome to persons when the maximum velocity exceeds 0.1 in./sec, and they are noticeable to persons if the velocity exceeds 0.01 in./sec. At a frequency of 1000 cycles/min, these velocities correspond to amplitudes of motion of 0.01, 0.001, and 0.0001 in., respectively. At other frequencies of operation the permissible amplitude of motion will be different. Note that the motion which may be noticed by persons is approximately $\frac{1}{1000}$ of that which is likely to cause damage to machines. Usually it is also necessary to impose a limit on the maximum acceleration that the foundations may experience. In some problems, such as when a stable base must be provided for precision machinery or calibration equipment, it may be necessary to restrict the acceleration to less than $10^{-4} g$.

The foundation engineer will find it necessary in all problems to work closely with the client to establish design criteria suitable to the particular problem at hand.

Concepts from Basic Dynamics

The response of a single degree of freedom mass-spring-dashpot system to a periodic applied load is given by the response curves in Fig. 15.2. The key characteristic determining the response of such a system is the undamped natural frequency f_n :

$$f_n = \frac{1}{2\pi} \left(\frac{k}{M} \right)^{1/2} \quad (15.3)$$

where k is the spring constant and M is the mass.

If the operating frequency f is much less than the undamped natural frequency f_n , then the applied force is resisted primarily by the spring, and damping and inertia are of little importance. The amplitude of motion in this case is simply the static response:

$$f \ll f_n \quad \rho_d = \frac{Q_0}{k} \quad (15.4)$$

If $f \gg f_n$, then the applied force is resisted primarily by inertia and the spring and damping are of little

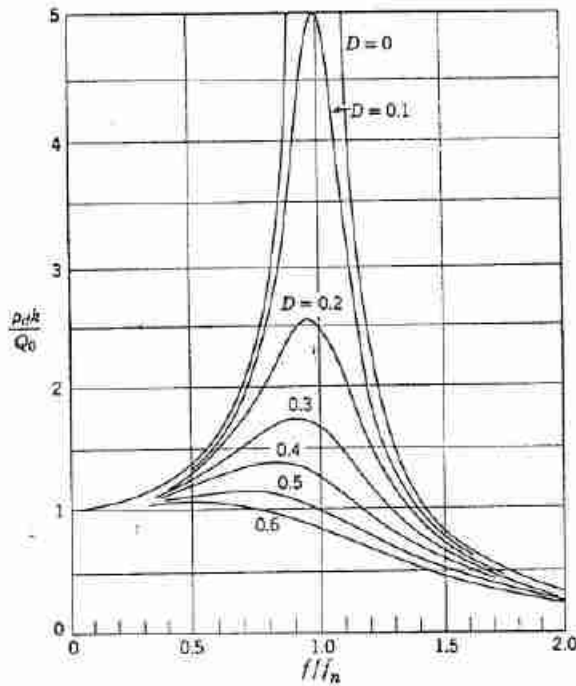


Fig. 15.2 Response of mass-spring-dashpot system.

importance. In this case the amplitude of motion is given by

$$f \gg f_n \quad P_d = \frac{Q_0}{(2\pi f)^2 M} \quad (15.5)$$

If $f \approx f_n$ then the system is said to be in resonance. The motions at resonance are determined by the damping ratio D , the ratio of the actual damping to the critical damping.

Design criteria for a dynamically loaded foundation are often written in such a way as to avoid resonance. If the damping present in the system is small, the motions at

Analysis	Factors Required	
Approximate estimate for resonant frequency	k and M	
Approximate estimate for motions at frequencies well away from resonance	$\ll f_n$	k
	$\gg f_n$	M
Upper limit for motion at frequencies near resonant frequency	D and k or M	

Fig. 15.3 Summary of parameters required for dynamic analysis.

resonance may be very large, and it is indeed prudent to avoid the resonant condition in order to meet the specifications upon permissible dynamic motions. However, if moderate to large damping is present in the system, it may be possible to operate near the resonant condition and still keep the dynamic motions within permissible limits.

Figure 15.3 summarizes the way in which the various parameters of a lumped system influence the response of the system. The approach to dynamic analyses and to design differs depending on the amount of damping present in the system. Hence the magnitude of damping that may exist in actual foundations is considered first in the following subsections. When damping is so small that resonance must be avoided, it becomes necessary to estimate the natural frequency, which requires that the spring constant and the mass be known. Since it is easier to make a reasonable estimate for the mass, it is considered next. Finally the spring constant, which is at the same time the most important and the most difficult parameter for the engineer to evaluate, is discussed.

Choice of Damping for Equivalent Lumped Systems

The dashpots of a lumped system represent the damping of the soil. There are two types of damping: loss of energy through propagation of waves away from the immediate vicinity of the footing, and the internal energy loss within the soil owing to hysteretic and viscous effects. The use of dashpots in the lumped system does not necessarily imply that the engineer believes that soil has viscous properties. Rather, dashpots are used in order to derive simple and useful mathematical expressions for the response of the lumped system. Damping ratios are chosen to represent an equivalent amount of damping, and not to represent a particular type of damping.

The damping due to wave propagation is often termed *radiation damping*. Each time that the foundation moves downward against the soil, a stress wave is originated (see Fig. 15.4). As this wave moves away from the foundation it carries with it some of the energy put into

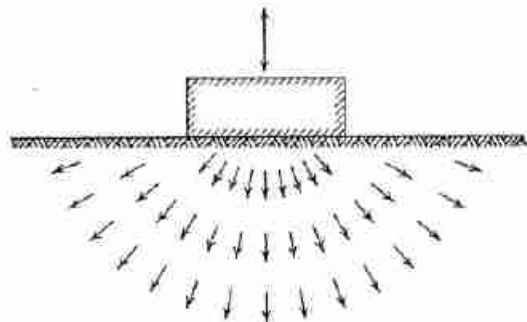


Fig. 15.4 Waves radiating away from vibrating foundation.

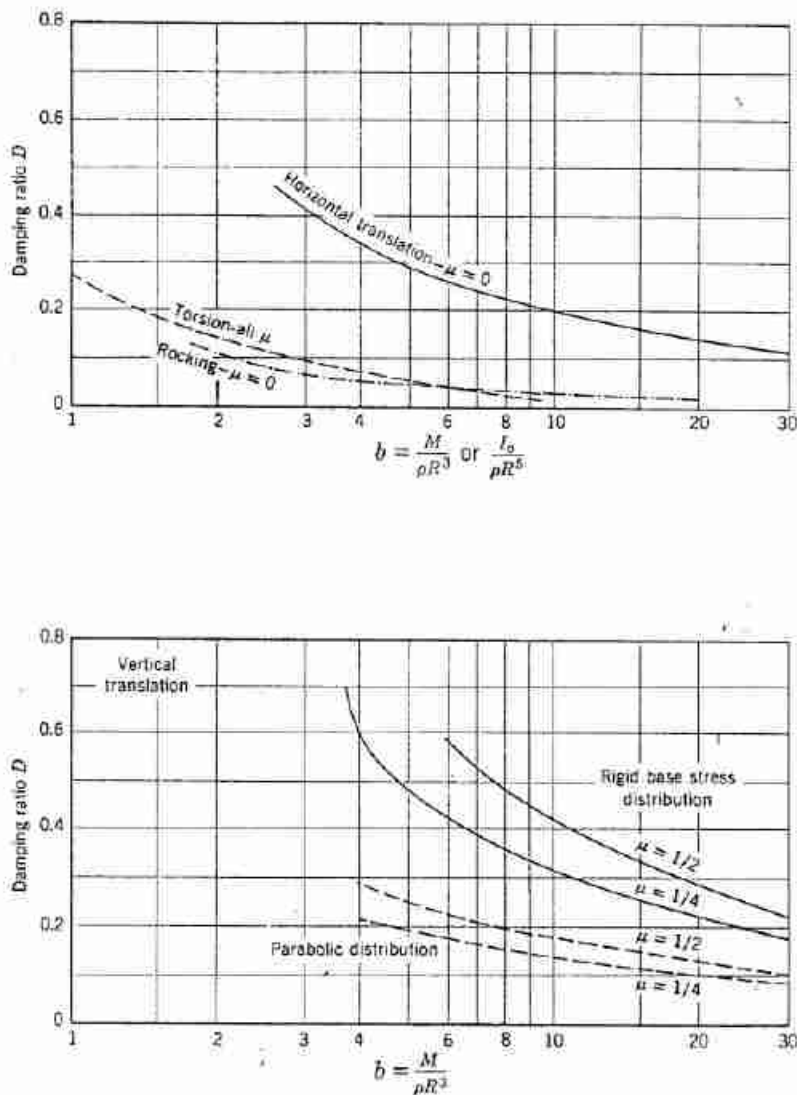


Fig. 15.5 Equivalent damping ratio for circular bases.

the soil. Since this energy is then not available to participate in a resonance phenomenon, a damping effect is introduced. The existence of radiation damping has been revealed by the theory for a rigid disk resting on an elastic half-space (Richart, 1960). This theory may also be used to evaluate an equivalent value of damping ratio. Figure 15.5 gives equivalent damping ratios for the case of circular foundations. The key parameter is the *mass ratio* b , defined as

$$b = \frac{M}{\rho R^3} \quad \text{for translation} \quad (15.6a)$$

and

$$b = \frac{I_0}{\rho R^5} \quad \text{for rotation} \quad (15.6b)$$

where

M = the mass of the foundation block plus machinery

I_0 = the mass moment of inertia of the foundation block plus machinery, evaluated about the vertical axis through the center of gravity for torsional motion, or about a horizontal axis through the centroid of the bottom of the foundation in the case of rocking

ρ = mass density of the soil

R = radius of the soil contact area at the foundation base

Note that the damping ratios are different for each mode of motion. Damping is most important for relatively

light foundations, and is much greater for translations than for rotations. Values of D for rectangular foundations may be estimated by entering Fig. 15.5 with an equivalent radius given by

$$R = \begin{cases} \left(\frac{BL}{\pi}\right)^{1/2} & \text{for translation} \\ \left(\frac{BL^3}{3\pi}\right)^{1/4} & \text{for rocking} \\ \left[\frac{BL(B^2 + L^2)}{6\pi}\right]^{1/4} & \text{for twisting} \end{cases} \quad (15.7)$$

where

- B = width of foundation (along axis of rotation for case of rocking)
- L = length of foundation (in plane of rotation for case of rocking)

The internal loss of energy due to hysteresis has already been discussed in Chapter 10. The magnitude of this energy loss is a function of the magnitude of the strains experienced by the soil. For the level of strains usually permitted under machine foundations, this hysteretic energy loss is equivalent to a damping ratio D of about 0.05.

Approximate values for the combined effects of radiation and internal damping can be obtained by adding $D = 0.05$ to the values of D given in Fig. 15.5. For horizontal translation and especially for vertical translation, internal damping appears to be relatively unimportant in comparison to radiation damping. For rotational motions, however, the radiation damping is small and the internal damping then becomes a significant part of the total damping.

Choice of Mass for Equivalent Lumped System

Clearly, the mass for an equivalent lumped system should at least include the mass of the foundation block plus the mass of the machinery. At first glance it might appear that an additional mass term should also be used to represent the inertia of the soil underlying the foundation block.

Actually, there is no such thing as an identifiable mass of soil which moves with the same amplitude and in phase with the foundation block. At any instant of time various points within the soil are moving in different directions with different magnitudes of acceleration. The use of an "effective mass" is justified only to the extent that a mass larger than that of the foundation block plus machinery is needed to make the response curve of the lumped mass fit the response curve of the actual system. If an "effective mass" is used, it must be regarded as a totally fictitious quantity which cannot be meaningfully related to any actual mass of soil.

The simplest assumption that can be made when

choosing the mass of the lumped system is simply to take this mass equal to that of foundation and machinery and to ignore any "effective mass" of the soil. Moreover, for most foundation problems this simple assumption will give the resonant frequency and dynamic motion within 30% accuracy. Whitman and Richart (1967) provide estimates for the "effective mass" which may be used in those few cases where greater accuracy is justified.

Evaluation of Spring Constant

The determination of a spring constant for use with a dynamically loaded foundation involves essentially the same steps as determination of the load-settlement relationship for a statically loaded foundation. In each case the key is to subject a small mass of soil to the same initial stresses and stress changes as will be experienced under the actual foundation. In the case of dynamically loaded foundations, this means that the soil should be subjected to an initial static stress equal to the stress expected under the actual foundation as a result of the dead load of the foundation plus geostatic stresses, and to stress changes approximately equal to those expected as the result of the dynamic loading. The frequency with which the stress change is applied to the specimen is relatively unimportant.

The various methods described in Sections 14.8 to 14.10 may all be used for estimating a spring constant. The most commonly used approach is to employ formulas from the theory of elasticity. Formulas applicable to rectangular foundations are given in Table 15.1 and values of the coefficients appearing in these formulas are given in Fig. 15.6. The shear modulus G appearing in these equations can be evaluated by the methods described in Chapter 12. This is most often done by measuring the shear wave velocity, either *in situ* or upon laboratory samples using a resonant technique. The

Table 15.1 Spring Constants for Rigid Rectangular Base Resting on Elastic Half-Space

Motion	Spring Constant	Reference
Vertical	$k_z = \frac{G}{1 - \mu} \beta_z (BL)^{1/2}$	Barkan (1962)
Horizontal	$k_x = 2(1 + \mu)G\beta_x (BL)^{1/2}$	Gorbunov-Possadov (1961)
Rocking	$k_\phi = \frac{G}{1 - \mu} \beta_\phi BL^2$	Gorbunov-Possadov (1961)

Note. Values for β_z , β_x , and β_ϕ are given in Fig. 15.6 for various values of L/B .

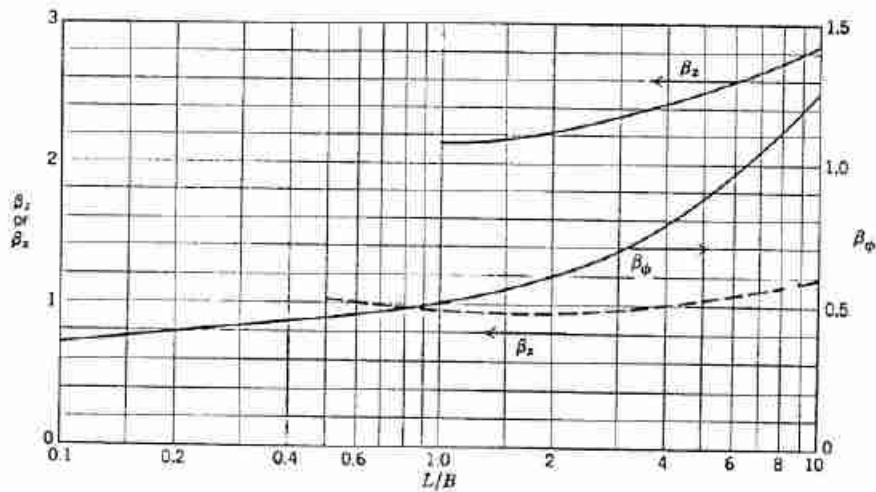


Fig. 15.6 Spring constant coefficients for rectangular foundations.

Poisson's ratio μ to be used in the equations can usually be estimated with satisfactory accuracy as 0.35 for soils of low saturation and 0.5 for fully saturated soils. Another satisfactory approach is to perform a small plate bearing test, using an initial dead load stress equal to that expected under the actual foundation plus a small repeated live load stress. The force-settlement ratio after about 10 cycles of this loading gives the spring constant for the small loaded area. The methods described in Section 14.10 must then be used to extrapolate the spring constant to the actual size of the foundation.

It should be apparent that the engineer must exercise considerable judgment in the selection of a spring constant, so as to take into account the effect of partial embedment of the foundation, stratification in the soil, etc.

Settlement Caused by Vibrations

The dynamic stresses within the soil beneath a machine foundation will cause settlement of the foundation, and excessive settlements must be avoided by proper design. As in the case of settlements resulting from a single static load, vibratory induced settlements of foundations on sand result partly from volume decrease but primarily from shear strains.

The best approach for predicting the magnitude of vibratory-induced settlement in a given case is to subject a sample of the soil to the initial stresses and dynamic stress changes expected below the foundation. Permissible settlements as a result of vibrations are essentially the same as permissible static settlements as discussed in Section 14.2.

In the absence of a detailed testing program, several design principles may be used to minimize the likelihood

of excessive settlements. The sum of the static and dynamic bearing stresses is often held to less than one-half of the usual permissible static bearing stress. Another approach is to subject the soil to vibrations more intense than those to be expected under the actual foundation. Such vibratory compaction may be accomplished by vibratory surface rollers (see Section 15.2). Vibroflotation may also be used to compact soil (D'Appolonia, 1953). A typical requirement is that the soil should be densified to greater than 70% relative density.

15.2 DENSIFICATION BY DYNAMIC LOADS

In many problems, such as the design of machine foundations, the engineer must ensure that vibrations do not cause significant densification of soil. On the other hand, vibrations are often used deliberately to densify soil, as in vibratory compaction. Figure 15.7 shows a vibratory roller compacting a sand fill. Vibratory

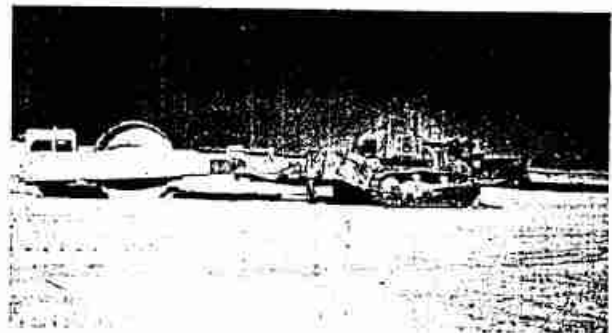


Fig. 15.7 Vibratory compactor.

compaction, which has long been used to densify granular soils, is now often used for compacting clayey soils as well. This section will be concerned primarily with densification of sands.

Laboratory Studies

Figure 15.8 shows a form of test which has frequently been used in the laboratory to study densification of sand by vibration. A container, open at the top, is filled with sand in a loose condition. Sometimes a weight is placed upon the surface of the sand. The container is subjected to vibrations for several minutes, and then the vibrations are stopped while the depth of the soil is measured and a new unit weight computed. Then an increased level of vibration is applied, and so on.

Figure 15.9, obtained when such a container was vibrated by a shaking table causing periodic vertical motion, shows typical results of such tests. The sand initially was at about zero relative density. Very little densification occurred until the accelerations increased nearly to 1g, and most of the densification occurred when the acceleration was at or about 1g. A peak density was attained when the acceleration reached 2g, but further increase in acceleration caused the sand to become less dense. In this particular sand, several different combinations of displacement and acceleration were used to achieve each acceleration, and, as shown in the figure, the results were substantially independent of the combinations employed.

Results of tests such as these have often been taken to imply that peak acceleration is the primary variable controlling densification (e.g., see Barkan, 1962). However, large accelerations alone, in the absence of significant changes in stress, may not cause densification (Ortigosa and Whitman, 1968). On the other hand, as discussed in Chapter 10, increase in stress produces relatively little densification of sand until the stresses become large enough to crush grains. Clearly some combination of events is producing the large observed densification of sand during vibration. The events during the vibratory test may be established by considering the

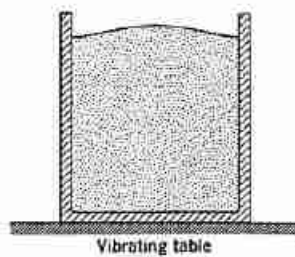


Fig. 15.8 Common laboratory test for study of densification of sand during vibration.

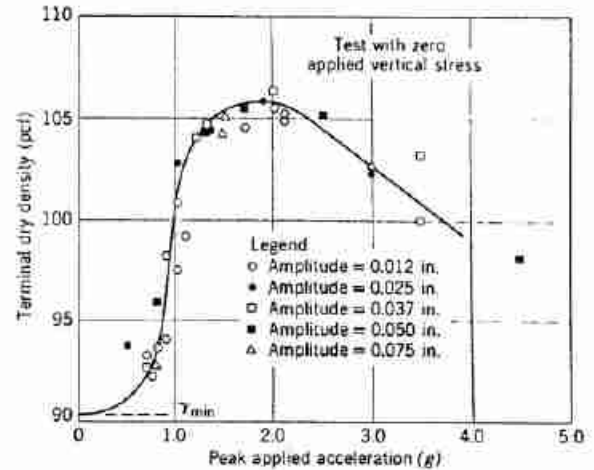


Fig. 15.9 Typical results obtained during laboratory study of densification by vibrations. (From D'Appolonia and D'Appolonia, 1967).

dynamic equilibrium between forces at various times during a cycle of motion (see Fig. 15.10).

When the container accelerates upward, the inertia force acts to increase the stress above the static value. When the table accelerates downward, the inertia force is opposed to the weight of the soil. Thus, if the peak acceleration of the container is 0.5g, the vertical stress at any depth within the soil fluctuates between 1.5 and 0.5 times the geostatic stress.

However, if the peak acceleration of the container exceeds 1g, then events during the test are much more complicated (see Fig. 15.11). At the point in each cycle where the downward acceleration of the container reaches 1g, the vertical stress within the soil drops to zero. Since sand cannot sustain tension, the sand is unable to follow the subsequent motion of the container and experiences *free fall* until it impacts against the container later in the cycle. Then the sand and container move upward together until separation once more occurs and the cycle is repeated.

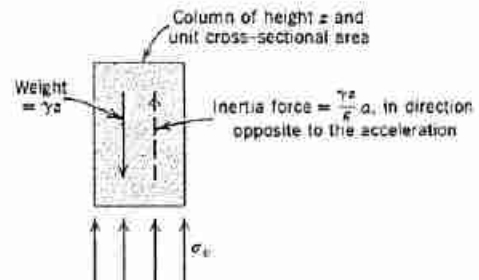


Fig. 15.10 Forces acting upon element of soil during vertical vibrations.

The occurrence of free fall is what distinguishes tests with accelerations of $1g$ or greater (where considerable densification occurs) from those tests with accelerations of less than $1g$ (where little densification occurs). During free fall, the particles become separated from one another and hence are free to seek positions of optimum packing when they fall back against a fixed surface. In a similar vein, it has been found that by sprinkling sand into a container it is possible to achieve a unit weight as great as that which can be achieved by vibration (see, e.g., Whitman, Getzler, and Hoeg, 1963). Thus, although the phenomena involved in vibratory densification are still poorly understood, the absence of effective stress during a part of each cycle of motion appears to be the key to efficient densification.

Vibrations are often used in tests to establish the maximum unit weight of a sand for purposes of studying relative density (see Section 3.1). From the foregoing discussion, it is evident that test conditions have a major influence upon the maximum unit weight obtained in a test. In relative density determinations, it is essential that standardized procedures be used to determine both maximum and minimum unit weight (see ASTM, 1967).

Vibratory Compaction

It is generally acknowledged that granular soils can be effectively compacted in the field using vibratory rollers,

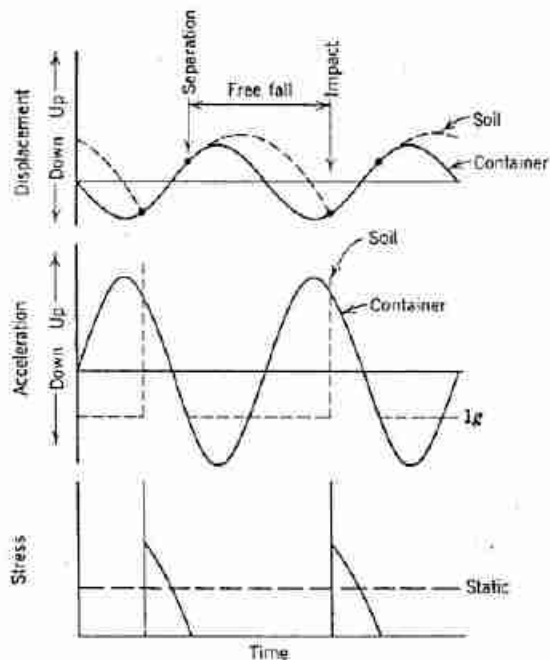


Fig. 15.11 Motions and stress during vertical vibration with peak acceleration greater than $1g$. Note. Drawn for peak acceleration of container equal to $2g$ at 25 cps.

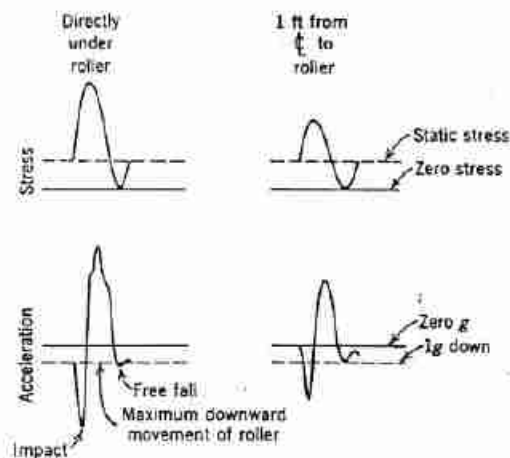


Fig. 15.12 Stress-time and acceleration-time at depth of 1.5 ft in sand beneath vibratory roller (From D'Appolonia et al., 1968).

but there is a lack of facts on the possibilities and limitations of such compaction. One study has been made by Forssblad (1965). The results given in this subsection are from D'Appolonia et al. (1968).

The typical vibratory roller, such as that shown in Fig. 15.7, consists of a drum supported by heavy springs from a frame. Inside the drum an eccentric weight rotates rapidly about the axle of the drum, producing a periodic force against the drum. The drum itself typically weighs about 2 tons, but the periodic force is several times larger so that the drum is raised free of the ground during each cycle and then slammed down against the ground producing large impact stresses. Figure 15.12 shows stresses and accelerations measured within sand beneath a roller during 1 cycle of motion. The impact of the roller against the ground and the subsequent rebound of

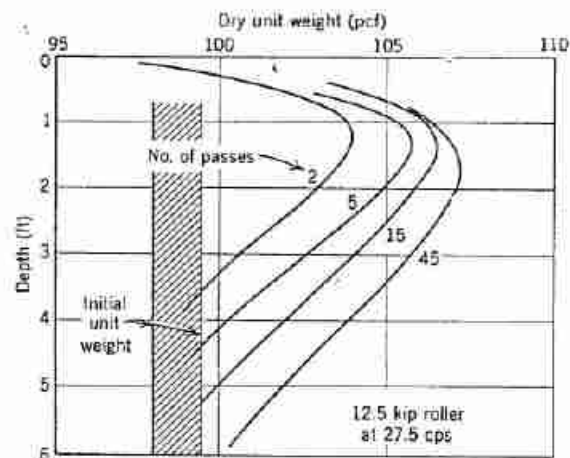


Fig. 15.13 Densification by vibratory roller (From D'Appolonia et al., 1968).

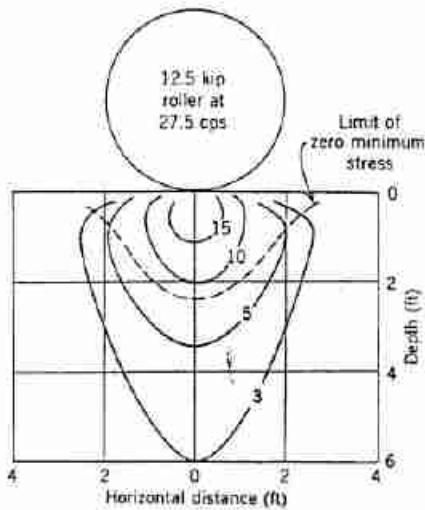


Fig. 15.14 Contours of maximum vertical dynamic stress beneath vibratory roller, psi (From D'Appolonia et al., 1968).

the soil into a state of free fall may be identified in these records. Jumping of particles from the surface of the sand is visible in Fig. 15.7.

The increase in unit weight with depth for various numbers of passes of the roller is shown in Fig. 15.13. The most efficient compaction occurs at a depth of about 2 ft, which, as is shown in Fig. 15.14, is the greatest depth at which zero effective stress occurs during rebound of the soil. By a great number of passes, some densification at a depth of 5 ft can be obtained, and this relatively inefficient compaction presumably results from many cycles of dynamic stress. The topmost 1/4 ft receives little compaction, probably because of the violent agitation (accelerations of more than 3g were observed) in this zone just after the center-line of the roller passed (compare with Fig. 15.9).

An interesting feature of these field observations was the large horizontal stresses built up as the result of several successive passes of the roller (Fig. 15.15). The resulting horizontal stresses exceeded the vertical geostatic stress.

It appears that the action of vibratory rollers with clays is quite different than with sands. Compaction of clay probably is accomplished by successive cycles of impact-caused stress.

Densification During Earthquakes

Earthquakes cause vertical acceleration of the surface of the ground, but these accelerations are too small (at most about 0.3g) to cause densification. Earthquakes also cause horizontal accelerations which, as indicated in Fig. 15.16, give rise to shear stresses. The direction of these shear stresses reverses many times during a strong earthquake as the direction of the acceleration reverses.

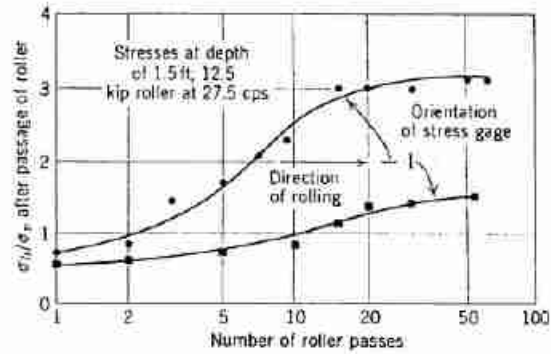


Fig. 15.15 Increase in horizontal stress beneath vibratory roller (From D'Appolonia et al., 1968).

Thus conditions in the ground during an earthquake are similar to those in a direct shear test with several reversals of the direction of shearing.

Subsidence of the ground has occurred during large earthquakes. Part of this subsidence is the result of tectonic movement of the underlying rock, but part results from densification of soil. In Valdivia, Chile, the subsidence due to densification during the 1960 earthquake amounted to more than 1 m. Some, but probably not all, of the subsidence during earthquakes is associated with the phenomenon of liquefaction (see Section 32.10).

15.3 DYNAMIC STABILITY OF SLOPES

When a slope is subjected to an earthquake, the shear stresses associated with ground acceleration (Fig. 15.16) will add to the shear stresses required for static equilibrium and may lead to temporary instability of the slope.

The key features of this problem may be studied by examining the problem of a block resting on an inclined plane (Fig. 15.17). If the block is to accelerate in a direction parallel to the slope, the shear force between the block and the slope must differ from T , the shear force required for static equilibrium. Since the shear

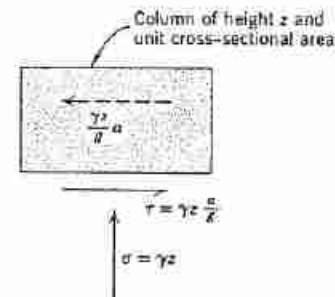


Fig. 15.16 Forces acting on element of soil during horizontal vibrations.

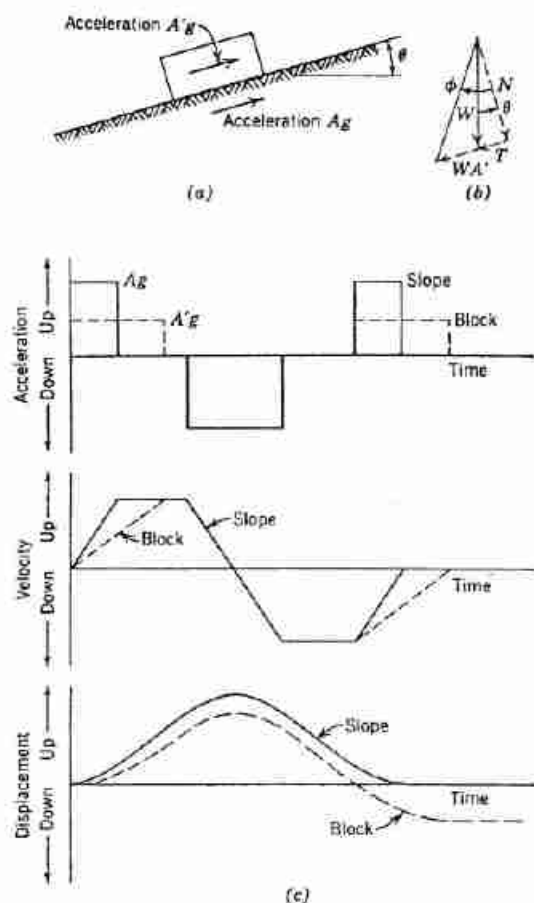


Fig. 15.17 Relative movement between block and slope during dynamic loading.

force is limited (it cannot exceed $N \tan \phi$, where N is the normal force and ϕ the friction angle), the acceleration the block can experience is limited:

maximum upslope acceleration:

$$\frac{W}{g} A'g = W' \cos \theta \tan \phi - W \sin \theta$$

or

$$A' = \cos \theta \tan \phi - \sin \theta$$

maximum downslope acceleration:

$$A' = \cos \theta \tan \phi + \sin \theta$$

If the maximum acceleration coefficient A of the slope is less than A' , then the block and the slope will move together without relative displacement. However, if $A' < A$, then relative displacement will develop as shown in Fig. 15.17c. The block cannot keep up with the slope as the slope accelerates uphill, and hence relative downhill displacement occurs. During downhill acceleration the block and slope are able to move together since A' is greater in this case.

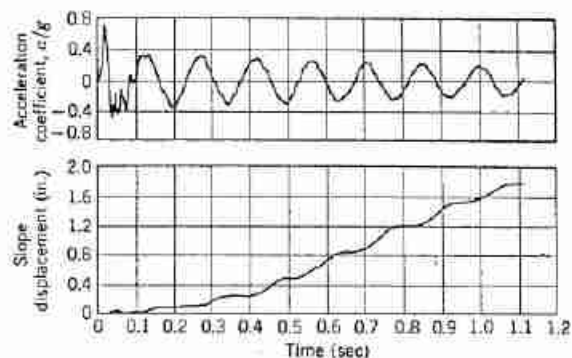
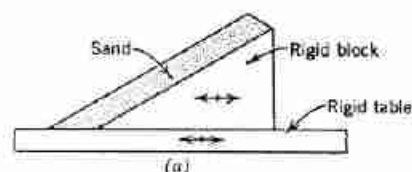


Fig. 15.18 Movement of sand slope during dynamic loading. (a) Schematic arrangement of sand bank for shaking test. (b) Acceleration and displacement of slope during shaking test. Monterey no. 20 sand, 31° slope (From Goodman and Seed, 1966).

A slope in sand, which behaves as an infinite slope (Section 13.9), will experience movements very similar to those of a block on a plane. Figure 15.18 shows downhill relative displacement each time that the applied uphill acceleration exceeds the acceleration corresponding to maximum shear strength. Test results such as these confirm the correctness of the theory for a material of constant strength in which very little strain is required to mobilize this strength.

This method of analysis has been developed in detail by Newmark (1965), who outlines methods for predicting maximum downhill movement during typical earthquake ground motions. The method can be applied in approximate fashion to slopes in materials other than sand. Application of the method will be discussed further in Section 31.8.

15.4 SUMMARY OF MAIN POINTS

The main point to be understood from this chapter is the role of inertia in modifying the stresses and displacements during dynamic loadings. This role has been illustrated for several relatively simple problems. Methods useful in certain practical problems have been presented, but the chapter has only introduced the complex and increasingly important subject of soil dynamics.

A. W. SKEMPTON



Dr. Skempton was born in Northampton, England, in 1914 and educated at Northampton School and Imperial College in the University of London, from which he graduated with the degree B.Sc. (Eng.) with first-class honors in 1935, and the degree of M.Sc. in 1936. In 1949 he was awarded the degree D.Sc. from Imperial College.

From 1936 until 1946, Dr. Skempton worked at the Building Research Station. In 1946 he established soil mechanics at Imperial College. From 1957 to 1961, Dr. Skempton was President of the International Society of Soil Mechanics and Foundation Engineering. In 1961 he was elected a Fellow of the Royal Society. He has been a Rankine Lecturer.

Dr. Skempton's interests have covered a wide range of problems in soil mechanics, rock mechanics, and geology, and in addition he has done extensive research into the history of civil engineering. Professor Skempton has made major contributions to soil mechanics on the fundamentals of the effective stress, pore pressures in clays, bearing capacity, and slope stability. Dr. Skempton has repeatedly shown his remarkable ability to identify the important components of a complex problem and to present a clear explanation of them. Under Dr. Skempton's leadership, Imperial College has become one of the top centers for soil mechanics in the world.